Energy Research and Development Division
FINAL PROJECT REPORT

21st CENTURY INSTREAM FLOW ASSESSMENT FRAMEWORK FOR MOUNTAIN STREAMS

Prepared for: California Energy Commission

Prepared by: University of California, Davis
Land, Air and Water Resources

Department of
LAND, AIR AND WATER RESOURCES
University of California, Davis
Climate Change • Sustainable Agriculture
Environmental Quality • Landscape Processes

MARCH 2011

CEC-500-2013-059

PREPARED BY:

Primary Author(s):
Gregory B. Pasternack, Principal Investigator
Anne Senter

University of California, Davis
Department of Land, Air and Water Resources
Davis, California 95616

Contract Number: **500-02-004**

Prepared for:

California Energy Commission

Joseph O'Hagan
Contract Manager

Guido Franco
Project Manager

Linda Spiegel
Office Manager
Energy Generation Research Office

Laurie ten Hope
Deputy Director
ENERGY RESEARCH AND DEVELOPMENT DIVISION

Robert P. Oglesby
Executive Director

ACKNOWLEDGEMENTS

This research was supported and funded by the Public Interest Energy Research Program of the California Energy Commission through the Instream Flow Assessment Program of the Center of Aquatic Biology and Aquaculture of the University of California, Davis. This project involved a large collaborative effort that was only possible by gracious contributions of effort and resources by many people, including relicensing stakeholders, their consultants, our paid project staff, and UC Davis student volunteers. For the UC Davis contingent, we thank Andy Bookter for serving as lead project technician during the data collection phase; Rusty Barker, Ryan Dupuis, Huy Hoang, and Oliver Huang assisted with field data collection; Chris Monary, Huy Hoang, Oliver Huang, and Simon Park voluntarily contributed an unbelievable amount of time to blimp imagery georeferencing; Nicole De La Mora worked on hydraulic analyses; and Dylan Garner was a tremendous student GIS analyst. We are indebted to visiting student Huy Hoang for performing all 1D numerical modeling and collaborating on the project. He received financial and logistical support from the Student Exchange Program of the Tokyo University of Agriculture and Technology. Dr. Sara Yarnell (UCD) provided discussions and data about the Foothill yellow-legged frog, for which we are very grateful, even though we ended up deciding not to use it in the study.

This project would never have gone anywhere without all the help provided by kind people beyond our ivory walls. Rick Weaver (USFS) helped with preliminary planning for our field data collection campaign. Don and Debbie Shipley, operators of the River Rest Resort campground in Washington, California, facilitated our data collection logistics, provided river access at a crucial location, donated miscellaneous supplies, and helped with contacting other local residents who could help with specific needs. John Godfrey allowed us to locate a storage container on his property, come and go as needed, and also install and maintain a water level sensor. Many local landowners along the study reach graciously allowed us to access the river through their property. The study is indebted to all the folk of Washington, California.

We thank the following individuals who provided wisdom, guidance, and access to diverse resources: Tom Payne (TRPA), Thomas Studley (PG&E), Gene Geary (PG&E), and Jessica Erickson (NID). At PG&E, David Ward and Matt McPheeters provided hydrological data, while Thomas Studley and Gene Geary provided insights and information about aquatic resources. Jennie Garza (HDR/DTA) provided a CD containing diverse hydrological data available in the Drum-Spaulding relicensing process. Bill Morrow (NID), Jarvis Caldwell (HDR/DTA), and David Ward also helped coordinate the timing of the airborne LIDAR survey. Mark Allen (TRPA) provided all of the habitat suitability curves used in the study, which was a critical element for the project. Helpful reviews and feedback were provided by Prof. Allen James (University of South Carolina), Dudley Reiser (R2 Resource Consultants, Inc), Michael Barclay (HDR/DTA), Thomas Studley (PG&E), and Dr. Joshua Wyrick (UC Davis).

PREFACE

The California Energy Commission Energy Research and Development Division supports public interest energy research and development that will help improve the quality of life in California by bringing environmentally safe, affordable, and reliable energy services and products to the marketplace.

The Energy Research and Development Division conducts public interest research, development, and demonstration (RD&D) projects to benefit California.

The Energy Research and Development Division strives to conduct the most promising public interest energy research by partnering with RD&D entities, including individuals, businesses, utilities, and public or private research institutions.

Energy Research and Development Division funding efforts are focused on the following RD&D program areas:

- Buildings End-Use Energy Efficiency
- Energy Innovations Small Grants
- Energy-Related Environmental Research
- Energy Systems Integration
- Environmentally Preferred Advanced Generation
- Industrial/Agricultural/Water End-Use Energy Efficiency
- Renewable Energy Technologies
- Transportation

21st Century instream flow assessment framework for mountain streams is a report for contract number 500-02-004, conducted by the Center for Aquatic Biology at the University of California, Davis. The information from this project contributes to Energy Research and Development Division's Energy-Related Environmental Research Program.

For more information about the Energy Research and Development Division, please visit the Energy Commission's website at www.energy.ca.gov/research/ or contact the Energy Commission at 916-327-1551.

ABSTRACT

Society expects that science and technology should play a central role in balancing hydropower societal benefits with preserving healthy aquatic ecosystems in remote mountainous regions. River science is relatively young and rapid advances in data-collection, mechanistic-modeling, and spatial-analysis technologies are transforming assessment methodologies and the state of knowledge. The disparity between the latest advances in scientific river research and the use of relatively simple river assessment methods for management efforts, such as hydropower dam relicensing, has been growing. This study addressed the gap by showing the practical capability and cost-effectiveness of performing instream flow assessment over a large spatial extent and at high resolution in a mountain river using a combination of remote-sensing methods and 2D hydrodynamic modeling. The authors conducted analyses that yielded an interdisciplinary and spatially explicit perspective on the status of a ~12.2 kilometer testbed river segment on the South Yuba River between Lake Spaulding and the town of Washington, CA in the northern Sierra Nevada. The researchers investigated stage-dependent patterns and processes at multiple spatial scales of fluvial landform nonuniformity. The most important finding was that the geomorphology, hydraulics, and physical habitat of the river segment are linked across four spatial scales. Researchers identified a recurring pattern of discrete fluvial landforms at the scale of ~1-10 channel widths in length. The study linked hydraulics and the availability of preferred physical microhabitat for specific fish species' lifestages to the observed pattern of morphological units, which were linked to reach attributes, which in turn were determined by segment-scale attributes. Perhaps the most important insight for river management was that integrating spatially explicit geomorphology, hydrology, hydraulics, and physical habitat characterization could improve instream flow assessment. Such integration would provide a foundation for quantifying current conditions, explaining their origins, and predicting what is necessary for their maintenance and/or improvement.

Keywords: instream flow assessment, mountain river hydraulics, mountain river fluvial geomorphology, mountain river hydrology, mountain river physical habitat analysis, regulated rivers, human impacts on rivers.

Please use the following citation for this report:

Pasternack, G. B. and A.E. Senter. 2011. ***21st Century instream flow assessment framework for mountain streams.*** California Energy Commission, PIER. CEC-500-2013-059.

TABLE OF CONTENTS

LIST OF FIGURES

LIST OF TABLES

EXECUTIVE SUMMARY

Introduction

Environmental conditions in many mountain rivers throughout the world are degraded due to a complex array of historic and current societal uses overlain on natural dynamics. In the United States, there are no systematic frameworks for managing the diverse impacts on environmental conditions of rivers from human uses. In mountain rivers, many stakeholders view hydropower dam relicensing as a possible framework, expecting licensees to solve problems far beyond the actual impacts of licensed projects. In addition, hydropower dam relicensing involves making fixed decisions at a given moment that locks in operations for decades, with little to no flexibility for adjusting to changing conditions and uncertainties.

Rational, quantitative river assessment has been a rapidly growing component of the hydropower dam relicensing process. Today, river assessments are more quantitative and accurate than they have ever been. Unfortunately, river science is a very young discipline that is not ready or able to meet the purpose of characterizing natural systems and human impacts on them in the detail required to answer important policy and management questions. River science is presently in the midst of a paradigm shift. Under the old paradigm that began in earnest in the 1940s, diagnosing river conditions relied on a small number of carefully selected transects (or cross-sections) and simple empirical equations. At the dawn of the 21st century, a new paradigm is emerging in which advanced remote-sensing technologies and sophisticated computer simulation models are providing a more complete characterization of physical conditions at the 0.01-1 meter (m) spatial scale for even longer lengths of river channel. Today, new scientific theories lag behind technological developments by several years and practical use of those theories in hydropower dam relicensing are ~15 years behind that. On one hand, the process of hydropower dam relicensing would be facilitated by standardized methods and professional licensure. On the other hand, improved outcomes for river assessment in support of hydropower dam relicensing require greater flexibility, adopting new methods, and more continuing education of professionals.

Project Purpose

The primary goal of this study was to show the practical capability and cost-effectiveness of performing instream flow assessment of the physical conditions in a mountain river over a relatively large spatial extent and at a high resolution. Current practice today is based upon a very small sampling. On a practical level, this study served as a proving ground to find out what tools within the new paradigm are presently capable of meeting the needs of hydropower dam relicensing. Is it valuable to have ~1-centimeter (cm) resolution digital imagery of a river corridor? Can desktop personal computers handle simulations of rivers that require hundreds of thousands to millions of computational elements? Is it possible to overcome the technical challenges of complex methods and produce new scientific interpretations of river processes relevant to hydropower dam relicensing? These overarching types of questions motivated this scientific study.

The specific objectives of this project involved (1) using remote-sensing and 2D hydrodyanmic modeling as the foundation for a thorough instream flow assessment of a test section of a regulated mountain river, and (2) comparing key results from the first objective with results obtained using common methods under the old paradigm founded on transects. Water depth

and velocity are key indicators for instream flow assessment. Manning's equation for estimating flow in an open channel and 1D hydraulic computer models are commonly used to estimate/predict depth and velocity in diverse river management efforts, including hydropower dam relicensing. Therefore, the methodological comparisons in this study focused on the performance of these tools relative to 1-m resolution 2D hydrodynamic modeling. The comparison of instream flow assessment used identical depth and velocity values at designated points but varied the total number of points and the methods for upscaling from points to overall conditions. This alternate test isolated the effect of using transects for sampling hydraulics, which is a common approach used for instream flow assessment in hydropower dam relicensing. This study did ***not*** test the complete method known as the Instream Flow Incremental Methodology (IFIM) or the program suite known as Physical Habitat Simulation System (PHABSIM). The investigators did thoroughly study PHABSIM applications in recent hydropower dam relicensing studies and noted its limitations.

Many project components had to be completed to achieve the two specific project objectives of the study. The investigators conducted a thorough planning phase with a literature review, site selection, and historical analysis. They developed methods and performed data collection, map production, hydrological analysis, 2D modeling, 1D modeling, geomorphic analysis, transect-based sampling, 2D hydraulic analysis, hydraulic comparisons, 2D physical-habitat analysis, and physical-habitat comparisons. The report is organized by these steps. From data collection through writing the report took just 19.5 months. The author's estimate that the same analyses could be performed ~30 percent faster now that the methods have been developed.

Project Results

This study found that not only is it feasible to perform instream flow assessment under the new paradigm of river science, but that doing so enabled a previously unobtainable process-based linking of topography, hydrology, channel organization, hydraulics, and physical habitat. Processes cannot be represented by transects, so transect-based methods will never achieve a process-based outcome capable of relating ecological functions to physical conditions and dynamics. Furthermore, the study showed that processes are derived from the expression of landform heterogeneity at multiple spatial scales. In other words, the way a river behaves at a higher flow is not necessarily more intense than how it behaves at a lower flow, so more flow does not mean more river action. It is more like multiple personalities in that there are discrete ranges of flows for which the river behaves in a unique way with specific patterns of hydraulics, physical habitats, and processes. Unfortunately, even though this study spanned four orders of magnitude of flows, it was still unable to investigate large enough rare floods to capture all of the relevant "personalities." Understanding the behavior and impacts of high flows is critical to evaluating the resilience of low-flow habitats to infrequent extreme events. Licenses are often issued for decades, over which time extreme flow in a mountain river is virtually guaranteed.

The authors initially reviewed the scientific foundation of instream flow assessment, selected and characterized a study river segment, retrieved pre-existing data, and established project constraints. They updated literature reviews for instream flow assessment previously sponsored by the California Energy Commision with assessments from around the United States and newly published concepts for instream flow assessment influencing future directions. They selected a river segment on the upper South Yuba River between Lake Spaulding and the town of Washington, CA. The Yuba River watershed has been investigated

for over 100 years, generating ample documentation. Participants in the ongoing Drum-Spaulding relicensing effort contributed valuable data.

Data collection occurred opportunistically throughout the duration of the project, with the primary effort consisting of a major campaign from mid-June to mid-October 2009. The data that was collected included ~4-cm resolution kite-blimp imagery; LIDAR (light detection and ranging)-derived ground, water surface, emergent boulder, and canopy-top elevations; LIDAR-derived image intensities; ground-based topographic and bathymetric measurements; discharge and water surface elevation measurements; stage-discharge rating curve development; velocity observations; sediment substrate grain sizes; and streamwood occurrence. Embedded within each dataset are sources of uncertainty, so efforts were made to characterize those uncertainties.

A detailed topographic map is the most important and basic foundation for an environmental analysis of a river. Integrating diverse data sources with different uncertainties into a single digital elevation model involved performing careful quality assurance and quality control by way of substantial manual inspection of data products. The researchers developed a new method to extract LIDAR-derived emergent boulder points, which greatly enhanced the digital elevation model of the river. In the end, the topographic map of 12.2 kilometer (km) of river valley produced in this study is likely to be among the longest high-resolution maps of a remote mountain river in the world at this time.

Mountain river discharge includes flow releases from human-operated facilities as well as unregulated flows that accumulate (or accrete) downstream as watershed area increases. As a necessary precursor to 2D hydrodynamic modeling, the researchers analyzed accretionary flows to determine the hydrological processes responsible for controlling them and to obtain synthetic empirical equations for estimating ungaged contributions to the study river segment from gaged flows. They statistically generated equations for each hydrologic season (i.e., dry, wet, and snowmelt) and then distributed total flow accretion among tributaries on the basis of proportional watershed area.

2D hydrodynamic models predict the spatial pattern of water surface elevation, depth, velocity, and associated variables such as eddy viscosity and bed shear stress. In this study, the authors divided the river segment into two model areas and then created a low-flow and high-flow computational mesh with ~1x1 m^2 grid cells. These meshes had between 284,000-468,000 cells, which is an order of magnitude more than was commonly used in projects in 1995-2005. Researchers compared predictions of water surface elevations and depth-averaged velocity magnitude from the freeware 2D model known as SRH-2D against observations made at flows ranging from ~10-1000 cubic feet per second (cfs) (gaged). The quantitative assessment of uncertainty in the digital elevation model served as the baseline reference for judging model performance with water surface elevation prediction, and by that measure, the model performed very well. For velocity, model performance was compared against other published 2D model studies. Despite being used in one of the most difficult river settings that exist—a low-flow, complex, bedrock/boulder mountain channel—the 2D model from this study performed as well as others used in much simpler settings. Specifically, 2D models tend to show an average velocity error of ~20-30 percent, with the coefficient of determination (r^2) between observed and predicted being between 0.5-0.7. These performance criteria were met in this study.

This study used the Hoang 1D model to simulate cross-sectionally averaged water surface elevation, depth, and velocity at 105 cross-sections (~8 per km). This density of cross-sections was higher than commonly used in 1D model studies and therefore was a fair test of the most optimistic way that 1D modeling might be used for instream flow analysis. Boundary and input conditions for the 1D model were set to be as similar to the 2D model as possible. Researchers also tested a transect-based hydraulic sampling approach using 916-3175 points, depending on the discharge tested.

Thorough geomorphic analysis is often neglected in instream flow analysis in favor of a statement that a given river is "stable" and thus suitable for neglecting geomorphology and physical processes. In contrast, this study used 2D model results to invent and thoroughly demonstrate a new way to characterize the geomorphology of a river at a moment in time as well as to infer key physical processes for sustaining physical habitat. Starting from the 1-m resolution 2D model outputs, it was possible to identify laterally varying, flow-independent "morphological units" that served as the basic building blocks of geomorphic processes at reach and segment scales. Morphological-unit analyses confirmed that these basic building blocks are spatially organized with different types having statistically significant "preference" and "avoidance" for each other. This is a significant advance over the current use of laterally uniform mesohabitat classification. Geomorphic analysis also included descriptions of key processes for sediment transport and channel maintenance, which were assessed along with 2D hydraulic model outputs.

Having identified distinct morphological unit types, the next step involved characterizing the hydraulics of the river at different spatial scales. Different hydraulics were evident for different morphological units as a function of hydrologic season and flow. When hydraulic results were propagated through appropriate equations to obtain sediment transport regime metrics, the key finding was that the range of flows observed (~5000-7000 cfs gaged) was inadequate to reach dramatic channel-changing events (e.g., the 1997 rain-on-snow flood had a discharge of ~30,000 cfs gaged) given the boulder framework of the channel, but it did capture the process of gravel/cobble substrate redistribution among morphological units. Another important finding was that the limited range of observed flows did not provide evidence for the mechanism of stage-dependent flow convergence that provides one mechanism for rejuvenating relief between pools and topographic highs. Differences in velocities and bed shear stresses between morphological unit types decreased dramatically from 5000 to ~7000 cfs, but higher flows need to be observed to fully evaluate how and if the river segment rejuvenates itself. Further, there was no evidence in the 2D model that local scour around bedrock outcrops was a significant process for channel change for gaged flows <7000 cfs.

The comparison of 1D and 2D numerical models revealed that even with 105 cross-sections, the 1D model performed poorly at predicting cross-sectionally averaged hydraulics and morphological-unit-averaged hydraulics. The reason for the poor performance is that a mountain river has so many important hydraulic controls in terms of topographic highs and width constrictions that it is infeasible to capture them all with a suitably low-cost field data collection campaign that could justify the use of 1D model over a 2D model. Without capturing the channel controls, the model gets the bed slope and channel width controls wrong, and then calculates faulty hydraulics. In the few locations where the river has uninterrupted "uniform" plane bed and bank conditions, the 1D model performs well, but those conditions are rare in mountain rivers.

In addition to testing 1D versus 2D hydraulic predictions, this study also tested the ability of transect-based sampling to accurately predict hydraulic indicators. This test isolated a single question and only varied the number of points. In the transect-based methodology commonly used in hydropower dam relicensing, a transect is designated as a single mesohabitat type, with no laterally varying component, which was proven by this study to be inaccurate. To provide a generous sampling for the transect-based method, 30 cross-sections were obtained for the 13.52-km study segment, which is ~30 percent more than is commonly used. At the segment-scale, the analysis showed that transect-based sampling can yield reasonable reproductions of the majority of the depth and velocity statistical distributions, although the performance at the upper tails was poor, and performance decreased as discharge increased. Model performance at the morphological-unit scale was poor overall. The test demonstrated that during the lowest flow of 5 cfs, the transect method overestimated velocity in plane beds, pools, and inset channels by 595 cfs, 400 cfs, and 65 percent, respectively. At the highest flood flow, the transect-based method had errors of 0.8-21.2 percent. However, a flood flow is largely irrelevant to physical habitat area estimation for hydropower dam relicensing, because the flow is uncontrolled. The goal of instream flow assessment for hydropower dam relicensing is often to choose optimal regulated low flows or even the minimal possible flow. The poor performance when using ~1000-3000 points compared to a near-census of hundreds of thousands of points in estimating unit-averaged hydraulics was a cause for concern for the continued use of transect-based sampling in hydropower dam relicensing for mountain rivers. However, the performance at the segment scale was encouraging, so the results were mixed.

The authors assessed physical habitat availability in the study segment by combining habitat suitability curves (HSC) for one to four lifestages of rainbow trout, Sacramento sucker, and pikeminnow/hardhead with 2D model results. Researchers performed standard tests of total preferred physical habitat area and percent of wetted area of preferred physical habitat area for each species' lifestage as a function of hydrologic season and flow. Results of these tests show that there is significant variation in which flows are optimal for species between lifestages for each hydrologic season. . For the dry season, area and percent area summary metrics indicate that either 20 or 10 cfs, respectively, released past the Lang's Crossing flow gage, would yield the best overall balance of habitat conditions. For the wet season, 55 and 15 cfs, respectively, would provide the best conditions, with 140 and 25 cfs, respectively, for the snowmelt season. These values diverge so strongly because the wetted area increases significantly as discharge increases.

Researchers performed similar habitat-area analyses using the 1D model and transect-sampling methods to the extent feasible, and then compared all methods. The various methods estimated very different amounts of preferred habitat area. Further, for both the 1D model and transect-sampling methods, there was a large variation in results depending on how habitat quality was extrapolated from sampling sites to the entire river segment. Relative to 2D model performance, the next best outcome was obtained by using a transect-based approach without any statistical averaging. Because of the careful control over methods and independent evaluation of calculating hydraulics performance, it was possible to attribute the differences relative to the 2D modeling approach to inadequacies in 1D models and transect-based hydraulic sampling for use in complex mountain rivers.

This project achieved its goal of breaking new ground in developing spatially explicit, high-resolution instream flow analysis. A "proving ground" combined novel technologies, data-

processing methods, mechanistic models, and Geographic Information Systems (GIS)-based spatial and 3D analyses and identified which components would be the most useful. Based on the results of this study, having an accurate, high-resolution topographic map has to be the single most important tool to support instream flow assessment in the 21st century. Having a mechanistic hydrodynamic model capable of integrating flow inputs and detailed topography is the next most important tool. Although this study did not test IFIM and the PHABSIM software suite, two key tests of the common ways hydraulic data are extrapolated from transects to mesohabitats and ultimately to habitat area metrics found that the methods have some merit and some troubling inaccuracies. The fact that one style of IFIM uses highly accurate, direct measurements of velocity and depth at up to three different discharges cannot overcome two major problems. First, a few hundred sampling points per ~10-100 km of mountain river is inadequate to represent the range of depth and velocity combinations in that complex channel setting. There is no one standard way to pick transects for all morphological unit types that will capture their joint depth-velocity probability distribution. Second, the conventional assumption of laterally uniform mesohabitat classes on transects improperly blends hydraulics from different landform types, resulting in an extrapolation over incorrect habitat areas. No matter how good point measurements of velocity and depth are in the transect-based sampling, the inadequacy of mesohabitat-based extrapolation degrades the accuracy of the area estimates. Beyond assessing the performance of different habitat-area computational methods in a complex mountain river, this study made several new basic discoveries about landform organization and physical processes in mountain rivers.

River science is progressing so fast that it would be premature to standardize methods for instream flow assessment at this point. The authors predicted the likelihood that assessment will be reliant on transect-sampling (including transect and 1D model options in PHABSIM) for analysis of physical conditions will be ~50% in five years, ~10% in ten years, and ~0.1% in twenty years. At some point the philosophy of statistically quantifying habitat by way of a flow-habitat relationship will have to give way to a more effective spatial analysis of habitat and a process-based accounting of ecology. Also, technology is going to make spatial analysis so readily available that practitioners will demand its use. Low-flying remote sensing is going to yield very low-cost topographic data of rivers with 1-cm resolution that can be done over long river segments. Meanwhile, ever-better 2D and 3D desktop computer models will become available with parallelized computational capabilities, greater direct numerical simulation capabilities for smaller grid scales, and improved sub-grid models. Even if transect-based depth and velocity measurements are superior to predictions of those variables by models in the future, the measurements are inadequate for several reasons: there are not enough measurements to characterize morphological-unit scale metrics; they cannot capture the hydraulic complexity relevant to the spatial pattern of physical habitat; they cannot be used for geomorphic assessment; they must be coupled with poor-quality, laterally uniform mesohabitat delineations to estimate habitat area; they are estimation methods rather than the prediction methods needed to plan river restoration; and they can never move beyond statistical analysis to spatially explicit habitat evaluation. This case study of the upper South Yuba River also estimated habitat area and percent area of three fish species by lifestage as well as summary metrics that will be made available for use in hydropower dam relicensing. Future research could apply the spatially explicit modeling results for additional hydrological and ecological features such as habitat connectivity.

Benefits to California

Significant progress has already been made in improving the science and technology of instream flow assessment. Nevertheless, production of methods and theories in river science has accelerated and the gap between peer-reviewed river science and professional practice applying river science is widening rapidly. This study illustrated how professional practice can make a leap forward with respect to evaluating links between river flow, landform structure, physical processes, and fish habitat across 1-m to 10-km spatial scales. There are ~1400 dams within California's jurisdiction, and each one is relicensed periodically. Californians need all of the societal benefits provided by dams, but they also consistently vote in favor of laws, regulations, bonds, taxes, and user fees that promote environmental conservation and restoration. Instream flow assessment is an essential tool in the process of balancing the societal uses of rivers, including hydropower, with their ecological sustainability

CHAPTER 1:
Introduction

Dams and flow regulation are common in mountain regions. This societal use of rivers for electricity, water supply, and flood control is important for many human needs, but it does significantly impact the river corridor downstream of the dam (e.g. Power et al. 1996; Brandt 2000; Grant et al. 2003; Parker et al. 2003). Specific examples of impacts include flow regime alterations (i.e. changes to the magnitude, frequency, duration, timing/predictability, and rate of change of flow downstream of the dam [Poff et al. 1997]), blockage of downstream flux of sediment and associated chemical and biological constituents, physical alteration of the river corridor (e.g., incision, narrowing, bed coarsening, reduced in-channel topographic relief and variability, vegetation encroachment, and isolation of channel from floodplain (Williams and Wolman 1984)), and habitat degradation in terms of availability and quality of aquatic and riparian conditions required for diverse ecological functions (Moyle 1994). Further, dams do not occur as a sole impact, but are part of a complex assemblage of cumulative societal impacts that may also include mining, roads, logging, urbanization, agriculture, recreation, and human-induced accelerated climatic change (Moyle and Randall 1998; Reid 2001).

Many hydropower dams will be re-licensed with the Federal Energy Regulatory Commission in the next 15 years. Complex and evolving societal perceptions about nature make it necessary to balance disparate societal uses and ecological functions of regulated rivers (Arthington et al. 2006). A key issue for hydropower dam relicensing projects is the determination of how much water should be released down natural channels and according to what regime. The answer to this also interfaces with questions about the relative role of flow regulation in degrading river ecology relative to other non-flow (concurrent and historical) human uses of rivers. Across the suite of societal impacts on rivers, it may be necessary to actively rehabilitate sections of rivers in addition to or instead of re-regulating flows.

Ideally, scientific and technological tools ought to objectively quantify the scope of adverse impacts on aquatic species and habitats from instream flow changes caused by dam operations. That would include enumerating all organisms at risk, characterizing their relations with each other and habitat (i.e. the physio-chemical environment), predicting how life histories and species' interactions would respond to any specified management regime, and assessing management trade-offs with either index-based analysis (Sandoval-Soils et al. 2010) or cost-benefit analysis in dollars (Jackson et al. 2001). The science of instream flow assessment aims to achieve just such a comprehensive appraisal. Creative scientists have developed hundreds of instream flow assessment methods for diverse river settings and with different theoretical underpinnings (Tharme 2003; Payne 2004). Unfortunately, information will always be limited and science will always have uncertainty (Castleberry et al. 1996; Van Asselt and Rotmans 2002), so it may be useful to use several methods and develop scientific conclusions from a suite of tools.

Another complication is that the status of and resources for mountain science and instream flow assessment lag behind those for lowlands (Tinkler and Wohl 1998). People and societal interests are concentrated in low-lying coastal regions. The frequency and devastation of river and coastal flooding ensure that resources will be heavily biased toward lowlands (Perry 2000; Cartwright 2005). Given the available resources for mountain river assessment, mountain extents are so large that the resources become quickly diluted per unit area. Meanwhile, the dominant

physical aspect of mountain streams is that they exhibit a lot of spatial complexity (i.e. channel non-uniformity as explained in the next paragraph), necessitating high-resolution methods (Valle and Pasternack 2006). Achieving such resolution in field observations is slowed by the highly variable climatic and rugged topographic conditions in which mountain streams reside. Finally, in the absence of historic progress in mountain science, methods developed for lowlands have been widely adopted for use in mountains, even though the conditions in the latter often violate methodological assumptions (Tinkler and Wohl 1998).

The primary challenge lies in the fact that mountain river systems span vast regions characterized by multiple spatial scales of landscape organization and heterogeneity. Diverse riverine features include organized lateral and longitudinal patterns as well as random elements (Figure 1). This complexity poses a technical problem in terms of adequately representing all features with equal consideration. Ideally, a complete *census* of all existing features would be done to yield the most certain characterization of their conditions and dynamics. At this time, a complete census of mountain river features over a large region is unfeasible. The most common approach to coping with this is to implement sampling, and the gold standard approach is to use *cross-sections* (Figure 2). According to this approach, detailed information is gathered for a small number of features that span the system using an objective sampling scheme (random, uniform, stratified random, stratified uniform, or stratified conditional sampling scheme where conditional means subject to logistic constrains such as accessibility) or a deterministic scheme such as representative sampling based on habitat mapping. Once the data is gathered, then results for the sampled set are interpolated to the entire population within the sampled domain. Among the pros and cons of the approach (Figure 2), the most fundamental problem is that many important river patterns and dynamics are not expressed in cross-sections and the process-related assumptions that have to be made to use this scheme are poor. This issue is investigated thoroughly in this study.

In tandem with the wide adoption of systematic cross-sectional sampling, the perspective that an understanding of how rivers work requires a thorough investigation of physical processes, ecological functions, and how they interact across spatial and temporal scales has always existed. An important issue, though, is how much time, effort, and cost should be allocated to in-depth studies and the results that those studies produce compared to what might be termed more efficient studies that produce reasonable results using less time, effort, and cost. Traditionally, in-depth studies have involved experts making intense observations at a small number of sites over time and extrapolating knowledge gained from those few sites to an entire system. Advances in remote sensing, computer modeling, and field data collection in the late 20th century increased the sophistication possible using an in-depth approach, but left the problems of interpretive subjectivity and extrapolation of results into unknown regions (Figure 3).

One framework for reconciling these two different approaches is to recognize that different instream flow assessment questions require different levels of detail, and thus a hierarchical (aka nested) strategy that makes use of both is possible (e.g. Rosgen 1996; Thomson et al. 2001). A broad interpolative sampling strategy can be standardized to meet general instream flow assessment needs and then unsatisfied stakeholders can identify specific issues that require more thorough investigation. Stakeholders in environmental management desire regulatory certainty and thus scientific certainty, because it provides stability for economic growth. Regulatory certainty is promoted by standardization. Hierarchical strategies enable a balance of

standardization of current condition assessment and process-based scientific inquiry to get at root causes of current conditions. Many instream flow assessment efforts underway today involve this compromise.

Despite the possible satisfaction provided by a nested framework, mountain river science is progressing so rapidly that it is foreseeable to look beyond current nested schemes to instream flow assessment based on a complete river census. This was the purpose of this study; to work through the difficult basic and applied science of the future using the rapidly progressing tools available to us today.

Figure 1. Mountain rivers have multiple spatial scales of diverse features.

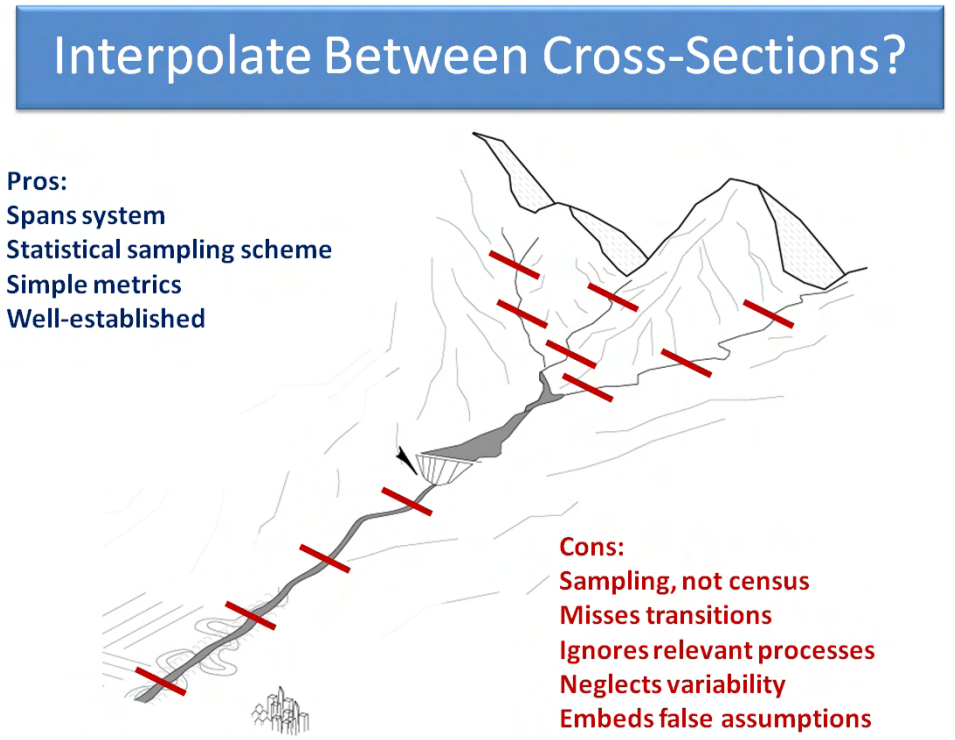

Figure 2. Common 20th-century approach for sampling river corridor conditions to obtain an instream flow assessment.

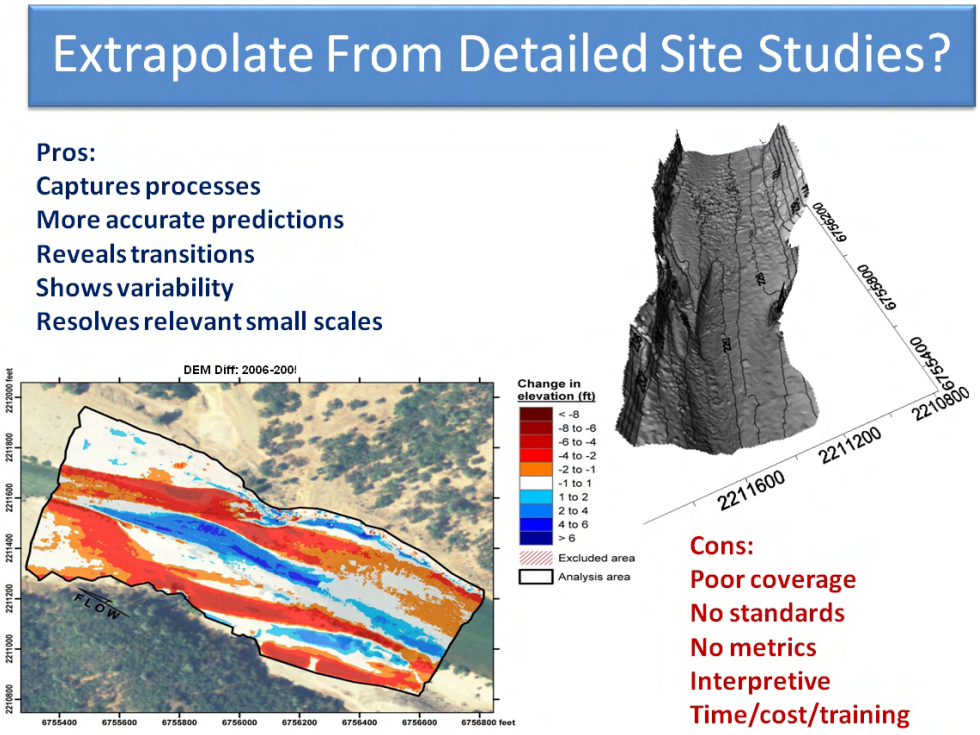

Figure 3. Process-oriented investigation of complexity of riverine hydroecology.

1.1 Project Goal and Objectives

"On the day we shipped the first [Atari] Video Console Systems, I said, 'Okay, that's done, now we have to get a product that will replace it.'" –Nolan Bushnell, founder of Atari

The primary goal of this study was to show the practical capability and cost-effectiveness of performing instream flow assessment over a relatively large spatial extent and at a high resolution compared to what is commonly performed in instream flow assessment practice today, and is consistent with a concept of achieving a near-census of the physical conditions in a mountain river instead of a much smaller sampling of a large area. The approach involved using the most advanced remote sensing methods, rapid field-observation technologies, and the latest, most efficient algorithms for 2D hydrodynamic modeling. All of this data was then processed using a Geographic Information System (GIS; ArcGIS 9.3) for comprehensive river evaluation using a variety of relatively standard methods. With such an extensive data set, other creative analyses may be explored at a later date but those will have to remain undone at this time. This report has a central focus, but also takes the opportunity to explore interesting scientific side questions that inform that focus.

In addition to pushing the present limits of spatially distributed, point-scale analysis, this study took the opportunity with the newest 2D mechanistic modeling approach to compare methods and results using two other standard approaches for sampling hydraulics. The first approach was a standard 1D numerical (mechanistic) hydrodynamic model that predicts water surface elevation and cross-sectionally averaged depth and velocity values at specified cross-sections. The second approach was a transect-based sampling scheme in which the test was not on the method of estimating point-scale hydraulics, but rather was on the effect of scaling up from the commonly-used small number of points distributed along transects to estimate hydraulics at larger spatial scales. These tests are not intended to be a comprehensive assessment, confirmation, or indictment of the validity and utility of current river-assessment methods such as Indicators of Hydrologic Alteration (IHA), Instream Flow Incremental Methodology (IFIM), or the Physical Habitat Simulation System (PHABSIM). In fact, currently practiced methods are not only diverse, but the use of any given method is not well standardized by its user base. The results of this study aim to provide insights that help inform and constrain underlying elements of some current practices, but most importantly to develop methods for what river assessment could do with data approaching a near-census of river conditions.

This study was not designed to explicitly test IFIM or PHABSIM in hydropower dam relicensing. The funding proposal describes comparisons of 1D and 2D hydraulic models, with reference to the Brown and Pasternack (2009) journal article that performed similar tests of outputs from hydraulic models and Manning's equation. Neither IFIM nor PHABSIM is a 1D or 2D model. Both are broader frameworks for conducting aspects of instream flow assessment that include several approaches for estimating or predicting hydraulics, but they are not themselves 1D or 2D models. Colloquially, some practitioners use the term "1D model" to mean PHABSIM, but this study does not do that. In considering whether to go beyond the scope of the project to perform such an evaluation, a literature review revealed that there is no professional consensus as to how IFIM and PHABSIM should be implemented, as exemplified by the range of methods and results available via manuals and reports from public and private entities. This study chose to conduct rigorous analyses of 1D and 2D hydrodynamic model results with no interest in mimicking other instream flow assessment methods. Therefore, a

focused set of tests was conducted with the intention of providing useful insights into the constraints on different tools for hydraulic prediction at multiple spatial scales. It is up to the reader to evaluate the uncertainties, assumptions, and methods of this study, and to decide whether these new results inform the current practice of using PHABSIM or any other instream flow assessment methodology that uses transect-based hydraulic observations and/or 1D hydraulic models.

1.2 Project Components

To achieve the goals of this project, a diverse and thorough set of analyses were required to generate the observation- and simulation- based inputs for GIS-based spatial analysis. A significant amount of background literature exists on instream flow assessment methods as well as on the setting of the selected study segment on the South Yuba River in the Sierra Nevada of Northern California. That information was part of the background information assessment (Chapter 0). A broad-based data collection campaign included data collection via remote-sensing methods as well as ground-based topographic and hydrologic methods (Chapter 0). These data were processed to obtain baseline maps of current conditions in the river, in terms of a digital elevation model, riparian canopy surface model, ~4-cm resolution aerial photography, and other GIS map products (Chapter 0). Next, it was necessary to conduct a hydrological analysis of the watershed area under investigation in order to characterize the role and spatial distribution of flow accretion in the study segment, and additionally to explore existing hydrologic data for possible climatic change impacts 1965-2009 (Chapter 0). With digital GIS maps and synthetic hydrologic flow accretion relations in hand, it was then possible to develop and test a 2D hydrodynamic model (Chapter 0), while the 1D hydrodynamic model used in the study was developed in collaboration with international collaborator Huy Hoang (Chapter 0). Taking advantage of the 1-m resolution, spatially explicit 2D model results, it was possible to make new scientific advances in characterizing the fluvial geomorphology of a mountain river at multiple spatial scales (Chapter 0). Geomorphic analyses were then used to aid a thorough hydraulic analysis of 2D model results (Chapter 0) and hydraulic comparisons of 1D numerical modeling and transect-based sampling against 2D modeling (Chapter 0). Finally, drawing on both hydraulic and geomorphic results, a physical habitat analysis was performed using common methods for 2D model outputs, and hydraulic habitat comparisons of 1D numerical modeling and transect-based sampling against 2D modeling were made (Chapter 0). Finally, conclusions integrate project results and experiences with respect to methodological findings, scientific findings, and management findings (Chapter 0).

CHAPTER 2:
Background Information

2.1 Literature Review

2.1.1 Instream Flow Analysis Approaches

Habitat units in rivers, also known as physical habitat, are defined as zones with characteristic physical attributes where organisms perform ecological functions, defined as the ways in which organisms interact with each other and their environment (Knighton 1998; Marcot and Heyden 2001; Moyle and Check 2004). A considerable number of physical habitat characterization methodologies (i.e. more than 200 according to Tharme 2002) (Tharme 2003) have been developed in the context of in-stream flow requirements. Still, reviews of the methods identify additional research needed to improve the understanding of the fundamental associations between aquatic ecosystems and physical factors (Payne 2004). From the perspective of assessing freshwater ecosystem services, approaches that relate ecological functions and physical processes help evaluate how hydrologic processes contribute in the creation and maintenance of habitats required by in-stream organisms (Degroot et al. 2002; Moir and Pasternack 2008).

Escobar and Pasternack (2009) reviewed a sample of the most commonly used approaches for characterizing physical habitat from the perspective of their emphasis on some key parameters over others (Figure 4;

Table 1). Their review stressed that existing approaches may be useful to produce detailed characterizations of parameters representing one or two habitat functions; however, they do not incorporate key parameters of the omitted habitat functions and therefore lack the capacity to represent hydraulic, geomorphic and ecologic interactions of physical habitat (Maddock 1999; Clarke et al. 2003). Also, methods issuing detailed characterizations require detailed input data at small spatial scales, such as the hydraulic-unit (10^{-1}–10^{0} channel widths) and geomorphic-unit (10^{0}–10^{1} channel widths) scales, making applications at the larger reach scale (>10^{2} channel widths) less likely due to time constraints associated with data input requirements and computer model set up and subsequent model simulations (Maddock 1999; Kondolf 2000; Pasternack 2008a).

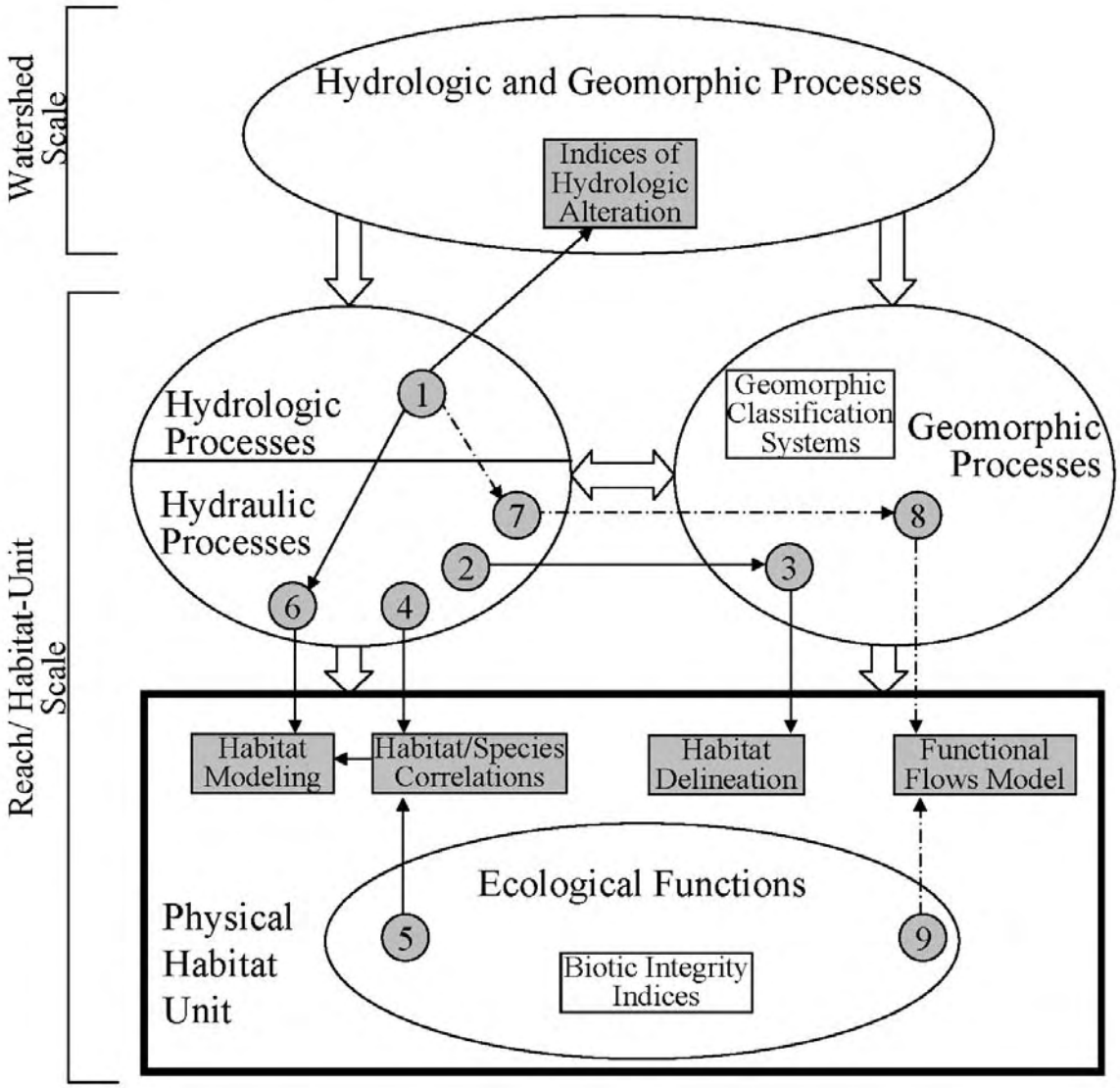

Figure 4. Different methods for assessing functions of physical habitat. Methods (grey boxes) use different ways to measure variables, or metrics, (grey circles) from a subset of hydrological, hydraulic, geomorphic and ecologic functions at the reach or habitat-unit scale. Other methods evaluating hydrologic or geomorphic functions (white boxes) may help infer ecological functions

without addressing them explicitly. The proposed new model based on 'functional flows' (grey box with dashed lines 8 and 9 leading to it) incorporates metrics from all functions. List of metrics: (1) Discharge, (2) Qualitative/quantitative hydraulics, (3) Qualitative/quantitative morphology, (4) Hydraulics measures (i.e. depth, velocity, grain size distribution), (5) Species response, (6) 1D/2D Hydraulic modeling, (7) Depth and slope time series, (8) Shear stress time series, (9) Ecological functions and their timing (from Escobar and Pasternack 2009).

Table 1. Examples of types of approaches for characterizing physical habitat (from Escobar and Pasternack 2009).

Approach	Process Considered			Spatial scale			Examples	Main characteristic
	Hydro	Geo	Eco	Habitat unit	Reach	Basin		
Biotic Integrity Indices	NO	NO	YES	X	XX	XX	Regional biotic integrity (Miller et al. 1988) Biotic integrity evaluation (Moyle and Randall, 1998)	Measures of species structure and function to monitor environmental changes
Geomorphic Classification Systems	NO	YES	NO	X	XX	XX	Rosgen classification (Rosgen, 1994) Channel morphology (Montgomery and Buffington, 1997) River Styles (Brierley and Fryirs, 2000)	Categorization framework to group morphological features
Indices of Hydrologic Alteration	YES	NO	NO			X	The Natural Flow Regime (Poff et al. 1997) IHA (Richter et al. 1996)	Statistical parameters of discharge to assess changes over time
Habitat Delineation	YES	YES	NO	X	XX		Reconnaissance survey (Thorne, 1998) Habitat mapping (Maddock, 1999)	Standard procedures to record geomorphic characteristics
Physical Habitat and Species Relations	YES	NO	YES	X	XX		Egg-to-smolt survival rates (McHugh et al. 2003) Fish guilds and hydraulics relations (Lamoroux and Cattaneo, 2006) Fish distribution from stream variables (Mugodo et al. 2006)	Statistical correlations of physical habitat parameters and biological measurements
Cross-sectional Habitat Modeling	YES	NO	YES	X	XX		PHABSIM (Bovee et al. 1998)	Analytical or 1D hydraulic modeling, cross sectional data, and habitat suitability curves to predict habitat availability
2D Habitat Modeling	YES	NO	YES	X			Numerical Habitat Model - NHM (Guay et al. 2000) FEWMS and GHSI (Pasternack et al. 2004) SHIRA (Weaton et al. 2004)	2D hydraulic modeling and topographic survey coupled to habitat suitability curves to predict habitat quality

Note: Approaches are grouped based on habitat processes and spatial scales considered. X indicates the scale at which it was developed, XX indicates other scales at which it has been applied.

2.1.2 VSP and Spatial Structure Concepts

The primary goal of all instream flow analysis approaches is to determine what is necessary to insure the viability of impacted species. With respect to anadromous salmonids, McElhany et al. (2000) developed the concept of the "Viable Salmonid Population" (VSP) to facilitate establishment of Evolutionarily Significant Unit (ESU)-level delisting goals and to assist in recovery planning by identifying key parameters related to population viability. As presented in Good et al. (2007), criteria for viable salmonid populations (VSP) are based on measures of population parameters that reasonably predict extinction risk and reflect processes important to populations: (1) abundance; (2) productivity; (3) diversity; and (4) spatial structure.

A population's spatial structure encompasses the geographic distribution of that population as well as the processes that generate or affect that distribution. A population's spatial structure depends fundamentally on habitat quality, spatial configuration, and dynamics as well as the dispersal characteristics of individuals in the population. Spatial structure is notable because it is relevant at all ecological scales, which are commonly defined as individual, population, species, and ecosystem scales. In the short term, demographic properties of a population

depend largely on the quality and quantity of habitat. In the longer term, genetic diversity, and the diversity of habitats that support genetic diversity, becomes increasingly important (McElhany et al. 2000; Kendall and Fox 2002; Williams and Reeves 2003).

Recently, the Lower Yuba Accord River Management Team (YARMT 2009) considered VSP for use at the scale of a single river, the 37.5-km lower Yuba River, rather than across a broader geographic region (Figure 5). In doing so, the YARMT developed specific performance indicators for spatial structure within a single river and articulated a suite of analytical steps (analytics) to address each performance indicator. At the highest level, the performance indicators may be summarized as follows:

- [Species X lifestage #] use most, but not all, of the available [lifestage #] microhabitat considered as being suitable at the 1-m^2 scale.
- Sufficient quality, number, size and distribution of mesohabitat patches, and migration corridors between mesohabitat patches, exist for [Species X lifestage #] to achieve its ecological function.
- Sufficient maintenance of watershed processes and regulatory management practices to create and maintain suitable habitat for all freshwater lifestages of relevant species.

For this last performance indicator in particular, specific sub-indicators were enumerated:

- The sequence of morphological units is non-random, indicating that the channel has been self-sustaining of sufficient duration to establish an ordered structure. Highly disturbed systems often degrade into homogeneity or randomness.
- Distribution of the diverse morphological units is within the range common to healthy gravel-bed rivers of comparable setting.
- Distribution of morphological units persists through time.
- Relief between riffles and pools persists through time.
- Microhabitat heterogeneity at the 0.1–1.0 channel-width spatial scale within morphological units is present and persistent through time.
- Flood flows occur every 5–10 years and are of sufficient magnitude to submerge the floodplain, drive channel migration and avulsion, and prevent willows from encroaching on the bankfull channel and constraining channel dynamics.

Although the focus of YARMT (2009) was on Pacific anadromous salmonids, the approach is transferrable to other species and their lifestages in other types of rivers. Within instream flow assessment, methods exist to characterize diverse microhabitat and mesohabitat species and life stages for almost any river. Also, there exist methods for evaluating fluvial and watershed processes relevant to aquatic and riparian ecology. The VSP-based assessment framework of YARMT (2009) is a new addition to the array of instream flow assessment approaches.

A notable aspect of YARMT (2009) is that it includes many state-of-the-art, high-resolution, geospatially explicit data collection and analysis methods of interest to this study. This study was proposed prior to the start of the drafting of YARMT (2009), but in fact, the Principle Investigator for this study was a co-author of YARMT (2009). Many of the goals articulated in

section 1.1 are also evident in YARMT (2009). Consequently, there has been a synergistic co-development of ideas and methods between activities for this study on the South Yuba River and those done by the YARMT on the mainstem lower Yuba River below Englebright Dam. This study has been completed ahead of the effort on the lower Yuba River, and will be used to inform those on-going activities.

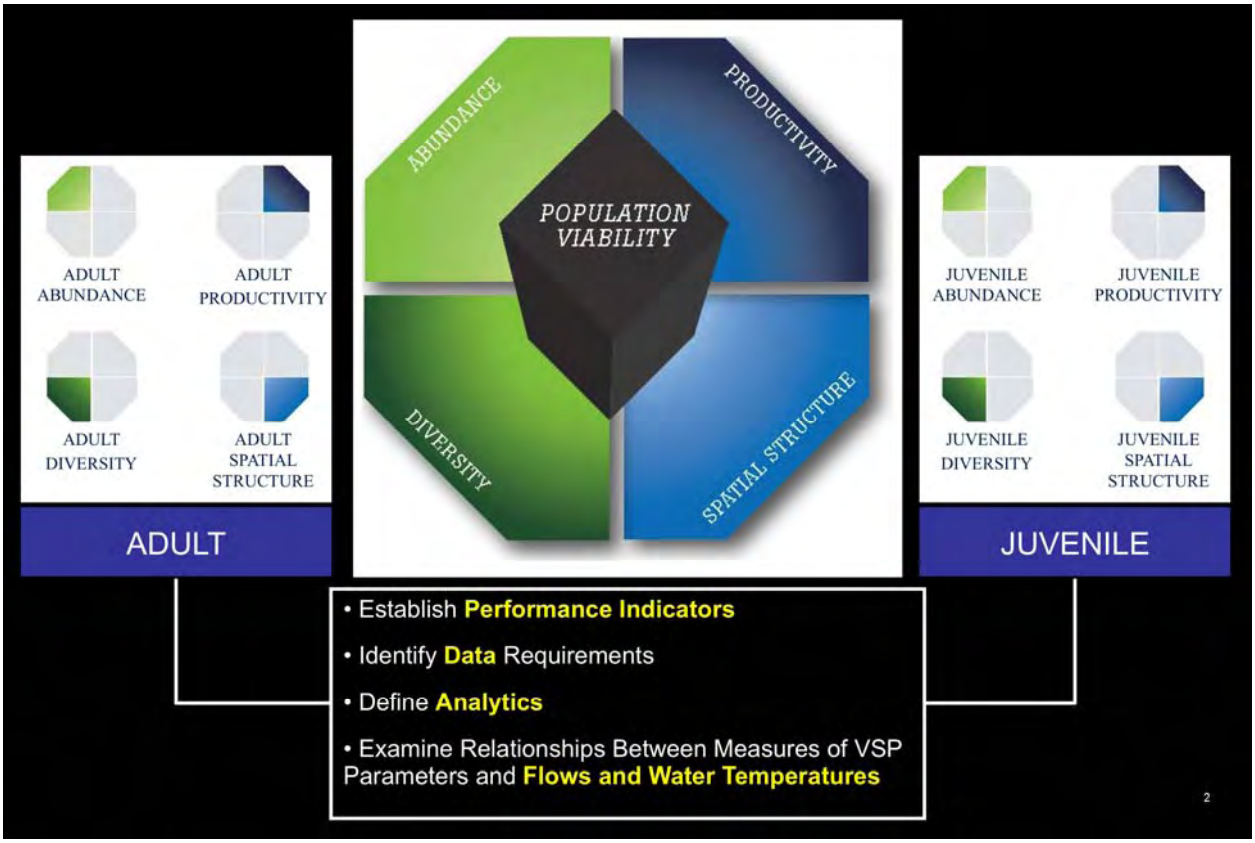

Figure 5. VSP framework adaptation for the lower Yuba River (YARMT 2009).

2.2 Study River Segment

As explained in detail in Chapter 0, a river segment is a section of river ~10^3-10^4 channel widths long that has characteristic attributes that are different from the river segments adjacent to it. It is the next scale up from the more commonly referenced scale of a reach. To achieve the purpose of this study, it was necessary to have a study area at the scale of a river segment.

2.2.1 Site Selection

The following selection criteria were established to pick a river segment to study, given in order of decreasing priority:

- Ability to conduct event-based monitoring (i.e. reasonable distance from UC Davis).
- ~50% of the stream length paralleled with road/trail access (4x4 truck or ATV).

- Enough management relevance to have biological field data.
- Presence of diverse morphological units, including waterfalls.
- Presence of one or more bridges to facilitate data collection.
- Nearby camping facilities for low-cost overnight stays.

The input of environmental consultants, hydro-facility staff, government regulators, non-governmental organizations, local landowners, and academics was obtained to help compare different possible study rivers. Scouting of several candidate rivers was done.

The selected study reach was on the South Yuba River between Lake Spaulding and the town of Washington, California (Figure 6, Figure 7). This reach met all of the criteria. The bottom of the study segment was within a two-hour drive for a UC Davis technician to respond to a high-flow monitoring event at a bridge over the river in Washington. Maybert Road ran along the north bank and had a good surface to the junction with Canyon Creek. Beyond that, Maybert was a more difficult path, but was open to a 4x4 truck along the entire length to the point where the bridge crossing back to the south side no longer exists. An ATV was necessary past that point and was available for use. Having Maybert along ~60% of the reach provided the opportunity for steady field data collection. Killer Fang Falls and Jolly Boy Falls were two relatively high waterfalls in the study segment that served as challenging tests of 2D model performance; several smaller steps 2-4 m high also helped test 2D model performance. In terms of existing information, the study segment was within the area under investigation for the Drum-Spaulding relicensing, so biological data were available. Also, there has been a huge amount of past research done in this river going back to Gilbert (1917), and continues in part due to the Upper Yuba River Studies Program, a component of the California Bay–Delta Authority Ecosystem Restoration Program. There were two local campgrounds near the study reach as well as several hospitable neighbors on the river who helped with equipment storage and river access. Integrated across all possible criteria, this study reach had tremendous value and high likelihood of success for demonstrating the next-generation instream flow assessment framework investigated herein.

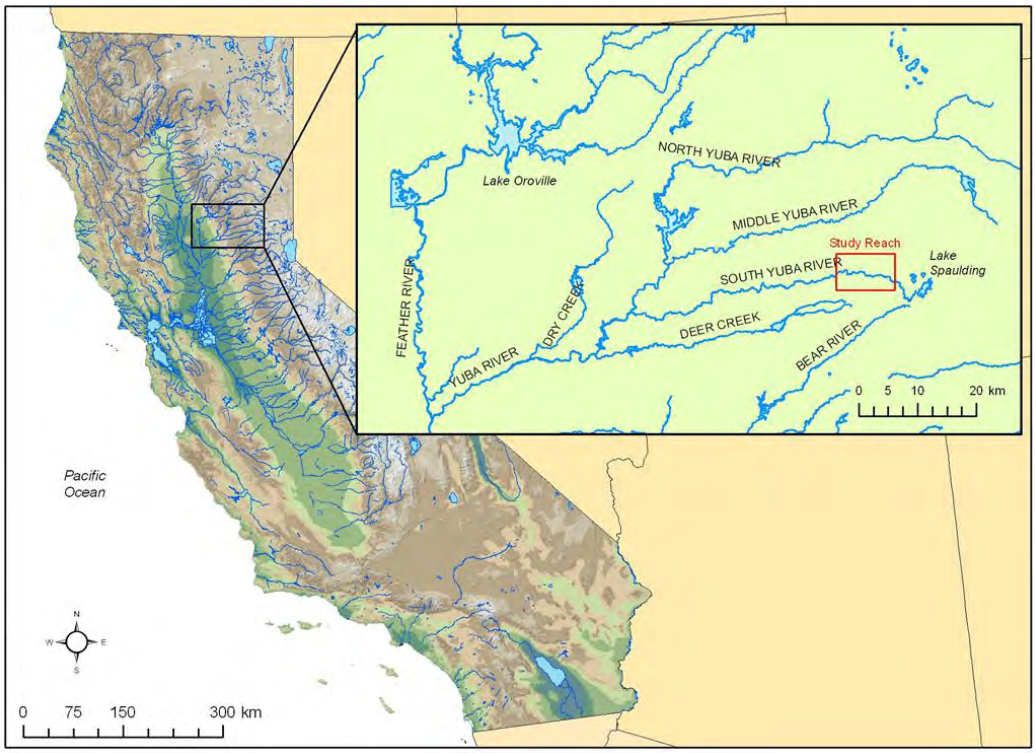

Figure 6. Map of California showing the region of the Yuba River and the location of the study.

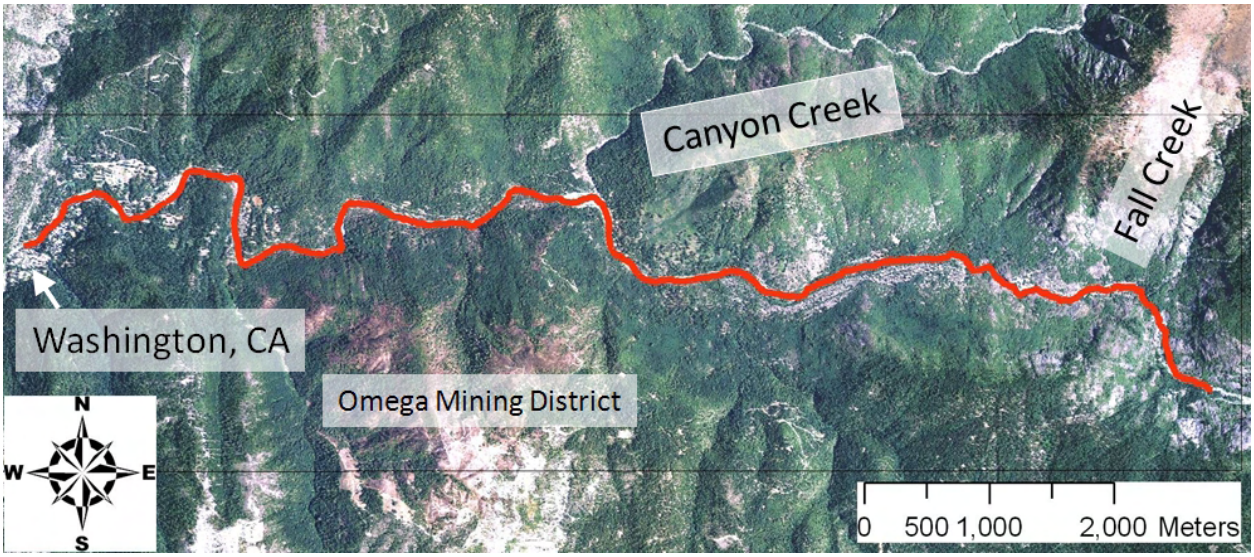

Figure 7. NAIP 2009 aerial photo of the 12.2-km long study segment (red polyline).

2.2.2 Upper South Yuba River

Watershed Characteristics

The South Yuba River watershed originates along the western slope of the Northern Sierra Nevada in California. The highest elevation in the watershed is English Mountain at 2552 m above mean sea level on the divide between the South and Middle Yuba Rivers. Bedrock geology is a combination of metamorphic sedimentary and volcanic rock, granitic batholith, and glacial till (Curtis et al 2005). The montane-Mediterranean climate is characterized by cool, wet winters and hot, dry summers (Storer et al 2004). Almost all precipitation occurs from October through April, with a temperature dependent snowline. Snow pack accumulates through the winter at high elevations. Heavy flooding can occur in the winter when weather systems driven by the Pacific Ocean El Nino Southern Oscillation produce warm rain-on-snow events. Spring runoff is dominated by snowmelt April-June as temperatures warm. Drought conditions prevail May-September with occasional convective thunderstorms at high elevations. Vegetation in the watershed includes chaparral, California black oak and live oak, ponderosa pine, sugar pine, white fir, red fir, and Lodgepole pine depending upon elevation, aspect, and topography (Barbour et al 2007).

Average annual precipitation at Lake Spaulding 1914-2003 was 173.88 cm (WRCC 2010), while the current 30-year average is 188.2 cm (NOAA 2010). Washington, California (39°21'38", 120°46'14" NAD27), the remaining gold-mining-era town in the area, is situated at the bottom of the study segment. Drainage area of the South Yuba watershed above Washington is 512.8 km^2. Tributaries within the study segment include Fall, Diamond, Canyon and Scotchman creeks, with Rucker and Jordan creeks discharging into the mainstem above the study segment but below Spaulding Dam. Spaulding Dam, ~20 km upstream of Washington and ~8 km upstream from the top of the study segment, captures 310.8 km^2 of the uppermost watershed, leaving a total of 202 km^2 of contributing watershed area to the study segment in addition to regulated releases and unregulated spills. Average daily flow releases out of Lake Spaulding gaged at Langs Crossing (USGS gage 11414250) 1965-2009 were 105 cfs, with a maximum of 24500 cfs (maximum gage capacity) and minimum 2.1 cfs. Outflow from the uppermost South Yuba catchment and accretionary flows from downstream tributaries resulted in 288.4 cfs average daily discharge at Washington gaged from 1943-1972 (USGS 11417000).

Gold Mining History

Gold was discovered in the North Fork American River watershed in 1848 at Sutter's Mill, and very quickly the California Gold Rush was underway. Miners established a camp in the upper South Yuba on the site of Washington, California in 1849 and began prospecting. Gold was found and within a year dams, flumes, and ditches were diverting water from the river channel so that bed sediments could be mined (Slyter and Slyter 1976). Mainstem channel mining returned sporadic findings, so the miners spread into local tributaries. Poormans Creek, located 1 km below Washington, yielded the largest amount of channel-bed gold in the area. Meanwhile, hydraulic mining was invented in 1853 just 20 miles away in nearby Nevada City, California. This technique used jets of highly pressurized water directed onto mountain topsoil to slough lower-grade gold-bearing paleo-sedimentary gravels from the mountain into gravity-separation sluice boxes. Two hydraulic mines within the study segment were Alpha and Omega Mines, located on mountain ridges along the south side of the river upstream of Washington (Figure 7, Figure 8). The exact upstream extent of hydraulic mining is uncertain, but mining

scars are evident on Google Earth imagery upstream of Diamond Creek. During the summer field campaign for this study, hydraulic mining equipment was found ~12 km upstream of Washington, California, which is well beyond Scotchman Creek. Major environmentally destructive consequence of hydraulic mining was that massive amounts of mountain top and hillslope sediments were flushed into the river and downstream, causing inundation and raising bed and floodplain elevations of lower reaches at such high rates that litigation eventually produced the Sawyer Decision of 1884, which banned the practice (PG&E 2010).

The Sawyer Decision did not stop all hydraulic mining along the South Yuba; the Omega Mining Company was found in contempt of the injunction in 1887. Debris dams were built throughout the greater Yuba watershed to capture these sediments near the source, including a debris dam built in 1895 on Scotchman Creek below Alpha and Omega Mines. The dam burst in 1896 and was rebuilt. It failed again, possibly dynamited, in 1905 and rebuilt again (Slyter and Slyter 1976). Today the dam is filled with sediment and supports a forested meadow on what used to be the reservoir surface. Licensed hard-rock mining continued in the upper watershed through the 1950's, and individual in-stream placer mining continued until suspended throughout the Sierras following a court order in summer 2009. River and hillslope topography and water diversions were not the only casualties of the early mining era. Massive amounts of energy were needed to power mining operations, which resulted in clear-cut logging throughout the upper South Yuba to supply the mines with steam energy and the working population with heating and cooking fuel (McKelvey and Johnston 1992).

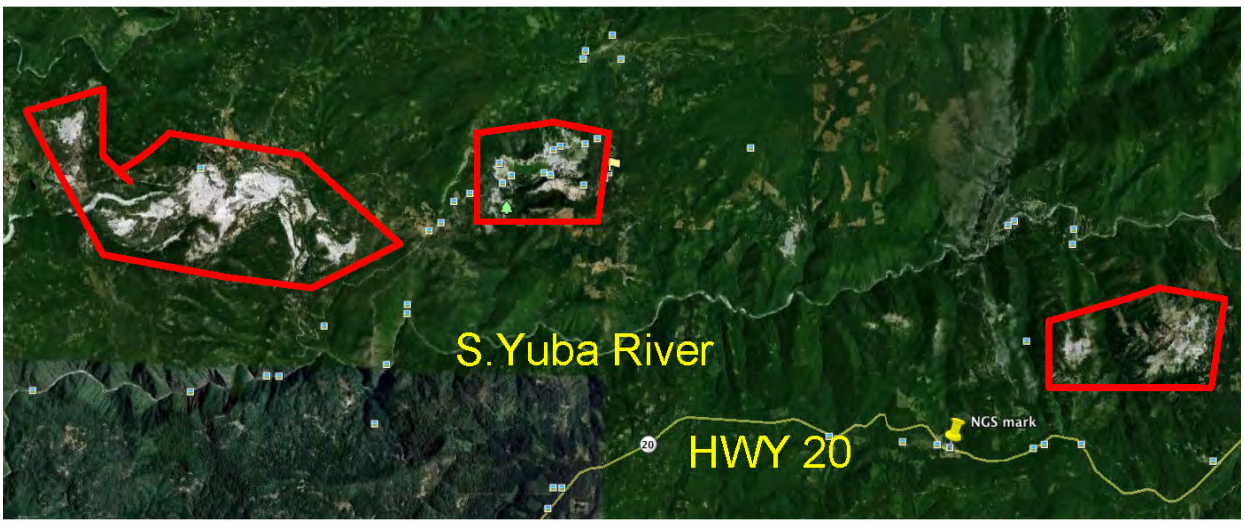

Figure 8. Google Earth image of the upper Yuba watershed showing three denuded areas caused by hydraulic mining. These areas exhibit badland erosion and have not recovered. Excessive sediment continues to enter the Yuba River from these locations. The red polygon in the lower right of the image is the Alpha and Omega Mining District.

Flow Regulation History

Significant alterations to the natural flow regime and channel configuration of the South Yuba began when gold was discovered. Earthen dams, wooden flumes and ditches were built to provide water for gold extraction. Hydraulic mining significantly increased the demand for

water. Entrepreneurs formed companies to provide water to miners. The South Yuba Canal Company emerged as a dominant water provider and by 1854 had built a 16-mile canal to send water from the South Yuba near current-day Lake Spaulding into the nearby Bear River watershed (Johnson 1997). By the 1870's the company had dammed numerous natural lakes in the high country, creating 20 storage reservoirs and providing water to mines and smaller canal companies through 450 miles of ditches. Canyon Creek subbasin, the largest tributary of the study segment, was highly regulated by 1873. Once hydraulic mining was banned in 1884, water conveyance companies sought other avenues with which to utilize water for profit, and began to provide water to farmers for irrigation and to towns for municipal and household use.

Meanwhile, efforts to develop an efficient water turbine to provide greater quantities of power to mining operations resulted in the invention of the Pelton Wheel water turbine in 1878- once again in Nevada City, California. By the late 1880's hydroelectric power generation became a serious goal for the mining companies. In 1896, a predecessor to the current-day Pacific Gas & Electric Company (PG&E) generated hydropower using water dammed and diverted from the South Yuba, and transmitted that electricity via copper wire six miles into Nevada City. Other hydroelectric projects were soon underway with the goal of transmitting power over much greater distances. After a series of mergers and acquisitions during a time of rapid expansion within the new industry, PG&E was incorporated in 1905 (PG&E 2010). Construction began on Spaulding Dam in 1913, PG&E's second major development. The upper South Yuba River above Spaulding Lake has been regulated since that date.

At a more local level, in 1921 Nevada County voters formed the Nevada Irrigation District in order to provide a steady supply of water to citizens, businesses, and farms in Nevada, Placer, and Yuba counties (NID 2005). Existing dams, storage reservoirs, and canals in the Canyon Creek subbasin became Nevada Irrigation District holdings. In the next three decades (1921–1951) improvements were made to dams, and more tunnels, flumes, and canals were built. In the 1950's, Nevada Irrigation District partnered with PG&E to develop the Yuba-Bear Hydroelectric Project, and in 1963, a 50-year license was granted to operate all facilities associated with the Yuba-Bear and Drum-Spaulding developments (Figure 9). Expansion, upgrades, and efficiencies occurred during the license period, such that 4 powerhouses, 35 dams and attendant storage units, canals and tunnels funnel water around the upper South Yuba watershed and into or out of Spaulding Dam (NID 2005). The north-side tributaries between Canyon Creek and Spaulding Lake—Fall, Rucker and Jordan creeks and their sub-basins—were regulated in the 1960's.

Nevada Irrigation District's holdings divert flow out of upper northwest South Yuba subbasins into Bowman Lake, Dam and Powerhouse facilities. The current license requires a minimum release of 5 cfs into Canyon Creek below Bowman. All other flows are diverted into the southeastern-running Bowman-Spaulding Conduit, which also captures most of the discharge from Fall, Rucker and Jordan creeks. Texas Creek, a Canyon Creek tributary, is also diverted into Spaulding Lake via the conduit. These diversions power a second hydropower plant as water enters the western side of Spaulding Lake. In addition, Spaulding Lake captures all other upper South Yuba tributaries including the upper mainstem along the southeastern boundary of the watershed. Diversions from Spaulding Lake power two hydropower facilities directly below the lake, which are then conveyed into the neighboring Bear River watershed, where many more water and power machinations occur among powerhouses, reservoirs, tunnels, canals, and diversions. The licensed minimum 5 cfs discharge into the mainstem South Yuba

comes from the low-level outlet in the dam, along with some leakage that occurs. Dam outflows change as needed based on weather forecasts, operational rules, and inflows into Bowman and Spaulding Lakes. The license for the South Yuba hydropower facilities is up for renewal in 2013. Continuity of operations requires a complex application process to the Federal Energy Regulatory Commission (FERC), currently well underway (NID 2005).

Present-Day Flow Regulation Regime

The upper South Yuba River that exists today is a heavily regulated system (Figure 9, Figure 10). The study segment receives minimum releases from Spaulding Dam of 5 cfs, and from Bowman Dam the river receives minimum releases of 2 cfs November-March and 3 cfs from April-October. There is also water entering the river segment from three other types of sources: (1) the unregulated downstream portions of regulated subbasins on Canyon, Texas, Fall, Rucker, and Jordan creeks, (2) the unregulated subbasins of Diamond Creek, Scotchman Creek, and from unnamed ephemeral tributaries, and (3) unknown quantities of groundwater discharging into the river along its length through bedrock fractures and along the bedrock-soil interface. These three sources of water are termed "accretionary flows", which is defined as additional ungaged water input to the river segment. Estimating accretionary flows turned out to be an important additional prerequisite to conducting the instream flow analysis aided by 2D hydrodynamic modeling.

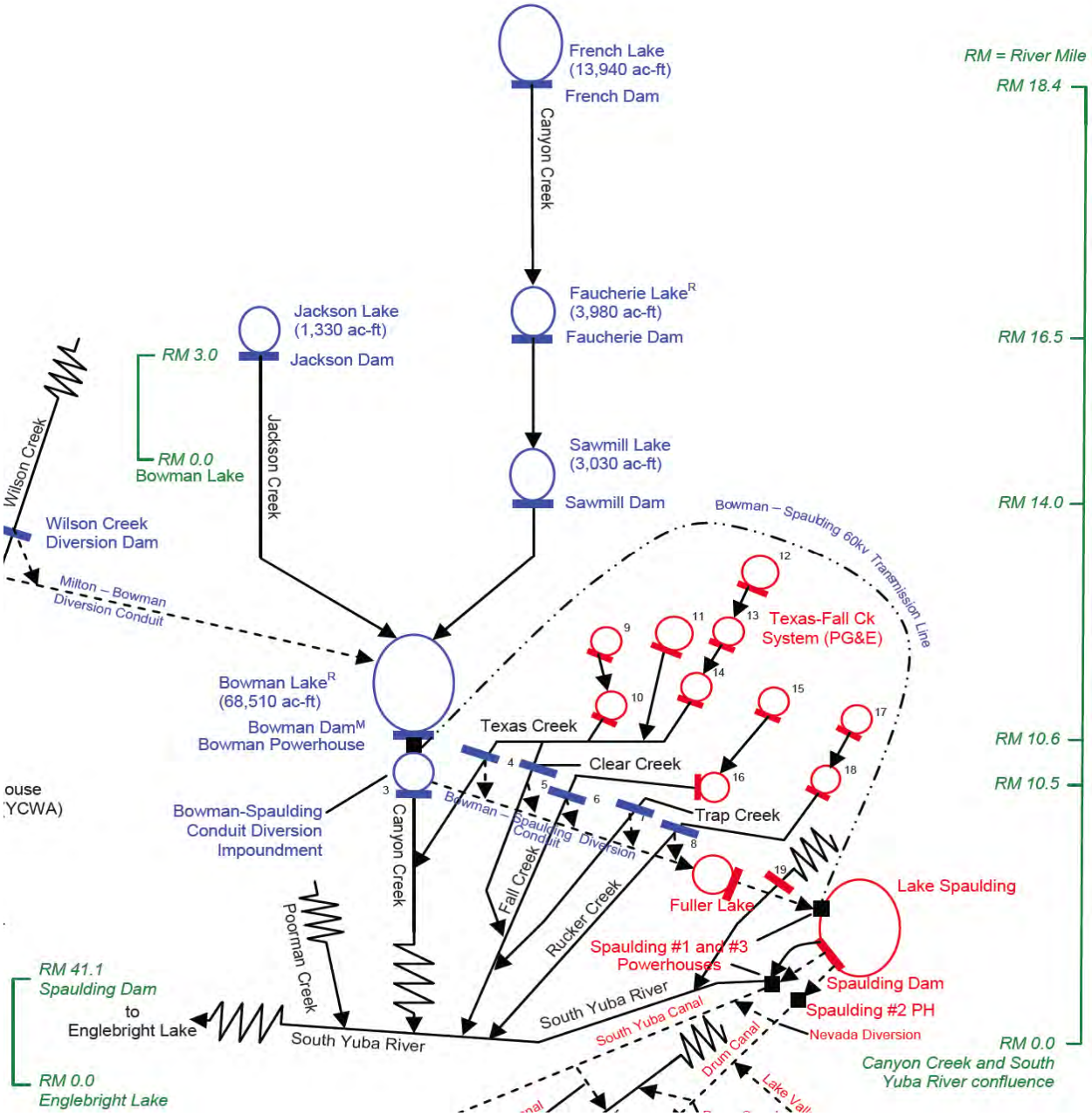

Figure 9. Schematic of Nevada Irrigation District operations (in blue) in the upper South Yuba River watershed (NID 2007).

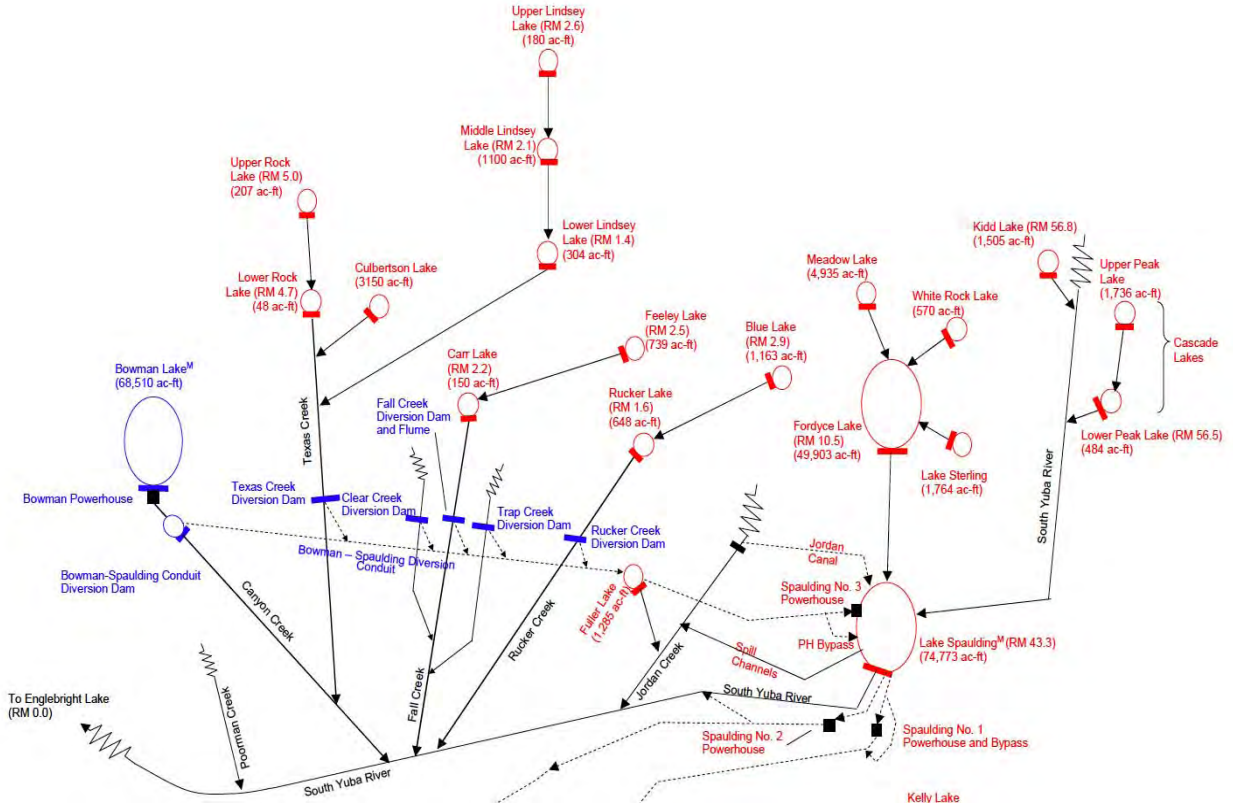

Figure 10. Schematic of PG&E operations (in red) in the upper South Yuba River watershed (PG&E 2007).

River Segment Characteristics

The lower boundary of the study segment was located in the town of Washington, California at the River Rest Campground. Topographic channel bed data were collected within the wetted channel for a total of 12.2 km in the upstream direction as measured along the valley centerline. Riverbed thalweg elevation ranged from ~780-1015 m above mean sea level. Notable tributaries entering the study segment were Fall, Diamond, Canyon, and Scotchman Creeks (Rucker and Jordan Creeks enter between Spaulding Dam and the upper end of the study segment). Seeps were observed throughout the segment during the 2009 field season.

The river corridor is confined by steep mountain hillslopes covered with second-growth coniferous forest. Cottonwood, willows, and alders were present in the riparian corridor. The most confined reaches of the river contained massive outcrops of bedrock blocks, which formed steep-sided canyons with deep pools. Less confined reaches varied in width, depending on valley floor constrictions and the presence of terraces. Bed materials ranged from sand to boulders >10 m in diameter. The combination of very high bed roughness and variation in width produced complex subcritical and supercritical flows.

Although flow regulation may affect some aspects of snowmelt recession, the timing and peak magnitude of floods, and summer low flows, floods, sediment transport, and channel change are normal events in the current regime. It remains difficult to determine how much of the bed

and floodplain sediment currently in the river corridor is mining debris versus natural sediment supply. In most regions of the Sierras, sediments derive from hard granitic rocks that have low sediment erodibility and modestly more erodible older metamorphic and sedimentary rocks. As a result, it is unusual to find such large quantities of coarse sediment in the study segment. There are two major historical drivers of current sedimentological conditions. A lot of alluvium derives from hydraulic mining, dredger mining, related activities, and the aftermath associated with cumulative anthropogenic impacts. Hydraulic mining sediments consisting of rocks ~0.5–2 m in diameter were littered along the study segment. The most material is downstream of Scotchman's Creek, which drained the Alpha and Omega Mines. The rocks had a distinctive look: fairly uniform in size, piled together along or near the channel banks, and sporting a greenish-gray patina of lichen or moss. Abandoned, rusty mining equipment was present along the banks and occasionally in the wetted channel throughout the study segment, including at the upstream boundary of the river segment, far upstream of Scotchman's Creek. Even in the absence of hydraulic mining, this river segment has an unusual geomorphic pre-existing basis for having a lot of coarse sediment. According to Professor Allen James of the University of South Carolina (who grew up in the region and has studied its physical geography for many years), Quaternary glaciations terminated in this area, so both glacial and sub-glacial meltwater processes were instrumental in sculpting the canyon and depositing large quantities of coarse sediment here (James, 1995).

2.3 Pre-existing Data Retrieval

2.3.1 Hydrological Data

The Drum-Spaulding relicensing stakeholders and contractors provided a plethora of hydrological information pertaining to regulated releases, diversions, and reservoir storage for upper South Yuba River operations. In addition, historical and current discharge data were obtained from United States Geological Survey (USGS 2010) internet archives (http://waterdata.usgs.gov/ca/nwis/).

The four professional streamflow gages relevant to the study site are

- South Yuba River at Langs Crossing (**SYLC**) 1.61 km (~1 mile) downstream of Spaulding Dam (USGS gage 11414250, 312 km^2).
- Canyon Creek below Bowman (**CCB**) (USGS gage 11416500, 73.3 km^2).
- South Yuba at Washington, California (**SYWA**) (discontinued USGS gage 11417000; 513 km^2).
- South Yuba at Jones Bar (**SYJB**) (USGS gage 11417500, 798 km^2).

Each of these gages has operated over different time periods, complicating hydrologic analysis. CCB has been in operation since January 5, 1927, and SYLC since December 1, 1965. SYWA was operated from April 1, 1942, to October 11, 1972. SYJB has operated since October 1, 1940.

As explained in Chapter 0, these data were used to investigate the role of accretionary flow coming from unregulated flow such as baseflow (perennial low flow), throughflow (discharge near the bottom of a hillslope but not directly into the channel), direct overland flow (runoff), and seepage (slow release of water through bedrock cracks) on a seasonal basis. That

investigation yielded a characterization of three seasonal flow regimes and equations for estimating tributary inflows into the 2D model of the study segment.

Precipitation data were obtained from NOAA http://www.cnrfc.noaa.gov/rainfall_data.php), the Western Regional Climate Center (http://www.wrcc.dri.edu/), and the California Data Exchange Center (http://cdec.water.ca.gov/).

2.3.2 Habitat Suitability Curve Data

Habitat suitability curves (HSC) are a representation of the univariate probability density function for a specific species and lifestage occurring along the gradient of the independent variable, with the range of frequencies of occurrence rescaled such that the peak of the distribution occurs at a value of one. For instance, there exist depth and velocity HSC for spawning rainbow trout, showing the distribution of suitability of specific depth and velocity values.

This study did not involve creation of habitat suitability curves or "bioverification" of existing curves (i.e. independent testing of the validity of HSC in the study segment) on the basis of any independently collected biological observations. Instead, this study involved assessing what happened when such curves were combined with different kinds of hydraulic estimation, simulation methods, and averaging approaches as well as what kinds of results and conclusions can be made when integrated with high-resolution imagery and 2D hydraulic modeling datasets representing geomorphic, hydrologic, hydraulic, and ecological processes.

PG&E and their consultants Devine Tarbell & Associates and Thomas R. Payne & Associates provided HSC for Sacramento Sucker (*Catostomus occidantalis*), Rainbow Trout (*Oncorhynchus mykiss*), and Pikeminnow/Hardhead (*Ptychocheilus grandis/Mylopharodon conocephalus*) fish species including fry, juvenile, adult, and spawning lifestages. These curves were used in the Drum-Spaulding relicensing process, and represent the most contemporary and relevant data for the system. They were applied with only common-sense scrutiny and no independent corroboration.

2.3.3 Pre-existing Base Map Imagery

The 2005 and 2009 National Agricultural Imagery Program (NAIP) 1-m resolution images of the upper South Yuba River were used as underlying red-green-blue color images for all GIS ArcMaps built for this study. NAIP images were available free of charge from the website: http://www.fsa.usda.gov/FSA/apfoapp?area=home&subject=prog&topic=nas

2.4 Project Constraints and Logistical Considerations

One of the concerns that commonly arises when there is a comparison of the potential costs and benefits of employing different methods for instream flow analysis is the practicality of doing a study based on a near-census of river conditions. That led to a desire to make this study as transparent as possible, including reporting on the difficulties involved in the work. Ultimately, it proved feasible for a team consisting of one principle investigator, one full-time technician, one three-month visiting scholar, and a group of part-time undergraduate students to complete the project. Consequently, a professional company with a team of experienced technical staff would likely achieve the same outcome quicker and better.

It was understood before the project began that a number of challenging issues could hinder the ability of the research team to maximize the potential for this study. There were many possible variables to observe and questions to test within the realm of relevance to the research. The study was conducted in a remote, mountainous region. Driving to the downstream boundary of the study segment took a minimum of two hours from Davis, California. The most efficient way to collect as much data as possible during the field campaign was to establish a base camp at the River Resort Campground in Washington, California. This location was conveniently located at the bottom boundary of the study. Forty-hour work weeks were completed over the period of four days and included travel time to and from the field site, initial set-up time at the base camp (tents remained up throughout the primary field campaign), travel time to the day's initial start location (which changed daily) and work time. Managing logistics was required every day, such as next-day planning and equipment maintenance. Camp keep-up and cooking were not considered working hours. Developing work and camp routines was very important, as was being mindful of personal and equipment safety issues, as all data collection was conducted within the wetted channel of a dynamic river. Personal flotation devices and kayaking helmets were worn for safety when appropriate.

Developing relationships with local landowners was important. The high water bankfull river corridor itself is the property of the State of California and therefore all individuals have the right to be within the river corridor. Nevertheless, in numerous cases the easiest access to the river was through riverside property. Much support was received in this area, though there were instances where individuals did not allow access to the river through their property and alternative egress points had to be used.

Working conditions were challenging. Total station surveying equipment, real-time kinematic (RTK) global positioning system (GPS) equipment, kite-blimp equipment, and echosounding equipment had to be carried to the banks, set-up, and deployed following specific protocols. Total station surveying challenges included finding appropriate locations to establish control points for best field of view. Every day required multiple survey set-ups because sight lines were short. Equipment breakdowns and malfunctions cut into data collection time occasionally.

The campground provided electricity to the campsite, so all equipment was charged nightly. Occasionally, equipment malfunctioned or was not properly charged, so that device could not be used the next day. Most of the equipment used rechargeable batteries, so extra batteries were generally available if other batteries ran out. Late in the field season, the base camp was moved upstream to the end of Maybert Road. Two 90 Amp-hour deep-cycle marine batteries and power inverters were used to recharge equipment. In turn, those were recharged back in Washington, California each weekend. The change in location cut down travel time to upper reaches by over one hour.

The biggest challenge for running the RTK-GPS was maintaining constant satellite linkage so that control points, surveying, and echosounding data could be collected. The steep mountain hillslopes and sheer bedrock canyons greatly reduced the skyview, which blocked the number of satellites available within the available sky-view for the system to link to. Only the United States Global Position System satellites were available during this study, whereas additional global navigation satellite system (GLONASS) satellites could be valuable in a mountain region for subsequent studies. Many hours were spent waiting for satellite coverage. RTK GPS connectively was a major challenge during echosounding data collection as was working in unwadable pools, which increased fatigue. Two crew-members positioned themselves on

opposite sides of a pool; often one side was a sheer bedrock wall with little available space for footing. The pontoon was maneuvered across the pool for as long as satellite connectivity was maintained.

Kite-blimp digital photography used helium to loft the blimp, so a helium tank had to be carried to the channel bank on the days when this procedure was scheduled. The blimp material was thin-sheet rubber, vulnerable to puncture. It was tethered to a crewmember by sturdy kite string and could be lofted and reeled in, but from the ground there was little control as to how the blimp reacted to wind conditions. It was quickly discovered that the best time of day to loft was early mornings when wind conditions were most stable and calm. Caution was also needed, as the possibilities of the blimp drifting into a nearby tree were constantly present.

The field team collected topographic data for ~900 m of channel length per week over a 15-week period of fully crewed, full-time work as well as an additional 6-8 weeks where the team leader and one assistant took periodic trips to infill data gaps. Considering data collected via survey total station, RTK-GPS, and echosounding equipment as well as airborne LIDAR (light detection and ranging) points and 2-3 cm resolution digital camera photographs of the entire study segment, there were a large number of data points to acquire, manage, perform quality assurance/quality checks on, and develop into coherent data files to be thoroughly analyzed.

Data analysis presented its own challenges. Producing final digital elevation and surface models took ~4 months due to careful calibration between LIDAR and ground-based datasets, removal of poor-quality points, and other data validation checks. Determining the best strategy to construct 2D models for this study then took another ~4 months of trial and error. Once built, 2D models took up to 14 days to run—the lower the flow, the longer the total computational time. The study segment was split into two approximately even sections to speed model runs. Analyzing the seasonal flow regimes led to a large series of runs, 42 in total. Once results were produced, upper and lower runs with the same discharge were combined to yield a total of 21 runs. Running all models took ~4 months with the existing limited computer capacity available at that time. In contrast, 1D models were run by our collaborator Huy Hoang and were done intermittently over a period of 2.5 months. Finally, analyzing the data to produce results and to develop and format tables, figures, and interpretations took another 5 months.

CHAPTER 3:
Data Collection

The primary data needs for this study included remote sensing imagery and all the components necessary for developing and testing 1D and 2D numerical hydraulic models of the study segment. Some of the needed imagery was available at no cost on the internet, as previously described in section 2.3.3. Newly acquired imagery during this study included high-resolution kite-blimp photos and LIDAR intensity data. No pre-existing data was suitable for use to prepare a 2D model, so an intensive field campaign was conducted to collect topographic, bathymetric, hydrologic, hydraulic, and substrate data. Additionally, streamwood data was collected opportunistically during the field campaign.

The initial field campaign involved four months (mid-June through mid-October 2009) of on-site labor to survey topography, map bathymetry, and collect kite-blimp imagery. A four-person field crew was used and consisted of a data collection team leader, a graduate student, and two undergraduate students. This team camped out in Washington, CA for several days at a time and did as much mapping as could be achieved over the course of ~30 hours of data collection each week. Once upstream of the end of Maybert Road, the rate of progress slowed due to the increased number of logistics associated with a remote field site. Ultimately, data were collected for 12.2 km of extremely rugged terrain under difficult surveying conditions. Before and after the summer field campaign, fieldwork was conducted opportunistically to obtain hydrologic and hydraulic data under diverse flow conditions.

For all data collection and geospatial analysis, work was performed natively in SI units (International System of Units; metric). The coordinate system used was California State Plane, Zone 2 (Meters) with the NAD 83 Datum for horizontal coordinates and the NAVD 88 Datum for vertical coordinates. Whenever data had to be collected in (or were available only in) a geographical coordinate system, it was transformed to the projected system with the Geoid 03 model. The area for which data were collected is shown in Figure 11. Available time limited the upstream extent of the project.

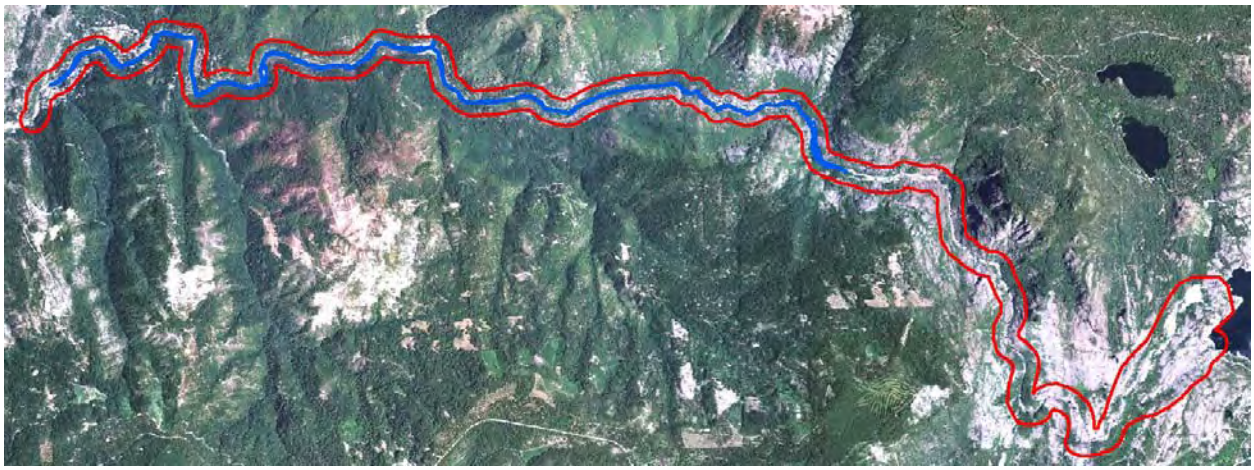

Figure 11. Study area extents for LIDAR (red) and ground-based (blue) surveys.

3.1 Kite-Blimp Imagery Data Collection

Obtaining high-resolution aerial imagery of the South Yuba River study segment was a primary objective of the study designed to enable diverse geomorphic and ecological analyses. The approach involved lofting an ~3'x6' (oblong ellipsoid) tethered Helikite helium kite-blimp (Figure 12) with an attached 14.7 megapixel Canon Powershot SD990 Image Stabilizer digital camera. This type of kite-blimp will handle only a light load and is height limited by string weight and weather conditions. Deployment occurred June through November 2009 during low flow with very low turbidity to allow digital image capture of channel features. Kite-blimp altitude varied between 70 and 110 m to obtain images that encompassed the entire channel width (i.e. the wider the channel the higher the altitude). Images that spanned the channel width were easier to georeference in ArcGIS. The camera had the capability of being locked into a "continuous shooting" mode that took pictures automatically every ~1–10 seconds, depending on flash and memory settings. Photos were later examined to pick the best ones to georeference in ArcGIS. Resolution varied with blimp altitude, but was in the range of 25–45 mm (Figure 13). With the presence of any ambient wind, minimal control of roll, pitch, and heading was possible, so early morning low-wind conditions were best for kite-blimp usage. Without a perfectly horizontal platform, the resulting oblique photos were somewhat distorted. Camera lens distortions were also present and not corrected for later.

Procedurally, the kite-blimp was first prepped for flight according to a standard protocol. The kite-blimp was carried in a tarp-sleeve for protection. Kite-blimp, helium, and accessories toolbox were brought to the loft location. The kite-blimp was arranged for inflation, and the flexible but sturdy framework that stabilized the unit was properly aligned. The kite-blimp was secured to a crewmember, and then filled with helium. Next, the camera was set to the ambient light and focal length conditions by taking a photo manually to check for brightness and focus. The camera was mounted onto the kite-blimp and continuous shooting initiated. Then the kite-blimp was lofted to the desired altitude and positioned over the river by boating, wading, or swimming into the channel with the tether attached with a quick release mechanism to a field-crew member. The kite-blimp was carried up or down the river until the batteries ran out, which was evident by the discontinuation of flash bursts. The kite-blimp was reeled in and the data disk retrieved from the camera. Finally, the images were saved to a netbook computer and examined for visual quality on-site. On occasion a group of photos were washed out due to brightness, in which case the reach was reshot another day. This procedure was repeated intermittently over several weeks until the entire study segment was imaged.

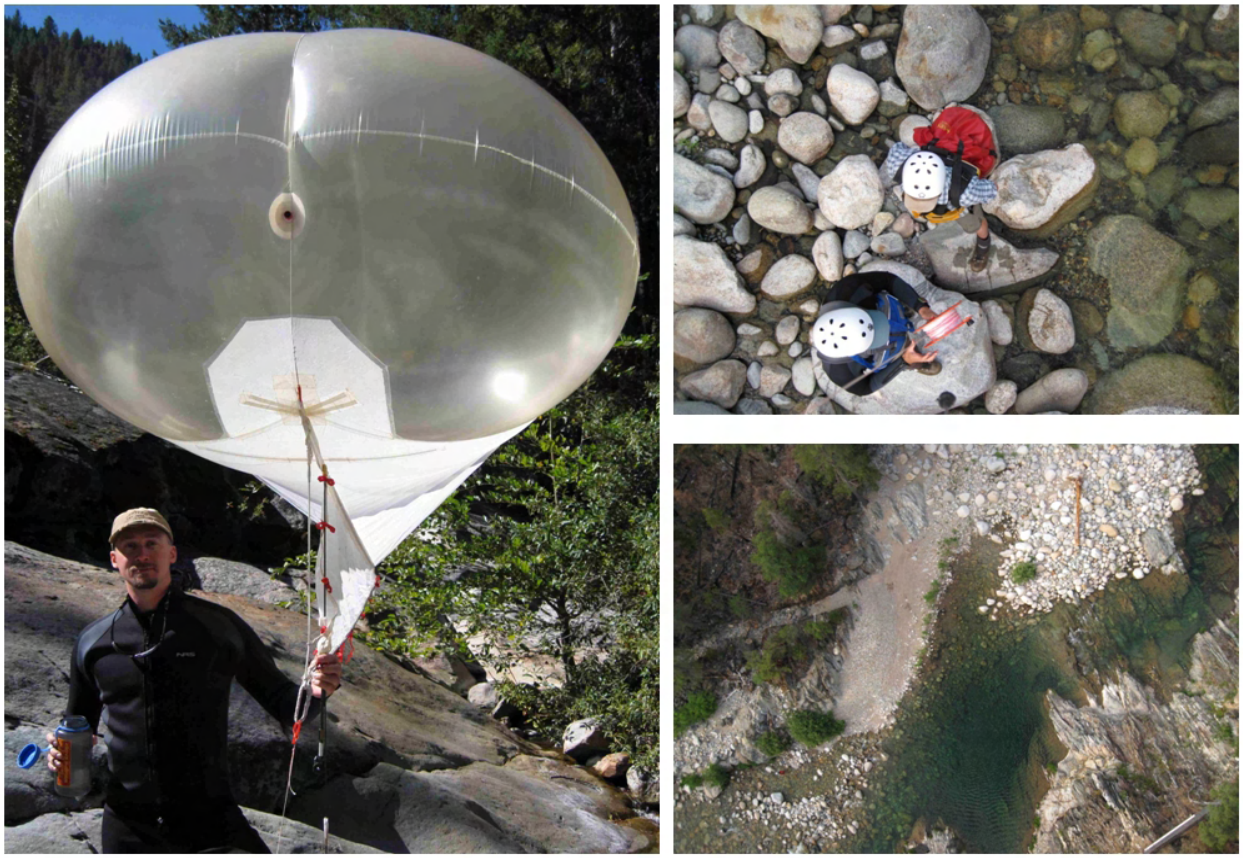

Figure 12. Aerial kite-blimp digital photography system. Left, inflated blimp, camera (not shown) attaches to screw mechanism at bottom of rod (below hand in photo). Right, top, blimp has been lofted with continuous shooting enabled; photos early in a series show blimp ascent. Right, bottom, typical photo chosen for georectification, altitude 70–110 m.

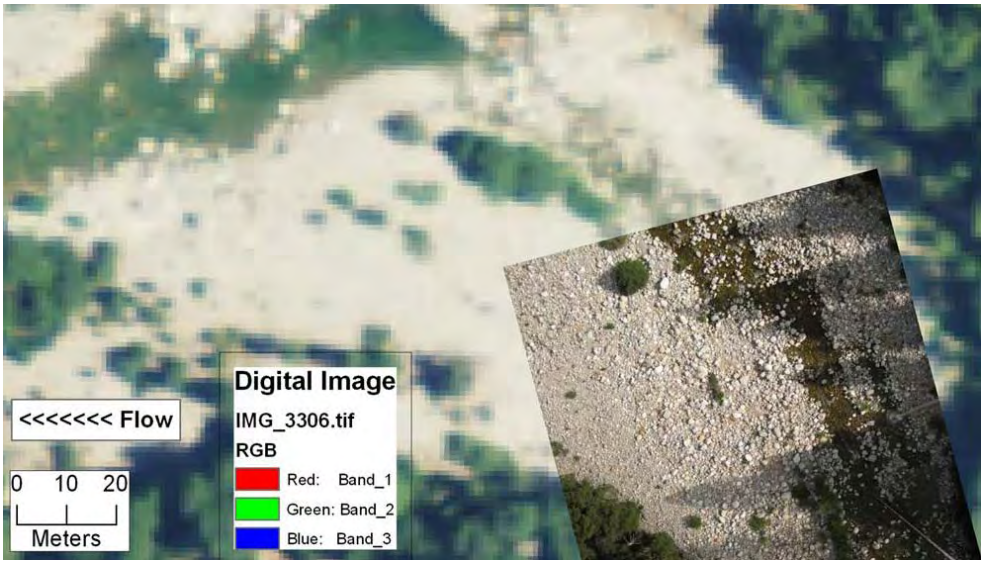

Figure 13. Visual comparison of 2009 imagery from 1-m NAIP versus cm-scale kite-blimp camera. Blimp photo shows area 100 m upstream of Canyon Creek confluence.

3.2 LIDAR Data Collection

Airplane-based Light Detection and Ranging (LIDAR) technology offers one of the most expedient and cost-effective ways to capture reasonably accurate, wide-area terrestrial ground elevation, water surface elevation, and canopy top elevation data. By merging laser ranging, RTK-GPS positioning, and inertial attitude technologies, airborne laser mapping directly measures the shape of the earth's surface beneath the aircraft's flight path. Elevation data are generated at the rate of thousands of points per second flying at an altitude of ~900 m, with each individual point representing the average elevation over an area of ~0.3x0.3 m^2 (~1 ft^2). Spatial resolution depends on the number of passes, and effort is necessary to insure consistency between flight lines through proper calibration. While many laser points will hit a tree-canopy (when present), others pass through holes between the foliage and reach the ground. The strength of the return signal varies with the absorptive ability of the surface; for instance tree and water surfaces return weaker signals than ground surfaces. All returns are registered by time-to-return and a digital dataset is created simultaneously. Most data sets include *first returns* that bounce off of canopy without hitting the ground and thus have a slightly faster return than any other returns, and *last returns*, which are classified by signal-strength identification and return time as ground points. The product received for this study was a dataset with an average of 1 point every 0.74 m (1 pt per ~2.5 ft) and a vertical accuracy of ~0.15 m.

The LIDAR survey generated several different types of data. First returns were used in a standard procedure to obtain a canopy height raster. Ground returns (including those on emergent boulders within the wetted channel) were used along with field-obtained survey data to create the topographic map of the river corridor. A subset of carefully selected and quality-checked water surface returns was used along with ground-based observations to characterize the water surface elevation for the summer baseflow level. Finally, the LIDAR survey yielded the intensity of the LIDAR return signal at each point, and this was converted into a GIS raster grey-scale image of the river corridor, which served as another base image for GIS analyses. This type of LIDAR image can be used to construct a polygon shapefile of the water's edge, since the intensity of LIDAR returns from water were dramatically lower than from land. However, with so many emergent boulders in the study segment and extremely shallow flows during field data collection, it was not used to construct the water surface edge in this study.

The LIDAR vendor was Airborne 1 Corporation (El Segundo, California). To tie the data set into the same geographic position system (GPS) datum as the study, LIDAR data was collected using the same National Geodetic Survey (NGS) benchmark as was used by the field crew for the ground-based survey, as well as an additional NGS benchmark suitable for their flight plan. The date of LIDAR mapping was timed for baseflow discharge in collaboration with local hydro-facility staff at Spaulding Dam. LIDAR data was acquired over the period of 1–2 hours one morning during July 15–18, 2009 (Figure 14). During that period, the discharge at Langs Crossing averaged 9.4 cfs, except for a brief late-night release that did not impact LIDAR data collection, because no night flights were made. Canyon Creek below Bowman Lake releases average 4.5 cfs over the same timeframe. The LIDAR coverage area spanned 20 river-valley kilometers from Spaulding Dam to an endpoint downstream of Washington, California.

Airborne 1 performed quality assurance and quality checks (QA/QC) on their data by comparing LIDAR topographic observations against RTK GPS topographic observations on the

same flat stable surface, which happened to be Highways 20 and 80 along the ridgeline of the watershed. In addition, a UC Davis technician made a comprehensive QA/QC comparison of LIDAR data and field-surveyed topographic data wherever the two methods yielded points within a horizontal distance of 5-cm of each other. Additional QA/QC was conducted for sloped and rough surfaces to constrain uncertainty in how LIDAR may perform in the natural, complex setting of a bedrock-boulder-cobble river corridor.

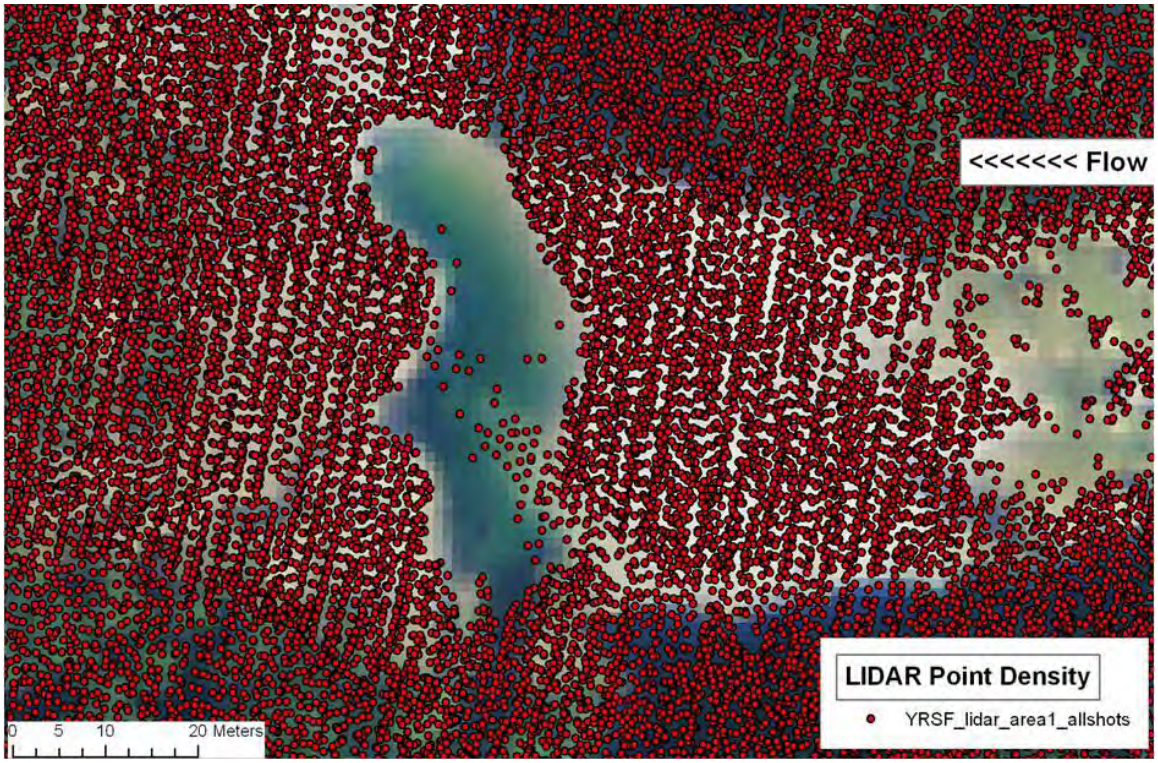

Figure 14. Example of raw LIDAR data collected showing few returns in deep pools, but many returns in shallow waters that contain many emergent boulders.

3.3 Topographic Data Collection

A topographic map is a representation of the elevation pattern of a land surface. Because topography is one of the most fundamental variables controlling ecosystem processes on Earth, it is essential to have a good topographic map to understand the landscape. Topographic maps are particularly important for river science, because landform configuration directs the speed and direction of water flow and sediment transport. In turn, flow and sediment help define instream habitat conditions, and are major drivers of landform change over time. Repeated topographic mapping can be used to characterize how rivers change through time. Both habitat conditions and channel dynamics are important considerations in river management, particularly in regulated rivers that are actively managed for multiple needs and interests. Two common management activities, instream flow assessment and river rehabilitation, that occur on regulated rivers would be greatly aided by detailed topographic maps.

Methods for topographic data collection have progressed rapidly in the last decade, so that now highly detailed datasets may be obtained at relatively low-cost. The preferred remote methods for topographic data collection recommended in this study are airborne LIDAR mapping of the terrestrial river corridor and boat- or platform-based echosounding of the submerged river channel. Where those are ineffective (e.g. shallow, wadable submerged areas, submerged areas with excessive bubbles, and terrestrial forests with inadequate canopy openings), a combination of Real-Time Kinematic Global Positioning System (RTK-GPS) and total station surveys are recommended. The LIDAR and echosounding methods are capable of obtaining very high densities of data, because sampling at a native rate higher than 1 point per second (1 Hz). The RTK GPS and total station surveys collect data at a user-specified interval that is much less frequent.

The ground-based RTK-GPS and total station topographic survey of the study segment was performed during typical minimum discharges under the regulated flow regime (mid-June through October 2009) and was conducted in all wadable areas within the wetted channel. The South Yuba study segment was primarily boulder-cobble bedded with a surface roughness spanning four orders of magnitude (10^{-2}–10^{2} m). Ground-based mapping to resolve every grain-scale feature within the wetted channel was infeasible. In the absence of LIDAR capable of collecting underwater topographic data or hydrographic surveys, data are often collected on a 1-m grid in gravel-bed rivers (Brasington et al. 2000), but no such standard has been set for boulder-cobble streams. Valle and Pasternack (2006) reported that a point density of 1–10 points per m^2 might be preferable for bedrock-boulder rivers in order to capture the high rate of variability across geomorphic, hydraulic and ecological spectrums. In this study, remote methods collected data at a higher resolution than 1 point per meter. It proved effective to isolate and use LIDAR observations of emergent boulders in wadable areas, so it was not necessary to map those in the ground-based effort. Given that only the wetted channel bed in shallow wadable areas (excluding emergent boulders) needed to be mapped, a compromise point density of 1 point every 5 m on an approximate grid was used (Figure 15). In addition, points were collected along the wadable thalweg at ~1-m spacing. This insured that the survey captured the deepest areas throughout the study segment, even in shallow wadable areas. Finally, water edges were mapped for each total station setup to collect the water surface elevation at summer baseflow throughout the study segment.

Topographic surveying was conducted using three survey instruments: a Leica TPS1200 Robotic total station, a Topcon GTS-603 total station, and a Trimble R7 RTK-GPS unit. Because of its automation and speed, the majority of the topographic survey was performed using the Leica total station (Figure 16). The survey was performed using standard surveying procedures used in similar geomorphic and ecohydraulic studies (Pasternack et al. 2004, 2006; Sawyer et al. 2010), except for the point sampling scheme. The survey was collected over such a large elevation range that it was crucial to use scale factors (to constrain the distortion across the projected coordinate system) when surveying in the projected coordinate system. These were obtained for several locations in the study segment using the CORPSCON v.6 freeware geographical coordinate conversion software program.

An initial network of control points was established using the RTK-GPS linked with an on-site base station located on NGS benchmark (KS2040) on Highway 20, ~9 km uphill from Washington, California by road, but within 5 linear km of the river at the bottom of the study segment (Figure 17, Figure 18). At each initial survey location, two control points were located

in proximity to serve as a station point and backsight point for total station surveys. To traverse between less frequent RTK-GPS control points, a second set of temporary control points was established using the total station and the bedrock locations marked with small hammer-drill holes and/or whiteout. The total station surveys were performed using a standard backsight setup on a control point. The back sight accuracy was checked before and after each survey setup was used. The vertical and horizontal accuracies of the total station surveys (Leica and Topcon), as determined by back sight check, were 1.0 cm and 3.5 cm, respectively. The horizontal and vertical accuracies of checks on the RTK-GPS survey were 1.5 and 2.6 cm, respectively. During surveys, observers progress as fast as can be achieved safely, so an additional error of 0.5–5 cm horizontal and 0.5–2 cm vertical can occur by not holding the survey pole exactly vertical. Overall, there is a very high confidence that individual point measurements were within the 0.15-m vertical accuracy required by the U.S Army Corps of Engineers' rigorous Class 1 standard.

After QA/QC checks, the resulting ground-based total station and RTK-GPS data set included 23,282 channel bed points, 4,039 thalweg points, and 781 water's edge points that provided both bed and water surface elevations.

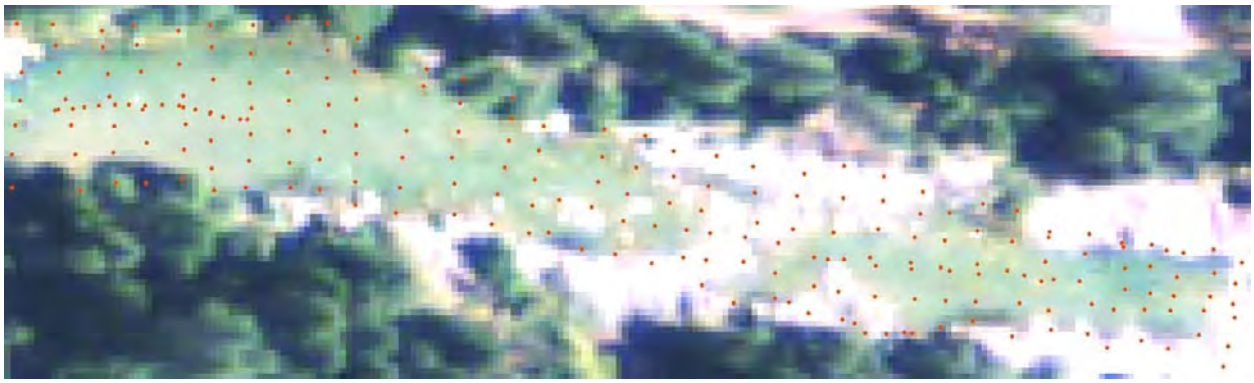

Figure 15. Example of ground-based topographic points collected on a ~5-m grid. Notice the thalweg points collected on a 1-m interval on the left side of the photo.

Figure 16. Leica robotic total station used to survey the majority of the wadable riverbed.

Figure 17. Trimble R7 RTK GPS base station supporting bathymetric and topographic surveying.

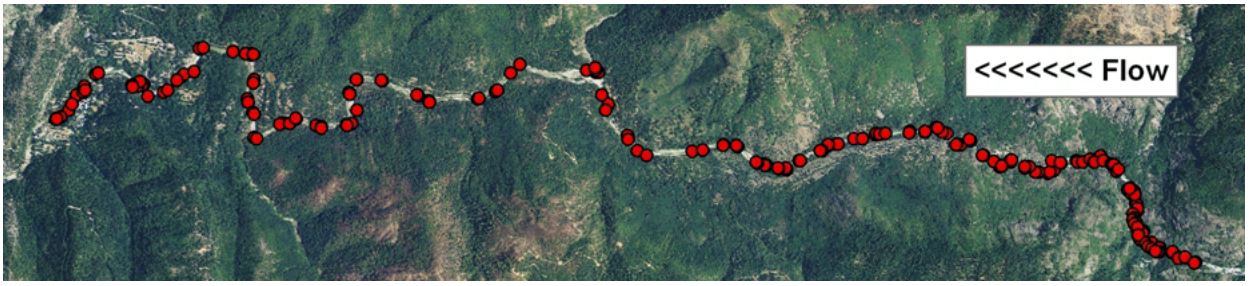

Figure 18. Distribution of surveying benchmarks established by the research team in the study segment.

3.4 Bathymetric Data Collection

Bathymetric data was collected for unwadable areas (pools and chutes primarily) mid-June through November 2009 during the lowest flows of the year using a pontoon-mounted echosounding system designed to be lightweight enough to carry from site to site in the river, while still being stable enough to function in currents of up to 5 m/s (Figure 19). A spool of nylon rock climbing webbing was held on either side of the pontoon to enable surveyors to maneuver it in deep areas, even holding firm position in fast, rough current. It was also possible to swim it around in slow currents. Unwadable cross-section data were collected every ~5 m on the longitudinal profile with additional points along either side of the wetted channel and in lines down the channel (Figure 20). The pattern was less precise than wading, because it depended on the ability to maneuver the pontoon. No thalweg was discernible in pools with slow-moving water, so no effort was made to survey such a feature.

The echosounder was an Ohmex Sonarmite with a depth range of 0.3–75 m and an accuracy of within 2.5 cm RMS (root mean squared). The sensor's parameter for speed of sound was set based on the observed range of water temperatures during the field campaign. The echosounder was periodically checked for accuracy. Echosounder output was transmitted to the Trimble R7 RTK-GPS where position, depth, bed elevation, and water surface elevation were recorded every 5 seconds. Position data were obtained from the RTK-GPS, which was receiving corrections by radio from the base station located on a pre-established benchmark (Figure 17). A total of 8,440 bathymetric observations were collected. The average horizontal and vertical accuracies for the bathymetry survey were 1.8 and 3.0 cm, respectively.

Figure 19. Bathymetric surveying system used to map unwadable areas. Left, echosounder being prepared for use; pontoon was built using common hardware supplies. Right, echosounder pulled across a pool. Team moved up or downstream ~5 m for the next traverse with echosounder in continual collection mode.

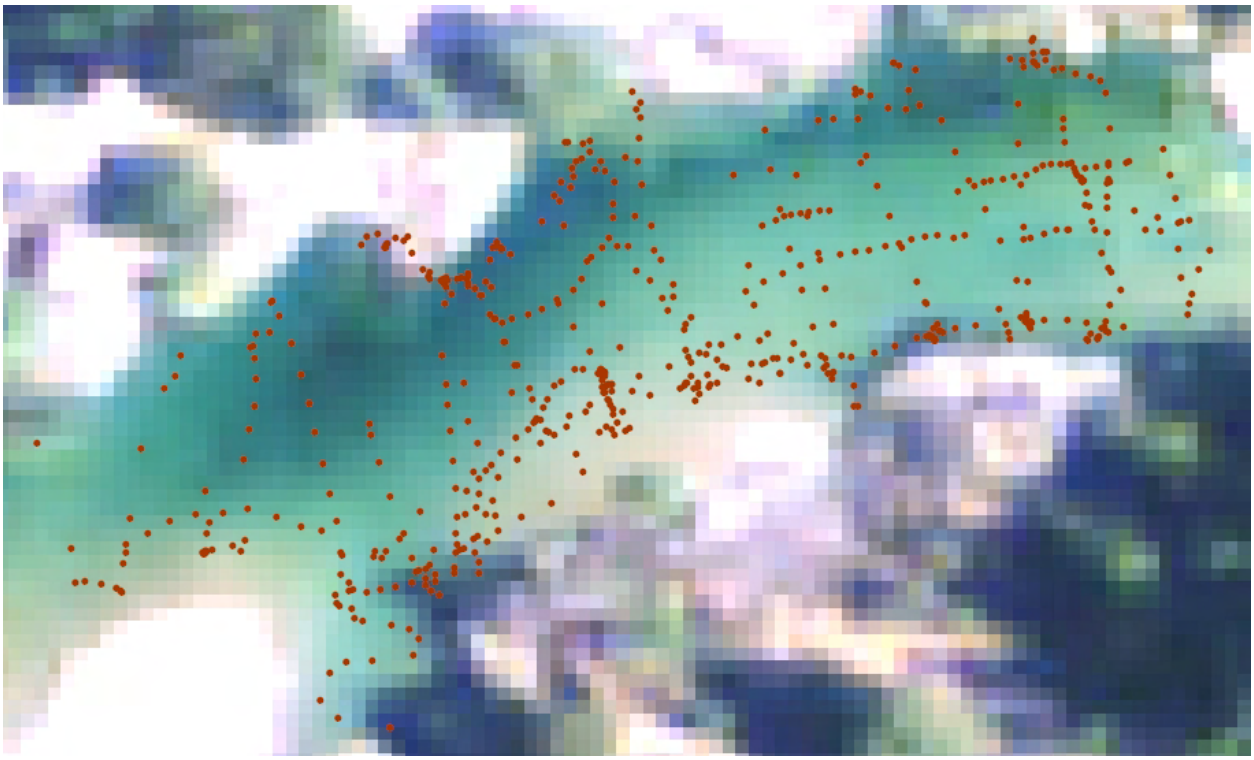

Figure 20. The pattern of echosounder points collected in a single pool in the study segment. In the NAIP image, white areas are bedrock cliffs, the elongated green area is the pool, and mixed white/gray/green areas are vegetated or partially vegetated hillslopes. The underlying 1-m resolution 2009 NAIP image has ~3-5 m georeferencing accuracy, so some points falsely appear to be out of the water.

3.5 Discharge Measurement

The primary sources of pre-existing hydrologic data for this study were the discharge records for Langs Crossing below Spaulding Lake on the upper South Yuba River (SYLC), the discontinued record on the upper South Yuba River at Washington, CA (SYWA), and Canyon Creek below Bowman Lake (CCB). The USGS provided final QA/QC'd daily flow records at these stations, excluding data from the current water year, which is still undergoing checks. When needed to facilitate fieldwork, real-time flow rates at the gages were obtained graphically from http://www.dreamflows.com. This source did not provide tabulated data, but PG&E and the Nevada Irrigation District provided preliminary 15-minute flow data tables for the 2009 and 2010 water years.

To assess the current condition of flow accretion in the study segment and to measure discharge on the date of velocity observations for 2D model validation, direct measurements of discharge were made at suitable cross-sections with an acoustic Doppler current profiler (ADCP). Wading-based discharge estimation using a current meter, top-setting wading rod, and the velocity-area method was not done, due to the lack of suitable cross-sections meeting standard requirements (i.e. average width and depth, relatively flat bed with little vegetation, few boulders, and no eddy currents; see Chapter 8.0, Geomorphic Analyses for detailed analysis and discussion of channel characteristics).

The sensor was a Sontek River Mini-ADCP Surveyor (Figure 21). This instrument has a 20-cm blanking region in the downward vertical direction from where it sits in the water and 15-cm vertical cells below that point. The bottommost 15-cm vertical cell is usually discarded from analysis (more if the bed is extremely rough, as it was in this study). The distance from each bank and bank slopes were also recorded and input into the software. For the surficial, bed, and lateral blanked areas of the cross-section, River Surveyor software extrapolated observed values to obtain a best estimate of discharge for the full geometric channel dimensions. Given the data gaps in the vertical profile, it was preferable to use the sensor in deep enough water to minimize the amount of extrapolated discharge. With a depth of 2 m, the region of estimated discharge was ~18% of total depth, so it was preferably to use it in at least that depth of flow. That limited suitable locations to the morphological units defined later as pool and transition (section 8.3). ADCP measurement cross-sections were further constrained to those with flows as parallel to the banks as possible and those not in meander bends. Site accessibility by truck and navigability by the kayaker were other factors that limited direct measurements of discharge.

ADCP discharge measurements were made at three locations: (1) on Canyon Creek in the pool at the Maybert Road bridge to evaluate flow accretion in the Canyon Creek sub-basin, (2) on the South Yuba in a pool just downstream of the confluence with Canyon Creek, (3) and on the South Yuba at the River Rest campground in different spots, depending on river stage. The sensor, its accessories, and a netbook computer were mounted onto an Equinox kayak (model 124) suitable for discharge measurement in a small river setting. At the start of discharge measurement for each cross-section, the magnetic declination was set, the depth sensor's atmospheric pressure was zeroed, and the water temperature was entered. Six to ten discharge measurements were made at each cross-section and measurements meeting quality criteria were then averaged to obtain the final discharge estimate. For each discharge measurement, the standard procedure recommended by the manufacturer was used to collect data. The kayak was

held in a facing-upstream, parallel to flow position and paddled across the river at the slowest possible speed, ideally a fraction of the ambient water velocity.

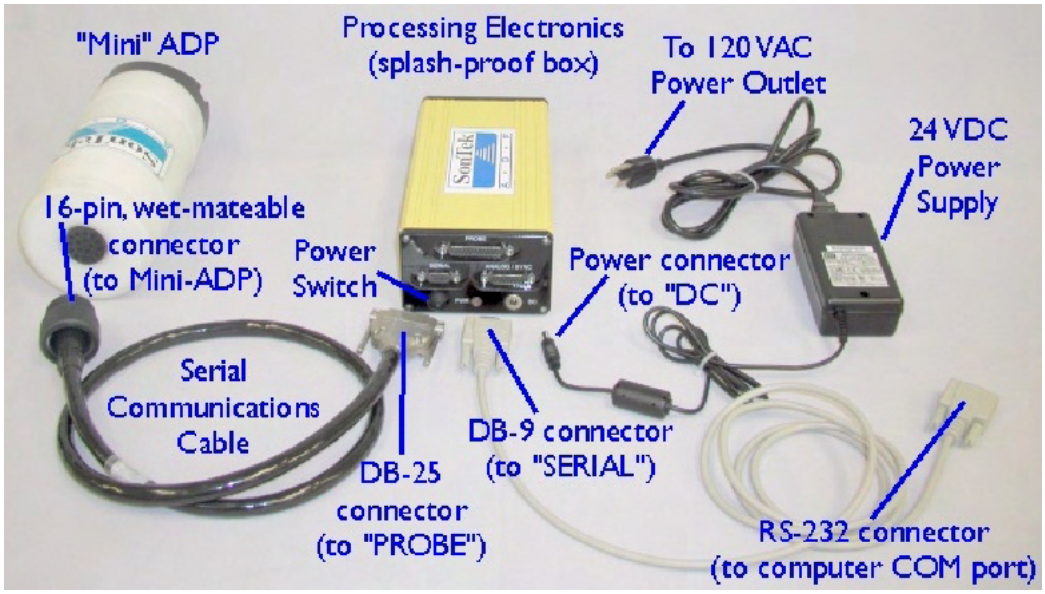

Figure 21. Components and connections for the Sontek Mini-ADCP River Surveyor System

3.6 Water Surface Elevation (WSE) Data Collection

The purpose of collecting WSE data was to validate WSE output from the 2D hydraulic model. Validation may be done by comparing either WSE or depth, and since it was faster and more accurate to measure WSE, that was the approach used in this study. WSEs for the summer baseflow level were mapped using data from LIDAR returns (28,012 points), ground-based surveys (782 points), and bathymetric surveys (8,440 points). The LIDAR WSE returns were carefully culled in GIS to remove the most uncertain points, including those on land, on emergent boulders, returns with very low intensities, and in such shallow water that the points might be bed elevations rather than WSE. However, these WSE data only captured a single flow condition, summer low flow. It was also necessary to collect WSE data for as many other flow conditions as possible to validate the 2D hydraulic model. Whenever hydraulic data was collected, WSE was also collected.

The Leica TPS 1200 total station had a red-light reflectorless capability that enabled distal collection of topographic measurements for a distance up to 300 m. This feature was used to observe the water surface elevation at the water's edge on the far bank within view of each set up on numerous occasions when flow was at different levels, including each of the highest observed discharges in spring 2009, winter 2010, and spring 2010. The procedure involved sighting the crosshair on the mean position of the water's surface up against a rock on the water's edge at the upstream limit of view and recording position. The crosshair was moved downstream along the edge and shots were taken for several suitable natural reflectors at the water line until the downstream limit of view was reached.

3.7 Stage Gaging Station at Washington, California

2D modeling required knowledge of the WSE at the downstream end of the model domain to match the total discharge passing that point, which is known as the stage-discharge relation. A stage-discharge relation is specific to the shape of the cross-section, so it has to be updated after every physical change to the dimensions of the river that impact stage at the gaging station. Such changes are normally caused by floods, but they can also be caused by in-channel gold dredging and other manmade disturbances. As a result, the pre-1972 stage-discharge relation for the SYWA gage was of no use. No other stage-discharge data were available.

Based on evaluations of access, study goals, and site conditions, the stage gaging station was located just upstream of the River Rest Resort on a bedrock outcrop located on the left bank on private property with permission of the land owner (Figure 22). River Rest provided electricity for hammer-drilling into the bedrock to install the "superstrut" that held the piping firm to the bedrock wall.

Water surface elevation at the end of the study segment was monitored at 15-minute intervals with an automated station. Two different sensors were used over time. The sensor used in 2009 was a Global Water Instrumentation, Inc. WL15 vented (i.e. atmospherically corrected) pressure transducer with a 4.572 m (15') range and an accuracy of 4.572 cm (1%) over the temperature range of the site. The sensor used in 2010 was an In-Situ, Inc. Level Troll 500 vented pressure transducer with a 3.5 m range and accuracy of 3.5 mm (0.1%) over the temperature range present at the site. The accuracy of each sensor was confirmed locally prior to installation by putting the sensor into different water depths in a swimming pool. On-site, camouflage-painted PVC plastic pipe was secured to a steep bedrock face with a "superstrut" pipe clamp system bolted into the rock face in two places (Figure 22). Under the water the sensor was shielded from velocity-induced pressure using additional piping that baffled the flow without hindering equilibration of water levels. The sensors recorded water depth and these were corrected to water surface elevation on the basis of an independent topographic measurement of the water surface elevation at the start of data collection for each sensor.

The stage gaging station was established on May 13, 2009, and began recording at 5:15 pm. In 2009 snowmelt happened quickly and by May 13 gaged flow (SYLC+CCB) was 1055 cfs (some years, flows remain high through June). The station was operated until June 16, 2009, at 9:15 am at which point the gaged flow was down to 25 cfs and a decision was made to remove it for lack of further utility during the low-flow period and vandalism risk. As a result, the automated gaging station for 2009 captured flows ranging in gaged discharge from 25–1055 cfs.

This range was substantially increased by manual WSE measurements made with the Leica total station (section 3.6). The WSE of the baseflow condition was measured several times in July 2009. By coincidence, the very first two days of data collection for this study, May 4–5, 2009, were the days on which peak snowmelt discharge occurred, which turned out to be the highest discharges in the 2009 and 2010 water years. At the time of WSE measurement on May 4, the combined gaged flow was 1184 cfs. The peak passed overnight and at the time of next measurement on May 5, the combined gaged flow was 7086 cfs. Capturing this one value on the second day of the project expanded the range of 2D modeling possible by a factor of six!

The approach taken to create a stage-discharge rating curve was to inspect the timing of WSE shifts in the stage record relative to discharge shifts in the SYLC and CCB records to determine

the lag time between a discharge value upstream and the occurrence of the corresponding stage downstream. Lag time depends on flow velocity and thus is discharge-dependent. The best estimate for both SYLC and CCB records was four hours. To build the rating curve, the following steps were taken:

- Made a scatter plot between WSE recorded at Washington, California and the total gaged discharge (SYLC+CCB) shifted by four hours into the future.
- Identified slope breaks in the WSE-to-discharge relation to stratify the data into subsets for fitting simpler and more accurate regression equations.
- Performed discharge-stratified regression analysis to obtain the synthetic stage-discharge relation for use in the 2D modeling study.

The 2009 rating curve provided the data required for the 2D modeling study, but another rating curve was constructed in 2010. The purpose of repeating the effort was to see how different the relation would be under a different hydroclimatological condition (i.e. different years bring different precipitation cycles, snowpack, and snowmelt conditions). Even when stage data is regressed against the discharge measured at the same location, there can be annual variations caused by a wide range of hydrological phenomena that cause "hysteresis"- a difference in stage-discharge curves on the rising limb versus the falling limb of a hydrograph (Park 1992). In this study, local discharge was not used, but rather gaged discharge far upstream. Since local stage responds to local discharge, which in turn responds to both gaged flows and flow accretion, then it is expected that each year there would be substantially different rating curves associated with the strong temporal variability in hydroclimatology. Consequently, making a stage-discharge rating curve toward the end of the study after 2 D models have already been run served the purpose of illustrating such variability.

For a 2D model of a lowland river (i.e. not mountainous), uncertainty in the local stage-discharge relation might cause catastrophic impacts on hydraulic prediction due to "tailwater" effects. Specifying a downstream WSE that is too high when channel slope is low may cause simulations to back-flood long stretches of river upstream. Specifying a downstream WSE that is too low in a lowland setting causes 2D simulations to accelerate flows excessively downstream.

In an extremely steep mountain river, the effect of specifying the downstream WSE as too low or too high has minimal consequences. In the case of the study segment on the South Yuba River, the downstream terminus of the 2D model occurs 57 m downstream of a step in the bed in a reach controlled by an inset channel (Figure 23) (see morphological unit definitions in section 8.3). Therefore, specifying a wrong WSE only propagates up to the bottom of this hydraulic control and has no effect upstream of it, because the step itself is the control for what occurs upstream. The crest of the step at the top of the channel slope acts like a submerged weir backing water up into the transition and pool units upstream of it. At high flow when the step is washed out, flows are transcritical to supercritical, which again serves as a barrier for upstream influence of downstream WSE effects (Figure 23).

In summary, the stage-discharge relation observed for 2009 between local WSE at the end of the study segment and the combined gaged flow upstream was used to drive the 2D hydraulic model used in this study. Although the uncertainty associated with flow accretion analysis

created uncertainty in the local stage-discharge relation at the end of the study site, the river was so steep that uncertainty in WSE at the end of the model had no effect on predicted hydraulics for the whole river, except for the final 57 m, which ends at the first hydraulic control upstream of the end of the model.

Figure 22. Stage gaging station established in Washington, California upstream of River Rest Resort.

Figure 23. The first bed-step hydraulic control 57 m upstream of the gaging station. Errors in downstream water surface elevation do not propagate past this feature. Flow shown is 1055 cfs. Photo taken on river left near the stage gage shown in Figure 22.

3.8 Velocity Data Collection

The purpose of collecting water velocity data was to validate velocity output from the 2D hydraulic model. Because the study segment consisted of reaches with cobble/boulder and bedrock channels, most of the assumptions associated with standard velocity measurement methods (which are oriented toward discharge estimation) are violated. In this study, new methods were developed for the setting. These efforts were complementary to a similar on-going study for the gravel/cobble bedded lower Yuba River in collaboration with the Yuba Accord River Management Team. The outcome was two new data collection methods for wadable and unwadable conditions that provided a foundation for 2D model testing and validation during this study.

3.8.1 Velocity Sampling Constraints

Traditionally, water velocity observation in a river with complex flow patterns would be made using a point-based velocity sensor, such as a Price AA current meter or a Marsh McBirney electromagnetic current meter. Observations are often made along cross-sections, but can also be done at any location for which velocity is desirable to know (e.g. Pasternack et al. 2004; Pasternack et al. 2006a; Sawyer et al. 2010). When estimating mean column velocity, observations are made at an elevation 0.4*depth up from the bed (0.6*depth from the water's surface) or an average is taken of observations made at elevations of 0.2*depth and 0.8*depth up from the bed. These positions are obtained using a top-setting wading rod. For 2D model validation of velocity (not stream discharge gaging), the sensor should be oriented in the direction of the velocity vector, not perpendicular to the cross-section.

This standard approach was ***not*** used in this study. First, given a 2D model spanning 12.2 km, there is no feasible number of ground-based observations that can be made to fully validate that scale of spatial pattern using traditional methods. Second, the river was too shallow or the flow too complex (bubbles, standing waves, tortuous paths) for boat-based ADCP measurement in the majority of morphologic units. At higher flows where a boat and ADCP system might be viable, the flow was too dangerous to be utilized. Third, there were so many emergent boulders present in wadable areas that collecting multiple cross-sectional profiles of velocity was impractical. Discharge measurement in wadable areas using the velocity-area method at wadable flows was thus not done. Generally, the only place where cross-sections were possible was in a straight pool exit (transition morphologic unit), but submerged large boulders disrupted flow in these units as well. Fourth, with such a complex pattern of bed roughness and range of subcritical to supercritical flows, the notion that there exists a persistent, unchanging log-velocity profile was visibly erroneous for most locations. These challenges required the researchers to explore other equally valid approaches that might replace wadable velocity data collection.

3.8.2 Velocity Spatial Sampling Strategy

For 2D model testing in this study, it was decided that the most useful purpose of performing point-based velocity measurement was to check the ability of the model to accurately predict velocity over the range present in the river over all flows, regardless of any information about local conditions at the point of observation. Such a test would involve making a direct scatter plot of the observed versus predicted variable, which is an effective validation approach for any hydrologic or hydraulic model. Such a test provides quantitative information on a model's ability to correctly predict the lowest velocities in the slowest areas, the mid velocities in mid-speed areas, and the highest velocities in the fastest areas.

To achieve a high-quality scatter plot test, the purpose of velocity data collection during this study was to collect data across the widest possible range of speeds and to obtain a uniform distribution of velocities in support of an evenly distributed scatter plot. In terms of an experimental design to collect this data, no *a priori* knowledge of the spatial pattern of velocity was available to create a sampling scheme in advance of data collection. The data were collected before the models were run to eliminate the possibility of any bias. Also, if a uniform or random statistical sampling scheme were made in GIS prior to data collection, it would be problematic in the field, because it would be highly unlikely to achieve a uniform distribution of velocity measurements across the range of velocities present on any given day. Such sampling schemes could be biased toward low velocities, as the spatial extent of low velocity is much higher than that of high velocity.

The range of near-surface velocities was 0–2.5 m/s in the study segment, so when collecting data by wading (section 3.8.4), locations were sought out to yield ~1–3 measurements per day within ~0.2 m/s bins divided evenly within the velocity range. For boat-based data collection (section 3.8.5), it was less feasible to control what velocity ranges were being sampled. Since the only criteria for locating wading measurements was that of achieving reasonable sampling of each velocity bin, there was no need for a statistical sampling design. Since the goal was to collect the full range of velocities with an adequate number of samples, any location was equally as good as any other, as long as the full range of velocities was measured (Figure 24). Therefore, the focus of sampling was to target locations with needed velocities and as the dataset grew, to focus on obtaining data to fill in the gaps of the less represented speeds.

Blending the data from the two different measurement methods (wadable and boat-based) yielded a final statistical distribution of surface velocities samples with more samples in the 0–1.2 m/s range and fewer in the 1.2–2.4 m/s range (Figure 25). The absolute area of safely accessible locations with higher velocities was smaller than lower velocity, safer areas, so it took more effort to locate and sample the higher velocities, yielding fewer total samples. At high flows, areas with surface velocities >2.4 m/s were present, but could not be sampled safely. Achieving a sampled range of 0–2.4 m/s was a successful outcome of the velocity sampling campaign.

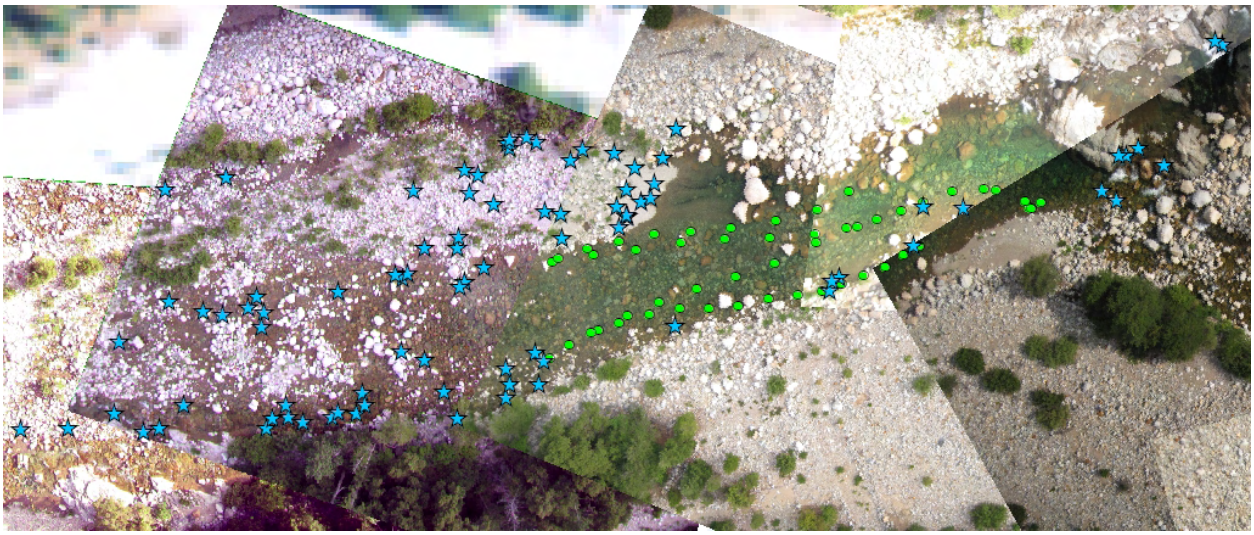

Figure 24. The reach just below the Canyon Creek confluence was used for velocity observations by wading (blue stars) and by kayak (green circles), because it had easy access, good surveying sight lines, and several morphological units present in close proximity. Note that digital images were acquired at lowest flows, while velocity points were collected at higher flows, so observations that appear to be on dry surfaces were not so at time of sampling.

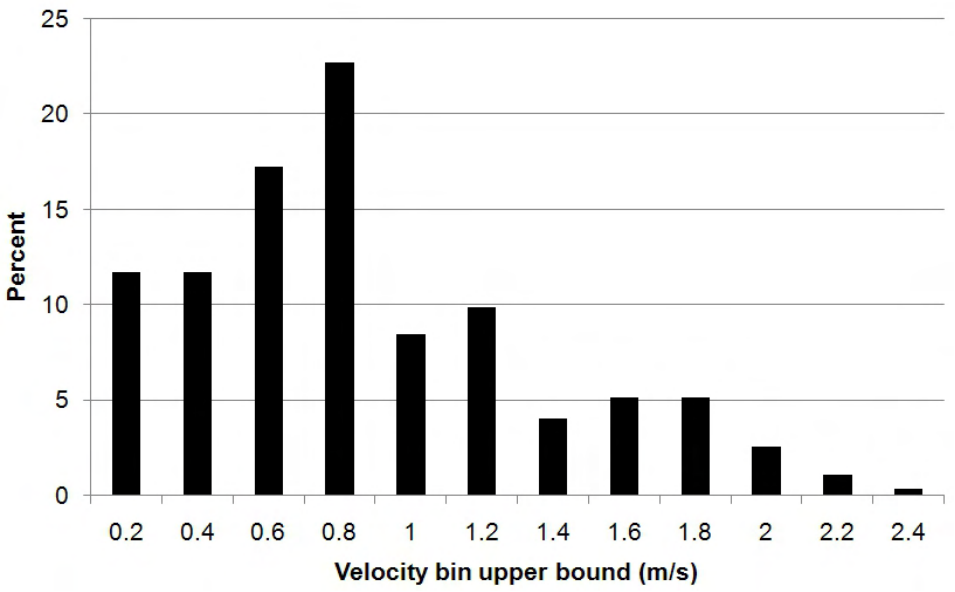

Figure 25. Histogram of surface velocities sampled in the data collection campaign.

3.8.3 Near-Surface Velocity Measurement

Because estimation of mean velocity was difficult to measure in the field, the researchers decided to measure near-surface velocity instead, and to rely on the strong correlation between surface and mean column velocity to compare observations with 2D model predictions. It is well known that mean column velocity is ~0.7–0.8 times near-surface velocity. For example, Pasternack et al. (2006) collected full vertical velocity profiles over an artificially constructed gravel bed in a river and found that the slope of the least squared regression equation between the observed mean column velocity and observed near-surface velocity was 0.71, with a sample size of 23 and a coefficient of determination (r^2) of 0.672 (Figure 26). Although the magnitude of the slope coefficient may change with different depth:bed material ratios, the existence of this fundamental relation is persistent and reliable. An advantage of making a velocity measurement near the water's surface is that it is fast, enabling a greater quantity of points to be measured per unit of effort.

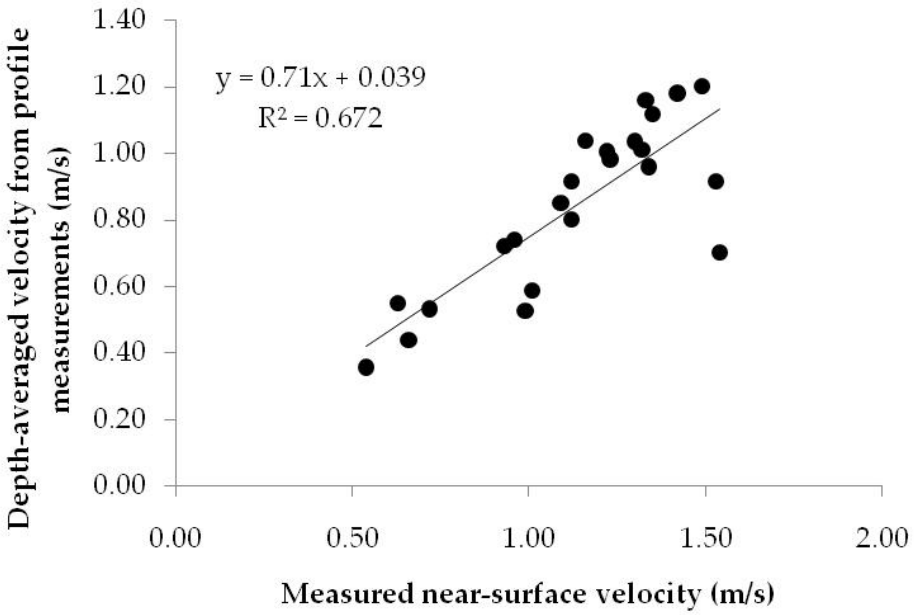

Figure 26. Field data from the lower Mokelumne River, California depicting the relationship between near-surface and depth-averaged velocity, with a slope coefficient of 0.71 and a coefficient of determination of 0.67.

3.8.4 Wading Point-Velocity Observations

There exist wadable areas of the upper South Yuba River over a wide range of flows. Velocity measurements in wadable areas present on any given day were made using a Marsh-McBirney Flo-Mate 2000 (MMB) sensor that was freshly calibrated by the manufacturer just prior to starting this study. Measurement error is reported by the manufacturer to be ±33 mm/s root mean squared. This sensor has been used often in the past to test 2D model performance (e.g. Pasternack et al. 2004; Pasternack et al. 2006a; Elkins et al. 2007; Brown and Pasternack 2008; Moir and Pasternack 2008; Sawyer et al. 2010).

The areas along the river where near-surface point velocity observations were made were selected for accessibility and good sight lines for surveying positions. One site was below the junction of Canyon Creek and the South Yuba (Figure 24), because it was possible to make ADCP-based discharge measurements at the mouth of Canyon Creek and right below the junction, to have a good characterization of input discharges for running the 2D model for the flow on the velocity data collection day. The procedure for data collection involved wading into the stream to an area with a visible range of velocities, observing near-surface velocities at 30 Hz with the MMB, and recording final velocities averaged over 40 seconds. The position of each measurement was surveyed while the measurement was taken, using either the Leica total station or Trimble RTK-GPS, to achieve highly accurate horizontal positioning (Figure 27). A total of 140 measurements were made, but of those it was determined that seven measurements were made at step locations with strong vertical velocity components not suitable for 2D model testing. This resulted in a total set of 133 wading observations available for testing against 2D model predictions.

The dates of velocity data collection were January 7, 2010; March 9, 2010; May 5, 2010; May 24, 2010; and June 22, 2010. The corresponding SYLC+CCB were 22, 30.5, 100, 480, and 935.6 cfs, respectively. This represents a wide range of discharges from near baseflow to overbank flood.

Figure 27. Near-surface velocity data collection during wet season on March 9, 2009.

3.8.5 Kayak-based Leica Total Station Velocity Reconnaissance

A new approach for rapid reconnaissance of the 2D velocity vector was developed during this study. Traditional point-based velocity observation is time-consuming, thus unable in most cases to span large areas in a reasonable amount of time and at low cost, and it does not yield a test of flow direction. Use of 2D and 3D velocity sensors can be problematic, because of the need for precise compass positioning to compare against 2D model velocity vectors. Drawing on the long-standing oceanographic method of using drogues to track water currents, previous studies have demonstrated the potential of small differential GPS units to obtain surface velocity in rivers (Stockdale et al. 2007). However, differential GPS is not accurate enough to test 2D models and there is financial risk in losing them in rough currents.

In this study, two trials were done in which a total station prism was mounted onto a manned whitewater kayak. The boater was positioned into the current and used floating debris to maintain a speed and heading consistent with the ambient surface flow field. Total station measurements were taken every 3–5 seconds. From these highly accurate positions, a 2D velocity vector was obtained between adjacent positions. This approach enabled testing of both velocity magnitude and direction. As the kayak was partially submerged into the water column, the observed velocity magnitudes were near-surface measurements analogous to those made

with the MMB in wadable areas, but the kayak was not limited to wadable areas. Instead, the kayak method was used to collect (coincidentally) an equal amount of data as obtained with the MMB, but in nonwadable areas. From a sampling perspective, the kayak-based rapid reconnaissance method was highly successful.

In a contemporaneous 2D model validation study on the lower Yuba River, >5,800 points were observed using this method—except all positions were recorded using an RTK-GPS, not a total station (Barker et al. 2010). Plotting these velocities against model results found the slope of the least-squared regression equation to be 1.01 and a coefficient of determination (r^2) of 0.784. Based on the peer-reviewed literature (e.g. compare against Lane et al. 1999; Gard 2003; Pasternack et al. 2006a), the resulting model performance was among the highest ever found for a direct observed-versus-predicted test of a 2D model (Figure 28). By the time the method was adopted for the South Yuba study (spring 2010), it was too late to collect a larger dataset over a wide range of flows. Nevertheless, the method did double the total number of observations for velocity validation. The method for using the kayak-based positional velocity data to test the 2D model was identical to that for the MMB (see Section 6.2.4).

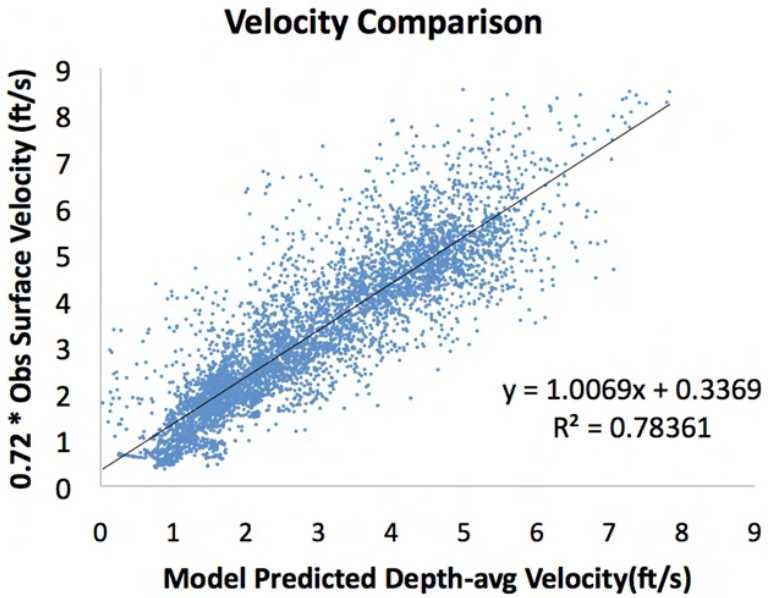

Figure 28. Kayak-based RTK GPS positioning velocity test of a 2D model for the lower Yuba River with >5,800 points, slope coefficient of 1.0069 and coefficient of determination of .7836 (Barker et al. 2010)

3.8.6 Morphological Unit Stratified Sampling

At least 25 MMB observations were made in each of the safely accessible morphological units (see Section 8.4, Table 2). Kayak observations helped to increase the number of observations in plane bed units, whereas transitions and pools would have had few to no velocity measurements without boat-based measurements. Chutes were narrow, deep, and fast, yet small in area, so they proved both unwadable and infeasible to sample using the boat-based method. By the time a kayak entered the standing waves at the onset of a chute, turned into

position, and matched speed with the flow, the kayak was no longer in the chute. Steps were defined as abrupt elevational drop >2 m between the brink of the step and baseflow water surface elevation below, so these units were not selected for velocity validation, since there was no expectation that a horizontal-oriented 2D model would capture velocities at features dominated by a vertical drop. As it turned out, a few measurements made at steps had the correct peak velocity for the step, but the model-predicted peak velocity occurred downstream of the exact location of the measured peak velocity, indicating the influence of the missing 3rd dimension in causing faster flow acceleration than the model can mimic without an explicit vertical dimension.

Table 2. Distribution of velocity observations by morphological unit and data collection method.

	# of Observations		
Morphological Unit	Marsh-McBirney	Kayak	Total
Plane bed	48	39	87
Inset channel	32	0	32
Floodplain	29	2	31
Steep inset channel	25	0	25
Chute	3	0	3
Transition	3	43	46
Step	0	0	0
Pool	0	56	56
Total	140	140	280

3.8.7 Substrate Data Collection

No quantitative measurements of substrate were made in the field, because sedimentary particle sizes were extremely heterogeneous over five orders of magnitude (0.001 to 10 m) and portions of the riverbed were bedrock. Two approaches to grain size analysis were considered. First, georectified kite-blimp imagery (aided by 2009 LIDAR intensity imagery and NAIP imagery) was used in ArcGIS 9.3 to digitize polygons around all bare bedrock surfaces. The bed was visible through the water everywhere except the deepest pools, which were assumed to be mantled in sand and gravel alluvium based on field experience. A polygon of the whole river corridor was clipped with the multi-part bedrock polygon to yield a polygon of the sediment-mantled bed.

For the sediment-mantled bed, grain size analysis was done on a morphological-unit stratified basis. Where bed sediments within a morphological unit were adequately resolved in the kite-blimp imagery, rectified image clips were extracted (Figure 29) and put through the "Cobble cam" freeware MATLAB code of Warrick et al. (2009) to estimate grain size attributes, including mean size and standard deviation. Seven floodplain unit images were ultimately analyzed and reported in section 8.8.3. This autocorrelation-based approach required just the image and the value of its pixel resolution as input. Based on extensive testing by the developers, results have

at minimum an irreducible error of 14% compared to observations. Applying the algorithm took only a few minutes to analyze hundreds to thousands of grains within a selected image, compared to the labor and difficulty of trying to measure particles sizes varying from sand to boulders. A standard Wolman pebble count method (Bunte and Abt 2001) was considered infeasible due to the extremely heterogeneous nature of the study segment. Ground-based measurement would be costly, time consuming, uncertain as to sampling method if the Wolman method was not used, and unlikely to span the spatial domain achieved with the kite-blimp imagery.

Where the Cobble cam algorithm was not applicable, image resolution appeared sufficient to enable a random statistical sampling of particle grain sizes visible in rectified blimp images using the ruler tool in ArcGIS 9.3 (Figure 30) and the mean and standard deviation metrics computed from that data. Insufficient time and resources were available to conduct analyses using this method during the study.

Figure 29. Alluvial floodplain image, with ~3 cm resolution, analyzed for grain size distribution.

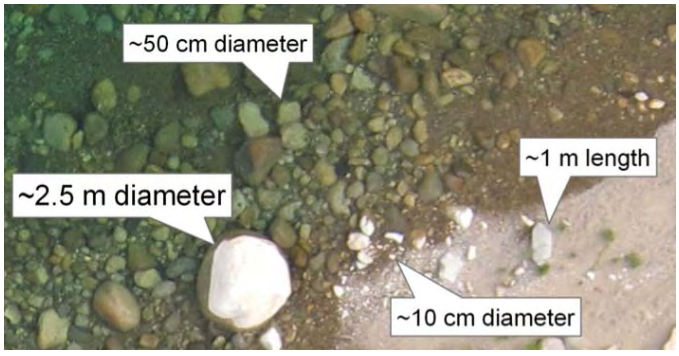

Figure 30. Rectified blimp image showing resolved characteristic grain sizes.

3.9 Streamwood Data Collection

Streamwood measurements were obtained whenever a wood piece >10 cm diameter and >1 m length was encountered during daily total station surveys. A code of 'wood' was entered along with the data points for separability during the data analysis phase of the project. Because the primary task of the study was to obtain topographic data, most streamwood pieces that resided outside of the wetted channel on the floodplain were not surveyed by instrument. Kite-blimp images were georectified and used in many analyses, including identification of streamwood.

Streamwood analysis was peripheral to the main study objectives, so it will be pursued opportunistically after this study ends. Partial results with the available data are detailed in section 8.8.4.

- ArcGIS 9.3 Editor tool was used to digitize polygons around all visible streamwood pieces in the upper half of the study area.
- Two-dimensional areas of each polygon were obtained using the Calculate Geometry ArcTool, then streamwood diameter estimated to calculate volumetric quantity.
- Future analyses will identify longitudinal distribution, morphologic unit distribution, and latitudinal position within the river corridor once all streamwood is digitized.

CHAPTER 4:
Map Production

To create the topographic map, the following items were obtained through data collection: LIDAR flight and data file tiling scheme polygon shapefile, LIDAR data coverage polygon shapefile, LIDAR intensity images (first and last returns), LIDAR bare earth last-return point file (ASCII format), echosounder/RTK-GPS bathymetry point file, RTK-GPS survey point file, Leica total station point file, and Topcon total station point file. In this section the details of the steps used to produce the topographic map are presented in the format they were written as the steps were done. Building the topographic map and digital elevation model were the most important steps for the entire study. Although it is not fixed through time, landform topography is a master variable underlying geomorphic-hydraulic-ecologic linkages.

4.1 Point and Polygon Shapefile Procedure

1. View the LIDAR intensity imagery and manually draw the following: A) a shoreline shapefile, B) a shapefile of isolated wetted areas not connected to the main channel, and C) a shapefile of gravel bars and islands in the river.

2. Rename ASCII-based LIDAR point files to .csv. Use a text or spreadsheet editor capable of handling the full size of each file to add a row with the following text column headers to the first line of the file: {X,Y,Z}. Use ArcCatalog to create a 3D point shapefile from each LIDAR point file. Check that the correct horizontal and vertical datums have been applied in ArcMap.

3. View echosounder and LIDAR data and digitize polygons covering areas with no data. Back-channels and side-channels may exist in areas where no points are present (water absorbs LIDAR, so generally no returns from water). For bank areas with few or no points, use judgment to determine if interpolation is acceptable in that area or if a critical data gap exists and field-based surveying is needed, or if manually point additions are acceptable.

4. Clip the shoreline shapefile with the island shapefile to create a wetted channel shapefile.

5. Merge the wetted and side channel shapefiles to create a wetted area shapefile.

6. Clip the LIDAR data coverage shapefile with the wetted area shapefile to obtain a land area shapefile.

7. Divide the total map area into a set of smaller mapping units, with each containing 8-10 lidar tiles. This is a necessary step, because ArcGIS has trouble building a map of the whole set at once because of the excessive number of data points. Use the autotrace tool in the Editor toolbar to create a boundary for each mapping area; use the Snap tool in Editor to be sure the boundary exactly matches the data boundary for the overall map or there can be edge effects when creating TINs and contours.

8. Divide echosounder point file into subsets that match the map area boundaries. Make sure the points include a small amount of channel outside the end boundaries or else there may be undesirable edge effects in the map. This also helps, because when QA/QC is performed on individual echosounder points later when using the Editor Toolbar, this ensures that any corruption to a file does not lose all the edits.

4.2 Process LIDAR Points

1. Extract LIDAR points that are on land into "landshp_tile#" file for each tile using the Spatial Analyst->Extract->Clip tool.

2. Extract LIDAR points that are on water into "watershp_tile#" file for each tile using the Spatial Analyst->Extract->Clip tool.

4.3 QA/QC Bathymetry and Survey Data

1. Review field notes and correct any data issues mentioned (e.g. incorrect survey rod height).

2. Review Bathymetry and Survey Data in ArcGIS. Compare to available imagery (e.g. NAIP 2009, LIDAR intensity and elevation hillshade, and georeferenced high-resolution aerial photos).

3. Correct skewed data where possible. If data skew cannot be determined or a method of correction cannot be determined, then list data as erroneous and delete from master file.

4.4 Compare Overlapping LIDAR, Survey, and Bathymetry Points

Each dataset is obtained using a unique method that makes it difficult to say with certainty that any one represents the true elevation. LIDAR "point" elevations are actually averages over an area that is hit with a signal, while total station and RTK GPS points are locations where the tip of a pole touched the ground. Commonly, averaged areas tend to be higher than points, because people tend to push tips down between particles and because the average covers a larger protruding area. That difference is not an error, just a measurement difference.

LIDAR-based topographic measurement has a commonly cited vertical accuracy of within 15 cm for large flat surfaces, such as roads and airport runways. For a natural rough surface, the measurements deviations are therefore expected to greater than 15 cm. For a gravel bed surface with particle sizes ranging from 0–20 cm, it is expected that deviations in LIDAR-based topographic measurements will vary by up to 20 cm just due to the effects of that roughness, so the mapping goal of having points accurate to within 15 cm is within the noise of the bed roughness, though on the high side of it. The two effects are not additive. Further, when a LIDAR measurement averages across a sharp topographic boundary, like the side of s cliff or the side of a boulder, then the measurement deviation can be large compared to a point observation at the top or bottom of the boundary. In light of these concepts, the goal of the analysis steps reported in this subsection was to look for any large deviations and try to account for them, but generally to ensure that the data conforms to the goals of the project.

1. Identify the LIDAR, bathymetry, and ground survey point files that will be compared and create 3D point shapefiles of each dataset.
    a. Create one shapefile that includes both survey and bathymetry data.
2. Add a field to each shapefile's attributes table that contains the elevation data for the points. This is the field that will be compared.
3. Perform a spatial join (Arctoolbox->Analysis Tools->Overlay->Spatial Join) to create a new point shapefile that contains comparable points and both elevation fields. The target is the point shapefile you want to end up with, the feature set is the data you want

to merge. Set a horizontal distance or intersection of 0.3 m to find matching points in the datasets.

4. Add a new field to the merged shapefile.
5. Use field calculator to difference the two fields and obtain the deviation value.
6. QA/QC resultant point file, eliminate any high deviation (>5 m) caused by steep stream banks, large boulders, or first return LIDAR data (i.e. vegetation).
7. Perform statistics on raw deviations and absolute values of deviations to determine how much of the data falls within <3m and <5m difference thresholds.

4.5 Calibration of Bathymetry and Survey Data

There was a significant (0.97 m) and consistent deviation between the LIDAR and bathymetry/survey datasets collected for the South Yuba. The LIDAR dataset was believed to be more accurate due to the short period of data collection (one day) and use of National Geodetic Survey (NGS) benchmarks to ground truth the dataset. The bathymetry/survey dataset used a control network originating from a NGS benchmark, but was progressively surveyed upstream from the initial control points over a four-month period. Therefore, the potential for propagating survey inaccuracies was greater for the bathymetry/survey dataset. Calibrated ground-based data retained some bias compared to LIDAR data (Table 3, Figure 31).

1. Create regression relationships between the LIDAR and bathymetry/survey datasets for each LIDAR Area 1–4.
    a. Use the LIDAR/Survey comparison points obtained from the Spatial Join in step 4.4.
    b. In Excel, plot the LIDAR data versus the Survey data and fit a trendline to the data. R^2 values for the trendlines were 0.997–0.998.
2. In Excel, adjust the bathymetry/survey data using the above regression equations. This produced two elevation columns: Z and CalZ.

Table 3. Percent of topographic elevation deviations between LIDAR and ground-based surveying datasets, after calibration of ground-based data to LIDAR that meet various thresholds of performance.

Threshold (m)	% Data Within
0.025	9%
0.05	18%
0.1	43%
0.25	85%
0.5	98%

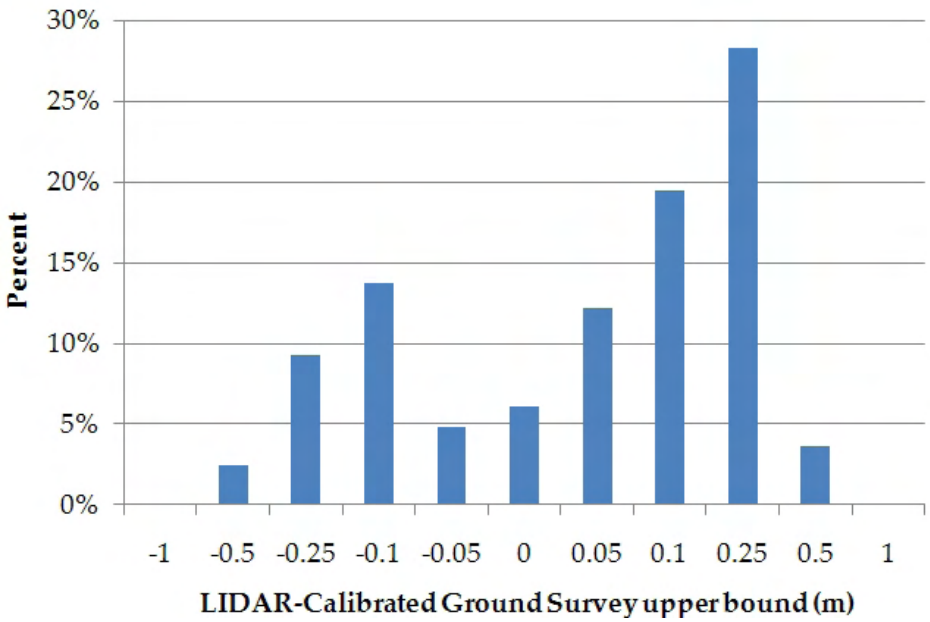

Figure 31. Histogram of deviations between topographic datasets after calibration of ground-based data, showing a slight high bias of the lidar data.

4.6 Build Preliminary Topography TIN

1. Create a boundary area shapefile for the study reach.
2. Create a boundary file with a 15-meter buffer around the boundary area polygons.
3. Create a shapefile within each boundary area with the bathymetry and survey data for that area.
4. Build preliminary TIN using 3D analyst.
    a. Use the LIDAR land.shp tile, bathymetry, and survey files for that area.
    b. Use the buffered boundary area polygon as a hard clip.
5. Create a shapefile of 0.25-meter contours

4.7 Build a Water Surface Elevation TIN

The water surface elevation of the study reach at summer base flow was useful for hydrodynamic analyses, to validate the 2D model, and to extract boulders from the LIDAR dataset.

1. Create a water surface elevation (WSE) point shapefile from the survey and bathymetry data.
    a. In Excel, add the echosounder depth reading to the bathymetry elevation to obtain the bathymetry data WSE.

b. Save file as a .csv

c. In ArcCatalog, right click select Create Feature Class → From XY Table

2. Create a water surface elevation point shapefile from the wetted area LIDAR data.

    a. Reverse Step 4.1.6 and clip the wetted area LIDAR points into a shapefile.

    b. Cut out LIDAR points using the islands polygon shapefile from Step 4.1.1 c.

    c. QA/QC this shapefile.

        i. Use all available imagery (LIDAR, NAIP, Aerial, etc) to select only the LIDAR points on the water surface

3. Build a WSE TIN using 3D Analyst and the above WSE point shapefiles.

4.8 QA/QC Contours For Each Boundary Area

1. View contours and points together.
2. Delete any outlier individual point that is more than 3 feet different than the points around it.
3. When data is collected over the same area at different times and large flows or long time intervals have passed, then it is necessary to check to see if the lines of data are significantly different due to erosion or deposition. If that is the case, then one or the other data must be deleted. In some instances, the set that had fewer points might be deleted to yield a robust representation of the surface as it was at the time of greater data availability. Alternately, one might choose the more sparse data if it was newer and the most recent surface was desirable over what might be a more accurate one.
4. Where in-channel data had a small data gap along the bank (<2 m), such as limited bathymetry data, then it was determined acceptable to augment a few points to fill in the gap and prevent the LIDAR data from interpolating irregularly into that space.

    a. Add an augmented data point shapefile (with Z)

    b. Add points in the gap, interpret the existing point data (LIDAR and/or survey) around it to identify a suitable elevation

    c. Assign that elevation to the augmented points by double clicking on each point, then right clicking, choosing properties, and typing the elevation.

5. Re-build TIN and contour and then repeat steps 1-4 as many times as necessary to resolve evident problems.
6. Build final TIN and contour shapefile, QA/QC the augmented points, and adjust as necessary until solution appears reasonable as understood from an expert field perspective.

4.9 Extract Instream Boulders from LIDAR dataset

In the above steps, the LIDAR dataset has been split into land and wetted areas. This process has not accounted for any instream boulders surveyed by LIDAR. This next step is one method of extracting those boulder returns from the LIDAR dataset (Note: .shp file names used here are generic, for procedure description only).

1. Map wetted area LIDAR points over WSE TIN in ArcGIS.
2. Extract WSE elevation for each wetted LIDAR point.
    a. Open the Attribute Table of wetlidarpoints.shp
    b. Export (Options → Export) the table as a .txt file (this is save the original xyz, primarily z, coordinates if you decide to delete them in the next step)
    c. If x,y,z coordinate columns are titled Point_X, Point_Y, and Point_Z, then rename or delete them because three new columns with those names will be generated shortly.
    d. In 3D Analyst, Convert → Feature to 3D
    e. Use the Add XY Coordinates tool
    f. Open the Attribute Table, the table should now contain the original coordinates (if you didn't delete them) and a new set labeled Point_X, Point_Y, and Point_Z
        i. The xy coordinates are the same, but the new Point_Z is taken from the WSE.tin
3. Export data from Attribute Table to a .txt file (see 4.9.2.b).
4. Compile the x, y, LIDAR Z, and WSE Z into one .csv file.
5. Open in Excel and calculate the difference between LIDAR Z and WSE Z.
6. Cut out points with elevation differences <0.33m and >10m. The resolution of this method is 0.33m at best and there are no boulders >10m (bedrock is >10 m in some cases but it should already be identified as ground).
7. Save file as .csv
8. In ArcCatalog, create a point shapefile from XY coordinates (Create Feature Class → From XY Table).
9. Map the new shapefile and QA/QC new difference points.
    a. Check the boulder points with available imagery (LIDAR, NAIP, Aerial, etc). Ensure that the extracted boulder points make sense for the field site from the perspective of expert field knowledge.
    b. Use Properties → Symbology to color code boulderpoints.shp, this will allow visual identification of points with large LIDAR/WSE elevation differences.

c. It is helpful to map contours of the LIDAR first returns (vegetation) as these contours can be used to ensure boulder points are not trees or shrubs.

10. The boulder points were incorporated into the topographic TIN and were used to represent boulders in the 2D model. To create model elements representing boulders, polygons were created from the boulder points first. To incorporate the boulder points into the topographic TIN, create boulder polygons and convert the perimeter of those polygons into 3D points. Steps 4.10 to 4.12 describe some methods of accomplishing these tasks.

a. Create Boulder Polygons

1. Buffer the Boulder.shp created in Step 4.9 with a variable buffer distance (Note: .shp file names used here are generic, for procedure description only).
    a. Create two separate boulder shapefiles, one for boulders with elevation difference <1m and one with elevation differences >1m
    b. Buffer the <1m Boulder.shp using the elevation difference as the buffer distance
    c. Buffer the >1m Boulder.shp with a 1 meter buffer distance
2. Merge the <1mBoulderpolygon.shp and >1mBoulderpolygon.shp
3. Use Dissolve to combine all buffer polygons in the new BoulderBuffer.shp, creating single polygons for boulder clusters
4. Aggregate polygons to eliminate any gaps in the center of boulder clusters.
    b. Aggregate Distance = 0.01m, Minimum Hole Size = 6 m^2 (these are arbitrary values, use what makes sense or works for the specific study site).

c. Create Boulder Perimeter Breaklines

1. Open final boulder polygon shapefile from Step 4.10 in SMS
2. Convert Shapes to Feature Objects (Mapping: Shapes → Feature Objects)
3. Select all Arcs
4. Redistribute Vertices to 0.5m spacing (Feature Objects: Redistribute Vertices…)
5. Select all Vertices
6. Convert Vertices to Nodes (Feature Objects: Vertices->Nodes)
7. Save As, Shape Files (.shp), Export as Feature Points-> Point Shapefile
8. Map the resultant boulder vertices.shp and the topographic TIN (topo.tin) in ArcMap
9. Use 3D Analyst to Convert → Feature to 3D using the topo.tin for the elevation (Z) values, creating boulder vertices3d.shp

d. Create Final Topographic TIN with Boulders

1. In ArcCatalog, copy and rename (topo_bldrs.tin) the topographic TIN
2. In ArcMap, use 3D Analyst to Add Feature to the topo_bldrs.tin
3. Add Boulder.shp and boulderverticies3d.shp
4. QA/QC topo_bldrs.tin to ensure boulder and boulder perimeter points were interpolated properly

CHAPTER 5:
Hydrologic Analysis

The watershed supplying runoff to the study segment of the South Yuba River ending at Washington, CA includes many regulated catchments and some unregulated areas (section 2.2.2; Figure 9, Figure 10). The uppermost area of the South Yuba is regulated by Lake Spaulding. The upper area of the largest tributary, Canyon Creek, is regulated by Bowman Lake and several upstream facilities. The three major tributaries on the north side of the river (Rucker, Fall, and Texas creeks) have facilities to capture flow and divert it to Lake Spaulding. Unregulated areas contributing flow to the upper South Yuba include the portions of the north-side creeks below diversions, any flows from the total watershed areas of all upstream regulated portions that exceed the holding and diverting capacity of existing facilities, and all the flows from the unregulated south-side tributaries of Diamond and Scotchman Creeks.

An early assumption of this study was that unregulated summer baseflow would consist of summer releases from Spaulding Dam with a minimum flow release requirement of 5 cfs and from Bowman Dam a minimum 3 cfs. Other incremental amounts of flow coming out of tributaries visually looked small. However, as various analyses were being undertaken, it became clear that the assumption was wrong, because 8 cfs of total discharge could not account for preliminary results. Therefore, it was necessary to undertake a suite of analyses to determine the role of unregulated flow in the study segment and adjust the experimental design of the study to account for the role of unregulated flows.

Because the study segment was within the area between the gages at SYLC and SYWA, it was possible to do a direct analysis of flow accretion between those stations. However, SYLC did not start operating until December 1, 1965, and SYWA was discontinued on October 11, 1972. As a result, historical flow accretion over a ~7-year period was available for analysis. The short timeframe of overlap between those gages left open the question of whether characteristics of flow accretion 1965–1972 were relevant and representative for current conditions, given climatic variability, adjustments to flow regulation, and changes to land use and land cover. To assess that uncertainty, an analysis of flow accretion was done between SYLC and SYJB, which overlap over the entire record for SYLC, including the period of this study. In both of the above analyses, gaged CCB flows were subtracted from the downstream gage (either SYWA or SYJB) to isolate the effects of accretion relative to the flows reported for SYLC. Ungaged flows downstream of CCB on Canyon Creek were part of the investigated accretionary signal. Through hydrologic analysis of these gage data, answers were sought for the following questions.

First, with regard to the historical analysis of SYLC versus SYWA between 1965 and 1972:

- What were the raw statistical attributes of flow accretion between SYLC and SYWA?
- Were there seasonal variations in flow accretion, and if so, what water-delineated seasons were evident?
- For each identified season, what was the empirical equation relating total flow accretion to SYLC flows?

Second, for the SYLC versus SYJB analysis:

- What were the season-stratified statistical attributes of flow accretion 1965–1972, 1965–2009, and 2003–2009?
- Does flow accretion scale with watershed area?
- How does historical flow accretion compare to modern flow accretion?

Third, has the Yuba River watershed experienced a "secular trend" (defined as an underlying unidirectional shift in magnitude ignoring short-term fluctuations) in hydrologic metrics caused by historical climatic change?

Fourth, based on the results of the above analyses, what methods could be employed so that accretionary flows are properly apportioned to tributaries?

Fifth, how did direct observations of flow accretion compare to historical values and synthetic regression relation predictions?

Finally, what was the stage-discharge relation at the end of the 2D model study segment?

Answering the above questions produced important insights about the relative significance of flow regulation for different times of the year. More importantly, it yielded the estimates of ungaged tributary inflows required for use as inputs into the 2D hydrodynamic model. Ultimately, these estimates had uncertainties that contributed to the overall scope of limitations to what conclusions could be reached in the study.

5.1 SYLC to SYWA flow accretion

Using the 2,507 mean daily flow values during the period of overlapping record between 1965–1972, statistical analysis found a large amount of accretionary flow between SYLC and SYWA (excluding gaged flows from CCB), but more importantly that it was not uniformly proportioned to SYLC gaged flows (Figure 32). The average of daily flow accretions over the period of record was 110 cfs, which represents an average addition that was 6.44 times the SYLC gaged flow. The maximum accretion was 5,210 cfs, which was 66.6 times the SYLC gaged flow for that day. These results indicate that a large proportion of the water reaching Washington, CA for much of the year is untallied.

Analysis of the time series of flows and flow accretions revealed a strong seasonality in both variables in the system (

Table 4, Figure 33, Figure 34). In the dry season (August 1 through November 30), flow was normally low and accretion ~3.2 times SYLC gaged flows on average. However, when it rained during the dry season, flow accretion rose at the fastest rate of any season. Considering that unregulated releases from Spaulding or Bowman dams were unlikely during dry season regardless of the amount of runoff, runoff from dry-season rainstorms would come from the unregulated watershed areas at lower elevations, which would have a fast overland response to intense rainfall. Rainstorms in September through November are often the remnants of monsoons, typhoons, and tropical storms that come across the Pacific, yielding tightly focused, intense bursts of rain. For example on October 13, 2009, a typhoon remnant precipitated 3.59 inches of rain in one day at the Blue Canyon, CA weather station (elevation 5280 ft), 8 km from Spaulding Dam (elevation 5200 ft). These events are rare in the historical record, so the flow data has a lot of low values and only a few high values. Of 790 flow accretion observations, 97% of values are < 100 cfs. Only two observations exist for accretions >500 cfs and an additional three for flows > 300 cfs. That presents a problem for high-quality statistical analysis, leaving high-flow estimation more uncertain. Based on the available data, a 2nd-order polynomial statistical regression equation was obtained with an r^2 of 0.75 (Figure 33, top). According to that equation, a SYLC gaged flow of 45 cfs corresponds with a SYWA accretionary flow addition of 612 cfs. No SYLC regulated releases higher than 45 cfs were observed during the dry season in the historical record.

In the wet season (December 1 through March 31), flow was higher than in the dry season and average accretionary flows were ~10.3 times the SYLC gaged value (

Table 4). According to Kattelmann (1997), streamflow associated with elevations <1500 m in the Sierras (Lake Spaulding elevation ~1600 m) is generated directly by rainstorms, while that associated with elevations >2500 m is generated on a delay because precipitation is stored on land as snow and not released until temperatures rise and snow begins to melt in the spring. The wet season produces much more low-elevation rain than the dry season, so its flow accretion was substantially (~3x) higher (

Table 4). The statistical regression relation between accretionary flow and SYLC gaged flow for the wet season was even stronger than that for the dry season (Figure 33), with an r^2 of 0.83 (though there is a highly unbalanced number of points as a function of increasing SYLC flow magnitude). The regression relation breaks down once SYLC flows are >~350 cfs, though they rarely occurred in the limited historical record analyzed. Rain-on-snow events and large rainstorms over the whole basin could be the cause of high flows at SYLC at a time when Lake Spaulding was near capacity. Presumably, above this discharge, flow increases stem primarily from Lake Spaulding overflows that outpace further increases in accretionary contributions. This would decrease the relative magnitude of ungaged accretionary flows. Based on the regression relation, a SYLC gaged flow of 45 cfs in the wet-season is associated with an estimated accretionary flow addition of 338 cfs at SYWA. This amount is roughly half the amount for that gaged flow in the dry season. Despite this less flashy response, the regulated wet season flows dominated by flow accretion go much higher (~350 cfs) than dry season flows (~45 cfs).

The snowmelt season (April 1 through July 31) was the most complicated and uncertain to quantify. During the snowmelt season an array of hydroclimatological processes take place, causing different runoff patterns to overlap, which led to counterintuitive thresholds in the relation between flows at SYLC and SYWA. Average flow accretion magnitude was ~3.5 times the SYLC gaged value, resembling the dry season (

Table 4). However, closer analysis revealed the existence of three different flow ranges over which flow accretion was distinct (Figure 34). SYLC gaged flows >200 cfs indicate that flow in the study segment is dominated by runoff from the upper watershed either being released from or spilled over Lake Spaulding. The average flow accretion under this regime was just 0.2 times that of SYLC gaged flows, an order of magnitude lower than the season-average. When SYLC gaged flows are >200 cfs, snowmelt water from the upper watershed overwhelms any rain-induced runoff generation that may be occurring in the unregulated lower watershed. Since snowmelt begins as the wet season ends, the likelihood of rain diminishes as snowmelt peaks. SYLC flows between 100 to 200 cfs have an average flow accretion ratio of 2.2 and a range from 0-8, a transitional condition when several different processes can play a role simultaneously, such as a late May rainstorm during heavy snowmelt runoff. Finally, when SYLC flow is <100 cfs, unregulated lower-basin flows dominate the runoff response in a way that is similar to the wet season, yielding a mean flow accretion ratio of 4.3 and a maximum of 20.3. However, this flow domain shows some influences of the late snowmelt runoff regime, with some individual daily flow values having flow accretion ratios of 0–1.

The presence of a complex, overlapping, discharge-dependent transition between regulated snowmelt-dominated runoff and unregulated rainfall-dominated runoff means that a synthetic empirical relation between SYLC flows and accretionary flows has to be conditional on the SYLC flow range and is not a linear relationship across the flow domain. For low SYLC releases, accretionary flows make ~3x more contribution to discharge at SYWA than SYLC, but once the gaged flow goes above 100 cfs, accretionary flows drop as rain-driven runoff drops, even as gaged flows are pushed higher by upper watershed snowmelt runoff. Once gaged flow goes above 200 cfs, flow accretion becomes a fractional component of runoff.

In summary, statistical analysis of historical data found that three distinct flow regimes exist corresponding with seasonal hydroclimatology. The wet and dry seasons have simple regression relations that represent the total amount of flow accretion for SYLC gaged flows. Dry season response is associated with rare storms that cause a strong, flashy response. Wet season response is associated with winter rainstorms, during which time the majority of precipitation is stored on land as snow, mediating the strength of the accretionary response. Finally, in the snowmelt season, a mix of different processes yield a complex accretionary flow response that does not grow simply with increasing gaged flows. Above a threshold, unregulated rain-driven runoff decreases abruptly and snowmelt-driven runoff from the regulated watershed takes over. With only 7 years of overlapping flow records, it was not possible to characterize the rain-to-snowmelt runoff-response transition as precisely as desired.

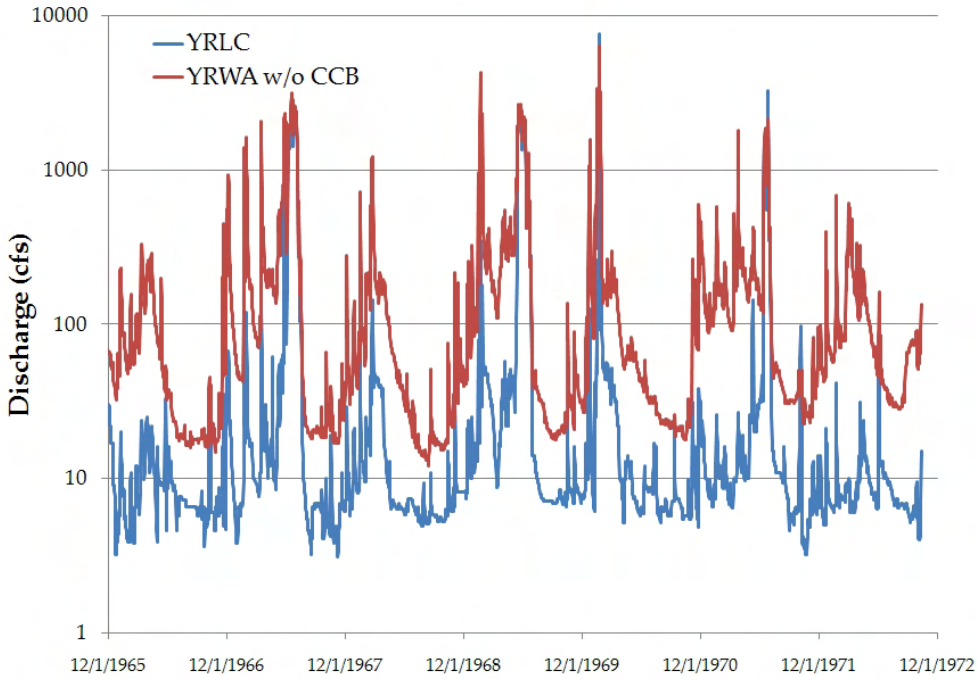

Figure 32. Hydrographs for SYLC (YRLC on graph) and SYWA without CCB (YRWA w/o CCB on graph) showing significant downstream flow accretion.

Table 4. Season-stratified statistical description of accretionary flows.

	Hydrologic Season		
	Snowmelt	Dry	Wet
Statistic	Apr 1-Jul 31	Aug 1-Nov 30	Dec 1-Mar 31
Count	644	673	1057
Median	2.77	2.52	9.48
Mean	3.5	3.16	10.27
Standard Deviation	3.15	2.23	7.07
Minimum	0	0.12	0.13
Maximum	20.26	21.49	66.61

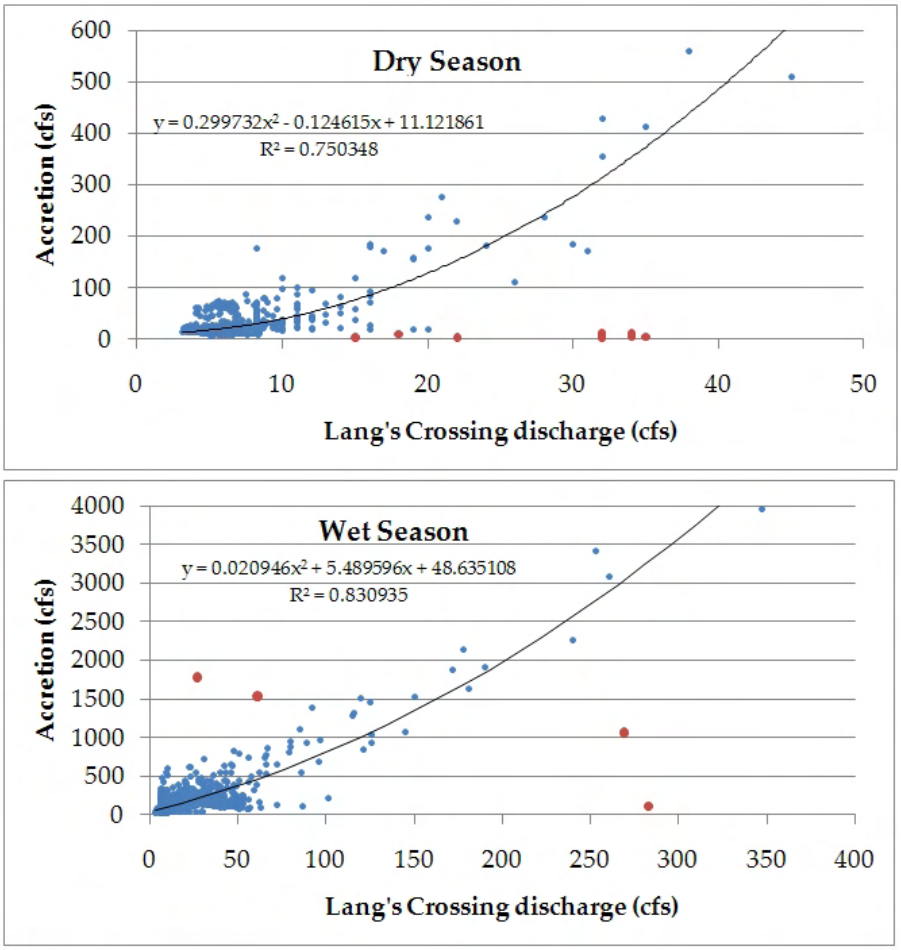

Figure 33. Season-stratified regression analysis showing strong predictability of flow accretion as a function of SYLC gaged flows for wet and dry seasons. Red points are outliers excluded from the final regression equation.

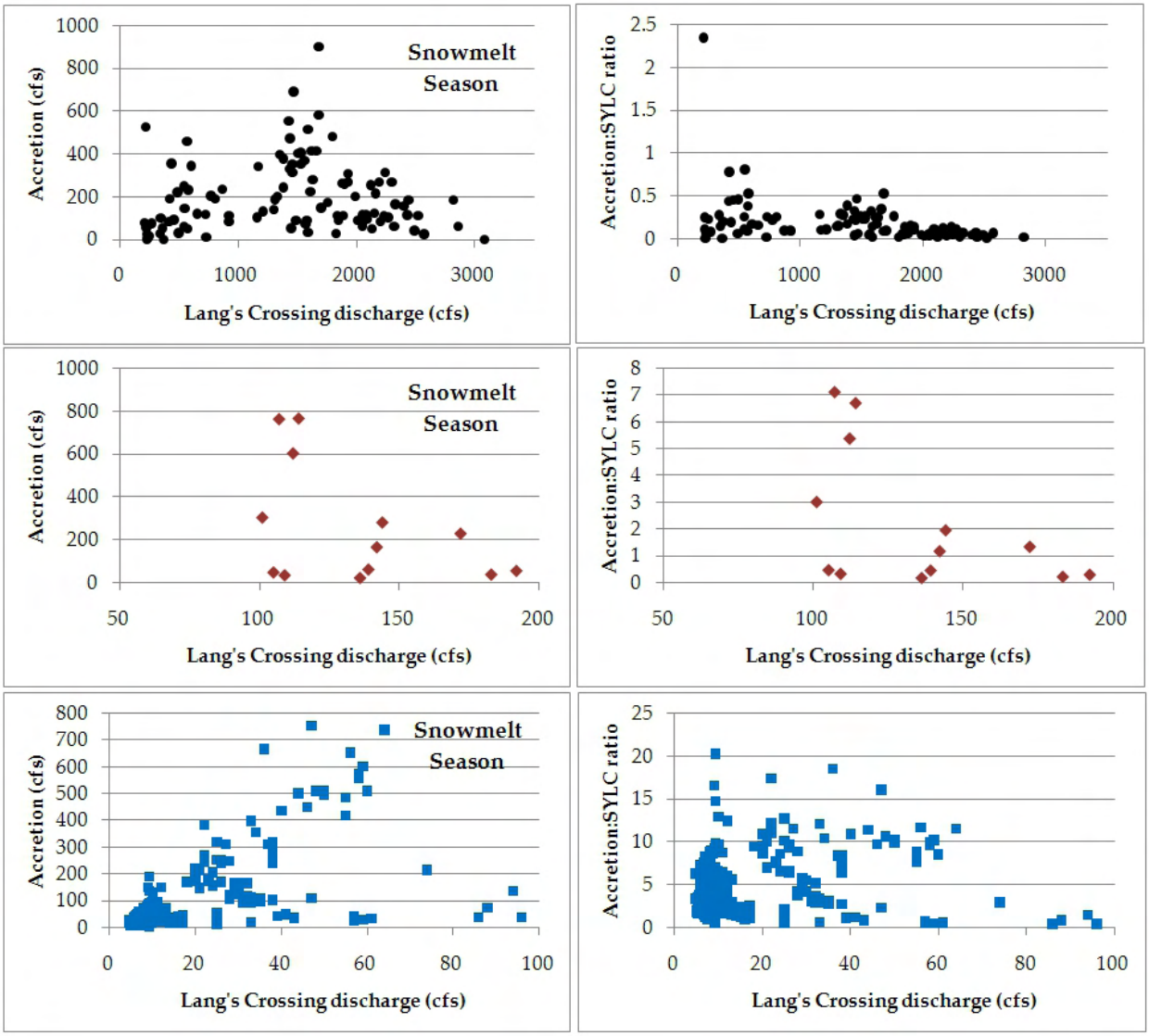

Figure 34. Season-stratified regression analysis showing distinct domains of flow accretion as a function of SYLC gaged flows for the snowmelt season, but no simple function within each domain. The top plots represent Q>200 cfs, middle plots 100<Q<200 cfs, and bottom plots Q<100 cfs. The bottom plots show a quick-response rain relation driven by the unregulated lower-basin (correlated linear flow response between 10–65 cfs) and an upper basin response associated with Lake Spaulding releases (scatter points with accretions <250 cfs regardless of SYLC flows).

5.2 SYLC to SYJB flow accretion

The same analyses performed to understand flow accretion between SYLC and SYWA were performed for the larger watershed between SYLC and SYJB, because the latter datasets overlapped for the entire duration of the SYLC gage record. Table 5 presents the key findings from the analysis. The SYJB analysis yielded the same pattern of relative flow accretion among seasons, with the dry season having a slightly lower mean accretion ratio than the snowmelt season and the wet season having ~3 times the ratio as the other seasons.

Since SYJB is downstream of SYWA it has a larger watershed area and thus higher accretion ratios. After subtracting out the watershed areas of SYLC and CCB, the ratio of watershed areas for SYJB:SYWA is 3.2:1. In comparison, the ratio of the mean accretion ratios for SYJB:SYWA for the 1965-1972 comparable period is 2.9:1. That suggests that there is a close relation between watershed area and accretion ratio, with a slight decrease in water yield with increasing area, which is well known in the hydrological literature (e.g. Dendy and Bolton 1976).

Stratification of SYJB daily accretion ratios into three different time periods revealed that the period 1965-1972 had higher accretionary flows than has recently occurred using an identical number of data values in the years 2003-2009 (Table 5). The three hydrologic seasons of 2003–2009 have 38–48% lower flow accretion ratios than in the years 1965–1972. Compared to the whole record since 1965, the 1965–1972 period had 13–23% higher accretion ratios. Many factors might play a role in these differences, such as hydroclimatological variability, increased capturing of flow for societal use, and increased forest cover. However, some of the variation might be specific to the non-SYWA drainage area. In terms of hydropower facilities, efforts were undertaken in the late 1960s to improve the effectiveness of diversions to Lake Spaulding, but that happened during the period of analysis. It is possible that these changes could cause a secular decrease in accretionary flows. Determining changes in land use and land cover that may have occurred 1972–2009 were outside the scope of this study. Hillslope areas of hydraulic mining, such as the Alpha and Omega mining districts, are still denuded and contributing excessive sediment to the river (Figure 8). Some other areas are also logged (Figure 8), but much of the upper South Yuba watershed is in Tahoe National Forest, so it is possible that canopy density has increased over time as a result of fire suppression and managed logging. In terms of climatic change, enough data exists to do a separate analysis, which is the purpose of the next section.

Table 5. Ratios of ungaged accretionary flow to gaged SYLC flow for different historical time periods and the percent changes between time periods.

	Hydrologic Season		
Metric	Snowmelt	Dry	Wet
SYLC versus SYWA comparison			
1965-1972 mean accretion ratio	3.5	3.16	10.27
SYLC versus SYJB comparison			
1965-1972 mean accretion ratio	9.81	8.65	32.47
1965-2009 mean accretion ratio	8.51	7.42	25.02
2003-2009 mean accretion ratio	6.05	4.51	18.12
Percent change in hydrologic accretions 1965-2009 compared to 1965-1972	-13	-14	-23
Percent change in hydrologic accretions 2003-2009 compared to 1965-1972	-38	-48	-44

5.3 Historical Climatic Change Analysis

A deeper understanding of the role of potential secular trends in hydroclimatology would help clarify the importance of accounting for the difference in observed accretion ratios between 1965–1972 and 2003–2009 at SYJB in developing the synthetic accretionary flow relations between SYLC and SYWA. The key question is whether the observed difference is a secular trend or an artifact of temporal variability. If the former were true, then an adjustment would be required to the SYWA accretionary flow relations. However, if the system is dominated by non-secular temporal variability, then there is no way to know whether the future will be more like the 1965–1972 period or the 2003–2009 period, in which case the synthetic flow accretion relations developed from the 1965–1972 historical analysis has less uncertainty.

Because all of the gages on the South Yuba are influenced by flow regulation, the assessment of secular trends in historical hydroclimatology was performed using data from the unregulated North Yuba River at Goodyear's Bar. At this location, USGS gage #11411500 captures the response of a 648-km^2 unregulated catchment. Using the daily discharge record, three commonly used metrics for identifying secular changes in hydrology associated with climatic change were calculated and tested: (1) calendar day of peak discharge, (2) percent of total water-year streamflow occurring April through July, and (3) calendar day of flow center of mass (McCabe and Clark, 2005; Stewart et al., 2005). For each metric, the p-value and coefficient of determination (r^2) of the relation between the metric and number of years from 1939–2010 (71 years) were calculated. The p-value was compared against the standard of statistical significance, $p < 0.05$. Although a correlation among 71 points might be statistically significant, a more rigorous test would also require an $R^2 > 0.2$ to provide a baseline amount of explanation and preferably an $R^2 > 0.5$ to show a strong explanatory trend.

Tests for a response of the North Yuba River at Goodyear's Bar streamflow to climatic change found no statistically significant effect (Figure 35). All three test metrics: (1) calendar day of peak snowmelt, (2) April-July percent of streamflow, and (3) calendar day of flow center of mass- showed a wide scatter of points when plotted against years since 1939, which is characteristic of the dominance of interannual variability over any secular trend. P-values were all higher than 0.1, showing no statistically significant trends in any metric. No relation had an $r^2 > 0.1$, indicating that years since 1939 have no explanatory power in accounting for the temporal variability in the test metrics.

Based on the analysis of the unregulated North Yuba River, there is no *historical* basis for expecting future hydroclimatology in the Yuba watershed to be any different than the variation in the known historical conditions since 1939. Temporal variability in hydrologic metrics appears to dominate the unregulated flow record. Hopefully, results from mechanistic regional climate modeling at a <5-km resolution including dynamical downscaling necessary to resolve Yuba-specific processes will be available soon to provide climate forecasts that can guide future analysis (e.g. as is possible using the Weather Research and Forecasting model). Such a study is nearly complete using the Goodyear Bar catchment (Pasternack et al. submitted).

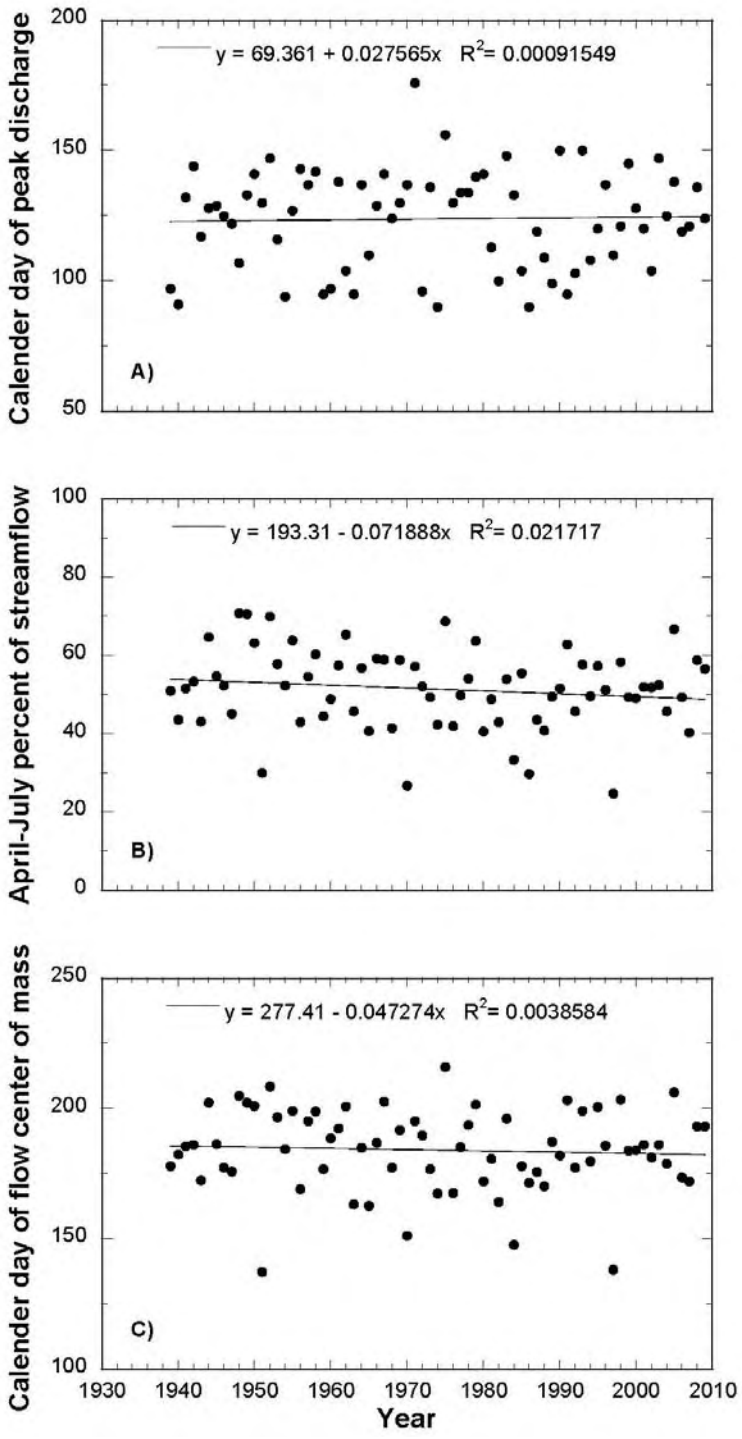

Figure 35. Analysis for historical climate change trends in the unregulated North Yuba River gaged at Goodyear's Bar. No secular trend exists and temporal variability is the dominant feature of the record. (From Pasternack et al. submitted).

5.4 Synthetic Flow Accretion Relations

The results of hydrologic analyses indicate that accretionary flows are a vital component of the flow regime in the South Yuba River. Using the historical flow records of 1965–1972, highly significant statistical regression equations were created for dry and wet seasons. For the snowmelt season, relations were stratified by SYLC gaged flow. Observations across all seasons in the historical record had so much scatter that the best approach involved using the mean accretion ratios as a scaling factor to estimate flow accretion based on SYLC gaged flows. For the snowmelt season, this approach yielded threshold shifts at specified SYLC discharges and thus there is no one-to-one flow relation during this season. This is a result of the complexity of overlapping hydroclimatological mechanisms (section 5.1). Matching the observed conditions was more important than yielding a single simple relation.

Using this framework, the equations for calculating flow accretion (FA) (in English units of cubic feet per second) were

Dry season: $$FA = (0.299732*SYLC^2) - (0.124615*SYLC) + 11.121861 \quad (1)$$

Wet season: $$FA = (0.020946*SYLC^2) + (5.489596*Q) + 48.635108 \quad (2)$$

Snowmelt Season: $$\text{if } SYLC < 100 \text{ cfs}, FA = 4.24*SYLC \quad (3a)$$

$$\text{if } 100 < SYLC < 200 \text{ cfs}, FA = 2.19*SYLC \quad (3b)$$

$$\text{if } SYLC > 200 \text{ cfs}, FA = 0.2*SYLC \quad (3c)$$

To get to the total flow at SYWA, the equation used was

$$SYWA = FA + SYLC + CCB_i \quad (4)$$

where CCB_i is the typical CCB gaged flow for the i^{th} season. For the dry season of the study period (August 2009-November 2009), the actual observed CCB_{dry} was commonly 4–7 cfs with an average of 6.0 cfs. Two large rainstorms occurred in October 2009. For the wet (December 2009-March 2010) the actual observed CCB_{wet} was commonly ~4.5–12 cfs with an average of 7.5 cfs. For the snowmelt seasons (April-July 2009 and April-July 2010) the actual observed CCB_{snow} was commonly was ~5–15 cfs for the majority of the time that no major snowmelt runoff was present and > 100 cfs when it was. All of these values are higher than the required minimum flows from CCB, which are 2 cfs November-March and 3 cfs April-October.

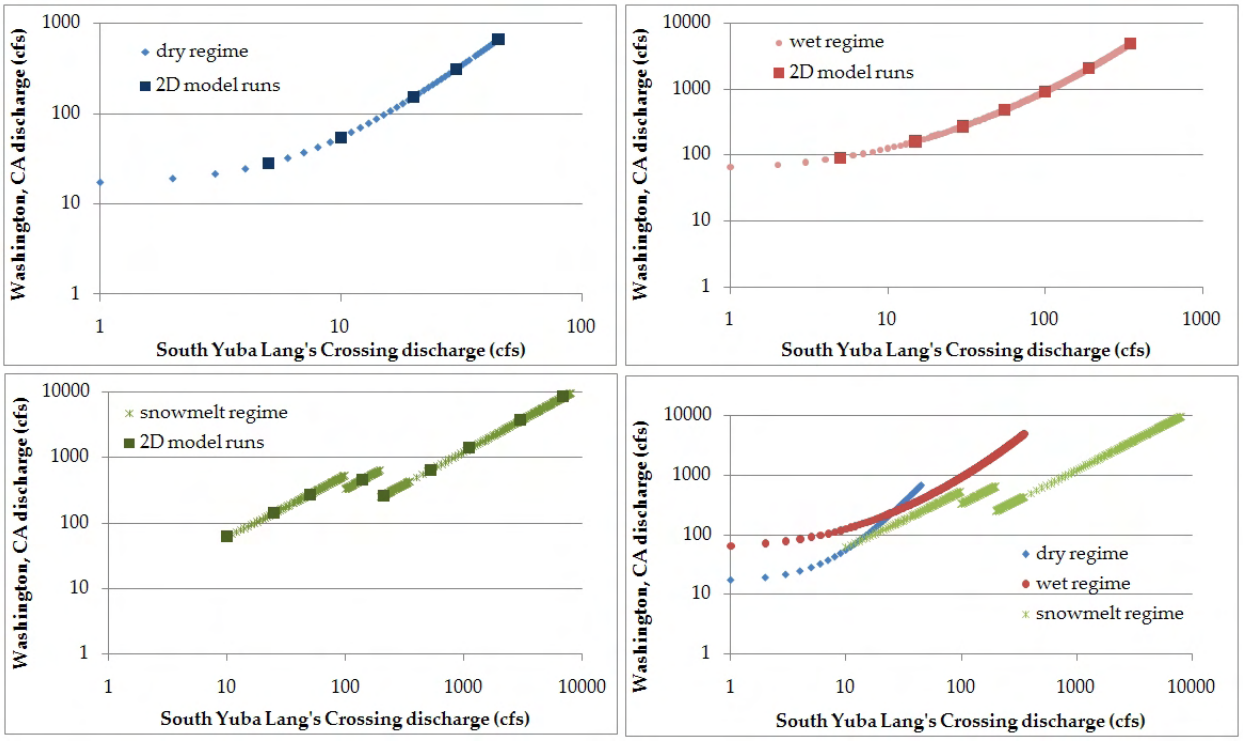

Figure 36. Season-stratified synthetic flow regimes for estimating the discharge of the South Yuba River at Washington, California based on gaged flows at Lang's Crossing, and accounting for flow accretion and gaged flow inputs on Canyon Creek below Bowman Lake.

5.5 Distributing Flow Accretion to Tributaries

Based on the comparative analysis of flow accretion at SYWA and SYJB, there was a consistent relation between accretion ratio and watershed area. As a result, the total flow accretion estimated for SYWA was divided among the key tributaries according to their watershed areas (

Table 6). Values for the watershed areas of these tributaries were obtained (in units of acres) from Figure 2 (PDF document page 78) of Appendix A of UYRSPT (2007). Among these areas, the largest contributor is lower Canyon Creek, which is fed by its own large tributary, Texas Creek (Figure 9).

Table 6. Watershed area of each major tributary between SYLC and SYWA.

Tributary*	Area (km^2)	Area (acres)	% of Total Area
Rucker Creek	11.87	2932	10%
Fall Creek	27.64	6829	23%
Lower Canyon Creek	57.43	14191	47%
Diamond Creek	12.68	3134	10%
Scotchman Creek	12.61	3116	10%
Total Area	122.22	30202	100%

*Tributaries ordered in the downstream direction from Spaulding Dam

5.6 Direct Flow Accretion Observations

Analyzing historical gage data to develop synthetic flow accretion relations was a useful way to take advantage of available data to meet project needs. An effort was made to collect discharge observations in 2010 to evaluate current flow accretions and test the utility of the synthetic relations based on 1965–1972 data. As explained in section 3.8.1, wadable cross-sections were unsuitable for discharge gaging, including at the key locations for evaluating flow accretion. Instead, discharges were estimated in the field using a boat-based ADCP system, as described in section 3.5. This technology was tested in several locations at different flows, but site conditions were also unfavorable to its use at the most important location, in Washington, California at the exit cross-section for the 2D model. At this location there are standing waves at most discharges, making lateral transit by kayak in an upstream position difficult. The cross-section was also deep across most of the width, so wadable discharge measurements could not be done either. Kayak measurements were attempted in the next pool downstream of the exit cross-section, but it had undercut bedrock banks with bypass flow and could not be measured properly with the ADCP. Washington Creek junction with the South Yuba was 300 m downstream of the exit cross-section, and the channel in between the two was too shallow and filled with boulders, had flows oriented cross-channel, or had undercut bedrock banks with bypass flow.

The two locations where flow accretion was checked by direct observation were (1) on Canyon Creek in the pool just upstream of its confluence with the South Yuba River in the vicinity of the Maybert Road bridge and (2) on the South Yuba River just downstream of the confluence with Canyon Creek in a transition type morphological unit (see definition in section 8.3). There is no backwater influence of the South Yuba on Canyon Creek, as the tributary is separated from the mainstem South Yuba by waterfalls after a small flow diversion structure that provides drinking water to Washington, CA. ADCP flow measurements at the mouth of Canyon Creek were divided by the CCB gaged flows for the same 15-minute time point (provided by Nevada Irrigation District) to calculate Canyon Creek flow accretion. This value was compared against the Canyon Creek flow calculated using the gaged CCB value plus the Canyon Creek fraction of flow accretion estimated using the appropriate seasonal regression equation for the date of flow observation. A similar suite of calculations were made for the South Yuba River above Canyon Creek by subtracting the observed Canyon Creek flow from the observed combined Canyon Creek and Yuba River flow just downstream of their confluence. These observations were

compared against the sum of SYLC gaged flows plus the tributary proportional flow accretions for Rucker, Fall, and Diamond creeks estimated using the appropriate synthetic seasonal flow relation for the dates of observation.

By the time the hydrologic analysis was far enough along to demonstrate the need for direct observations, it was already the snowmelt season of 2010. Based on project priorities, it was only possible to collect observational discharge data during the 2010 snowmelt period. The observations were made on May 5, May 24, June 22, and July 19. Discharge measurements on July 19 were taken only on Canyon Creek. Combined SYLC and CCB gaged flows that were observed spanned 13.3 to 936 cfs. Because the topographic map and 2D model were made using SI units, ADCP measurements and associated analyses were performed in SI units as well.

The following questions were evaluated using this observation data:

- How do snowmelt synthetic flow relations based on the 1965–1972 period compare to direct observations made in snowmelt season 2010?
- Are flow accretions presently observed in the study segment?
- Do the snowmelt synthetic flow relations based on the 1965–1972 period show systematic bias in the prediction of flow accretions?

For each data collection date on Canyon Creek, ADCP discharge values were higher than gaged releases (

Table 7), so flow accretion ratios greater than one were observed for every measurement. Flow accretion ratios ranged from 1.12–9.93. Two low-accretion ratio values of 1.12 and 1.19 were observed during releases of 456 cfs and 300 cfs, respectively, from Bowman Lake. Two high-accretion values of 7.36 and 9.93 occurred on days when baseflow-type conditions of 9.96 cfs and 4.31 cfs, respectively, were gaged. The prediction of Canyon Creek total discharge for June 22 (1.12 ratio) using the synthetic regression relations was under-predicted by -5% from the observed value using the ADCP. Prediction versus observed in this case was very closely matched. Total discharge for May 24 (1.19 ratio) and July 19 (9.93 ratio) was under-predicted -45% and -34%, respectively. These two ratios are far apart, with the 1.19 ratio suggesting little accretionary input while the 9.93 ratio suggests quite high accretion input, yet both are under-predicted. Total discharge for May 5 (7.36) was over-predicted by 161%. Three of four discharge measurements on Canyon Creek were under-predicted, with two of the three (-5% and -45%) occurring during high flow releases. Under-predictions suggest that there was more unregulated watershed runoff than expected based on the 1965–1972 synthetic flow relations. The over-prediction, on the other hand, suggests less unregulated runoff than expected based on the 1965–1972 synthetic flow relations. The variability in predictions suggests that there is no systematic bias in current-day 2010 flow accretion predictions using the 1965–1972 synthetic flow relations. Although three observations under-predict accretion an average -27.3%, one of those predictions was just -5% from its prediction. If the large, 161% over-prediction is included in an average of the four values, the average becomes +19% with a standard deviation of 96.2%. The large over-prediction coupled with three under-predictions suggests that variability in current-year hydroclimatic factors (e.g. percent of snowpack remaining on a given day, daily temperature fluctuations within the melt-freeze cycle, and snow-melting rate) dominates over the influence of any interdecadal secular drying trend.

ADCP discharge measurements for South Yuba River above Canyon Creek were higher than gaged releases in two of the three days of data collection (

Table 7). No discharge measurements for this parameter were collected on July 19, so this dataset consists of three discharge measurements compared to the four measurements from Canyon Creek. Flow accretion ratios ranged from 0.85 to 3.53. No days of measurement were at baseflow conditions. The accretion ratio was highest at 3.53 when flow was 318.2 cfs, which under-predicted the 1965-1972 synthetic flow relation discharge by -20%. Two low-accretion ratios of 0.85 and 1.01 were calculated for flows of 154 and 487 cfs, respectively; with expected discharge values over-predicted 126% and 7%, respectively. Gaged discharge predicted discharges similar to those collected on Canyon Creek, yet only the June 22 predicted discharges were somewhat similar to one another, +7% versus -20%. Overall, one value was a small under-prediction, one was a small over-prediction, and one had a large over-prediction, which is similar to the range of Canyon Creek discharge data.

The observations that were made confirm the existence of significant flow accretions and demonstrate that the synthetic relations based on the 1965–1972 record do not systematically over-predict actual flow accretions, with four of seven values under-predicted, one value very close to zero, and two high over-predictions. The historical analysis showed that flow accretions vary significant during the snowmelt season (Figure 34), so whether historical conditions or adjusted present-day conditions are used, there may be too much inherent variability to derive consistently precise and accurate predictions. The mean difference in flow accretion between 1965–1972 and 2003–2009 is small relative to the variability in flow accretion. The analysis would have benefitted from more discharge measurements, but this was not the central focus of the overall project. Additionally, more advanced ADCP technology now exists for shallow rivers, but it was not available for this study.

5.7 Stage-Discharge Relation

2D modeling requires knowledge of the WSE at the downstream end of the model match the total discharge passing that point, which is known as the stage-

Data collected in 2009 yielded a stage-discharge relation for flow ranging from (0.42475–200.65 m^3/s). The relation is stratified into four discharge ranges for empirical fitting, with breaks at 10, 25, and 45 m^3/s (

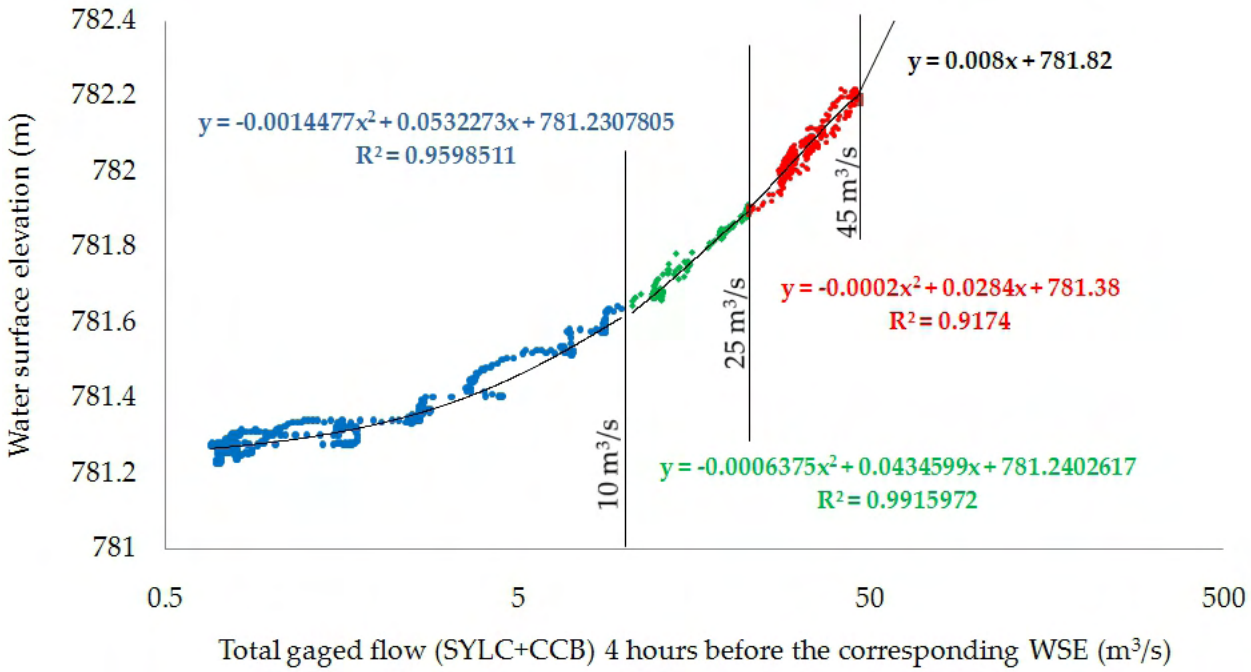

Figure 37). Regression analysis found that the three discharge ranges ending at 45 m^3/s with 15-minute observational data could be fit with 2nd-order polynomial equations with r^2 values >0.91.

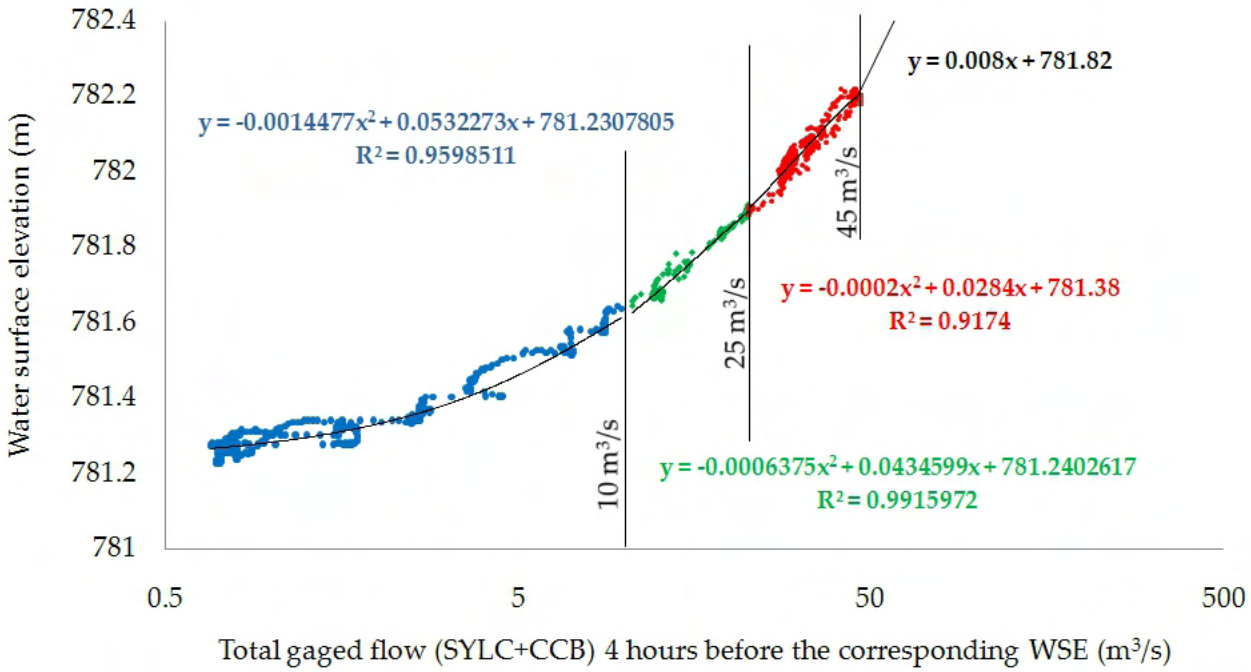

Figure 37 shows the equations. For flows ranging from 45–200.65 m^3/s, there were only two observations available at either end of the range, so a line was fit between them. Stage-discharge points for gaged flows <10 m^3/s show some hysteresis, but above 10 m^3/s that is not evident.

Table 7. Direct observations of flow accretions and testing of synthetic relations.

Metric	South Yuba River above Canyon Creek	Canyon Creek at terminus
May 5, 2010		
Gaged flow (m^3/s)	2.549	0.282
Observed Q using ADCP (m^3/s)	9.01	2.075
Observed flow accretion ratio	3.53	7.36
1965-1972 flow accretion ratio	4.24	n/a
Expected Q using snowmelt regression (m^3/s)	7.21	5.41
% difference expected to observed	-20%	161%
May 24, 2010		
Gaged flow (m^3/s)	5.097	8.495
Observed Q using ADCP (m^3/s)	4.36	10.14
Observed flow accretion ratio	0.85	1.19
1965-1972 flow accretion ratio	0.2	n/a
Expected Q using snowmelt regression (m^3/s)	9.86	5.53
% difference expected to observed	126%	-45%
June 22, 2010		
Gaged flow (m^3/s)	13.592	12.9
Observed Q using ADCP (m^3/s)	13.78	14.45
Observed flow accretion ratio	1.01	1.12
1965-1972 flow accretion ratio	0.2	n/a
Expected Q using snowmelt regression (m^3/s)	14.75	13.74
% difference expected to observed	7%	-5%
July 19, 2010		
Gaged flow (m^3/s)	n/a	0.122
Observed Q using ADCP (m^3/s)	n/a	1.213
Observed flow accretion ratio	n/a	9.93
1965-1972 flow accretion ratio	n/a	n/a
Expected Q using snowmelt regression (m^3/s)	n/a	0.8
% difference expected to observed	n/a	-34%

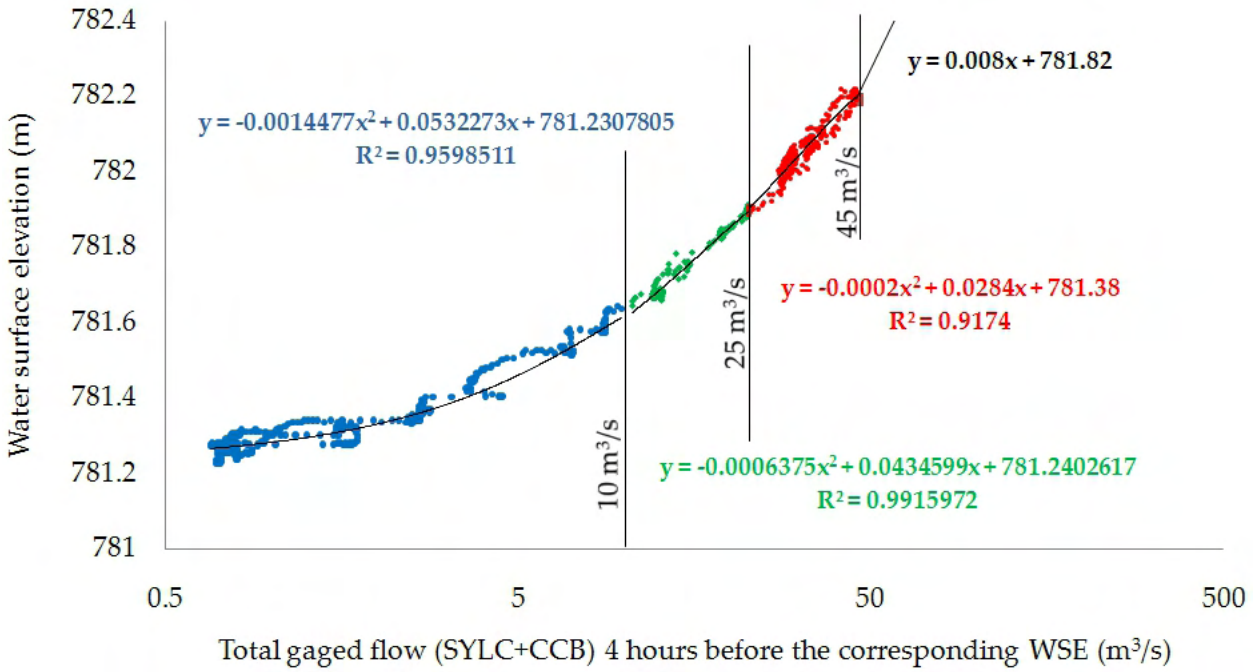

Figure 37. Stage-discharge relation for the downstream terminus of the 2D model, based on direct observations. Discharge is not the local value at the cross-section, but the upstream gaged values.

5.8 Hydrologic Uncertainties

In this study, hydrologic analysis was a critical step necessary to understand the relative roles of gaged and ungaged flows influencing the study segment. Ungaged accretionary flows at Washington, California are several times bigger than the gaged flows, making them an essential requirement of hydraulic and physical habitat analysis. Using the available data, robust synthetic equations were developed to estimate flow accretion at Washington and distribute it among source tributaries. Considering all factors, secular differences 1965–1972 versus 2003–2009 were not accounted for, because there was no way to quantify the amount of change due to (1) ephemeral temporal hydroclimatological variability, (2) hydropower facility upgrades and operational adjustments affecting withdrawals and releases, and (3) land use and land cover changes affecting water losses and the runoff/precipitation ratio. There is substantial certainty that no historical secular trend is associated with human-induced climatic change, though that could change in the future. Furthermore, it was found that for the snowmelt season at least, the mean difference in flow accretion between 1965–1972 and 2003–2009 is small relative to the variability in flow accretion, so making further adjustments cannot overcome the remaining sources of uncertainty in the data to yield a significantly improved synthetic prediction. Considering that streamflow gages are maintained at hydropower facilities upstream of the study segment, it is unfortunate that ungaged areas exist downstream, impacting the level of certainty of instream flow analysis.

The following assumptions influence the results of this study:

- Gaged flows are accurate estimates of actual flows.

- Ungaged accretionary flows between SYLC and SYWA for past, present, and future conditions are represented by those quantified in the 1965–1972 record.
- Season-stratified accretionary flows are represented by the regression relations presented in section 5.6.
- Total accretionary flow may be distributed among the major tributaries in proportion to their watershed area; this shifts inputs from any small tributaries not considered as well as those from throughflow and groundwater (that are distributed along the entire length of the study segment), to the locations where the major tributaries enter the study segment of the upper South Yuba River.

CHAPTER 6:
2D Hydrodynamic Modeling

At this moment in the development of river science, a paradigm shift is taking place. Traditionally, analysis of rivers has relied on cross-sections, longitudinal profiles, and top-view observations to obtain characteristic geometric values. The cost, slow-speed, and limitations of traditional topographic and bathymetric surveying methods precluded the use of detailed maps in quantitative river assessment. These assessment methods have been fine-tuned to get the most out of available data, but with the advent of digital elevation modeling and geographic information systems as well as an array of faster, inexpensive, detailed, and increasingly accurate mapping technologies, it is possible to re-conceive what should be involved in performing river assessments. That is the purpose of the next component of this study, which is described in this section.

Two-dimensional (depth-averaged) hydrodynamic (2D) models have existed for decades and are increasingly used to study a variety of hydrogeomorphic processes (Bates et al. 1992; Leclerc et al. 1995; Miller and Cluer 1998; Cao et al. 2003; Brown and Pasternack 2008; Sawyer et al. 2010). Recently, their use in regulated river rehabilitation emphasizing spawning habitat rehabilitation by gravel placement has been evaluated (Pasternack et al. 2004; Pasternack et al. 2006a; Wheaton et al. 2004a; Elkins et al. 2007). 2D models have also been applied to better understand the relative benefits of active river rehabilitation versus flow regime modification (Jacobson and Galat 2006; Brown and Pasternack 2008) on regulated rivers. In several of the above examples, 2D models were used to quantify the spatial pattern of physical habitat for individual fish species in specific life stages at specified discharges and/or to quantify the spatial pattern of sediment transport potential at specified discharges (see also Moir and Pasternack 2010). Notably, those previous studies were limited to short river areas, usually consisting of 1–10 geomorphic units over 50–2000 m of channel length. That may be adequate to reveal local processes and test site-scale project designs, but it is not adequate for comprehensive instream flow analysis of a long river segment.

As stated in section 1.1, the primary goal of this study was to show the practical capability and cost-effectiveness of performing instream flow assessment over a relatively large spatial extent and at a high resolution. It is hypothesized that achieving a near-census of the physical conditions in a mountain river would enable a better predictive linkage between river landforms, flow and transport processes, quality and distribution of physical habitats, and diverse ecological functions. Today, it may be infeasible to quantitatively link these facets across the spatial and temporal scales at which they occur, but new methods in river science are emerging so quickly that it such goals may be foreseeable in the near future. Mechanistic, predictive modeling will be a key tool in reaching this objective.

In this study, a 2D model was developed, tested, and applied to the South Yuba River study segment to explore opportunities and constraints in using a 2D predictive tool to provide a mechanistic foundation to instream flow analysis. Not only was the size of the model notable, but also the application of it to a steep mountain river. Previous site-scale 2D models in mountain rivers include Rathburn and Wohl (2003) and Harrison and Keller (2007). Those studies yielded mixed results in terms of model performance, with the earlier study showing difficulties in predicting fine-sediment deposition and the later study successfully explaining channel-maintenance mechanisms.

The specific questions that were exclusive to the 2D model component of this study included the following with respect to a steep mountain river with a high ratio of bed roughness to water depth:

- How accurate is a 1-m resolution 2D model in predicting WSE and velocity magnitude?
- What are the characteristics of hydraulics at segment, reach, and morphological-unit spatial scales as a function of discharge?
- What is the joint probability distribution of depth and velocity at the segment and morphological-unit scales as a function of discharge?
- Can 2D model results be used to delineate morphological units at the sub-width spatial scale, and would such units have statistically significant associations amongst themselves?
- Does flow convergence and divergence explain the spatial pattern and resilience of morphological units?
- How does sediment transport change as a function of discharge?
- What are the quantities, qualities, and spatial structures of physical habitats for different fish species in different life stages at the segment and morphological-unit spatial scales as a function of discharge?

By linking landform, processes, and habitats, the application in this study of a 2D model aims to demonstrate the capability of providing a more holistic assessment of instream flow conditions than may be obtained using current standard methods, while also providing a far more detailed characterization founded on mechanistic principles. The underlying philosophy is that it is not enough to know the answer to a question, but that the answer should be based on mechanistic principles rather than simply on empirically derived point data extrapolated across long longitudinal rivers. The reason for this stringency is that river systems are dynamic. With an inflexible estimate such as those found in some of today's river assessments, there is no ability to predict change, understand why it happens, or adapt to it. A mechanistic prediction enables all of those vital capabilities, and it even provides a framework for active management of flow and channel form (Wheaton et al. 2004 a,b). These are the hopes for what 2D modeling can offer instream flow assessment. A primary motivation for this study was to assess whether 2D models prove accurate enough to be reliable, thus pushing river science forward in the use of 2D modeling.

Many different 2D hydrodynamic models exist, each with different trade-offs. Examples of specific models include SRH-2D, FESWMS, HIVEL, RMA2, TUFLOW, TELEMAC-2D, FLO-2D, RIVER2D, MIKE-21, and MD_SWMS. Models vary based on the coordinate system they use (Cartesian or curvilinear), the exact form of the fluid-mechanics equations they solve, the numerical solution method (finite difference, finite element, or finite volume), ability to handle supercritical and/or subcritical flow, robustness of wetting/drying algorithm, ability to solve steady and/or unsteady flows, method(s) for handling turbulence closure, and differences in ancillary features and add-ons. Often the specification of one model or another simply rests on user experience, availability, and cost, because model results are usually similar among them all. Direct comparisons of FESWMS vs. SRH-2D for 5 gravel-bed river sites in the Central Valley

of California yielded an almost identical outcome (Pasternack, unpublished data). FESWMS does better with very high velocities, but SRH-2D is dramatically more computationally efficient. For this study, the key criteria were (a) ability to cope with supercritical and transitional flow conditions, (b) expandability to cope with a large computational mesh, and (c) model speed and stability.

6.1 2D Model Development

In this study, the 2D model known as Sedimentation and River Hydraulics—Two-Dimensional model (SRH-2D) v. 2.1 was used to predict hydrodynamics. The Surface-water Modeling System (SMS) v. 10.1 graphical user interface (Aquaveo, Inc.) was used for pre- and post-processing model inputs, parameters, and outputs. SRH-2D v. 2.1 focuses specifically on 2D modeling of river systems by using the depth averaged St. Venant equations:

$$\frac{\partial h}{\partial t}+\frac{\partial hU}{\partial x}+\frac{\partial hV}{\partial y}=e \qquad (5)$$

$$\frac{\partial hU}{\partial t}+\frac{\partial hUU}{\partial x}+\frac{\partial hVU}{\partial y}=\frac{\partial hT_{xx}}{\partial x}+\frac{\partial hT_{xy}}{\partial y}-gh\frac{\partial z}{\partial x}-\frac{\tau_{bx}}{\rho}+D_{xx}+D_{xy} \qquad (6)$$

$$\frac{\partial hV}{\partial t}+\frac{\partial hUV}{\partial x}+\frac{\partial hVV}{\partial y}=\frac{\partial hT_{xy}}{\partial x}+\frac{\partial hT_{yy}}{\partial y}-gh\frac{\partial z}{\partial y}-\frac{\tau_{by}}{\rho}+D_{yx}+D_{yy} \qquad (7)$$

where t is time, x and y are horizontal Cartesian coordinates, h is water depth, U and V are depth-averaged velocity components in x and y directions, respectively, e is excess rainfall rate, g is gravitational acceleration T_{xx}, T_{xy}, and T_{yy} are depth-averaged turbulent stresses, D_{xx}, D_{xy}, D_{yx}, and D_{yy} are dispersion terms due to depth averaging, $z = z_b + h$ is water surface elevation, z_b is bed elevation, ρ is water density, and τ_{bx}, τ_{by} are the bed shear stresses (friction). Bed friction is calculated using the Manning's roughness equation as follows:

$$\begin{pmatrix}\tau_{bx}\\ \tau_{by}\end{pmatrix}=\rho C_f\begin{pmatrix}U\\ V\end{pmatrix}\sqrt{U^2+V^2};\quad \mathrm{C_f}=\frac{gn^2}{h^{1/3}} \qquad (8)$$

where n is the Manning's roughness coefficient. This 2D model is capable of simulating steady, unsteady, subcritical and supercritical flows. With several waterfalls present in the study segment, having these capabilities was crucial. 2D models of the same type as SRH-2D are not morphodynamic; they cannot explicitly simulate channel changes, such as longitudinal profile adjustments or bed material coarsening.

In order to solve these St. Venant equations a finite-volume numerical method is needed, and that requires the use of a computational mesh. SMS software was used to build such meshes. In designing a mesh, there are three primary choices that have to be made: (1) model domain, (2) mesh structure, and (3) mesh-element resolution. Answers to these choices depend on the range of flows to be modeled, the resolution of topographic survey data, and the complexity of channel morphology.

6.1.1 Computational Mesh Design

Computational mesh design involves a creative process of selecting a model domain (area of river to be simulated), specifying the structure of the numerical system for efficient solution, and setting the resolution of the model in a way that is consistent with the needs of the scientific questions and the capabilities of the available data inputs.

In terms of model domain, one option is to simulate the entire width of the river corridor and accept much longer computational times than strictly required for low flows, because so much extra dry area is being modeled. The advantage is having a single mesh for all runs, but depending on available time it may time-prohibitive. In this study, it was decided to create one smaller mesh that was more efficient for lower flows and another mesh capable of running all flows, but primarily used for higher flows. The other aspect of model domain was deciding whether to model the entire 12.2-km river segment as a single mesh or to break it up into multiple meshes run independently. The advantage of multiple meshes is that they can be run in parallel reducing the total duration of each simulation, but that could be problematic because a stage discharge relation is necessary for the terminus of each mesh. A work-around when there is only one stage-discharge relation (at the end of the river segment) and the choice is made to break a river segment into two or more models is to use the downstream model's water surface elevation prediction for its upstream boundary as the downstream input for running the upstream model. For this study, it was decided to break the river roughly in half, with the upstream mesh going for the top of the mapped area down to a point upstream of the junction with Canyon Creek and the downstream mesh spanning from that end point down to Washington, California (Figure 38). Some observations were made at the downstream boundary of the upstream model, but many values were taken from the downstream model's solution at the upstream boundary.

In terms of the spatial organization of the mesh, there exists the concept of a "structured mesh". A structured mesh is one in which there is a uniform Cartesian grid that enables high-speed computation. An unstructured mesh is one in which the grid may deform to better represent the underlying complexity of a natural surface. Locations of abrupt widening are an example where an unstructured mesh is needed. Also, in some situations it is preferable to use a lower resolution over large floodplains and a higher resolution in the channel, which requires using both structured and unstructured mesh areas. In the case of the South Yuba River, the river was confined by proximal hillsides, so it was decided to use as uniform of a mesh element size as possible. Consequently, suitable areas were given a structured mesh with predominantly quadrilateral elements for the entire river width, and where necessary, unstructured mesh areas with both quadrilateral and triangular elements were placed in between structured mesh areas. Mesh nodes were assigned elevations by standard TIN interpolation of the total set of DEM (x,y,z) topographic points imported from GIS into hydrodynamic modeling software as a comma-delimited text file.

In terms of mesh-element resolution, the decision of how to proceed depends on factors such as channel complexity, size and number of emergent boulders and islands, and the required resolution of outputs to answer specific scientific questions. In this study, the final topographic data set included mixed resolutions. LIDAR data from open areas of the river corridor, including on in-channel boulders, had points on a ~0.3x0.3 m^2 grid, while ground-based data had points on a ~5x5 m^2 grid. Bathymetric data was intermediate in resolution. The primary factor used to constrain grid size was that at low flow there are thousands of emergent boulders

and boulder clusters in the wetted channel. These features play a critical role in creating 2D hydrodynamic complexity in reality, so any resolution that ignored those features was deemed untenable. At first, meshes with a ~2-m internal distance were tested under the difficult challenge of simulating the low summer baseflow, but model results were poor quality due to too many emergent boulders and boulder clusters falling entirely within a single cell or with just 1–2 nodes representing what should have been individual boulders. Next, meshes with ~1m internodal spacing were tested. For the 1-m test starting from a dry condition, it took ~14 days for a single low-flow run to converge on a solution, but the results showed that this resolution represented the majority of the boulders identified in the LIDAR data. Reducing the mesh down to a ~0.5-m internodal spacing was considered by the researchers as that spacing would likely yield the best boulder representation, but halving the size of the meshes would require four times as many mesh elements, possibly requiring 40-60 days to solve a single low-flow model, which was considered too time-intensive for this study. Several other exploratory mesh constructions were considered and tested, such as unstructured meshes with higher resolution in the vicinity of boulders and lower resolution away from them, but this approach yielded unstable model runs. Unstructured, uneven resolution meshes with "holes" in them (i.e. forced dry areas regardless of flow) at each emergent boulder were also attempted, but were also found to be unstable. In the end, meshes with ~1-m internodal spacing were found to produce the best compromise of model performance and run time, so those were used in the study.

A common concern with mesh resolution in the emerging subdiscipline of ecohydraulics is the extent to which the resolution of a computational mesh should conform to the scientific questions associated with organisms <0.5 m long, such as fry and juvenile fish. Motile aquatic organisms have the option of choosing their location and orientation in the flow to balance needs/wants against energy expenditure. For each size of organism, there exist correspondingly sized flow obstructions that create 3D eddies with resting habitat. 2D hydrodynamic models can simulate 2D eddies (Crowder and Diplas 2000), but no one has carefully tested the accuracy of 2D eddy simulation to confirm their suitability for use in evaluating and quantifying eddy habitats. Further, most 2D models (including the SRH-2D features used in this study) use a simple fluid-mechanics approach to coping with turbulence that causes momentum to spread too effectively to generate the sharp "eddy fence" boundaries that exist in natural mountain streams, especially at the sub-meter spatial scale (MacWilliams et al. 2006). Finally, most natural eddies are not 2D, but are fully 3D. Rotational eddies behind emergent flow obstructions include a "whirlpool" suction effect at the onset of the eddy and a "boil" upwelling further downstream. The stronger the shear in rotational eddies between the ambient flow and the slackwater in the lee of the obstruction, the greater the 3D effect. Eddies caused by submerged bed protrusions cause vertical eddies flowing over the top of the obstruction, while complex 3D obstructions, such as logs, roots, and branches protruding into the middle of the flow, cause complex 3D eddies. All of these velocity structures impact 2D modeling, and the smaller the mesh resolution attempted, the more uncertain the prediction becomes. Consequently, even though there is a strong scientific interest in resolving sub-meter fluid mechanics for instream flow assessment, the physics of real mountain rivers violates the mathematical assumptions of 2D hydrodynamic models at the sub-meter spatial scale. A user can choose to specify <0.5-m mesh resolution, but in reality there is no substantive meaning to doing so—one is not actually resolving the fluid mechanics at that scale by making this choice. The consequence is that an assumption is made that there is a link between habitat utilization by small organisms and the

hydraulics at the >1-m spatial scale. There is high uncertainty in this assumption, but this is the state of the art at this time, and nevertheless uses more accurate mechanistic equations than those in 1D models. Some more sophisticated 2D and 3D models exist to handle micro-turbulence structures, but topographic and bathymetric data would have to be collected at the same scale. Red-LIDAR now provides topographic data at a sub-meter scale, but some issues exist between theoretical and actual results using LIDAR (section 3.2). Currently there is no proven method for bathymetric measurement at the centimeter scale in natural mountain rivers, although it may come soon with the improvement of green-LIDAR technologies.

The final suite of 2D models included four computational meshes with 1-m intermodal spacing (Figure 38). The downstream low- and high- flow meshes had 331,593 and 467,272 elements, respectively. The upstream low- and high- flow meshes had 284,461 and 396,615 elements, respectively. For each flow-regime simulation, the results from the two reaches were merged to create a single dataset file for evaluation in GIS.

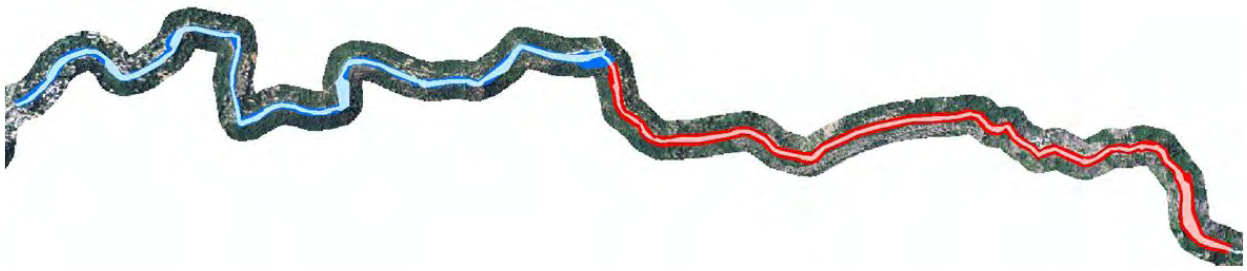

Figure 38. The study segment was divided into two modeling areas (blue and red), and then a low-flow and high-flow mesh was created for each area (low=light blue and red, high=light+dark blue and red). Underlying the meshes is a clipped 2005 NAIP image.

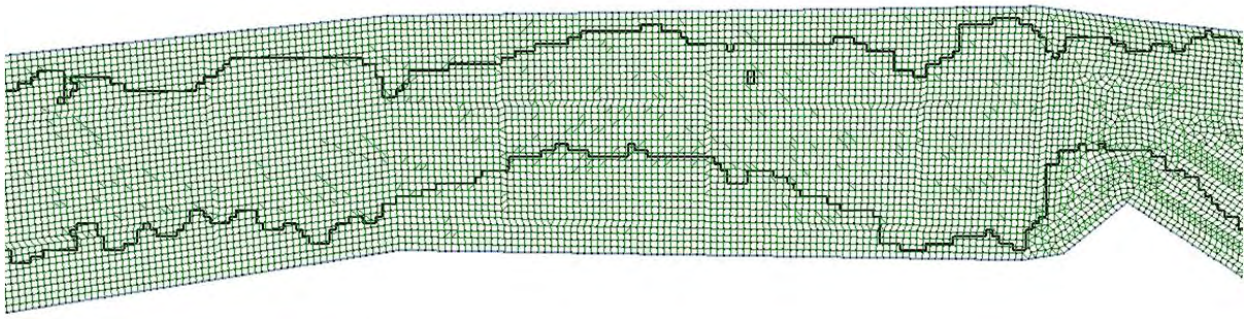

Figure 39. Sample of an area of the highflow downstream computational mesh. Black line is wetted boundary, green quadrilaterals and triangles are computational elements (~1x1 m^2). Some of the illustrated area has a structured grid, with the far right illustrating an unstructured grid.

6.1.2 2D Model Inputs

To run a 2D model, discharge at the upstream boundary and at all tributary inflow junctions is needed along with the corresponding WSE at the downstream boundary. A thorough hydrological analysis (Chapter 0) determined that significant accretionary flows were present.

The mechanisms for these additional inputs varied, depending on the timing of three different flow regimes (dry season, wet season, or snowmelt season; section 5.1). To determine the total amount of accretionary flow, season-specific synthetic regression relations were developed (section 5.6), and the total accretionary flow was distributed to the major tributaries according to their relative watershed areas. For the upstream 2D model, the inflow at the upstream boundary equaled the Lang's Crossing gaged flow value plus the estimated Rucker Creek accretionary flow. Fall Creek and Diamond Creek inputs were assigned based on their estimated accretionary flow values. For the downstream 2D model, the inflow at the upstream boundary equaled the Lang's Crossing gaged flow value plus the estimated accretionary flows for Rucker, Fall, and Diamond Creeks. The Canyon Creek input equaled the CCB gaged flow plus the estimated lower Canyon Creek accretionary flow. The Scotchman Creek input was assigned based on its estimated accretionary flow value.

The town of Washington, California withdrawals water from Canyon Creek just before the tributary joins the mainstem South Yuba River and withdrawals are not monitored in real-time for Washington usage. The local water operator estimated that 10,000 gallons of water use per day (0.0155 cfs) is used during non-irrigation periods and up to 50,000 gallons per day (0.0774 cfs) during peak use in the summer. These values are <0.6% of gaged flows in Washington, California and do not include accretionary additions, so this withdrawal was not included in the 2D model. If withdrawals increased substantially, future model runs could reduce Canyon Creek tributary inflow by that amount.

Because there is no discharge gage in Washington, California, the WSE-the downstream flow boundary was constructed using data from 2009 matching gaged discharge of SYLC and CCB with the observed downstream WSE (

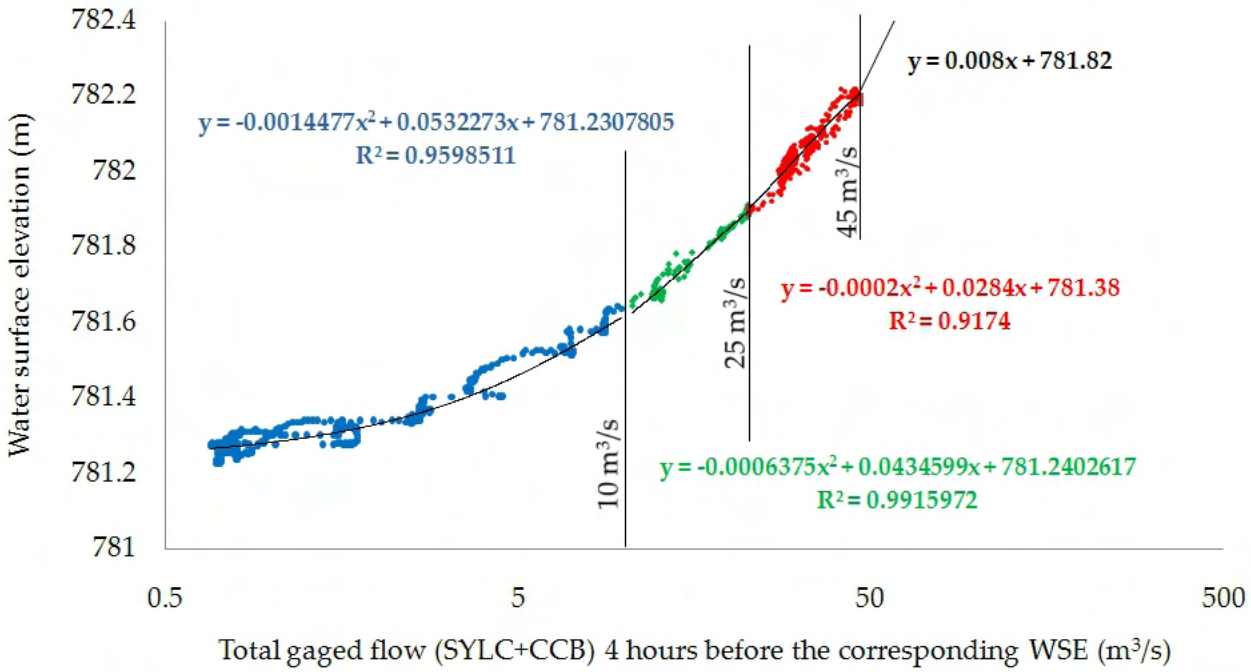

Figure 37). The result is a high-quality stage-discharge relation, but this approach does not account for flow accretion explicitly. It assumes that the flow accretion observed in 2009 is representative of other years, which is unlikely to be the case. Given the uncertainty in the 1965–1972 flow-accretion analysis, it could take more than a decade of observations to generate suitable stage-discharge relations, because there is so much temporal variation in flow accretions (Figure 33 and Figure 34,

Table 7). Additional explanation might come from groundwater monitoring and/or a better understanding of local hydrometerological mechanisms. These are fundamental uncertainties for instream flow analysis in mountainous streams with ungaged tributaries at this time.

The complete arrays of specific discharge and downstream WSE inputs to every 2D model simulation are given in sections 6.2 (validation simulations) and 6.2.5 (synthetic simulations).

6.1.3 Bed Roughness Boundary Condition

The two primary bed roughness model parameters in SRH-2D are approximated using variable Manning's n for a gravel/cobble bed and isotropic kinematic eddy viscosity (E). Roughness associated with resolved bedform topography (e.g., rock riffles, boulders, gravel bars, etc.) was explicitly represented in the detailed channel DEM. Two-dimensional model predictions are highly sensitive to DEM inaccuracies (Bates et al. 1997; Hardy et al. 1999; Lane et al. 1999; Horritt et al. 2006), requiring high-resolution topographic mapping as a data collection method. The bed-roughness parameter can vary spatially in a 2D model to account for variable bed sediment facies. However, local roughness deviations (< 0.005) are expected to be insignificant relative to the limitation of field-measurement accuracy in cobble/boulder bedded rivers comparable to the South Yuba. 2D models have been reported to be sensitive to large (> 0.01) variations in n values (Bates et al. 1998; Lane and Richards 1998; Nicholas and Mitchell 2003).

Bed roughness was initially assessed for the base flow condition, for which the most WSE data was available. For unresolved roughness elements smaller than resolved bedform topography, Manning's coefficient (n) was initially guesstimated as 0.06 for deeper areas and 0.08 for shallow areas, with both values consistent with the USGS photo library of Manning's n values for different site conditions (http://wwwrcamnl.wr.usgs.gov/sws/fieldmethods/Indirects/nvalues/index.htm) (Figure 40). After simulating the base flow for the whole river, WSE tests showed that the model was under-predicting depths and that the differentiation between deep and shallow areas was insignificant. It was determined that the greater relief between bed crests and troughs was the dominant control on longitudinal WSE variation, not local bed roughness. As a result, a few higher values of roughness coefficients were tested and it was found that a uniform value of 0.10 worked best (i.e. yielded the lowest deviations between observed and modeled WSE values; see section 6.2). Higher n-values yielded excessive depths, lower values yielded insufficient depths.

In rivers with simple, uniscalar roughness associated with bedforms, Manning's roughness coefficients decrease with increasing depth and increasingly uniform flow conditions. However, 2D modeling studies in gravel-bed rivers characterized by multiple spatial scales of landform heterogeneity have found that roughness does not decrease with increasing depth (Brown and Pasternack 2008; Pasternack 2008b; Sawyer et al. 2010). As water rises in these rivers, the water column makes contact with new types of roughness elements such as boulder clusters, bedrock outcrops, vegetation, and valley width variations. As a result, high roughness is maintained through increasing discharges. Based on assessment of the types and scales of channel roughness present at different observed flows, the confined, cobble/boulder South Yuba matched this latter profile, so the roughness value of 0.1 was maintained through all investigated flow regimes. Further, because this value was high, a judgment was made that it would be adequate to represent the roughness associated with inundated vegetation at high flows. Vegetation was one of several roughness elements associated with landform

nonuniformity present over the range of scales investigated, but it did not seem any rougher than cobble clusters and small boulders not explicitly represented in the model's topography. This assumption was evaluated using WSE and velocity observation at higher flows that inundated vegetation (see sections 6.2.3–6.2.4).

Figure 40. Comparison of USGS photo of Rock Creek near Darby Montana with n=0.075 (left, viewing upstream) and a steep inset channel site in the study area (right, viewing downstream). However, model tests indicated multiple scales of channel nonuniformity not captured with this n-value, which suggests higher roughness than is evident in this photo comparison of a single site in the South Yuba project area against a reference USGS photo.

6.1.4 Eddy Viscosity Turbulence Closure Parameterization

In a study of 2D model sensitivity for a bedrock channel, Miller and Cluer (1998) showed that 2D models are particularly sensitive to the eddy viscosity parameterization used to cope with turbulence. In the model used in this study, eddy viscosity (E) was a variable in the system of model equations, and it was computed using the following standard equations developed from many studies of turbulence in rivers (Fischer et al. 1979; Froehlich 1989):

$$E = e^{*} H \cdot u_{*} \tag{9}$$

$$u_{*} = U\sqrt{C_{d}} \tag{10}$$

$$C_{d} = g\frac{n^{2}}{H^{1/3}} \tag{11}$$

where H is water depth, e is the eddy viscosity coefficient (assigned a value of 0.6 for this study based on several past investigations (e.g. Wheaton et al. 2004b; Brown and Pasternack 2008), u* is shear velocity, U is depth-averaged water velocity at a point, C_d is a drag coefficient, g is the gravitational acceleration constant, and n is the Manning's n roughness parameter value at a point. These equations allow E to vary throughout the channel, which yields more accurate transverse velocity gradients. However, a comparison of 2D and 3D models for a shallow gravel-bed river demonstrated that, even with this spatial variation, rapid lateral variations in velocity are not simulated to the degree that occurs in natural channels, presenting a fundamental limitation of 2D models like FESWMS and SRH-2D (MacWilliams et al. 2006). This study included some visual assessment of the occurrence of eddies between observation and simulation, but there was no formal velocity direction validation. The kayak-based method would be suitable for that, but it was not adopted until too late to achieve such a goal.

6.1.5 2D Model Result Outputs

The raw model outputs are hydraulic variable values at all computational mesh nodes. The variables are WSE (m), depth (m), velocity component in the east-west direction (m/s), velocity component in the north-south direction (m/s), velocity magnitude (m/s), Froude number, and bed shear stress (Pa). Because the mesh nodes are not evenly spaced (section 6.1.1), it was necessary to re-sample them into an equal-area grid for further analysis. To do this, model results at computational mesh nodes were used to build TIN-based surface models that were then re-sampled to 0.5-m resolution raster grids. These grids provided an equal-area basis for further analysis. The 0.5-m grids were not used for any statistical testing that might be problematic because of the over-densification of data relative to the original topographic survey point density that is much lower. The dense gridding was only used for calculations that require equal-area analysis, such as computing the average velocity for each morphological unit.

6.2 2D Model Validation

Two-dimensional models have inherent strengths and weaknesses, thus uncertainty in modeled results needs to be understood and accepted (Van Asselt and Rotmans 2002). Brown and Pasternack (2009) compare and contrast the uncertainties among 1D, 2D, and 3D models. Previous studies using 2D hydrodynamic models for gravel-bed rivers have validated 2D modeling for use in that setting and provide valuable information regarding model utility and uncertainty (Pasternack et al. 2004, 2006; Wheaton et al. 2004a; MacWilliams et al. 2006; Elkins et al. 2007; Brown and Pasternack 2008). However, in this study the river setting is far more complex. The South Yuba study segment has waterfalls, extensive areas of emergent boulders and cobble/boulder clusters, gravel bars and islands, and vegetation. Manning's n was set to minimize the deviation between the observed and predicted longitudinal profile of water surface elevation, and final model values were within the physically realistic realm. Predicted and observed conditions at independent locations were compared to provide an assessment of model capability and uncertainty.

The ability of 2D models to accurately predict depth, velocity, and bed shear stress in a gravel/cobble bed river was tested in the most detail by Pasternack et al. (2006) on an artificially constructed riffle-pool section of the lower Mokelumne River, CA. Depth error was primarily attributable to inadequacies in the DEM, which in that case had a relatively high resolution of 1 point per 1.14 m^2, but which was still too low to resolve small humps and depressions influencing point measurements. Error in 2D model velocity prediction averaged 29%. More than half of this error was attributable to depth prediction error. Despite depth and velocity error, 56% of tested 2D model predictions of shear velocity were within the 95% confidence limit of the best field-based estimation method. Ninety percent of the error in shear velocity prediction was explained by velocity prediction error. Using different testing approaches, Pasternack et al. (2006) and Macwilliams et al. (2006) came to the same conclusion; that bed shear stress that was predicted using depth-averaged velocity over-predicts actual bed shear stress in a systematic way, and that multiplying the shear-stress estimate by a factor of 0.51 yields the best adjustment.

A suite of model tests was performed to characterize the uncertainty in the 2D model of the South Yuba study segment. Table 8 and Table 9 provide information about each 2D model

validation simulation. Tests included mass conservation checks at three cross-sections in each validation simulation, baseflow WSE validation, and velocity validation for all flows.

In contrast to prior 2D modeling studies done at the site scale, this study undertook the challenge of maintaining the same focus on 1–10 m process-scale details, but increasing the domain of the effort an order of magnitude and in a remote and rugged mountainous region. Given the constraints on data collection at this scale, the evaluation of 2D model performance is as much a test of the data collection effort to generate model inputs as it is a test of the numerical model itself. Ultimately, the 2D model was found to have a similar level of uncertainty as typically seen with 2D models in general, even though the model was applied in a far more challenging setting and over a much larger domain, which is a highly promising outcome. Still, the larger the spatial extent and the more diversity of data-collection methods that are used, the more risk there is of adding more and different types of uncertainties into the analysis.

Table 8. 2D model input and parameter values for validation runs using downstream meshes.

				Discharge Inputs (m^3/s)			
Flow Simulated	n	e	WSE (m)	South Yuba River	Canyon Creek	Scotchman Creek	Total Discharge
Low-flow mesh							
Baseflow	0.1	0.6	781.25	1.2025	1.1528	0.222	2.5773
1/7/10	0.1	0.6	781.26	1.795	1.6452	0.3238	3.764
3/9/10	0.1	0.6	781.273	2.5299	2.2762	0.4529	5.259
High flow mesh (may be used for any flow)							
5/5/10	0.1	0.6	781.45	9.005	2.075	0.4318	11.5118
5/24/10	0.1	0.6	781.63	4.36	10.14	0.5088	15.0088
6/22/10	0.1	0.6	782.12	13.7786	14.45	0.2619	28.4905

Table 9. 2D model input and parameter values for validation runs using upstream low-flow mesh.

				Discharge inputs (m^3/s)			
Flow simulated	n	e	WSE (m)	SYLC plus Rucker Creek	Fall Creek	Diamond Creek	Total Discharge
Low-flow mesh							
Baseflow	0.1	0.6	867.93	0.4922	0.4868	0.2235	1.2025
3/9/10	0.1	0.6	868.499	1.0782	0.995	0.4567	2.5299

6.2.1 Mass Conservation Checks

In a river with a highly complex terrain, there is a risk of poor model performance with mass conservation, especially at low flows. Achieving good mass conservation means that the river discharge at the downstream boundary of a model is nearly the same as the sum of the

discharges assigned to the upstream flow boundaries. Ideally, what comes out should exactly equal what goes in, but that is numerically impossible, because computers calculate approximations of solutions to analytical equations. It is also important to consider as a reference for evaluating the significance of model uncertainty that stream gages and other discharge measurement methods themselves have uncertainty, and, sometimes substantial error. Flumes and weirs are typically in the 0.1–3% uncertainty range (Ackers et al. 1978), while stage-gage relations are in the 5–10% error range (USGS 1992). In comparison, the error in mass conservation in a 2D model can be anywhere in the 0.01–2% range, so typically smaller than the uncertainty in the gage measurements. For each simulation, mass conservation was checked at three cross-sections inserted into the models relative to the specified flow inputs, with one located near the top of the model, one midway through it, and one near the end. Table 10 shows that flow losses between cross-sections was very low. Mass conservation losses increased in the downstream direction, because error accumulates with the extent of the domain, especially with such a complex river setting. Considering the uncertainty in specifying flow accretions, mass conservation was not a problem for the simulations performed in this study.

Table 10. Mass conservation checks at three cross-sections in each 2D model validation test.

	2D model flow loss (%)		
Flow simulated	XS1	XS2	XS3
Downstream low-flow mesh			
Baseflow	0.019	0.47	0.83
1/7/10	0.022	0.41	0.6
3/9/10	0.021	0.19	0.36
Downstream high-flow mesh			
5/5/10	0.021	0.08	0.15
5/24/10	0.02	0.09	0.13
6/22/10	0.008	0.04	0.07
Upstream low-flow mesh			
Baseflow	-0.001	1.07	1.9
3/9/10	0.002	0.44	0.79

6.2.2 Baseflow WSE Validation

The first key test of model performance was the test of the ability of the 2D model to match the LIDAR-measured baseflow WSE. In past studies, typically 10–100 WSE or depth observations were used to test model performance (Lane et al. 1999; Gard 2003; Wheaton et al. 2004b; Pasternack et al. 2004, 2006; Harrison and Keller, 2007; Brown and Pasternack, 2008; Moir and Pasternack 2008), with Stewart (2000) having the most with 80-160 per model. In this study, the dataset of LIDAR-measured water surface elevations on the date of the LIDAR survey was compared against the 2D model predictions. The intercomparison dataset consisted of 17,198 pairs of LIDAR and 2D model points, which is two to three orders of magnitude more than previous studies. Given that there is elevational uncertainty in the LIDAR data (Table 3), the

expectation for the test is that the elevational uncertainty in model WSE predictions should be about the same as the uncertainty in the topographic data itself. The LIDAR survey was instrumental in having such a robust dataset with which to compare to model point data.

The results of the test found that the uncertainty in baseflow WSE (Table 11) was lower than the uncertainty in LIDAR topographic elevations relative to ground-based topographic elevations (Table 3). The mean deviation (including positive and negative values) between LIDAR estimated and 2D model predicted WSE was -0.028 m, with the mean of the absolute value of deviations 0.12 m. One-half of the WSE point deviations were within 0.1 m of the corresponding LIDAR data point (Table 11). When WSE deviations were stratified by morphological unit type (section 8.4), model performance varied by type. Transitions showed the best matching, while pools showed the worst (Table 12). The histogram of deviations shows a near equal balance of points with over- versus under-predictions (Figure 41). Over-predictions beyond 0.1 m were uniformly distributed up to 0.5, whereas under-predictions were predominantly in the 0.1–0.25 m bin. Surveying methods for a highly heterogeneous bed and water surface condition, such as in a remote mountain river, are not as precise as for an easily accessed lowland river. Model performance for comparable metrics can then be expected to have variability of about the same scale. Model-predicted WSE variability was smaller than observed bed topographic variability.

Table 11. Percent of baseflow WSE deviations meeting different thresholds of performance.

Threshold (m)	% Data Within
0.025	14%
0.05	34%
0.1	51%
0.25	91%

Table 12. 2D model WSE performance stratified by morphological unit type.

Morphological unit	*n*	Absolute Value Median WSE Deviation	% Data Within 0.05 m	% Data Within 0.1 m
Transition	4402	0.067	40%	60%
Plane bed	3814	0.093	35%	51%
Inset Channel	2059	0.101	21%	50%
Chute	553	0.104	23%	49%
Steep Inset Channel	807	0.123	19%	40%
Pool	5539	0.13	36%	45%

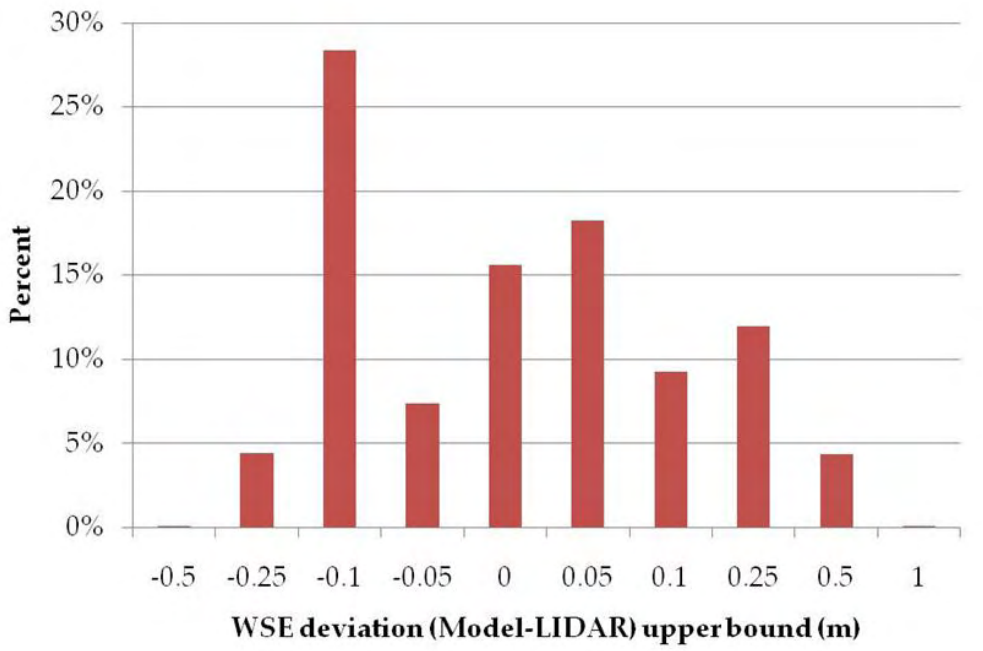

Figure 41. Histogram evaluating 2D model WSE performance, with deviations centered on zero.

6.2.3 WSE Validation at Various Flows

An analysis of WSE model performance was done for the moderate flows observed on May 5, 2010, May 25, 2010, and June 22, 2010. For each date, WSE observations were made along the bank within view of the Leica total station and its reflectorless surveying capability. Because the priority for these observation dates was velocity and discharge observation, the total number of WSE observations is limited to 27 points, compared to the 17,198 points from the baseflow analysis. This small dataset is insufficient to yield conclusions with any certainty, but is included for completeness. Using the observed points, all 2D model predicted WSEs except one were too low. The mean deviation was -0.16 m. All of these data except one point were within 0.31 m of the observed values (

Table 13). The performance is worse than observed for the baseflow WSE validation (Table 11). One component of the difference in error may stem from the variability inherent in the calibration between ground-based and LIDAR-determined elevations (Table 3). However, the high-flow WSE deviations exceed those, so that cannot account for the whole difference. Another factor is that the number of points for the analysis is very small. Finally, it is possible that channel roughness might be higher for this range of higher flows, but then the velocity ought to be over-predicted for these flows, and as the next subsection reports, that was not the case. To get a 0.16 m increase in WSE by adjusting the channel roughness parameter takes a much larger parameter value than is realistic.

Table 13. Percent of WSE deviations at various flows meeting different thresholds of performance.

Threshold (m)	% Data Within
0.025	1%
0.05	9%
0.1	30%
0.25	88%
0.35	99%

6.2.4 Velocity Validation for Various Flows

After the test of baseflow WSE, the next important test evaluated the overall performance of the 2D model to predict velocity magnitude. For this test, the 2D model values of velocity magnitude at each observational location for all flows and morphological units were put into a single scatter plot. In hydrological modeling, it is very rare for modelers to show head-to-head scatter plots, and in hydraulic modeling it is not always done either. One argument against a raw scatter plot is that it does not convey an understanding as to why individual points are deviating from a one-to-one line. Instead, cross-sectional comparisons are often used to illustrate the lateral pattern in velocity deviations, which may then be explained by the role of the eddy viscosity assumption and/or patterns of topographic variability (Pasternack et al., 2004, 2006). However, in this study cross-sectional data collection was not considered viable (section 3.5). A head-to-head scatter plot of observed versus predicted velocity magnitude provided the most rigorous test of model performance with velocity prediction.

To obtain a benchmark for what 2D model performance is typical for scatter plot tests, a survey of past studies using this type of test was conducted. Studies by Lane et al. (1999), Gard (2003), Pasternack et al. (2006), and Moir and Pasternack (2008) typically used 20-100 test points per model, with Stewart (2000) using 80-160 test points per model. In these studies, r^2 values varied widely from 0.4–0.6, with the exception of Stewart (2000) with values of ~0.8–0.9.

The procedure for performing the test was to make a scatter plot of observed surface velocity as a function of 2D model predicted velocity, then perform a least square regression analysis to get the r^2 value. Next, the surface velocities were adjusted by a scaling coefficient <1.0 until the slope between the two was as close to 1.0 as possible. This scaling step had no effect on the r^2 value, but did change the value of the slope parameter (m) in the resulting slope-line equation. Finally, the scaling coefficient was assessed to determine if it was in the range typically reported from studies that measure the ratio between observed mean and surface velocities, which is ~0.65–0.8. For the lower Mokelumne River, Pasternack et al. (2006) found a scaling value of 0.71 by least square regression (Figure 26).

The results of the 2D model velocity test found that model performance was good relative to common benchmarks reported in the literature. The r^2 value for the scatter plot was 0.607 (Figure 42), which is on the high side of literature values. Given 273 points, this value is statistically significant above the 99.99% confidence level. The least-squares-regression optimal scaling coefficient for relating mean and surface velocities was found to be 0.74, which is very close to the field-observed value of 0.71 from Pasternack et al. (2006). After applying that scaling factor, the mean deviation between observation-based and predicted depth-averaged velocities

was -0.07 m/s and the mean of the absolute values of deviations was 0.18 m/s. In terms of error percent, the median error was 28%, which is in the same 20–30% range reported in the literature cited above as benchmarks for this study. Only 20% of points were within 10% error, while 94% were within 100% error (Table 14). When test results were stratified by morphological unit, significant differences were observed, and they were not the same as those found for the WSE tests. Whereas model-predicted pool WSE values were the least accurate, their velocity values had the strongest r^2 value (

Table 15). This r^2 value of 0.8 is on par with the best results reported for 2D model velocity tests by scatter plot in the literature. The only unit type with no correlation between observed and predicted velocities was the steep inset channel, and even then the median error of 25% was within the range of the other unit type median errors. Steep inset channels had the highest bed roughness (Chapter 8.0), which likely explains the randomness of the error as a function of observed velocity magnitude.

Velocity tests found no distinction in model performance based on the discharge. As stage increases, the zone of the river containing any given velocity bin was observed to shift outward. Since the floodplain is composed of the same coarse bed material as the perennial channel, this shift did not cause any threshold change in processes. Consequently, model performance within safely measurable velocity bins (depth-average values of 0–2 m/s) is independent of discharge in the study segment.

This study tested a 2D model in the most challenging hydraulic and geomorphic conditions to date reported in the literature. A primary goal of this project was to test the limits of 2D modeling capabilities in a mountain river context. 2D model performance for all morphological units other than step/waterfalls was similar to studies reported in much simpler gravel-bed rivers. Only a few observations were made on steps/waterfalls, and the outcome was that the model performed poorly for those units; there is too little data to present quantitative statistics and interpretation, and was not an objective for this study. There is no escape from the inherent limitations of a 2D model that are already well known and were discussed earlier (e.g. simplistic turbulence closure, sensitive to the resolution of topographic mapping, can't simulate sub-meter hydraulics accurately, can't handle flow through wood-jams and other "strainers"), but the finding that 2D models performed as well in this remote, highly heterogeneous river corridor as in easy accessible, simple channels is noteworthy.

Table 14. Percent of 2D model velocity predictions meeting different thresholds of performance.

Error %	% Data Within
5	9%
10	19%
25	46%
50	81%
100	94%

Table 15. 2D model velocity magnitude performance stratified by morphological unit type.

Morphologic unit	N	Median Error (%)	r^2
Chute	3	21	n/ a
Pool	56	30	0.8
Transition	46	27	0.79
Plane bed	86	24	0.64
Floodplain	31	29	0.57
Inset channel	31	36	0.41
Steep inset channel	20	25	0.06

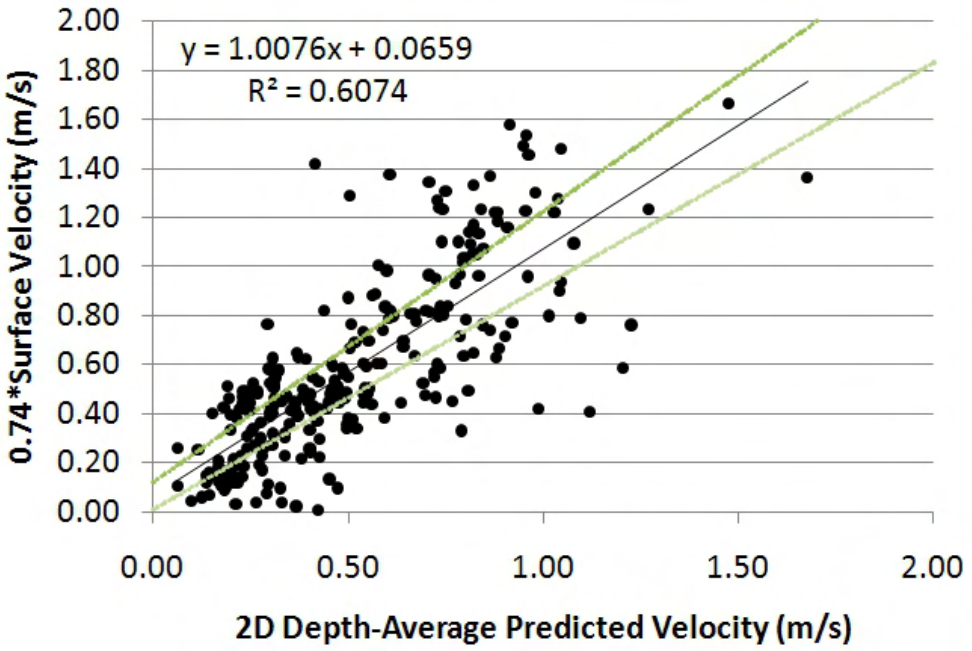

Figure 42. Scatter plot test of 2D model velocity magnitude performance relative to observed surface velocities. Green lines are 95% confidence limits.

6.2.5 Synthetic 2D Model Simulations

After characterizing the uncertainties in the 2D models of the study segment of the South Yuba River through a substantial suite of 2D model validation tests, the next step involved performing simulations of unobserved flow conditions. As explained in section 5.1, the South Yuba River exhibits three distinct seasonal flow regimes, wet (November-March), snowmelt (April-July), and dry (July-October). The study plan did not originally propose to perform simulations of seasonal hydrologic conditions, but the hydrologic analysis led to that requirement in order to follow the science as it unfolded. With a goal of evaluating specific fish life stages as they occur during specific times of the year, it would be inappropriate to lump annual hydrology into a single flow regime. To span the hydraulics associated with each of the

three flow regimes, five to nine discharges were simulated, depending on how wide of a range of discharges was relevant to each hydrologic season. The dry season only spanned 5–50 cfs on the SYLC gage, so fewer incremental 2D simulations were modeled. The discharges selected in dry, wet, and snowmelt seasons were based on SYLC flows and were spaced in roughly equal intervals to cover the hydrologic regime (

Table 16,

Table 17,

Table 18, Figure 36).

For each SYLC gaged flow chosen for synthetic simulation, the corresponding relevant CCB gaged flow was assigned. For example, for the dry season used as the value for CCB, since that was the typically observed flow for that study. The minimum required flow is lower, but often facility operators do not use lowest value permitted, in case the gaging is inaccurate, causing them to violate requirements. The SYLC 1103 and 6971 cfs snowmelt season flows were actual WSE data were collected by the research team, so actual CCB values were used simulations. The CCB gaged flow for the intervening 3000 cfs simulation was between those for the SYLC 1103 and 6971 cfs values. For the combined SYLC flows, the stage-discharge relation (

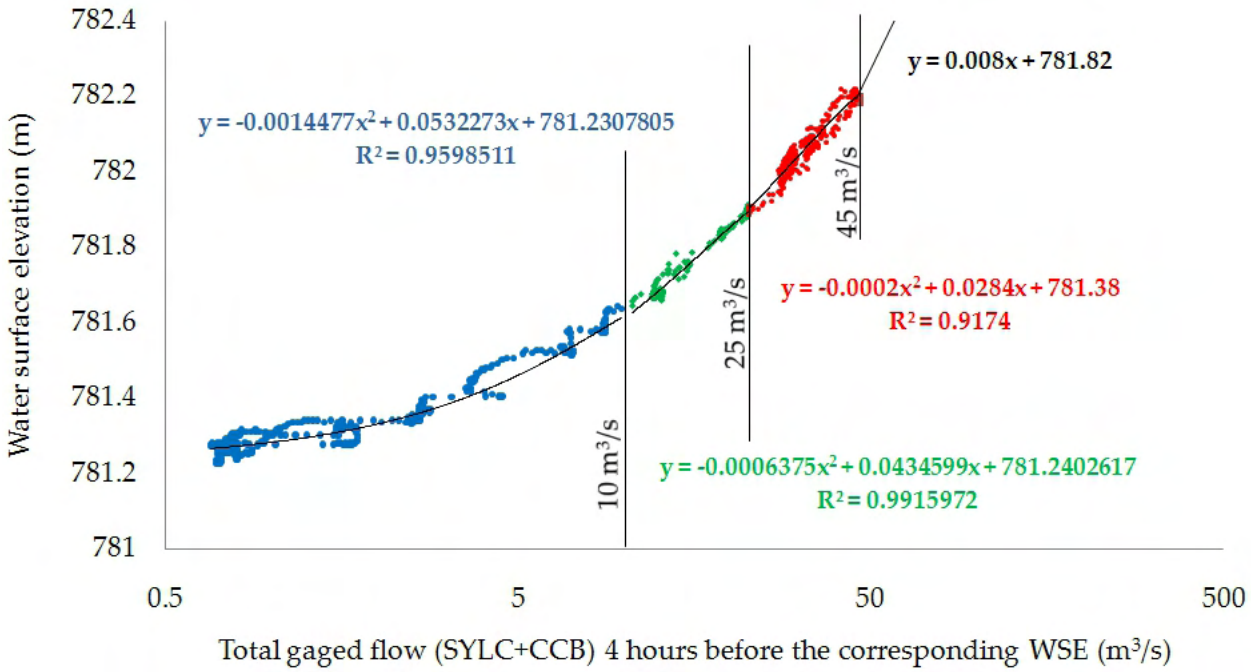

Figure 37) was used to estimate the downstream WSE for the downstream model. For the SYLC gaged flows, the season-stratified synthetic flow accretion relations (Figure 33; equations 1–4) and proportional watershed areas were used to estimate major tributary inflows (see section 5.5). The downstream 2D model for each flow was performed first to obtain the WSE at the upstream boundary of the downstream model from the downstream model output. This value was input as the downstream boundary WSE for the upstream 2D model at the corresponding flow. There was no suitable location for direct stage-discharge gaging for the upstream model and since the primary range of flows occurred within the first 2 weeks of the project, there was no time to assess where such 2D model breaks would be located.

Other nuances to the use of SMS 10.1 and SRH-2D v. 2.1 were relevant, but are beyond the scope of this report. Every measure was taken to perform the highest quality 2D model simulations with the data and tools available. Technological advances continue to enable more efficient model development and faster model run times.

Table 16. 2D model input and parameter values for dry season simulations.

Downstream models			Discharge inputs (m^3/s)			
SYLC (gaged cfs)	CCB (gaged cfs)	WSE (m)	South Yuba River	Canyon Creek	Scotchman Creek	Total discharge
5	5	781.25	0.3591	0.381	0.0526	0.7927
10	5	781.25	0.7649	0.6718	0.1164	1.5531
20	5	781.27	2.1202	1.8516	0.3755	4.3473
30	5	781.28	4.2002	3.829	0.8097	8.8389
45	5	781.3	8.6791	8.2907	1.7893	18.7591

Upstream models			Discharge inputs (m^3/s)			
SYLC (gaged cfs)	CCB (gaged cfs)	WSE (m)	SYLC plus Rucker Creek	Fall Creek	Diamond Creek	Total discharge
5	5	867.7255	0.191	0.1152	0.0529	0.3591
10	5	867.83	0.3927	0.2551	0.1171	0.7649
20	5	868.0299	0.9196	0.8229	0.3776	2.1201
30	5	868.2095	1.6114	1.7745	0.8143	4.2002
45	5	868.4278	2.9579	3.9215	1.7997	8.6791

Table 17. 2D model input and parameter values for wet season simulations.

Downstream models			Discharge inputs (m^3/s)			
SYLC (gaged cfs)	CCB (gaged cfs)	WSE (m)	South Yuba River	Canyon Creek	Scotchman Creek	Total Discharge
5	10	781.25	1.0678	1.3024	0.2238	2.594
15	10	781.27	2.0653	2.0886	0.3964	4.5503
30	10	781.29	3.6565	3.3723	0.6783	7.7071
55	10	781.32	6.5618	5.7905	1.2093	13.5616
100	10	781.38	12.5891	11.0212	2.3578	25.9681
190	10	781.49	27.7204	24.8687	5.3984	57.9875
350	10	781.62	64.7502	60.634	13.2516	138.6358

Upstream models			Discharge inputs (m^3/s)			
SYLC (gaged cfs)	CCB (gaged cfs)	WSE (m)	SYLC plus Rucker Creek	Fall Creek	Diamond Creek	Total Discharge
5	10	867.8857	0.3522	0.4905	0.2251	1.0678
15	10	868.0238	0.7978	0.8688	0.3987	2.0653
30	10	868.1672	1.4878	1.4866	0.6822	3.6566
55	10	868.3491	2.6953	2.6503	1.2163	6.5619
100	10	868.5622	5.0503	5.1674	2.3714	12.5891
190	10	868.8034	10.4598	11.8311	5.4296	27.7205
350	10	869.16	22.38	29.0421	13.3281	64.7502

Table 18. 2D model input and parameter values for snowmelt season simulations.

Downstream models			Discharge inputs (m^3/s)			
SYLC (gaged cfs)	CCB (gaged cfs)	WSE (m)	South Yuba River	Canyon Creek	Scotchman Creek	Total Discharge
10	10	781.26	0.8006	0.8526	0.125	1.7782
25	10	781.28	2.0016	1.7068	0.3126	4.021
50	10	781.32	4.0031	3.1305	0.6252	7.7588
140	10	781.43	7.6712	4.3626	0.8957	12.9295
210	10	781.51	6.4543	0.842	0.1227	7.419
525	10	781.7	16.1358	1.6802	0.3068	18.1228
1103	81	782.17	33.901	5.229	0.644	39.774
3000	108	782.52	92.2046	11.0414	1.7529	104.9989
6921	165	783.44	212.716	23.089	4.044	239.849

Upstream models			Discharge inputs (m^3/s)			
SYLC (gaged cfs)	CCB (gaged cfs)	WSE (m)	SYLC plus Rucker Creek	Fall Creek	Diamond Creek	Total Discharge
10	10	867.8372	0.4009	0.274	0.1258	0.8007
25	10	868.0165	1.002	0.6851	0.3144	2.0015
50	10	868.1927	2.0041	1.3702	0.6288	4.0031
140	10	868.4566	4.8072	1.9631	0.9009	7.6712
210	10	868.4832	6.062	0.2689	0.1234	6.4543
525	10	868.7	15.1549	0.6723	0.3085	16.1357
1103	81	868.93	31.84	1.412	0.648	33.9
3000	108	868.9891	86.5999	3.8416	1.763	92.2045
6921	165	870.18	199.786	8.863	4.067	212.716

CHAPTER 7:
"1D Model" Hydraulic Sampling

7.1 "1D Model" Concepts

As summarized in section 2.1.1, instream flow assessments of all sorts have been done using a diversity of approaches by practitioners with widely varying educations and experiences. It is common for key terms and jargon to be used in discussions of instream flow assessment, but in fact they often mean different things to different subsets of practitioners. As a result, it is necessary to clarify some terms and concepts before moving forward, especially because this study was not done from within the relicensing practitioner community, but rather as a broader academic exercise.

Among the approaches that use hydraulic variables to quantitatively determine instream flows, IFIM and the PHABSIM program suite (Waddle 2001) (or its more recent software derivatives) are now commonly used in FERC relicensing (e.g. DWR 2004) and physical habitat assessment more broadly (e.g. Hatfield and Bruce 2000). It is beyond the scope of this study to describe and explain PHABSIM. Gallagher and Gard (1999) found that PHABSIM-predicted weighted usable area has significantly related to redd densities and locations at microhabitat and mesohabitat scales for Chinook salmon spawners in California. Moir et al. (2005) subsequently tested PHABSIM's predictive ability for Atlantic salmon at one riffle-pool site in Scotland and found a statistically significant correspondence between predicted habitat and conditions fish utilized. Nevertheless, according to Lamb et al. (2004), even though PHABSIM is favored for its scientific basis, "there is little body of evidence in the peer reviewed literature that tests the assumptions of the model." Thus, there are promising results at specific sites, but continued evaluation and awareness of uncertainties is warranted.

Discussing PHABSIM in concrete terms is complicated by the on-going competition among advocates and critics of different methods of obtaining hydraulic information at different spatial scales and resolutions (e.g. Leclerc et al. 1995; Geist and Dauble 1998; Parasiewicz 2007; Williams 2010). In one common approach used right now, PHABSIM involves obtaining hydraulic variables at points on cross-sections. Colloquially, the term "1D" is used in river science to describe any approach that involves cross-sections, because the primary emphasis of analysis is between cross-sections along the length of a river, not assessment of lateral variations. The PHABSIM software suite is intended to provide a statistical sampling of river hydraulics using the set of points where observations and estimations are made, not as a cross-section intercomparison tool, so the "1D" moniker is a misnomer. Ghanem et al. (1996) argued that the method should be termed a "zero-dimensional approach", because it involves no spatial component at all. PHABSIM hydraulic methods actually sample 2D hydraulics (lateral and longitudinal), but the gap between cross-sections is often larger than what is used in a 2D hydrodynamic model, as detailed in Chapter 0. Also, PHABSIM hydraulic methods are not designed to represent near-continuous hydraulic patterns, whereas a 2D hydrodynamic model is meant for that very purpose.

Hydraulic engineers limit the term "1D model" to refer to a numerical method for solving a set of fluid-mechanics equations that are simplified to yield just the cross-sectionally averaged values of water surface elevation and velocity along the length of a river (Brown and Pasternack 2009). This type of 1D model is available as one option for computing hydraulics in the

PHABSIM program suite and its recent derivatives. However, the moniker "1D model" used in instream flow assessment is not limited to that choice, but is used for any and all methods that rely on cross-sections. Even though PHABSIM does not necessarily include a hydraulic numerical model, the final product is a predictive statistical relation between flow and weighted useable habitat (Hatfield and Bruce 2000).

7.2 Methodological Comparison Goals

At the beginning of Chapter 0, the rapid transition in river science toward digital elevation modeling and associated analytical methods was discussed. An important step in the paradigm shift is to make the best effort possible to compare different methods, evaluate the sources of uncertainty, and decide the circumstances under which the existing paradigm is adequate to meet current needs. According to a needs analysis for instream flow assessment by Cox (2007), "Methodological assessment, standardization, and comparison studies were identified as a priority research need across the range of stakeholder groups and were seen as a means of increasing both the procedural efficiency and ecological effectiveness of FERC licensing." This study was sponsored to provide such an assessment as part of its future visioning, and this report has aimed to do so.

Unfortunately, comparison is confounded by the fact that different paradigms are built on incommensurate ideas and methods, and thus yield different quantities and types of results and interpretations. As practitioners develop new, creative analyses unique to the results produced by each method, comparison becomes even less feasible. There is no one definitive metric that indicates whether an approach is satisfactory or if two particular approaches are similar, because analyses are built in a step-by-step fashion, with each step including choices about assumptions, methods, and interpretations. It is reasonable for different practitioners to make different choices based on their experience and local project needs.

Previous studies (Waddle et al. 2000; Wu and Mao 2007; Brown and Pasternack 2009; Sawyer et al. 2010) have found reasonable comparisons at the site scale when considering channel landforms that are orthogonal to the banks and poor comparisons when flow has a strong oblique component. Hydraulic differences become amplified when extrapolated through nonlinear habitat suitability curves or sediment transport equations, but that can be offset by lumping calculated values into broad habitat or transport-regime categories (Brown and Pasternack 2009). In a study focusing specifically on habitat, Wu and Mao (2007) concluded that PHABSIM and RHABSIM are "less capable of simulating microscale or complex river environments accurately". None of these previous efforts attempted the scale of comparison performed in this study, and none focused specifically on remote mountain regions.

In this study, the methodological-assessment component involved comparing many hydraulic and physical habitat metrics in an effort to illustrate how different approaches perform and to "triangulate" an overall conclusion coming at the problem from different directions. Given the breadth, complexity, and timeline of the undertaking, no pre-conceptions as to what the outcome would be were formulated at the start of the study. As academic scholars with no stake in the outcome, the study's investigators had no preference or bias for a particular outcome in the comparison. The lead investigator has recently published journal articles relying on 1D methods (e.g. Escobar and Pasternack 2009) and 2D methods (Elkins et al. 2007), and a combination of both (Brown and Pasternack 2008; Brown and Pasternack 2009; Sawyer et al. 2010), so the approach was to let the results speak for themselves, however they turned out.

The scientific questions asked in the methodological assessment revolved around the topic of characterizing hydraulics and habitat in a long river segment of a remote mountain river with a high ratio of bed roughness to water depth. Specific questions are detailed in Chapters 0 and 0, but the broad questions involved the following:

- Head-to-head, when mechanistic numerical models are made for long river segments using standard approaches, do 1D and 2D models yield similar cross-sectionally averaged depths and velocities?
- How do transect-based estimates, 1D numerical models, and 2D numerical models compare in prediction of morphological-unit averaged hydraulics as a function of discharge?
- How do transect-based estimates, 1D numerical models, and 2D numerical models compare in prediction of morphological-unit averaged physical habitat indices as a function of discharge?
- How do transect-based estimates, 1D numerical models, and 2D numerical models compare in prediction of physical habitat area as a function of discharge?

7.3 "1D Model" By Transect Analysis

A common method used as part of IFIM and the PHABSIM software suite involves selecting representative cross-sections along the river to sample point-scale (i.e. microhabitat) river hydraulics as an estimate of the river's population of hydraulics. At the selected locations, hydraulic observations are typically made at 1–3 discharges (Payne and Bremm 2003; Moir et al. 2005). The hydraulic simulation program IFG4 within the suite of PHABSIM tools is then used to estimate hydraulics across the full flow range of interest (Ghanem et al. 1996; Waddle 2001), with the aim of having estimations within <10% tolerance limits (Milhous et al. 1989; Elliott et al. 1996). Hydraulic estimations are then used for habitat predictions, which is the topic of Chapter 0. Overall, this approach is deemed a "1D model", even though it does not use a 1D numerical model. Notably, Ghanem et al. (1996) and Williams (2010) provided thorough critiques of this transect-based sampling approach used as one option with the PHABSIM program suite.

In this study, a transect-based, hydraulic sampling method was done to evaluate how well a small number of transects could capture the population of hydraulic and physical habitat conditions in a long river segment. The approach used to obtain the transect locations and number of transects closely mimics that used in current hydropower dam relicensing efforts (Williams 2010), and in particular was based on the method described for the Yuba-Bear and Drum-Spaulding relicensing process (NID and PG&E 2008; http://www.eurekasw.com/DS/default.aspx), with some modifications related to substituting the morphological-unit definitions and delineation approach of this study (explanation pending in sections 8.4–8.6) in place of the mesohabitat classification used in relicensing. Figure 44 illustrates the "1D model" transect-selection procedure.

Normally, the justification for using a 1D method instead of a 2D model is that it is simpler, cheaper, requires less data inputs, and yields the same flow-habitat relationship outcome anyway. For that foundation to be true, the number of cross-sections used in this study needed

to be on par with the number used in a professional instream flow study at a typical cost today. In this study, the baseflow thalweg length for the model domain was 13.52 km. Over that distance, instream flow assessments often collect data from one to two cross-sections per km for a range of ~13-26 total cross-sections in this domain. According to Payne et al. (2004), 18-20 transects is suitable to characterize hydraulics well enough to define weighted usable area relationships. This study did not investigate that particular criteria, but the number of transects recommended is a useful benchmark to consider. For the 37.42 km of the lower Feather River, the PHABSIM instream flow study used 29 transects (DWR 2004). That is equivalent to 10 transects in 13.52 km. For the PHABSIM joint instream flow relicensing study for the Yuba-Bear and Drum-Spaulding projects (http://www.eurekasw.com/DS/default.aspx), hydraulic measurements and estimations were made for 81 transects along ~66-km of the South Yuba River. That yields a sampling of 17 transects per 13.52 km. Thus, there is a consistent pattern of professional practice in the region that served as a benchmark for this study.

Based on these and other references, a total of 30 transects were selected within the 13.52-km upper South Yuba river segment for this study. This yielded almost double the density of cross-sections for the Yuba-Bear and Drum-Spaulding relicensing study, which was more transects than is commonly used in consulting/relicensing practices for the Sierra region (Payne et al. 2004). Further details on the specific cross-sections that were selected and their suitability for representing the morphological units in the river segment are presented in section 8.6, because the selection hinged on the number of morphological units in the study segment and their relative abundance. The important point is that if the professional recommendation calls for ~18-20 transects to adequately sample and represent the hydraulics of a river segment, then the use of ~30% more transects should be adequate to test a transect method against a 2D model with 1-m high-density predictive data results. Therein lies the primary question and test:

- Does a sampling of depth and velocity values at a 0.5-m spacing along 30 transects (chosen to represent channel-unit diversity according to the recommended professional methodology) yield a similar probability distribution function as the population of hydraulic values at the segment-scale in a remote mountain river over a wide range of discharges?
- Does a sampling of depth and velocity values at a 0.5-m spacing along 30 transects (chosen to represent channel-unit diversity according to the recommended professional methodology) yield similar average and standard deviation metrics for the morphological-unit averaged depths and velocities compared to the same metrics for the whole population of depths and velocities in the river segment?

The first question tests the overall effectiveness of the sampling, while the second question addresses a common step in habitat analysis in which hydraulics are upscaled to mesohabitat averages and then the averages are used in subsequent calculations. Sometimes the hydraulics are propagated through to habitat indices first, before the averaging is done, but either way this tests the effect of averaging on the robustness of the statistical sample of the population of hydraulics.

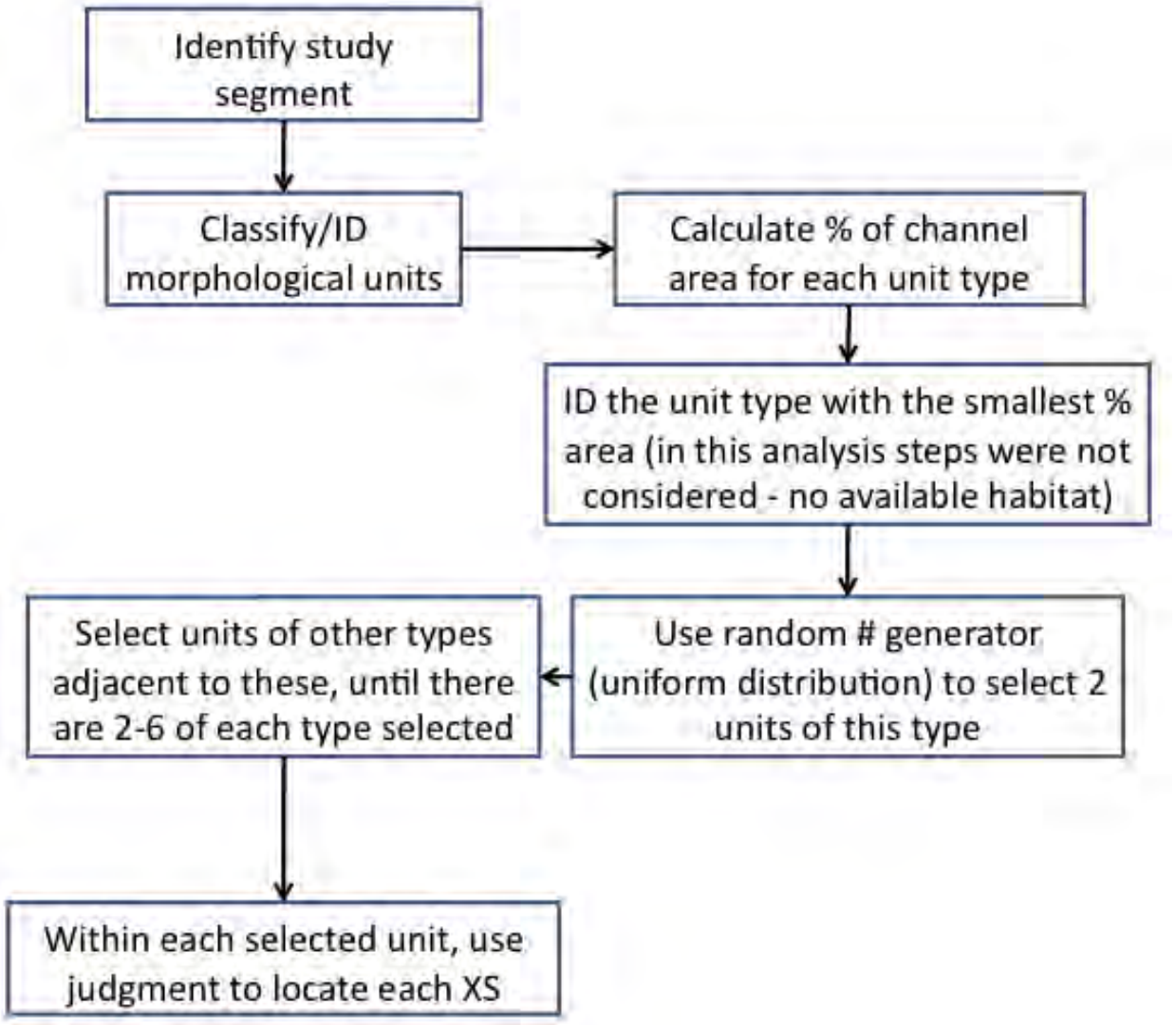

Figure 43. Methodology to select transects for geomorphic, hydraulic and ecological analyses. This was based on the draft-published methodology reported for the Drum-Spaulding relicensing effort (NID and PGE 2008).

7.4 1D Hydraulic Model

1D models such as HEC-RAS and MIKE11 can consider unsteady conditions and non-uniform conditions to the extent that the non-uniformities are captured by cross-sectionally averaged metrics. PHABSIM has a 1D numerical model module as one option for computing hydraulics. 1D models cannot explicitly account for transitional dynamics where no cross-sections are measured. Nor do they account for complex lateral variation in longitudinal flow, though this can be extrapolated with the use of velocity adjustment factors by back-solving Manning's equation to get laterally varying Manning's n values, or for secondary flow processes (i.e. fluxes orthogonal to banks) that may occur at or between measured cross sections (Darby and Van de Wiel 2003; Nelson et al. 2003). 1D models use a standard step method to iteratively solve the energy equation from one cross section to the next to calculate water surface profiles. These

models solve the energy equation for steady gradually varied flow and are also capable of calculating subcritical, super critical, and mixed flow regime water surface profiles (Brunner 1998).

Like 2D models, 1D models are quite similar among the different codes in their predictions, so it which particular model was selected for use in this study was not considered an essential element in the selection of the model. The deciding factor was familiarity with whichever 1D-model was used. Visiting scholar Hoang Quang Huy was a collaborator on the project, and the 1D numerical model that he developed was the one used in this study (Hoang et al. 2009). The numerical model was built based on the Saint-Venant equations for unsteady flow (Cunge et al. 1980). Equation (12) is the continuity equation, and Equation (13) is the dynamic equation of the Saint-Venant equations, which were solved by a modified Two Step Lax-Wendroff Scheme (Lax et al. 1960).

$$\frac{\partial A}{\partial t} + \frac{\partial Q}{\partial x} = 0 \tag{12}$$

$$\frac{\partial Q}{\partial t} + \frac{\partial}{\partial x}\left(\frac{Q^2}{A}\right) + gA\frac{\partial h}{\partial x} = gA(S_0 - S_f) \tag{13}$$

where A is cross-sectional area (m^2); Q is flow rate (m^3/s), t is time (s); x is longitudinal distance downstream (m); h is depth (m); S_0 is bed slope and S_f is friction slope.

The boundary conditions required to run the 1D numerical model were the discharge entering the upstream boundary (same as used for 2D model, see section 6.2.5), the associated downstream water surface elevation (same as used for 2D model, see section 6.2.5), and channel topography at designated cross-sections. The selection of the location and number of cross-sections for a 1D numerical model can be done in numerous ways.

One goal of this project was to understand how a 1D numerical model performs at hydraulic prediction for a long segment of a mountain river, when applied using a standard method. When 1D numerical models are done at the site-scale (~1–10 channel widths long) for any purpose (not just instream flow assessment), it is common to have tightly spaced cross-sections located at representative locations every 0.5–1.5 channel widths and at any evident hydraulic controls for the site. However, when a hydraulic model is used for river segments of greater length, there is no way to know where all of the relevant river features are located (especially in a mountain stream with highly complex, submerged terrain). With ground-based surveying technology in a remote-mountain setting it would be cost-prohibitive to measure cross-sections even at all the obvious locations. Even if LIDAR data were available for the terrestrial river corridor and suitable for dense cross-sections, bathymetric data is often lacking, especially in remote mountain regions where site conditions preclude or make some forms of data collection very difficult. This is a key reason why transect-based hydraulic estimation using observations/estimations is used over 1D numerical modeling for long river segments (Waddle, 2001). Nevertheless, given the goal of methodological comparison between 1D and 2D numerical models, it was necessary to select a suitable standard approach for how 1D numerical modeling is used in professional practice.

As in the transect-based hydraulic sampling component of the study, it was necessary to refer to the literature to determine an appropriate set-up (number of cross-sections and their spatial

pattern) for a 1D numerical model as a means for sampling hydraulics. Several examples of 1D numerical model studies exist for long segments of gravel-bed rivers, but very few exist for steep bedrock, boulder, and cobble-bed rivers. Partridge and Baker (1987) used a 1D numerical model to study flood hydraulics in a 4.4-km, bedrock-confined segment of the Salt River in Arizona. The study included 23 unevenly spaced cross-sections (equivalent to 71 per 13.52 km). Using the ratio of bed roughness to water depth, occurrence of bed steps, and width variability at bankful flow as benchmarks of channel complexity, gravel-bed rivers are not as complex as bedrock-mantled mountain rivers, but recent studies show that gravel-bed rivers do exhibit processes governed by channel non-uniformity (MacWilliams et al. 2006; Sawyer et al. 2010; White et al. 2010). URS Corporation (2004) conducted a 1D numerical model for 11.33 km of the gravel-bed Merced River in California. The study included 40 cross-sections (equivalent to 48 per 13.52 km) spaced 50-832 m apart. Water surface elevation verification consisted of 36 points observed during a low flow and three points observed during a flood. Gibson et al. (2010) performed a 1D numerical model for 32.2 km of the gravel- and sand-bedded Cowlitz River as part of an evaluation of sedimentation of material derived from the Mount St. Helens eruption of 1980. Sediment transport prediction is a highly nonlinear function of depth and velocity, so the need for accurate hydraulics is crucial. In that study, 95 unevenly spaced cross-sections were used, which is equivalent to 40 per 13.52 km. These and other studies provide a reasonable reference of ~40–50 cross-sections per 13.52 km for a common professional standard for 1D numerical modeling to obtain river hydraulics.

To be sure to have a more robust basis for methodological comparison, the 1D numerical model in this study used 105 cross-sections along the 13.52-km mainstem of the river (~8 per km), which is double the reference value. Further details on the specific cross-sections that were selected and their suitability for representing the morphological units in the river segment are presented in section 8.6, because the selection hinged on the number of morphological units in the study segment and their relative abundance.

The model parameters that were used were set to match the same values as those of the 2D model wherever possible. A global Manning's n roughness value of 0.1 was used. Initial values of discharge and water depth to start a simulation were 0 m^3/s and 1 m, respectively. The time step was t = 2 s.

Model outputs consisted of the water surface elevation, cross-sectionally averaged velocity, and cross-sectionally averaged depth. These values are the direct outputs from a 1D numerical model, so they were used for hydraulic and ecologic analysis. It is possible to use cross-section geometry to distribute depth across the channel by subtracting each point's bed elevation from the WSE for its cross-section. Methods exist to distribute velocity, but they require more questionable assumptions (Ghanem et al. 1996). The goal for this study was to evaluate how 1D hydrodynamic models perform using their native outputs, not with further extrapolation based on more assumptions. Along with many other specific tests, that one would also be interesting, but it was only possible to do a limited number of methodological comparison tests given the scope of the project.

Because of the adverse field conditions described in section 3.8.1, it was not possible to collect high-quality velocity data by wading across methodologically inappropriate cross-sections and measuring velocities to calculate mean cross-sectional velocity for comparison with the 1D numerical model. Instead, the approach taken here is similar to that of Brown and Pasternack (2009) in which the 2D model was validated and the 1D model is compared against that

validated model. The hydraulic analyses investigated the differences between the two types of models and then sought to understand the cause of the differences. Each model has sources of uncertainty and the goal was to expose those and allow readers to think critically about each approach.

Figure 44. Sample area of the study segment showing variable cross section spacing (black dots) overlain on the map of morphological units (e.g. larger unit areas in this reach are blue=pool, yellow=steep inset channel, and green=plane bed).

CHAPTER 8:
Geomorphic Analyses

Geomorphology is the study of the landforms on the surface of the earth. Geomorphic analyses involve mapping the shape of landforms to describe their spatial patterns, observing landforms over time to record their changes, exploring the drivers and mechanisms of landform change, and evaluating the responses of biological, chemical, and hydrological processes to geomorphic change. A common practice in geomorphology involves focusing on specific spatial scales at which landforms have characteristic features (Grant et al. 1990; Rosgen 1996; Thomson et al. 2001). In the study of rivers, these scales are proportional to channel width (W) and include catchment (entire watershed scale), segment (10^3-10^4 W), reach (10^2-10^3 W), morphologic (or geomorphic) (10^0-10^1 W), and hydraulic (10^{-1}-10^0 W) units. Spatial scales are referenced to channel width, because many observers have recognized a similarity of forms among systems of different absolute size that are governed by the same underlying processes. Note that in this study the reach length is defined as 10^2-10^3 W, and that a gap exists for channel lengths of 10^1 to 10^2 W. This smaller 10^1-10^2 W is considered by some geomorphologists to be an assemblage of geomorphic units, while others simply call it a reach also (because they are not investigating the larger spatial scales beyond that, and so do not require larger scale categories).

The baseflow thalweg is 13.52 km long, while the valley centerline of the study area is 12.2 km long. The wetted channel has a width of ~10–50 m as a function of morphological unit type and investigated stage range (section 8.1), so the scale of its entirety is 10^3 W. This scale is consistent with the study area being considered as a single segment composed of several reaches and even more smaller-scale unit types. Both segment lengths (13.52 km and 12.2 km) are used in this report, depending on the analysis.

Dense topographic data, ~1-cm scale kite-blimp imagery, a GIS-based environmental informatics system, and ~1-m resolution nodal results from 2D modeling were leveraged to yield detailed, multi-scalar analyses (segment, reach, and morphologic unit scales) with greater spatial variability at each scale than has been traditionally possible using classical cross-section and longitudinal-profile geomorphic methods. The availability of spatially distributed 2D modeling results enabled representation of all areas of the wetted channel with equal emphasis.

Geomorphic analysis for instream flow assessment is often limited to a determination of whether the study area is “stable” or not. Traditionally it is has been thought that rivers possess the capability of adjusting their attributes to accommodate flow and sediment transport regimes so that sediment in- and out-fluxes are balanced and landform conditions are “stable”. However, in reality geomorphic drivers and boundary conditions are much more independently dynamic and fast changing than classically envisioned, such that landforms may always be in a state of adjustment in response to external drivers and internal free oscillations that is normal and appropriate. Rather than thinking of landforms as “stable”, it is more appropriate to think of them and the ecosystem functions they are associated with as resilient in the face of change. Knowledge of historic, pre-human baseline conditions or regional reference conditions is limited and may not be as useful in understanding natural geomorphic and ecosystem services as once envisioned. In light of this natural complexity, a geomorphic assessment of conditions after a large dam or other facility is built and operated may not be as simple as documenting geomorphic instability and attributing that to human impacts relative to the presumed stable baseline conditions.

Rather than compare human-impacted conditions to theoretical baseline or reference conditions, a more effective approach is to deduce the geomorphic processes in a system under different regimes and evaluate the implications for resiliency of ecosystem services. Through a mechanistic understanding of environmental systems, it may be possible to manage flows and/or rehabilitate an ecosystem to achieve resiliency in cases where it has been lost or it is desirable to be instilled, even if it was not historically present.

In light of these concepts, the scientific questions that were addressed by geomorphic analysis included the following

- At the segment-scale, what are the values of wetted channel area, wetted width, and water-surface slope as a function of discharge?
- Based on thresholds in segment-scale attributes and the locations of tributaries, what is the delineation of reaches for the segment?
- At the reach scale, what are the values of wetted channel area, wetted width, and water-surface slope as a function of discharge?
- Does the study segment exhibit geometric organization at the reach scale?
- What are the morphological unit types present in the upper South Yuba river segment?
- Can 2D model results be used to rationally delineate morphological units in a mountain river?
- Are the morphological units delineated with a 2D model naturally organized into a coherent spatial structure that is non-random? If the structure is deterministic, then is it periodic or non-periodic? Are there systematic variations in morphological-unit organization and spacing along the segment?
- Is the longitudinal distribution of emergent boulders structured or random?
- Is there evidence of stage-dependent flow convergence as a mechanism for controlling sediment redistribution and fluvial landforms in the river segment over the range of discharges observed?
- What are the stage-dependent sediment transport regimes in the study segment?

Answering these questions sheds light on the resiliency of the channel to flood disturbances, societal flow adjustments, and instream bed alteration. That helps to set reasonable expectations for the sustainability of physical habitat conditions over time.

8.1 Segment-Scale Analysis

Segment-scale stage-dependent fluvial characteristics were explored by subjecting the digital elevation model and 2D model results to top-view and longitudinal profile analyses. These methods ascertain how segment-scale channel geometry and flow interact. Results for segment-scale hydraulic patterns are presented in Chapter 0.

8.1.1 Plan-view Analysis

The upper South Yuba River study segment had a wetted area of 261,397 m^2 and an average channel width of 13.74 m during the 2009 summer baseflow regime of approximately 10 cfs discharge at SYLC and 5 cfs at CCB. Wetted channel area and average channel width increased with discharge, except for the 210 cfs stage in the snowmelt regime (

Table 19). This fluctuation in response variables is evident through all discharge-dependent results for the snowmelt regime in the study, because SYWA outflow dips as SYLC inflow increases over a narrow range. This is the condition in which there is a threshold shift in runoff-contributing mechanisms and areas (explained in section 5.1). The fact that wetted area and average width increase through the whole discharge domain investigated suggests that the canyon floor is not full at the highest flow modeled. That means that there are more spatial scales of landform variability present in the system than have been captured by the study, even though the study spans three orders of magnitude of discharge. This insight was checked in several of the subsequent analyses.

Table 19. Wetted channel area and width as a function of season and flow.

Dry (cfs)	Area (m^2)	Average Wetted Width (m)
5	187,080	13.7
10	198,471	15.5
20	253,787	18.9
30	295,294	21.9
45	344,483	25.9
Wet (cfs)	Area (m^2)	Average Wetted Width (m)
5	226,555	16.7
15	254,029	18.9
30	285,995	21.4
55	325,174	24.6
100	369,243	27.9
190	425,183	32.5
350	499,551	38.5
Snowmelt (cfs)	Area (m^2)	Average Wetted Width (m)
10	216,244	16.0
25	253,122	18.8
50	292,641	22.0
140	332,720	25.2
210	311,832	23.9
525	377,081	29.2
1103	433,858	33.8
3000	514,476	40.7
6921	610,780	48.8

8.1.2 Longitudinal Profile Analysis

The first step in this analysis was to create a thalweg point set and polyline. During the 2009 field campaign, thalweg locations in all wadable sections of the river study segment were measured in 1–2 m intervals. Surveyed points were projected into ArcGIS as (*x*,*y*,*z*) data and digitized into a multi-part polyline with gaps where no data was gathered. For unwadable areas (typically points with depths >1.5 m), thalweg locations were extracted from the 2D model results for the 2009 summer baseflow simulation. To do this, a 1x1 m^2 raster was generated of the product of the depth raster times the velocity raster. This product raster clearly illustrated the location of the thalweg. As a test, field-observed locations were compared against the 2D model predicted locations, and were found to overlap for the majority of the study segment (Figure 45). Once this raster was visually validated, additional points were manually added in unwadable pools, chutes, and steps as needed to follow the thalweg path. After all the points were created, polyline features were digitized and then all polyline features were merged and

dissolved to yield a single continuous thalweg line for the entire study segment. The thalweg point set and the thalweg polyline were the foundation for analyses that required longitudinal positioning or referencing. Another shapefile was built using the valley centerline. Points were distributed every 10 m along the centerline, and then polylines were created perpendicular to the centerline at each point. These lines were buffered and converted into individual polygons, then clipped to the highflow boundary created for the topographic map. This process yielded 10-m rectangles that were used for width, morphologic unit, and slope analyses (see Figure 63). Some 10-m rectangles overlapped or underlapped at meander bends, creating triangles rather than rectangles, but no work was done to rectify this issue. It was decided that the overlaps and underlaps balanced each other out, and the data in these units were as important as in all other units, so all data were kept and analyzed as desired.

The longitudinal profile of the river was plotted with bed, baseflow water surface, and snowmelt 6921 cfs water surface elevations all shown for comparison. Regression analysis of the full segment returned average slopes of 1.65, 1.63, 1.63% for each profile, respectively (Figure 46). The range of bed elevations was 780.2–1016.1 m. Overall, the longitudinal profile had an elevation change of 235.9 m over 13.52 km.

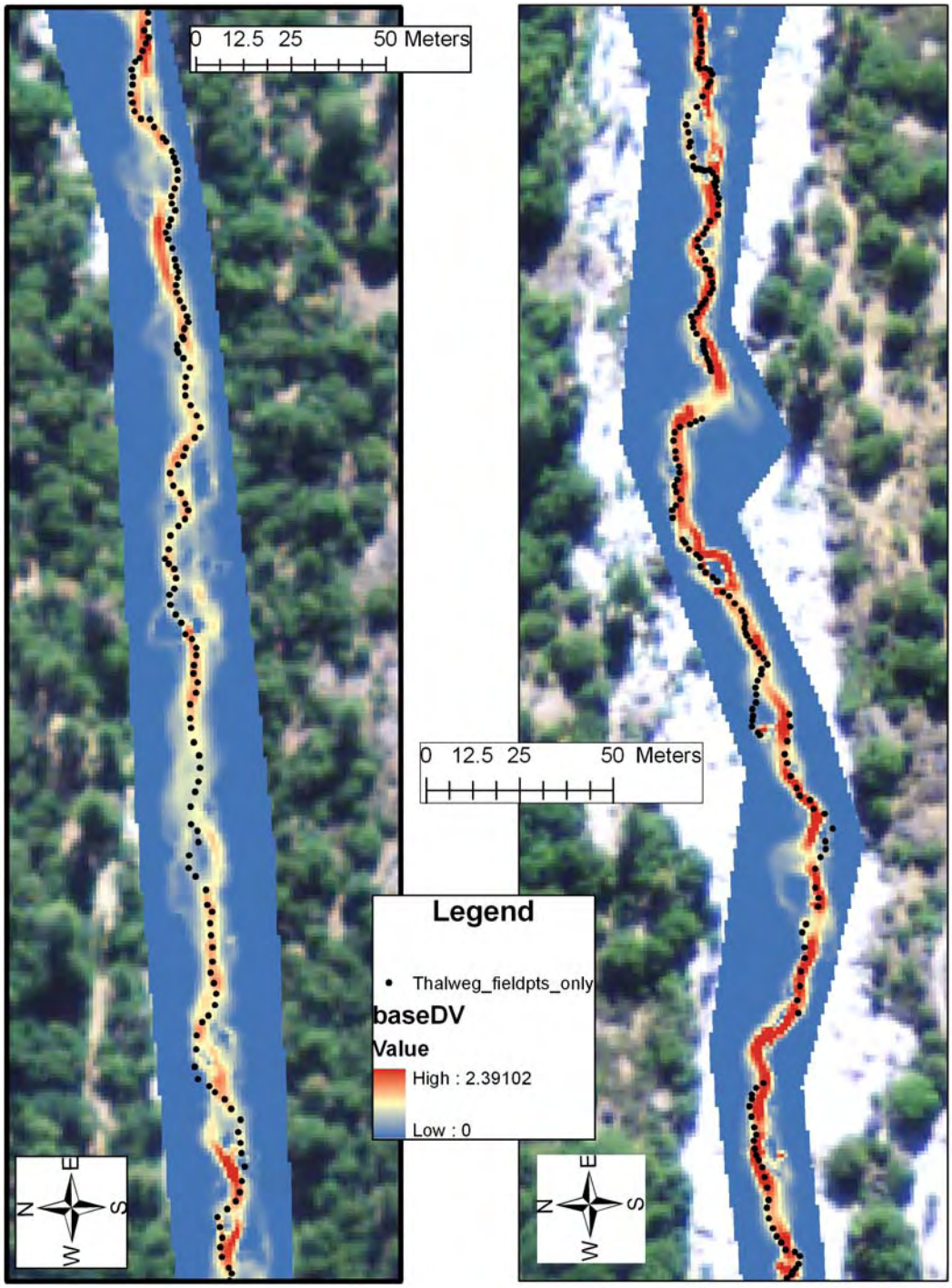

Figure 45. Comparison of field-observed (black dots) and 2D-model-predicted (pixels with shades of red) thalweg pathway showing a close visual match. Left image is a cobble/boulder-strewn reach, whereas the right image is a bedrock dominated reach.

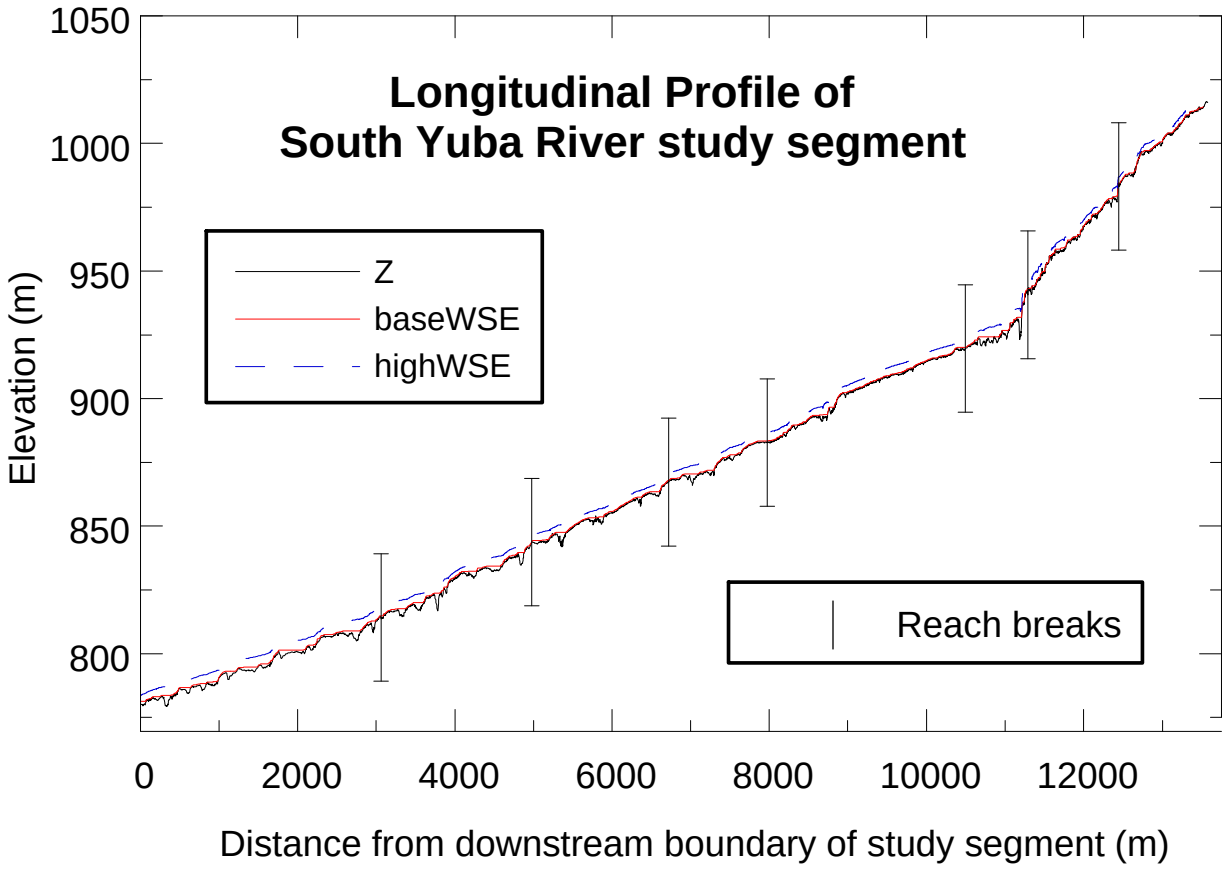

Figure 46. Longitudinal profiles of bed, baseflow water surface, and highest water surface (6921 cfs on SYLC gage). Reaches are numbered from downstream to upstream (see Figure 47).

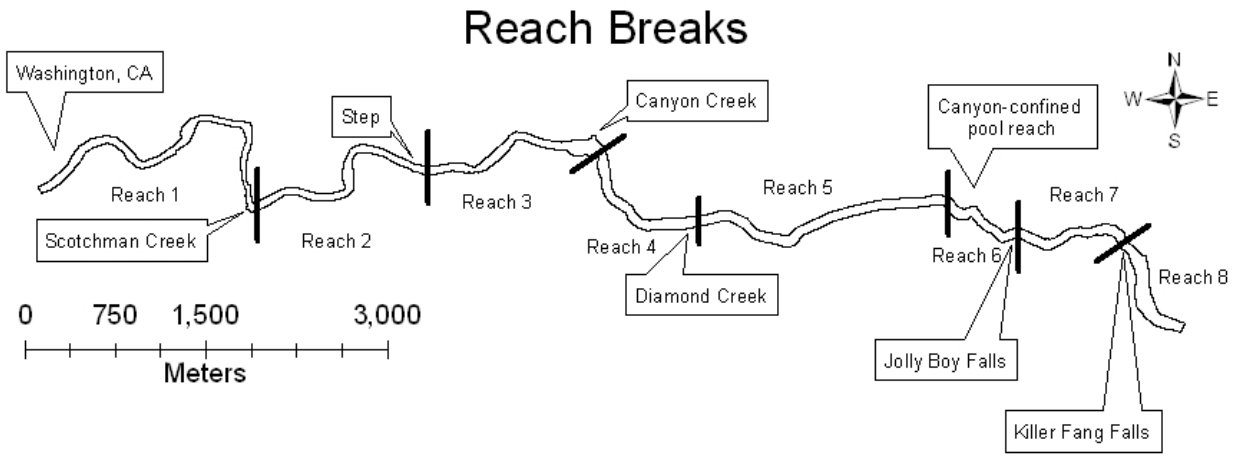

Figure 47. Plan view of reaches with notable morphologic controls.

8.2 Reach Characteristics

A reach is a length of river with a characteristic set of attributes controlled by the balance of sediment transport capacity, sediment supply, and topography. These governing factors are expressed through the following variables: discharge from mainstem-tributary confluences, impacts of man-made structures and activities, valley width, bed slope, and bed material type (or absence of it). Major changes in these underlying variables may be used to delineate reaches in a river segment.

Inspection of the longitudinal profile and field-based knowledge led to a delineation of eight reaches (Figure 46, Figure 47, Figure 48). Tributaries form the upper boundary of four reaches; two boundaries were at significant steps, and one at a significant change in channel morphology. Average reach widths were calculated for the baseflow WSE using modeled dry 10 cfs water surface elevations, as width analyses were not conducted on baseflow shapefiles. Dry 10 cfs approximates the discharge from Langs Crossing during summer 2009 water surface elevation direct observations. The modeled water surface elevations from snowmelt 6921 cfs discharge at Langs Crossing were used for highflow WSE calculations (

Table 20). Slopes were calculated for changes in channel bed elevation, modeled baseflow water surface elevation, and highest modeled water surface elevation (Table 21).

- A brief description of each reach follows (Figure 46, Figure 47, Figure 48).
- Reach 1 begins at the downstream boundary of the study segment with a bed elevation of 814.1 m and ends at the upper edge of channel influences of Scotchman Creek, a distance of 3,059.8 m. A difference in elevation of 33.9 m returns a bed slope of 1.07%. Scotchman Creek joins the South Yuba in the middle of a meander. The tributary flows into the upper end of a pool on river left, with a gravel bar formation along river right in the downstream direction as well as extending upstream; a consequence of the tributary itself and therefore included in the reach. Unregulated Scotchman Creek is an active source of hydraulic mining debris; ~1 km upstream is a full debris dam that shows signs of potential failure. Still-scarred mountain ridge tops are at the top of this sub-basin, where hydraulic mining at Alpha and Omega Mines took place in the mid- to late-1800's in the search for gold.
- Reach 2 ends just above the only step below Canyon Creek (i.e. greater than 2-m elevation drop from brink to baseflow WSE). An elevation gain of 26.6 m over 1,920.1 m returns a bed slope of 1.44%. A bedrock outcrop dominates the wetted channel at the top of this reach, creating two significant steps that are expressed laterally, with one step on each side of the outcropping bedrock within the wetted channel.
- Reach 3 ends just above the convergence of Canyon Creek with the South Yuba main stem, with an elevation gain of 23.55 m over a distance of 1,738.9 m for a bed slope of 1.39%. Canyon Creek is the largest tributary in the study segment, and is regulated. A massive gravel bar is located on river left across from the confluence and extends upstream and downstream. A backchannel behind the gravel bar is wetted during highest modeled flows.
- Reach 4 ends just above the influence of Diamond Creek, gaining 15.5 m over 1,254.1 m for a bed slope of 1.40%. Diamond Creek is unregulated, and its hillsides were also hydraulically mined for gold. Omega Mines lies on the ridge tops between Scotchman and Diamond Creeks.
- Reach 5 has few pools, gaining 36.8 m in elevation over 2,523.6 m for a bed slope of 1.53%. It is the most homogeneous stretch of the study segment, where fewer bedrock outcrops and canyons are expressed within the river corridor, and below the beginning of a canyon-confined reach. The upper boundary of this reach exhibited significant change in channel morphology not associated with a tributary or step.
- Reach 6 consists of a series of pools confined by canyon walls and ends at the top of Jolly Boy Falls, gaining 21.0 m in elevation over 794.2 m for a bed slope of 1.99%. Jolly Boy Falls is the highest step of the study segment with a fall of ~6 m from upper brink to downstream channel. The deepest pool of the reach, ~9 m deep at baseflow, exists directly below the step. Buildings, mining equipment, and a crane at the top of the canyon wall suggest are a remnant of instream gold mining activity to get at the alluvial-bedrock interface where gold often settles. James et al. (2002) report that the morphology

of the Yuba Gorge (Spaulding Dam to at least Jolly Boy mine and possibly as far downstream as Washington, California, the lower extent of this study's study segment) was set by glacial plucking and subglacial meltwater during two to three glacial advances that occurred during the Quaternary period.

- Reach 7 runs from Jolly Boy Falls to the top of Killer Fang Falls just upstream of Fall Creek, gaining 42.5 m in elevation over 1,157.1 m for a bed slope of 3.30%. Fall Creek's influence extends to the downstream end of the pool below Killer Fang Falls. The slope increases markedly in this reach at more than 3 times the slope of Reach 1 and more than twice the slope of all other downstream reaches except Reach 6.
- Reach 8 ends at the top of the study segment, gaining 32.9 m in elevation over 1129.5 m for a bed slope of 2.81%. Four steps were clustered together at the lower end of the reach. The upper section of this reach was significant for having the only bi-threaded channel of the study segment. Some mining occurred in this reach also, as was evident from the characteristic look of mined rock (section 2.2.2). It was discussed during field data collection in this reach whether the side channel was a product of mounded mining debris in the wetted channel bisecting flow in a wider pre-mining channel, or not. The conjecture remains an open question at this time. It is also possible that instream miners pushed around pre-existing glacially-derived sediment to access different parts of the canyon floor. The key indicator according to James (2005) would be the amount of quartz in the gravel fraction of the existing channel sediment, which was not assessed in this study.

Overall the study segment bed slope increased by a factor of three, with a low of 1.07% in reach 1 between the downstream boundary of the study segment in Washington, California and Scotchman Creek, and a high of 3.3% in the reach upstream of Jolly Boy Falls to Killer Fang Falls. Bed slope changed most significantly above Jolly Boy Falls as can be seen in the segment-scale long profile (Figure 46).

Bed elevation, baseflow WSE and high-flow WSE slopes varied by as little as 0.01% and by as much as 0.2% (Table 21). Baseflow WSE slope was greater than bed elevation in four reaches, an indication of heterogeneity throughout the study segment. Reach 6 exhibited the most variation in slope, increasing by 0.09% from Z to baseflow WSE, and 0.2% from Z to high-flow WSE. This reach is dominated by pools stepping down in elevation through canyon walls with a significant backwater effect near the bottom of the reach extending upstream ~300 m (Figure 48). The canyon walls constrain the ability of higher discharges to spread laterally, so depth and velocity increase disproportionately, increasing slope at a higher rate. Reach 4 shows a significant backwater effect also but does not exhibit similar slope variations and is not dominated by canyon walls. The delineation between reaches 6 and 7 occurs at an abrupt change in slope at Jolly Boy Falls, while the upstream delineation of Reach 7 ends above Killer Fang Falls. Reach 7 slope does not change between bed and baseflow WSE, but decreases by 0.11% at high-flow WSE, which may be due to the constraints of major step features at each end of the reach. Reaches 3, 4, and 5 also exhibit a decrease in slope at high-flow WSE, suggesting a smoothing as hydraulic features drowned when WSE rises.

Baseflow slopes were marginally higher than bed slopes in reaches 1, 2, 6, and 8 (Table 21). Average widths in these reaches were not the highest or the lowest, so bed undulations may have been a greater control than widths (

Table 20). Conversely, baseflow slopes were marginally lower than bed slopes in reaches 3, 4, 5, while reach 7 slope remained static. Average widths in these reaches were either highest as in reaches 4 and 5, or lowest as in reaches 3 and 7. Taking the average and standard deviation between bed elevation, baseflow WSE, and high-flow WSE shows that reaches 3, 4, 5, and 7 have some of the lowest average differences between bed and base slopes, suggesting that bed undulations were less of a factor than in reaches 1, 2, 6, and 8. Calculated baseflow WSE - Z have high coefficient of variation values (Table 22), which means that variation in bed elevation plays a dominant role in low flow water surface elevation behavior regardless of bed versus baseflow slope or widths.

The ratio between average low and high flow widths per reach shows that reaches 2, 3, and 7 have the greatest floodplain capacity within the range of modeled flows. Reaches 2 and 3 have similar slopes and are concurrent in the lower half of the study segment. Reach 7 is bounded by two large steps, has the greatest slope of all reaches, and the largest ratio of high/low width of 4.3. While steep, it also has width capacity. Reaches 4 and 5 have the lowest high/low width ratios at 2.3 and 2.5, respectively, yet have the greatest widths at baseflow. These reach floodplain boundaries are confined as flows increase, but must have a less rough bed with fewer obstructions at low flows.

As discharge increases, water surface slope smoothed out visually but remains closely linked to the bed slope. As the ratio of depth to the amplitude of bed-undulation increases local vertical causes of backwater and flow acceleration are flooded out. This phenomenon can be seen in the reach profiles, where bed variations become less important as geomorphic controls when discharge increases (Figure 48). Variations in slope cannot be attributed to average widths so bed forms continue to be a dominant control even at the highest modeled flow. Morphologic roughness within the flooded channel is greater than depicted in the modeled flows of this study because surveying collected data at ~1–5 m intervals, while the models were gridded at 1-m intervals then interpolated between nodes using TINs. The coefficients of variation for high-flow WSE - Z are much smaller than those for baseflow WSE - Z, suggesting that widths vary much more during low flows than during high flows.

Table 20. Average channel width per reach at dry 10 cfs (~baseflow) and highest modeled flows.

	Average width per reach		
Reach	Dry 10 cfs	Snowmelt 6921 cfs	Ratio high/low
1	17.0	50.7	3.0
2	14.7	53.9	3.7
3	12.7	47.4	3.7
4	19.9	46.3	2.3
5	19.6	48.5	2.5
6	14.2	46.7	3.3
7	13.3	57.0	4.3
8	14.4	45.9	3.2

Table 21. Reach slopes for bed topography, baseflow WSE (dry 10 cfs), and highest flow WSE (6921 cfs).

	Slope %		
Reach	Z	baseWSE	highWSE
1	1.07	1.08	1.11
2	1.44	1.45	1.45
3	1.39	1.37	1.33
4	1.40	1.38	1.36
5	1.53	1.52	1.52
6	1.99	2.08	2.19
7	3.30	3.30	3.19
8	2.81	2.85	2.83

Table 22. Average, standard deviation, and coefficient of variation by reach between bed elevation and baseflow WSE, and between bed elevation and high flow WSE.

	baseWSE - Z (m)			highWSE - Z (m)		
Reach	Average	Standard devation	Coefficient of variation	Average	Standard devation	Coefficient of variation
1	1.07	0.83	77.1	4.40	1.15	26.2
2	1.02	0.92	89.9	3.80	1.24	32.5
3	0.79	0.72	91.4	3.39	0.97	28.7
4	0.68	0.60	88.9	3.58	0.95	26.6
5	0.52	0.35	67.4	3.50	0.61	17.5
6	1.27	1.41	111.2	4.72	1.50	31.7
7	0.73	0.52	71.9	3.54	1.09	30.9
8	0.44	0.32	73.6	2.78	0.64	23.2

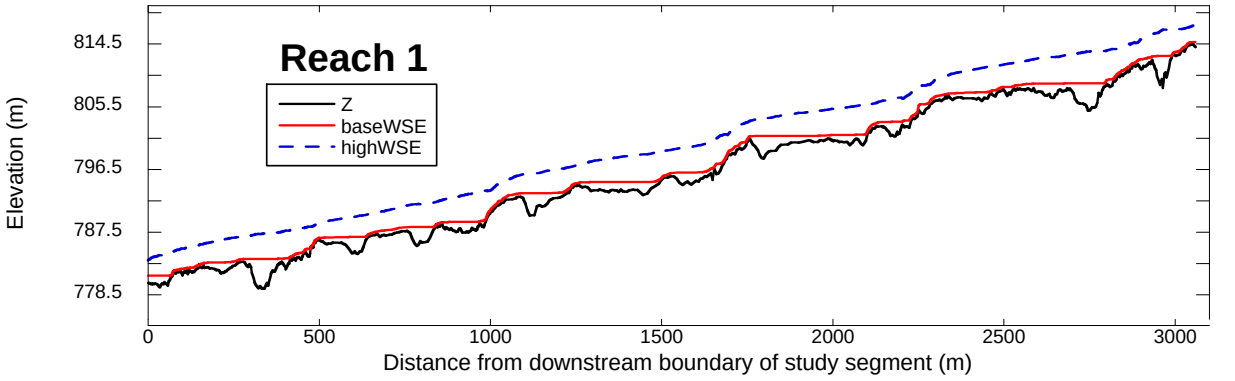
Reach 1
Z
baseWSE
highWSE
Elevation (m)
814.5
805.5
796.5
787.5
778.5
0
500
1000
1500
2000
2500
3000
Distance from downstream boundary of study segment (m)

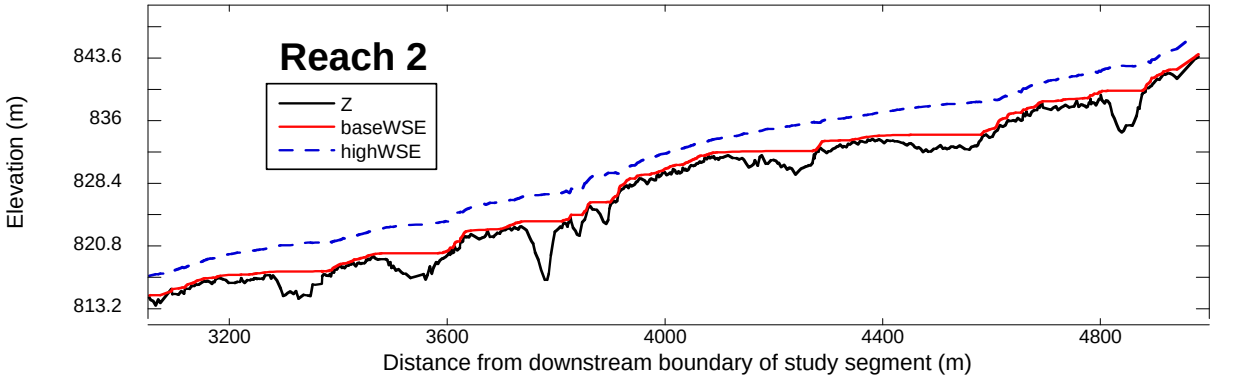
Reach 2
Z
baseWSE
highWSE
Elevation (m)
843.6
836
828.4
820.8
813.2
3200
3600
4000
4400
4800
Distance from downstream boundary of study segment (m)

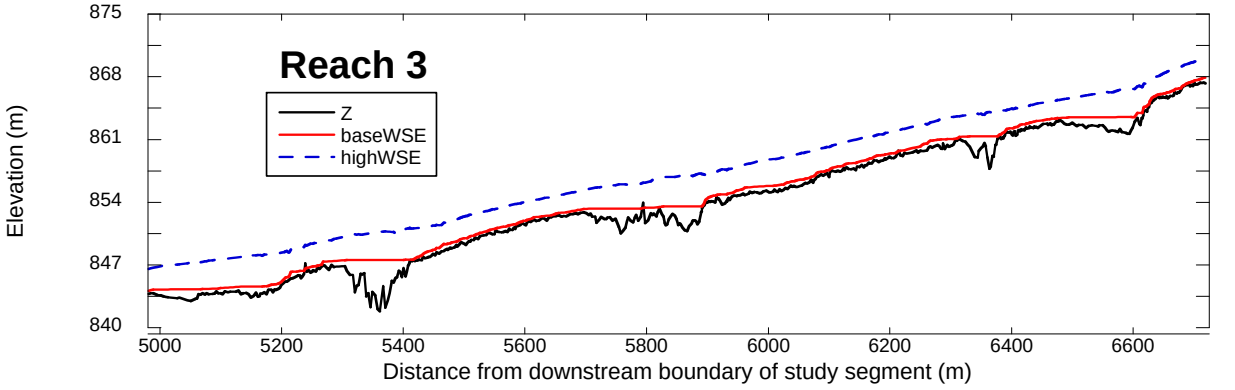
Reach 3
Z
baseWSE
highWSE
Elevation (m)
875
868
861
854
847
840
5000
5200
5400
5600
5800
6000
6200
6400
6600
Distance from downstream boundary of study segment (m)

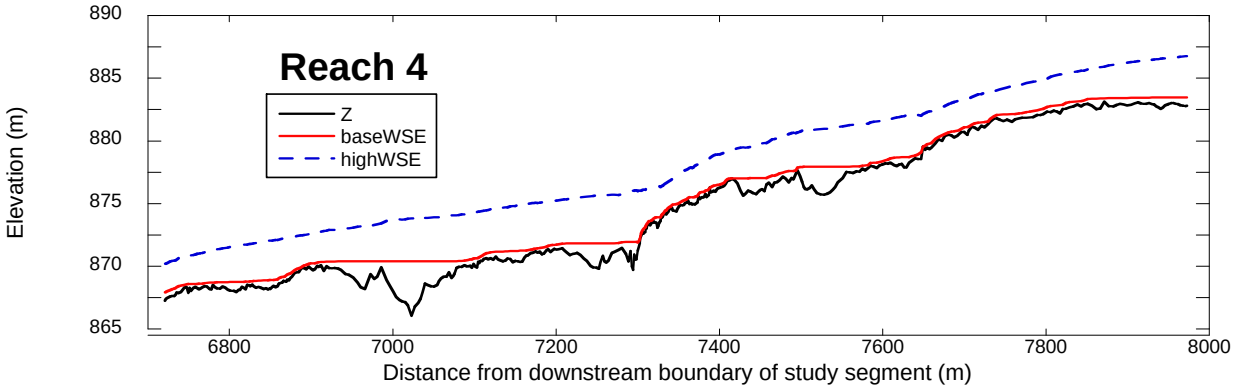
Reach 4
Z
baseWSE
highWSE
Elevation (m)
890
885
880
875
870
865
6800
7000
7200
7400
7600
7800
8000
Distance from downstream boundary of study segment (m)

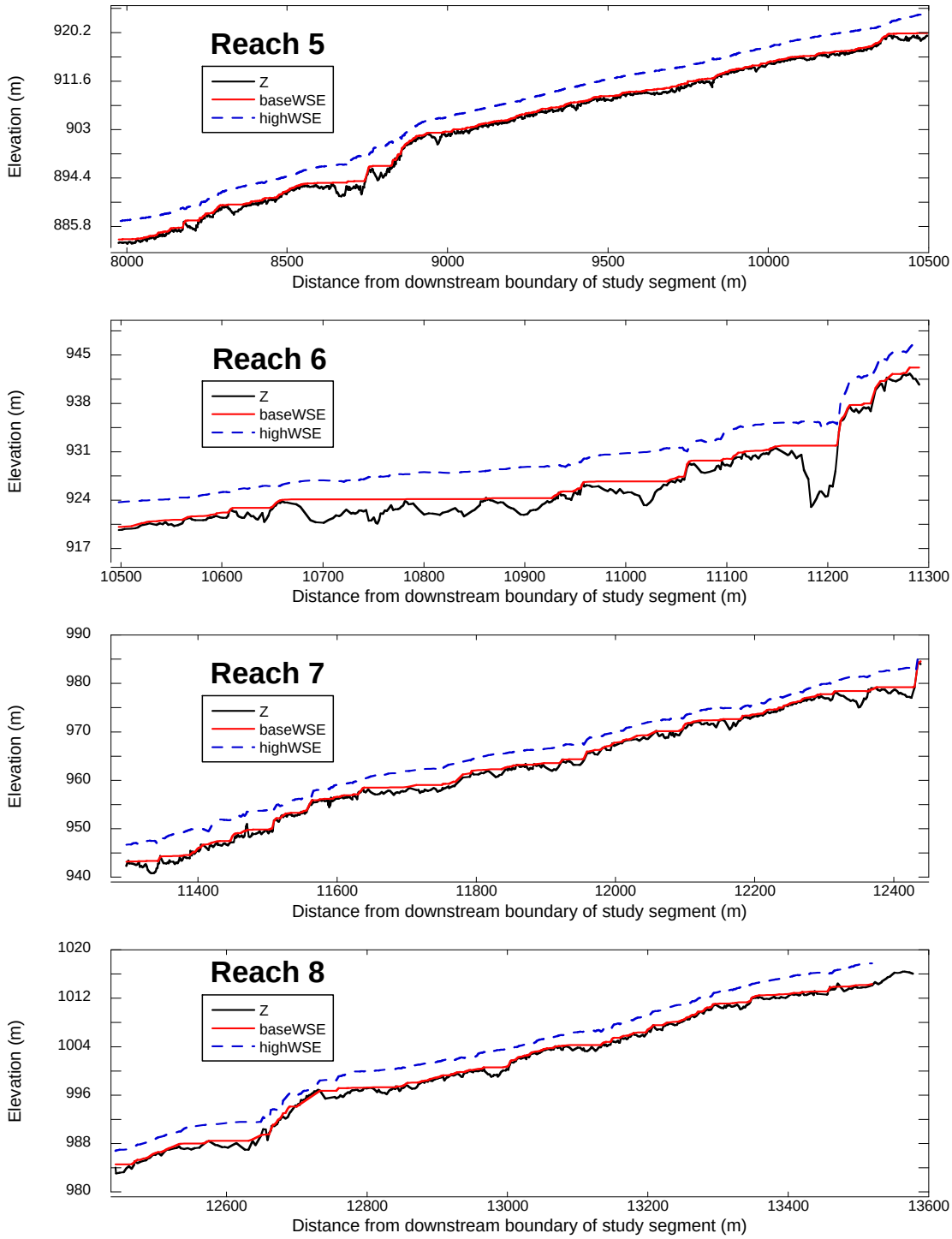

Figure 48. Bed elevation, baseflow water surface elevation, and high flow water surface elevations plotted by reach.

8.3 Reach-scale Geometric Organization

To better understand geometric organization in the upper South Yuba River at the reach scale, a suite of cross-covariance analyses were performed to assess the phasing of undulations in wetted width and bed elevation as a function of flow. Such phasing can serve as a topographic control on flow, landform organization, and physical habitat distribution. Where phasing exists, physical habitat is likely to persist, because the phasing is resilient against disturbances.

Wetted widths from dry 10 cfs and snowmelt 6921 cfs model results were used in this analysis along with the channel thalweg for three selected reaches. Cross covariance is a measure of bivariate similarity of two spatial series. Positive cross covariance is indicative of a strong positive relationship where both series show deviations about the mean at the same lag distance. Negative cross covariance occurs when one series deviates below the mean while the other deviates positively.

Reaches 1–3 were selected for this analysis, delineated by channel slope (Figure 48). The overall slope of each reach was removed from the bed elevation data through a procedure known as detrending. A moving average approach through the reach lengths was employed where the window size (e.g. reach length) was manually varied until residual correlation was a minimum. Flow widths from the hydrodynamic model at dry 10 and snowmelt 6921 cfs were extracted from GIS along the river corridor and normalized by the average width. Detrending of the flow width was not needed, because the series was stationary with respect to first and second order statistical moments. The normalized width residuals and detrended thalweg residuals were then analyzed in GS+ using a lag distance of 10 m (~20% of average channel width at 6921 cfs).

For the three reaches shown, the organization of cross covariance is slightly oscillatory depending on the scale analyzed (Figure 49). Peaks and troughs associated with positive and negative cross covariance typically occur at about a separation distance of 350 m, corresponding roughly to 7 channel widths which is the average pool spacing within the study area. Further work is being pursued that links the spatial organization of channel geometry with specific hydraulic and geomorphic mechanisms.

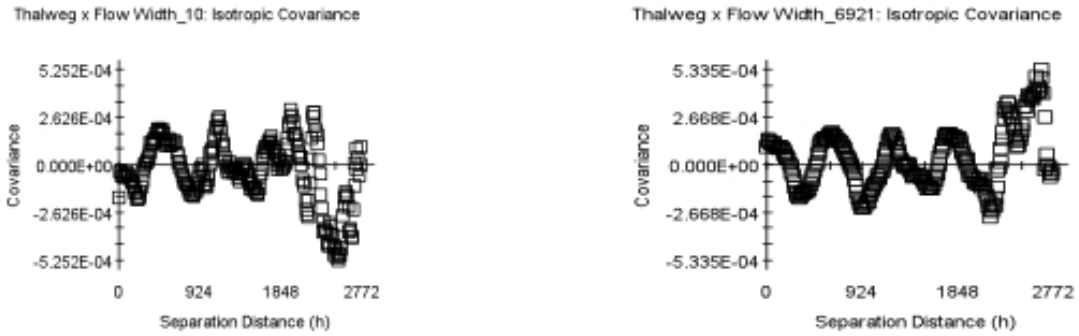

Reach 1
Stations 0 to 2,776

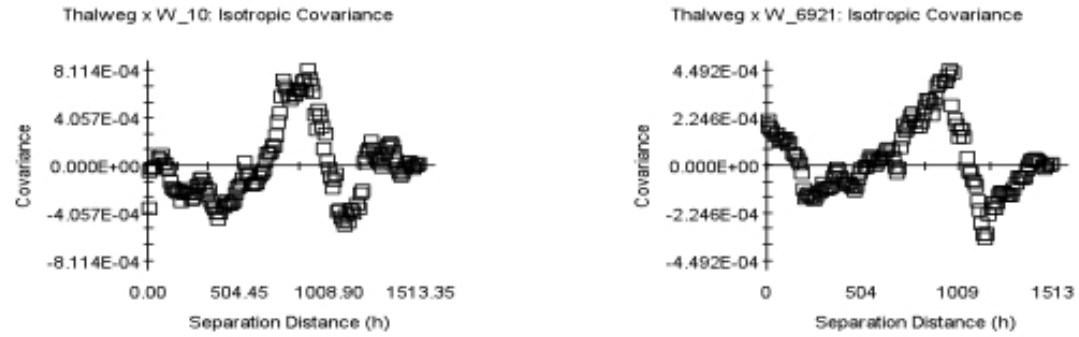

Reach 2
Stations 2,776 to 4,330

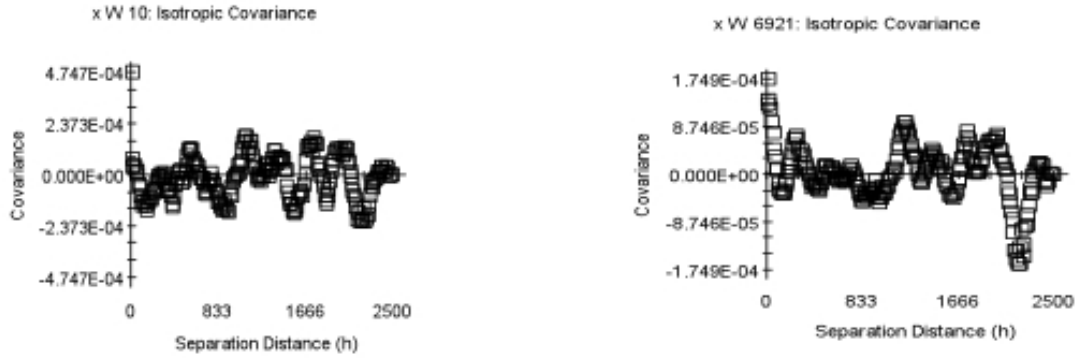

Reach 3
Stations 4,330 to 6,810

Figure 49. Reach-scale cross-covariance analysis showing deviations about the mean.

8.4 Morphologic Unit Definitions

The literature contains many definitions of and nomenclatures for riverine landform patterns (Grant et al. 1990; Beechie et al. 2006). Most landform definitions currently in use are qualitative in nature, because the processes that control these channel patterns are still not well understood (Benda et al. 2005). Conceptually, hydrogeomorphic variables such as discharge, sediment supply, channel slope, valley slope, entrenchment ratio, and channel bed material grain size influence the organization of landforms in a river. However, these variables may have different relative importance in each system, so a uniform classification approach may not be applicable.

A ***morphological unit*** is a discernible landform in the river valley that is typically visible at the spatial scale of 1-10 channel widths.

Morphological units are revealed by their topographic form and the hydraulics generated as water moves through the channel. Ideally, a digital elevation model of an exposed riverbed could be analyzed numerically to delineate individual fluvial landforms, but no technology has achieved that yet. As illustrated in Figure 50, the hydraulics of flow over a landform most closely reflect its topographic variation at a low flow (Pasternack et al. 2006b). If flow is too low, then too little of the bed may be underwater to have any hydraulics. As discharge increases, higher momentum enables flow to launch out from the landform and ignore more topographic controls (Pasternack et al. 2006; Wyrick and Pasternack 2008). As a result, the velocity field and derivative hydraulic metrics have decreased spatial variation. Consequently, good morphological unit delineation requires a low flow within the bankfull channel and perhaps within ~0.2–0.4 of bankfull dimensions, based on experience. Using a flow of that magnitude, water depth and velocity are strong indicators of underlying landform features. Even though low-flow hydraulics help infer morphological-unit patterns, the key point is that once identified, the morphological units themselves are not stage-dependent. They are landforms; the hydraulics just help identify them.

Independent from the morphological units are the discharge-dependent micro- and meso-habitats. Parasiewicz (2007) defines habitat as the area where an organism can be observed for a significant portion of its diurnal routine. In this study, the term physical "microhabitat" is defined as the localized depth, velocity, temperature, and substrate at a point in a river without regard to the surrounding conditions. It is often possible to empirically relate ecological function to physical microhabitat variables (Bovee 1986), but doing so provides a limited understanding of how and why fluvial-ecological linkages are spatially related. Parasiewicz (2007) suggests that the natural mobility of fish and their behavioral response to observers makes it difficult to know if an observation at the point scale is representative of their microhabitat preference. For less-mobile organisms, the term "occurrence" is used over "preference" to denote an observation of an organism where it is unclear if the organism chose to be there or was pushed there by the flow. The term physical "mesohabitat" is defined as the interdependent set of the same physical variables over a morphological unit at a given discharge. Parasiewicz (2007) prefers to use the term hydromorphic unit in place of physical mesohabitat to emphasize that this is a set of physical attributes. There is a general lack of studies that nest the microscale requirements of aquatic species within the mesoscale context of an assemblage of morphological units, but Moir and Pasternack (2008) is one example of such a study. Geist and Dauble (1998) also report the importance of considering morphological units, because they help to explain the role of hyporheic flow differences in salmon spawning habitat

utilization. The MesoHABSIM methodology for instream flow assessment eschews microhabitat analysis altogether, in favor of a coarser-scale analysis that may be easier to scale up to the watershed level (Parasiewicz 2007).

Previous studies have provided justification why morphological units should be able to explain fluvial-ecological relations. First, they are considered to be the "fundamental building blocks of rivers systems" (Brierly and Fryirs, 2000). At the mesohabitat scale, the concept of physical biotopes has been proposed as a framework for classifying streams based on their physical characteristics that are typically linked to instream habitats (Padmore et al., 1998). Newson and Newson (2000) stated that a "biotope approach represents an important linking scale between the detail of microscale habitat hydraulics and the need for network-scale appraisals for management of channels and flows." Furthermore, mesohabitat delineation may be a good predictor of fish utilization patterns (Geist and Dauble, 1998; Hanrahan, 2007). Finally, the type and distribution of morphological units have been found to be sensitive to land use within the watershed (Beechie et al., 2003). In terms of practicality, the mesohabitat scale provides a manageable resolution of analysis that balances scientific detail with the potential for catchment-scale application (Padmore et al., 1998); the study of the form, function and distribution of morphological units is therefore useful both in terms of scaling-up to watershed scale estimates of habitat capacity and for assessing how this might be impacted by human activity (Reeves et al., 1989; Beechie et al., 2001).

The approach used in this study was to delineate in-channel morphologic unit types quantitatively using the 2D-model summer 2009 baseflow hydraulics and then inspect the unit types to assign names to them consistent with geomorphic lexicon. To do this, 1x1 m^2 depth and velocity rasters were generated from SRH-2D model results and then ArcGIS Spatial Analyst was used to generate trial morphological unit patterns with a variety of possible depth and velocity thresholds. Resulting trial patterns were overlain on ~4 cm resolution kite-blimp imagery and a visual inspection made to determine if each trial pattern made sense. The co-author who performed the analysis had four months of daily ground-based experience with the river that also aided evaluation and interpretation of trial patterns. Even though this approach was subjective in setting the thresholds, once those were established, ArcMap Spatial Analyst objectively delineated the resulting spatial pattern of morphological units. By way of comparison, this approach is similar to supervised cluster analysis in that the expert defines the number of units. The difference in the approach used in this study is that supervised cluster analysis involves selecting the beginning centroids of clusters ("seeds") and having the boundaries be calculated mathematically. The choice of seeds can impact the final cluster delineations, which is not desirable. In the preferred approach, the boundaries are selected based on experience with the study segment, iterative trial, and consultation with local river scientists and managers; then the centroids are calculated mathematically. The boundaries are more important than the centroids, so carefully choosing those is more important than carefully choosing the centroids.

Figure 51 shows a flow chart illustrating the quantitative hydraulic thresholds in depth and velocity that were used to delineate morphological unit types and the names assigned to each unit. Figure 52 sets the morphologic unit into a phase-space plot of the hydraulic domains, showing that every possible combination of depth and velocity returned from the low flow 2D model was considered. Steps were defined by elevational differences rather than depth and velocity, and thus are not present in the two just-discussed figures; they are described in section

8.5. Since 2D models do not simulate steps well, they cannot be used to delineate them. 3D models would be able to achieve this.

In addition to these unit types, one sub-aerial morphological unit was also delineated. This unit consisted of the lightly vegetated active river corridor, which was composed of a combination of coarse cobble and boulder alluvium and bedrock. Colloquially, it was termed "floodplain", for lack of a better word, even though it does not meet the semantic lowland-oriented definition for landforms of that designation. This unit type was manually delineated using georeferenced blimp imagery, LIDAR-derived DEM contours, and visual evidence of a slope break between the active river corridor and the soil-mantled, forested hillside in NAIP imagery.

The units may be geomorphically defined as

- ***Pool***: topographically low area of the channel bed with the largest negative deviation from average slope.
- ***Step***: abrupt elevational drop >2 m between the brink of the step and baseflow water surface elevation below.
- ***Transition***: gradual increase or decrease in slope typically occurring between pools and other units.
- ***Chute***: rapid expansion in cross-sectional area causing a hydraulic jet to issue into a larger body of water.
- ***Plane Bed***: Flat areas of the river bed on a relatively low slope with variable bed roughness and water velocities. Figure 40 (left photo) illustrates a classically defined plane bed area consistent with the definition of Montgomery and Buffington (1997). Aquatic biologics use the term "pocket water" to describe these areas. In this study plane bed was often found along the periphery of other unit types.
- ***Inset Channel***: For the topographically high areas of the riverbed, these are the geometric channels within the wetted area, and thus they concentrate flow and have a higher velocity.
- ***Steep Inset Channel***: Same morphology as inset channel, but tilted with a significantly higher slope.
- ***Floodplain***: Lightly vegetated sub-aerial active river corridor bounded by the soil-mantled hillside and composed of exposed bedrock and very coarse alluvium. The word "floodplain" is not strictly appropriate, but for lack of something more appropriate it was used colloquially.

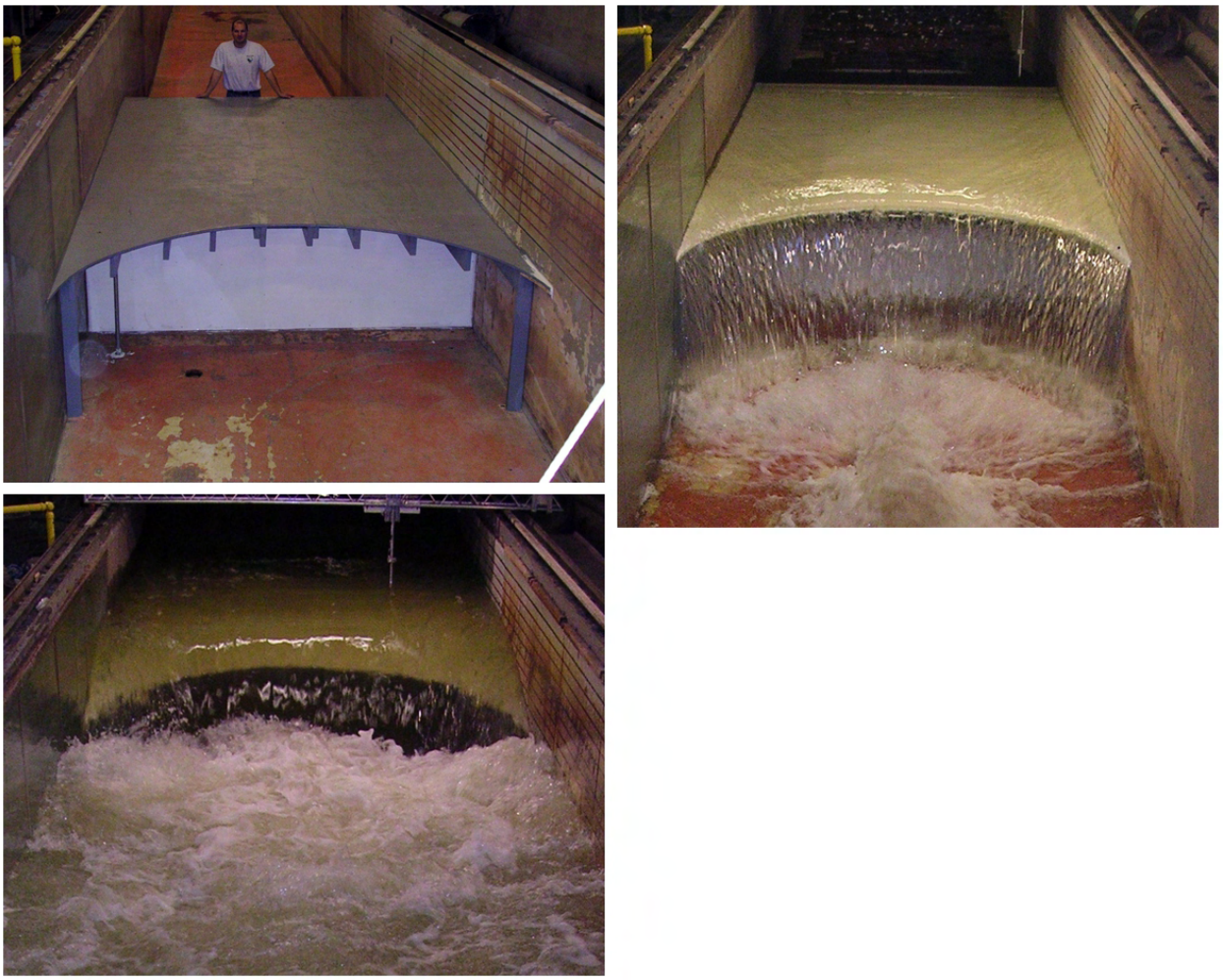

Figure 50. Illustration of stage-dependent hydraulics over an artificial morphological unit. The lower the discharge, the closer the hydraulics reflect the spatial structure of the underlying landform. In the case shown, the landform is a simple semi-circular bed step. In the high-flow run (lower left), the high velocity of the water launches it out over the step and the high tailwater depth drowns out step height. In the low-flow run, step characteristics are much more evident (upper right).

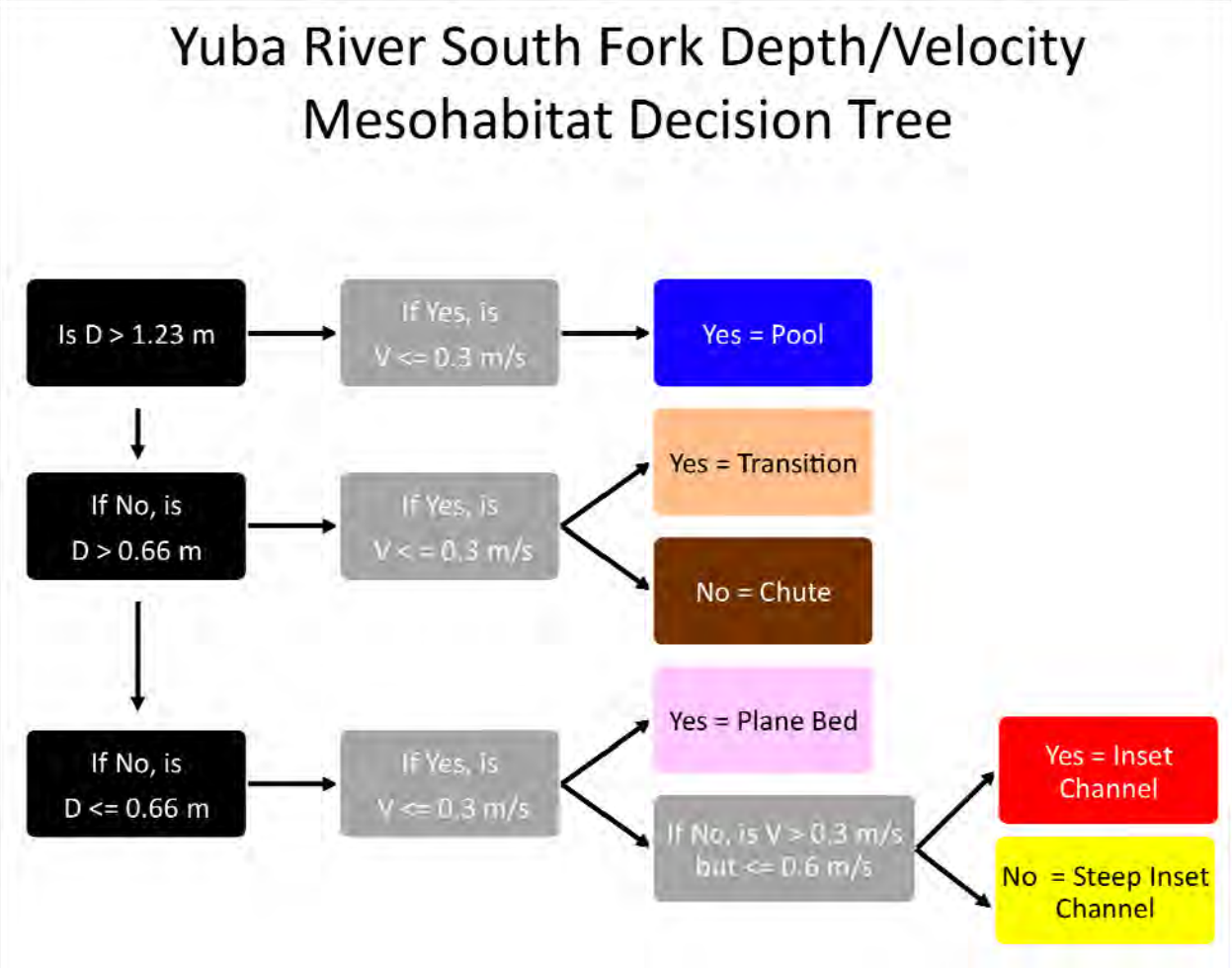

Figure 51. Decision tree showing the quantitative hydraulic thresholds used to delineate morphological units in the study. There were no areas where D>1.23 m and V>0.3 m/s in the summer 2009 baseflow simulation. Steps were manually delineated based on geomorphic indicators and thus are not present in this tree.

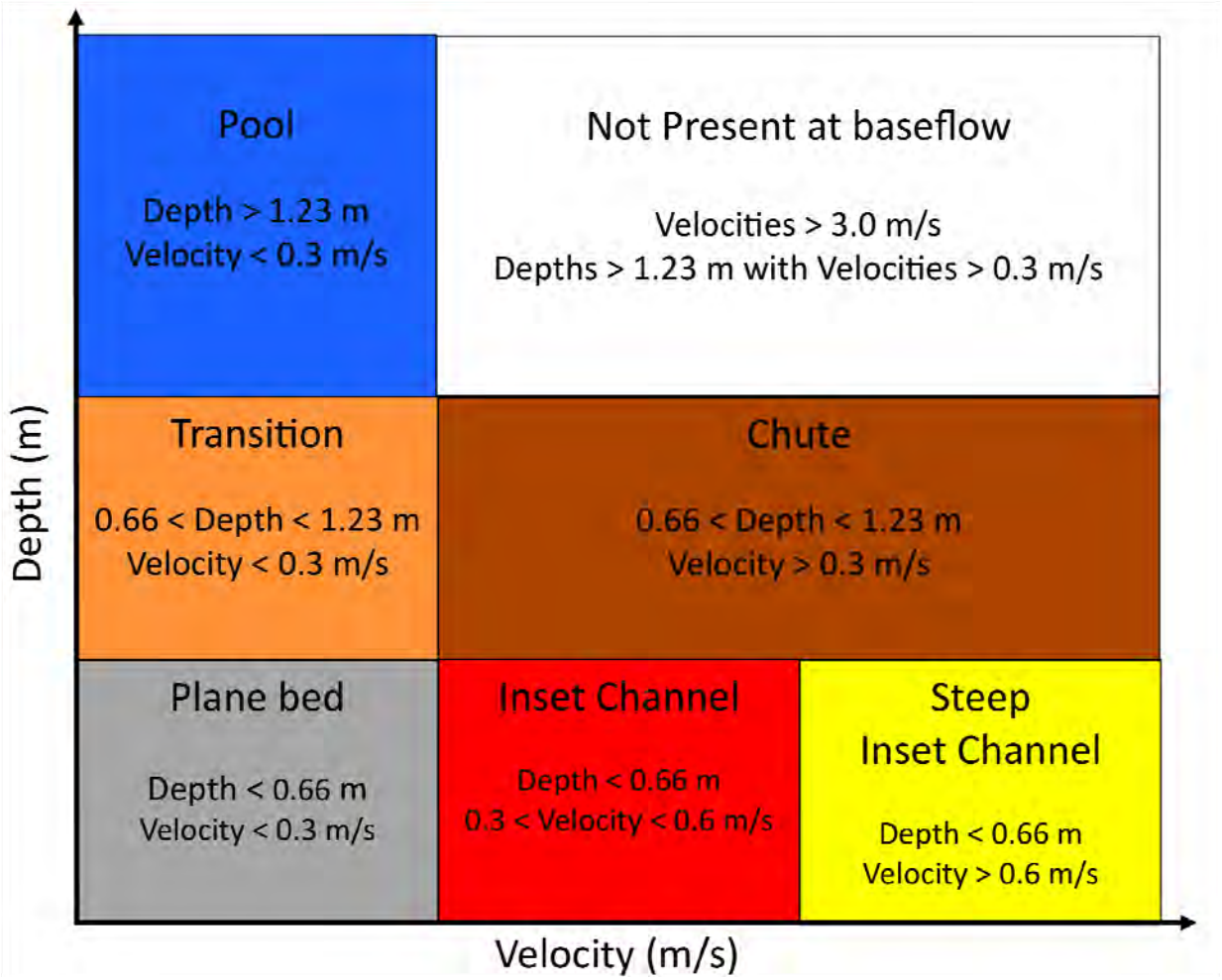

Figure 52. Phase-space plot of depth and velocity showing morphologic-unit hydraulic domains.

8.5 Morphologic Unit Delineation Procedure

The following steps were performed in ArcGIS to build morphologic unit shapefiles. First, georeferenced SRH-2D summer 2009 baseflow depth and velocity results (x,y,z) (z = depth and velocity, respectively) were imported into ArcMap and converted to shapefiles (e.g. Figure 53). Next, a boundary file was added, TINs were created via the 3D Analyst ArcTool, and converted to rasters (e.g. Figure 54). Conditional statements were developed using the previously described quantitative parameters in conjunction with the velocity and depth rasters in the Spatial Analyst Raster Calculator, which delineated the extent of each morphological unit throughout the study segment.

There was one exception to this procedure. The delineation of steps, of which there were just ten, was done manually because steps were further defined by elevational change >2 m between the brink of the step and the low flow WSE below. The procedure of delineating steps was done in ArcMap by editing the morphological unit polygon shapefile. This method resulted in a morphologic unit map (e.g. Figure 55, Figure 56) for the wetted channel that was used in many geomorphic, hydraulic, and ecologic analyses. Morphologic unit delineations were

visually compared against field experience, and photos were selected to represent each unit type (e.g. Figure 57, Figure 58, Figure 59, Figure 60, Figure 61).

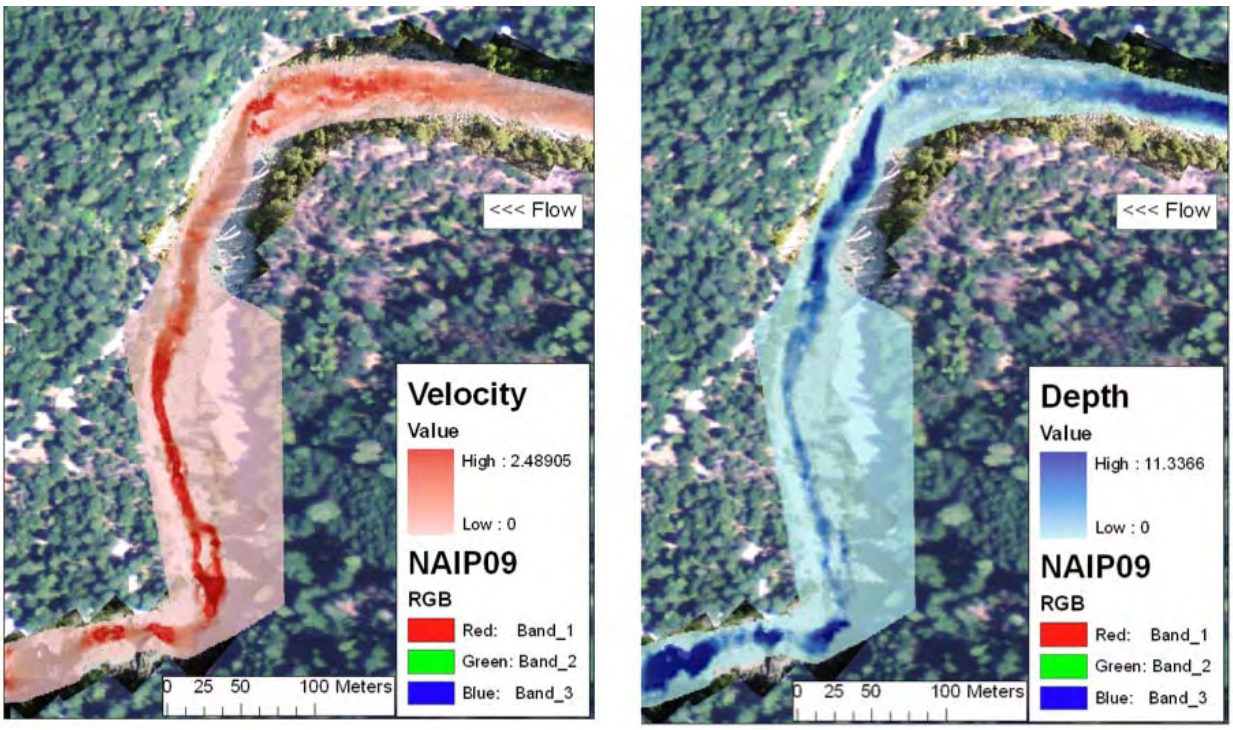

Figure 53. ArcMap velocity (left frame) and depth (right frame) rasters showing continuum of values returned by SRH-2D modeling of baseflow conditions. Colored areas show extent of 2D model domain, with the lightest color having a value of zero.

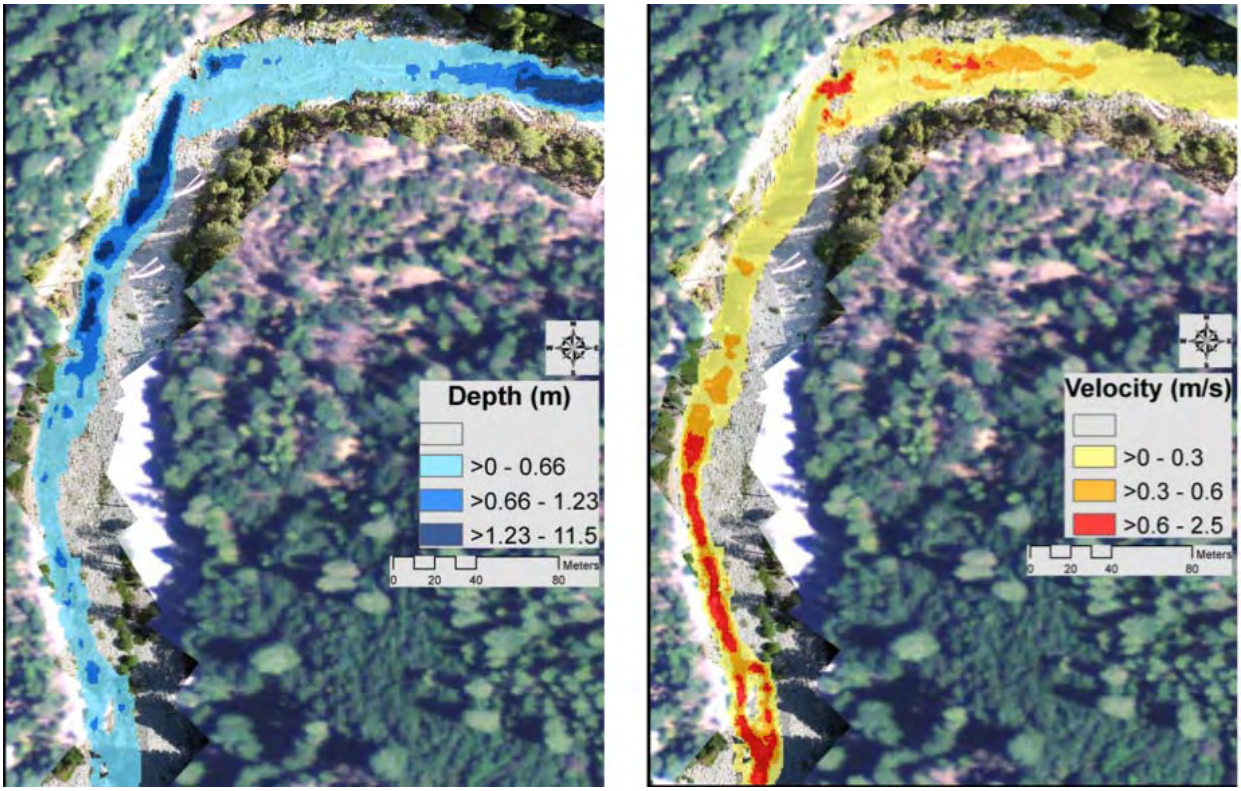

Figure 54. Wetted channel shapefiles derived from rasters and stratified by depth (left frame) and velocity (right frame). Note underlying high-resolution digital photos in-channel compared to 1-m resolution NAIP imagery. Shapefiles have a degree of transparency so that visible channel conditions can be seen.

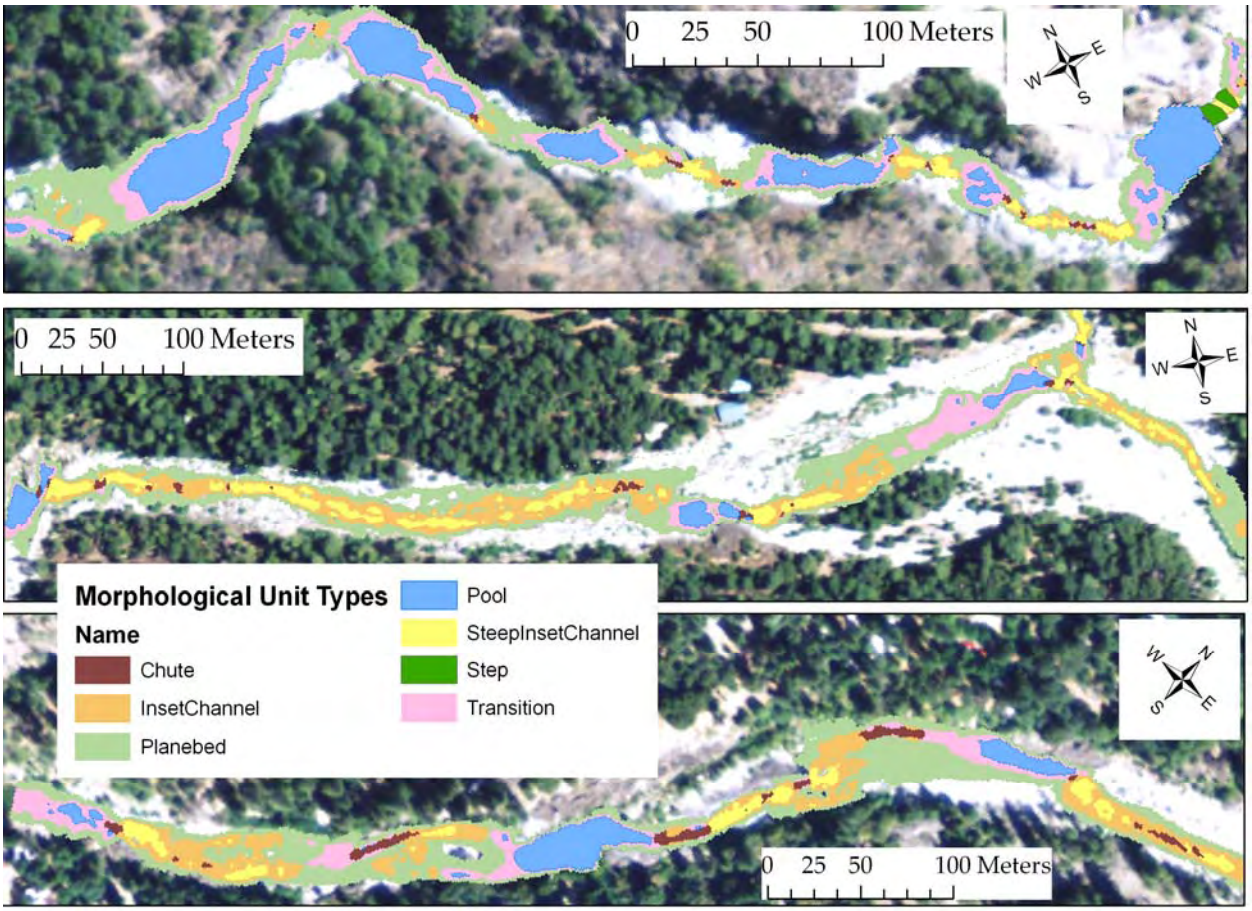

Figure 55. Morphologic units defined by quantitative binning of depth and velocity. Note underlying NAIP imagery and ~4 cm resolution kite-blimp aerial imagery.

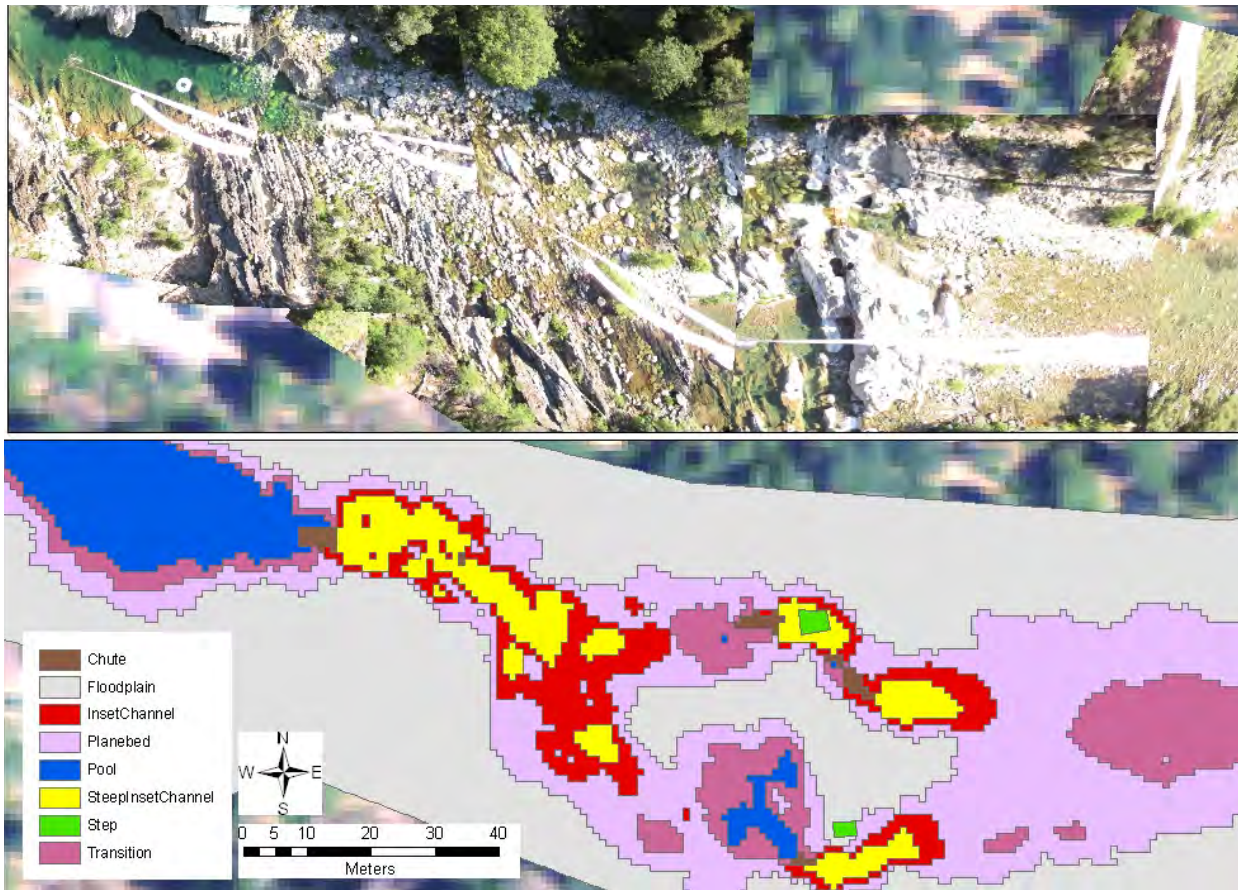

Figure 56. Representation of morphologic units. The two images show same reach, same scale. Upper image are a series of five georectified kite-blimp aerial images, lower image shows morphologic units as defined by depth and velocity variations. Note that the steps (depicted in green) were hand-drawn, as differences in elevation played a primary role in the designation of this unit.

Figure 57. Step morphologic unit. Oblique and vertical (aerial) aspects of a step, highlighting the difficulty of aerial imagery to detect significant elevational drops. Notice how difficult it is to recognize the step from the vertical angle.

Figure 58. Top left image shows steep inset channel unit followed by a small area of inset channel, then transition zone and into a pool. Top right image shows a crew member at edge of two morphologic units; transition to the right, plane bed to the left. Aerial image shows upper images, as well as (circle) steep inset then chute mid-image where turbulence is evident.

Figure 59. Crew members surveying topography in a steep inset channel. Chute exists directly downstream as turbulence diminishes, with transitions to either side of the chute. Pool in the lower portion of the aerial image (flow direction also to right) is depicted in Figure 60.

Figure 60. Pool with bedrock canyon walls (downstream to lower right in both images). From top of canyon wall (left) and aerial view (right).

Figure 61. Oblique upstream image (left) of inset channel at forefront and plane bed mid-image. Plane bed occupies river right, transition on river left. Aerial image (right) has arrow pointing to same inset channel. Downstream in right image, plane bed occupies channel edges along both sides, with transition present though middle of channel. Inset channel follows, with steep inset channel beginning at far right of image.

8.6 Transect-based and 1D Numerical Model Sampling of Morphologic Units

As explained in section 7.2 a primary goal of this study was to perform a methodological comparison among transect-based empirical analysis, 1D numerical modeling, and 2D

numerical modeling for instream flow assessment in mountain rivers. The methods for 1D and 2D numerical modeling were already explained in detail. For the transect-based analysis, the full method could not be explained in Chapter 0 without reference to the morphological units, so now the methodological explanation will be completed.

8.6.1 Morphological-unit Representation With Transects

For the transect-based analysis, a total of 30 cross-sections were selected within the 13.52-km river segment, a higher density of cross-sections than is commonly used in consulting/relicensing practices for the Sierra region (Payne et al. 2004). Total and percent areas of each morphologic unit type at baseflow discharge were calculated (Table 23), and then a minimum of three cross-sections per type was selected over six morphologic unit types (Figure 62). No step units were selected, as this unit type is commonly avoided for instream flow assessment, since it is not easily measured or modeled (and some consider it to have little habitat value for species of interest, though that is a questionable assumption. Studies have been done to show macroinvertebrate utilization of substrate and cover beneath steps to take advantage of the air bubbles there, so fish may also be attracted, since their food source is there).

The 30 selected transects were given a length that exceeds channel width at the highest flow observed. Points were distributed along transects in 0.5-m intervals. Because morphological units are laterally variable in size and shape, in every instance, the points along transects established to represent one unit type also contained points within other unit types. For example, in this study transition and/or plane bed units commonly flank a pool, so some points designated along a pool-transect may actually reflect the conditions in these other units. Nevertheless, in an effort to match how transects are commonly used for instream flow assessment associated with relicensing efforts, for which mesohabitat classes do not change across a channel, all points along a pool-designated transect were treated as if they were pool points.

Table 23. Morphologic unit total area at observed summer 2009 baseflow, percent and number of cross-sections selected per morphologic unit for transect-based analyses.

Morphologic Unit	Area (m^2) during baseflow conditions	# Distinct Units	% Area	# XS
Step	488.82	10	2.61	0
Chute	4784.12	326	25.55	3
Steep inset channel	18725.98	578	100.00	5
Pool	25804.28	153	137.80	5
Transition	28834.65	1099	153.98	5
Inset channel	47259.00	1892	252.37	6
Plane bed	135500.17	1291	723.59	6
Total	261397.02	5349	1395.91	30

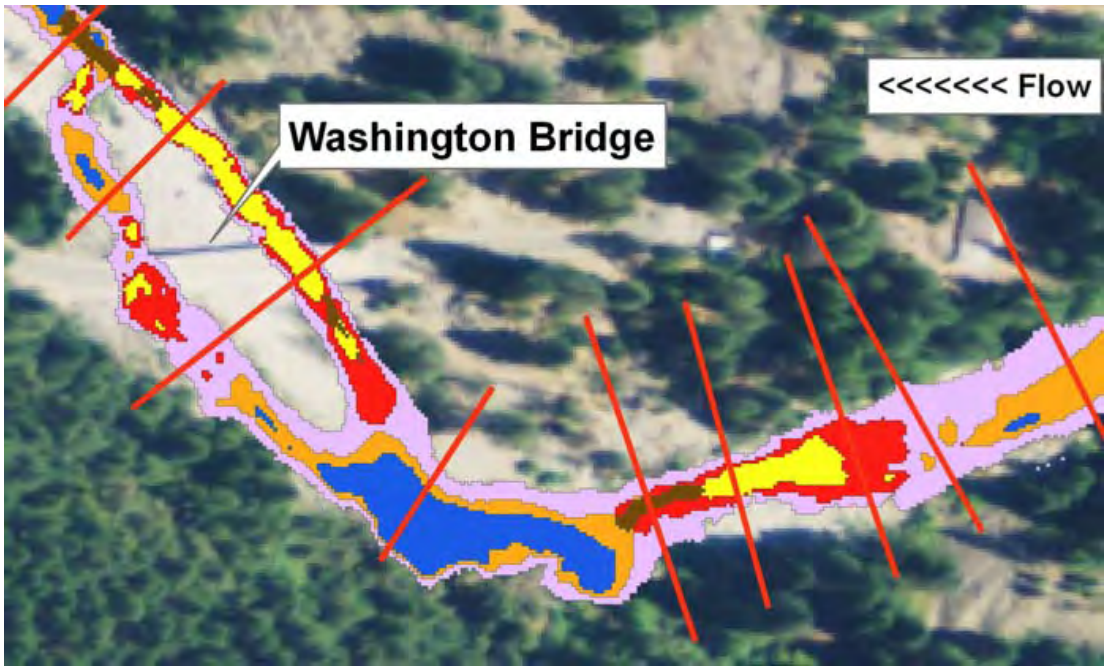

Figure 62. Some transect locations and associated morphologic units at one of the accessible sampling areas (see section 7.2). Brown = chute; orange = transition; yellow = steep inset channel; red = inset channel; light purple = plane bed; blue = pool.

8.6.2 Morphological-unit Representation With 1D Numerical Model

For the 1D numerical model, the number of morphologic units represented by the 105 cross-sections were 12 chute, 14 pool, 16 plane bed, 17 transition, 19 inset channel, 27 steep inset channel, and 0 step. The baseline cross-sectional spacing used here involved roughly uniform spacing (not exact, because model breaks around waterfalls required different spacing in different areas) as well as additional feature-based cross-sections (see section 8.6 for their selection method and locations). These criteria yielded a mean spacing of 130 m, with a minimum of 14 m and a maximum of 288 m (Figure 44). Once cross-sections were established, points were distributed along those lines in 0.5 m intervals and elevations were sampled at each point from the ground-based survey topographic TIN of the river corridor.

8.7 Morphologic Unit Analysis

A central question in fluvial geomorphology at the 10^0-10^1 W spatial scale is whether morphological units are naturally organized into a coherent spatial structure that is non-random. If the structure is indeed deterministic, then is it periodic or non-periodic? Traditional analyses in which morphological units are defined to be channel-wide and only change longitudinally are commonly reported to have a characteristic spacing. For example, pools are spaced 5–7 channel widths in riffle-pool sequences (Knighton 1997).

At the segment and reach spatial scales, the South Yuba River was composed of an unequal number of unequally distributed morphological units. Each unit type has a characteristic set of discharge-independent geomorphic attributes that explains its hydraulic conditions at the

summer 2009 baseflow. In terms of their spatial organization, analyses found that morphological units were preferentially ordered down the river segment in a nonrandom structure, with most unit types having a "preference" for adjacency to only a few other unit types (see section 8.7.3). In this usage, the term preference means co-occurrence at a higher frequency than would occur if occurrence were random. Since units are inanimate objects that cannot choose their location, the concept of a "preference" relates to the role of underlying, stage-dependent, physical processes that control unit type sequencing. A natural order to the sequencing is indicative of underlying natural laws in processes.

8.7.1 Morphological Unit Statistics

Morphological unit types in the South Yuba River study segment exhibit an unequal abundance, with each unit type having unique geomorphic attributes. Just over half of the wetted area of the geometric channel consists of a plane bed. From plane beds flows have carved out other units via sediment transport processes (e.g. Figure 55, Figure 56). The next most abundant unit type is the inset channel, which is an inner channel readily evident at low flow. After that transition, pool, and steep inset channel types follow in order of abundance. The least aerially abundant unit types are chute and step.

Given the variable shape and size of morphological units, it is difficult to calculate the slope of every individual unit, so an approach was developed using the valley center 10-m polygons. First, the length of the river was divided into river-wide 10-m long rectangular polygons (Figure 63; section 8.1.2). Next, the summer 2009 baseflow water surface elevation slope of each polygon was calculated by taking the change in WSE through each box divided by 10 m. Find relative percent area of each morphological unit in each rectangle by developing area measures of each unit in each rectangle. Remove all WSE slope values <0, as these would be local anomalies and were not considered applicable to this analysis. For each morphological unit type, the rectangles in which that unit type comprised >60% of the wetted area of the box were selected, and the average slope of all rectangles meeting this criteria was calculated. The results show that steep inset channel has ~4 times the slope of inset channel, confirming the decision to delineate those as independent types (

Table 26). Pools have a surprisingly high slope, consistent with the value for plane bed. Transition has the lowest slope.

The wetted width of the river was analyzed by morphological unit to characterize stage-dependent unit shapes. The valley center 10-m polygons were used for this analysis. For each discharge, the valley center shapefile was clipped with the wetted area polygon shapefile and the length of each clipped rectangle was calculated. The representative morphological unit type for each rectangle was identified.

Morphological units show significant differences in width at low flow and that difference decreases with increasing flow. Step and steep inset channel units were the narrowest at the lowest flow, while pools and transitions were the widest. Pools were almost twice as wide as steps. At the highest flow modeled, pools and steps were the narrowest units, while steep inset channel and inset channel were the widest. This indicates a "reversal" in width, which is one indicator of a possible shift in underlying hydrogeomorphic controls over that flow range. However, even though results indicate a reversal, the difference in widths between the widest and narrowest is only 24.7%, so at this stage the reversal is still relatively weak, even though flow is higher by almost three orders of magnitude.

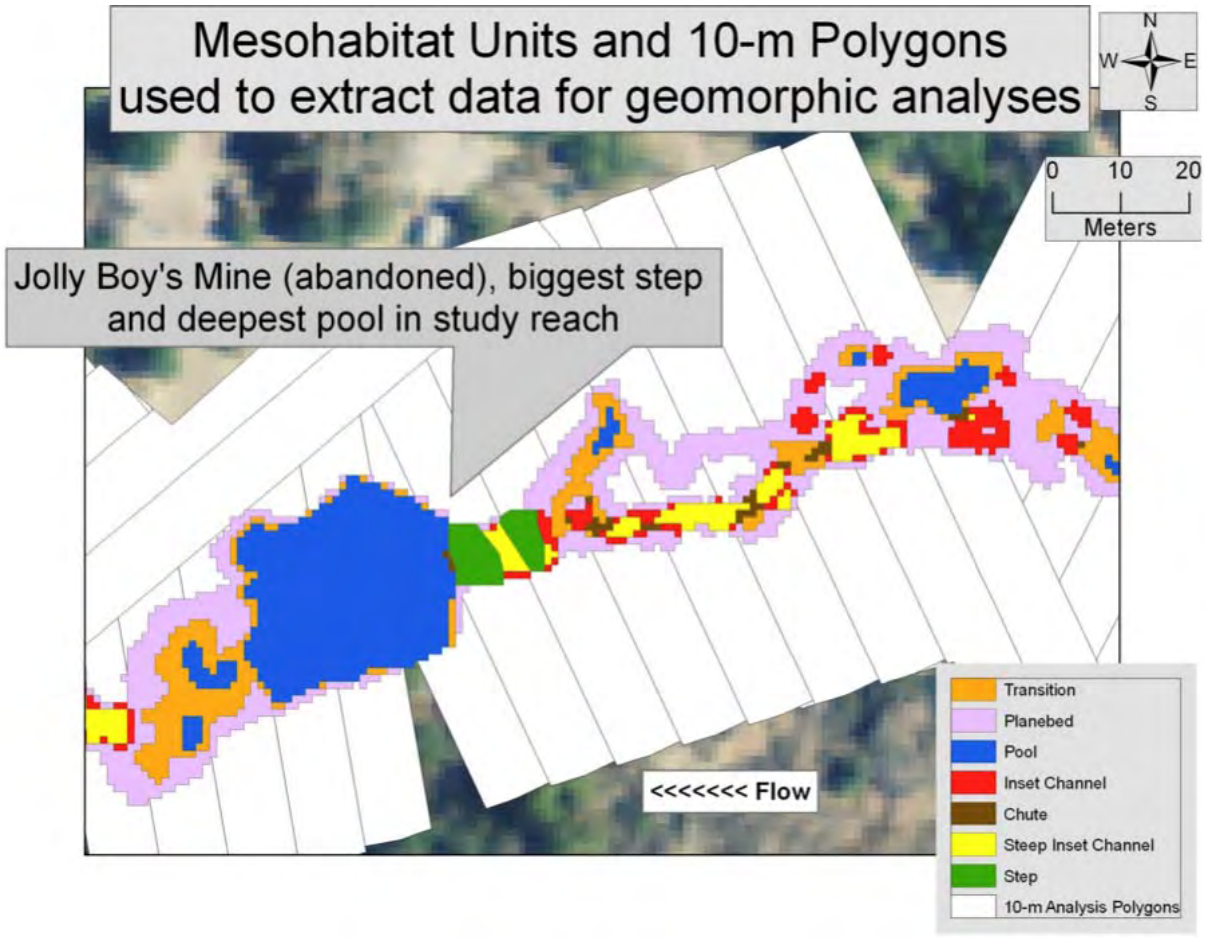

Figure 63. Equally spaced, 10-m long, rectangular polygons used to extract various metrics at the spatial scale of ~1 W. Note that some rectangular polygons overlap and others underlap (missing parts of the channel). Variations were considered to cancel each other out, so all values were

used in analyses no matter if it appeared that data were missing or duplicated. These variations occurred due to the sinuosity of the channel.

Table 24. Average width per morphologic unit per 2D modeled flow.

Dry	Chute	Inset Channel	Plane bed	Pool	Steep Inset Channel	Step	Transition	Average
5	12.60	13.28	14.85	18.37	10.73	9.65	16.72	13.74
10	14.94	15.91	17.04	19.13	13.48	10.72	17.34	15.51
20	19.39	19.36	20.07	21.19	17.93	13.19	21.00	18.88
30	23.15	22.45	23.78	23.54	22.67	14.64	23.38	21.94
45	28.06	26.24	27.43	26.33	28.22	18.26	26.68	25.89
Wet	**Chute**	**Inset Channel**	**Plane bed**	**Pool**	**Steep Inset Channel**	**Step**	**Transition**	**Average**
5	16.98	16.91	17.79	19.76	15.03	11.44	19.07	16.71
15	19.56	19.29	19.81	21.16	18.09	13.63	20.78	18.90
30	22.34	21.84	23.09	23.02	21.61	15.07	23.02	21.43
55	25.88	24.82	26.10	26.04	26.04	18.21	25.40	24.64
100	30.29	28.51	29.35	27.78	30.82	20.46	28.39	27.94
190	35.08	33.68	34.04	31.35	36.56	23.49	33.17	32.48
350	41.38	39.90	38.50	36.62	44.36	29.62	38.94	38.47
Snowmelt	**Chute**	**Inset Channel**	**Plane bed**	**Pool**	**Steep Inset Channel**	**Step**	**Transition**	**Average**
10	15.68	16.15	17.14	19.23	13.86	11.18	18.41	15.95
25	19.11	19.42	19.98	21.03	17.87	13.45	21.06	18.85
50	22.64	22.40	23.42	23.25	22.27	16.76	23.46	22.03
140	25.94	25.92	27.17	25.34	26.81	19.36	26.19	25.25
210	23.27	25.07	26.49	23.75	24.27	19.16	25.31	23.90
525	29.09	31.09	31.10	27.31	31.25	24.43	30.43	29.24
1103	33.96	36.10	35.60	30.75	37.23	28.10	34.56	33.76
3000	40.80	43.48	42.31	36.40	45.28	35.61	41.18	40.72
6921	49.21	51.26	49.46	43.89	54.52	43.74	49.31	48.77

Table 25. Width increase (m) between low and high flow per season.

	Chute	Inset Channel	Plane bed	Pool	Steep Inset Channel	Step	Transition	Average
Dry	15.46	12.96	12.57	7.95	17.48	8.60	9.97	12.14
Wet	24.40	23.00	20.71	16.87	29.33	18.18	19.87	21.76
Snowmelt	33.53	35.11	32.31	24.65	40.66	32.56	30.90	32.82

Table 26. Average summer 2009 baseflow water surface slope for each morphologic unit type.

Morphologic Unit	Average Slope (%)
Step	12.07
Steep inset channel	4.10
Inset channel	1.10
Chute	0.94
Plane bed	0.38
Pool	0.31
Transition	0.05

Table 27. Average stage-dependent wetted width for dry 5 cfs and snowmelt 6921 cfs flow per morphological unit type.

	Wetted width (m)	
	Dry	Snowmelt
Morphologic Unit	5 cfs	6921 cfs
Step	9.7	43.7
Steep Inset Channel	10.7	54.5
Chute	12.6	49.2
Inset Channel	13.3	51.3
Plane bed	14.9	49.5
Transition	16.7	49.3
Pool	18.4	43.9

8.7.2 Morphological Unit Longitudinal Distribution

The previous section established that morphological units are geomorphologically differentiated. The next question is whether they are spatially organized or randomly located along the study segment. By definition, if they are randomly located, there is equal probability of them being located in any particular location. When that is the case, then the type of statistical distribution that is present is called a uniform distribution. The presence of a uniform distribution is indicated by having a straight-line cumulative distribution function when cumulative probability of occurrence is plotted against distance upstream or downstream. Deviations of the slope from a straight-line trajectory indicate a higher or lower occurrence in a region of channel relative to the uniform expectation, where a steeper slope would indicate a higher occurrence and a lower slope would indicate a lower occurrence.

Probability and cumulative distribution functions of the morphologic units shows that steps were predominately observed at the top of the segment (80% within top 3 km), plane bed occurred uniformly throughout the study having a nearly straight-line cumulative distribution, and all other types were found preferentially lower in the segment (Figure 64, Figure 65). Chutes had the strongest downstream preference. Fewer pools were found in Reaches 4 and 5, which also had the lowest width ratios between high/low flows and the smallest increases in

WSE from Z to baseflow WSE to high-flow WSE (

Table 20, Table 22). Inset channels and steep inset channels were more abundant in the lower 6 km.

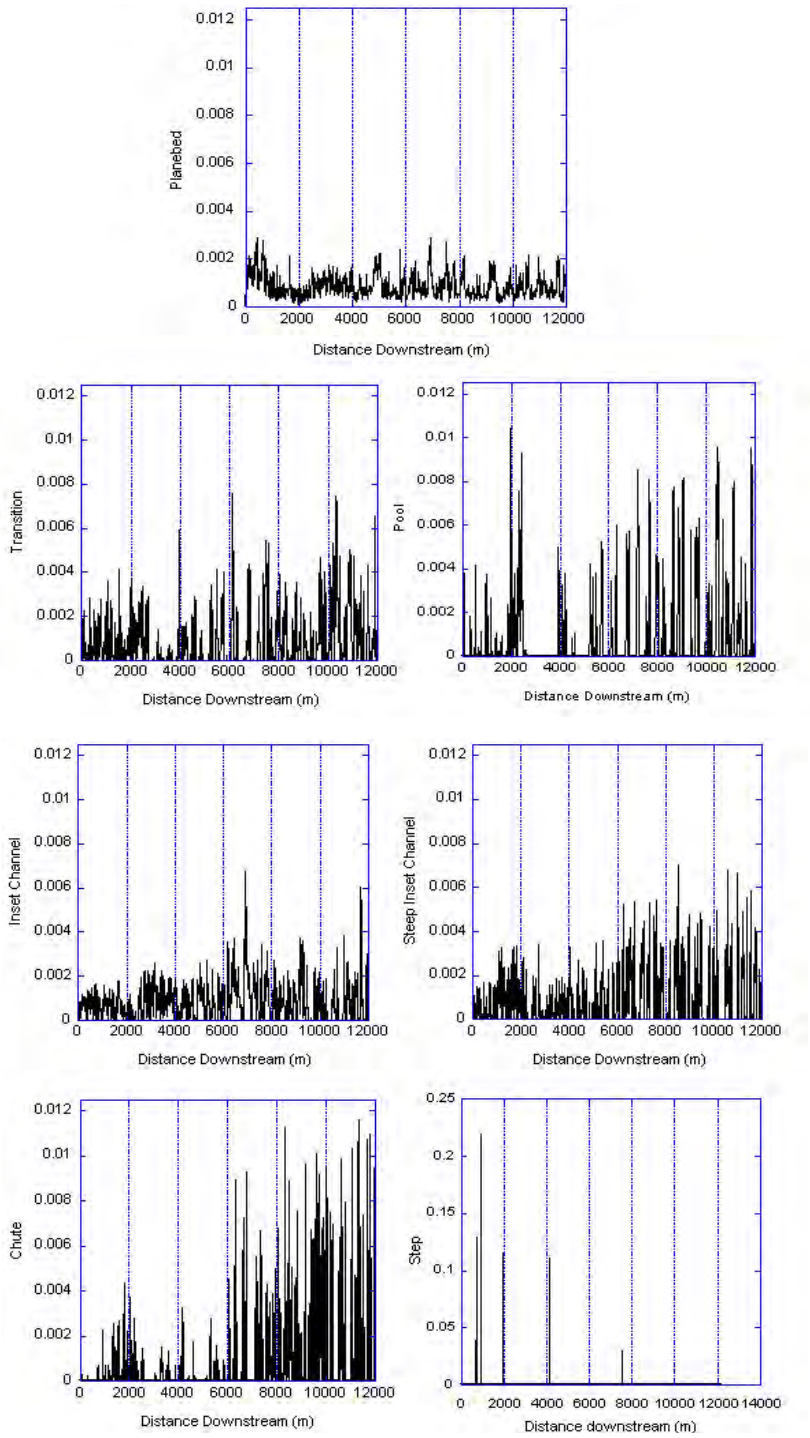

Figure 64. Probability distribution function for morphologic units. In all graphs the y-axis is percent. Note origin starts at top of study segment rather than bottom, also that Step y-axis scale is different.

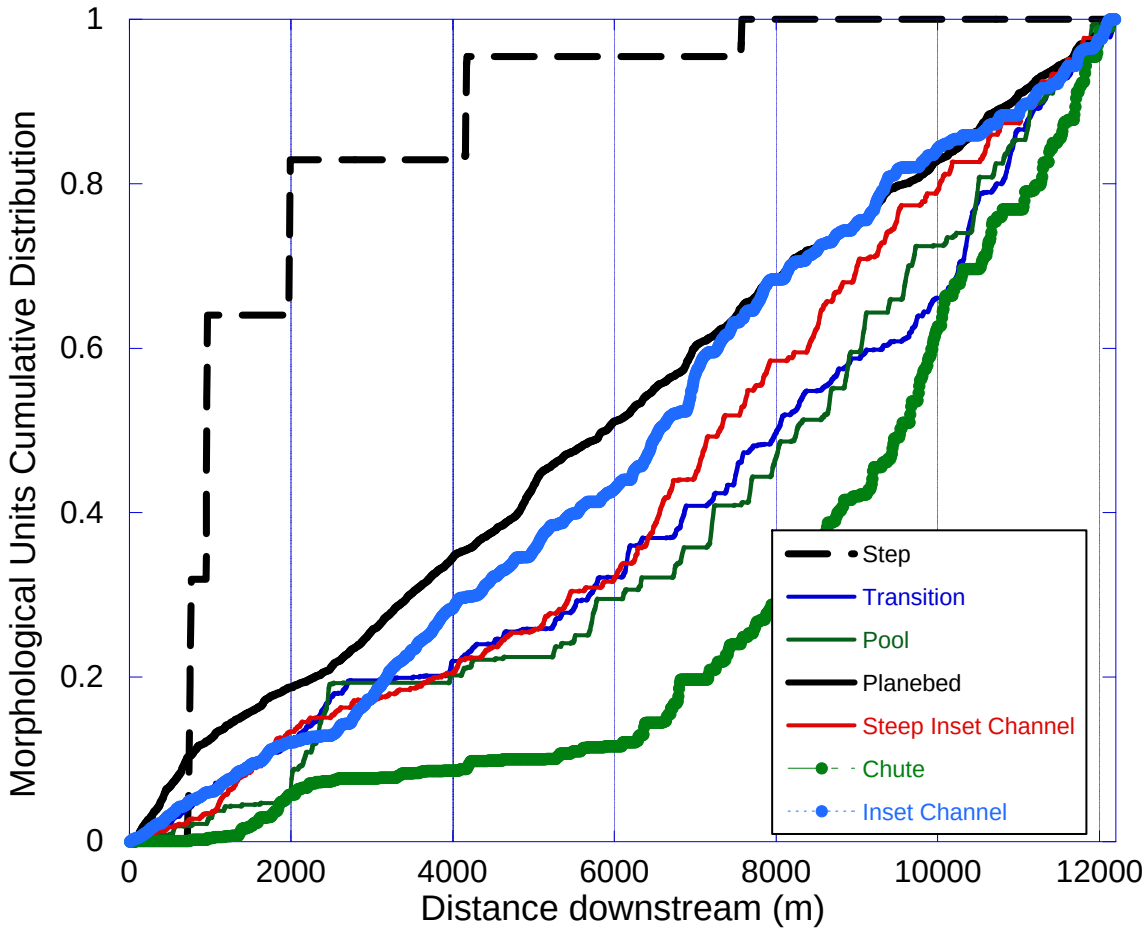

Figure 65. Cumulative distribution of morphologic units. Note that the upstream boundary starts at the origin.

8.7.3 Morphological Unit Organization Analysis

An underutilized approach to investigating morphological unit organization is the transition probability analysis method of Grant et al. (1990). This approach evaluates the frequency that each morphological unit is adjacent to every other unit, and then compares that against the expectation associated with a random system. This approach should become more valuable now that detailed spatial datasets of fluvial landforms are becoming readily available. As a result of lack of use, there is no baseline as to what constitutes a "normal" transition probability matrix, so an important first step is to apply the method for diverse natural and regulated streams and derive that.

Because the morphological unit conceptualization used in this study involves both lateral and longitudinal adjacency of units, a new procedure had to be developed to investigate transition probabilities, which in this analysis become non-directional adjacency probabilities. To determine how many units of one morphologic type were adjacent in any direction to another type, the Select by Location ArcGIS selection tool was used. This tool allows the user to specify

criteria for selection. For this analysis, a 12.2 km shapefile was selected with all instances of morphologic units represented by individual polygons, and then a specific morphologic unit shapefile separate from the all unit types shapefile (e.g. plane bed only) was selected to intersect with the full shapefile polygons. This led to the selection of all polygons of the specified unit type (from the morphologic unit shapefile containing all polygons of all unit types) that shared a common boundary with the individual morphologic unit type shapefile (Table 28). For instance, a plane bed unit was adjacent to an inset channel unit 1113 times and to a pool 178 times, so 43.3% of the entire plane bed adjacency was associated with inset channels and only 6.9 % associated with pools. This type of adjacency is not one-to-one. That is, unit type A will be adjacent to X number of unit type B, while unit B will be adjacent to unit type A, a different Y number of times. That happens because a single type A polygon can be long and touch multiple unit B polygons, whereas in the inverse, all those B polygons are only touching the one type A polygon. In other words, there is no way to count each individual transition, which would have to be one-to-one, and instead the metric that is counted is number of unique adjacencies. If five unit A polygons touch the same unit B polygon, then that counts as one adjacency, but in the inverse it counts as five adjacencies.

The way Grant et al. (1990) evaluated the likelihood that the transition probabilities were nonrandom was to randomly generate a sequence of units (with each unit equally likely to occur next in order of selection), calculate the random transition probabilities, and then compare the real transition probabilities to those. A possible issue with that method is that the outcome is sensitive to the specific sequence created at random. Conceivably, one could repeat the step several times and compare the real transition probabilities to the average of random ones. Conversely, if one were to use a near infinite number of random sequences, then in the limit, by definition, the transition probabilities available for this analysis must converge on 100/7, or 14.3%, since there is equal probability of any unit type randomly going to any of the other six unit types (with seven total unit types to choose from). As a result, it is possible to designate a "preference" or "avoidance" to adjacency to a unit type on the basis of whether the percent of adjacencies to it (Table 28) are higher or lower than 14.3%. This is the approach used here.

Results of this analysis show that there is a strong organizational structure evident in the adjacency probabilities (Table 29, Table 31). All units have a higher than random adjacency to plane bed, which is understandable, since plane bed is present at the margins of most of the wetted area. Excluding plane bed, inset channel and steep inset channel show an organizational proximity to each other. Similarly, transition and pool as well as pool and chute both show preferential connection. Chutes also tend to be adjacent to inset channel and steep inset channel. Steps tend to be associated with inset channel and steep inset channel. This last one is remarkable, since people commonly conceive as steps ending in a plunge pool. In this case that association is less common than randomly expected and steps are part of sequences of the steeper unit types.

Another test compared the percent of adjacencies for a unit type to the relative percent area of the other unit types (renormalizing total area to exclude the area of the unit type being tested). Conceptually, the more channel area that a unit type has relative to the others, the more likely that another unit is going to be adjacent to it. As a result, it is possible to design a "preference" to be adjacent to a unit type B on the basis of whether the percent of adjacencies of type A to it (Table 28) are higher than type B's percent of total area (

Table 19) renormalized to exclude the area of the type A (since A cannot be adjacent to itself).

Using this percent area reference, the results are somewhat inverted from those observed for the random percent test. In the random test, plane bed comes up as significant simply because it has so many adjacencies. In the area test, plane bed adjacency is not significant, because the calculation recognizes its abundant area explicitly. On the other hand, since step is so rare in the segment, any adjacency to it is disproportionate to its area and it appears more significant than it is. The random test did not show this bias. Of interest is that both tests yield a similar result for the adjacency preferences for transition, pool, and steep inset channel. The area test amplified the significance of chute, somewhat like the step area effect, but this result seems more meaningful, because chutes occur as a large number of small polygons but with a small total area. That means that chute can have many adjacencies, despite its low area, and that seems to be what the area test is suggesting. Step has both a low number and a low area, so its results may not be as significant, whereas the chute results may be significant.

Table 28. Transition probabilities showing number and percent of unit transitions.

	# of starting units that are adjacent to this unit type							
Starting unit	Plane bed	Inset channel	Transition	Pool	Steep inset channel	Chute	Step	Total Transitions
Plane bed	0	1113	347	178	697	208	25	2568
Inset channel	1847	0	320	8	1440	522	33	4170
Transition	1082	281	0	811	41	340	7	2562
Pool	83	7	153	0	3	67	5	318
Steep inset channel	354	578	40	3	0	167	13	1155
Chute	234	310	235	68	170	0	6	1023
Step	9	9	5	3	7	4	0	37
Total transitions	3609	2298	1100	1071	2358	1308	89	11833

	% of total transitions from the starting units to another unit							
Starting unit	Plane bed	Inset channel	Transition	Pool	Steep inset channel	Chute	Step	Total %
Plane bed	0	43.3	13.5	6.9	27.1	8.1	1	100
Inset channel	44.3	0	7.7	0.2	34.5	12.5	0.8	100
Transition	42.2	11	0	31.7	1.6	13.3	0.3	100
Pool	26.1	2.2	48.1	0	0.9	21.1	1.6	100
Steep inset channel	30.6	50	3.5	0.3	0	14.5	1.1	100
Chute	22.9	30.3	23	6.6	16.6	0	0.6	100
Step	24.3	24.3	13.5	8.1	18.9	10.8	0	100

Table 30. Occurrence of starting units that are adjacent to this unit type. Highlighted cells indicate adjacency is more frequent than by random chance alone.

Starting unit	Plane bed	Inset channel	Transition	Pool	Steep inset channel	Chute	Step
Plane bed		3.0	0.9	0.5	1.9	0.6	0.1
Inset channel	3.1		0.5	0.0	2.4	0.9	0.1
Transition	3.0	0.8		2.2	0.1	0.9	0.0
Pool	1.8	0.2	3.4		0.1	1.5	0.1
Steep inset channel	2.1	3.5	0.2	0.0		1.0	0.1
Chute	1.6	2.1	1.6	0.5	1.2		0.0
Step	1.7	1.7	0.9	0.6	1.3	0.8	

Table 31. Occurrence of starting units that are adjacent to this unit type. Total area has been renormalized to exclude the percent area of the starting unit. Highlighted cells indicate adjacency is more frequent than would be present by relative percent area alone.

Starting unit	Plane bed	Inset channel	Transition	Pool	Steep inset channel	Chute	Step
Plane bed		1.2	0.6	0.3	1.8	2.1	2.5
Inset channel	0.7		0.6	0	3.9	5.6	3.5
Transition	0.7	0.5		2.9	0.2	6.5	1.3
Pool	0.5	0.1	3.9		0.1	10.4	7.6
Steep inset channel	0.5	2.6	0.3	0		7.3	5.6
Chute	0.4	1.6	2	0.7	2.3		3.1
Step	0.5	1.3	1.2	0.8	2.6	5.9	

8.7.4 Morphological Unit Spacing

Traditional research has reported that pools tend to be spaced every 5–7 channel widths down a river (Knighton 1998). To test that, the following analysis was done. The centroid of each pool polygon was located in ArcGIS and the perpendicular point on the thalweg at the position of each pool centroid was identified. The route distance from the downstream end of the thalweg to each point was determined, and the difference between route distances for adjacent thalweg pool points was calculated, which yielded a spacing metric.

The same procedure was repeated for the chute and steep inset channel unit types, which are also primarily distributed longitudinally. Plane bed was so ubiquitous that spacing was not considered a viable test for this unit type. Inset channel and transition had many laterally distributed polygons and very small polygon areas, so these units were also not analyzed for longitudinal spacing. As defined in this study, steps were too rare to analyze for spacing.

The key finding of the analysis was that during the summer 2009 baseflow, pools conformed to the expected average spacing. Specifically, they had a mean spacing of 6.9 average channel widths, with a median of 3.3 and maximum of 96 (Table 32). Although this average fit the

known empirical generalization from worldwide rivers, pool spacing was not periodic over the 12.2-km study segment. Some areas were mostly devoid of pools and others had a tight spacing of them.

By comparison to pools, chutes and steep inset channels were much more tightly spaced, with chutes an average 43.9-m apart and steep inset channels just an average 25.6-m apart. This is explained by the fact that pools have more total wetted area distributed among fewer individual units (Table 23). Although individual chutes and steep inset channels are smaller in area than pools, both have higher numbers of units, which translates into closer spacing.

Table 32. Longitudinal spacing at summer 2009 baseflow between unit locations for those unit types primarily distributed downstream and with less distribution across the channel.

Statistic	Pool	Chute	Steep inset channel
mean (m)	94.6	43.9	25.6
mean (W)*	6.9	3.2	1.9
median (m)	44.7	20.3	14.3
median (W)*	3.3	1.5	1
std dev (m)	156.3	71.9	38.2
min (m)	2	0.37	0.05
max (m)	1483.9	564.2	363
max (W)*	95.7	36.4	23.4
count	142	305	525

*Spacing divided by the mean channel width of 15.51 m for the dry 10 cfs simulation

8.8 Substrate Analysis

With the advent of high-resolution remote sensing methods, it has become feasible to investigate the relative distribution of bedrock, boulders, streamwood, and other features in mountain rivers. Performing manual grain size analysis of bed material sizes that range from <1–1,000 mm is extremely difficult and cannot be done with a single measurement tool. Visual substrate classification is considered inaccurate by sedimentologists (Bunte and Abt, 2001), and its particularly ineffective with such heterogeneous mixtures. The availability of ~0.6-m resolution LIDAR data and ~4-cm resolution kite-blimp imagery motivated efforts to extract these features through remote sensing and GIS methods. Rapid advances have recently been made in using imagery to estimate bed material grain size metrics (Warrick et al. 2009, Buscombe et al. 2010). Bedrock and alluvium coverage of the channel bed, boulder size and longitudinal distribution, grain size distributions, and streamwood distributions all contribute to understanding complex patterns in mountain rivers.

8.8.1 Bedrock Analysis

Bedrock was delineated using georectified kite-blimp images to digitize bedrock sections in the wetted channel and on the floodplain into a shapefile using the Editor tool. Deep pools or shadows precluded bedrock delineation for a small amount of the channel bed. Bedrock distribution is reported by morphologic unit area and percent distribution (

Table 33). Overall, 12% of wetted channel and 11.6% of floodplain were classified as bedrock. This finding suggests that there is a high sediment supply that mantles the majority of the bedrock. Within the channel, 53.7% of exposed bedrock is located in plane bed areas, while 14.7% is visible in pools. Almost the same amount of bedrock is exposed in transitions. Within each unit type, the units with the highest proportion of their bed as exposed bedrock are step, pool, and transition in descending order. The higher amount of exposed bedrock in pools suggests that even though pools are depositional zones for sediment at low flows, some floods must occur that scour pools down to bedrock and prevents alluvium from filling them in on the falling limb of those same floods. Similarly, the fact that inset channel and steep inset channel are >3x steeper than pools, but they have the highest proportion of coverage by alluvium, indicates that there must be some high flow under which they experience net deposition. These findings are evidence for the role of stage-dependent landform nonuniformity in controlling geomorphic patterns, but do not reveal the mechanism by which the patterns are formed and maintained.

Table 33. Bedrock occurrence within morphologic units and on floodplain at wetted baseflow conditions.

Bedrock Distribution	Area (m^2)
Bedrock within Chute :	648.8
Bedrock within Inset channel:	2913.7
Bedrock within Plane bed:	16819.9
Bedrock within Pool:	4585.3
Bedrock within Steep inset channel:	1565.2
Bedrock within Step:	290.7
Bedrock within Transition:	4474.0
Total Bedrock within Channel:	31297.6

Morphological Unit	% Bedrock
Chute	13.6
Inset channel	6.2
Plane bed	12.4
Pool	17.8
Steep inset channel	8.4
Step	59.5
Transition	15.5

Segment-scale Distribution	% Bedrock
% Wetted Channel that is Bedrock	12.0
% Floodplain that is Bedrock	11.6

8.8.2 Boulder Analysis

Boulder points and polygons were delineated using LIDAR as explained in sections 4.9–c. Boulders were analyzed in terms of numbers of boulders and area of boulders. The procedure involved using the equally spaced, 10-m long, rectangular polygons along the river segment and counting the points in ArcGIS to determine the number of boulder points in each 10-m rectangular polygon. The 10-m polygons were clipped to the wetted area at the 2009 summer baseflow and the percent area of each boulder/boulder cluster in each 10-m polygon was calculated. Next, the cumulative and probability distribution functions for boulder points and boulder area were derived. Boulder polygons and morphological unit polygons were overlaid to determine the relative abundance of emergent boulders by unit type (Figure 66).

Boulder numbers and area have very similar distributions (Figure 67, Figure 68). When boulder numbers are more abundant than boulder area, there are more small boulders present in that 10-m section. The largest area and number of boulders is located at ~1800 m above the lower study boundary in Reach 1. The total area of boulders was 20,645.5 m^2, and the total number of boulders was 34,113, for an average boulder area of 0.61 m^2.

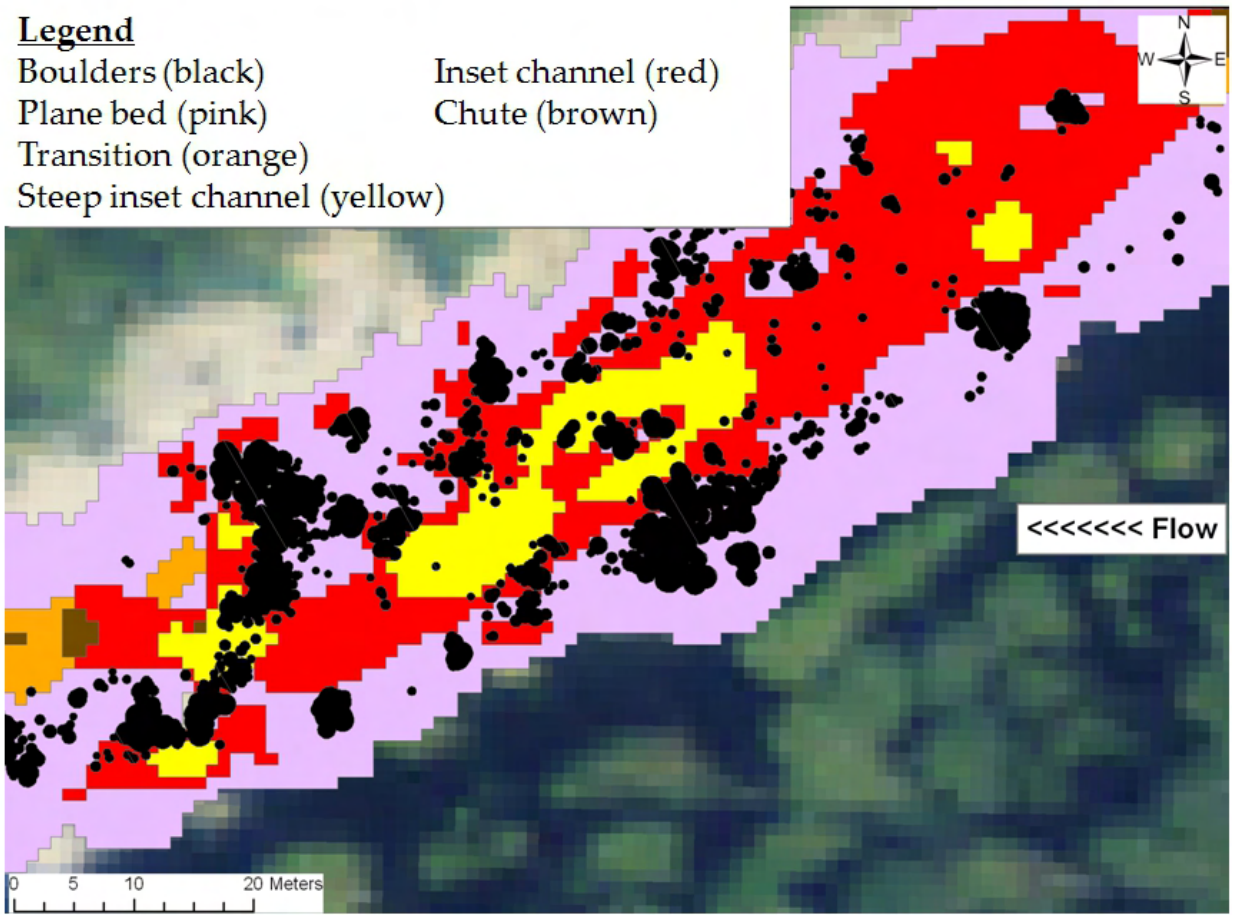

Figure 66. Example of the overlay of boulders and morphological units. Notice the clusters of boulders compared to individual boulders. Boulder dots vary in size according to diameter.

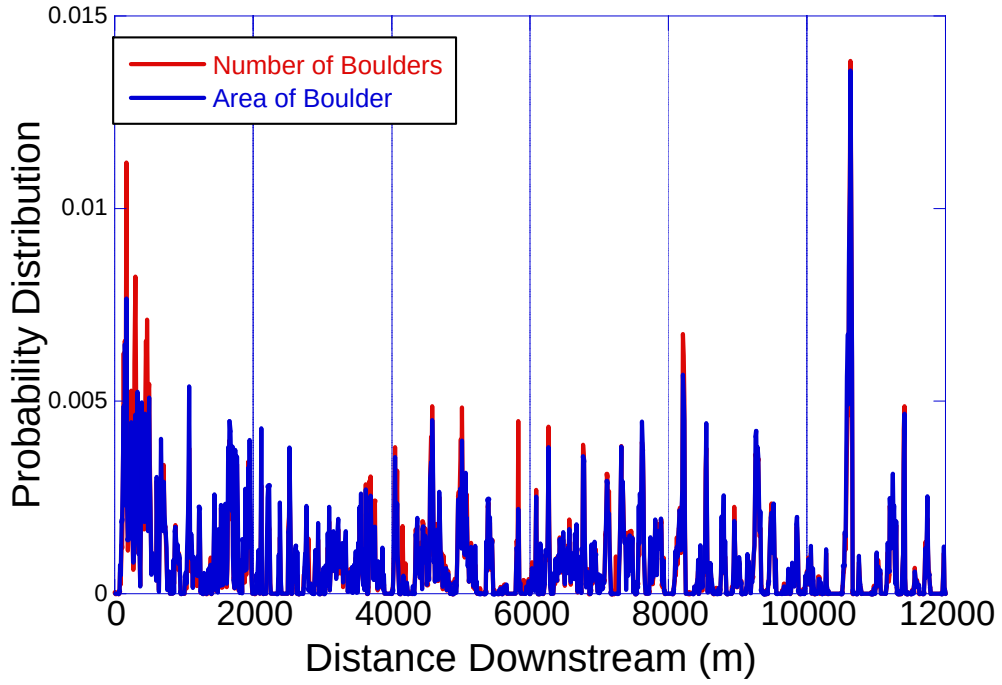

Figure 67. Probability distribution of number and area of instream emergent boulders. Note origin starts at upstream limit.

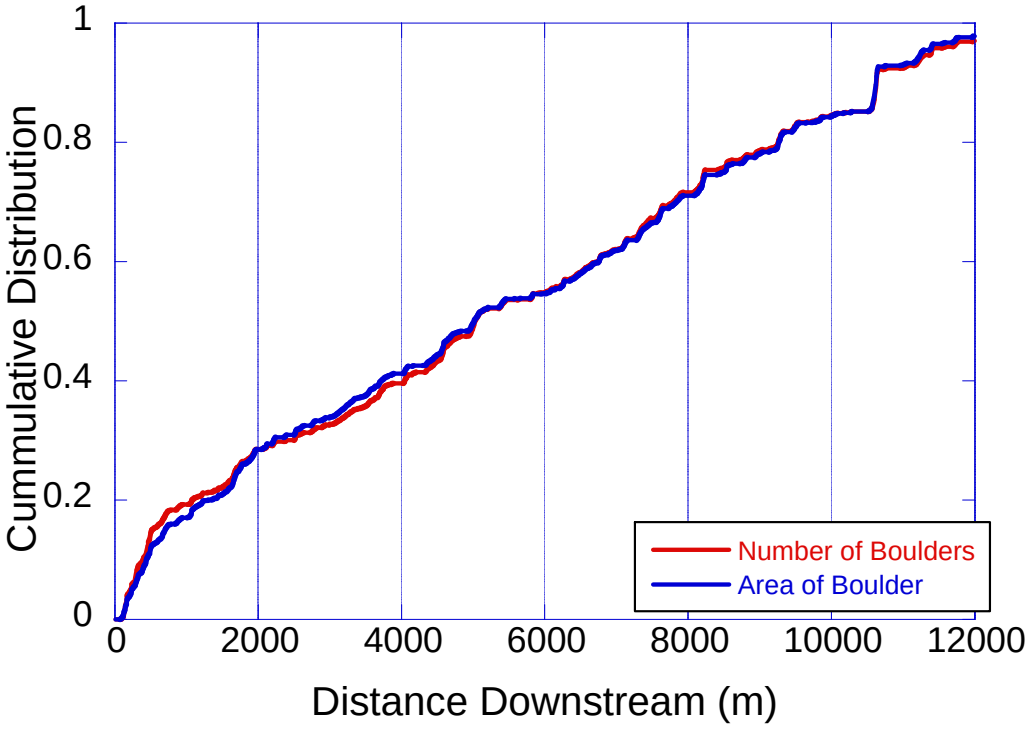

Figure 68. Cumulative distribution of number and area of emergent boulders.

8.8.3 Alluvium Analysis

A limited effort was made to characterize alluvial bed material grain size distributions. The primary potential purpose for doing so would be to quantify the availability of microhabitat by substrate class. However, in most areas the bed material was heterogeneous and had gravel-sized sediment intermixed, such that gravel occurrence did not appear to be a limiting factor on the ambient bed. As a result, the approach taken here was to use a recently introduced method to measure grain sizes without doing the laborious field work necessary to adequately characterize a grain size distribution across the length of the study segment. Instead, a remote-sensing based algorithm was applied to kite-blimp imagery to estimate average sediment size per morphologic unit. Morphological unit areas of less than 10 m^2 were not included in the analysis, as units of this size were at the lower limit of the minimum size needed for image analysis. At the time of these analyses, the researchers' ability to perform this method was limited to dry land where the bed material was clearest; more work is needed to understand limitations of water depth on image clarity and subsequent analysis. To begin the procedure, georeferenced kite-blimp aerial images were opened in ArcMap. The morphologic unit shapefile for floodplain was opened and the floodplain attribute table was used to eliminate all unit areas less than 10 m^2 so that a large enough area could be selected for analysis. Random numbers were generated within the range of number of polygons eligible for analysis. Randomly selected floodplain polygons were located and scrutinized to determine if sediment analysis could be performed on that particular polygon. Elimination of a polygon may occur due to position of unit in relation to position of image (i.e. along bedrock bank, in shadow, image lacking sufficient control points for high-quality georectification). Once an image was selected for analysis, it was exported as a rectified .tif image and opened in a photo manipulation program such as Gimp image software for cropping to an area of analysis free of water and vegetation. The Cobble Cam freeware MATLAB code of Warrick et al. (2009) was used to analyze the image, and yielded calculations of average sediment diameter, standard deviation, and standard error. The only input value needed for this program was pixel resolution, which provided a limit to the grain size that this program could analyze.

An image and blown-up inset of one image shows a typical area available for analysis (Figure 69). Mean floodplain sediment diameter ranged from 244-1264 mm. Overall mean sediment diameter for all analyzed images was 641 ± 321 mm (

Table 34). Difficulties were encountered with some of the analyzed images due to heavy shading, images out of focus at higher resolutions (as evident in Figure 69), brightness of image, size of selected location, and very large boulders acting as outliers that may skew final mean and standard deviations. Random selection was also difficult, for the above reasons as well as finding large enough areas to select images of the suggested minimum 150 x 150 pixels. After numerous images were rejected due to poor returns versus manually checking sediment diameters with the Arc ruler, it was decided that images 400 x 400 pixels were generally the smallest that would return reasonable results. Pixel sizes ranged from ~2.5-4 cm, so unobstructed areas that could be used for analysis needed to be about 10 m^2 for reasonable results.

A series of randomly selected in-stream wetted areas were also analyzed. These images did not return reasonable results. Subsequent efforts might utilize a deterministic selection process, where promising analysis locations are selected and then the morphologic unit layer is turned on to identify unit type.

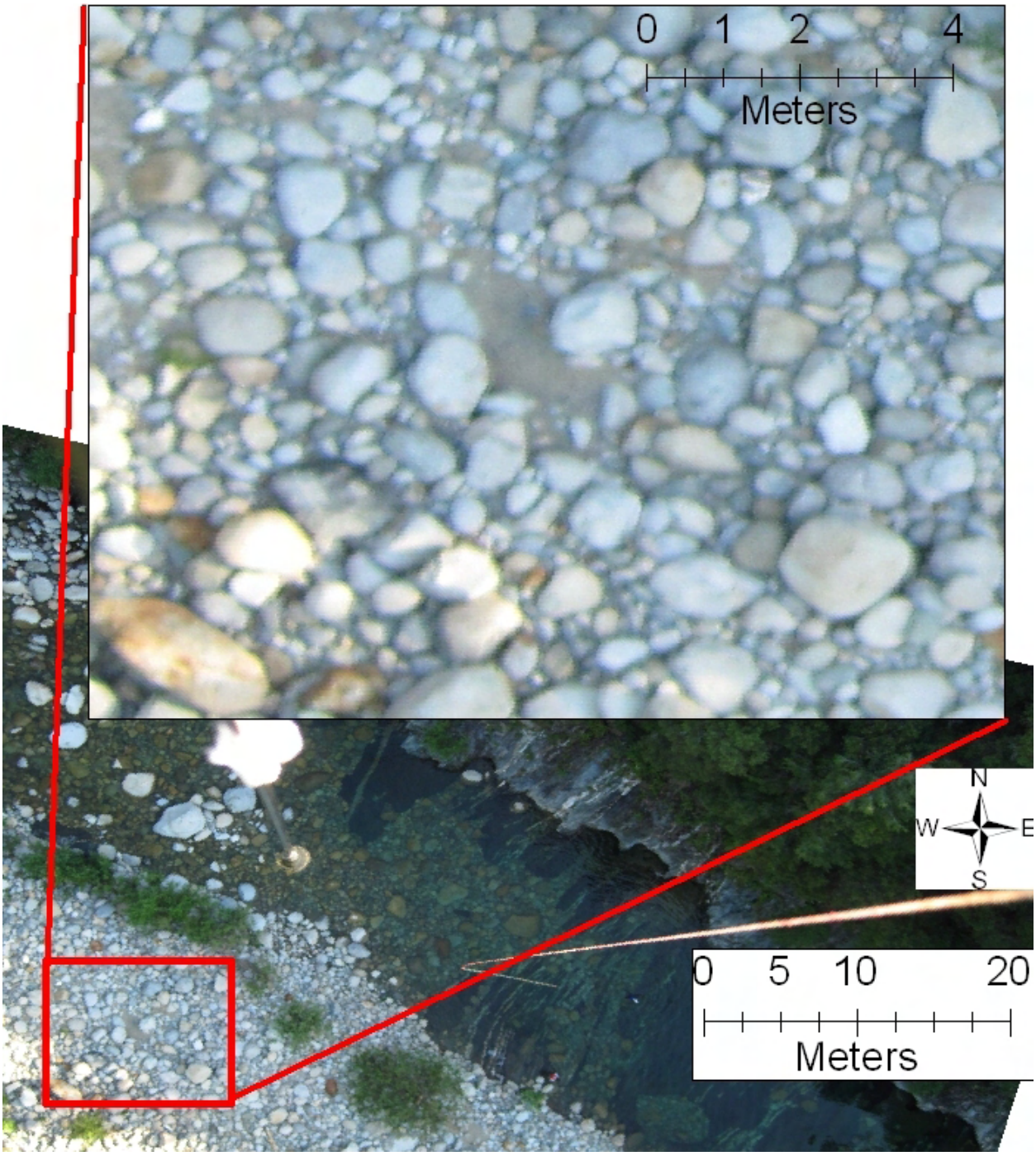

Figure 69. Image 0230 obtained from kite-blimp imagery, with selected sediment analysis location highlighted in red box. Pixel resolution of inset image was 1.9 cm. Grain size analysis returned a mean diameter of 1264 mm ± 522 mm.

Table 34. Grain size statistics from randomly selected kite-blimp images of the dry floodplain. Far right column presents statistics across all images.

Individual Image	Mean grain size (mm)	Standard Deviation (mm)	Grain Size Summary Statistics; All (mm)	
IMG_0230crop	1264	522	Mean	641
IMG_1077crop	538	116	Median	592
IMG_1246crop	699	128	Standard Deviation	321
IMG_1498crop	244	44	Range	1020
IMG_1569crop	592	88	Minimum	244
IMG_3295crop	424	48	Maximum	1264
IMG_3771crop	735	126	Count	7

8.8.4 Streamwood Analysis

Georectified kite-blimp images were used in conjunction with the ArcMap Editor tool to delineate the area and longitudinal distribution of streamwood pieces within the floodplain channel. Preliminary results are presented here, as the analysis was partially complete at the time of this report.

Studies that analyze streamwood abundance and distribution often are done in headwater reaches of stream order 1–3, whereas this study segment is of stream order five. Low-order reaches range in width but are generally small (i.e. 1–5 m average bankfull width). The South Yuba could be thought of as a medium-sized river with respect to wood pieces delivered to the wetted channel, where channel width is less than the upper quartile of available wood piece length (Gurnell et al., 2002). In the study segment, low flow channel width averaged ~15 m but increased to ~50 m at 6921 cfs. With many conifers of height >15 m along the stream corridor, streamwood did accumulate in the channel, but it is unlikely to remain in place during high flows unless a jam forms. Jamming opportunities are present with so many boulders (section 8.8.2), but jams are not currently present. One explanation for the absence of instream jams is that local residents remove wood that spans the river in an effort to protect their property and 'keep the river clean' of obstructions. Another possibility is that transport overcomes both supply and the roughness elements in the river that might allow streamwood to lodge in the channel. Streamwood was found in much greater abundance on channel banks where streamwood comes to rest when water levels drop.

The method used to delineate streamwood pieces started by opening the georectified kite-blimp images in ArcMap. With an approximate resolution of 1–4 cm per image, the task was to zoom in to a resolution where linear streamwood features could be accurately digitized using Arc Editor. All identifiable streamwood pieces were digitized, such that many identified wood pieces do not fit the definition of a streamwood piece of minimum 10 cm in diameter and 1 m in length. By digitizing all streamwood, a complete census of woody materials present in the bankfull channel has been accomplished up to Canyon Creek, a distance of ~6 km.

In 6 km, 3342 individual streamwood pieces were digitized, ranging in area from 0.005–9 m^2, for a total of 459 m^2. An average diameter of 14 cm (dividing the total area by total pieces for a third dimension) yields a volume of ~63 m^3, whereas a more conservative average diameter of 5 cm results in ~23 m^3 of streamwood over the 6-km reach. The largest streamwood piece was 9 m^2, and 92 streamwood pieces were greater than 1 m^2 in area. Streamwood was distributed throughout the study segment along both channel banks, and appear to have been deposited in those locations on the falling limb of a high flow as streamwood accumulated in eddies. Streamwood was clustered in some areas, showing where preferential depositional zones for streamwood might be located (Figure 70). One hundred-eleven wood pieces were digitized in Figure 70 (left), yielding a total of 3.21 m^2 in area. Notice the stacked positioning of streamwood on a bedrock shelf—the number of digitized pieces is likely less than actual. Two larger pieces in this image were measured using the Arc measuring tool at 14 cm by 1.45 m (far right side of image, middle) and 16 cm by 1.2 m (a piece in the upper right cluster).

This analysis shows that a high-resolution method can be used to rigorously locate and digitize the physical attributes and longitudinal distribution of streamwood in river channel.

Further analyses could include piece size distribution, longitudinal and latitudinal distribution with respect to bedrock exposure on the floodplain and in the channel, streamwood piece distribution per morphologic units, and distribution per 10-m in the downstream direction and with respect to slope. The 2D results could be used to evaluate specific hydrographs that transport and deposit wood across a very large channel segment.

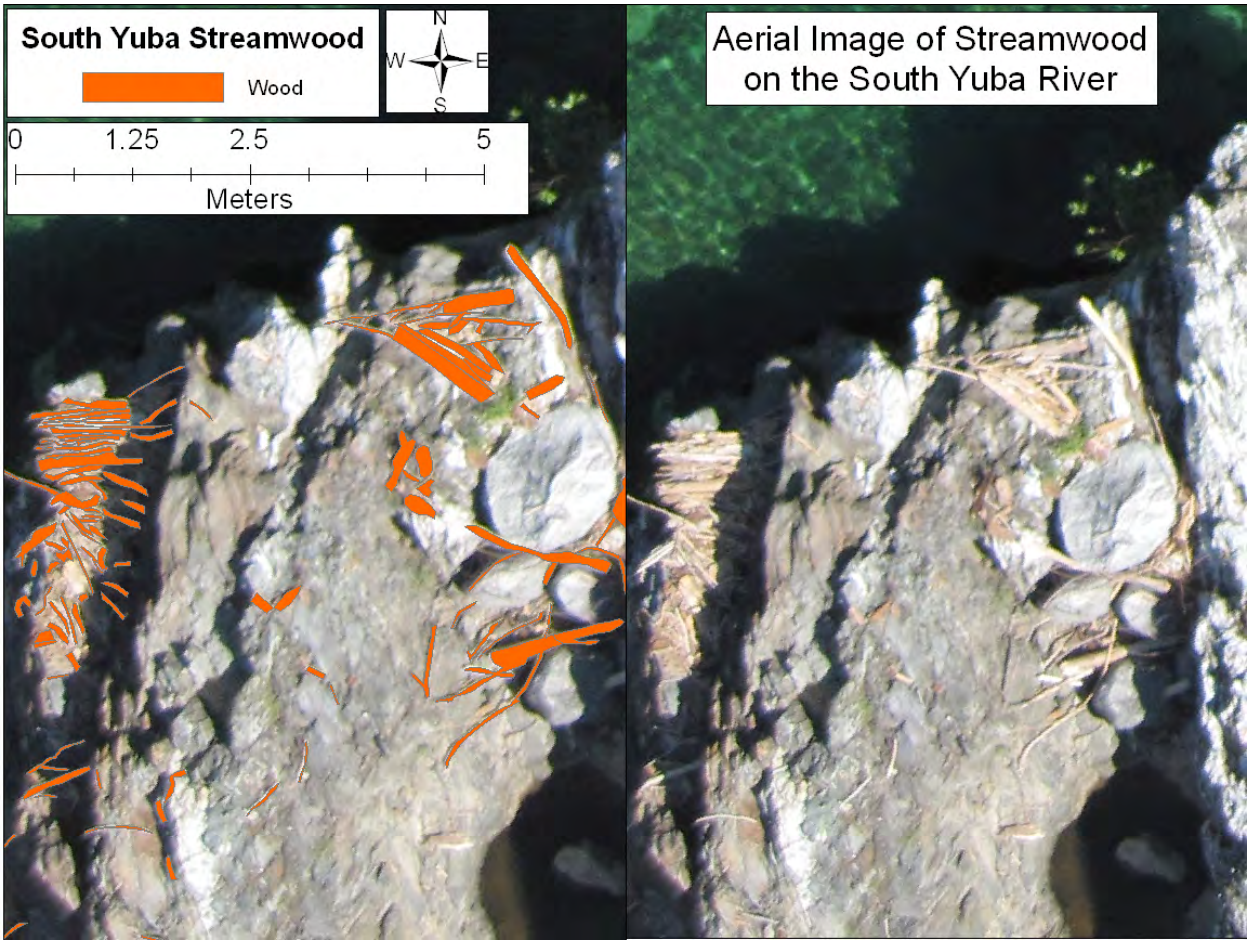

Figure 70. Kite-blimp image. Left image shows digitizing process, right image show wood pieces.

8.9 Assessing Channel Change Mechanisms

Each of the previous geomorphic analyses addressed issues related to the topic of spatial patterns of landforms and some of the materials that shape them across morphological-unit to segment scales. The dataset collected for this study captures only one moment in time, and therefore cannot be used to directly compute channel change, such as can be done using digital elevation model differencing methods (e.g. Heritage et al. 2009; Wheaton et al. 2010). Further, even with such direct change computations, there is still a need to explain the changes on the basis of a mechanistic understanding of physical processes.

White et al. (2010) used a literature review and a newly developed analysis of a gravel-bed river corridor to make the case that the presence of multiple scales of landform heterogeneity explains the majority of mechanisms associated with channel changes that allow morphological units to persist for decades in the face of a diverse flow regime that includes infrequent floods. Specific mechanisms included meander migration (Johannesen and Parker 1989; Pyearce and Ashmore 2005), particle queuing (Naden and Brayshaw 1987; Clifford 1993), bar instability (Wilkinson et al. 2008), pool scour by fluctuating bursts of turbulence associated with forced obstructions (Kieffer 1985; Lisle 1986; Kieffer 1989; Montgomery et al. 1995; Thompson 2001),

and flow convergence processes (MacWilliams et al. 2006; Sawyer et al. 2010). These mechanisms have been reported to exist in nature and a particular suite of geomorphic and hydraulic evidence is indicative of each one. Each mechanism also presents unique challenges for numerical prediction of their occurrence.

Ideally, a numerical model would exist for the simulation and prediction of each mechanism of channel change, but that has not been developed yet. High-resolution, spatially explicit, morphodynamic models that simulate how river landforms change through time are presently under development, but are unproven. These models are often programmed with only a subset of the actual mechanisms required or may focus on a single landscape context (e.g. large lowland meandering rivers, deltas, or landscape evolution of mountain ranges with minimal representation of channels and their processes). Simplified morphodynamic models (e.g. cellular automata models) that ignore momentum conservation violate observed interdependencies between depth and velocity as a function of stage in rivers and are not accurate enough for the questions under investigation. Mountain rivers with multiple complex sources of sediment input, exposed bedrock, and an extremely wide range of bed material sizes pose an exceptionally difficult problem for morphodynamic modeling.

In light of the long-standing limitation of morphodynamic models, the standard practice in geomorphology is to perform hydraulic modeling and infer mechanisms based on the combination of geomorphic observations and hydraulic predictions. Traditionally this was done using analytical/empirical calculations or 1D numerical models (Grant et al. 1990; Keller and Florsheim 1993), but most recently depth-averaged 2D numerical hydraulic models have been used to reveal hydrogeomorphic mechanisms (Miller 1994; MacWilliams et al. 2006; Harrison and Keller 2007; Pasternack et al. 2008; Sawyer et al. 2010). The standard procedure involves using a numerical model to characterize the spatial pattern of the bed shear stress regime responsible for channel change. In some studies shear stress has been shown to be directly correlated to scour depth (Wilcock et al. 1995), but in others there is only a relation between shear stress and the presence/absence of scour or deposition (Sawyer et al. 2010), or there is no relation of any kind (May et al. 2007). At a larger spatial scale, stage-dependent patterns of shear stress indicate relative changes in transport conditions among morphological units.

8.9.1 Flow Convergence Mechanism

One of the primary results of the analysis of the spatial organization of morphological units in the upper South Yuba River is that there exists oscillatory patterns in longitudinal trends of bed elevation and channel width. The maintenance of oscillatory relief in mountain rivers is of vital importance to mediating the dissipation of energy and providing ecological diversity. *Flow convergence* has been suggested as a physical mechanism of maintaining variable topography in both free and forced gravel bed rivers (MacWilliams et al. 2006; Sawyer et al. 2010; White et al. 2010).

Flow convergence is defined as the stage-dependent oscillatory focusing of high velocity jets through riffle and pools driven by multiple scales of landform variability (Figure 72, Figure 72).

According to this concept, under low-flow conditions, vertical variations in topography along the length of a river control channel cross sectional area and hydraulics, driving vertical flow convergence and determining local sediment transport capacity. In this situation, pools have deep, slow, divergent flow and low transport capacity; riffles have shallow, fast, convergent

flow and high transport capacity (Clifford and Richards 1992; Brown and Pasternack 2008). Transport rates for riffles are supply-limited in terms of mobile bed particle sizes. Under high flow conditions, longitudinal variations in wetted width control channel cross sectional area and hydraulics, driving lateral flow divergence over wide riffles and convergence over narrow pools (Sawyer et al. 2010). Flow convergence over narrow pools creates a zone of high velocity and shear stress at the pools (Carling 1991; Booker et al. 2001; Cao et al. 2003; MacWilliams et al. 2006). These high velocity zones cause mobilized sediment to be routed through or around pools and deposited as riffles downstream where flow diverges and velocity, shear, and transport capacity reduces (Leopold et al. 1964; Keller 1971; Lisle 1979; Booker et al. 2001; Repetto et al. 2002; MacWilliams 2006). As discharge increases, the effect of lateral flow convergence on velocity and shear stress increases (MacWilliams et al. 2006). At all discharges, flow divergence and deceleration is influenced by backwater conditions upstream of vertical and/or lateral constrictions (Buffington et al. 2005; Clifford et al. 2005; Pasternack et al. 2008). Notably, flow convergence routing does not include a mechanism related to fluctuation of turbulent intensities at forcing elements, so that has to be accounted for independently. Flow convergence can account for the role of bed particle size differences in scour location and timing when sufficient data is available to be used in conjunction with a 2D or 3D numerical model. As a result, it may be consistent with essential aspects of the particle queuing hypothesis (Naden and Brayshaw 1987; Clifford 1993). The key consequence of stage-dependent convergence and divergence is that different morphologic units within a reach may be formed and maintained by different discharges (Milan et al. 2001).

Two modeling studies have demonstrated the ability of 2D models to successfully simulate and predict the link between stage dependent flow convergence and riffle-pool maintenance on gravel/cobble bedded rivers. The first was the 2D versus 3D model comparison study of MacWilliams et al. (2006). More recently, a similar finding was presented by Sawyer et al. (2010), but in this case the study performed both modeling and channel-change observation to confirm the link in a specific flood (Figure 73). These studies provide confidence that mechanistic 2D hydraulic models have value in understanding geomorphic processes.

For this study on the South Yuba River, model results were analyzed for evidence of stage dependent flow convergence. The analysis was performed using metrics explained in the next subsection, but can be illustrated using velocity results for one site here. The photo sequence shown in Figure 74 is suggestive of flow convergence occurring just downstream of the bridge crossing in Washington, CA. At the lowest flow, the steep inset channel on river right has the highest velocity, the side-channel pool on river left has very low velocity, and the flow in the region downstream of the steep inset channel is also slow-moving. At highest flow, the constricted side-channel pool on river left is seen to have standing waves and velocities as high, if not higher, than the steep inset channel. Similarly, the region downstream of the steep inset channel is constricted and appears to have standing waves and high velocities.

The 2D model results for the summer 2009 baseflow and May 5, 2009 peak discharge (i.e. snowmelt 6921 cfs simulation) quantify the visual indicators for stage-dependent hydraulics downstream of the Washington Bridge. At baseflow, the steep inset channel has a peak thalweg velocity of 1.5–2 m/s, the side channel pool has a thalweg velocity of 0–0.5 m/s and the downstream pool has a thalweg velocity of 0–0.5 m/s. The areas of highest velocity in the map are all located on steep inset channel morphological units. At the peak observed flow on May 5, 2009, the velocities increased everywhere, the location of the peak velocities spread and shifted

some, and the range of thalweg velocities increased significantly to 2.5–3.0 m/s. However, there is no evidence for a full "reversal" of velocities, with pools having the highest velocity at the highest observed discharge. This illustrates how the analysis may be done at the site scale, but the comprehensive approach involved comparing morphological-unit averaged metrics that were assessed for stage-dependent shifts in peak values between units for the whole study segment.

The complete analysis of stage-dependent flow convergence processes is presented in Chapter 0.

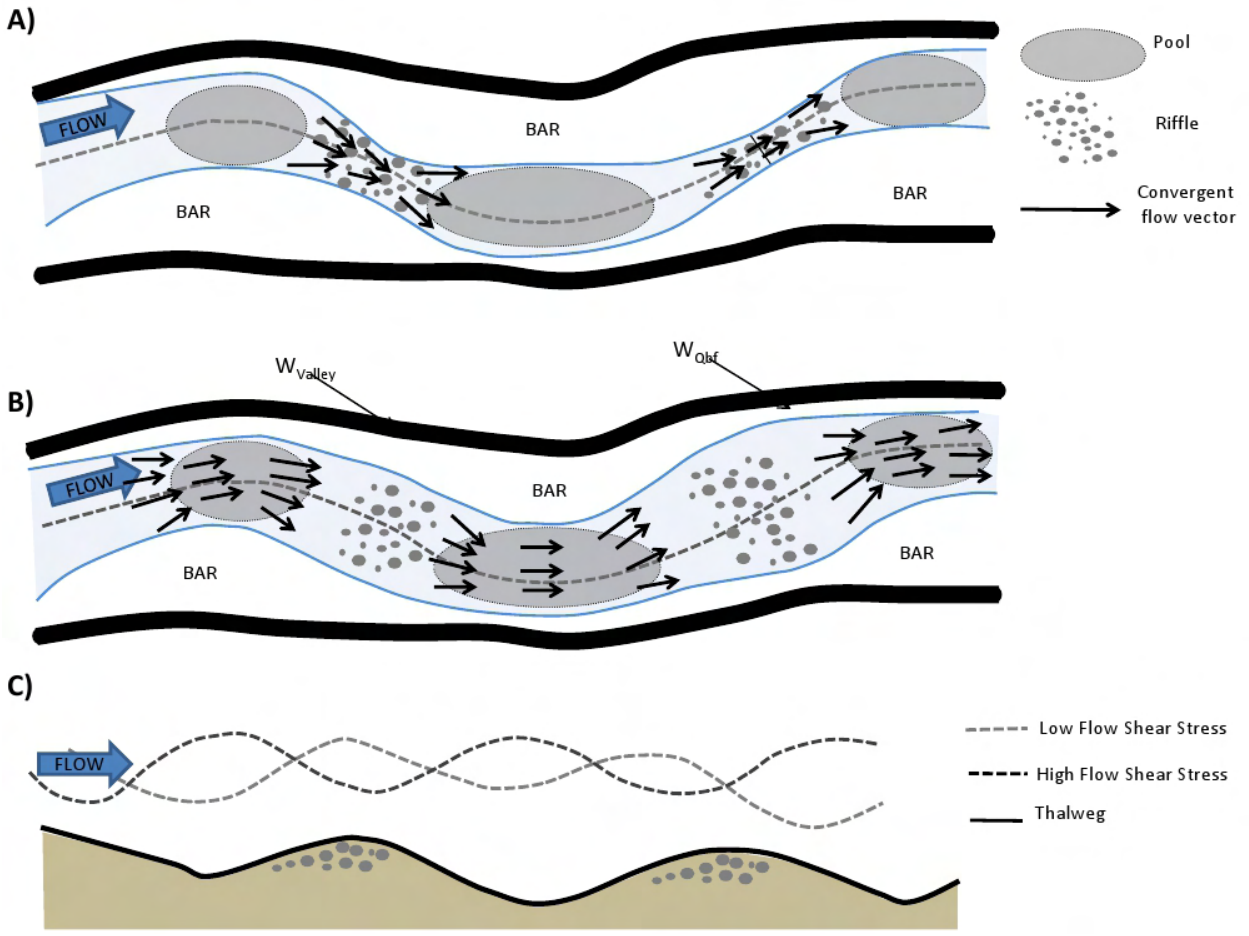

Figure 71. Conceptual diagram of oscillatory flow convergence within multiple morphologic units nested in the reach scale. A) planview of low flow convergence through riffle crests, B) planview of high flow convergence through pools upstream of the riffles, and C) longitudinal section of ideal oscillatory patterns of bed shear stress that are dependent on thalweg oscillations at low flow (A) and width oscillations at high flow (B). Note that at low flows riffles do not necessarily need to be narrower than pools, as vertical convergence (not represented in the above 2D conceptual diagram) can occur. This figure is courtesy of Rocko Brown and must not be reproduced without explicit permission.

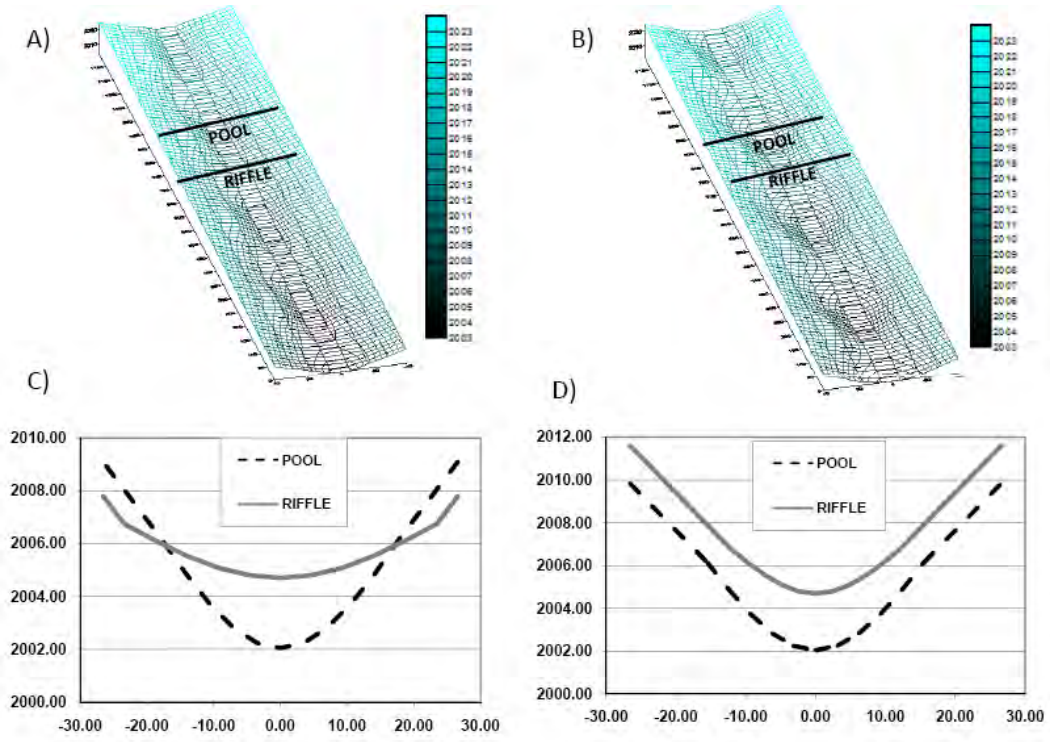

Figure 72. Sine generated synthetic terrains for A) in phase width and thalweg series and B) out of phase width and thalweg series. Cross sections for riffle and pool unit for C) in phase width and thalweg series and D) out of phase width and thalweg series. Case A/C would experience flow convergence at the depth for incipient motion, while case B/D would experience convergence at much greater depths indicating an unstable configuration. This figure is courtesy of Rocko Brown and must not be reproduced without explicit permission.

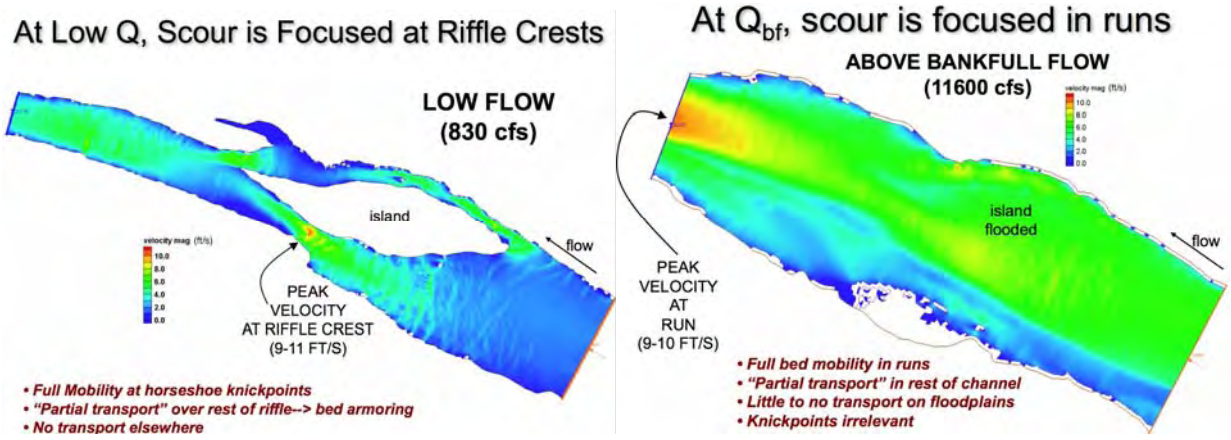

Figure 73. Demonstration from the lower Yuba River that 2D models can capture stage-dependent flow convergence. Left image shows convergence through a riffle at low flow and right image shows convergence through a run at two orders of magnitude higher flow for the same pool-riffle-run complex.

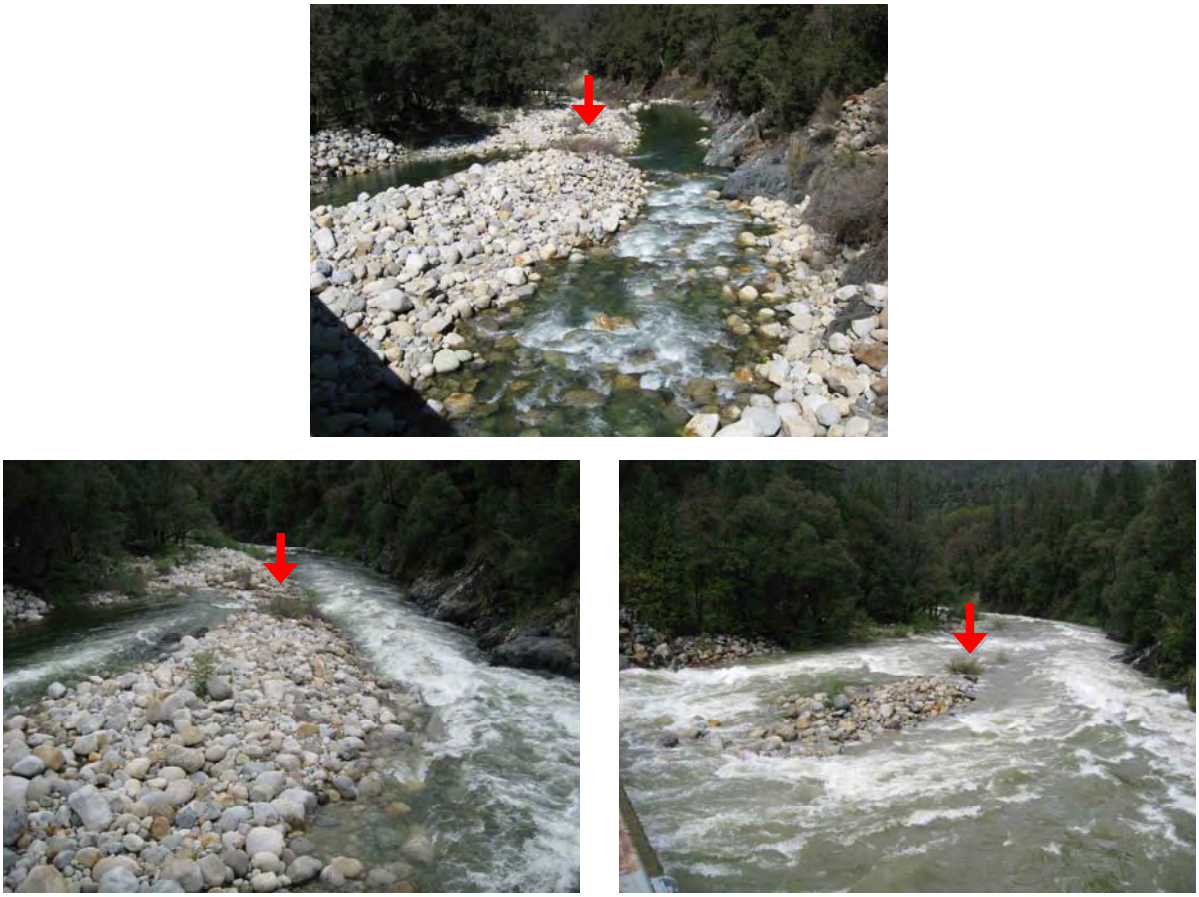

Figure 74. Downstream steep inset channel at summer 2009 baseflow dry season conditions (top), 1103 cfs on May 4, 2009 during snowmelt season conditions (left), and 6921 cfs on May 5, 2009 during snowmelt season conditions (right). Note position of willow in each image (red arrow).

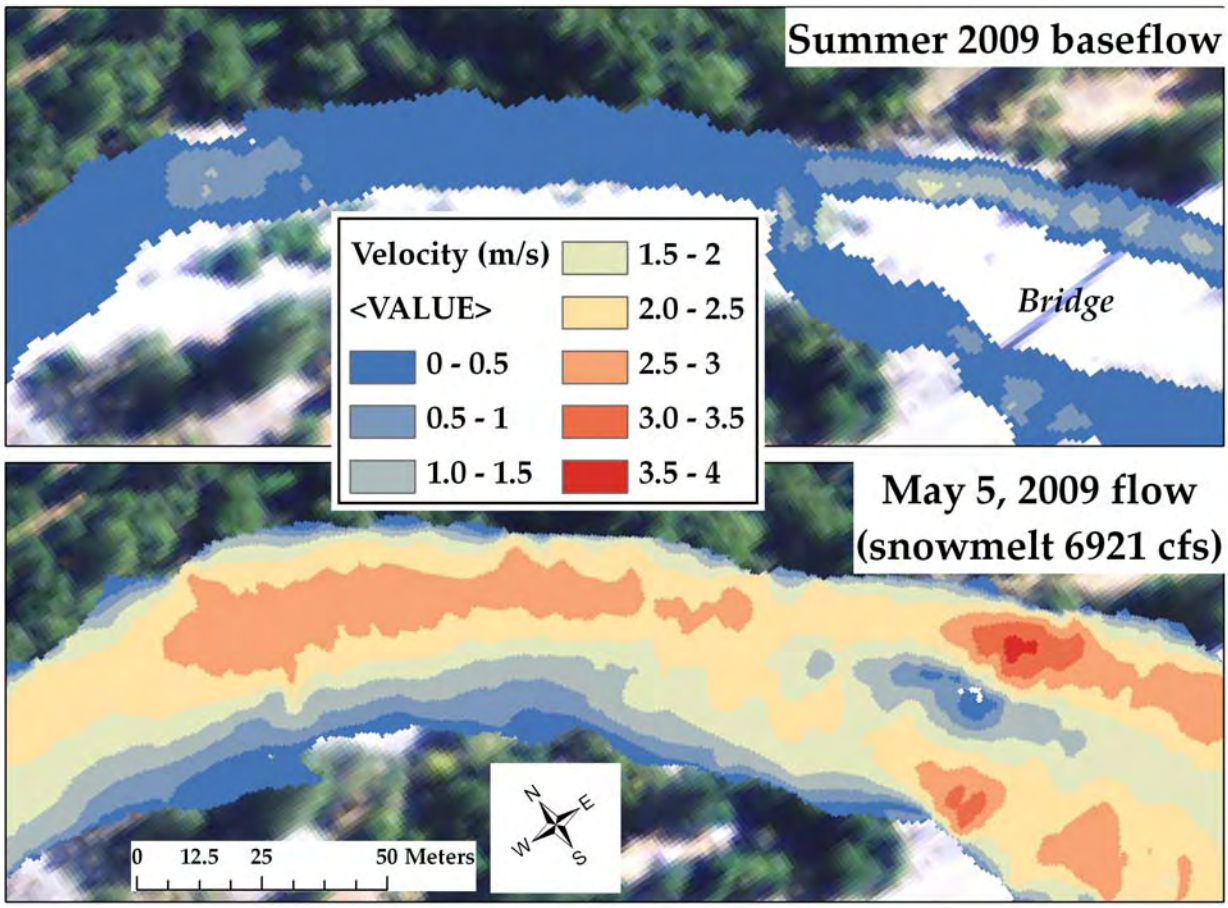

Figure 75. 2D model velocity results for Washington Bridge area as shown in previous figure. Flow is from right to left.

8.9.2 Sediment Transport Regime Calculations

The first step in making use of 2D model results to evaluate channel change mechanisms is to use depth and velocity model outputs to compute one or more metrics that indicate scour potential. Some studies assess scour of a representative bed material size, while others perform separate calculations for each size fraction. More recently, studies have found that a non-dimensional shear-stress variable called Shields stress may be used to characterize the sediment transport regime (Lisle et al. 2000) and patterns of scour and deposition (Sawyer et al. 2010). In this approach, a representative particle size of a heterogeneous mixture is needed for non-dimensionalization, which is commonly taken as either d_{50} or d_{90}, where $d_{\#\#}$ is the size that ##% of the surficial bed material is smaller than. For a highly heterogeneous bed, d_{90} is more appropriate.

In this study it was infeasible to quantify the spatial pattern of bed material sizes over the wide range known to exist. Spatial patterns of bedrock versus alluvium were mapped. Also, the locations and sizes of all boulders protruding out of the water by at least 0.3 m were mapped. Bed roughness was found to be uniformly high in 2D model testing, indicative of the role of multiple scales of grain clusters, bedform undulations, and bedrock outcrops in the channel.

Consequently, two different approaches were used with the 2D model to gain insight into mechanisms of channel change at the point scale.

The starting point for the two approaches involved using 2D numerical model outputs to calculate bed shear stress (τ_b) at each node in the 2D model according to

$$u^* = U\sqrt{C_d} \tag{14}$$

$$C_d = g\frac{n^2}{H^{1/3}} \tag{15}$$

$$\tau_b = \rho_w(u^*)^2 \tag{16}$$

MacWilliams et al. (2006) and Pasternack et al. (2006) reported that 2D models over-predict bed shear stress by a factor of ~2. This occurs because 2D models do not account for the vertical profile of velocity and because they are overly efficient in transferring momentum. On the basis of the statistical analysis reported in Pasternack et al. (2006), the raw τ_b dataset was multiplied by 0.51 to obtain corrected τ_b values. These values were then used to compute two sediment transport regime indicator variables.

First, a study objective was established to characterize the availability, transport, and fate of gravel-sized sediment commonly used for fish spawning. To achieve this, a representative bed-material size of 60 mm was set for a heterogeneous gravel/small cobble mixture and the nondimensional Shields stress (τ^*) was calculated as

$$\tau^* = \tau_b/(\rho_s - \rho_w)gd \tag{17}$$

where ρ_w is water density, ρ_s is bed particle bulk density, d is the representative grain size of the bed sediment mixture of interest, set to 60 mm in this analysis. Shields stress values were categorized based on transport regimes defined by Lisle et al. (2000), where values of $\tau^* < 0.01$ correspond to negligible transport, $0.01 < \tau^* < 0.03$ correspond to intermittent entrainment, $0.03 < \tau^* < 0.06$ corresponds to partial transport (Wilcock et al. 1996), and $\tau^* > 0.06$ corresponds to full transport of a carpet of sediment 1-2·d_{90} thick, where d_{90} is the size that 90% of the surficial bed material is smaller than. To be clear, beyond characterizing the Manning's roughness as explained in section 6.1.3, it is not necessary to know the initial ambient grain size distribution throughout the river segment to evaluate the pattern of the sediment transport regime. This approach is evaluating sediment transport capacity, so it is independent of sediment supply. It is reporting the potential for what could happen to gravel/small cobble throughout the system.

Second, instead of assuming a representative particle size and evaluating the sediment transport regime, the approach was taken to use the available hydraulic regime to estimate the local critical particle size at the incipient-motion threshold for a given point in the flow domain (d_c). This was done by setting a threshold of incipient motion and solving equation 15 for the particle size:

$$d_c = \tau_b/(\rho_s - \rho_w)g\tau^* \tag{18}$$

In this scenario, the critical Shield stress value for incipient motion must be selected, but there is more certainty in that. The value of critical Shields stress is sensitive to how loosely the bed is packed, but in the case of the South Yuba River study segment the bed showed an imbricated

structure and larger grains were often imbedded in a matrix of smaller ones. As a result, the critical value is very unlikely to be lower than 0.03. The most commonly used values are 0.03 and 0.045. Sawyer et al. (2010) performed the most directly relevant test in which 2D model predicted values of Shields stress were compared to observed changes to bed elevation in a gravel/cobble bed river and found that scour always occurred above the 0.045 threshold, but not the 0.03 threshold. Therefore, 0.045 was used in this study.

Despite all the measures taken in this study to try different approaches to characterize sediment transport regime with a 2D model, it is very important to appreciate that 2D models have uncertainty and a limited ability to predict sediment transport, because the latter is so strongly influenced by multiple scales of turbulence. Turbulence is poorly represented by the type of 2D model commonly used in instream flow assessment, including the SRH-2D model using for these analyses. The strength of the approach lies in the ability to characterize mean flow fields, so the interpretation of model results emphasizes that capability.

Results are presented as part of the 2D model hydraulic results in Chapter 0.

CHAPTER 9:
2D Model Hydraulic Analyses

Discharge has been called a 'master' variable that impacts many aquatic ecological processes. Some types of instream flow assessments use discharge to infer ecological effects of dam operations without quantifying the mechanisms by which discharge influences aquatic and riparian ecology (see section 2.1.1). When water flows through a stream channel of specified geometry, it yields fluid motion, or hydraulics. Hydraulics involves specific mechanisms that create, modify, and destroy physical habitat characteristics that contribute to biological processes and ecological functions such as individual reproduction, growth, and mortality as well as interspecies competition and predation. In this study, the concept of hydraulics has been simplified to mean the spatial patterns of water surface elevation, water depth, water velocity, and bed shear stress in a range of steady, nonuniform flows.

A central premise of this study is that instream flow assessment for the 21st century will blend high-resolution imaging, mapping, and 2D numerical modeling over the full extent of a river segment to yield a near-census of spatially distributed hydraulics, which will then enable the practice of evaluating the pattern of geomorphic, hydraulic, and habitat information. At present, spatial considerations are not included in many instream flow assessments. Ecological functions such as migration and predator avoidance hinge on the connectivity and adjacency of habitat units. To that end, it is important to understand how hydraulics affects morphologic units, which are the basis of the geomorphic and ecological analyses in this study. 2D model results will be presented first. In the next chapter, methodological comparisons between different methods of obtaining hydraulic estimation/prediction methods are presented.

Joint distribution plots of depth and velocity (i.e. phase-space plots) provide insights into underlying channel morphology. Stewardson and McMahon (2002) showed that depth and depth-averaged velocity are co-dependent variables, because channel hydraulics exhibit spatial organization. Besides showing how to obtain independent hydraulic variables from raw observations, they also used the joint probability distribution of the two codependent variables to show that it is possible to distinguish between two types of channels (i.e. two hydraulic signatures)—one in which depth and velocity are inversely related, and one in which they are directly related. The first relation, where velocity and depth are inversely related, occurs when the channel has a much stronger longitudinal variation in depth than a lateral variation. The second hydraulic signature when depth and velocity are directly related occurs when the channel has much stronger lateral variation in depth than longitudinal variation. Building on the concepts of Stewardson and McMahon (2002), Brown and Pasternack (2008) evaluated how hydraulic signatures shift over a range of discharges (Figure 76). They found that as flow increases, channel hydraulics shift from the inverse depth-velocity relation to the direct relation. The rate of the shift hinges on the roughness and topography of the area that becomes wetted with each incremental increase in flow. The overall effect of decreasing relative roughness and increasing prismatic channel conditions on hydraulic signatures as discharge increases is known (e.g. Clifford and French 1998), but its significance for geomorphic and ecological applications have not been sufficiently explored. The tests of Brown and Pasternack (2008) focused on a highly engineered reach directly below a large water-supply dam and adjacent to a large salmon hatchery, whereas this study looked at a steep mountain reach with a wider range of hydrogeomorphic conditions.

The presentation of results in this section parallels the scale-centric approach used in the geomorphic analysis section. Depth and velocity are reported at the segment scale and then at the morphological-unit scale (reach scale is excluded). Within each scale, statistical tables and plots are presented that focus on these specific questions:

- How do depth and velocity vary by season and discharge?
- How do depth and velocity vary by morphologic units?
- Is there evidence of stage-dependent flow convergence processes?

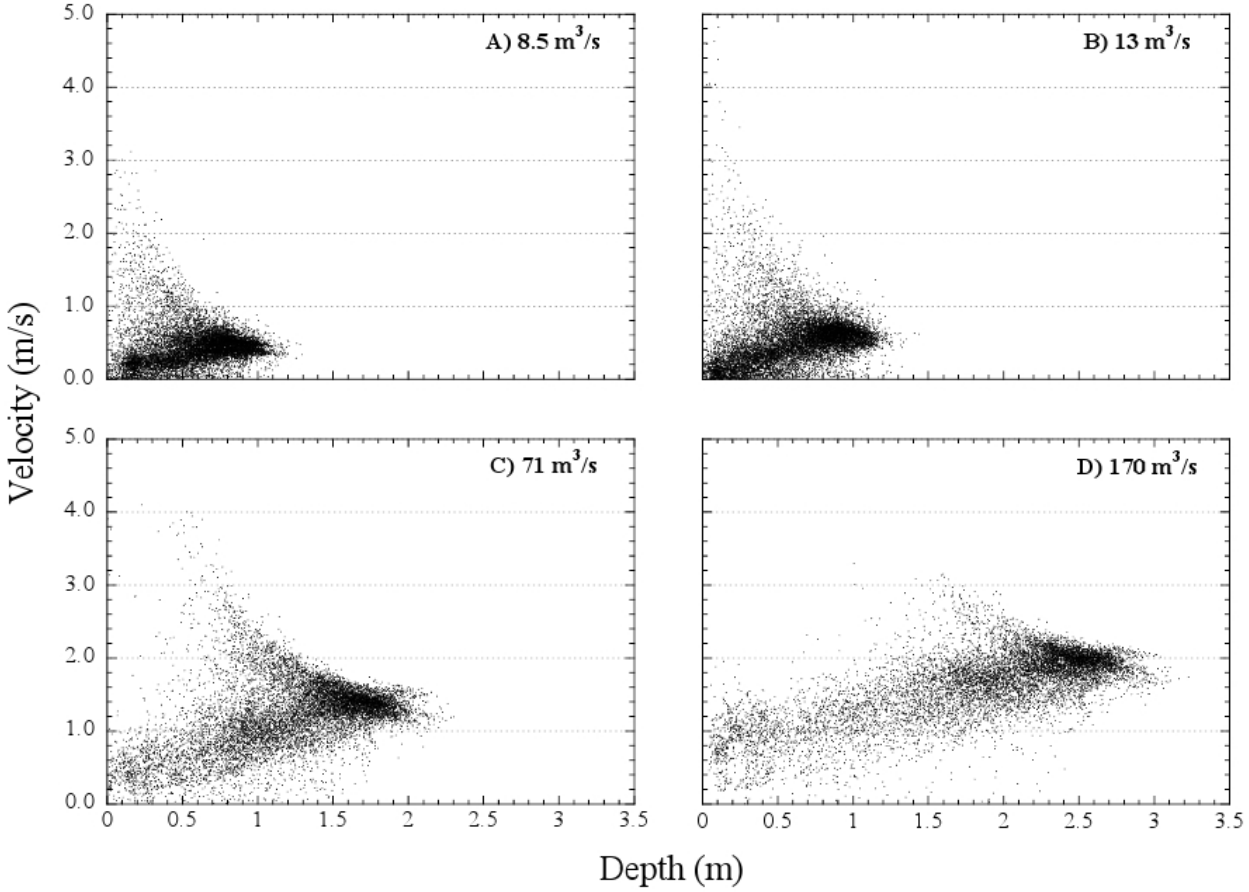

Figure 76. Stage-dependent joint probability distribution of depth and velocity at various flows on a small reach of the heavily regulated and engineered Trinity River below Lewiston Dam (from Brown and Pasternack 2008).

9.1 Segment Scale 2D Hydraulic Results

The first set of analyses addresses the above questions at the segment scale by lumping all data and analyzing it as a whole. For each set of 2D model results at ~1-m point locations, a TIN was created for depth and velocity. The point distribution on the TIN is not exactly equal. Then the TIN was sampled to a uniform 0.5x0.5-m^2 raster to yield points that represent equal areas. This uniform distribution of results is required to compare hydraulic results on an equal-area basis.

The number of 0.5-m gridded points in each raster increases with increasing discharge, with a minimum of 662,475 for dry 5 cfs and a maximum of 2,413,066 for snowmelt 6921 cfs. On average, depth and velocity increases as discharge increases, as does the standard deviation of each variable (

Table 35). Peak depth does not change as much as peak velocity over the observed flow range. Season- and flow-dependent depth maps illustrate the expansion of the wetted area as discharge increases (Figure 77, Figure 78, Figure 79). They also illustrate the location and spacing of pools. Similar maps illustrating season- and flow-dependent velocity patterns show a systemic expansion of higher velocities in the 2–5 m/s range, with the rate of increase therefore highest in the initially slow areas (Figure 80, Figure 81, Figure 82). In terms of depth averaged velocity, there is no evidence for a complete "velocity reversal" from lowest to highest discharge over the observed range of flows even though the range of flows spans over two orders of magnitude. Most likely, the observed flow range does not include high enough discharges to represent the infrequent, high-impact channel-forming floods. For example, the 1997 flood that is widely described by observers of that event to have significantly altered channel form had an estimated gaged flow at SYLC of 25,400 cfs (719.25 m^3/s), which is more than three times the highest observed flow in this study.

Season- and flow-dependent joint-distribution analysis of depth and velocity at the segment scale found that there was dependency. At lowest flow, there is an inverse relation between depth and velocity, with the majority of gridded points having depths within 0–2 m and velocities within 0–0.2 m/s (Figure 83). At the highest flow, there are overlapping distribution patterns, with the majority of points showing a direct relation and a subset of outlier points showing an inverse relation (Figure 84). The direct relation is evident in the joint histogram by the cluster of large bars, while the inverse relation is indicated by the wide spread of the flat bars. The majority of gridded points have depths and velocities between 0–4.6 m and 0–2.9 m/s, respectively. The fact that the highest observed discharge still exhibits a noticeable inverse relation indicates that (over the range of observed flows) the addition of more wetted channel area with increasing discharge preserves a baseline inverse relation for the segment, even as the thalweg transitions from an inverse to direct relation. In other words, the center of the channel may be drowning out, but the periphery is always growing. The added area has the inverse relation, while the central area has the direct relation.

Table 35. Segment-scale summary statistics for depth and velocity for all simulations. These metrics were calculated using the 0.5x0.5-m^2 rasters to have each point represent an equal area. Each flow has a different wetted area, so the number of points is different, ranging from 662,475 for dry 5 cfs to 2,413,066 for Snowmelt 6921 cfs.

	Depth (m)			Velocity (m/s)		
Flow	Average	St dev	Max	Average	St dev	Max
Dry						
5	0.58	0.81	11.45	0.15	0.17	1.77
10	0.57	0.77	11.54	0.20	0.20	2.31
20	0.63	0.77	11.69	0.31	0.27	3.14
30	0.70	0.77	11.87	0.41	0.32	3.70
45	0.82	0.81	12.12	0.56	0.39	4.41
Wet						
5	0.60	0.78	11.57	0.24	0.23	2.51
15	0.64	0.77	11.68	0.31	0.27	3.10
30	0.69	0.78	11.89	0.39	0.31	3.58
55	0.77	0.79	12.03	0.49	0.36	4.15
100	0.90	0.83	12.27	0.65	0.42	4.80
190	1.15	0.92	12.64	0.90	0.52	5.90
350	1.58	1.12	13.25	1.25	0.64	16.05
Snowmelt						
10	0.58	0.78	11.54	0.21	0.21	2.35
25	0.63	0.77	11.68	0.27	0.22	1.13
50	0.69	0.77	11.87	0.40	0.32	3.71
140	0.77	0.78	12.11	0.50	0.37	4.39
210	0.72	0.76	12.09	0.44	0.34	4.32
525	0.88	0.80	12.46	0.64	0.43	5.39
1103	1.11	0.87	12.89	0.89	0.51	6.53
3000	1.61	1.06	13.86	1.32	0.65	9.44
6921	2.23	1.34	15.20	1.77	0.81	9.72

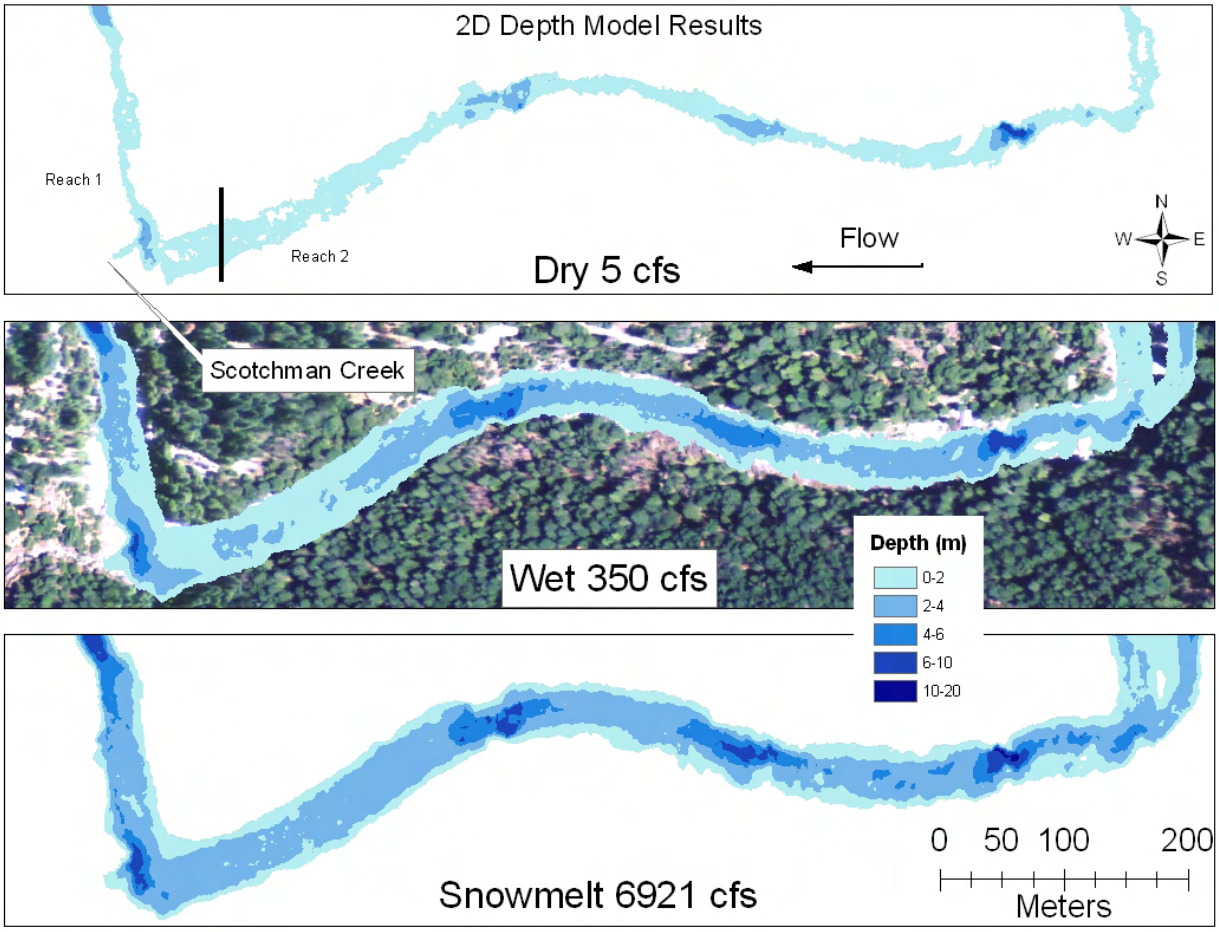

Figure 77. Example of season- and flow- dependent depth in the lower part of Reach 2.

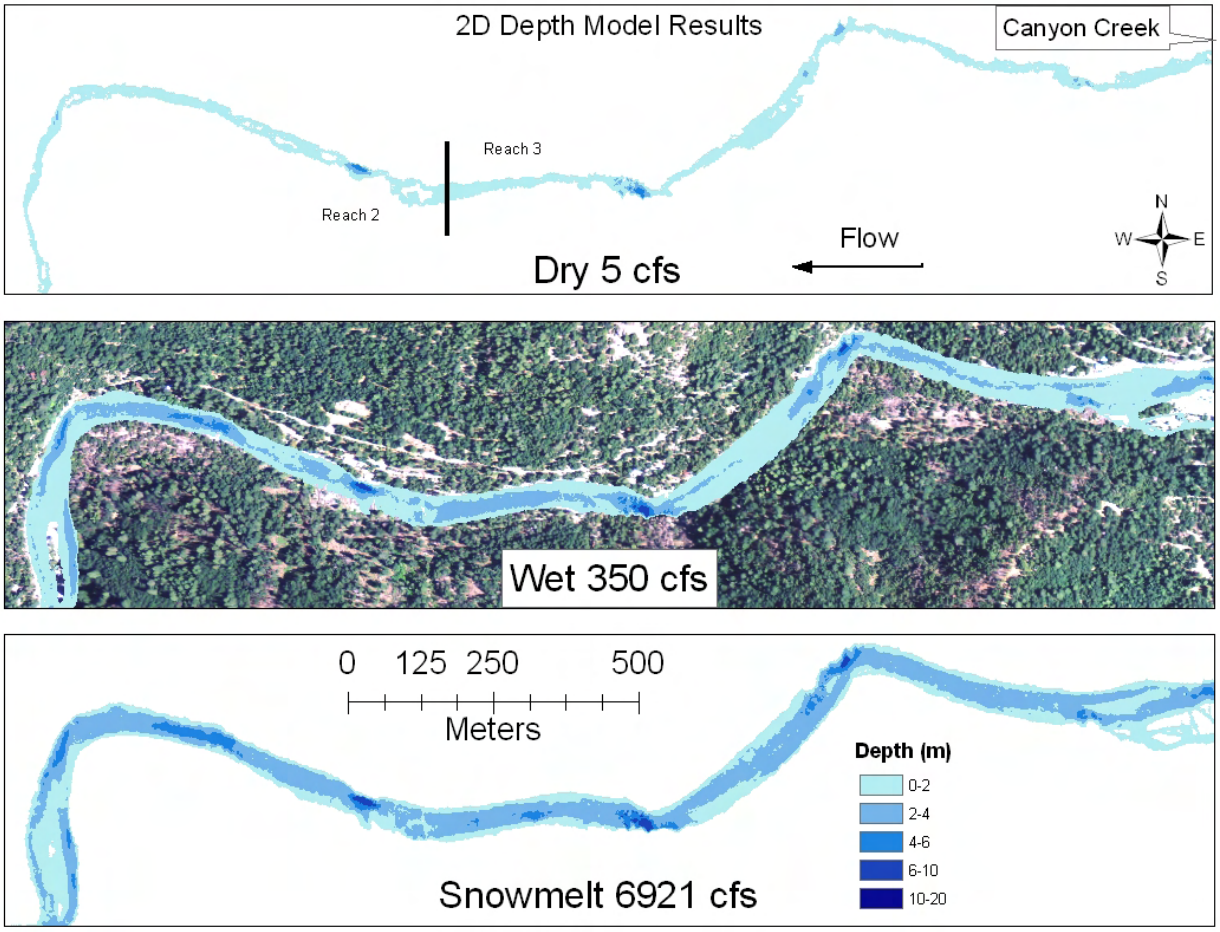

Figure 78. Example of season- and flow- dependent depth in the lower part of Reach 3.

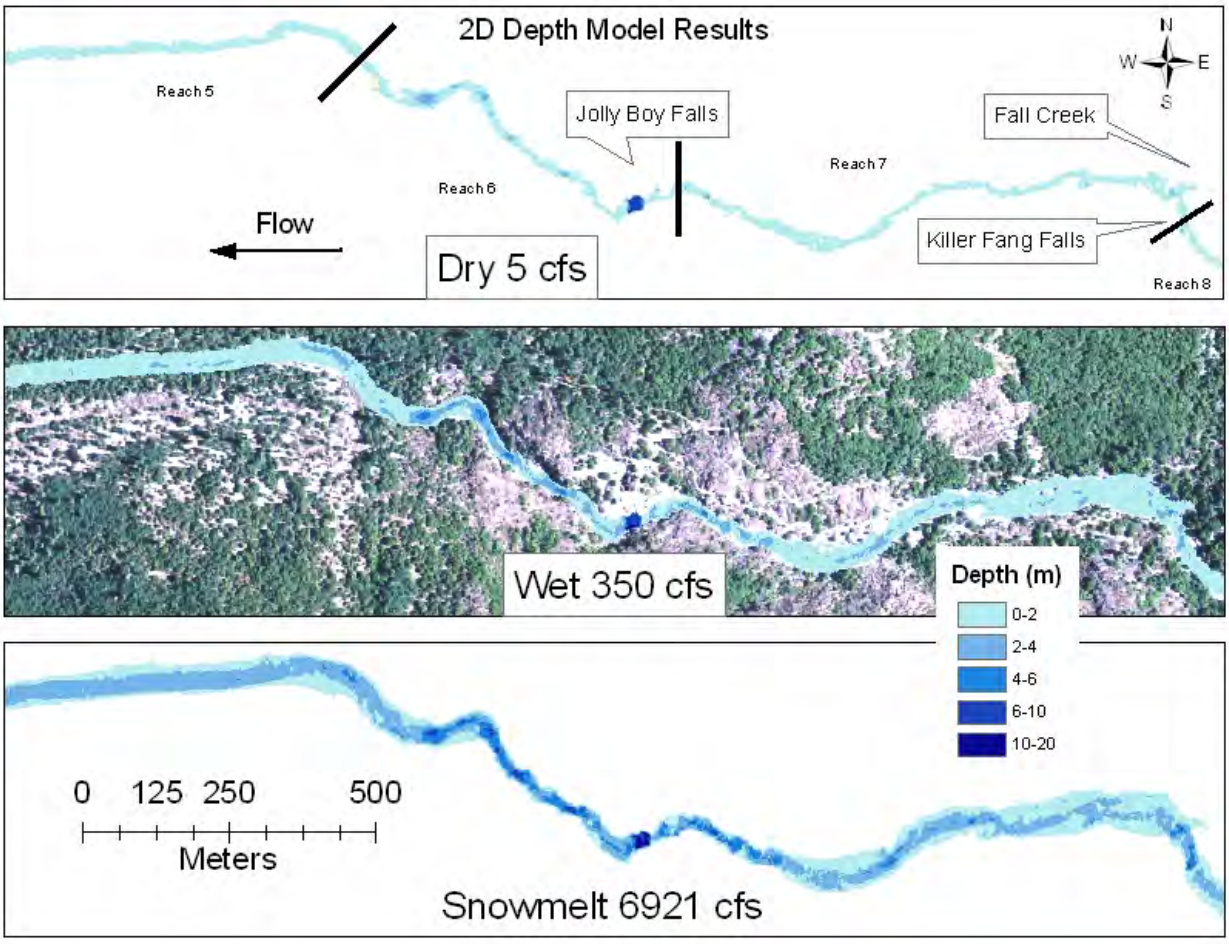

Figure 79. Example of season- and flow- dependent depth in Reaches 6 and 7.

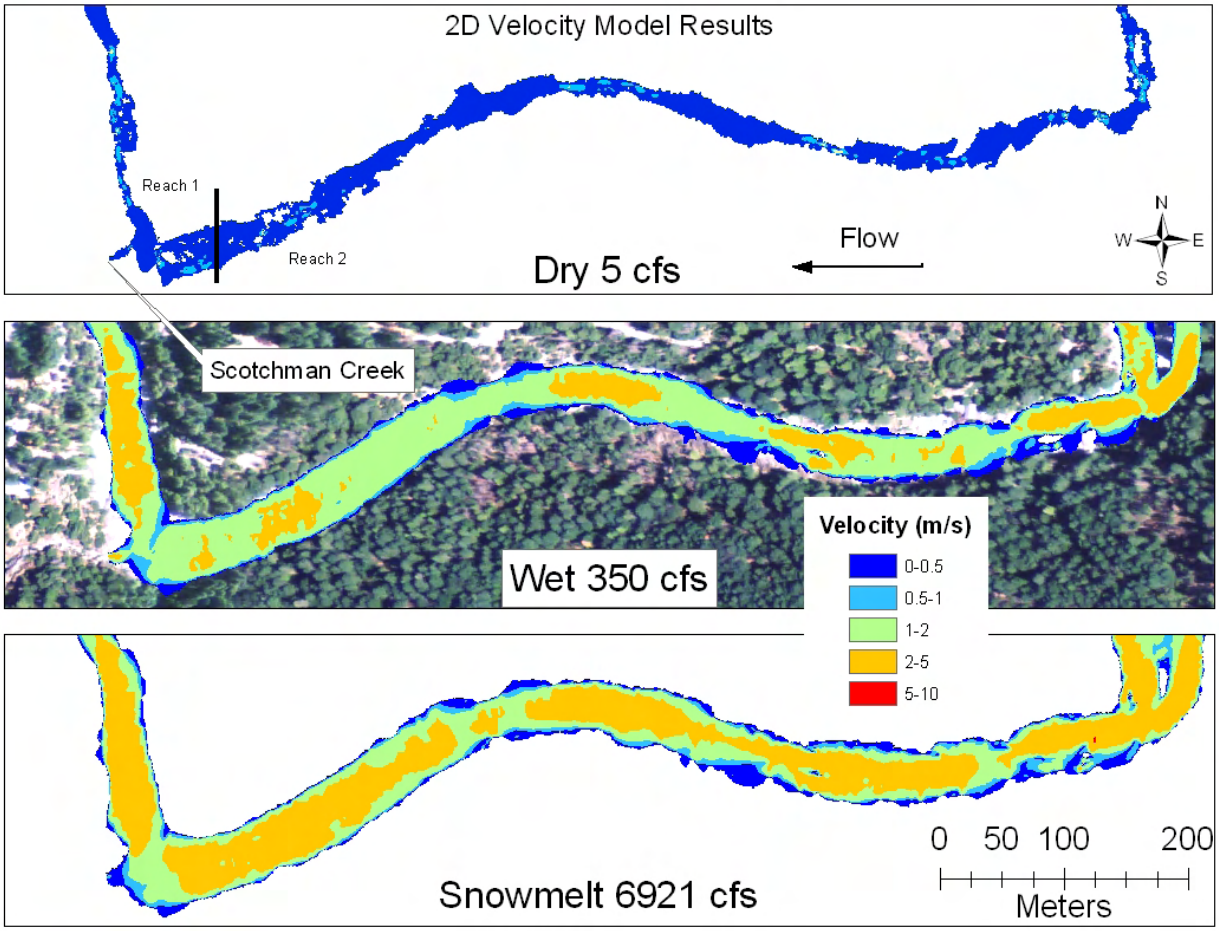

Figure 80. Example of season- and flow- dependent velocity in the lower part of Reach 2.

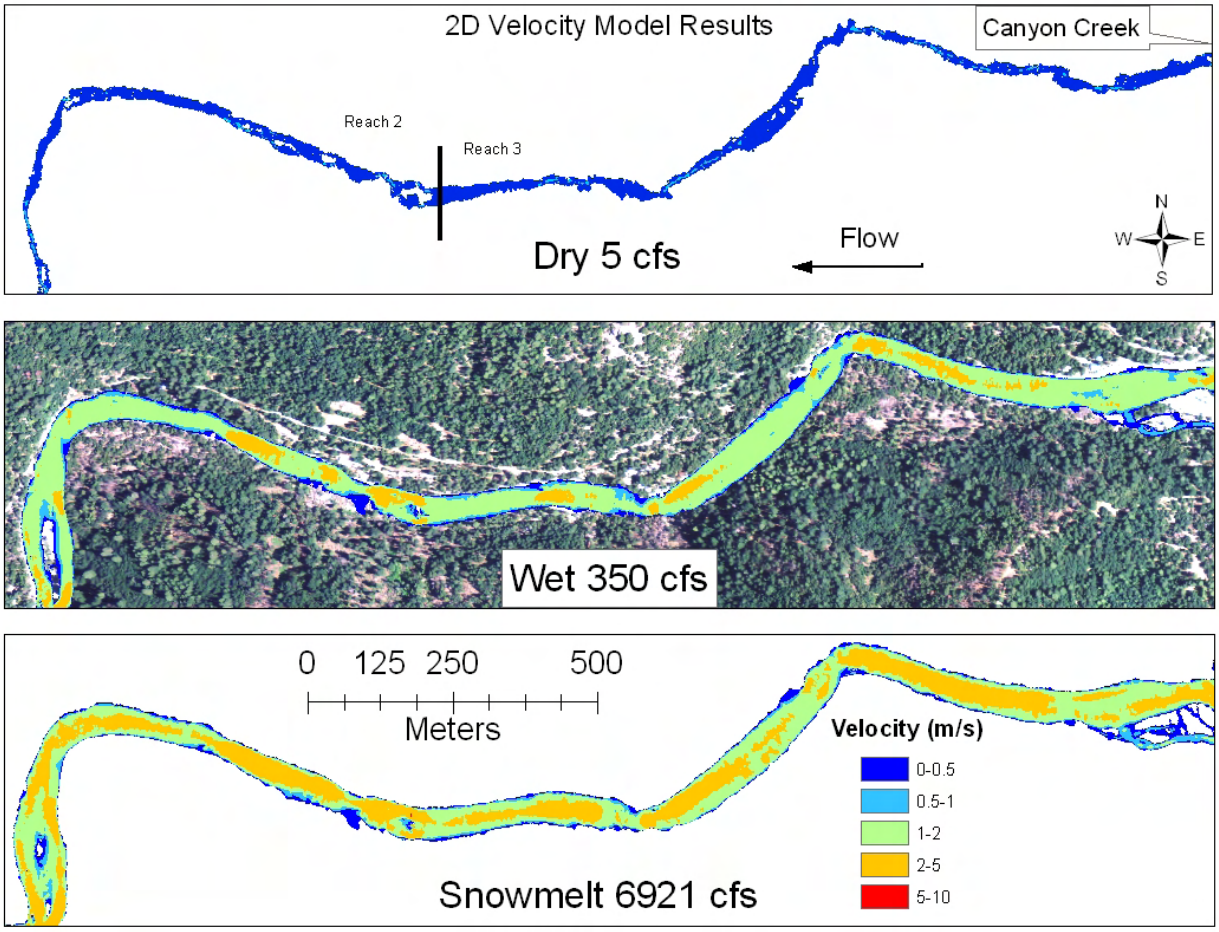

Figure 81. Example of season- and flow- dependent velocity in the lower part of Reach 3.

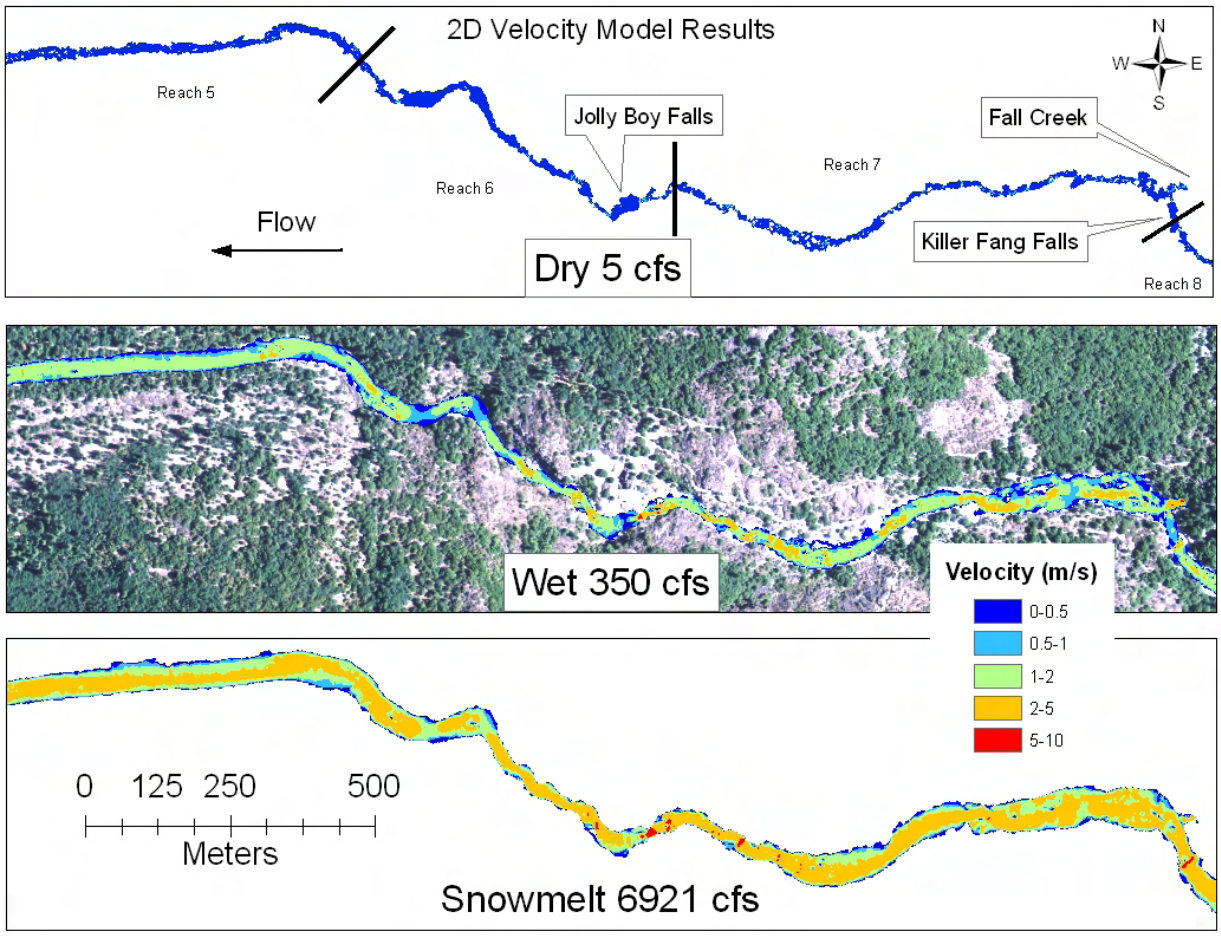

Figure 82. Example of season- and flow- dependent velocity in Reaches 6 and 7.

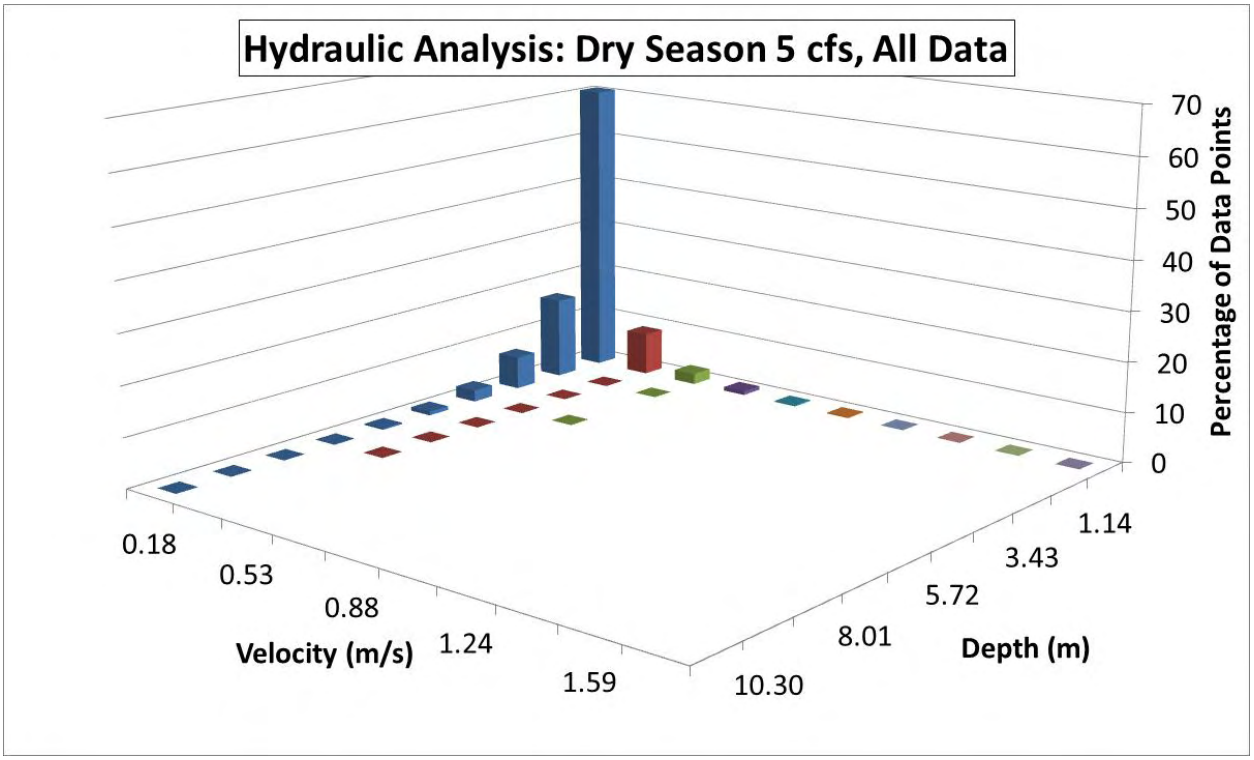

Figure 83. Segment-scale joint distribution of depth and velocity for all 2D model gridded points (n=662,475) in the lowest flow in the dry season.

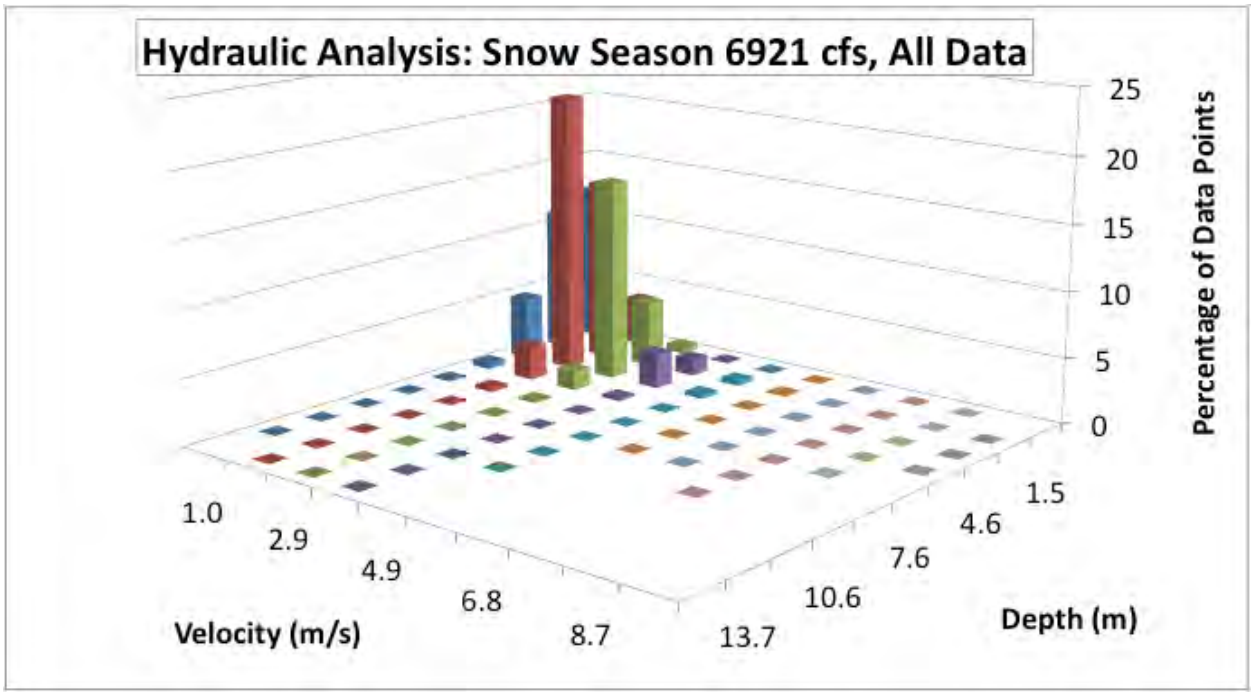

Figure 84. Segment-scale joint distribution of depth and velocity for all 2D model gridded points (n=2,413,066) in the highest observed flow in the snowmelt season.

9.2 Morphological Unit Scale 2D Hydraulic Results

9.2.1 Stage-Dependent Morphological Unit Average Conditions

Overall, average depth and velocity values increase as flows increase (Table 36, Figure 85, Figure 86, Figure 87). Differences in initial values at the low end of the discharge scale (i.e. between dry 10, wet 5, and snowmelt 10) can be attributed to the hydrologic analysis of Chapter 6.0 and subsequent regression equations (Eq. 1–3c) that take into account variance in accretion rates during different times of the year. Morphologic units are defined by velocity and depth, so some of the variances are constrained by boundary definitions of the units (Figure 51).

Lowest average depth was 0.166 m in inset channels with plane beds and steep inset channels 0.183 m, all from the dry 5 cfs run. Highest average depth was 5.48 m in pools during the 6921 cfs run. Standard deviation in depth values ranged from 0.115 m in steep inset channels in the dry 5 cfs run to 1.3194 m in pools during the 6921 cfs run. Lowest average velocity was 0.055 m/s in transitions followed closely by 0.056 m/s in plane beds, both from the dry 5 cfs model run. Highest average velocity was 2.738 m/s in steep inset channels during the 6921 cfs model run. Standard deviation in velocity values ranged from a low of 0.025 m/s in pools during the dry 5 cfs run to a high of 0.625 m/s in steep inset channels during the 6921 cfs run.

Rates of increase in average and standard deviations of depths are greatest in plane beds, inset channels, and steep inset channels. These units are initially shallower (Table 36), so any increases are disproportionately large in the early stages of discharge increases. Plane beds are located predominately along the margins of other morphologic units and are shallow, so when discharge increases, these units are always affected. Inset channels and steep inset channels are cross-sectionally constrained, and since discharge is a function of width and depth, when width is constrained depth will increase. The combination of disproportionate increase in depth due to shallowness and the width constraint are the main drivers of the greater rates of increase in average and standard deviation of depths. Pools and transitions tend to occur together (Table 31) and are the units with the greatest average widths, thus depths will increase more slowly. Chutes have greater initial depths and higher velocities, thus rates of increase are spread over two larger 'bins', which minimizes both rates of increase.

Pools, transitions, and plane beds exhibited the highest rates of increase in average and standard deviation velocity values compared to inset channels, chutes, and steep inset channels. The higher rates of increase are a result of lower slopes (

Table 26) and less constrained cross-sectional area in pools, transitions, and plane beds (

Table 24), which allows flow to spread out and dissipate in these units, particularly at low flows. Inset channel, chute, and steep inset channel velocities are initially higher because slope functions dominate these morphologic units and they are the units that are more constrained in cross-sectional areas. Slope continues to be the dominant physical driver in these units, so velocities remain highest as discharge increases but the rate of increase is lower.

As illustrated in Figure 80, Figure 81, and Figure 82, no modeled discharge, including that of snowmelt 6921 cfs, were large enough to reveal a systemic velocity reversal, where pool velocities became faster than steep inset channel velocities, but a separate analysis was performed to assess that on a morphological-unit basis (section 9.2.2). Rates of average velocity increase in transitions, pools, and plane beds far out-paced rates of velocity increase in inset channels, chutes, and steep inset channels (

Table 37). The highest rate of velocity increase between seasons occurs in pools, with snowmelt season 2.8 times greater than dry season. This hints at, but does not show that the hypothesis of stage-dependent flow convergence may occur in mountain river channels. Average depth, on the other hand, exhibits greater rates of increase in the shallower units of plane bed, inset channel, and steep inset channel. This drives an equalization of water surface slope.

A series of plots were developed so that averages and standard deviations of depth and velocity could be compared across flows in each season (Figure 88, Figure 89, Figure 90). Each set of plots is discussed in the following sections.

Table 36. 2D model results stratified by morphological unit from all simulations for three hydrological regimes. Discharge is the YRSF gaged input, not total discharge.

Average Depth (m)

Season	cfs	Transition	Plane Bed	Pool	Inset Channel	Chute	Steep Inset Channel
Dry	5	0.74	0.18	2.02	0.17	0.66	0.18
	10	0.83	0.21	2.12	0.22	0.77	0.25
	20	1.03	0.29	2.34	0.37	1.01	0.41
	30	1.23	0.42	2.55	0.52	1.24	0.57
	45	1.52	0.63	2.86	0.74	1.56	0.81
Wet	5	0.91	0.23	2.22	0.28	0.87	0.31
	15	1.04	0.29	2.35	0.37	1.02	0.42
	30	1.19	0.39	2.50	0.49	1.19	0.54
	55	1.39	0.54	2.72	0.64	1.42	0.70
	100	1.68	0.76	3.03	0.87	1.74	0.95
	190	2.18	1.14	3.55	1.26	2.28	1.37
	350	2.95	1.76	4.39	1.90	3.15	2.07
Snow melt	10	0.85	0.21	2.14	0.24	0.79	0.27
	25	1.02	0.28	2.32	0.36	0.99	0.40
	50	1.20	0.40	2.52	0.50	1.20	0.55
	140	1.41	0.56	2.73	0.66	1.41	0.71
	210	1.26	0.48	2.57	0.57	1.22	0.60
	525	1.64	0.78	2.96	0.87	1.61	0.90
	1103	2.09	1.16	3.43	1.25	2.08	1.29
	3000	2.93	1.90	4.33	1.98	2.95	2.04
	6921	4.01	2.87	5.48	2.94	4.08	3.05

Average Velocity (m/s)

Season	cfs	Transition	Plane Bed	Pool	Inset Channel	Chute	Steep Inset Channel
Dry	5	0.06	0.06	0.03	0.22	0.22	0.48
	10	0.09	0.09	0.06	0.32	0.33	0.64
	20	0.19	0.19	0.13	0.53	0.56	0.93
	30	0.31	0.31	0.22	0.70	0.76	1.14
	45	0.49	0.50	0.37	0.93	1.02	1.40
Wet	5	0.13	0.12	0.08	0.39	0.43	0.75
	15	0.20	0.19	0.13	0.53	0.57	0.93
	30	0.28	0.28	0.20	0.67	0.72	1.10
	55	0.40	0.42	0.30	0.84	0.91	1.29
	100	0.60	0.61	0.46	1.06	1.16	1.53
	190	0.93	0.93	0.78	1.38	1.52	1.84
	350	1.43	1.39	1.29	1.81	2.02	2.23
Snow melt	10	0.10	0.09	0.06	0.34	0.35	0.67
	25	0.18	0.18	0.12	0.51	0.54	0.91
	50	0.29	0.30	0.20	0.69	0.73	1.12
	140	0.41	0.44	0.30	0.86	0.90	1.31
	210	0.41	0.44	0.30	0.86	0.90	1.31
	525	0.56	0.64	0.42	1.07	1.06	1.50
	1103	0.86	0.96	0.70	1.38	1.39	1.81
	3000	1.43	1.52	1.27	1.89	1.92	2.26
	6921	2.11	2.15	1.99	2.44	2.49	2.74

Average Standard Deviation of Depth (m)

Season	cfs	Transition	Plane Bed	Pool	Inset Channel	Chute	Steep Inset Channel
Dry	5	0.21	0.16	1.19	0.13	0.24	0.12
	10	0.21	0.18	1.19	0.15	0.24	0.14
	20	0.21	0.22	1.19	0.19	0.25	0.18
	30	0.24	0.26	1.20	0.23	0.26	0.22
	45	0.28	0.33	1.19	0.28	0.30	0.28
Wet	5	0.20	0.20	1.19	0.17	0.24	0.16
	15	0.22	0.22	1.19	0.19	0.25	0.18
	30	0.23	0.25	1.19	0.21	0.26	0.21
	55	0.26	0.30	1.19	0.26	0.28	0.25
	100	0.31	0.36	1.20	0.31	0.32	0.31
	190	0.42	0.47	1.22	0.40	0.42	0.42
	350	0.62	0.66	1.30	0.57	0.60	0.62
Snow melt	10	0.21	0.18	1.19	0.15	0.24	0.14
	25	0.21	0.22	1.19	0.19	0.24	0.17
	50	0.22	0.26	1.18	0.22	0.26	0.21
	140	0.24	0.29	1.19	0.25	0.28	0.24
	210	0.23	0.28	1.19	0.23	0.27	0.21
	525	0.27	0.34	1.19	0.29	0.31	0.27
	1103	0.32	0.40	1.20	0.35	0.38	0.34
	3000	0.44	0.53	1.25	0.47	0.52	0.48
	6921	0.61	0.69	1.32	0.62	0.71	0.67

Average Standard Deviation of Velocity (m/s)

Season	cfs	Transition	Plane Bed	Pool	Inset Channel	Chute	Steep Inset Channel
Dry	5	0.04	0.06	0.02	0.10	0.11	0.20
	10	0.06	0.08	0.04	0.12	0.14	0.23
	20	0.11	0.14	0.08	0.14	0.18	0.27
	30	0.16	0.20	0.13	0.19	0.23	0.32
	45	0.23	0.28	0.20	0.25	0.29	0.38
Wet	5	0.08	0.10	0.06	0.12	0.16	0.25
	15	0.11	0.14	0.09	0.14	0.18	0.27
	30	0.15	0.18	0.12	0.18	0.22	0.31
	55	0.20	0.24	0.17	0.22	0.26	0.35
	100	0.26	0.32	0.23	0.27	0.32	0.40
	190	0.36	0.41	0.34	0.33	0.38	0.47
	350	0.48	0.51	0.48	0.39	0.45	0.53
Snow melt	10	0.06	0.08	0.04	0.12	0.14	0.23
	25	0.10	0.13	0.08	0.14	0.18	0.27
	50	0.15	0.19	0.12	0.18	0.22	0.31
	140	0.19	0.25	0.16	0.22	0.26	0.35
	210	0.19	0.25	0.16	0.22	0.26	0.35
	525	0.24	0.33	0.20	0.29	0.31	0.42
	1103	0.32	0.40	0.29	0.35	0.37	0.49
	3000	0.42	0.49	0.42	0.42	0.45	0.57
	6921	0.51	0.54	0.58	0.45	0.52	0.63

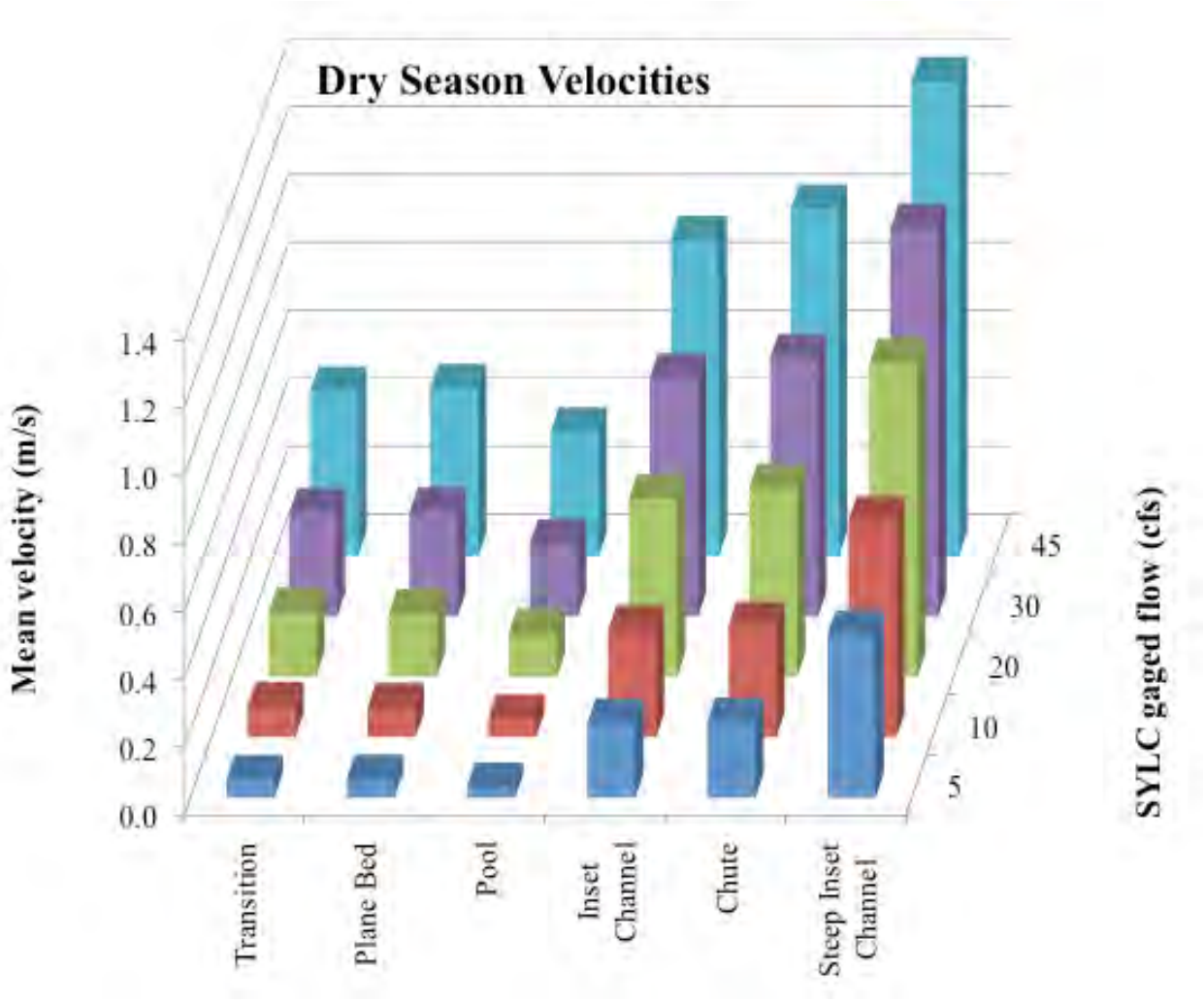

Figure 85. Flow-dependent average velocity of each morphological unit in the dry season.

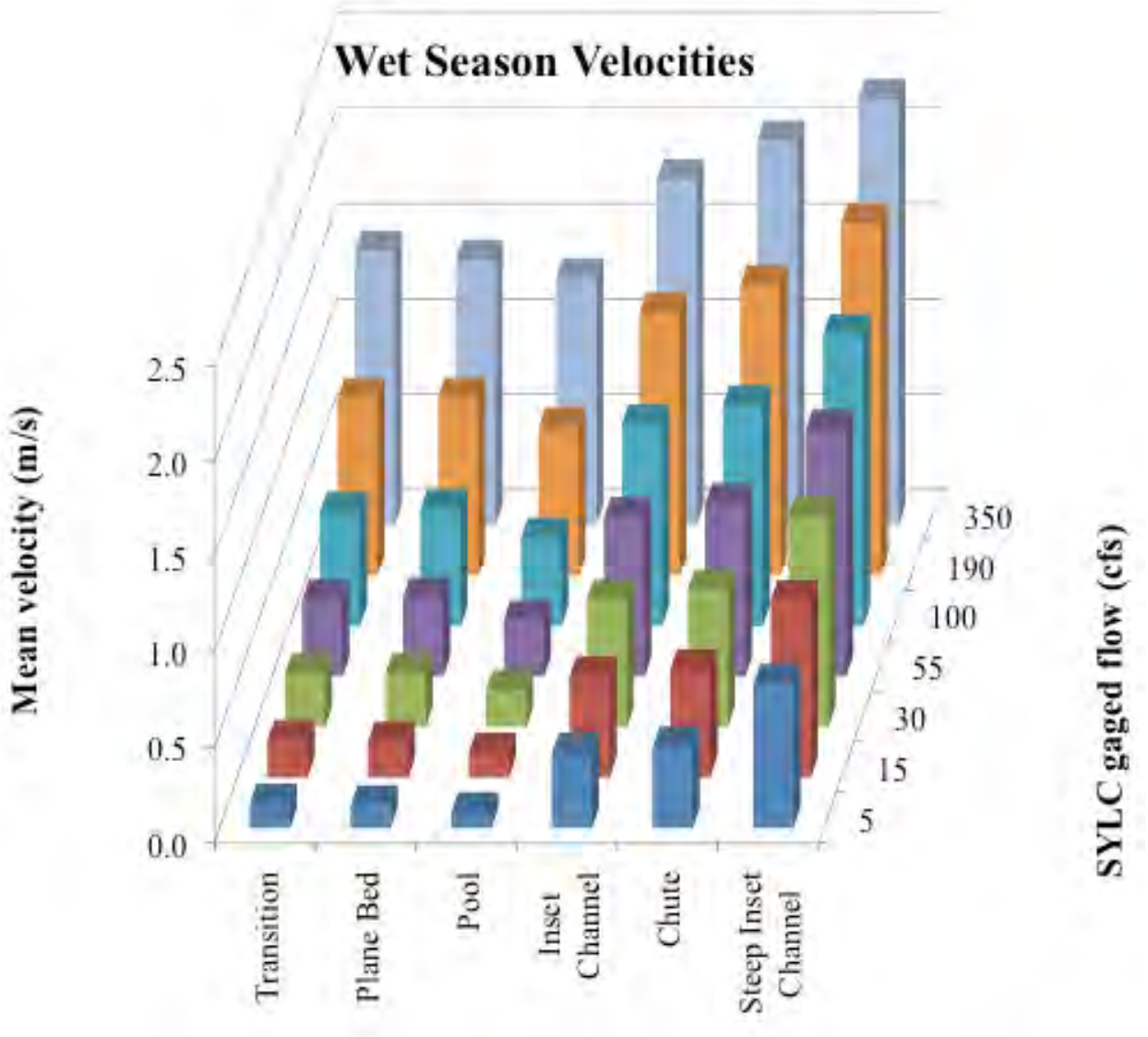

Figure 86. Flow-dependent average velocity of each morphological unit in the wet season.

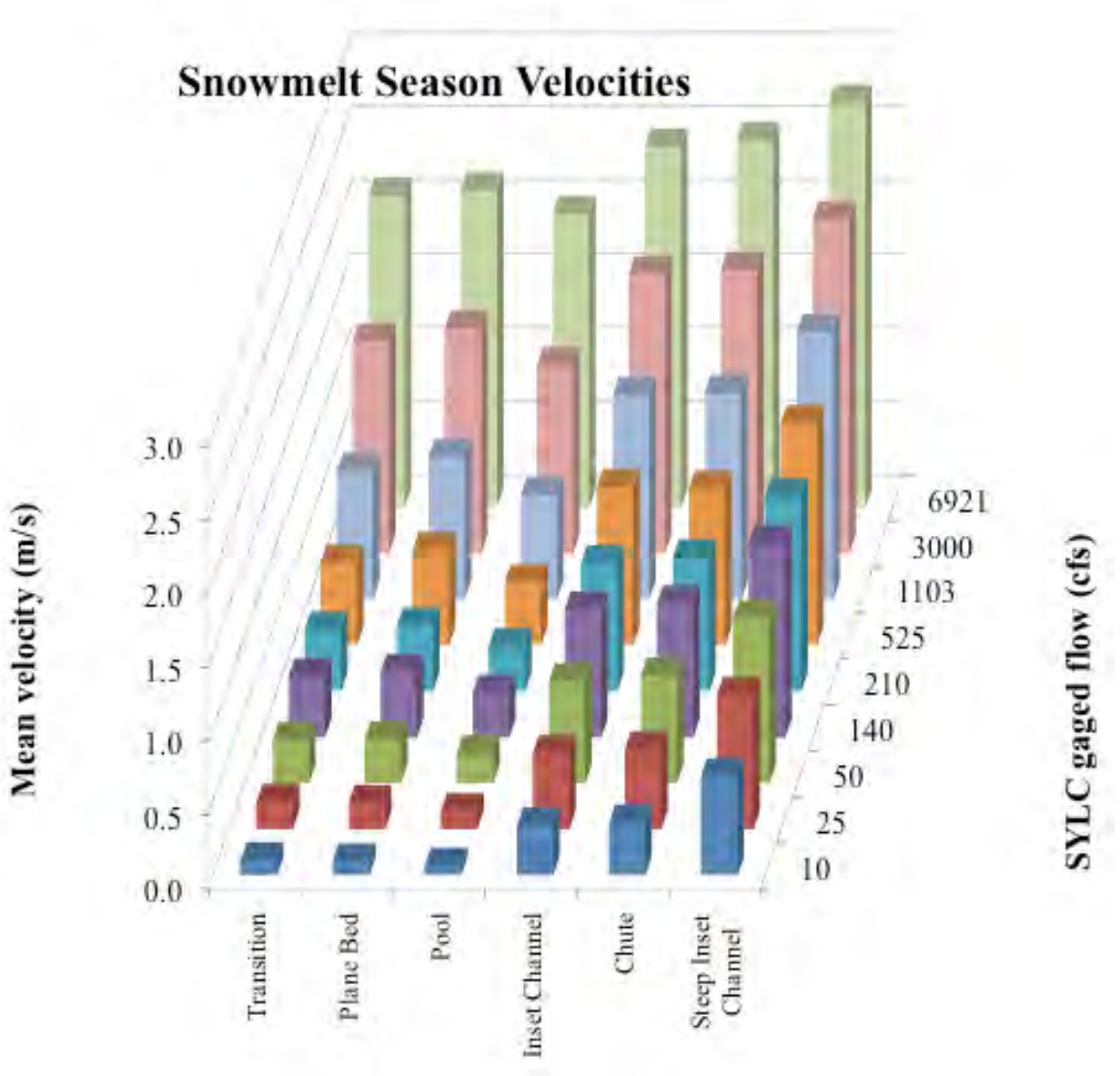

Figure 87. Flow-dependent average velocity of each morphological unit in the snowmelt season.

Table 37. Rate of increase between lowest and highest 2D model values regardless of flow regime (e.g. highest value of snowmelt 6921 divided by lowest value of dry 5).

	Rate of increase of parameter					
Variable	Transition	Plane Bed	Pool	Inset Channel	Chute	Steep Inset Channel
Average Velocity (m/s)	38.4	38.3	62.1	11.1	11.1	5.7
Average Standard Deviation Velocity (m/s)	13.1	9.4	23.1	4.3	4.5	3.1
Average Depth (m)	5.4	15.7	2.7	17.7	6.2	16.7
Average Standard Deviation Depth (m)	3.0	4.2	1.1	4.9	3.0	5.8

Dry Season Plots

Plotted dry season average velocities exhibit increases such that as flows increase, velocity increases proportionally (Figure 88). In some cases, such as steep inset channel, a power function yields a slightly better fit, $r^2 = 0.9974$ than a linear function $r^2 = 0.9837$, but both yield very strong coefficients of determination. Steep inset channels maintained highest velocities and standard deviations across all modeled flows, while pools were slowest. Transitions and plane beds had very similar velocities at every modeled dry season flow. Inset channel velocity standard deviations increase at a slower rate than all other morphologic units. Plane bed standard deviations increased at a faster rate than all other morphologic units.

Dry season average depth curves are best fit with either a linear function as in pool, inset channel, steep inset channel, and plane bed, or polynomial functions for transition and chute. The deviation in depth across all morphologic units was small. As flows increased, the width dimension of the wetted channel cross-sectional area grew faster than depth; therefore variation in depth increases would be small. Average standard deviations of depth converged, except for pools. Plane beds had the highest rate of increase in standard deviation, indicative of the large channel roughness (Manning's n) caused by emergent boulders. Emergent boulders create pockets of divergent and convergent flow, which impinges on velocity trajectory and yields greater degrees of depth deviation in comparison to other morphologic units.

Wet Season plots

Steep inset channels, chutes, and inset channels show highest rates of average velocity increases during the wet season, particularly at discharges below 50 cfs (Figure 89). The curvature of the data is best described by power functions with the exception of pools, where a linear equation fits best. The wet season average and standard deviations in velocity exhibit a similar pattern to the dry season flows, with steep inset channels having highest velocities, followed by chutes and inset channels. Transitions become slightly faster than plane beds at about 250 cfs. Standard deviations of steep inset channels, chutes, and inset channels have a slower rate of increase compared to plane beds, transitions, and pools. Inset channel standard deviation is overtaken by plane bed by 15 cfs, by transitions between 100-150 cfs, and by pools after 300 cfs. The slower velocity, lower slope, greater-average-width morphologic units of plane beds, transitions, and

pools all increase in average standard deviation more rapidly than the more constrained cross-sectional areas of steep inset channels, chutes, and inset channels.

For average depths, polynomial functions yield best fits. A polynomial function fitting the pool curve yields $r^2 = 0.9978$ compared to a linear fit of $r^2 = 0.9873$. No units have a significantly high enough rate of increase to overtake another unit. A small degree of differences in rate increases can be seen as the curves separate with higher flows. Chutes have the highest rate of increase in depth, while plane bed exhibits the highest rate of increase in standard deviation.

Snowmelt Season plots

Almost every snowmelt season plot exhibits a downward jog or flattening of the curve between 100 and 200 cfs before recommencing its upward trajectory (Figure 90). These zones and the curves above and below are directly related to the use of three accretionary flow equations during 2D snowmelt season model runs (Chapter 0, equations in section 5.4), compared to single equations used in the dry and wet season model runs. Note the semi-log plotting used to adequately represent data across three orders of magnitude. Power functions best describe all curves.

Average velocities of all units show marked increases as discharge increases. In dry and wet results (Figure 88, Figure 89), morphologic unit average velocities begin to diverge as flows increase. This can be seen between 5 cfs and 45 cfs in dry season, and between 10 cfs and 350 cfs during wet season. Snowmelt season velocities, on the other hand, begin to show a pattern of convergence as flows reach the 2D model limit of 6921 cfs, with transitions, plane beds, and pools increasing at higher rates than other morphologic units. Average velocity standard deviations also begin to converge, with inset channel an exception as it continues to diverge. Pools can be seen as the units with the greatest rate of velocity standard deviation.

Average depths and deviations follow a similar trajectory as seen in the dry and wet seasons. Transitions and chutes track one another as they both increase, and plane beds, inset channels, and steep insets cluster together while increasing. Depth average standard deviations remain more constant as a group, with steep inset channels, plane beds, and inset channels having the highest rates of increase.

Evidence of a velocity reversal may begin to show itself in the snowmelt season average velocity plots, but 2D modeled flows at greater SYLC discharges would be needed to determine if the trajectory seen in Figure 90 would continue, with the typically slower morphologic unit velocities overtaking the faster units (Figure 87,

Table 37).

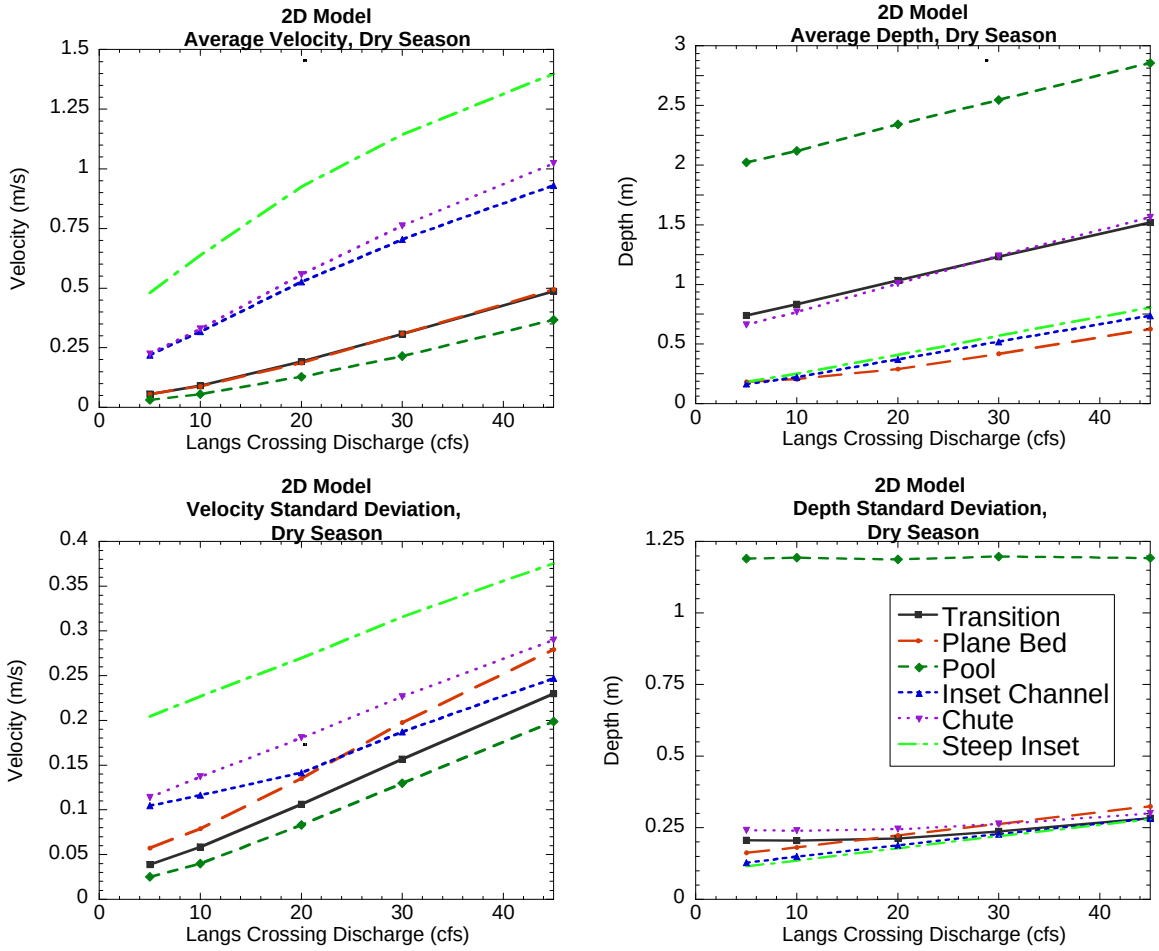

Figure 88. 2D velocity and depth variations during dry season.

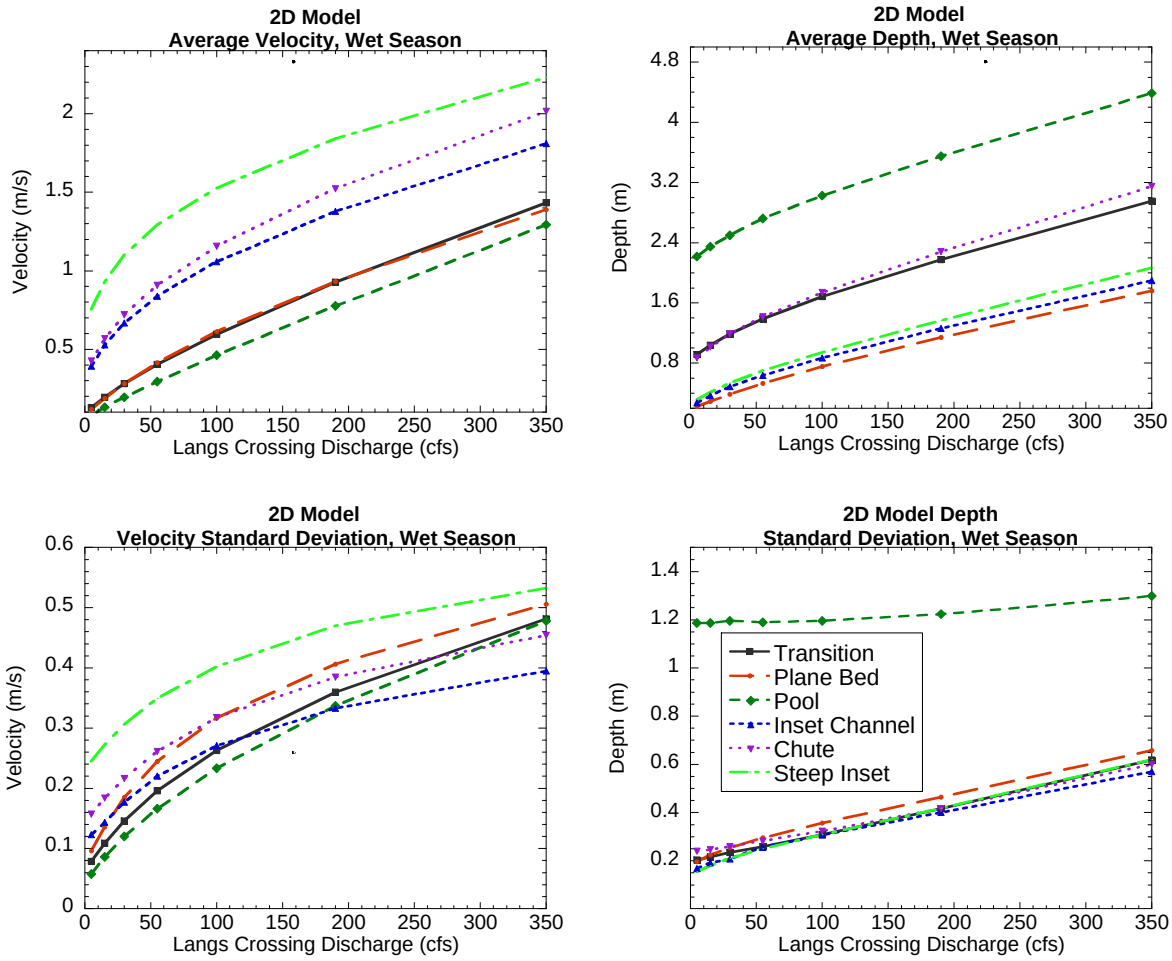

Figure 89. 2D model results of velocity and depth during wet season.

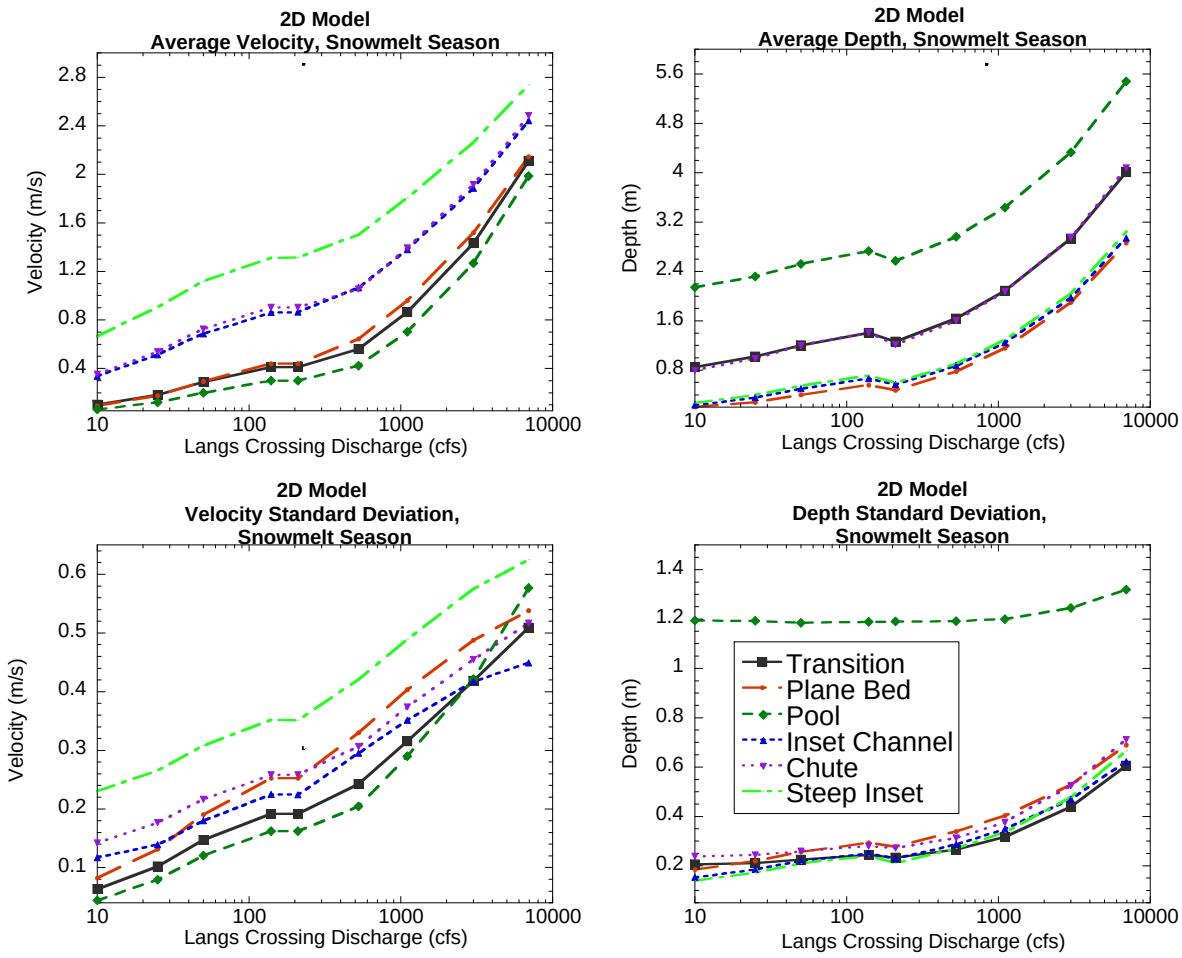

Figure 90. 2D model results of velocity and depth during snowmelt season, plotted in semi-log scale.

9.2.2 Depth-velocity phase space plots by morphological unit

Joint distribution of velocity and depth were plotted for each model run result. Because morphological units were established using the observed flow during summer 2009, the joint distributions illustrated for any given morphological unit for any given simulated flow below are not limited to the specified ranges in Figure 52. For example, at the defining flow, all chute points have a velocity >0.3 m/s. However, at dry 5 cfs, chute points might have velocities lower than 0.3 m/s.

Presented below are one low flow and one high flow set of morphologic-unit velocity and depth joint distributions for all morphological units to represent the analysis. Each morphologic unit plot has a unique set of velocity, depth, and percent ranges. Also, plot perspective changes to provide the best view of each unique dataset distribution. To make these 3D histograms, the program MATLAB was used. Using that program, the axes for all plots must have exactly 10 bins, with the even interval for each axis equaling the maximum point value divided by 10. Notice the difference in visual perception between the typical 2D figures presented in Figure 88, Figure 89, and Figure 90 and the 3D depictions of the same information. Hydraulic model run

results from each morphologic unit are depicted as depth-velocity joint distribution plots in Appendix A.

Dry 5 cfs joint distributions of velocity and depth

- Joint distributions of velocity and depth for the dry 5 cfs model run were plotted using Excel 3D bar charts. Each morphologic unit is represented by a plot; all plots for this model run are presented together as Figure 91.
- Transition depth data are relatively uniform across low velocities, becoming more normally distributed in the velocities 0.09–0.18 m/s, with a decrease in velocity and depth near maximum values. At high depths, velocities exhibit linear decay. Overall, transitions are fairly evenly distributed over all depths and velocities within a narrow range.
- Plane bed data exhibit an exponentially decaying function along the depth axis. Depth data have a much wider range and have maximum values are slightly higher values than transitions. Velocity data have a narrow range, with few velocities greater than 0.15 m/s. These tendencies can be seen in the hydraulic summary table (Table 36), where mean depth is 0.183 m, standard deviation 0.163 m, versus velocity mean of 0.056 m/s and standard deviation of 0.057 m/s. The majority of velocities in plane beds flow at less than 0.06 m/s.
- Pools show a log-normal distribution along the depth axis, while velocities show exponential decay. Most depths reside in the 1-4 m range, while velocities predominate below 0.06 m/s. Pool depths show normal distributions between 0.6–0.18 m/s velocities. Shallow pools have some velocities greater than 0.15 m/s, but the vast majority of pools have depths less than 3.4 m and velocities less than 0.15 m/s. Some pools have depths as great as 10.2 m, even at low flow.
- Inset channel data are expontentially distributed on the velocity axis and log-normally distributed on the depth axis.
- Chute data is predominately focused in the velocity range 0.2–0.5 m/s and depths less than 0.4 m. Exponential decay is noticeable in the depth data. The vast majority of velocities are less than 0.5 m/s, while most depths are less than 3.0 m. Chutes are areas where an expansion of width or depth occurs where velocities increase rapidly, often into a pool, which explains the higher velocities compared to other morphologic units.
- Steep inset channel has the highest range and the highest peak of velocities of all morphologic units. The velocity distribution is fairly normal with positive skewness. Exponential decay is present in the positive depth direction, while the majority of depths are <0.3 m.

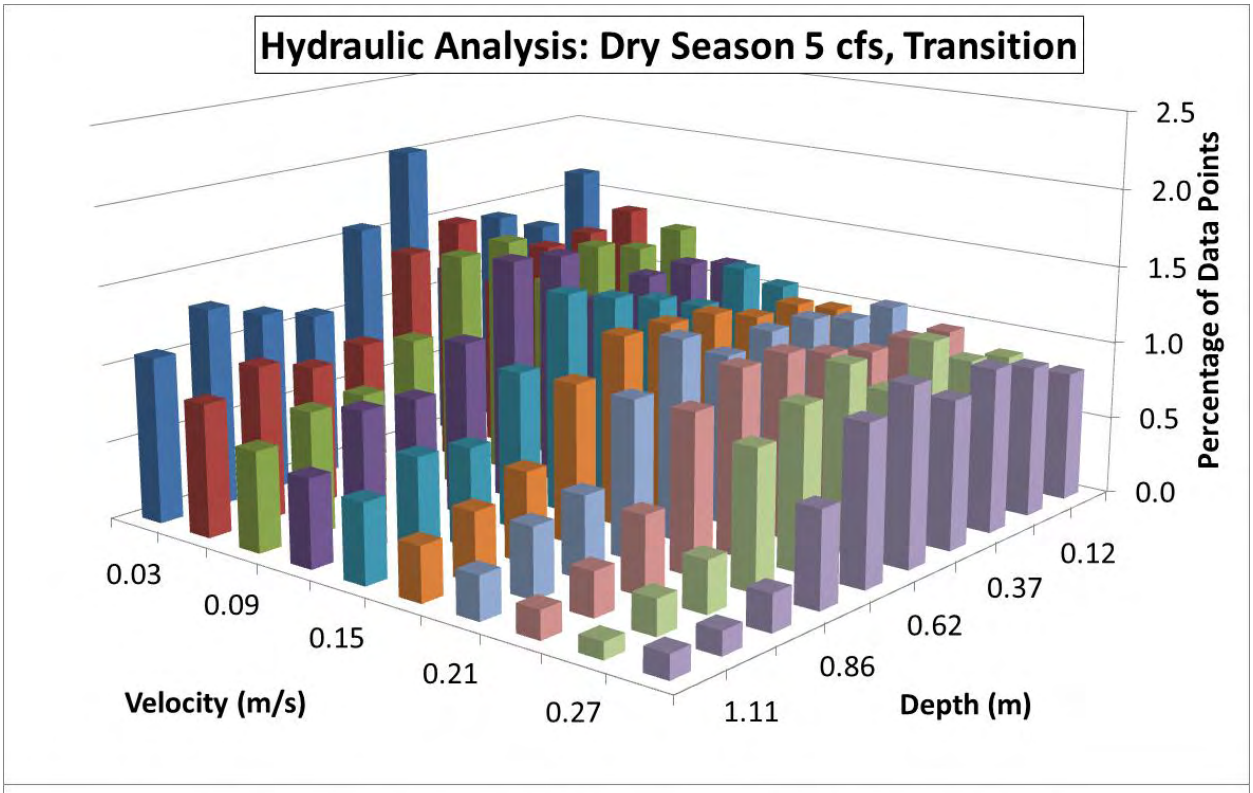
Hydraulic Analysis: Dry Season 5 cfs, Transition
2.5
2.0
1.5
1.0
0.5
0.0
Percentage of Data Points
0.03
0.09
0.15
0.21
0.27
Velocity (m/s)
0.12
0.37
0.62
0.86
1.11
Depth (m)

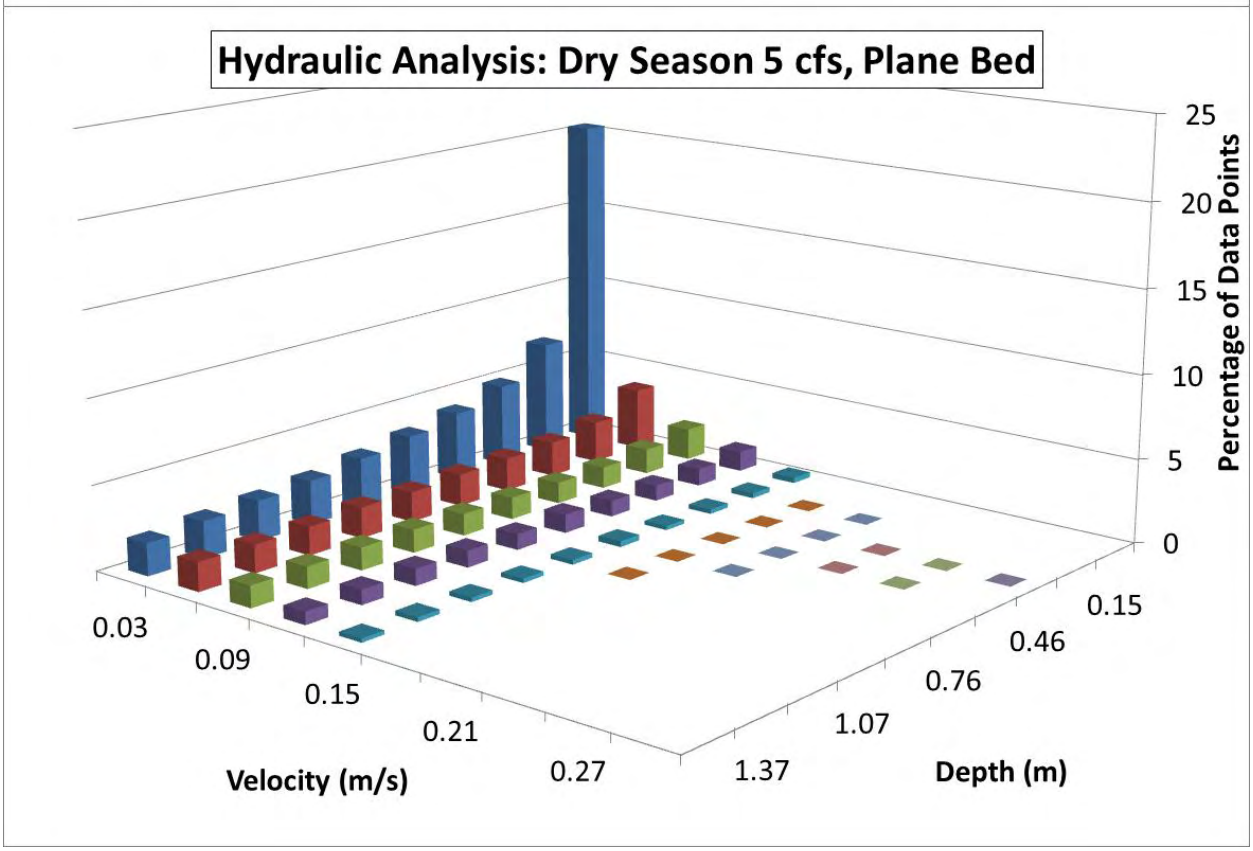
Hydraulic Analysis: Dry Season 5 cfs, Plane Bed
25
20
15
10
5
0
Percentage of Data Points
0.03
0.09
0.15
0.21
0.27
Velocity (m/s)
0.15
0.46
0.76
1.07
1.37
Depth (m)

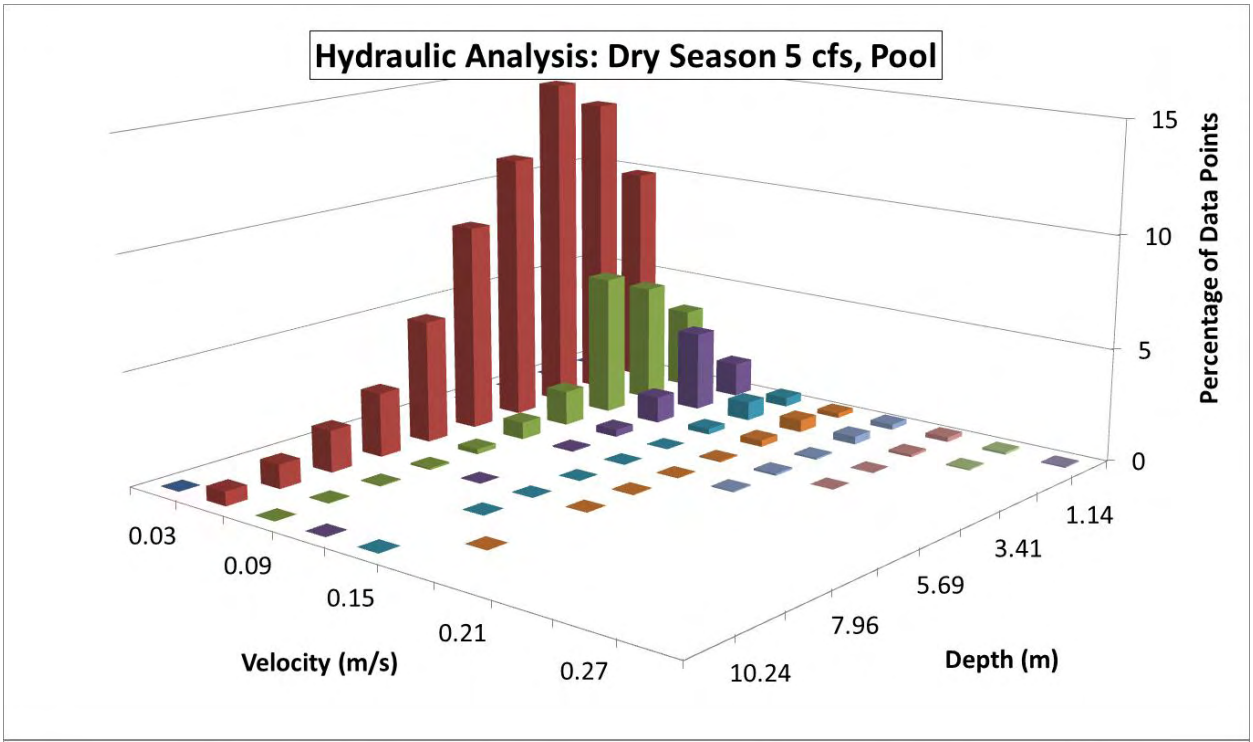
Hydraulic Analysis: Dry Season 5 cfs, Pool
Percentage of Data Points
15
10
5
0
0.03
0.09
0.15
0.21
0.27
Velocity (m/s)
1.14
3.41
5.69
7.96
10.24
Depth (m)

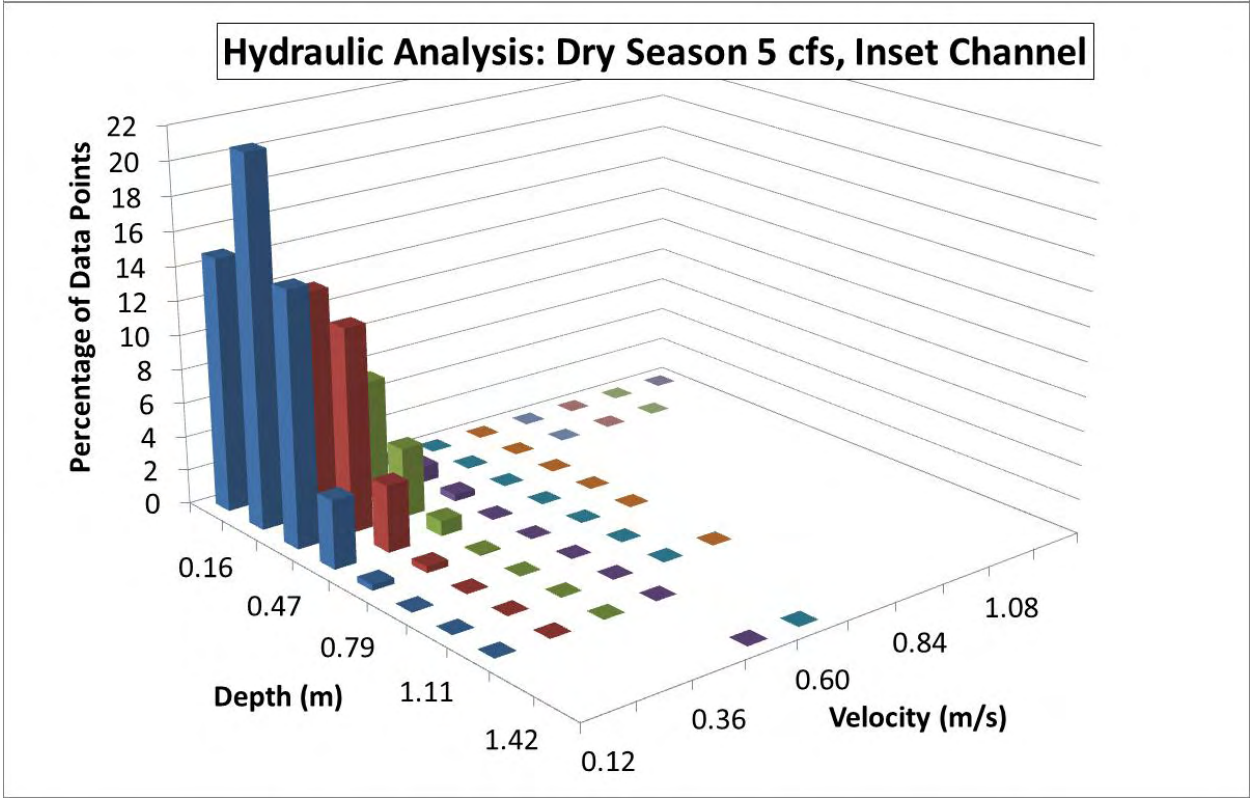
Hydraulic Analysis: Dry Season 5 cfs, Inset Channel
Percentage of Data Points
22
20
18
16
14
12
10
8
6
4
2
0
0.16
0.47
0.79
1.11
1.42
Depth (m)
0.12
0.36
0.60
0.84
1.08
Velocity (m/s)

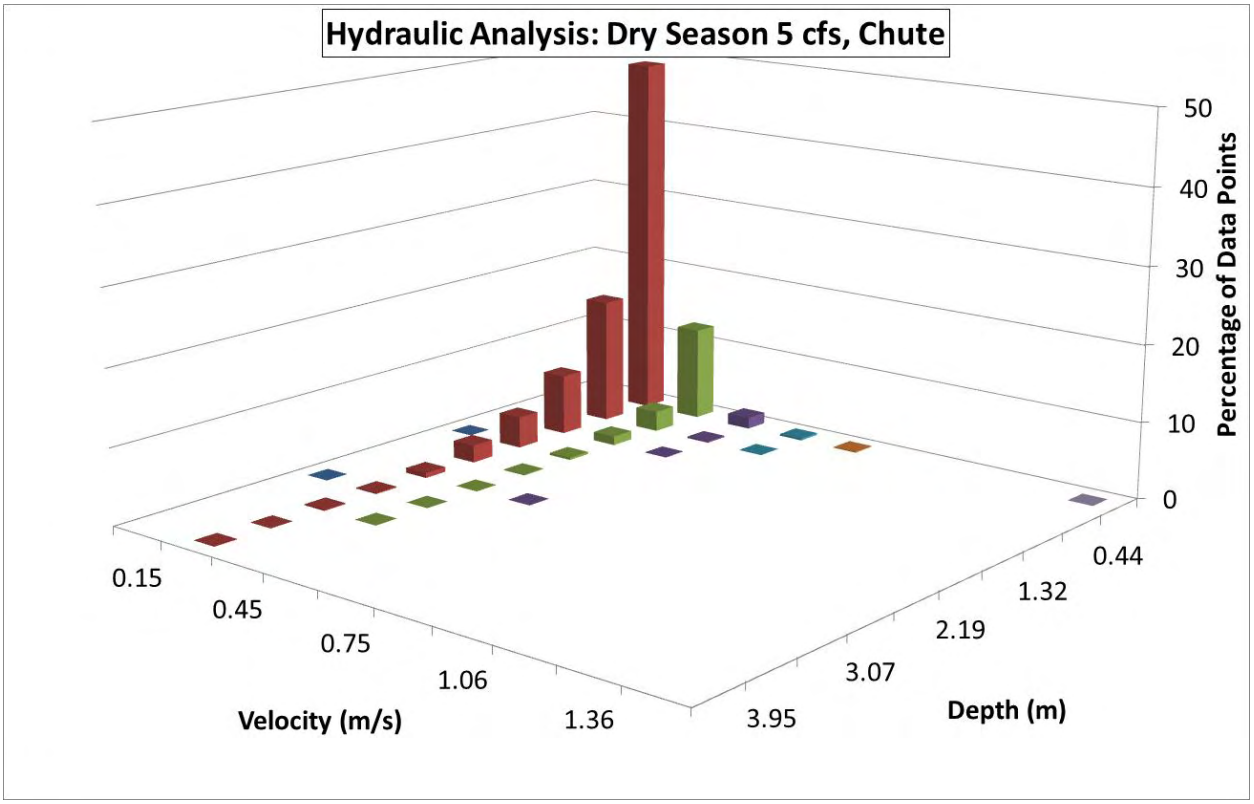

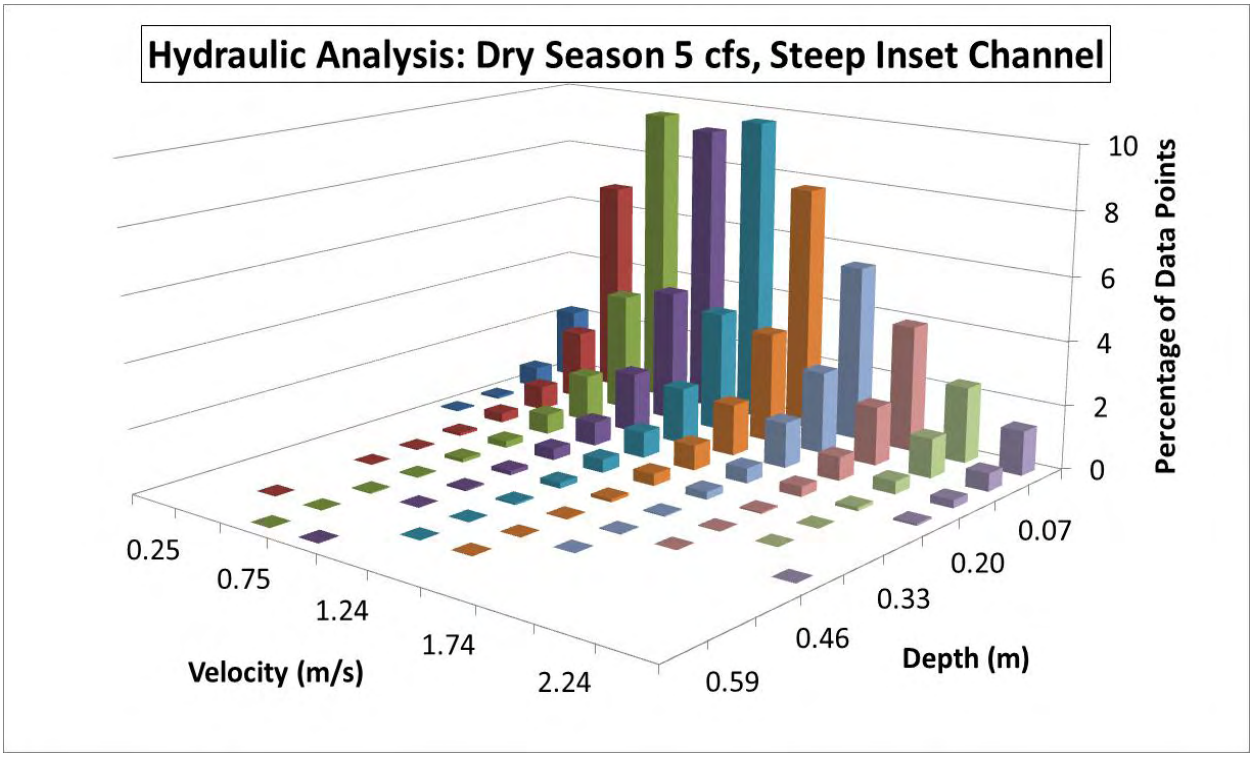

Figure 91. 3D depictions of 2D model results of average velocity and depth by morphologic units during dry season 5 cfs discharge at Langs Crossing. Note variance in velocity, depth, and percent occurrence scales with morphologic units.

Snowmelt 6921 cfs joint distributions of velocity and depth

- Joint distributions of velocity and depth for the snowmelt 6921 cfs model run were plotted using Excel 3D bar charts. Each morphologic unit is represented by a plot; all plots for this model run are presented together as Figure 92.
- Transition data exhibit a normal distribution in depth and velocity directions, with high kurtosis in both directions. The majority of velocities and depths have moved into faster and deeper bins rather than the preponderance of low bin values present in dry 5 cfs data. Most velocities are in the range of 3–6 m/s, and depths from 1–3 m compared to dry 5 cfs velocity and depth ranges of 0–0.27 m/s and 0–1.1 m. Velocities increased at a much higher rate than depths (

Table 37).

- Plane bed data show a normal distribution with high kurtosis in the velocity direction, centered on 3–6 m/s. Depth data show a normal distribution with high kurtosis and a long tail as depths increase. Depths are centered on 0.6–1.7 m. Depths range above 5 m at velocities between 2.9–6.7 m/s. Velocities range up to 8.6 m/s at depths less than 2.9 m.
- Pool data show a range of velocities similar to plane bed, where highest velocities exist up to 8.6 m/s at depths less than 2.9 m. Depths are much greater in pools, reaching above 13.7 m and exhibiting velocities as high as 7 m/s. The majority of velocities exist from 2.0–4.8 m/s, and the majority of depths range from 1.5–6.0 m.
- Inset channel data show a normal distribution in the velocity direction and an exponential decay in the depth direction (excluding the first depth bin). Depths dominate in the range of 1.2–3.0 m, while most velocities are located between 2.3–5.4 m/s.
- Chute data exhibit a normal distribution in the velocity direction and an exponential decay in the depth direction. Depths dominate the range 1.3–4.9 m, while most velocities are located between 2.3–4.7 m/s. Chute depths have a greater range than inset channel depths, while inset channels have a greater range in velocities.
- Steep inset channel data exhibit a normal distribution with high kurtosis in both directions. Velocities are concentrated between 2.3–5.3 m/s and as high as 6.8 m/s. Depths are concentrated between 1.2–2.9 m with greatest depth as high as 5.3 m.

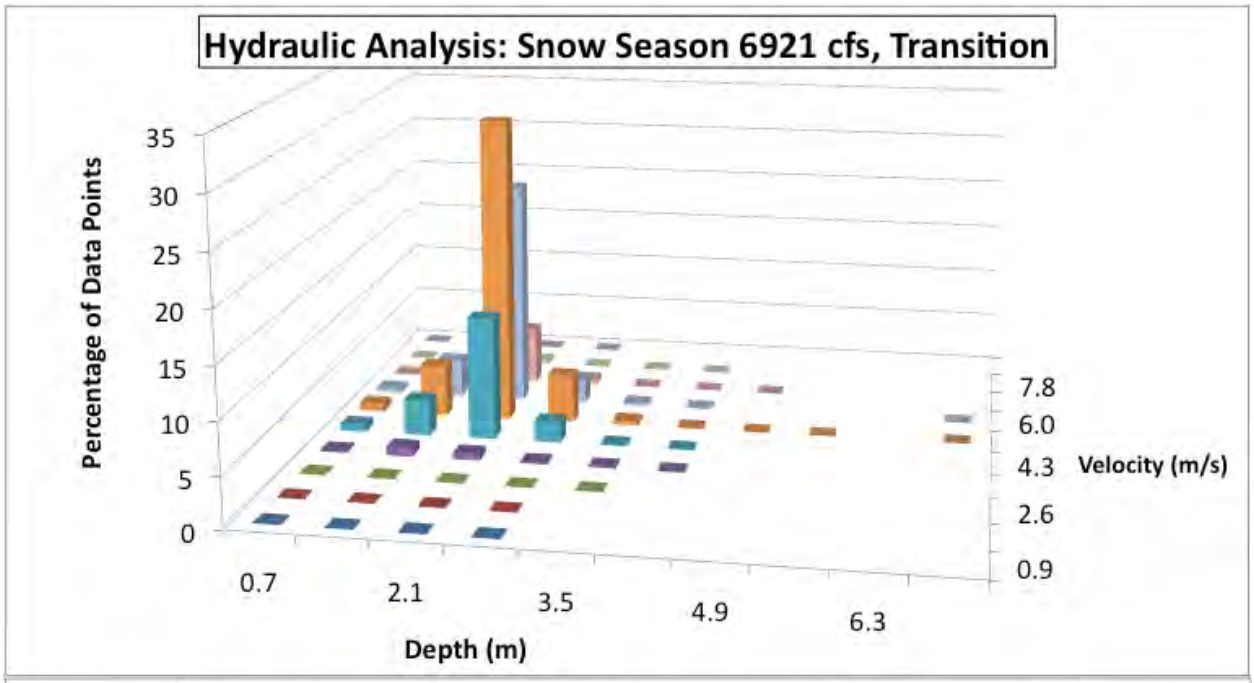
Hydraulic Analysis: Snow Season 6921 cfs, Transition
Percentage of Data Points
35
30
25
20
15
10
5
0
0.7
2.1
3.5
4.9
6.3
Depth (m)
7.8
6.0
4.3
2.6
0.9
Velocity (m/s)

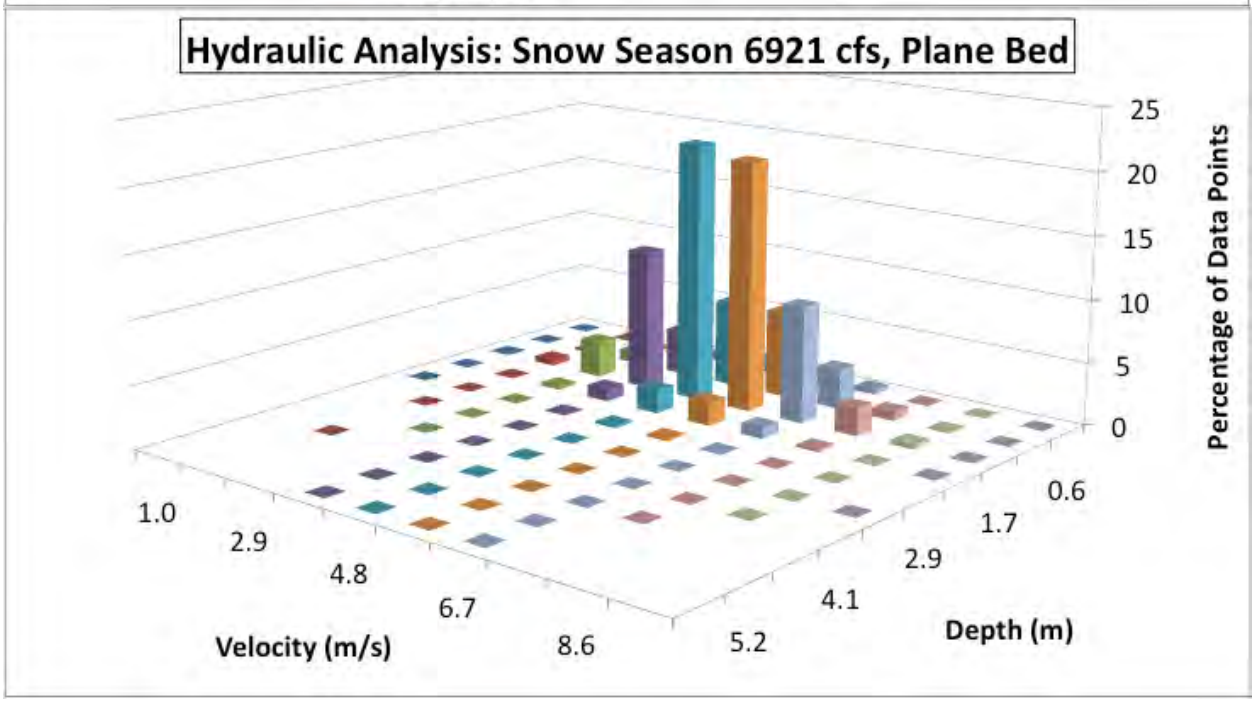
Hydraulic Analysis: Snow Season 6921 cfs, Plane Bed
25
20
15
10
5
0
Percentage of Data Points
1.0
2.9
4.8
6.7
8.6
Velocity (m/s)
0.6
1.7
2.9
4.1
5.2
Depth (m)

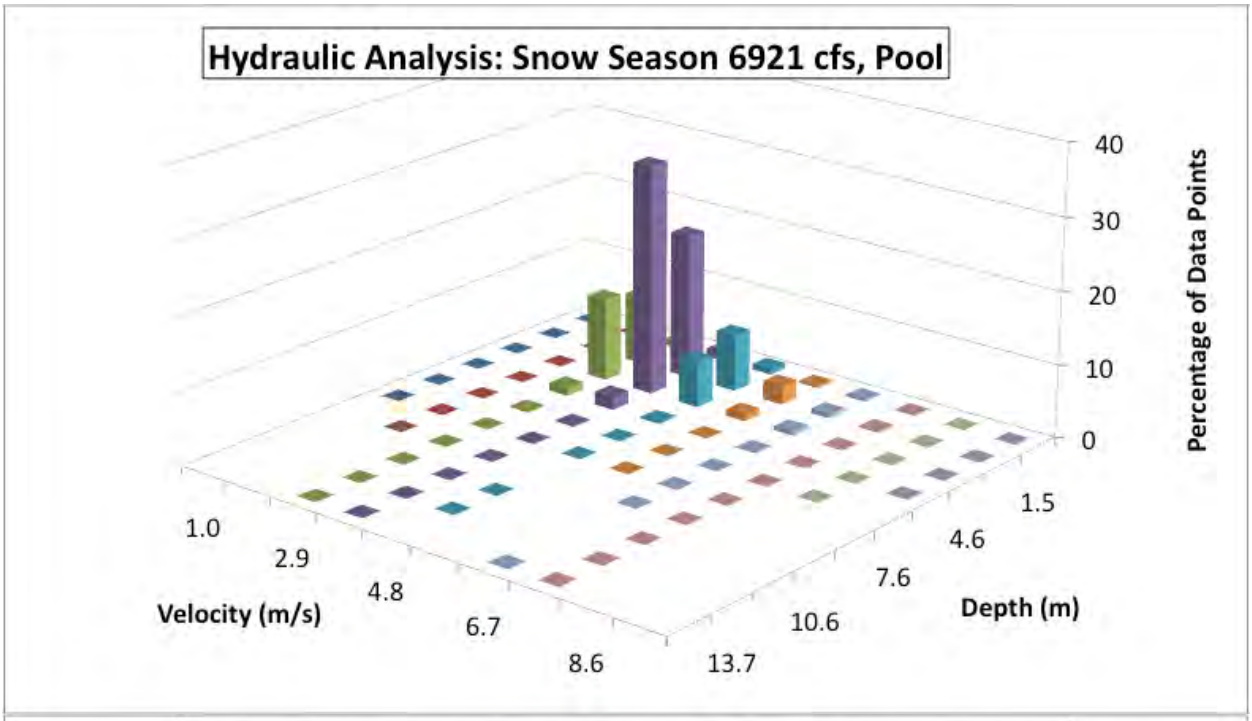
Hydraulic Analysis: Snow Season 6921 cfs, Pool
40
30
20
10
0
Percentage of Data Points
1.0
2.9
4.8
6.7
8.6
Velocity (m/s)
1.5
4.6
7.6
10.6
13.7
Depth (m)

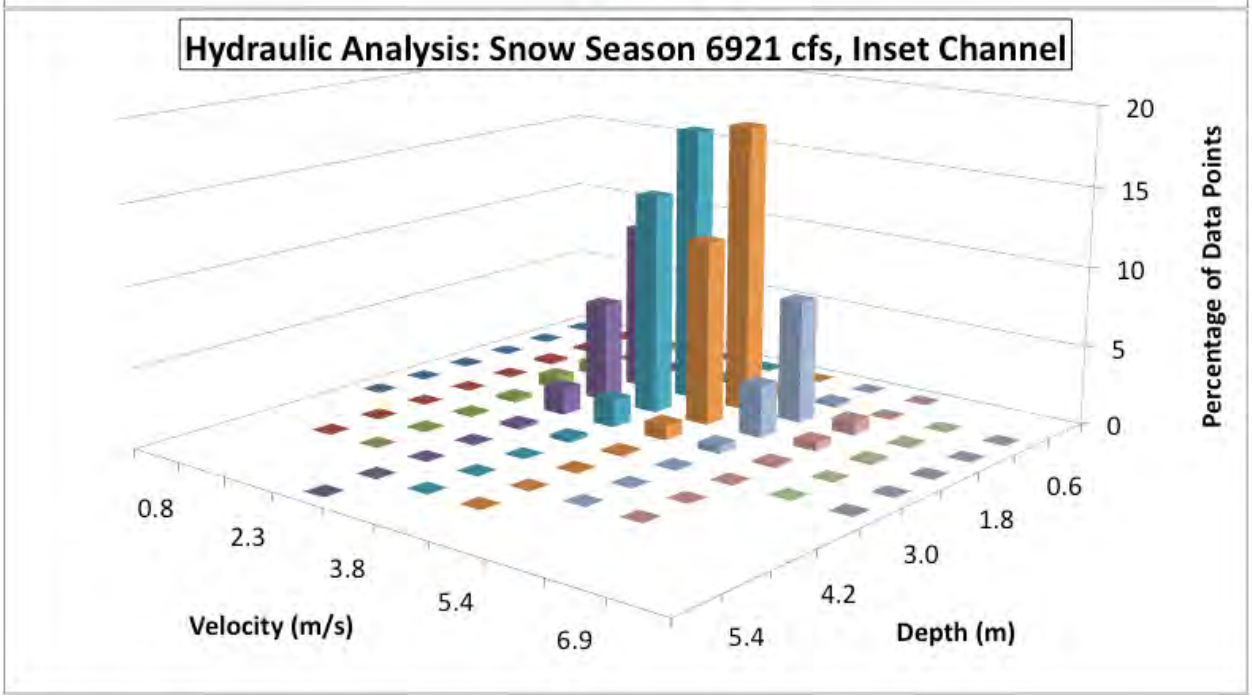
Hydraulic Analysis: Snow Season 6921 cfs, Inset Channel
20
15
10
5
0
Percentage of Data Points
0.8
2.3
3.8
5.4
6.9
Velocity (m/s)
0.6
1.8
3.0
4.2
5.4
Depth (m)

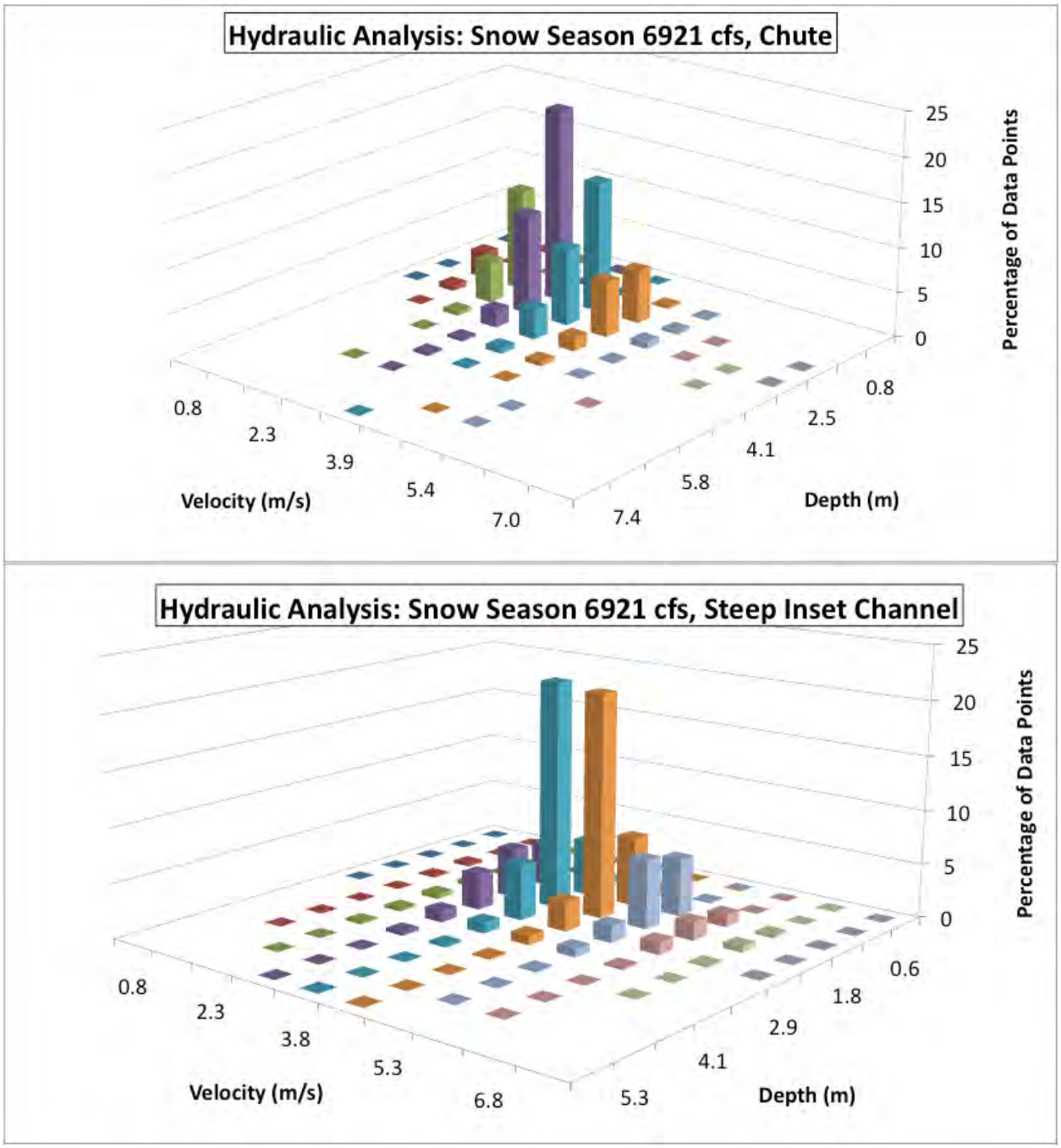

Figure 92. 3D depiction of 2D model results of average velocity and depth during snowmelt season discharges of 6921 cfs. Note variance in velocity, depth, and percent occurrence scales with morphologic units.

9.3 2D Sediment Transport Regime Results

Section 8.9.2 describes the calculations used to obtain two metrics that evaluate sediment transport mechanisms in the study segment. The critical bed material size metric is a measure of the competence of flow to transport sediment of a particular size range. The framework of the

river bed in the study segment is composed of small and large boulders (>256 mm), with gravel and cobble (2–256 mm) making up the interstitial matrix. In some places these smaller materials create a moderately thick surface covering, but they do not define the structure of the morphological units. Therefore, the key question this metric assessed was whether any flows in the observed range were competent enough to make the majority of the riverbed move its boulders. The second metric, Shields stress for a gravel/cobble mixture, is a measure of the bulk sediment transport regime for the fraction of riverbed composed of this material. The key question this metric assessed was whether any flows in the observed range were competent enough to redistribute gravel/cobble substrate used for rainbow trout spawning. Together, these metrics clarify the types of and potential for channel change in the study segment. The term *competence* is used here to define the upper limit of grain size capable of being moved by a discharge.

9.3.1 Flow-Dependent Critical Bed Material Size

At the segment scale, the critical bed material size metric reveals that the river is primarily capable of moving sand and gravel across all seasons and flows (Figure 93-Figure 98). In the figures, as the competence goes up, the bars shift in percentage from more of the channel being able to transport nothing larger than sand to nothing larger than gravel to nothing larger than cobble. For the dry season, sand transport competence dominates the SYLC 5 and 10 cfs flows, but at all higher flows gravel transport competence dominates (Figure 93). For the highest flow, a wetted area of ~15% is capable of moving cobble. Minimal boulder transport occurs in the dry season, so the structure and function of the channel is fixed during this part of the year. Sediment competence in the wet season is similar to the dry season, but because it spans a wider range of flows, transitions between sand, gravel, cobble competence are seen (Figure 94). At the highest wet-season flow, cobble competence dominates the channel, with almost 60% of the channel capable of moving cobble. Because the hydrology of the snowmelt season is so different form the other two seasons, flow competence is also different (Figure 95). During the snowmelt season, the smaller proportion of flow accretion means that cobble competence does not exceed ~30% until the flow is >1000 cfs, whereas in the wet season cobble transport competence at 350 cfs is closer to 60%. Above 3000 cfs, small-boulder competence is possible in about ~10% of the channel and at 6921 cfs the area of small-boulder transport has increased enough that the area of cobble transport has started to decline. However, even at 6921 cfs, the river is not pre-dominantly experiencing boulder transport, so the scope of channel change for the range of observed flows appears limited at the segment scale.

The spatial pattern of the critical bed material size metric was evaluated for evidence of stage-dependent flow convergence. Figure 96, Figure 97, and Figure 98 illustrate the spatial pattern of the metric for three different parts of the river segment. Although there is some variation in location of peak flow competence with increasing discharge, there is no “reversal” in which the areas of lowest competence at low flow become the areas of highest competence at high flow.

Taken together, the conditional statistical distribution of competence and the spatial pattern of competence provide very strong evidence that the maximum flow observed and modeled is too small to cause channel-changing process. The 1997 flood was known to produce this outcome and that event had ~4 times the flow of the largest one assessed in this study. At present, it is unclear what processes were occurring during that flood.

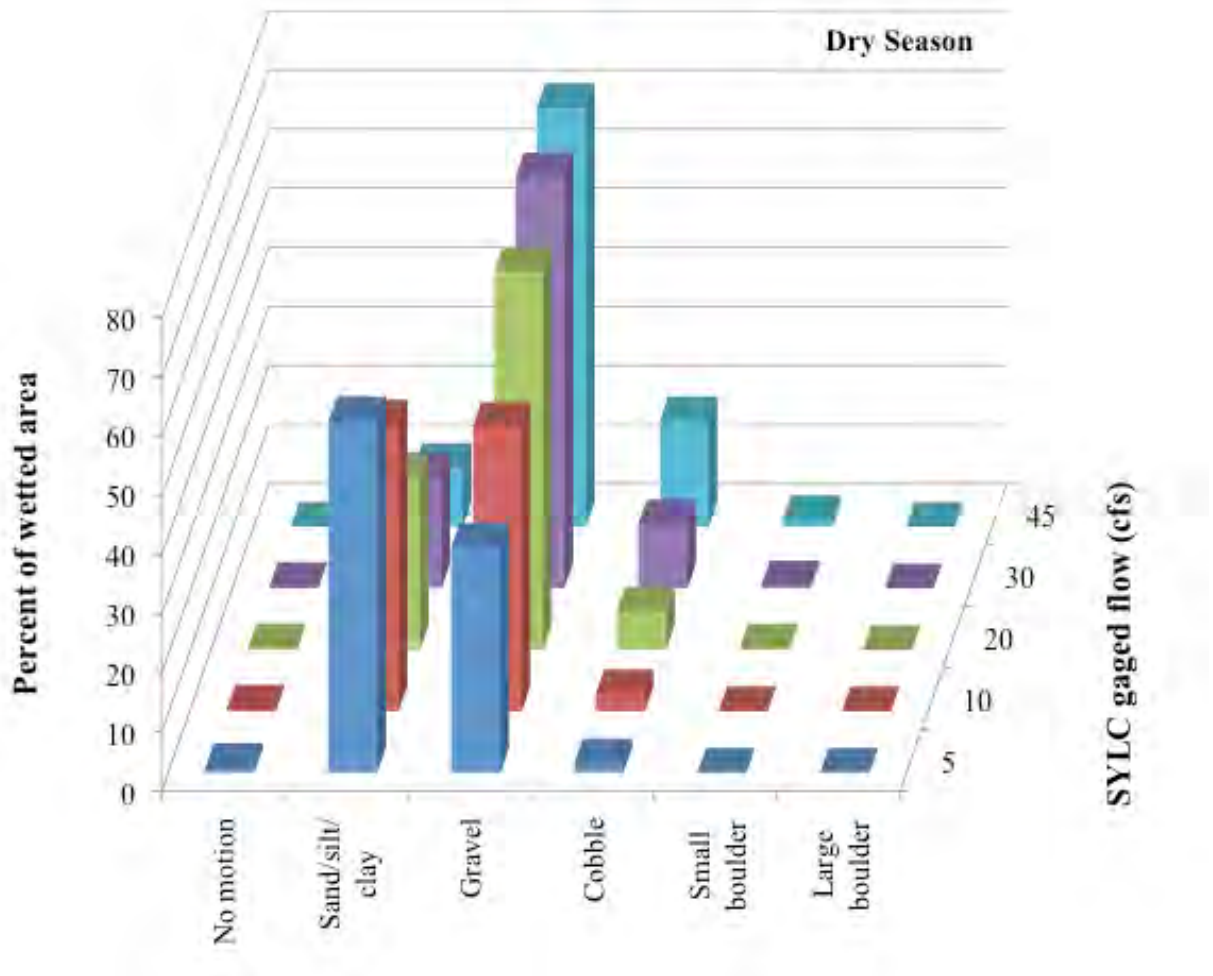

Figure 93. Flow-dependent percent of the wetted study segment with a sediment transport capacity to entrain the designated critical bed material size class during the dry season. The decline of sand/silt/clay bars does not mean that these are not transported, but that they are not the critical size. The plot shows a shift in the threshold of what can be moved—larger sizes with larger flows.

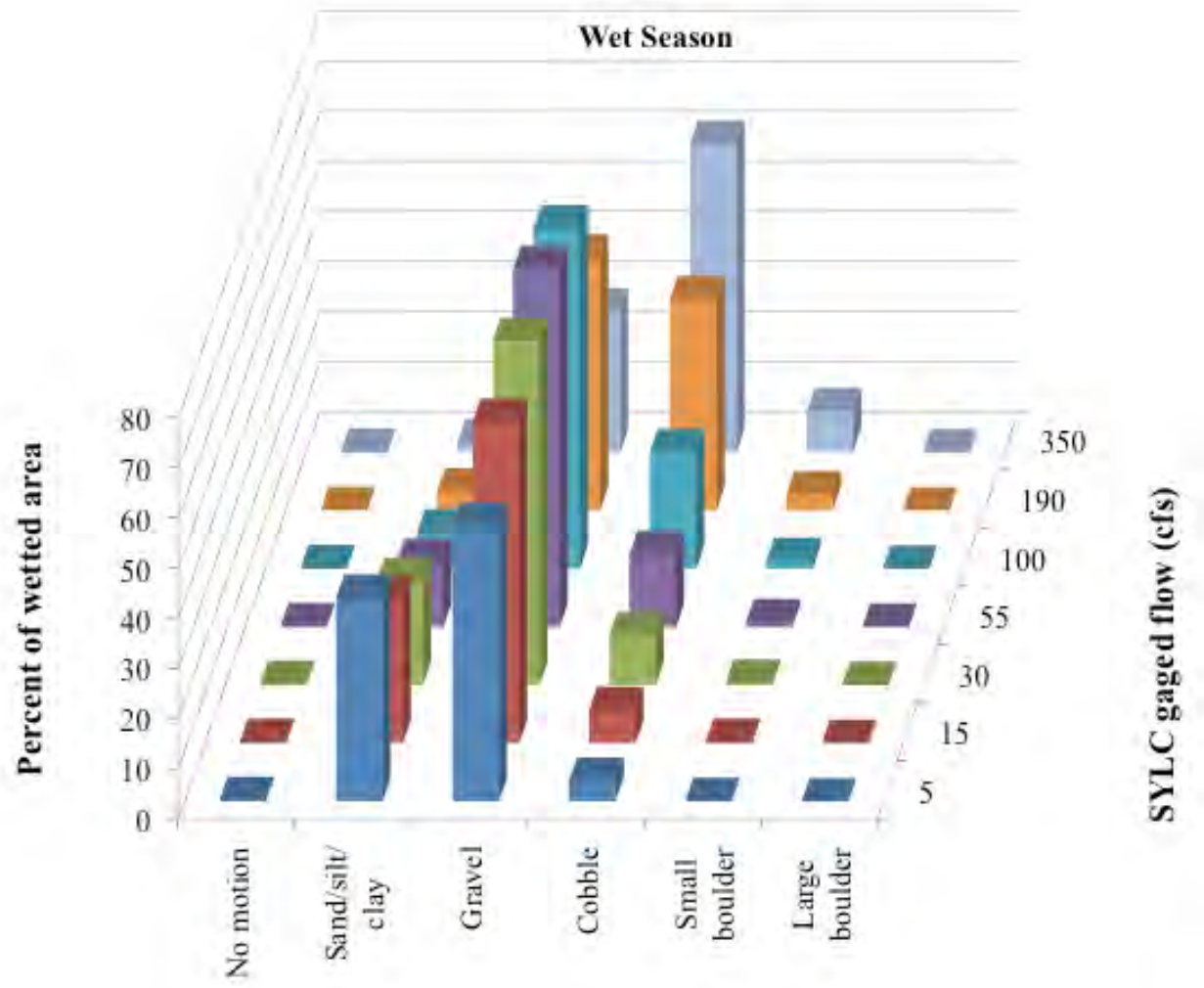

Figure 94. Flow-dependent percent of the wetted study segment with a sediment transport capacity to entrain the designated critical bed material size class during the wet season.

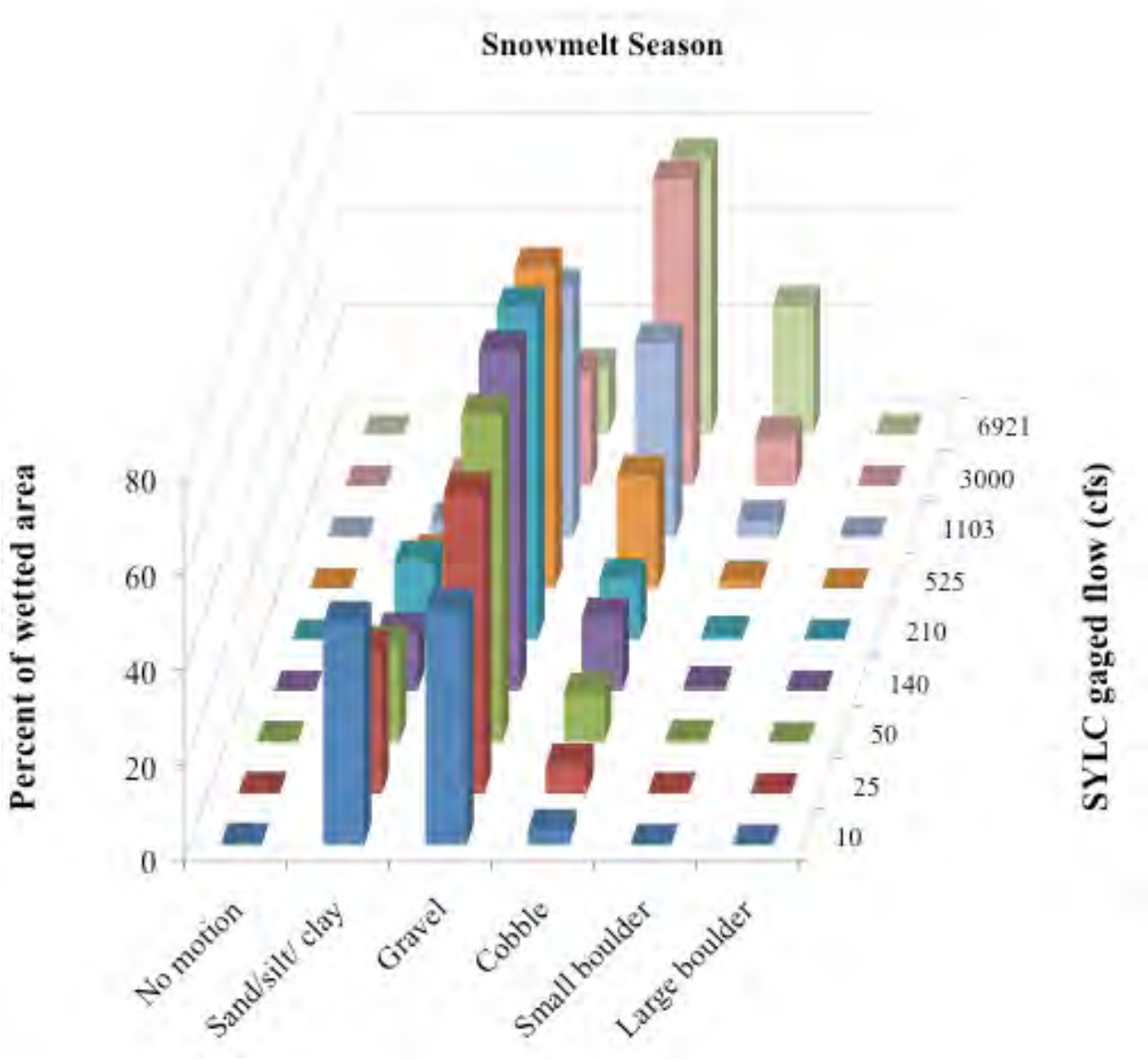

Figure 95. Flow-dependent percent of the wetted study segment with a sediment transport capacity to entrain the designated critical bed material size class during the snowmelt season.

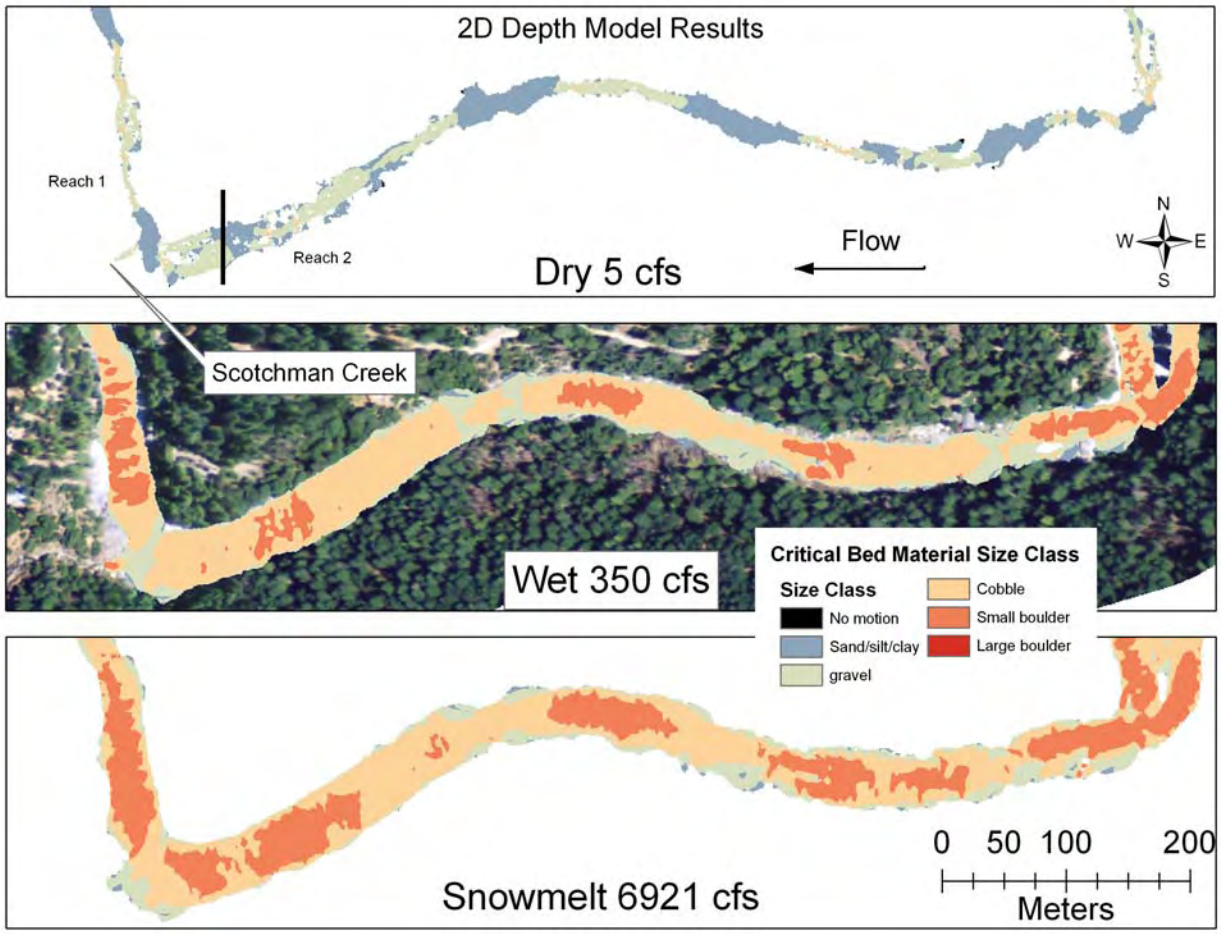

Figure 96. Season- and flow- dependent sediment transport capacity in the lower part of Reach 2.

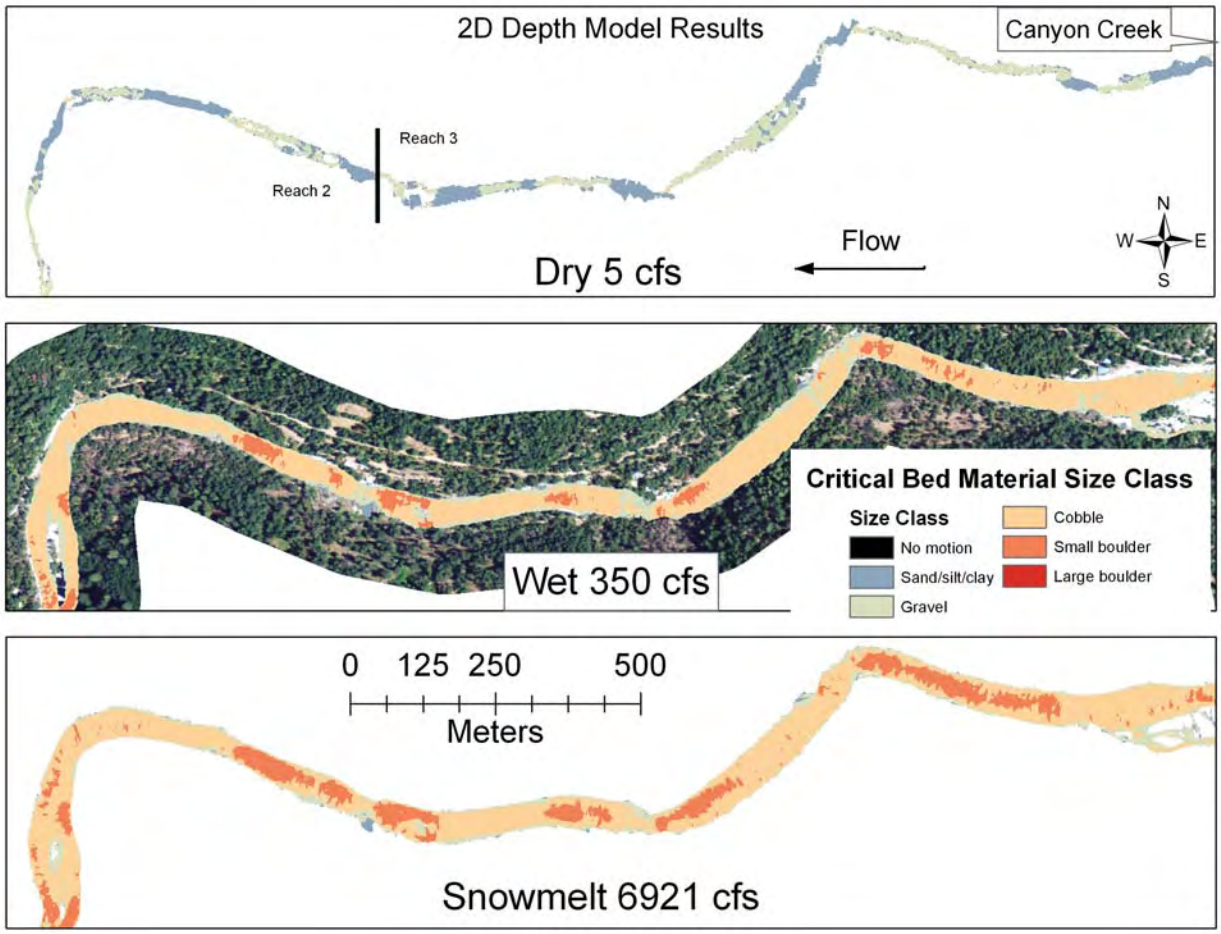

Figure 97. Season- and flow- dependent sediment transport capacity in the lower part of Reach 3.

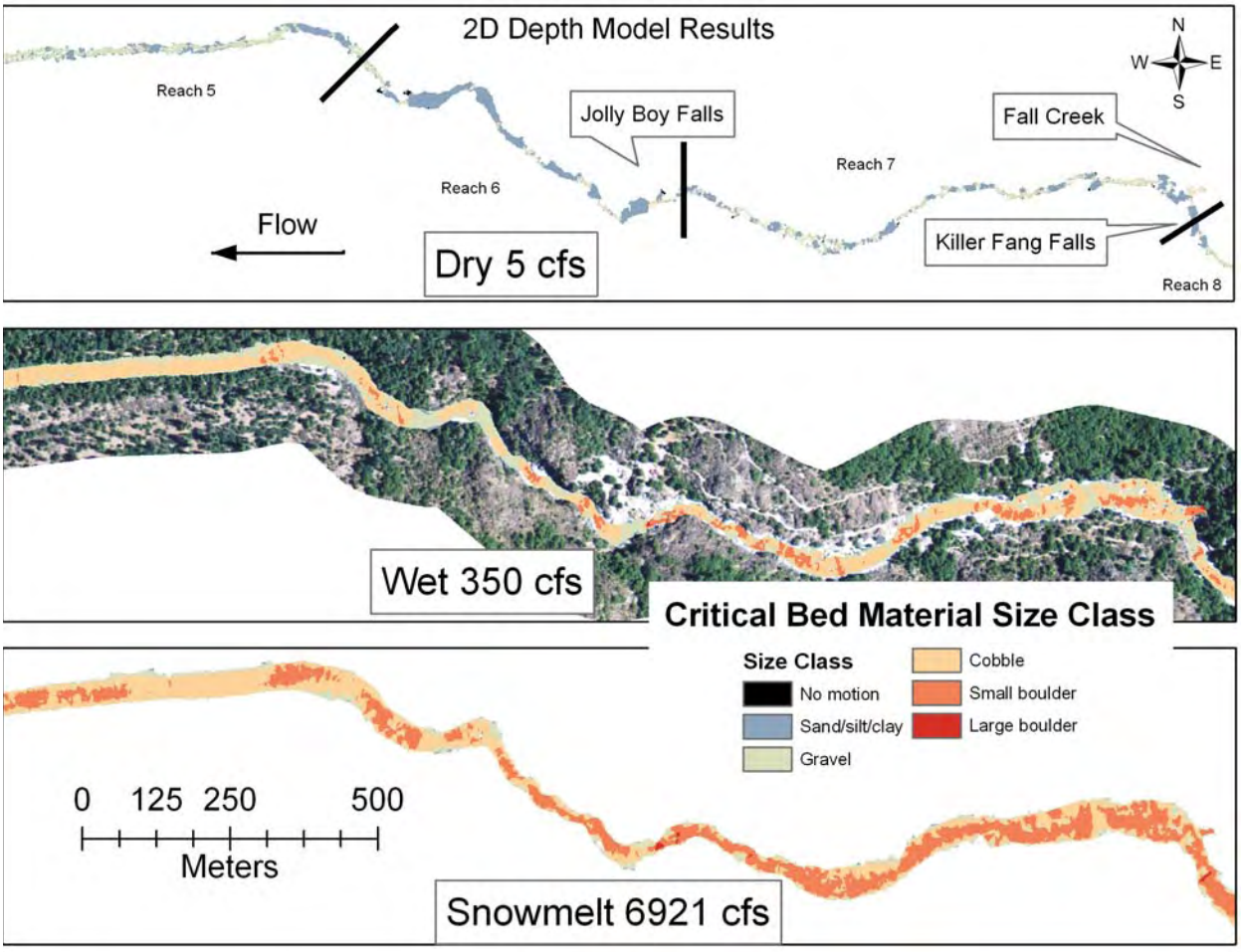

Figure 98. Season- and flow- dependent sediment transport capacity in Reaches 6 and 7.

9.3.2 Flow-Dependent Shields Stress for the Gravel Fraction

The Shields stress metric was used to determine whether any flows in the modeled ranges across each season were competent enough to redistribute gravel/cobble substrate used for rainbow trout spawning. During the dry season, transport of gravel/cobble was primarily rare to intermittent (Figure 99). During the wet season, flows >100 cfs were found to have significant transport in the gravel/cobble substrate fraction, while flows >190 cfs had predominantly full transport and channel altering conditions (Figure 100). The 350 cfs flow was predominantly channel altering across ~50% of channel area for gravel/cobble substrate, which corresponds to the percentages of gravel and cobble competence seen in Figure 94. During the snowmelt regime, flows >525 cfs were found to have significant transport, flows >1103 cfs had predominantly full transport and channel altering conditions, and flows >3000 cfs were predominantly channel altering (Figure 101). These results confirm that spawning substrates are redistributed and rejuvenated at much lower flows than those necessary to re-structure the channel's boulder framework. The landform response is that steep and fast-flowing units such as steep inset channel, inset channel, and chute have little gravel/cobble on their surface year-round. Meanwhile, the units of inset channel, plane bed, and transition have gravel/cobble on

their surfaces, but these materials have to be renewed with fresh supplies on the falling limb of the snowmelt season or else high flows would remove them permanently.

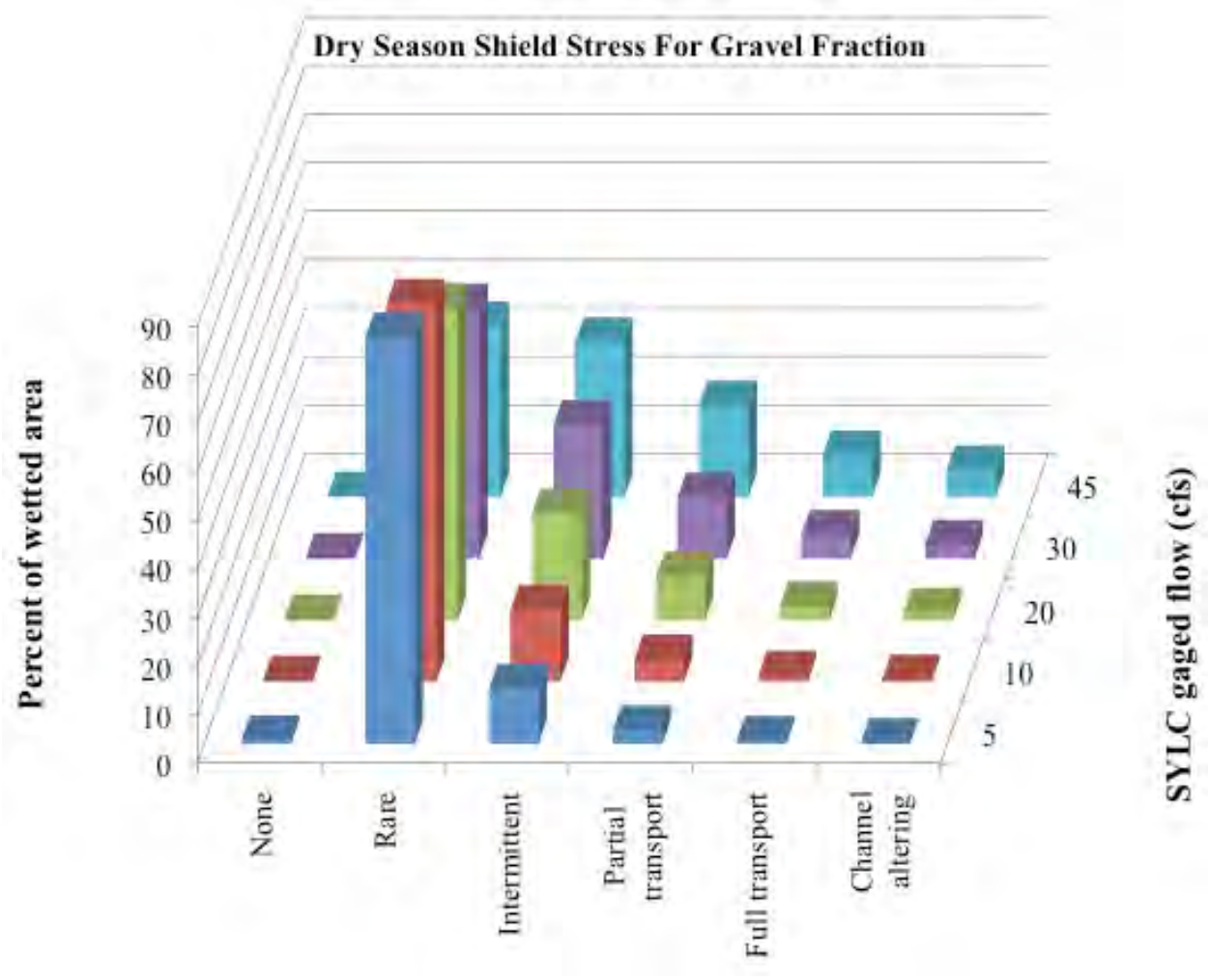

Figure 99. Flow-dependent percent of the wetted study segment with each gravel-fraction sediment transport regime during the dry season.

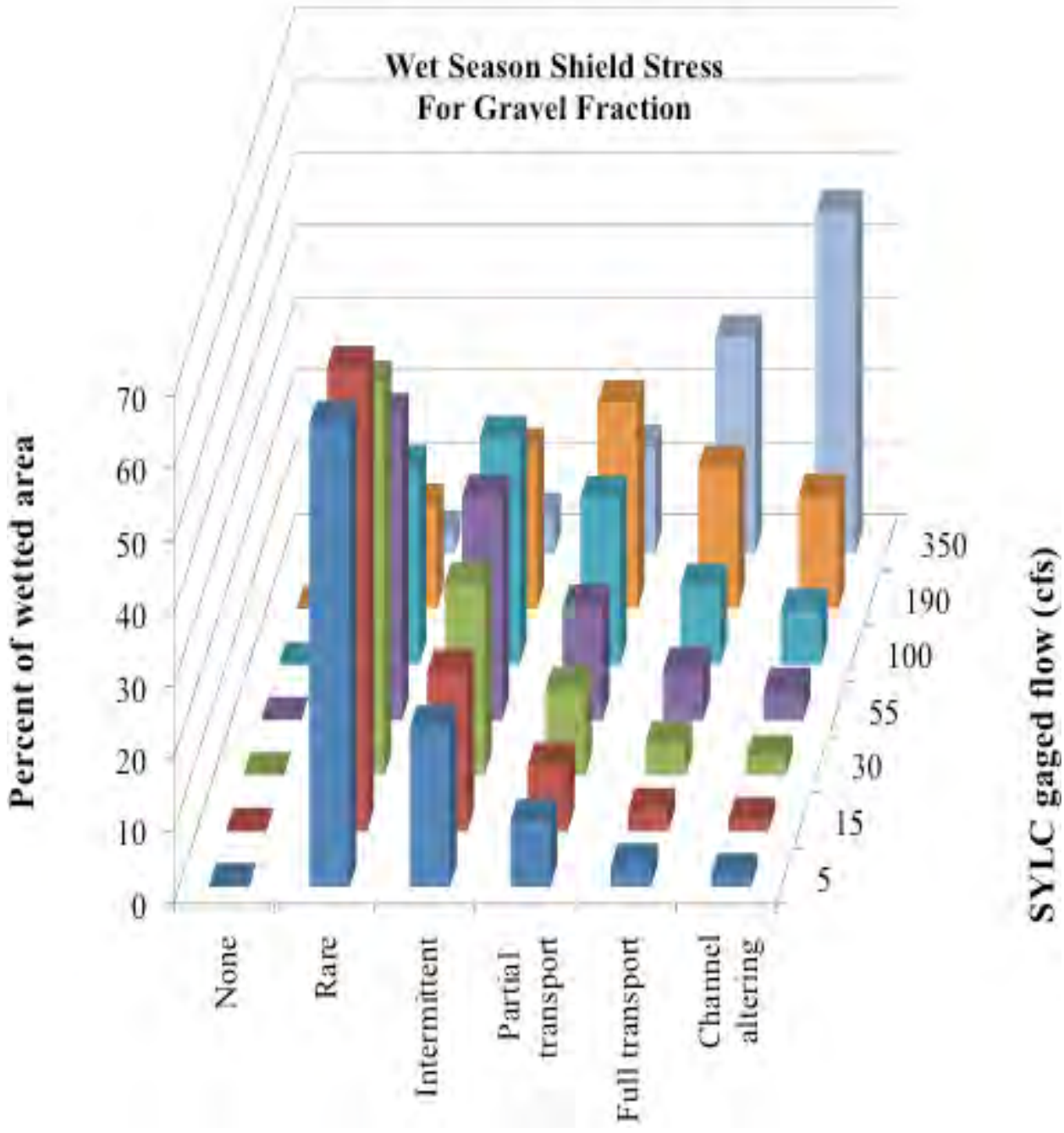

Figure 100. Flow-dependent percent of the wetted study segment with each gravel-fraction sediment transport regime during the wet season.

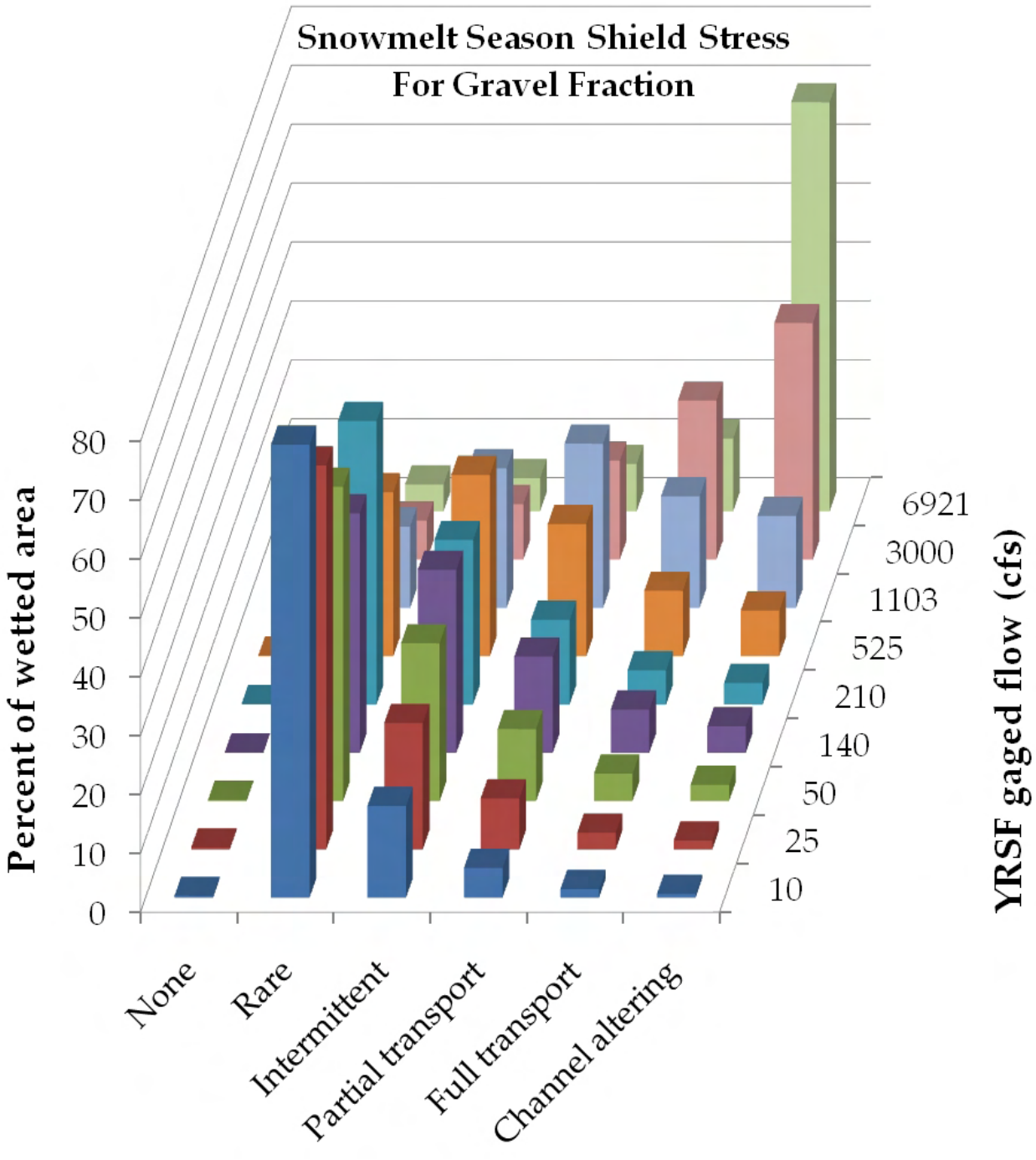

Figure 101. Flow-dependent percent of the wetted study segment with each gravel-fraction sediment transport regime during the snowmelt season.

CHAPTER 10:
Hydraulic Method Comparisons

10.1 1D Versus 2D Numerical Model Comparison

The 1D numerical model output consisted of cross-sectionally averaged water depth, velocity, and WSE predictions at 105 cross-sections for 21 discharge simulations. The morphological unit represented by each cross-section was also noted. To obtain a comparable dataset from the 2D model results, the following steps were taken. Along each of the 105 cross-sections, a point shapefile was created with points distributed in 0.5-m intervals across the channel for a distance beyond the maximum wetted width of the study segment. For each discharge, cross-section points were trimmed to the wetted width of that flow and then 2D model hydraulic outputs were interpolated to those points, using the Feature to 3D function in ArcGIS 3D Analyst, from the ~1-m resolution TIN previously made for each 2D model output variable. Then, the average and standard deviation of 2D model results at 0.5-m spacing along each cross-section were calculated for each hydraulic variable for each discharge. This was the same approach as used by Brown and Pasternack (2008).

10.1.1 Comparison of 105 Test Cross-Section Results Versus 2D Results

The most direct test of the differences between the 1D and 2D numerical models involved a comparison of predicted cross-sectionally averaged depths and velocities at the 105 cross-sections for all 21 discharges (105 x 21 = 2,205 points for comparison). The key result was that the 1D model yielded significantly higher depths and velocities than the 2D model (55% and 81% on average, respectively). The correlation between 1D and 2D model results was stronger for depth than velocity (Figure 102), but the slope of the regression relation was closer to 1.0 for velocity than depth. The 1D model tended to over-predict depth.

Given that a significant difference between 1D and 2D model results was found, the next step was to determine what explained that variation and whether that indicated a problem with the performance of one or both of the models. Factors that might contribute to performance issues are the geomorphic attributes used in the models to control flow, which include factors such as discharge, bed roughness, cross-sectional area, slope, and hydraulic controls not represented by the cross-sections. Both discharge and bed roughness were specified identically in the two models, so those are unlikely to explain the differences. However, it is theoretically plausible that the 1D model needs to be calibrated with a different bed roughness from the 2D model to yield optimal results, so that bears further consideration. Running the 1D model with a higher Manning's roughness would increase depth and decrease velocity, whereas using a lower value would do the opposite. No matter how Manning's roughness is adjusted, there is an inverse consequence between depth and velocity. What the model comparison found was that 1D depth and velocity results were ***both*** higher than 2D results. Therefore, an adjustment to Mannings roughness would not resolve the difference.

In terms of cross-sectional area, it is unlikely that much difference exists between the models to explain the results. The channel was sampled with a 0.5-m interval to calculate the area at each cross-section in the 1D model. Wetted widths ranged from ~10–50 m, so that yielded ~20–100 points for each cross-section to calculate area. A minimum of 20 points per cross-section is a reasonable number for estimating area.

That leaves the factors of slope and hydraulic controls not represented by the cross-sections. These are likely the ones that explain the differences between 1D and 2D model predictions. Slope affects velocity, because the elevation change through a morphological unit drives the change of potential energy into kinetic energy, which is the gravitational mechanism underlying velocity. The shorter the distance over which an elevational change occurs, the faster the shift in potential energy to kinetic energy, so the higher the velocity. That means that any inadequacies in the representation of elevation change through a reach could yield incorrect hydraulics.

However, the effect of slope is mediated by hydraulic controls. A hydraulic control is a local channel nonuniformity (usually an expansion or constriction in width and/or depth) that causes an abrupt change in the ability of flow to move past a point on a river. For example, everywhere that there is a bump up on the bed relative to the slope-subtracted mean bed elevation, water backs up behind the bump because the bump acts like a small dam (Clifford and French, 1998; Clifford et al., 2005). In the reach-scale longitudinal profiles of summer 2009 baseflow water surface elevation (baseWSE), reaches 1, 2, 3, and 5 are flat over deep pools and then steep over subsequent inset channels and steep inset channels (Figure 48). The flat-water surface is caused by water ponding behind the bed-bump obstruction as local bed elevation increases at the downstream ends of the pools. This ponding is termed a "backwater effect". A similar effect happens when a constriction is due to a lateral obstruction, such as a bedrock outcrop on one or both banks, or an island in the middle of the river. After such a constriction, flow accelerates out of it, causing a hydraulic jet. At any discharge, backwater and jet effects play a vital role in controlling patterns of hydraulics and thus physical habitat and sediment transport regime (Pasternack et al, 2008). Consequently, any inadequacies in the representation of hydraulic controls through a reach may yield incorrect hydraulics.

An inspection of the longitudinal profile of the bed represented by the full thalweg point dataset versus the 105 cross-sections used in the 1D model reveals the likely cause of the differences in 1D versus 2D model results, which appears to be associated with slope and hydraulic controls. Figure 103 and Figure 104 show that even with 105 cross-sections in 13.52 km of thalweg length, a large number of hydraulic controls associated with bed and width undulations are not represented in the 1D model. Absent an accurate representation of bed undulations, the slopes used to calculate 1D hydraulics between cross-sections were inappropriate for the majority of the thalweg length for which they are used.

The challenge in setting up a 1D numerical model for a remote mountain stream is that it is very difficult to identify all of the relevant hydraulic controls a priori, and then it is expensive to survey so many additional cross-sections. The more accurate a model one would desire to have, the smaller the scale of hydraulic controls that would have to be represented. In a visual reconnaissance of mountain stream, one can roughly locate riffles and pools, but it is much more time-consuming and difficult to locate accurate crest, trough, constriction, and expansion cross-sections. Even then, none of the sub-width hydraulic controls, such as boulders, boulder clusters, and streamwood can be dealt with effectively in a 1D numerical model. When 1D models are made for project sites at the geomorphic-unit scale (10^0–10^1 W, Chapter 0), there are usually 10–20 cross-sections for one site, which is adequate to cover physical processes at that scale. When 1D models are made for long river segments, the number of cross-sections used only goes up by a factor of 2–3 (e.g. URS Corporation, 2004; Gibson et al., 2010). As a result, in common professional use of 1D numerical models, upscaling is associated with a significant loss of resolution and hydraulic-prediction accuracy. Although it is theoretically plausible to

construct a 1D numerical model with cross-sections at all of the hydraulic controls, the practical outcome is that the commitment to the effort of mapping would be just as costly as going out and mapping the river with sufficient detail to run a 2D model. The benefit of the 2D model is realized in having explicit lateral variation in hydraulics, including velocity directions that are not parallel to the banks.

In contrast to the 1D model, the 2D model used all of the thalweg points and a high density of topographic and bathymetric observations (~0.3–5 m spacing) throughout the study segment for its underlying TIN-based digital elevation model. From this foundation, the model re-sampled the native resolution of points to ~1-m spacing of the computational mesh nodes. This density of nodes is sufficient to capture hydraulic controls and slopes at the reach and morphological-unit scales. With the benefit of the new LIDAR-based boulder mapping scheme developed in this study, even local boulder-scale hydraulic controls are explicitly incorporated into the 2D model (see sections 4.9–d). Microhabitats that require point sampling and computational mesh densities of < 1x1 m^2 were not meant a focus for this study's 2D model, but they are present in the vicinity of boulders, thanks to the new method. Plots similar to Figure 103 and Figure 104 that compare the 2D model and observational longitudinal profiles were made and found to have lines that overlap so well that they are indistinguishable. Statistically, the average and maximum errors between 2D model and observed thalweg point bed elevations were 0.004% and 0.27%, respectively. These are extremely low and acceptable errors, and serve as validation that interpolation of the DEM to the 2D model computational mesh was robust.

Based on the above discussion of hydrogeomorphological factors underlying the 1D and 2D numerical models, the difference in predictions between the two models appears to be attributable to inadequate slope and hydraulic control identification in the 1D numerical model. An argument can be made that careful selection of more cross-sections at identified hydraulic controls would mitigate this issue and produce better 1D results. Another argument might be made that the 105 cross-sections used in the 1D model in this study were arbitrarily selected rather than carefully selected based on field-knowledge of hydraulic controls (Chapter 7.0). The extent to which careful selection of the number and location of cross-sections at hydraulic controls is the current practice for instream flow assessments in mountain streams is unclear, but an assessment of the literature on 1D numerical models in river science and management shows little practice for siting cross-sections at hydraulic controls. In the remote Sierra region, many assessments use a transect-based approach to cope with limited accessibility to long sections of rough terrain and private property (Payne et al. 2004; Williams 2010), not a 1D numerical model approach. If a 1D numerical study purports to capture hydraulic controls, then an explanation of the types of controls and their representative spatial scale should be stated, as hydraulic controls exist over a continuum of scales. The challenge with knowing whether a representation is accurate is that one has to have an independently collected, higher-resolution sampling to compare the 1D model's sampling against. This study has that sampling, but none of the 1D numerical modeling studies reviewed for this report presented evidence demonstrating whether they accounted for hydraulic controls, and if so how. Thus, even though a 1D numerical model could be better designed for instream flow assessment, more effort is needed on the part of 1D model studies to show that such improvement is achieved.

The selection process for the 105 cross-sections for this study was similar to an in-field selection process that might occur for an instream flow assessment study. A sub-sample of 30 cross-

sections were obtained from the transect-based sampling scheme (Figure 62), and was based on field experience of the study segment (although not selected in the field). These cross-sections were located in the lower half of the study segment in accessible locations where it might be likely that a 1D model study would select cross-sections (Figure 62). The remaining 74 cross-sections were selected in the upper reaches where less accessibility might constrain field-based selection and were based on approximately equal spacing. Figure 103 and Figure 104 show that some of the 105 cross-sections do adequately represent hydraulic controls, but it also shows that even more hydraulic controls are not adequately represented. The results of this analysis suggest that hydraulic controls would be missed at a higher frequency as the number of cross-sections decrease. In this study, morphologic units represent hydraulic controls at the geomorphic-unit scale. Hydraulic variability is shown in the range of represented units, with a low of 12 chute cross-sections and a high of 27 steep inset channel cross-sections. Cross-sections were not selected at any steps as no model has the ability to adequately represent drops of >2-m from brink to WSE. Even within morphologic units, there is variation in depth and velocity (Figure 52), so the question of where to position a particular cross-section within a morphologic unit could be investigated further. Some amount of constriction and expansion is inherent in the morphologic units based on the binning method used to delineate these units, but further analysis of variation between observed width controls versus cross-section widths could yield even more understanding of the differences between ~1-m spacing and widely spaced cross-sectional representation of a river.

An additional consideration of the efficacy between 1D and 2D models centers around the question of how to obtain dense topographic measurements to thoroughly represent mountain river topography at the detail needed for the most robust results, as systematically discussed here. The manpower effort to collect 13.52 km of topographic data involved more than four months of work by a team of four people, which may not be feasible for a typical instream flow assessment project. It could be argued, however, that the number of hours of field work, analysis, and report writing were within the magnitude of effort that might be allocated to a project with similar goals by other organizations. Further, the cost involved may also be within range of that spent by others. Nevertheless, it is probable that the number of hours used for this project was higher than would be needed by a professional organization, as the number of experienced resources were fewer at the university level, but on the other hand, new methodologies and insights were obtained here at what might be a fraction of the cost associated with developing such a protocol in other public or private sectors. The differences between 1D and 2D models as discussed here suggest that a 2D-based approach using a dense topographic sampling scheme and performing in-depth geomorphic analyses as an integral component of modeling large river sections can provide detailed and robust results for scientists and resource managers.

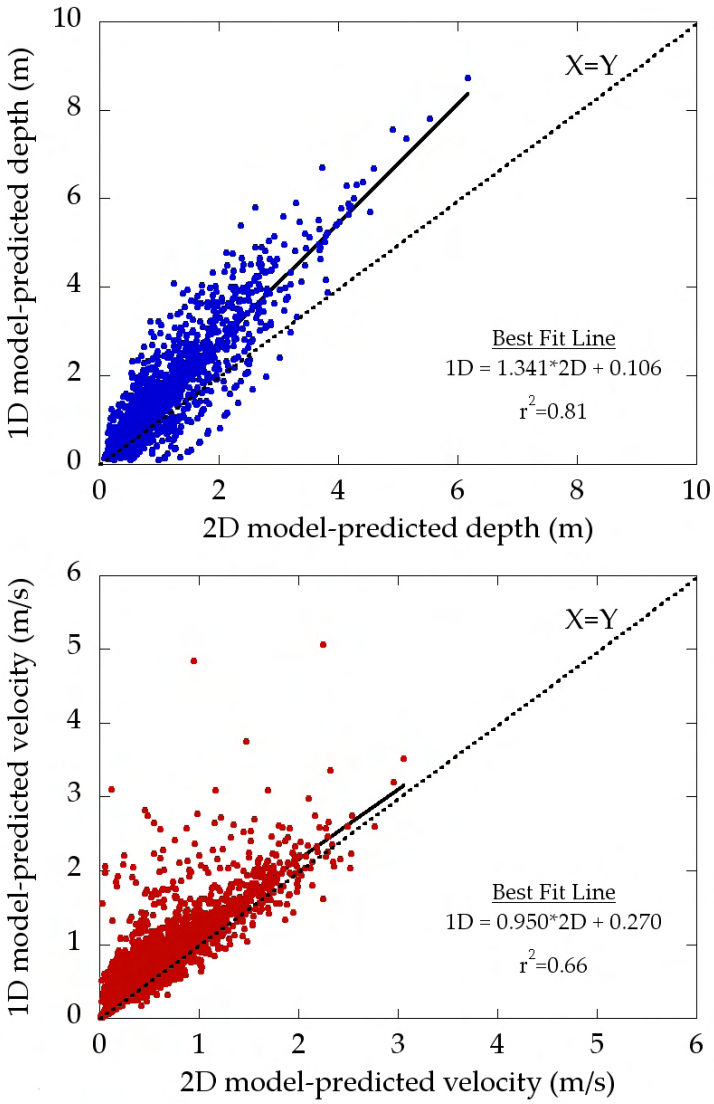

Figure 102. Direct comparison of 1D and 2D numerical model results at 105 cross-sections using all data points from 21 different simulations.

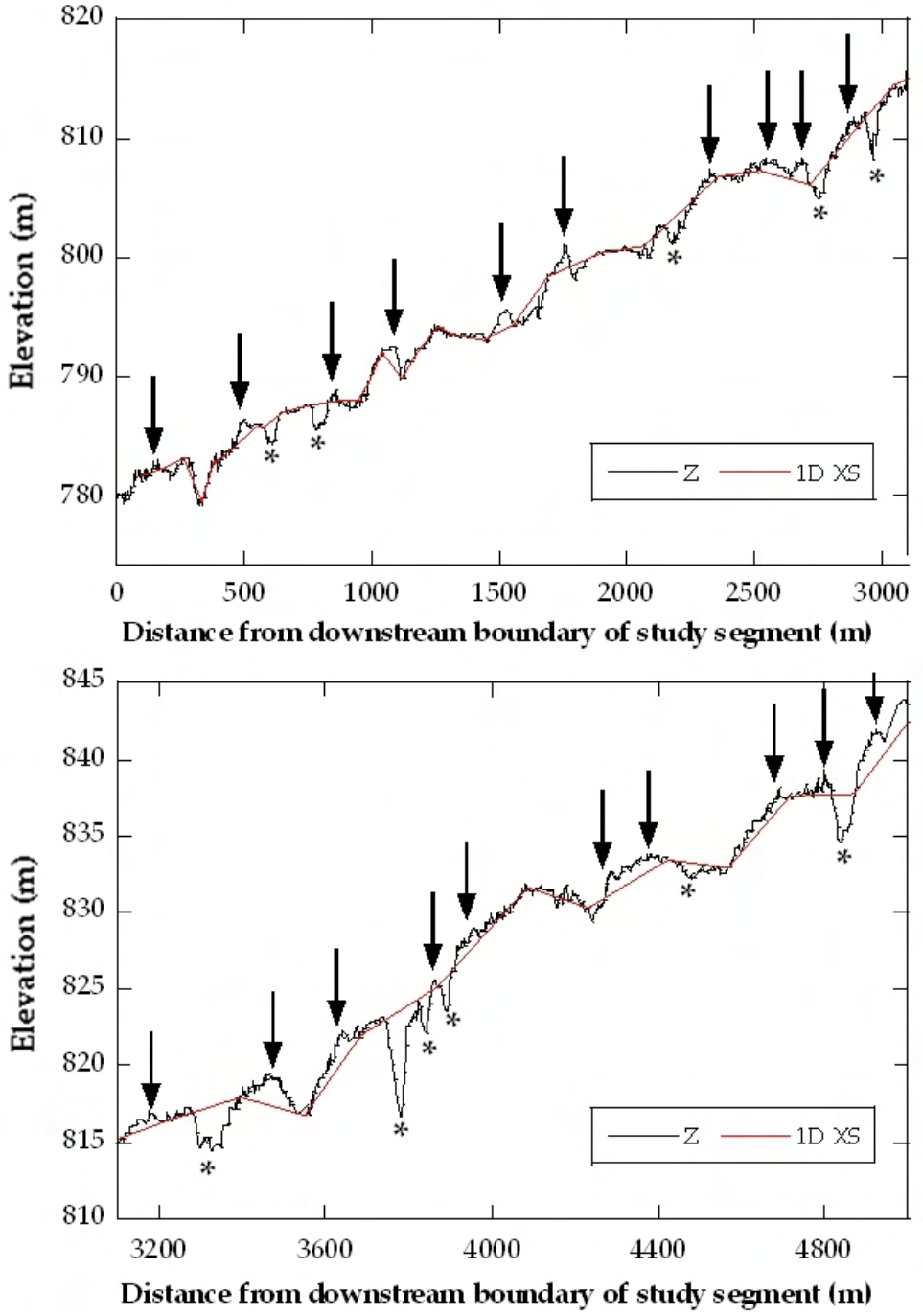

Figure 103. Reach-scale longitudinal profiles for the lower 5 km of the study segment, comparing observed elevations against elevations associated with the 105 cross-sections. It is evident that the cross-sections inadequately estimate slope and do not capture the full range of hydraulic controls. Missed crests and pools are denoted with arrows and asterisk, respectively.

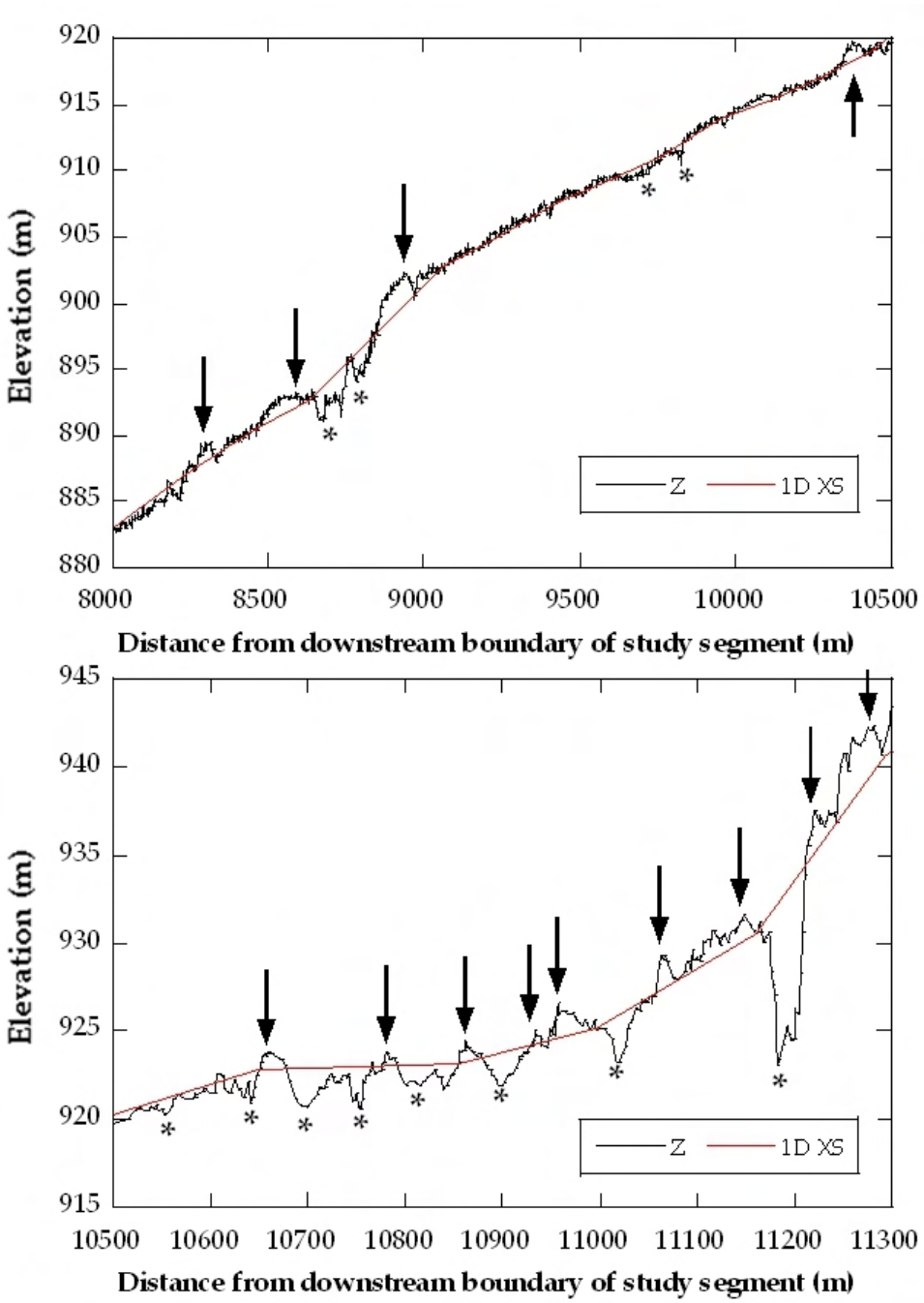

Figure 104. Reach-scale longitudinal profiles for the upper 8 to 11.3 km of the study segment, comparing observed elevations against elevations associated with the 105 cross-sections. 1D cross-sections are more adequate when no pools are present. Missed crests and pools are denoted with arrows and asterisk, respectively.

10.1.2 1D Model Results and Comparison to 2D Model Results by Morphological Unit

The 1D numerical model results exhibited variances in depth and velocity results compared to the 2D model results even though a large number of cross-sections were used (section 10.1.1).

Another analysis involved stratifying and averaging cross-section results by morphological unit. This test was used to investigate whether better 1D model performance might be found at the morphological-unit scale compared to the segment-scale results that used data from each 0.5 m point in each cross-section with no regard to morphological unit type. To address this possibility, the same morphological-unit hydraulic analyses presented in section 9.2 with 2D model results were performed with the 1D model results. The morphological-unit average and standard deviations for depths and velocities for the 1D model (

Table 38) show the range of values, which are illustrated graphically by flow for each hydrologic season regime (see Chapter 5.0 for hydrologic season details) in Figure 105-Figure 107. The comparative 2D model result velocity and depth table and plots are located in section 9.2.1 (Table 36, Figure 88-Figure 90). Differences between model results, divided by 2D results and multiplied by 100 to arrive at percent, are shown in

Table 39.

1D Model Dry Season Plots of Velocity and Depth Results

Plotted dry season average velocities increase mostly linearly, with chutes showing highest rate of increase between discharge at SYLC of 5–45 cfs, and plane beds showing lowest rate of increase (Figure 105). Standard deviations in velocity show a markedly different pattern, with large variations in steep inset channel velocities at lowest flows, which narrow rapidly as discharge increases. This suggests that flows may quickly fill-in the steep inset channels as discharge increases, smoothing variations. Transitions show unexplained fluctuations. Deviations increase for pools and chutes as discharge increases, whereas decreases are seen for plane bed and steep inset channels, and inset channel variations remain fairly static.

Pools and chutes have the highest average depths, which may be why velocity standard deviations are high as the variation in velocities could be greater within a larger water column. Conversely, plane bed, inset channel, and steep inset channels are the shallowest units, and they also have the least variation in depth as shown in the standard deviation plot. All units increase at an approximately equal rate in depth. Transition depths increase less rapidly than in all other units, and also show the least amount of standard deviation increase as discharge increases.

1D Model Wet Season Plots of Velocity and Depth Results

Wet season average velocity increases are best fit by power functions, with all units increasing as discharge at SYLC increases (Figure 106). Transitions have the most unusual pattern, with a drop-off in average velocity and a sharp increase in standard deviation between 190 cfs and 350 cfs. Pools shows the highest rate of increase in velocity and also have a higher standard deviation than units other than transitions after 100 cfs. Chutes have the highest velocities but taper off in terms of standard deviation increases as discharge increases. Depths increase at approximately equal rates in all units. Standard deviations also increase, with inset channel rate dropping slightly as discharge increases and transitions increasing at a faster rate than the other units.

1D Model Snowmelt Season Plots of Velocity and Depth Results

Recall that snowmelt season exhibits threshold behavior based on climate conditions and subsequent snowmelt patterns, thus three accretion equations were used in the 2D model simulations based on SYLC discharge (Chapter 5.0; equations in section 5.4).

All units show increases in average velocity as discharge increases, except for the anticipated dip at 210 cfs, which are also evident in the 2D model results (Figure 107). As discharge increases to the maximum-modeled YRSL discharge of 6921 cfs, velocities in all units converge. This convergence may be an indicator of the flow convergence mechanism (section 8.9.1, Chapter 9.0). Transitions have an unexplained jump in velocity standard deviation, in this case at a low SYLC discharge of 25 cfs. Pool velocity standard deviation has a high rate of increase, suggesting that velocity results vary widely at the 1D modeled pool cross-sections.

Depths increase as discharge increases, again with a dip at 210 cfs. Pool depths are greatest among all units, while pool depth standard deviation remains fairly even at all discharges. All other units show increases in standard deviations.

Differences Between 2D and 1D Velocity and Depth Model Results

Table 39 summarizes percent differences between 1D and 2D numerical models for key metrics stratified by morphological unit, including the average of all flow metrics and two representative flows. The lowest and highest SYLC discharges were selected because they represent the limits of both sets of model runs. The differences using morphological-unit averages do not have to show the same pattern of error found for the direct cross-sectional comparison reported in the previous section, because in this analysis the 2D model estimates of morphological-unit-scale metrics include results from all points within a unit, not just those at the 1D model's 105 cross-sections. The 1D model morphological-unit stratified results (Figure 105-Figure 107) show significant differences from those reported for the 2D model in section 9.2.1 (Figure 88-Figure 90).

Transitions, which exhibited fluctuations unlike any other units, deviate from the overall average depth 2D model results by -15.5%, whereas for velocity the overage average deviation from 2D results is a positive 50.5%. These values establish the overall negative and positive limits, respectively, for all units. This pattern of the most negative value holds for average depths at both the lowest discharge of 5 cfs and the highest discharge of 6921 cfs, but not for velocities. Chute overall average depths from the 1D model results deviate just -1.0% from 2D results, the best overall performance for 1D model depth results stratified by morphologic unit. Dry 5 cfs average depths show the highest variation of each unit, while snowmelt 6921 cfs show that variations diminish between 1D and 2D model results as discharge increases. Transition, pool, and chute 1D depths are under-predicted compared to 2D depths, while plane bed, inset channel, and steep inset channel depth are over-predicted. This result indicates that a smoothing function occurs in the 1D model across all units, with shallow units given more depth while deep units become shallower.

Most morphologic units over-predict the overall average velocities, with the exception of inset channels and steep inset channels, which are under-predicted. At the highest SYLC discharge of 6921 cfs, the difference between 1D and 2D average velocities diminishes in transitions, plane beds, and pools. It also narrows in steep inset channels, but by a smaller margin. Steep inset channels have the fastest velocities across all flows and seasons in the 2D model (Figure 88-Figure 90), but that does not hold for the 1D model where chute velocities vie with steep inset channels for greatest velocities (Figure 105-Figure 107). Transition, plane bed, and pool 1D model velocity results for dry 5 cfs flows have very large variances from 2D model results, with the average over-prediction for each greater than 400%. These morphologic units have the lowest velocities overall. This observation suggests that low flow 1D model simulations do not perform well when compared to 2D model results at the same flow. On the other hand, average velocity results from 1D model snowmelt 6921 cfs results are all within 22% of 2D model results, so as discharge increases, 1D model results converge toward 2D model results.

The 1D model depth and velocity results converge toward the 2D model results as discharge increases, as seen in the lower percent differences between 2D and 1D results at 6921 cfs (

Table 39). The difference between 2D and 1D model results is worst at the lowest discharge, because that is the condition under which the topographic controls that were missed in the 1D model have the greatest influence (Figure 103, Figure 104). The 1D model over-predicted 64% of the morphological-unit stratified metrics shown in the table; 61% of depths are over-predicted (11 of 18), whereas 67% of velocities were over-predicted. The absolute average variance of averages of all morphological units for the 6921 cfs flow was 11.3% for depth and 10.6% for velocity. The absolute average variance of averages of all morphological units for the 5 cfs flow was 45.1% for depth and 274.5% for velocity.

Table 38. 1D model results stratified by morphological unit for each flow and per hydrological regime. Discharge is YRSF gaged input.

Average Depth (m)

Season	cfs	Transition	Plane Bed	Pool	Inset Channel	Chute	Steep Inset Channel
Dry	5	0.46	0.30	1.50	0.26	0.46	0.29
	10	0.57	0.39	1.63	0.35	0.61	0.40
	20	0.79	0.56	1.91	0.56	0.92	0.62
	30	0.99	0.71	2.16	0.75	1.20	0.82
	45	1.26	0.94	2.52	1.00	1.56	1.10
Wet	5	0.66	0.42	1.74	0.42	0.75	0.47
	15	0.80	0.55	1.91	0.56	0.94	0.62
	30	0.95	0.68	2.10	0.71	1.14	0.78
	55	1.21	0.88	2.45	0.94	1.50	1.03
	100	1.43	1.09	2.73	1.16	1.76	1.26
	190	1.91	1.46	3.36	1.60	2.35	1.71
	350	2.67	2.03	4.34	2.26	3.31	2.41
Snow melt	10	0.59	0.40	1.66	0.37	0.65	0.41
	25	0.78	0.56	1.89	0.55	0.90	0.60
	50	0.96	0.72	2.12	0.73	1.15	0.80
	140	1.17	0.93	2.37	0.95	1.39	1.02
	210	1.04	0.89	2.19	0.86	1.18	0.91
	525	1.42	1.25	2.66	1.23	1.61	1.29
	1103	1.89	1.66	3.23	1.66	2.13	1.72
	3000	2.70	2.43	4.30	2.45	3.09	2.54
	6921	3.77	3.39	5.61	3.47	4.32	3.57

Average Velocity (m/s)

Season	cfs	Transition	Plane Bed	Pool	Inset Channel	Chute	Steep Inset Channel
Dry	5	0.33	0.39	0.16	0.36	0.40	0.54
	10	0.42	0.40	0.19	0.44	0.48	0.59
	20	0.41	0.51	0.31	0.61	0.66	0.72
	30	0.65	0.59	0.42	0.73	0.86	0.82
	45	0.87	0.70	0.59	0.88	1.06	0.98
Wet	5	0.46	0.42	0.23	0.49	0.55	0.64
	15	0.41	0.50	0.31	0.61	0.67	0.71
	30	0.62	0.57	0.40	0.71	0.82	0.79
	55	0.82	0.66	0.55	0.84	1.04	0.94
	100	0.98	0.79	0.70	0.97	1.15	1.07
	190	1.33	0.99	1.00	1.20	1.45	1.32
	350	1.28	1.27	1.44	1.50	1.81	1.65
Snow melt	10	0.29	0.40	0.20	0.45	0.50	0.60
	25	0.59	0.50	0.30	0.60	0.65	0.72
	50	0.63	0.59	0.41	0.72	0.82	0.81
	140	0.76	0.71	0.54	0.85	0.97	0.93
	210	0.66	0.69	0.48	0.79	0.83	0.86
	525	0.88	0.89	0.72	1.00	1.07	1.07
	1103	1.12	1.12	0.99	1.23	1.34	1.33
	3000	1.61	1.52	1.52	1.63	1.76	1.74
	6921	2.13	2.00	2.13	2.08	2.17	2.16

Average Standard Deviation of Depth (m)

Season	cfs	Transition	Plane Bed	Pool	Inset Channel	Chute	Steep Inset Channel
Dry	5	0.27	0.15	1.35	0.09	0.27	0.13
	10	0.27	0.16	1.37	0.10	0.30	0.15
	20	0.28	0.18	1.39	0.13	0.37	0.19
	30	0.32	0.21	1.40	0.17	0.45	0.22
	45	0.39	0.26	1.40	0.22	0.53	0.28
Wet	5	0.28	0.18	1.40	0.13	0.33	0.18
	15	0.28	0.19	1.40	0.14	0.38	0.20
	30	0.31	0.20	1.40	0.16	0.44	0.22
	55	0.40	0.27	1.44	0.24	0.53	0.30
	100	0.42	0.29	1.39	0.23	0.58	0.30
	190	0.55	0.39	1.43	0.32	0.67	0.42
	350	0.77	0.60	1.58	0.47	0.81	0.64
Snow melt	10	0.27	0.17	1.38	0.11	0.31	0.16
	25	0.28	0.17	1.39	0.13	0.36	0.19
	50	0.30	0.19	1.39	0.15	0.44	0.21
	140	0.32	0.21	1.36	0.18	0.49	0.23
	210	0.27	0.19	1.33	0.19	0.45	0.22
	525	0.33	0.22	1.28	0.24	0.56	0.27
	1103	0.41	0.26	1.26	0.29	0.65	0.33
	3000	0.53	0.35	1.27	0.37	0.79	0.46
	6921	0.66	0.50	1.37	0.45	0.95	0.59

Average Standard Deviation of Velocity (m/s)

Season	cfs	Transition	Plane Bed	Pool	Inset Channel	Chute	Steep Inset Channel
Dry	5	0.35	0.30	0.19	0.16	0.21	0.87
	10	0.46	0.20	0.21	0.15	0.22	0.47
	20	0.24	0.18	0.30	0.18	0.29	0.35
	30	0.36	0.17	0.35	0.18	0.38	0.25
	45	0.42	0.17	0.41	0.20	0.41	0.27
Wet	5	0.43	0.18	0.23	0.16	0.25	0.43
	15	0.24	0.18	0.29	0.18	0.30	0.33
	30	0.36	0.17	0.34	0.18	0.37	0.25
	55	0.39	0.18	0.33	0.21	0.42	0.26
	100	0.40	0.18	0.46	0.21	0.41	0.30
	190	0.60	0.20	0.54	0.24	0.41	0.39
	350	1.25	0.25	0.58	0.30	0.39	0.41
Snow melt	10	0.23	0.19	0.21	0.15	0.24	0.45
	25	0.67	0.19	0.30	0.17	0.28	0.40
	50	0.38	0.17	0.36	0.18	0.37	0.25
	140	0.37	0.18	0.43	0.17	0.40	0.25
	210	0.38	0.21	0.44	0.17	0.35	0.26
	525	0.38	0.24	0.58	0.18	0.39	0.28
	1103	0.36	0.25	0.61	0.20	0.37	0.35
	3000	0.41	0.27	0.74	0.24	0.36	0.40
	6921	0.47	0.32	0.94	0.30	0.39	0.46

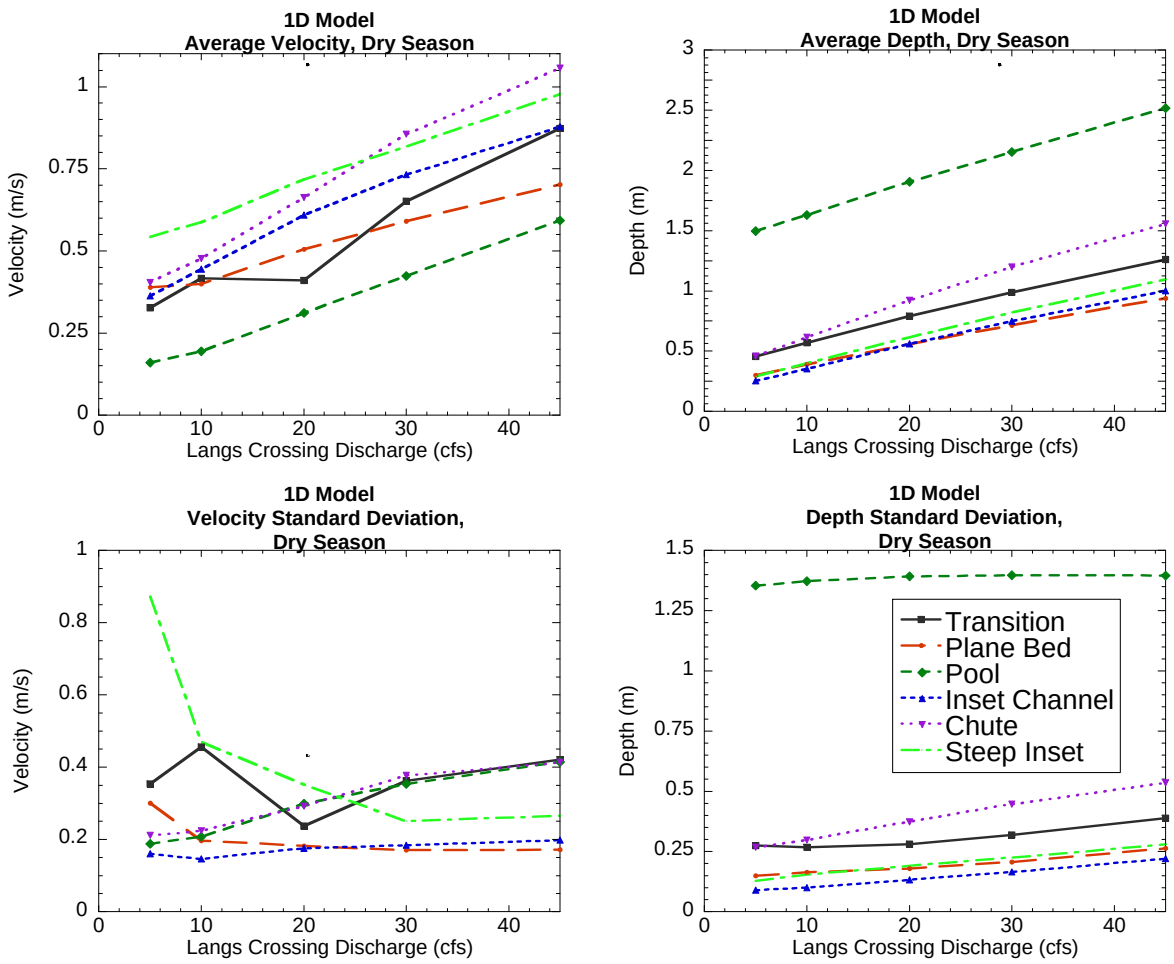

Figure 105. 1D model variation in average and standard deviation velocity and depth during dry season discharges.

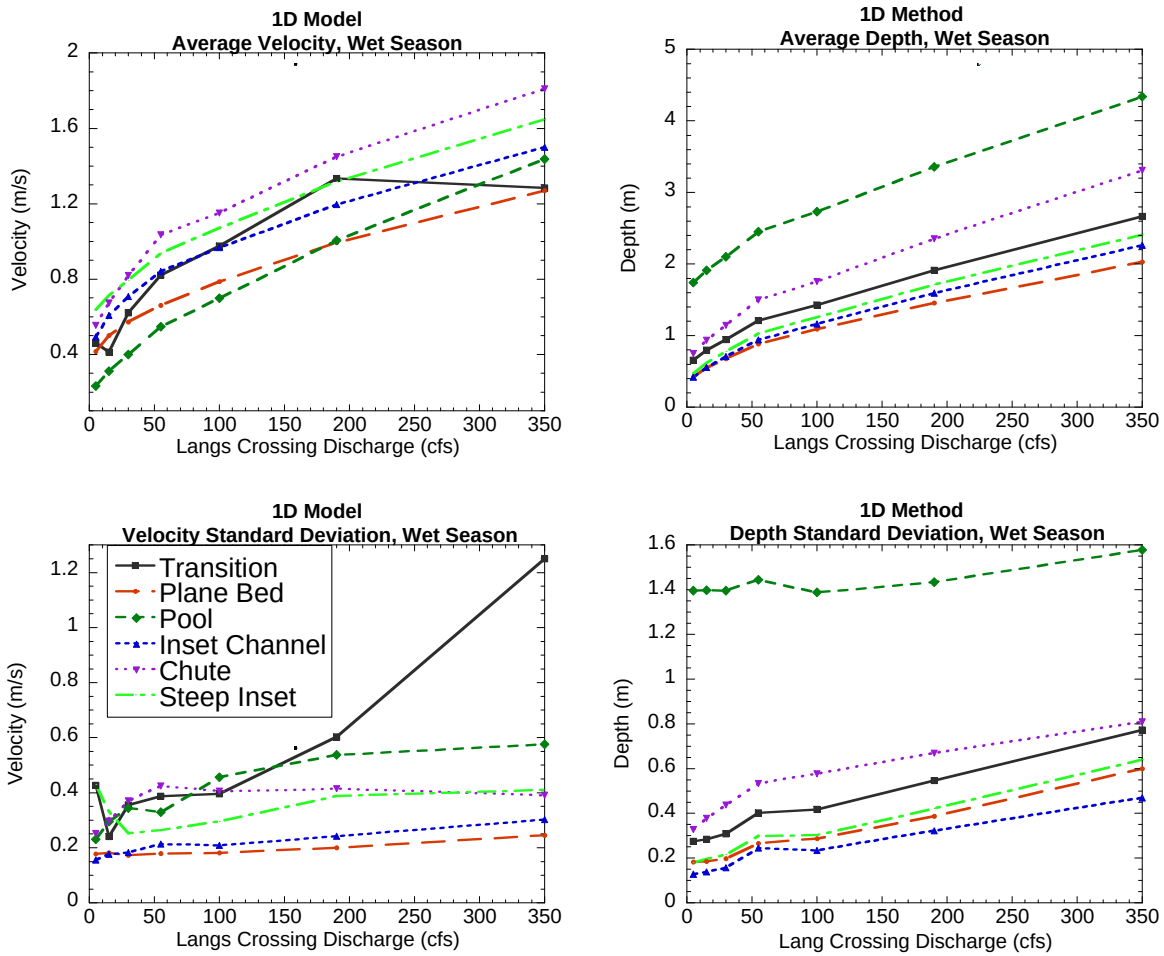

Figure 106. 1D model variation in average and standard deviation velocity and depth during wet season discharges.

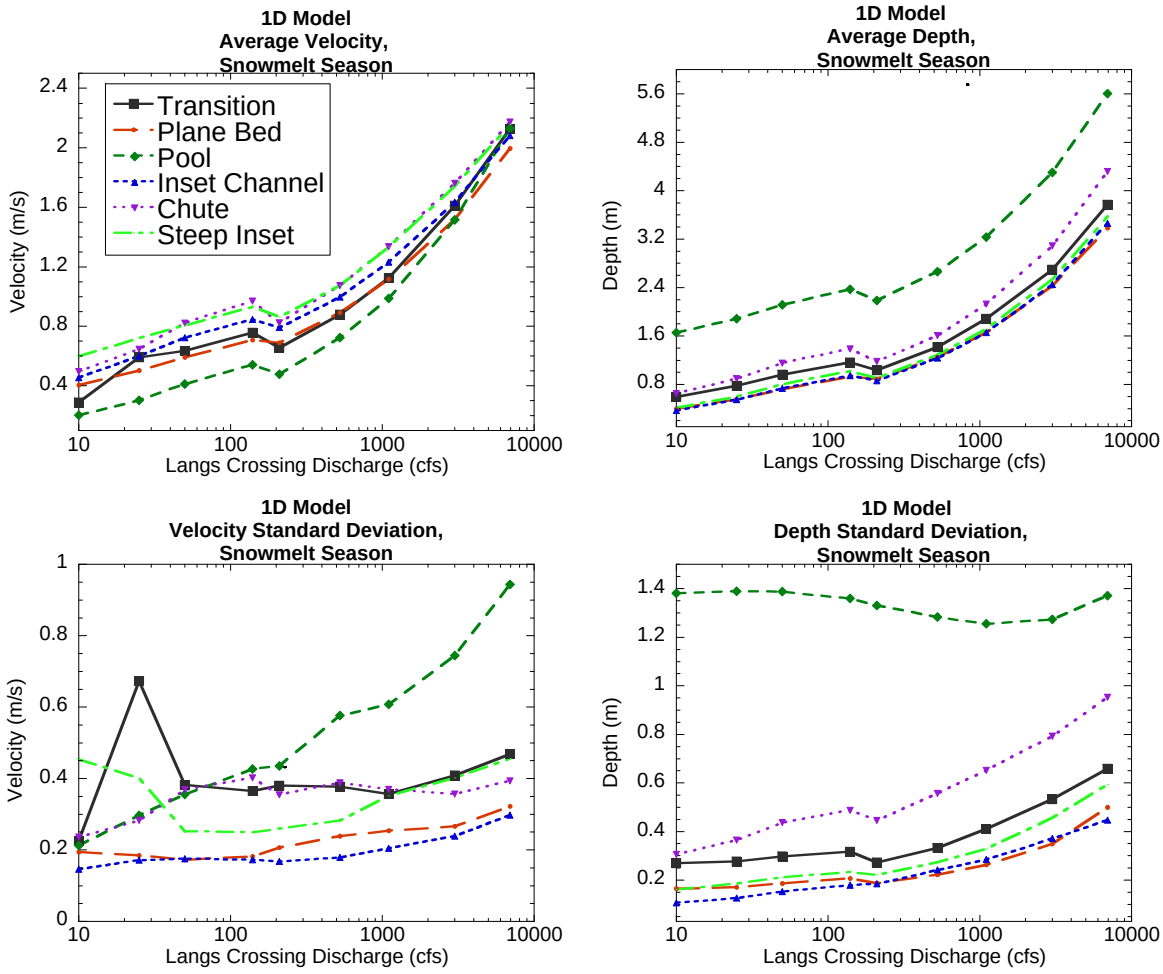

Figure 107. 1D model variation in average and standard deviation velocity and depth during snowmelt season discharges.

Table 39. Percent difference between average 1D and 2D depth and velocity model results, stratified by morphologic unit and inclusive of all seasons and discharges.

Metric	Percent difference calculated as 100*(1D - 2D)/2D					
	Transition	Plane Bed	Pool	Inset Channel	Chute	Steep Inset Channel
Depth metrics						
Average depth*	-15.5	43.8	-11.1	32.9	-1.0	32.6
6921 cfs average depth	-6.1	18.2	2.3	17.9	5.9	17.3
Dry 5 cfs average depth	-38.3	62.8	-26.0	53.7	-30.7	59.0
Velocity metrics						
Average velocity*	50.5	37.5	44.9	-3.6	2.8	-24.8
6921 cfs average velocity	0.8	-7.0	7.2	-14.8	-12.5	-21.2
Dry 5 cfs average velocity	493.6	594.7	400.2	64.9	80.5	12.8

*Calculated by taking the average of all morphological-unit average values for all seasons and all simulated discharges (n=21).

10.2 2D Transect Method versus 2D Model Analysis

The sampling scheme used in the 2D model approaches a near-census of hydraulics in the river at the ~1-m scale, yielding hundreds of thousands of wetted channel point values (exact value varies by season and discharge). As explained in sections 7.2 and 8.6, a transect-based sampling approach was employed to enable a methodological comparison between the hydraulic and habitat metrics obtain from 2D numerical modeling and transect-based sampling. By comparison to the 2D model's near-census, a dataset comprised of 30 transects with points distributed in 0.5-m intervals along each length is a small sampling (section 8.6, Figure 61, Figure 62), but it is representative of the recommended transect-based sampling procedure (Payne et al., 2004) and is double the density of transects used in reference studies (see section 7.2). The goal here was not merely to assess a final weighted usable area versus flow relationship, but to look at how the different approaches affect all of the steps of computation of an instream flow analysis, and to look at each method transparently through a scientific lens.

As discussed earlier, the transect-sampling approach involves making observations at 1-3 flows and then estimating hydraulics at other flows of interest. Two questions that arise are: (a) what is the accuracy of hydraulic estimation/prediction at the point scale between transect-based observation versus 2D modeling and (b) what is the ability of transect-based sampling to accurately represent the population of hydraulics? With regard to the first question, section 6.2 presented the results of 2D model performance, indicating that 2D models in remote mountain rivers perform similarly as those in lowland rivers—there is a strong correlation between prediction and observation, but for any given point subjected to sub-grid-scale topographic variability and turbulence, the hydraulics can deviate significantly. Transect-based analysis uses direct observations and has no predictive capability, so it is more accurate at the point scale; that is why it is commonly used for instream flow assessment. The remaining important scientific questions are therefore:

- Does a sampling of depth and velocity values at a 0.5-m spacing along 30 transects (chosen to represent channel-unit diversity according to the recommended professional

methodology) yield a similar probability distribution function as the population of hydraulic values at the segment-scale in a remote mountain river over a wide range of discharges?

- Does a sampling of depth and velocity values at a 0.5-m spacing along 30 transects (chosen to represent channel-unit diversity according to the recommended professional methodology) yield similar average and standard deviation metrics for the morphological-unit averaged depths and velocities compared to the same metrics for the whole population of depths and velocities in the river segment?

To isolate each question, two tests were designed in which the values for hydraulics were set to be the same between methods. To achieve this, the near-census of 2D-model hydraulics values was used to create TINs of depth and velocity, and then values for hydraulics at the transect sampling points were obtained from the TINs. This method holds hydraulic values fixed for the same locations, but the 2D model has the availability of vastly more points.

- The name "2D Transects" is used throughout the rest of the report and in figures and tables to describe the sampling of 2D-model hydraulics at 0.5-m intervals along the selected 30 transects.

10.2.1 Test of Transect-Based Hydraulic Sampling of Points At The Segment Scale

To test the first question, the probability density functions for the three hydraulic estimation/prediction methods were computed and compared for the lowest discharge (dry 5 cfs), a mid-discharge (dry 45 cfs that has a lot of flow accretion), and the highest discharge (snowmelt 6921 cfs) for the study. For each distribution, three key metrics (mean, standard deviation, and maximum) were also computed and compared. Overall, the transect-based sampling of the 2D model results performed reasonably well at representing the left and central regions of depth and velocity distributions, with similar distribution shapes and metrics for mean and standard deviation (

Table 40, Figure 108). However, transect-based sampling performed poorly at representing the right tail of the distributions. At the lowest flow, transect sampling overpredicted the mean depth by 29% and underpredicted the maximum depth by a factor of 2.25. As discharge increased, mean depth prediction improved, but maximum depth prediction got worse. For velocity, transect-based sampling yielded good estimates of mean and standard deviation for all flows, but performed poorly at estimating the maximum velocity, and that performance got worse as discharge increased (

Table 40). Relative to transect-based sampling, the 1D numerical model performed very poorly at representing the populations of depth and velocity in the study segment (

Table 40, Figure 108).

Table 40. Comparative metrics for the statistical distributions of segment-scale hydraulic variables for three flows. 2D=2D model results, 1D=1D model results, and T=transect-based hydraulic sampling of the 2D model results.

	Depth (m)			Velocity (m/s)		
Statistic	2D	1D	T	2D	1D	T
Dry 5 cfs						
Max	11.63	4.64	5.16	1.80	4.85	1.21
Mean	0.58	0.49	0.75	0.15	0.38	0.14
St. Dev.	0.81	0.65	0.99	0.17	0.50	0.17
Count	186095	105	916	186095	105	916
Dry 45 cfs						
Max	12.30	5.82	2.97	4.46	2.21	1.71
Mean	0.84	1.32	1.01	0.58	0.86	0.57
St. Dev.	0.82	0.77	0.93	0.39	0.34	0.37
Count	352122	105	1814	352122	105	1814
Snowmelt 6921 cfs						
Max	15.35	8.73	4.94	9.75	5.06	2.58
Mean	2.36	3.91	2.36	1.87	2.11	1.67
St. Dev.	1.34	1.04	1.41	0.77	0.50	0.64
Count	599378	105	3175	599378	105	3175

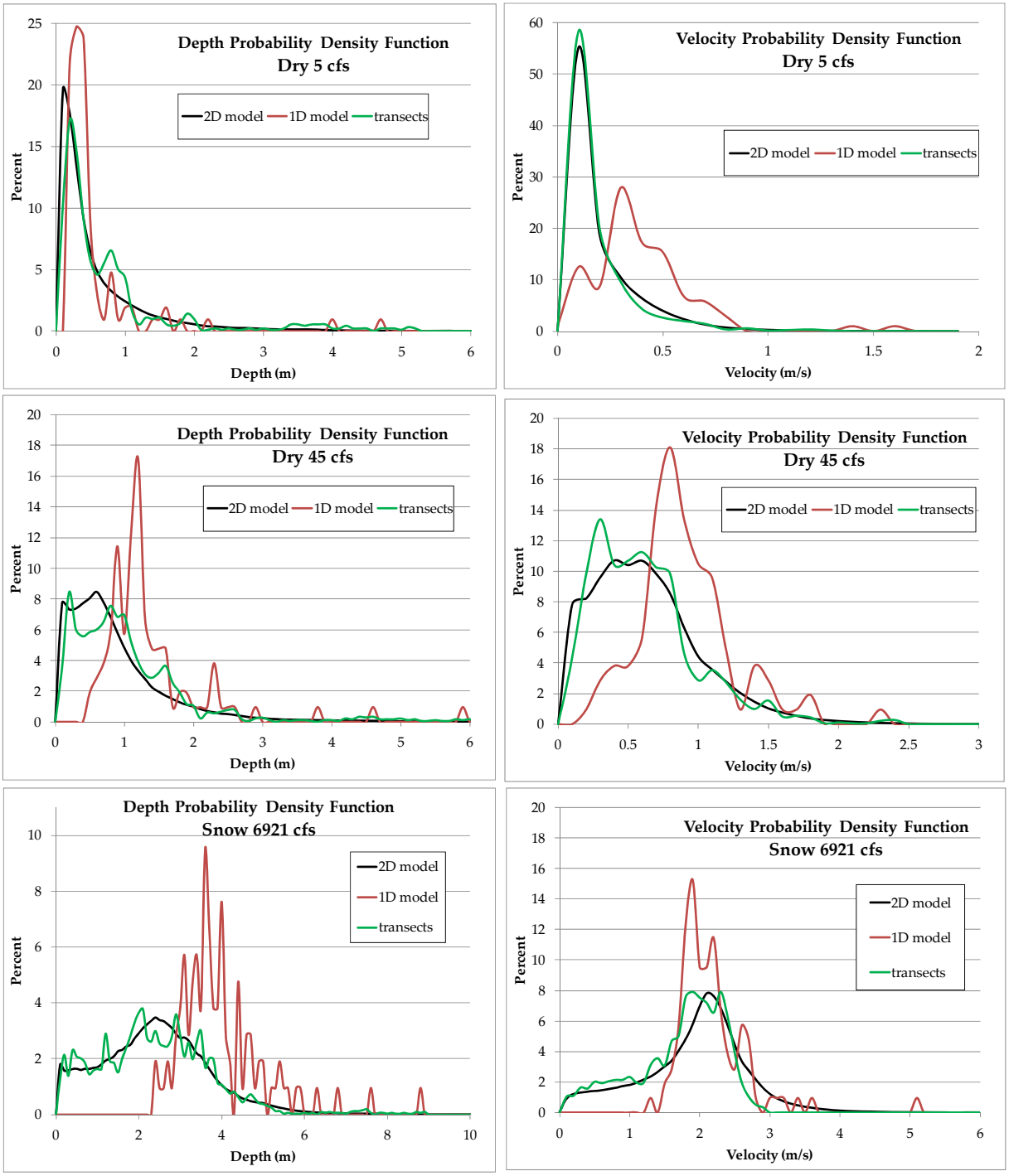

Figure 108. Probability density functions for the three different methods of computing segment-scale hydraulics for the study reach.

10.2.2 Test of Stratifying Transect Points By Morphological Unit

Transect-based sampling performed reasonably well at representing the segment-scale populations of depth and velocity. A common instream flow assessment approach involves averaging samples for a given mesohabitat (or in this study, a morphological unit) to arrive at the mesohabitat-averaged hydraulic values. In another variety of the approach, the averaging is not done until hydraulic values are extrapolated to habitat indices. Either way, a statistical averaging approach to upscaling is involved, so a test of the effects of averaging was of interest.

In this test, transect points were stratified by morphological unit and then the mean and standard deviation of the stratified subsets was computed. These were compared against the population of results from the 2D model. The results of morphological-unit averaging of depth and velocity values using transect-based sampling are illustrated in Figure 109-Figure 111 and

Table 41. The main result of the comparison is that transect sampling performed poorly at representing the population of the full 2D model results stratified by morphological unit (

Table 42). Whereas the results for 105 transects in the 1D-model over-predicted 64% of the depths and velocities in

Table 39, the 30 transects using 2D results tended to under-predict them, with 78% of metrics in the table under-predicted. The absolute average variance of the averages of all morphologic units at 6921 cfs for the transect-based approach was 33.2% for depth and 27.5% for velocity, versus 11.3% for depth and 10.6% for velocity in the 1D model results (

Table 39). At 5 cfs flows, the absolute average variance of the averages of all morphologic units for the transect-based approach was 17.2% for depth and 33.4% for velocity, versus 45.1% for depth and 274.5% for velocity in the 1D model results. 1D model predictions were closer to the 2D model results than the transect-based estimations for 53% of the table metrics, so by that measure the two methods performed almost equally. The one condition in which transects performed noticeably better than the 1D model was for velocity prediction of dry 5 cfs. Further analysis of other seasonal flow simulation results was not conducted, which may have revealed further insights into the performance differences.

Table 41. 2D Transect Method results stratified by morphological unit from all simulations for three hydrological regimes. Discharge is the YRSF gaged input.

2D Transect Method Summary Depth and Velocity Values

Average Depth (m)

Season	cfs	Transition	Plane Bed	Pool	Inset Channel	Chute	Steep Inset Channel
Dry	5	0.67	0.28	2.14	0.17	0.51	0.21
	10	0.73	0.34	2.17	0.23	0.61	0.32
	20	0.86	0.47	2.27	0.36	0.77	0.46
	30	0.98	0.59	2.42	0.46	0.90	0.45
	45	1.20	0.77	2.52	0.57	1.06	0.59
Wet	5	0.79	0.39	2.21	0.29	0.69	0.39
	15	0.87	0.47	2.26	0.36	0.78	0.45
	30	0.98	0.56	2.39	0.45	0.88	0.44
	55	1.10	0.69	2.47	0.51	0.95	0.51
	100	1.32	0.87	2.53	0.66	1.17	0.69
	190	1.69	1.17	2.76	0.93	1.40	0.98
	350	2.02	1.74	2.89	1.36	2.01	1.55
Snow melt	10	0.74	0.36	2.19	0.25	0.64	0.34
	25	0.86	0.46	2.25	0.35	0.76	0.45
	50	0.97	0.57	2.39	0.44	0.88	0.44
	140	1.11	0.69	2.48	0.51	0.96	0.51
	210	0.97	0.59	2.37	0.45	0.87	0.41
	525	1.23	0.81	2.46	0.59	1.05	0.62
	1103	1.53	1.09	2.62	0.84	1.28	0.85
	3000	2.12	1.68	2.92	1.34	1.81	1.44
	6921	2.41	2.32	3.31	1.95	2.63	2.08

Average Velocity (m/s)

Season	cfs	Transition	Plane Bed	Pool	Inset Channel	Chute	Steep Inset Channel
Dry	5	0.04	0.09	0.02	0.25	0.13	0.61
	10	0.08	0.13	0.04	0.34	0.20	0.50
	20	0.16	0.24	0.09	0.46	0.39	0.68
	30	0.25	0.34	0.16	0.55	0.55	0.60
	45	0.41	0.50	0.27	0.68	0.77	0.75
Wet	5	0.11	0.17	0.06	0.40	0.29	0.60
	15	0.16	0.24	0.09	0.47	0.40	0.68
	30	0.23	0.31	0.14	0.54	0.51	0.62
	55	0.33	0.43	0.22	0.59	0.66	0.67
	100	0.50	0.59	0.34	0.77	0.89	0.84
	190	0.81	0.85	0.61	1.00	1.21	1.07
	350	1.18	1.29	1.00	1.32	1.59	1.41
Snow melt	10	0.08	0.14	0.04	0.36	0.22	0.53
	25	0.15	0.23	0.08	0.46	0.37	0.66
	50	0.23	0.32	0.14	0.53	0.52	0.59
	140	0.33	0.43	0.21	0.59	0.65	0.67
	210	0.24	0.34	0.15	0.53	0.51	0.57
	525	0.43	0.54	0.29	0.69	0.76	0.79
	1103	0.68	0.79	0.51	0.93	1.03	0.97
	3000	1.18	1.26	0.95	1.32	1.51	1.35
	6921	1.57	1.70	1.48	1.71	1.85	1.71

Average Standard Deviation of Depth (m)

Season	cfs	Transition	Plane Bed	Pool	Inset Channel	Chute	Steep Inset Channel
Dry	5	0.25	0.16	1.37	0.10	0.23	0.11
	10	0.29	0.17	1.39	0.12	0.25	0.22
	20	0.36	0.22	1.42	0.18	0.34	0.26
	30	0.44	0.26	1.44	0.24	0.43	0.35
	45	0.50	0.33	1.51	0.32	0.59	0.42
Wet	5	0.31	0.19	1.40	0.14	0.28	0.23
	15	0.36	0.22	1.43	0.18	0.34	0.27
	30	0.39	0.25	1.43	0.22	0.41	0.33
	55	0.47	0.29	1.49	0.29	0.53	0.39
	100	0.54	0.37	1.62	0.35	0.66	0.47
	190	0.66	0.50	1.79	0.48	0.93	0.62
	350	1.07	0.67	2.11	0.72	1.22	0.87
Snow melt	10	0.30	0.18	1.38	0.13	0.26	0.22
	25	0.35	0.21	1.42	0.17	0.32	0.25
	50	0.41	0.25	1.43	0.23	0.41	0.33
	140	0.46	0.29	1.48	0.29	0.51	0.38
	210	0.43	0.25	1.44	0.23	0.41	0.33
	525	0.51	0.34	1.56	0.33	0.58	0.41
	1103	0.62	0.42	1.71	0.42	0.80	0.54
	3000	0.82	0.56	1.97	0.60	1.11	0.75
	6921	1.41	0.92	2.30	0.92	1.37	1.08

Average Standard Deviation of Velocity (m/s)

Season	cfs	Transition	Plane Bed	Pool	Inset Channel	Chute	Steep Inset Channel
Dry	5	0.03	0.04	0.01	0.09	0.04	0.22
	10	0.04	0.06	0.02	0.10	0.06	0.39
	20	0.08	0.10	0.05	0.17	0.11	0.48
	30	0.13	0.13	0.09	0.24	0.18	0.55
	45	0.19	0.19	0.15	0.31	0.27	0.56
Wet	5	0.06	0.08	0.04	0.12	0.08	0.43
	15	0.08	0.10	0.06	0.17	0.11	0.48
	30	0.11	0.13	0.08	0.23	0.18	0.55
	55	0.16	0.16	0.12	0.29	0.24	0.56
	100	0.22	0.22	0.19	0.34	0.30	0.56
	190	0.32	0.32	0.32	0.45	0.40	0.54
	350	0.52	0.43	0.49	0.56	0.52	0.57
Snow melt	10	0.05	0.06	0.03	0.10	0.06	0.40
	25	0.08	0.09	0.05	0.16	0.10	0.48
	50	0.12	0.13	0.08	0.23	0.18	0.55
	140	0.15	0.15	0.12	0.29	0.23	0.55
	210	0.11	0.13	0.08	0.23	0.16	0.53
	525	0.18	0.19	0.16	0.31	0.27	0.55
	1103	0.27	0.25	0.28	0.37	0.38	0.54
	3000	0.41	0.37	0.47	0.46	0.48	0.53
	6921	0.68	0.61	0.69	0.59	0.52	0.65

Table 42. Percent difference (2D Transect minus 2D model)/2D model of depth and velocity model results, per morphologic unit inclusive of all seasons and discharges.

Metric	Percent difference calculated as 100*(2D Transect - 2D)/2D					
	Transition	Plane Bed	Pool	Inset Channel	Chute	Steep Inset Channel
Depth metrics						
Average depth*	-24.0	9.6	-14.9	-23.9	-31.8	-22.9
6921 cfs average depth	-40.0	-18.9	-39.6	-33.8	-35.4	-31.6
Dry 5 cfs average depth	-9.3	53.3	5.6	1.8	-18.2	15.1
Velocity metrics						
Average velocity*	-20.1	-7.3	-26.8	-25.3	-26.7	-39.5
6921 cfs average velocity	-25.6	-20.7	-25.6	-29.8	-25.7	-37.5
Dry 5 cfs average velocity	-18.7	59.6	-36.7	15.8	-42.9	26.7

*Calculated by taking the average of all morphological-unit average values for all seasons and all simulated discharges (n=21).

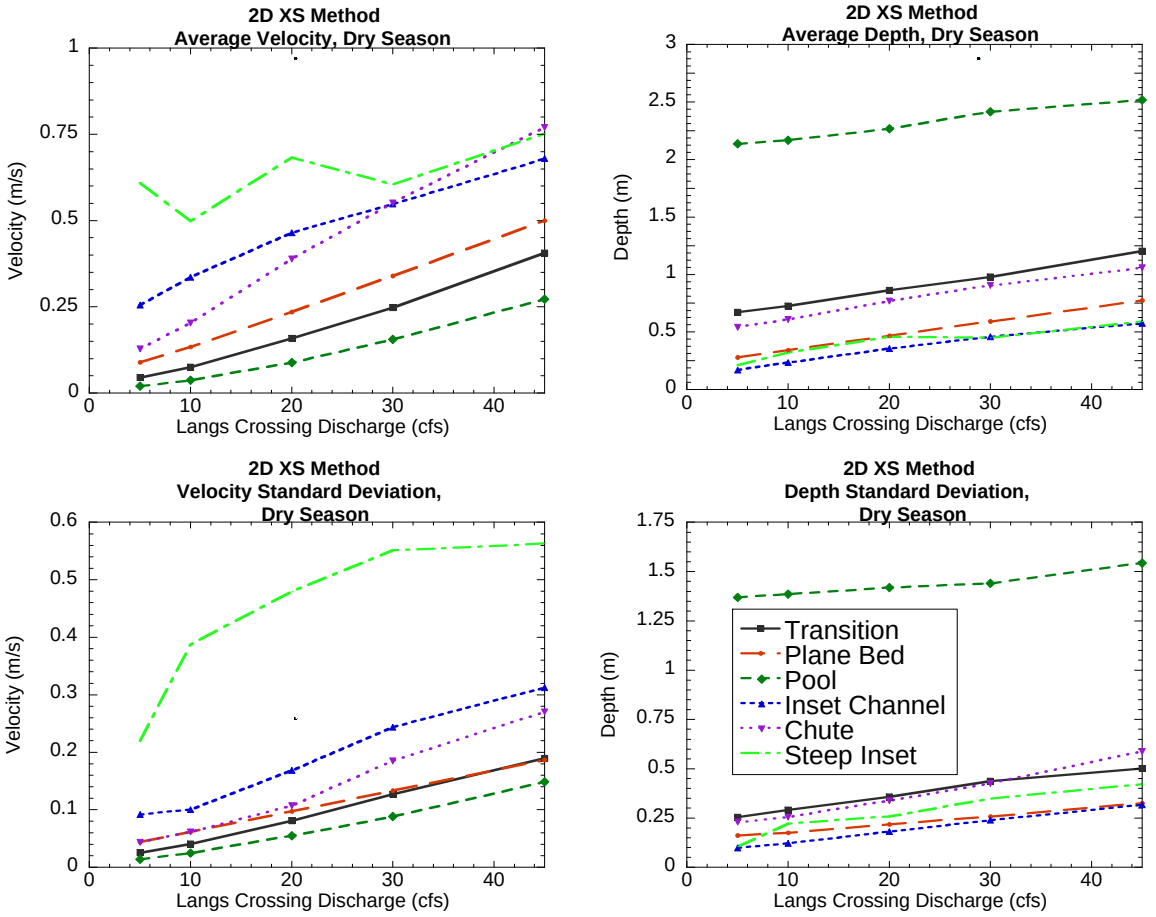

Figure 109. 2D transect method velocity and depth variations during dry season discharge.

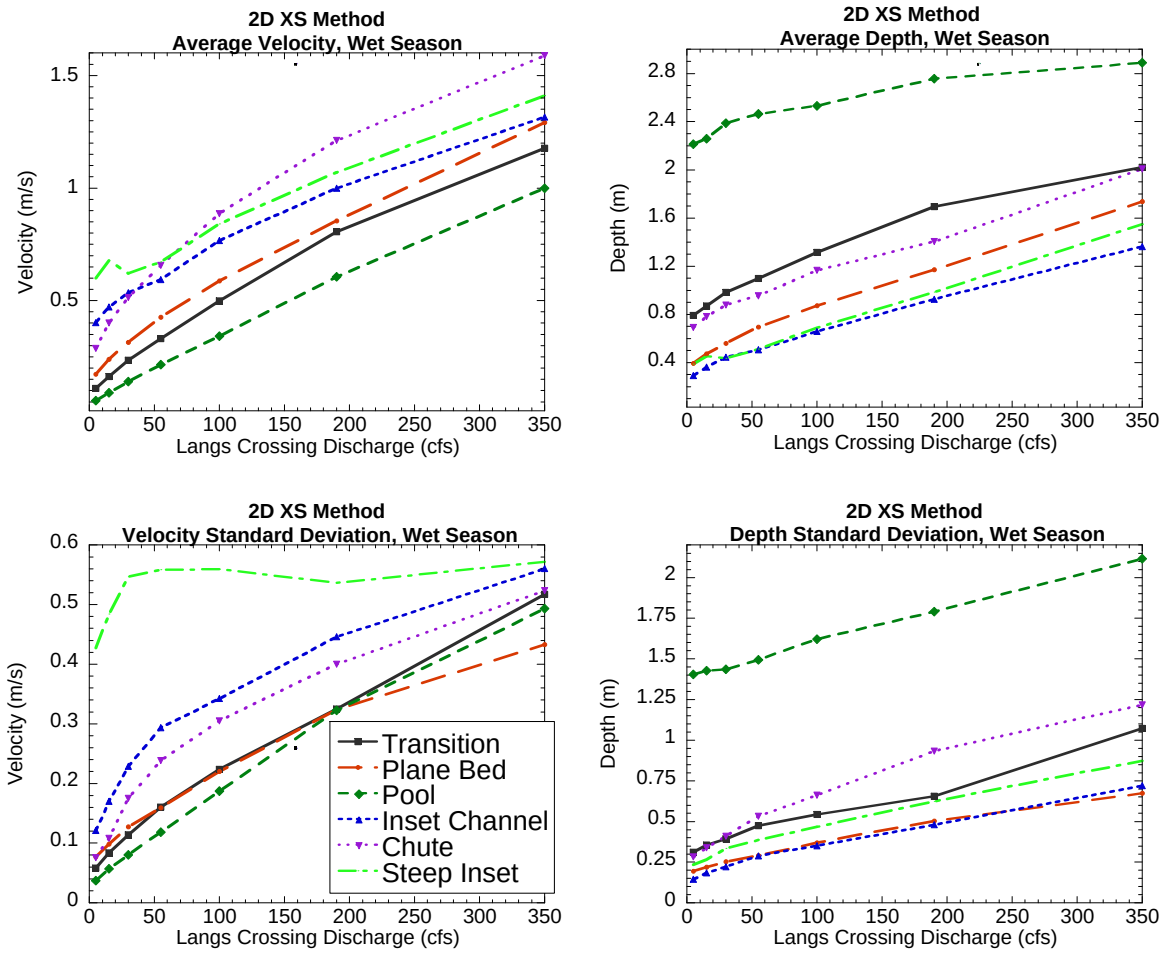

Figure 110. 2D transect method velocity and depth variations during wet season discharge.

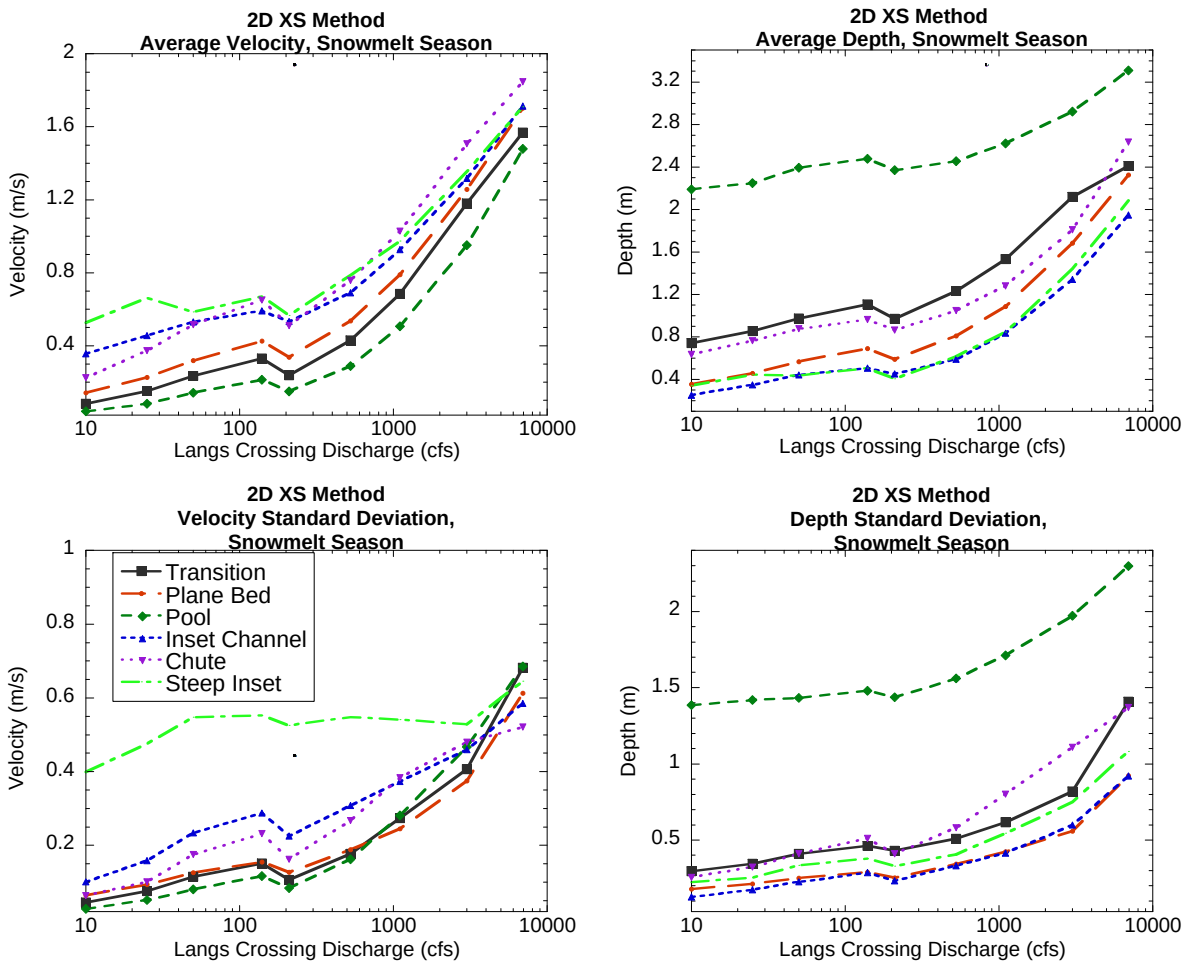

Figure 111. 2D transect method velocity and depth variations during snowmelt season discharge.

10.2.3 Transect-Sampling Comparison Interpretation

Three key results were found in this intercomparison: (1) transect sampling performed reasonably well at representing the majority of depth and velocity distributions, (2) transect sampling performed very poorly at representing high values at all flows, with performance worsening as flow increased; and (3) transect sampling performed poorly at estimating the statistical metrics of morphological units.

The explanation for why the 30 transects underpredict some depths and velocities compared to the full 2D model results (

Table 40 and

Table 42) is thought to have to do with the procedure used to select representative transects. In picking the exact transect location within a selected morphological unit, no particular strategy was used other than making sure to obtain the specified number of transects. In looking at the locations of cross-sections, for units that had simple shapes, the tendency appears to have been to locate each transect across the middle of that particular morphologic unit. This tendency was especially notable for pools and transitions. Considering that flow tends to decelerate into pools and accelerate out of it, the middle of a pool is the location where velocity is lowest and most uniform. As a result, transect sampling that emphasizes the middle of pools might miss the diversity of hydraulics present in pools. The same considerations might apply for the other unit types as well.

It is important to note that this 30-transect comparison used double the density of transects for the Drum-Spauling and Yuba Bear relicensing efforts for the entire South Yuba channel, to be a thorough methodological comparison. Within the study river segment, this study used ten times more transects than the relicensing effort used. Overall, representation of morphological-unit average hydraulics using the transect-based method results were better than 1D numerical model results. The margins of difference were smaller between depth results across methods than for velocity.

The conjecture that a small number of points (30 transects x 0.5-m spacing versus ~1-m spacing for 13.52 km of river, with exact numbers of points varying with season and discharge) accurately represents the statistical distributions of depth and velocity in a complex mountain river segment is plausible (central majority- yes; upper tail- no), while the conjecture that the same set accurately estimates the average depth and velocity of individual morphological units has been found to be incorrect for a complex mountain channel. Similarly, the number of points from transect-based sampling failed to capture the diversity of hydraulics within morphological units, as indicated by the difference in standard deviation values in Table 36,

Table 38, and in

Table 41.

CHAPTER 11:
Ecologic Analysis

The goals of ecological analysis are to evaluate biological conditions, processes, and interactions across three broad scales (individual, population, and community) as well as to characterize abiotic-biotic linkages relevant to each scale. For each of these goals, there are analyses to address the normative state of an ecosystem and others to assess human societal uses of an ecosystem that cause impacts on the normative state. Because a comprehensive approach that spans all of ecology is beyond the feasibility of instream flow assessment, it is common to identify a small subset of ecological "indicators" that can be used to diagnose the status of a system. Often the indicator is a particular species or subset of species (Willson and Halupka 1995), but more recently the idea of having key physical variables or processes serve as indicators has been promoted (Richter et al. 1996; Poff et al. 1997).

Following the approach of YARMT (2009), this study evaluated the ecological status of the selected study segment on the South Yuba River through the use of a wide array of "spatial structure" performance indicators and analytics (see sections 2.1.1 and 2.1.2). YARMT (2009) also includes a broad-based biological assessment, but purely biological topics are beyond the scope of this investigation. Although this study provides an evaluation of the spatial structure of the South Yuba River study segment, the broader purpose was to develop and test new methods to guide future maturation of instream flow assessment as a science-based tool for river management applications.

Many analyses of ecological spatial structure have already been addressed in the hydrological, geomorphic, and hydraulic analyses chapters (Chapters 5.0, 8.0, and 9.0, respectively). Specific examples relevant to spatial structure in those sections include: 1) the hydrologic analysis section quantified the magnitude, timing, and duration of regulated and unregulated water sources; 2) the geomorphic analysis section characterized the spatial organization of morphological units; and 3) the hydraulic analysis section revealed the stage-dependent joint distributions of depth and velocity at the segment and morphological-unit scales (with this last effort constituting a physical mesohabitat characterization of hydraulics). Along with many other specific analytics, these results provide a depth of understanding to the ecological status of the river.

In instream flow assessment practice today, the relationship between weighted usable area and discharge for individual species' lifestages is often the centerpiece of physical habitat evaluation, and therefore the focus of instream flow assessment (Bovee 1982; Gore and Nestler 1988; Waddle 2001; Booker and Acreman 2007). A common method for obtaining the relationship is to use the Instream Flow Incremental Methodology (IFIM) and the Physical Habitat Simulator System (PHABSIM) software suite. A computer package is readily available (http://www.fort.usgs.gov/Products/Software/PHABSIM/). The use of PHABSIM to obtain a statistical sampling of hydraulics for each morphological unit has already been described in sections 2.1.2, 7.1, and 7.2. After that, the procedure involves steps to linking point-scale hydraulics with habitat suitability curves for individual species' lifestages to arrive at the weighted usable area for a given flow.

All methods have proponents and detractors, so it is expected that IFIM and the PHABSIM software suite would have critics, too. Criticisms of PHABSIM include the inability of the

hydraulic estimation procedure to describe relevant variability between transects, deficiencies with the method of lateral extrapolation of velocities, the reliance on statistical sampling for habitat quantification, evidence of bias in transect selection, the absence of spatially explicit analysis, the dependence on habitat suitability curves, the exclusive focus on point-scale data with poor upscaling, exclusion of hyporheic flow effects at the morphological-unit scale, and the lack of a mechanistic foundation in river processes (Thomas and Bovee 1993; Geist and Dauble 1998; Ghanem et al. 1996; Kondolf et al. 2000; Moir et al. 2004; Moir et al. 2005; Parasiewicz 2007; Williams 2010). For over a decade, some have advocated for substituting site-scale 2D models in place of individual transects, while remaining in the larger IFIM concept for doing instream flow assessment (Leclerc et al. 1995; Guay et al. 2000; Tiffan et al. 2002; Gard 2003). 2D models have also found value beyond instream flow assessment in river rehabilitation, where they have been shown to provide accurate predictions of species utilization of high quality habitat for anadromous salmon spawning (Wheaton et al. 2004a; Wheaton et al. 2004b; Elkins et al. 2007; Pasternack et al. 2004). Nevertheless, there is a lot of uncertainty remaining for instream flow assessment, driving further methodological development and methodological comparison.

The purpose of this chapter is to continue to develop the results of the study to encompass physical habitat analysis as an important indicator of instream flow needs. After presenting some methods (sections 11.1–11.2), the chapter has four substantive sections presenting the following, in order: (1) results of physical habitat analysis using the 2D model, (2) methodological comparison of metrics between transect-based and 2D model methods, (3) methodological comparison of metrics between 1D and 2D numerical model methods, and (4) summary of the physical habitat analysis. Across all analyses and comparisons, one goal was to evaluate how the differences found in hydraulic metrics (Chapter 0) propagated through to physical habitat metrics and habitat area-flow relations. By design, the methods and results presented in this chapter do not exactly parallel the formal procedure in the PHABSIM manual or other documents, because the goal was to use all of the new information from the hydrological, geomorphic, and hydraulic analyses to dictate the appropriate physical habitat methodology for this river segment. IFIM applications (with or without the use of the PHABSIM software suite) are not well standardized in practice, in part because flexibility is needed to account for unique local contexts. As this study sough to be forward-looking, it was appropriate to remove constraints on what could be done. Nevertheless, several of the analyses are appropriately comparable to common practice today. Specific scientific questions are presented in the first paragraph of sections 11.3, 11.4, and 11.5 below.

11.1 Habitat Suitability Curves

This study did not collect biological data, but instead made use of the recently developed habitat suitability curves for multiple lifestages of Sacramento sucker (SS), rainbow trout (RT), and Pikeminnow/hardhead (PH) fish species that were provided by PG&E and their consultants Devine Tarbell & Associates and Thomas R. Payne & Associates (see section 2.3.2). The curves are suitable for use on the upper South Yuba River. They were generated in English units, and were converted to metric units for this study. The curves are presented in table and figure formats below (Table 43, Figure 112, Figure 113). Because the hydrological analysis (Chapter 0) revealed that the year is divided into distinct hydrological seasons with different stage-discharge relations, it was necessary to account for the timing of species' lifestages relative to those seasons to yield meaningful habitat-flow relationships. A literature review was

performed to determine which species' lifestages occurred during the periods of the year defined as dry, wet, and snowmelt seasons in this study (

Table 44).

Table 43. Velocity, depth, and associated habitat suitability values used to build habitat suitability curves.

Sacramento Sucker Adult			
Velocity (m/s)	Suitability	Depth (m)	Suitability
0	1	0.607	0
0.457	1	0.610	1
0.460	0	1.433	1
		1.436	0

Sacramento Sucker Juvenile			
Velocity (m/s)	Suitability	Depth (m)	Suitability
0	1	0.195	0
0.366	1	0.198	1
0.369	0	0.884	1
		0.887	0

Rainbow Trout Adult			
Velocity (m/s)	Suitability	Depth (m)	Suitability
0	0	0.152	0
0.152	0.8	0.701	1
0.213	1	0.945	1
0.396	1	1.158	0.6
0.549	0.5	1.524	0.3
0.762	0.2	9.144	0.3
1.219	0		

Rainbow Trout Juvenile			
Velocity (m/s)	Suitability	Depth (m)	Suitability
0	0.5	0.061	0
0.091	1	0.366	1
0.213	1	0.671	1
0.366	0.6	0.792	0.5
0.457	0.3	1.219	0.1
0.686	0.1	9.144	0.1
1.067	0		

Rainbow Trout Fry			
Velocity (m/s)	Suitability	Depth (m)	Suitability
0.006	0	0.0732	0
0.009	1	0.0762	1
0.165	1	0.4877	1
0.168	0	0.4907	0

Rainbow Trout Spawn			
Velocity (m/s)	Suitability	Depth (m)	Suitability
0	0	0.046	0
0.183	1	0.183	1
0.610	1	0.457	1
1.219	0	0.914	0

Pikeminnow/Hardhead Adult			
Velocity (m/s)	Suitability	Depth (m)	Suitability
0	0.82	0.201	0
0.061	1	0.799	1
0.274	1	5.486	1
0.649	0.22		
1.067	0		

Pikeminnow/Hardhead Juvenile			
Velocity (m/s)	Suitability	Depth (m)	Suitability
0	1	0.152	0
0.076	1	0.204	1
0.533	0.25	1.119	1
0.792	0	2.655	0.1
		5.486	0.1

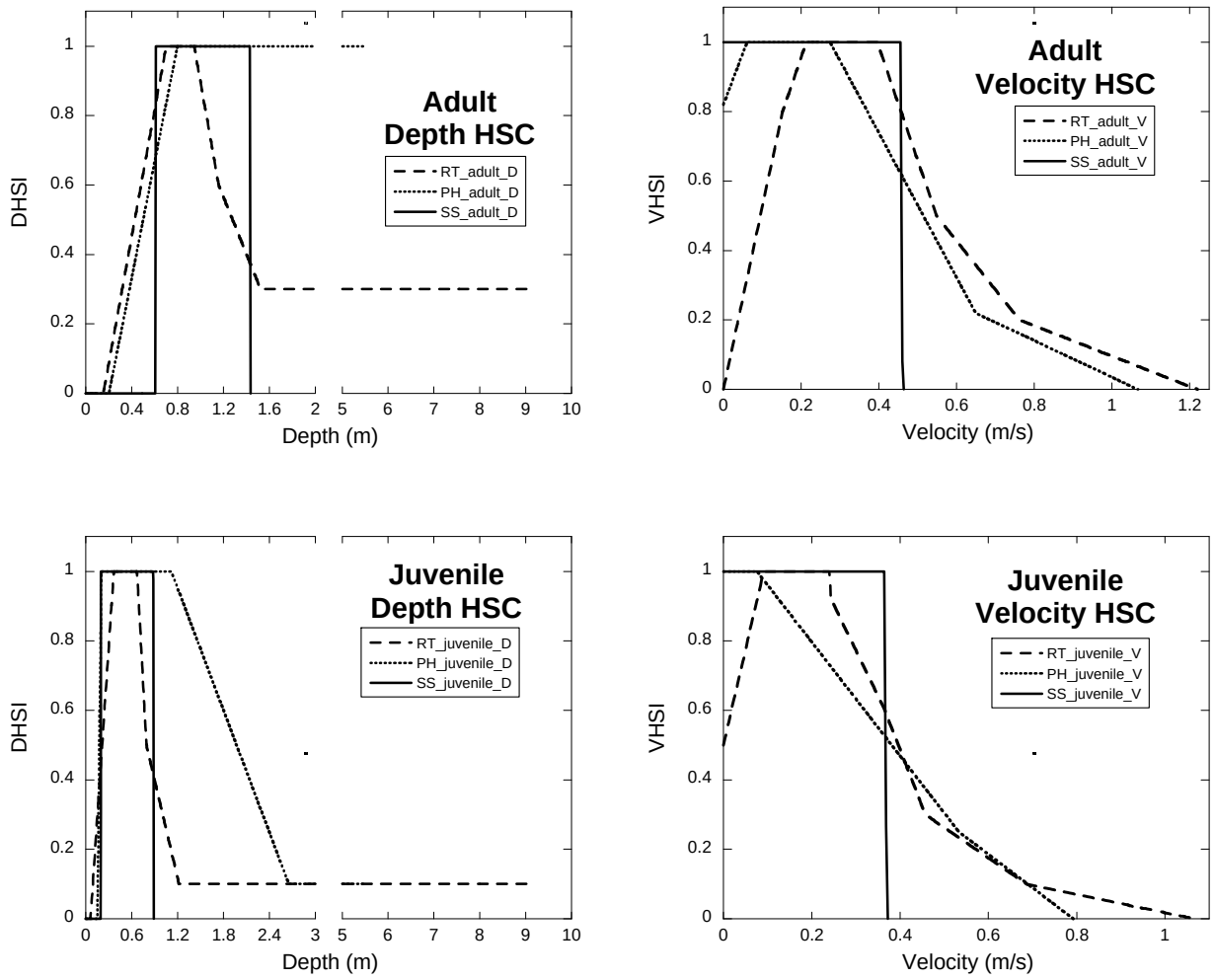

Figure 112. Depth and velocity suitability ranges plotted as habitat suitability curves for adult and juvenile lifestages. RT = rainbow trout, PH = Pikeminnow/hardhead, SS = Sacramento sucker.

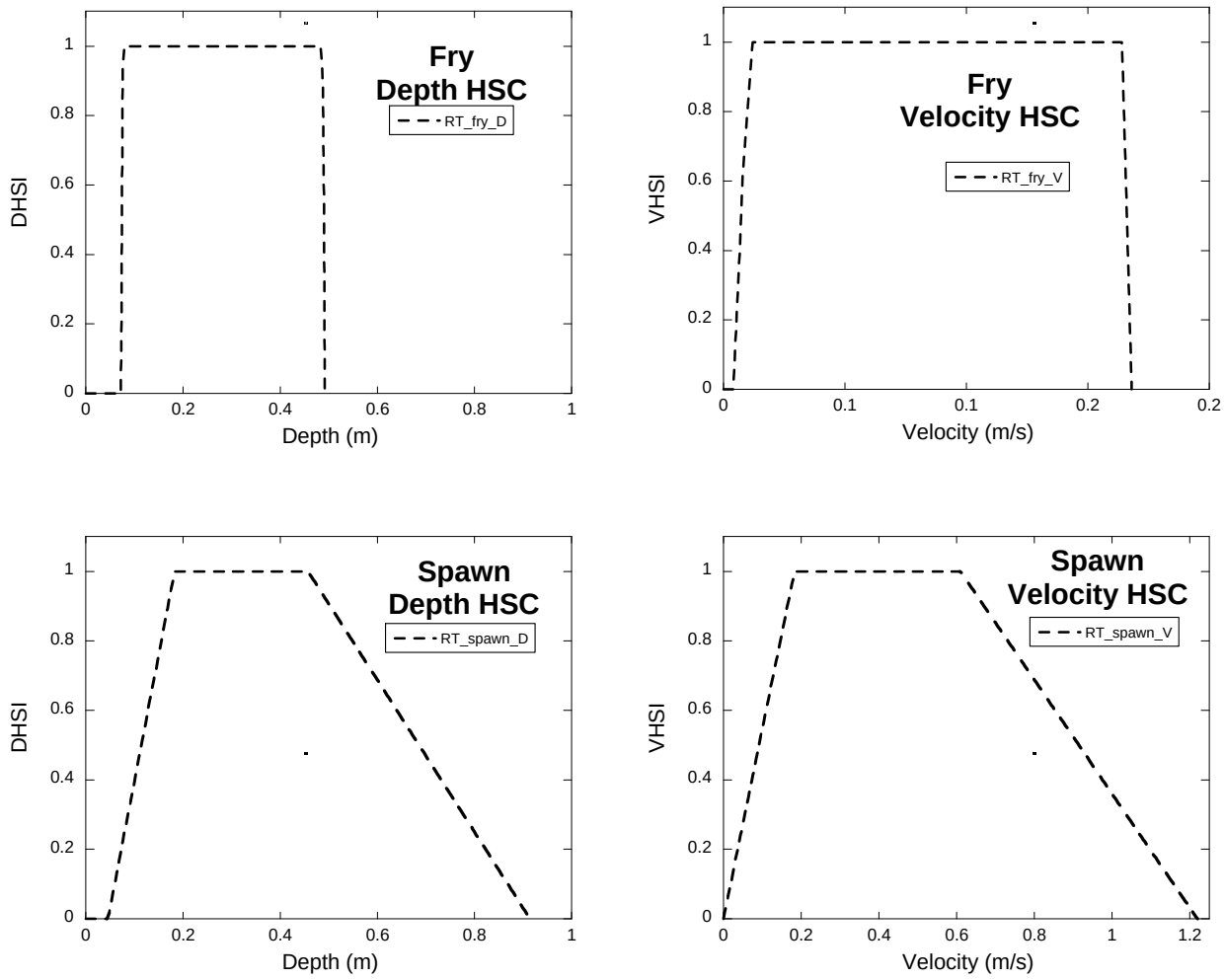

Figure 113. Depth and velocity suitability ranges plotted as habitat suitability curves for fry and spawning lifestages. RT = rainbow trout.

Table 44. Species lifestages per season that were modeled for the study.

	Habitat suitability curve lifestage occurrence by season		
	Dry (Aug 1-Nov 30.)	Wet (Dec 1-March 30)	Snowmelt (April 1-July 31)
	Sacramento Sucker (SS)		
Adult	x	x	x
Juvenile	x	N/A	x
	Rainbow Trout (RT)		
Adult	x	x	x
Juvenile	x	x	x
Fry	x	N/A	x
Spawn	N/A	x	x
	Pikeminnow/Hardhead (PH)		
Adult	x	x	x
Juvenile	x	x	x

11.2 Physical Habitat Quality Model

Each habitat suitability curve was transformed into a set of conditional linear equations that were applied to depth and velocity results for each hydraulic prediction/estimation method, to yield a prediction of the physical habitat quality per species at specified lifestages within each season and across all flows within seasons (

Table 44). These calculations returned a value at each 2D model result node of a depth habitat suitability index (DHSI) and a velocity habitat suitability index (VHSI). To represent the joint distribution of DHSI and VHSI, a global habitat suitability index (GHSI; also sometimes called a combined suitability index, CSI) was calculated as the geometric mean to give depth and velocity equal weighting (e.g. Leclerc et al. 1995; Cavallo et al. 2003; Pasternack et al. 2004; Elkins et al. 2007).

$$GHSI = \sqrt{DHSI \cdot VHSI} \tag{17}$$

To isolate the effect of hydraulics on habitat and simplify experimental design, no cover, temperature, or substrate quality habitat suitability curves were used, with the except that anywhere the bed was bedrock, the spawning habitat GHSI value was forced to zero. An important consideration with regard to other microhabitat variables is that they serve as downward modifiers on the hydraulic habitat GHSI variable. The maximum value for GHSI is 1.0, so adding one or more additional terms whose values are ≤1.0 can only decrease habitat quality further. Thus, gaining insight on the differences in GHSI values produced with different hydraulic methods was chosen as the most important issue relevant to this study. Other data that could influence habitat quality such as LIDAR-based canopy cover was collected and prepped for analysis, but time-constraints and limited resources dictated that other analyses were beyond the scope of the study.

For the 2D model, DHSI, VHSI, and GHSI values were computed at all wet nodes in the computational mesh. For the 1D numerical model, these values were calculated for cross-sectionally averaged depth and velocity values for a total of 105 values. For the transect-based analysis, values were calculated at each wet 0.5-m spaced point along the selected set of 30 transects.

For the 2D model results, GHSI values and a boundary layer were imported into ArcMap 9.3, with (x ,y) data projected into the NAD_1983_StatePlane_California_II_FIPS_402 (m) coordinate system, and z data representing each nodal GHSI value. ArcToolbox 3D Analyst was used to transform (x, y, *GHSI*) data into a TIN. The TIN was converted into a floating point raster with 0.5x0.5 m^2 pixels, which was then classified into an integer raster where GHSI ranges were assigned to one of five categories (Table 45). Without explicit bioverification data, it is uncertain whether this binning scheme is valid, but it is the one Pasternack et al. (2008) bioverified for lower Yuba River Chinook salmon spawning, so it was used here as well. The advantage of binning data into categories instead of assessing raw numbers for a weight usable area calculation as is commonly done is that it strongly reduces the impact of hydraulic uncertainty by smoothing values to fewer significant figures. With this simplification, uncertainty assessment is reduced from testing the accuracy of each GHSI value to the determination of whether each point is correctly binned. This is an example of how uncertainty can be reduced, even as it is propagated through diverse nonlinear calculations (Pasternack et al. 2006a; Brown and Pasternack 2009). A color scheme was used to identify the GHSI categories in images developed using ArcMap (Figure 121, Figure 122, Figure 123, Figure 124). A complete set of data tables of % GHSI binned values for all species, lifestages, and seasons are available in Appendix B. Also in Appendix B is a complete set of the joint distribution of GHSI bin values and SYLC discharge. Appendix C contains a set of maps developed in ArcGIS that provide a visual representation of the GHSI % distribution of each species' lifestages at three flows and in three locations within the study segment. These images show a range of flow conditions in

multiple reaches for each species lifestage, arranged so that the reader can visualize the spatial component of GHSI results.

In bioverifying habitat quality categories for Chinook salmon spawning, both Elkins et al. (2007) and Pasternack et al. (2008) reported that medium and high quality habitat bins were "preferred" by spawners, while the remaining bins were "avoided" (Table 45). These determinations involved comparison of the percent of utilized points versus the percent of available area within each habitat quality category using an electivity index (e.g. forage ratio) that divided utilized by available. There are many possible ways to compute an electivity index. The Elkins et al. (2007) study result was complicated in that low quality habitat was preferred in the degraded river state, but after river rehabilitation was completed, low quality habitat was strongly avoided. Based on the illustrated distinction of preferred versus avoided habitat on the lower Yuba and Mokelumne Rivers, the 0.6–1 and 0.4–0.6 GHSI bins were lumped together to obtain a single "preferred" habitat category and the remaining GHSI bins were lumped together to obtain a single "avoided" habitat category. The effect of flow on the amount of physical habitat was evaluated by comparing the amount of preferred habitat (i.e. GHSI>0.4; hereafter referred to as preferred habitat) for all species and life stages for every modeled discharge (

Table 16,

Table 17,

Table 18).

This is a key point for all habitat-area analyses that follow. Whereas many studies calculate a weighted usable area value for each measurement unit by multiplying the GHSI value times the area it represents, this study took a different approach. In this study, GHSI values were binned into a binary function (avoided or preferred), and then only preferred areas were further analyzed. This is a significant deviation from common practice, but it was done for an important reason—to account for uncertainty. All methods of hydraulic sampling and mesohabitat delineation (or morphological unit delineation) have uncertainty. When hydraulics is combined with habitat suitability curves, the uncertainty increases through nonlinear error propagation. The weighted usable area computation does not address this important problem. Meanwhile, the binning approach used in this study greatly reduces uncertainty by reducing the specificity of the numerics. Instead of there being amplified error in each specific weighted usable area value, the preferred approach only has error in the binning, and since there are only two bins, the likelihood of error is reduced substantially. The choice to prefer a method that accounts for uncertainty is a key feature of the analytical approach that follows, and is consistent with the effort throughout the report to embrace uncertainty, as it is unavoidable.

Table 45. GHSI range, habitat value, and color scheme for image depiction.

GHSI Bins	Habitat Value	Color Scheme for Images
0.6-1	High Quality	Blue
0.4-0.6	Medium Quality	Green
0.2-0.4	Low Quality	Yellow
0-0.2	Very Poor Quality	Red
0	Non-Habitat	Gray

Lumped GHSI Bins	
0.4-1	Preferred Habitat (medium + high quality)
0-0.4	Avoided Habitat (low, very poor, and non-habitat)

11.3 2D Model Microhabitat Analysis

A primary goal of this study was to showcase the opportunities and constraints for developing instream flow assessments of the furture to embrace a near-census approach with spatially explicit analyses. The geomorphic and hydraulic analyses presented several new ways to conceive of instream flow assessment. This section continues that perspective by drawing on those analyses to get to a segment-scale microhabitat analysis of the South Yuba River study segment. Whereas the earlier sections also included morphological-unit scale analyses and more spatial analyses of 2D model results, this section does not include those elements, for lack of time. Instead, significantly more effort went into methodological comparison of physical habitat metrics than was done for hydraulic metrics, because there are so many ways to propagate

hydraulics to address habitat and because there were so many species and lifestages to address (see the next two sections). The questions addressed in this section include the following:

- What is the segment-scale statistical distribution of microhabitat GHSI values for each species' lifestage as a function of discharge for each hydrological season?
- What is the spatial pattern of GHSI in characteristic sections of the study segment for each species' lifestage as a function of discharge for each hydrological season?
- How much area of preferred habitat exists for each species' lifestage as a function of discharge within each hydrological season?
- How do different metrics for combining all of the results of different lifestages into a single habitat-discharge function compare for each hydrological season?

11.3.1 Explanation of 2D model tables, figures, and analysis metrics

SRH-2D hydrodynamic model development and validation produced a suite of depth and velocity values across the study segment that are described in detail in Chapter 0. Microhabitat analysis involved applying habitat suitability curves to determine habitat quality on a 0.5-m grid.

Figure 114, Figure 115, Figure 116, and Figure 117 are 3-D graphical representations of RT snowmelt season lifestages of the full range of % distribution of 2D model GHSI categories, including those of low, very poor, and non-habitat (i.e. avoided habitat). These graphs are useful in visualizing how GHSI bins change with respect to flow, species, and lifestage (see Appendix B for tables). A complete set of the GHSI binned data and % distribution graphs are presented in Appendix B. These figures are not discussed further, but can be used in conjunction with

Table 48.

Table 48 reports only the percent per unit area where the GHSI value was equal to or greater than 0.4, whereas Appendix B 3-D graphs show all percentages of GHSI binned values, from 0–1.0. Tables at the beginning of Appendix B give the values associated with the 3-D graphs, thus reporting the full spectrum of results. Results of GHSI ≥ 0.4 are those of interest to this investigation, thus the decision was made to include the full set of results only in the appendices.

Figure 118, Figure 119, and Figure 120 are 3-D graphical representations of dry season adult, juvenile, and fry lifestages using the percent per unit area metric (e.g.

Table 48). Seasonal 3-D graphs are not available other than those for dry season included below.

Vivid examples of the spatial distribution of all GHSI habitat across large reaches of the study segment can be seen in Figure 121, Figure 122, Figure 123, and Figure 124, where rainbow trout adult, juvenile, fry, and spawner instream spatial GHSI distributions provide the opportunity to attain a clear conceptual understanding of the variation in percent habitat at different flows (see Appendix C for all species' lifestages). In each figure, the top panel typically represents the highest percent of preferred habitat per unit area, the second panel shows a mid-range percent preferred habitat, and the lower panel allows visualization of a very low percent of preferred habitat. Each species lifestage is represented a total of 9 times, with the lifestage represented not only at three flows, but also in three reaches. Image sets are ordered by reach, with the first set depicting the upper end of Reach 1 and the lower end of Reach 2. The second image depicts the upper end of Reach 2 and the lower end of Reach 3. This image stops just below Canyon Creek, which is the approximate halfway point in the study reach. These first two images encompass much of the accessible river near Washington, California. The third image depicts all of Reach 6 and 7, parts of upper Reach 5 and lower Reach 8, and includes Jolly Boy, Killer Fang Falls, and the confluence of Fall Creek with the mainstem South Yuba River. Appendix C holds all RT, SS, and PH lifestages as described here. Inspection of available graphics in the appendices will help the reader visualize GHSI distributions of each species lifestage at various modeled flows.

Total area of preferred habitat (

Table 46) is useful for interpretation of biotic abundance, but was also converted into a percentage per unit area, which can be viewed as an efficiency of habitat metric, in the sense of having more preferred habitat per unit area (

Table 48).

Table 47 and

Table 49 are companion tables, where averages per flow weighted by lifestage is used as a simple metric. Averages were calculated by adding the total area or percent of each lifestage together (e.g. SS adult +RT adult +PH adult) then dividing by the number of lifestages present in the season to achieve equal weighting. If a lifestage contained just one value, that value was used to represent that lifestage. To further parse the data, a non-parametric rank ordering was performed within each species lifestage in a season (e.g. SS adult area ordered 1 thru 5 to represent the five flows used in the dry season, and ordered from high to low amount of area), then the rankings summed across each flow (

Table 47,

Table 49). The largest area or percent of preferred habitat received a rank of 1, the next largest a rank of 2, and so on. If a species lifestage had the same amount of preferred habitat at multiple flows, each received the same rank number, and the next numbers were skipped such that a group of 5 might be ordered as such: [1 2 2 4 5]. With this approach, the smallest sum is then considered to be the most highly preferred habitat, inclusive of all species and lifestages present within that season. This approach eliminates the disparity between, for instance, a high of preferred RT fry habitat at 38,013 m^2 compared to a high of preferred RT adult habitat at 151,607 m^2. In the rank order test, both of these values received a '1' because they represent the highest amount of area for that particular lifestage.

The left-hand column of

Table 46 and

Table 48 list the amount of available wetted area (m^2), which varies by season even if discharge from SYLC is the same (e.g. dry and wet 5 cfs). Using seasonality (dry, wet, snowmelt) as a control to develop species' lifestage GHSI values (

Table 44) is a direct result of the hydrological analysis of Chapter 0. The concept of flow accretion within a watershed was used to develop understanding of physical processes that play important roles in stream ecology. No other variable is as important to riverine health than water itself, and a close second is the abundance, distribution, and occurrence of that water within the wetted channel. Recall that each season has its own accretionary flow equation(s) (section 5.4). These equations were the product of a thorough analysis of available historical and current hydrologic records. The analyses revealed distinct seasonal thresholds between SYLC gaged discharges and discharge at Washington, California, shaped by the Mediterranean-montane climate regime present throughout the Sierra Nevada. Seasonal climatic variations result in cumulative discharge variations within the South Yuba River study segment, which then translates into differences in wetted area across seasons.

Finally, a summary of metrics table assigns a point to the highest value in each column in

Table 47, which represents highest absolute area values and

Table 49, which represents highest area percentages. In addition, another metric is developed in this table that uses the weighted # of occurrences with highest individual area or percent divided by total number of species in a lifestage, then summed within lifestage. For example, each adult and each juvenile occurrence of highest area during dry season is assigned a weight of 0.33 because there is a one in three possibility of a particular species having the highest area. Conversely, dry season RT fry is assigned a weight of 1.0, as it is the only representative of the fry lifestage. Thus, dry 5 cfs total # of occurrences with highest individual area only occur for RT fry, so the total for that flow equates to 1.0 (see

Table 46 and

Table 48 for lifestage representations). Alternately, in dry 45 flows, two of three adult lifestages have the highest available preferred area during this flow, thus the metric total for dry 45 is 0.66 (0.33 + 0.33). This metric seeks to understand which flows are most highly utilized across species and lifestages.

In

Table 50, light gray highlights indicate preferred flow for absolute area (as defined in section 11.2), light blue for area percentages, and boxed for highest total across both area and percentages. These metrics indicate the flow in a season at which the highest estimated area, percent, or weighted average of preferred area or percent habitat is available for a species' lifestage.

The difficulties of averaging 'best' conditions across species' lifestages becomes apparent when close attention is paid to the area of GHSI>0.4 results of each method. Areas vary greatly, yet once averaging occurred, the information of individual lifestages becomes smoothed out and results converge to the species and/or lifestages, which command the most area. The weighted averages and ranked order analyses were developed to balance this tendency.

A key question considered here is what patterns emerge as the data is resolved into various metrics?

11.3.2 Interpretation of 2D model results

2D model results by area

The area of GHSI>0.4 (i.e. preferred habitat) varies by species and lifestage as well as by flow (

Table 46). Distribution of available area for Sacramento sucker (SS) adults show the peaks of available habitat at 48,980 m^2 during 25 cfs snowmelt season, 48,912 m^2 during 30 cfs dry season, and 48,535 m^2 during 15 cfs wet season (see gray highlights in

Table 46). Less preferred habitat becomes available as flows increase, but also as flows decrease, such can be seen between dry 5 and dry 45 cfs. Rainbow trout (RT) adult area at dry season 30 cfs has preferred area of 147,333 m^2, which is more than triple that of the highest Sacramento sucker preferred habitat. The highest amount of preferred area for RT occurred during snowmelt season 140 cfs with 161,654 m^2. The highest and lowest flows (snowmelt 6921 cfs and dry 5 cfs, respectively) provide relatively little preferred habitat for RT, but conversely RT has the median to maximum value at all flows and lifestages. Pikeminnow/hardhead (PH) adult GHSI>0.4 area is distributed similarly to RT. Both RT and PH adult areas peak in snowmelt 140 cfs flows.

Amount of preferred habitat for SS juveniles is higher at all flows compared to SS adults. RT juvenile area is greater at lower flows and decreases more rapidly at higher flows than for RT adult. Area is highest for PH among the three species at low flows across all lifestages. RT had the only fry habitat suitability curves. Fry have low amounts of preferred habitat, peaking at lowest flows in dry and snowmelt seasons. RT also had the only spawning habitat suitability curves of the three species. Preferred habitat peaked for spawning RT at wet season 55 cfs flows with 141,870 m^2, and in snowmelt season at 140 cfs with 143,143 m^2. Snowmelt season had 7 of 8 occurrences of the highest area for a species' lifestage, with snowmelt 140 cfs with three of those highest areas utilized by RT and PH adults and by RT spawners.

Weighted average area peaked in the dry season at 30 cfs flows, with 80,636 m^2 (see gray highlights in

Table 47). For snowmelt season, 210 cfs flows had the highest weighted average at 96,333 m^2, while wet season had the overall highest weighted average preferred habitat area at 30 cfs flows with 127,375 m^2. Wet season available preferred habitat areas were relatively large across all lifestages, whereas in snowmelt season SS juvenile and RT fry are relatively low (see

Table 46), which explains why 7 of 8 of the highest areas were found in snowmelt season yet the wet season weighted average is higher.

Ranked order results varied from equal weighting averages in the dry and snowmelt seasons, with dry 20 cfs and snowmelt 50 cfs accumulating the lowest rank number, which indicates highest preference (

Table 47). Ranked order returned the same preference for wet 30 cfs as equal weighting average.

2D model results per unit area (percentage)

Available preferred area was normalized by wetted area per flow, providing a percent per unit area metric that can be considered an expression of habitat efficiency (

Table 48). In dry season, 10 cfs provided the highest amount of preferred habitat per unit-wetted area for SS adult and all three species' juvenile lifestages (see blue highlights in

Table 48). The lowest % area of preferred habitat occurred for SS adults, which peaked at 19–20% in all seasons. RT fry peaked at 20.3% during dry season 5 cfs releases. RT adults have the most %-preferred habitat in the mid- to higher flows in all seasons, peaking at 50 cfs in snowmelt season before falling to 11.4% and 5.7% preferred habitat in wet and snowmelt season highest flows, respectively. PH adults have a similar pattern to RT, but peaked at lower flows in dry and snowmelt seasons. Juveniles across all species prefer lower flows than RT and PH adults. RT fry preferred the lowest flows, while RT spawners as preferred flows at the low end of the discharge spectrum.

In wet season, 15 cfs had the highest weighted average %-preferred area of all seasons at 46.8% (

Table 49). Snowmelt season 25 cfs provided the next highest seasonal weighted average with 35.6%, while dry season highest occurred at 10 cfs with 34.3%. When ranked, snowmelt 25 and dry 10 cfs results were the same as using the weighted average method. But for wet season, a rank order tie occurred between wet 5 and 15 cfs. This result shows the power of ranking first or second; both flows ranked either 1 or 2 in four of six of the possible categories (SS adult, RT and PH juvenile, RT spawner; see

Table 48).

3-D graphical representation of all dry season species and lifestages can be seen in Figure 118, Figure 119, and Figure 120. These figures depict the values from

Table 48, providing the opportunity to visualize the tabular data.

2D model results, summary table (

Table 50)

In analyzing the 2D model results for GHSI habitat suitability and preferences, metrics have been used to attempt to give weight to highest area or percent within season *and* across seasons; within a species lifestage *and* across other species' similar lifestages; and highest overall per species lifestage *and* highest overall per flow; as well as a total of totals, which sums the individual considerations (as detailed in

Table 46-

Table 50). This breadth of analyses show that results differ when considering total area of preferred habitat versus the percent of preferred habitat per unit area (

Table 50). Using the metrics methods described in 11.3.1, a synthesis of all 2D model results tables suggests that it is difficult to assign one flow as 'the best' when considering multiple species and lifestages. Nevertheless, the results of these analyses may be useful in guiding recommendations for Spaulding Dam flow releases aimed at providing the most habitat to the most species and lifestages during a specified season. Conversely, flows could be adjusted for very specific species or lifestage goals when conditions warrant it.

Specifically, the boxed flows in

Table 50 indicate one perspective on the overall 'best' flow, which takes into consideration flow with highest area per lifestage as well as area and % area metrics. Dry season 10 cfs, wet season 55 cfs, and snowmelt season 25 cfs received the highest overall totals and thus represent the flows that might best serve the most lifestages of the species present during the months of that specific season, when considering solely a physical habitat approach to instream flow assessment. Each season likely needs flow variations to serve other ecological functions (e.g. Escobar and Pasternack 2009). Interestingly, each boxed flow also represents the flow most preferred for either the area methods or the area % methods, but never for both.

Taking a range of flows approach, dry season flows of 10-20 cfs appear to provide the most preferred habitat to the most species and lifestages during the dry season months of August-November. Wet season flows of 15 and 55 cfs were most preferred for specie' lifestages during the months of December-March. Snowmelt season flows of 25 and 140 cfs may be most advantageous for species' lifestages present during the months April-July.

Having performed multiple analyses to deconstruct GHSI results from 2D model near-census velocity and depth data, the variation within these results does show how difficult it may be to select one analysis method over other methods. Depending on how one values total habitat area versus percent habitat area, a decision could be made for which set of flows to use. That is the step where a combination of expert guidance and stakeholder participation is crucial. There is also the potential to do further tests with the spatial pattern of habitat to assess patchiness and the effects of that on migration-related energy conservation and density-dependent competition and predation. In this regard, this analysis is an illustration as to why so many instream flow assessment methods are in use, as others struggle with similar decision considerations. Even though flow allocation decisions may be difficult to make regardless of methodology, the fact remains that the 2D model near-census approach taken here used a dense and diverse observational data set to predict velocity and depth values at ~1-m intervals in contrast to other instream flow assessments that rely on fewer data observations at transects. Unfortunately, there was insufficient time to fully develop a suite of spatial analyses to take advantage of the spatially explicit dataset, but therein lies one of the exciting challenges of river science in the 21st century.

Table 46. Area where 2D model results returned GHSI>0.4.

Area (m^2) GHSI > 0.4, 2D Model Results

		ADULT			JUVENILE			FRY	SPAWN
Dry (cfs)	Available Wetted Area (m^2)	SS	RT	PH	SS	RT	PH	RT	RT
5	187080	33,770	44,510	78,599	66,679	90,912	105,438	38,013	na
10	198471	39,476	70,581	93,106	73,579	106,654	124,103	35,109	na
20	253787	48,912	117,376	119,311	68,980	119,189	149,702	25,430	na
30	295294	45,781	147,333	138,633	57,985	112,572	158,217	21,734	na
45	344483	34,716	151,607	146,174	43,788	89,315	132,390	15,307	na

		ADULT			JUVENILE			FRY	SPAWN
Wet (cfs)	Available Wetted Area (m^2)	SS	RT	PH	SS	RT	PH	RT	RT
5	226555	43,622	88,028	102,735	na	112,748	134,028	na	110,464
15	254029	48,535	117,653	119,379	na	118,376	149,574	na	127,772
30	285995	47,243	142,775	134,954	na	114,446	157,834	na	137,661
55	325174	39,625	157,861	147,322	na	100,664	149,047	na	141,870
100	369243	28,653	138,499	137,622	na	75,928	112,395	na	126,796
190	425183	17,738	86,856	88,286	na	51,508	72,279	na	90,992
350	499551	12,780	56,962	52,541	na	33,944	47,647	na	63,720

		ADULT			JUVENILE			FRY	SPAWN
Snowmelt (cfs)	Available Wetted Area (m^2)	SS	RT	PH	SS	RT	PH	RT	RT
10	216244	40,635	74,541	95,333	73,711	108,321	126,601	34,277	101,269
25	253122	48,980	114,626	118,164	70,214	120,104	149,204	26,218	127,458
50	292641	47,886	145,684	137,537	59,482	114,606	159,535	21,985	139,338
140	332720	39,407	161,654	149,580	48,692	98,391	148,731	17,508	143,143
210	311832	46,643	155,818	143,694	54,574	107,913	157,489	20,348	142,941
525	377081	29,855	145,544	142,755	37,413	77,959	119,222	12,349	128,785
1103	433858	17,634	93,481	96,287	22,668	50,268	73,273	6,890	93,541
3000	514476	10,698	46,420	44,121	13,877	27,253	38,261	4,629	51,265
6921	610780	7,932	34,852	31,815	11,072	21,055	29,492	3,947	43,767

* Highlighted boxes indicate flows at which the highest estimated area of preferred habitat is available for the species' lifestage in each season

Table 47. Equal weighting average area (m^2) and rank order (lowest rank equals highest amount of preferred habitat) from 2D model results where GHSI>0.4.

2D Model area (m^2) GHSI>0.4 results, Weighted Average and Rank Order to test for most preferred flow scenario

Dry (cfs)	Equal Weighting Average	Rank Order
5	59327	28
10	68092	21
20	77751	15
30	80636	17
45	71545	24

Wet (cfs)	Equal Weighting Average	Rank Order
5	103993	25
15	118979	15
30	127375	12
55	127220	14
100	107516	24
190	72393	36
350	48425	42

Snowmelt (cfs)	Equal Weighting Average	Rank Order
10	77148	34
25	90193	24
50	95725	21
140	94034	27
210	96333	23
525	81346	41
1103	54575	54
3000	29026	64
6921	23280	72

* Highlighted boxes indicate the flow during each season with the highest estimated area using each metric.

**Lowest rank order indicates highest ranked area of preferred habitat

Table 48. Percent where 2D model results returned GHSI>0.4.

% Wetted Area GHSI > 0.4, 2D Model Results

		ADULT			JUVENILE			FRY	SPAWN
Dry (cfs)	Available Wetted Area (m^2)	SS	RT	PH	SS	RT	PH	RT	RT
5	187080	18.1	23.8	42.0	35.6	48.6	56.4	20.3	na
10	198471	19.9	35.6	46.9	37.1	53.7	62.5	17.7	na
20	253787	19.3	46.2	47.01	27.2	47.0	59.0	10.0	na
30	295294	15.5	49.9	46.9	19.6	38.1	53.6	7.4	na
45	344483	10.1	44.0	42.4	12.7	25.9	38.4	4.4	na

		ADULT			JUVENILE			FRY	SPAWN
Wet (cfs)	Available Wetted Area (m^2)	SS	RT	PH	SS	RT	PH	RT	RT
5	226555	19.3	38.9	45.3	na	49.8	59.2	na	48.8
15	254029	19.1	46.3	47.0	na	46.6	58.9	na	50.3
30	285995	16.5	49.9	47.2	na	40.0	55.2	na	48.1
55	325174	12.2	48.5	45.3	na	31.0	45.8	na	43.6
100	369243	7.8	37.5	37.3	na	20.6	30.4	na	34.3
190	425183	4.2	20.4	20.8	na	12.1	17.0	na	21.4
350	499551	2.6	11.4	10.5	na	6.8	9.5	na	12.8

		ADULT			JUVENILE			FRY	SPAWN
Snowmelt (cfs)	Available Wetted Area (m^2)	SS	RT	PH	SS	RT	PH	RT	RT
10	216244	18.8	34.5	44.1	34.1	50.1	58.5	15.9	46.8
25	253122	19.4	45.3	46.7	27.7	47.4	58.9	10.4	50.4
50	292641	16.4	49.8	47.00	20.3	39.2	54.5	7.5	47.6
140	332720	11.8	48.6	45.0	14.6	29.6	44.7	5.3	43.0
210	311832	15.0	50.0	46.1	17.5	34.6	50.5	6.5	45.8
525	377081	7.9	38.6	37.9	9.9	20.7	31.6	3.3	34.2
1103	433858	4.1	21.5	22.2	5.2	11.6	16.9	1.6	21.6
3000	514476	2.1	9.0	8.6	2.7	5.3	7.4	0.9	10.0
6921	610780	1.3	5.7	5.2	1.8	3.4	4.8	0.6	7.2

* Highlighted boxes are the flows at which the highest percent of preferred habitat per unit area is available.

Table 49. Equal weighting average percent (%) and rank order (lowest rank equals highest % preferred habitat) from 2D model results where GHSI>0.4.

2D Model GHSI>0.4 results, Weighted Average % Area and Rank Order to test for most preferred flow scenario

Dry (cfs)	Equal Weighting Average	Rank Order
5	31.7	21
10	34.3	13
20	30.6	16
30	27.3	23
45	20.8	32

Wet (cfs)	Equal Weighting Average	Rank Order
5	45.9	12
15	46.8	12
30	44.5	14
55	39.1	22
100	29.1	30
190	17.0	36
350	9.7	42

Snowmelt (cfs)	Equal Weighting Average	Rank Order
10	35.7	21
25	35.6	15
50	32.7	20
140	28.3	37
210	30.9	28
525	21.6	47
1103	12.6	56
3000	5.6	64
6921	3.8	72

* Highlighted boxes indicate the flow during each season with the highest estimated area using each metric.

**Lowest rank order indicates highest ranked % of preferred habitat

Table 50. Analysis metrics of 2D model results. Boxed flow indicates overall preferred flow (right column). Grey highlights indicate area analysis preferred flow; blue indicates % area preferred flow.

2D Model Results	Area (m^2) Metrics				% Area Metrics				Most Preferred Flows, All Metrics	
Dry (cfs)	weighted # occurrences with highest individual area*	Equal Weight Average	Rank Order	Most Preferred flow using Area metrics only	weighted # occurrences with highest individual %*	Equal Weight Average	Rank Order	Most Preferred flow using % Area metrics only	TOTAL All Metrics	Dry (cfs)
5	1.00			1.00	1.00			1.00	2.00	5
10	0.33			0.33	1.33	1	1	3.33	3.66	10
20	0.66		1	1.66	0.33			0.33	1.99	20
30	0.33	1		1.33	0.33			0.33	1.66	30
45	0.66			0.66	0.00			0.00	0.66	45
Wet (cfs)	weighted # occurrences with highest individual area	Equal Weight Average	Rank Order		weighted # occurrences with highest individual %	Equal Weight Average	Rank Order		TOTAL All Metrics	Wet (cfs)
5	0.00			0.00	1.3		0.5	1.83	1.83	5
15	0.83			0.83	1.0	1	0.5	2.50	3.33	15
30	0.50			0.50	0.7			0.66	1.16	30
55	1.66	1	1	3.66	0.0			0.00	3.66	55
100	0.00			0.00	0.0			0.00	0.00	100
190	0.00			0.00	0.0			0.00	0.00	190
350	0.00			0.00	0.0			0.00	0.00	350
Snowmelt (cfs)	weighted # occurrences with highest individual area	Equal Weight Average	Rank Order		weighted # occurrences with highest individual %	Equal Weight Average	Rank Order		TOTAL All Metrics	Snowmelt (cfs)
10	1.33			1.33	1.66			1.66	2.99	10
25	0.66			0.66	1.66	1	1	3.66	4.32	25
50	0.33		1	1.33	0.33			0.33	1.66	50
140	1.66			1.66	0.00			0.00	1.66	140
210	0.00	1		1.00	0.33			0.33	1.33	210
525	0.00			0.00	0.00			0.00	0.00	525
1103	0.00			0.00	0.00			0.00	0.00	1103
3000	0.00			0.00	0.00			0.00	0.00	3000
6921	0.00			0.00	0.00			0.00	0.00	6921

*This metric uses the weighted # of occurrences with highest individual area or percent divided by total number of species in a lifestage, then summed within lifestage. For example each adult and each juvenile occurrence of highest area during dry season is assigned a weight of .33 because there is a one in three possibility of a particular species having the highest area. Conversely, dry season RT fry is assigned a weight of 1, as it is the only representative of the fry lifestage. Thus, dry 5 cfs total # occurrences with highest individual area only occur for RT fry, so the total for that flow equates to 1. Alternately, in dry 45 flows, two of three adult lifestages have the highest available preferred area during this flow, thus the metric total for dry 45 is 0.66 (0.33 + 0.33).

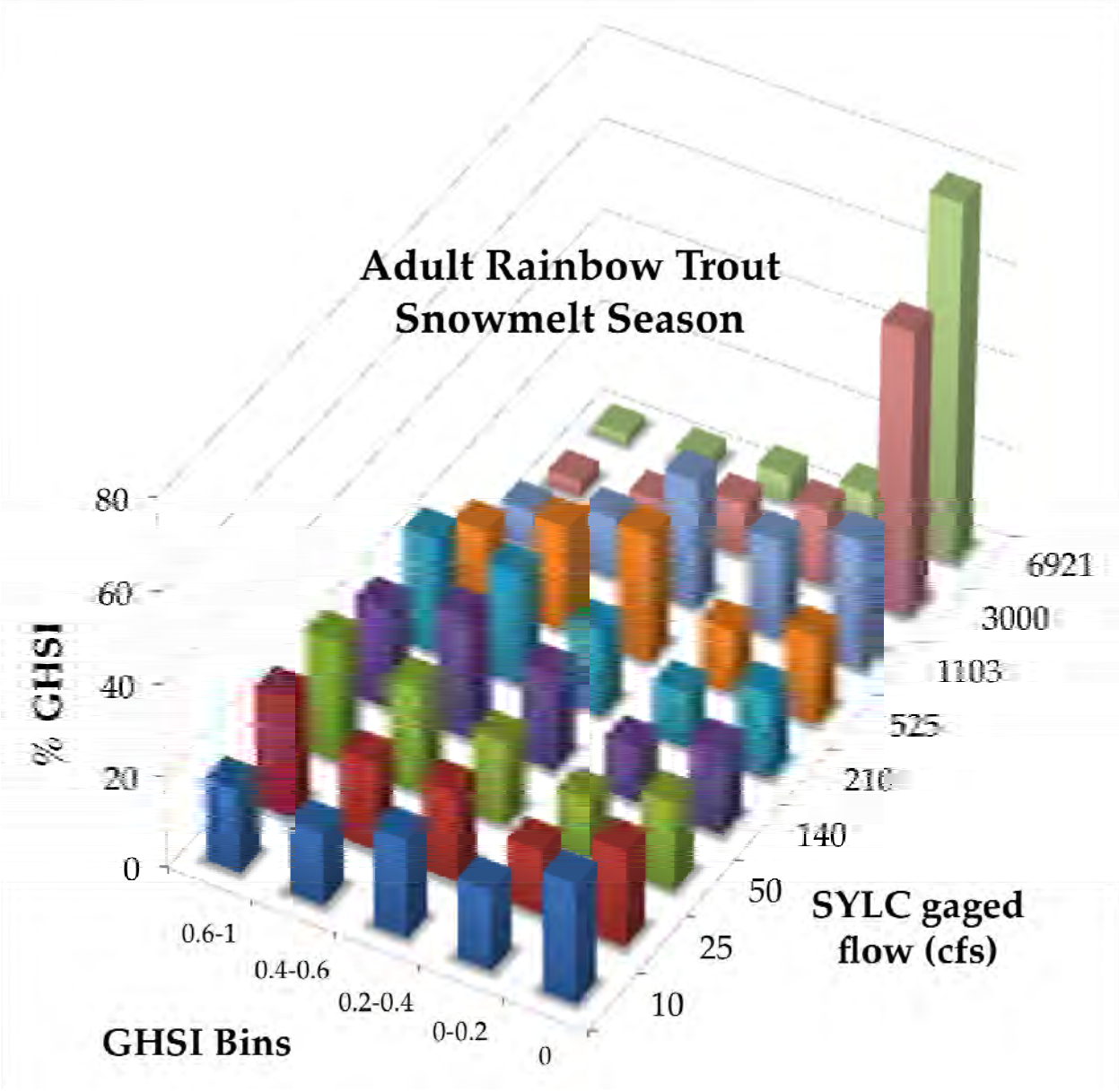

Figure 114. Snowmelt season rainbow trout adult lifestage 3-D graphical representation of 2D model results as GHSI binned distributions.

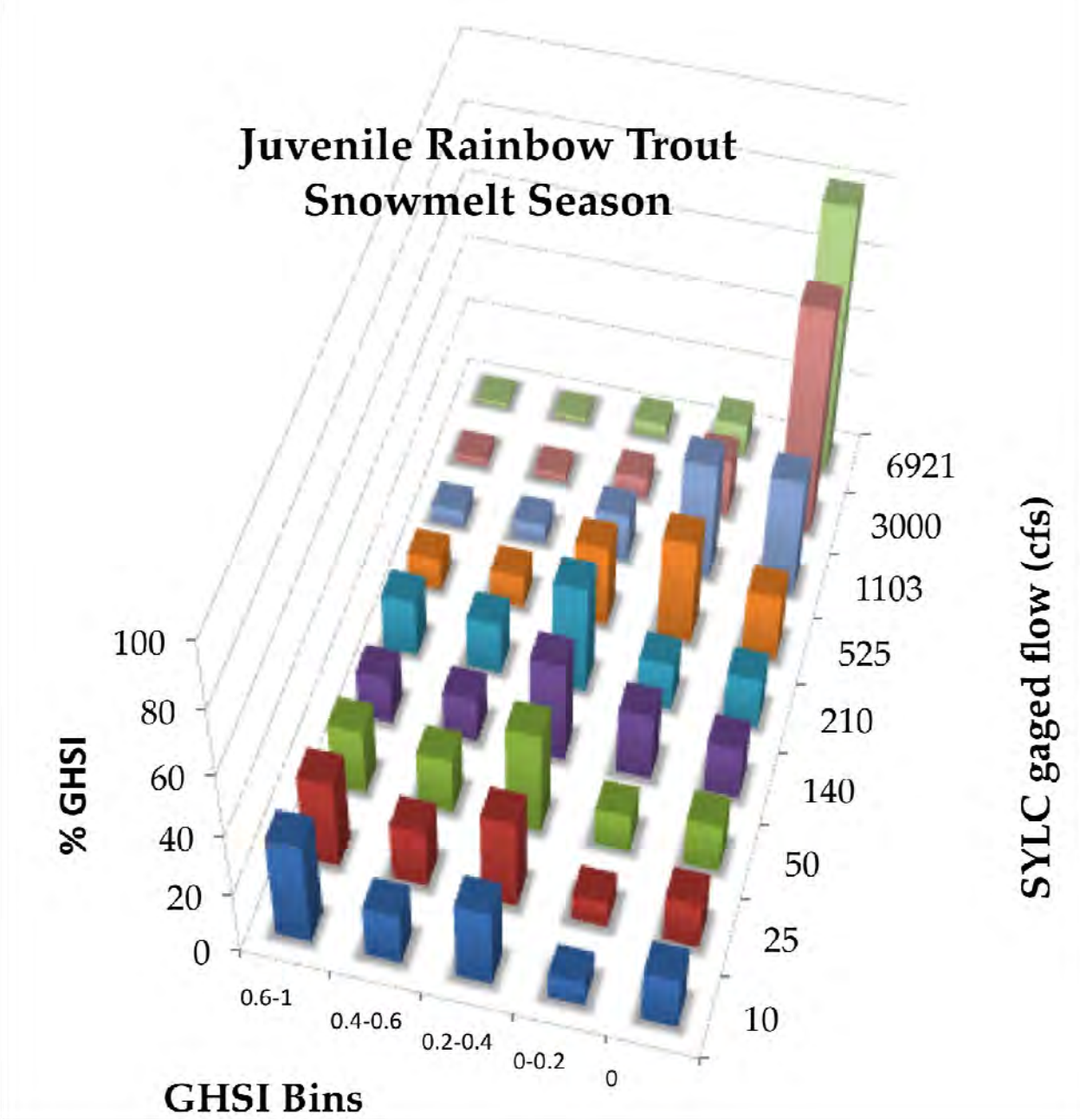

Figure 115. Snowmelt season rainbow trout juvenile lifestage 3-D graphical representation of 2D model results as GHSI binned distributions.

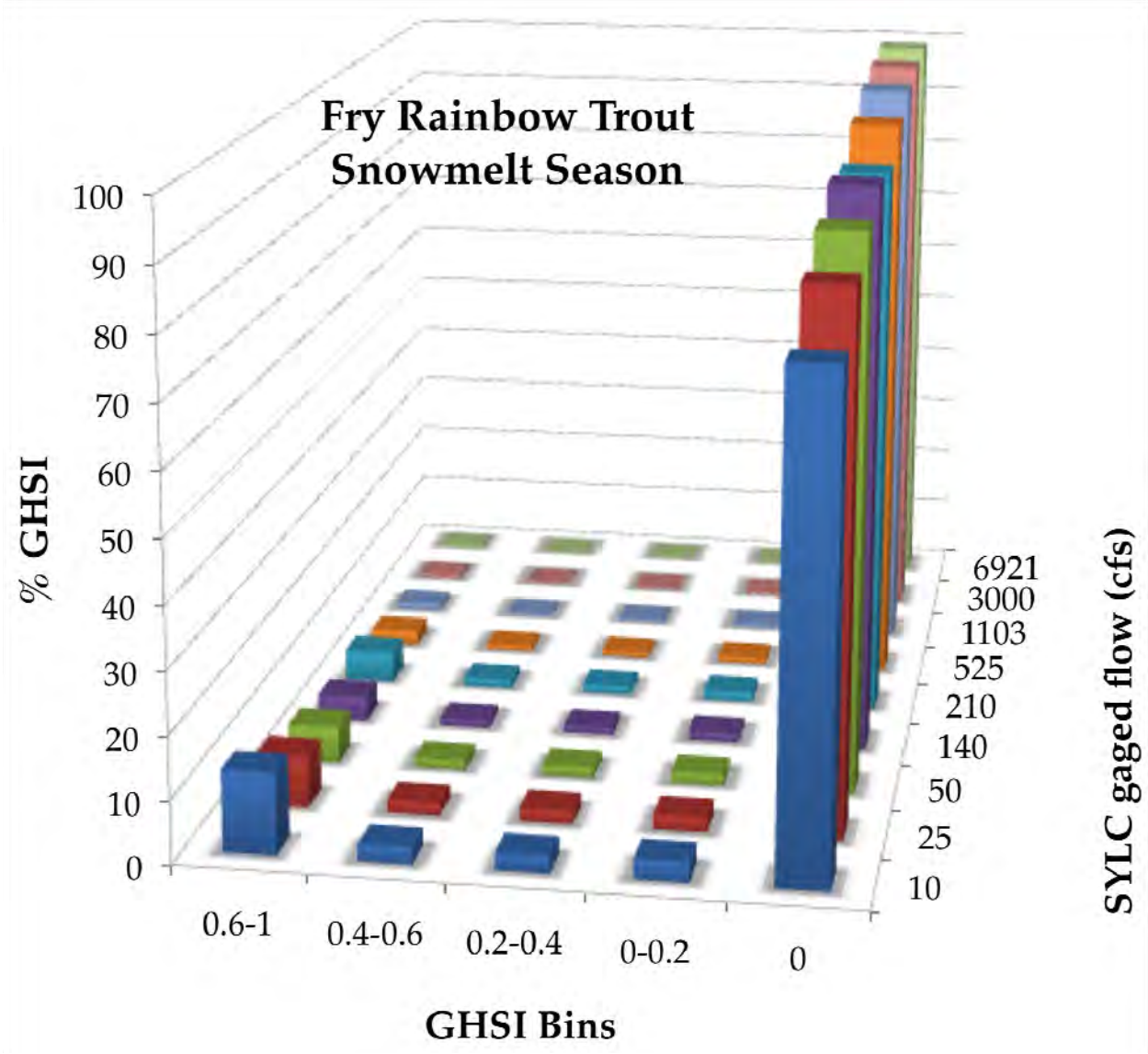

Figure 116. Snowmelt season rainbow trout fry lifestage 3-D graphical representation of 2D model results as GHSI binned distributions.

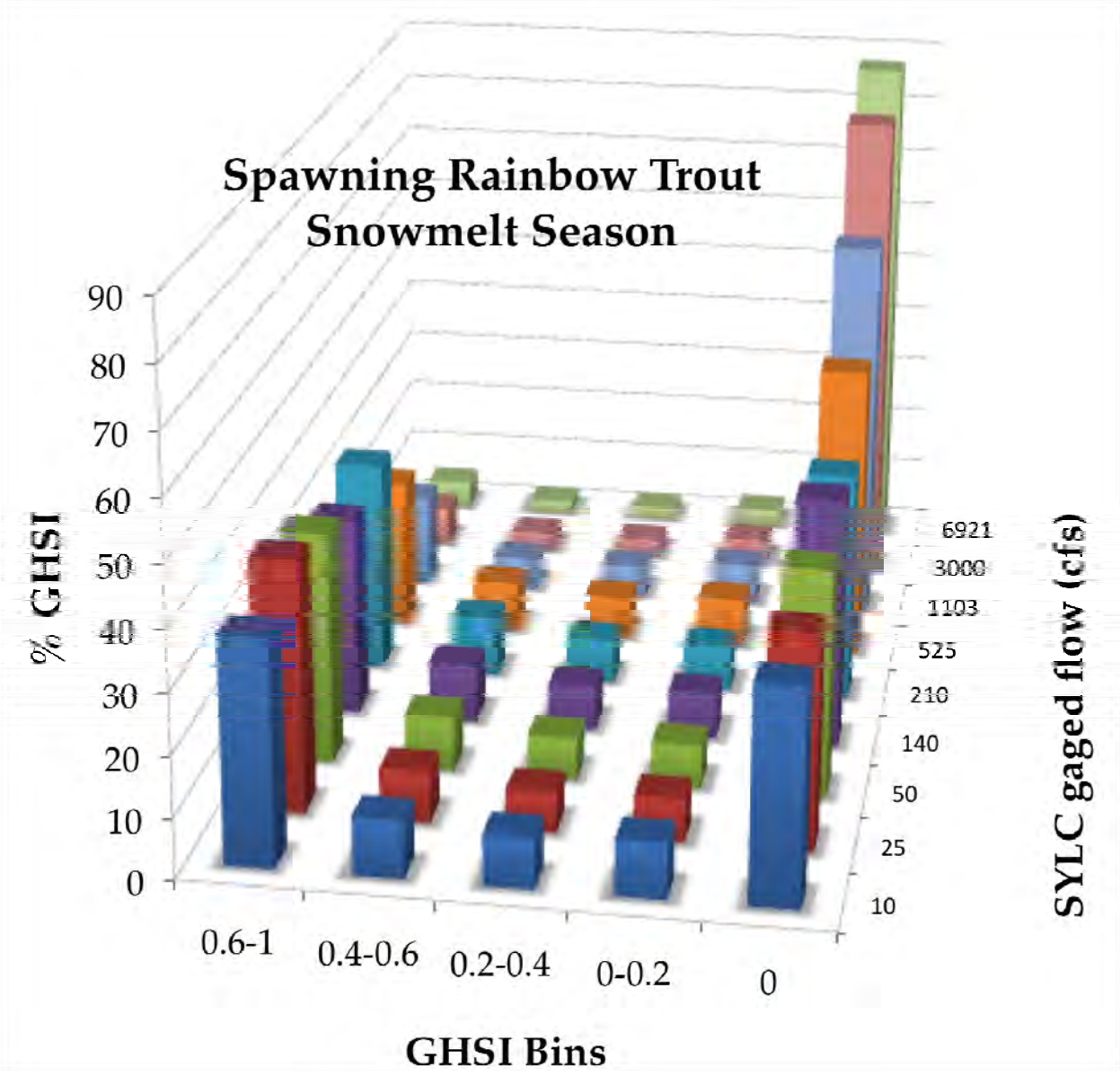

Figure 117. Snowmelt season rainbow trout spawning lifestage 3-D graphical representation of 2D model results as GHSI binned distributions.

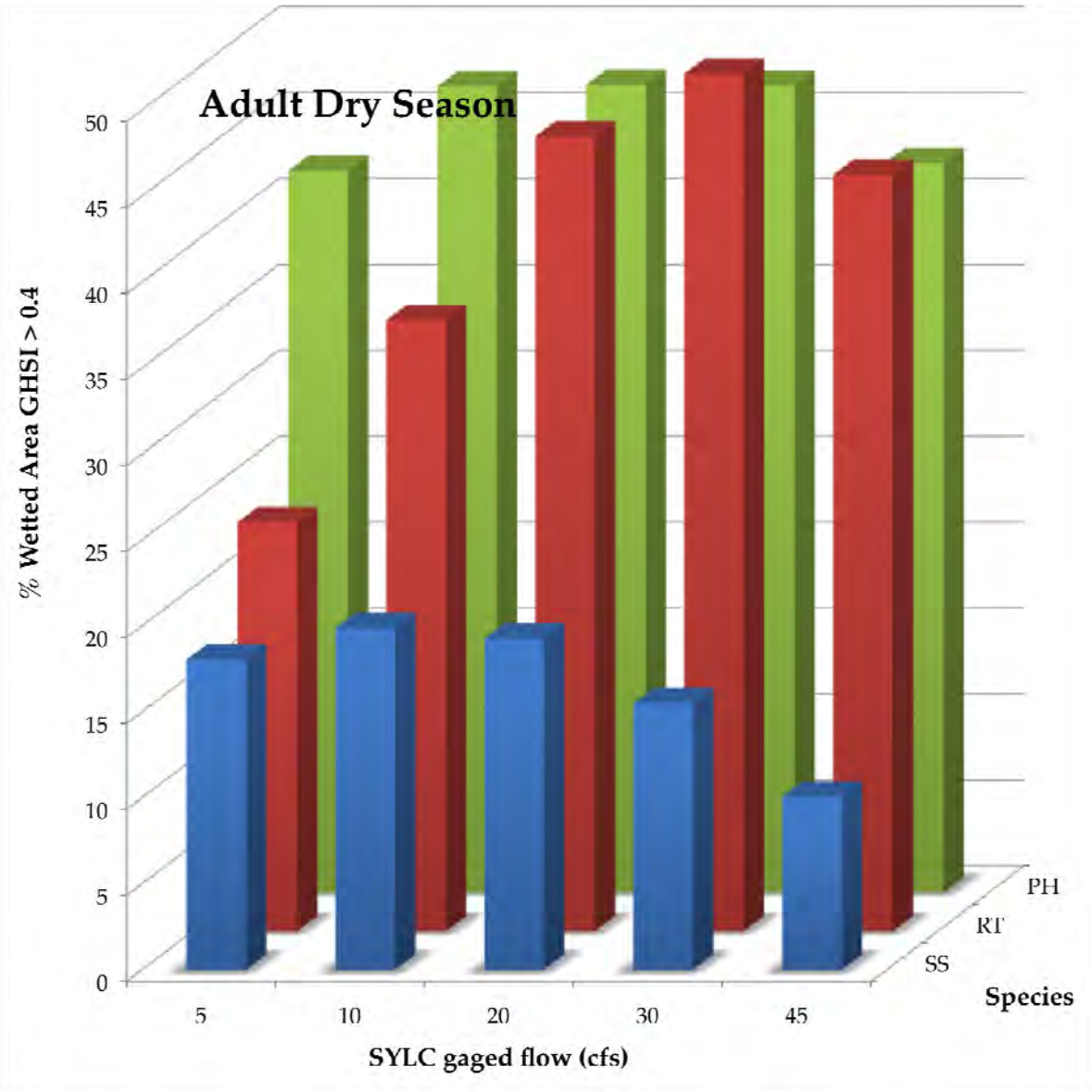

Figure 118. Dry season adult lifestage flow-dependent percent of the wetted study segment where the 2D model returned values of GHSI>0.4.

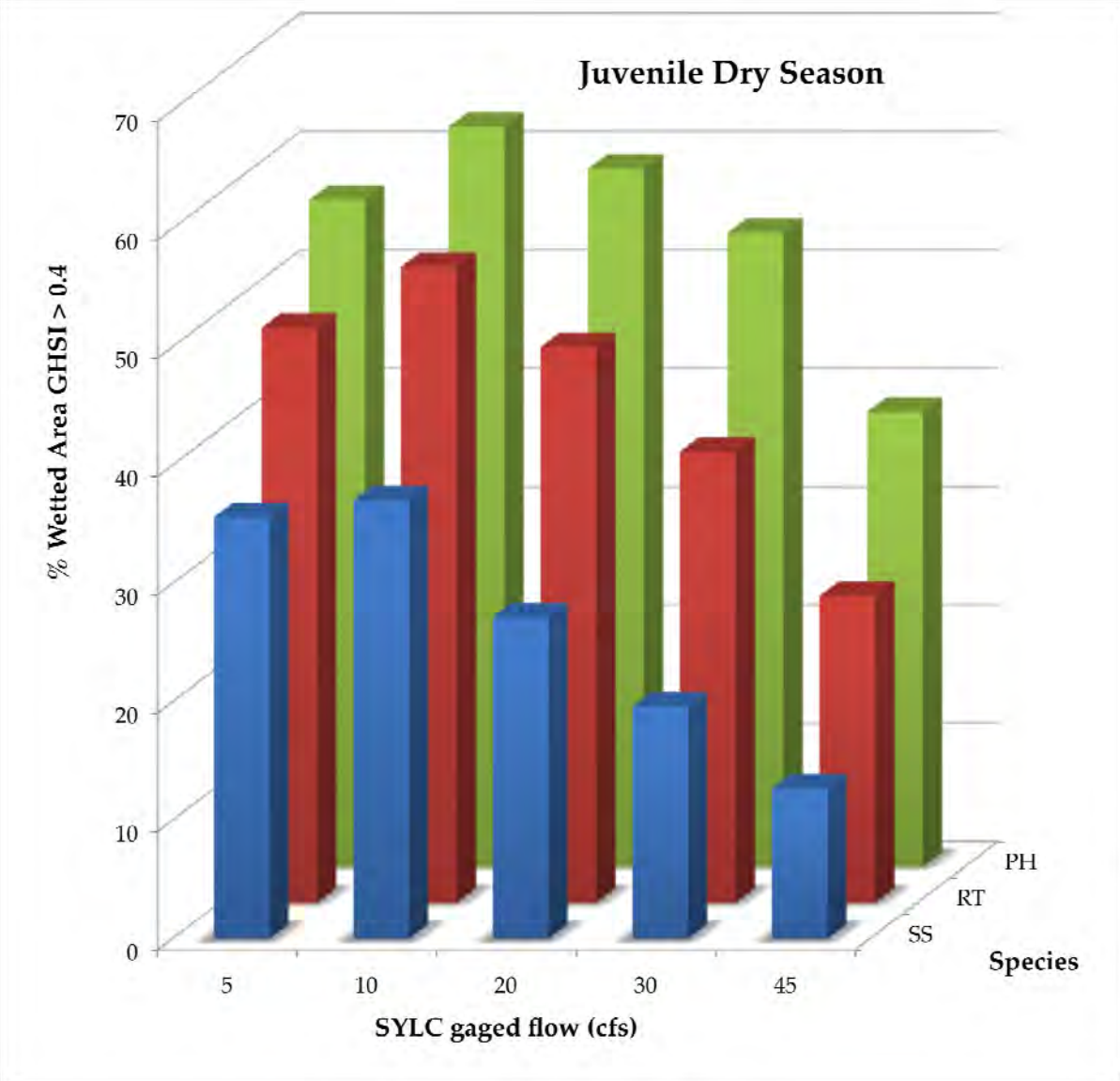

Figure 119. Dry season juvenile lifestage flow-dependent percent of the wetted study segment where the 2D model returned values of GHSI>0.4.

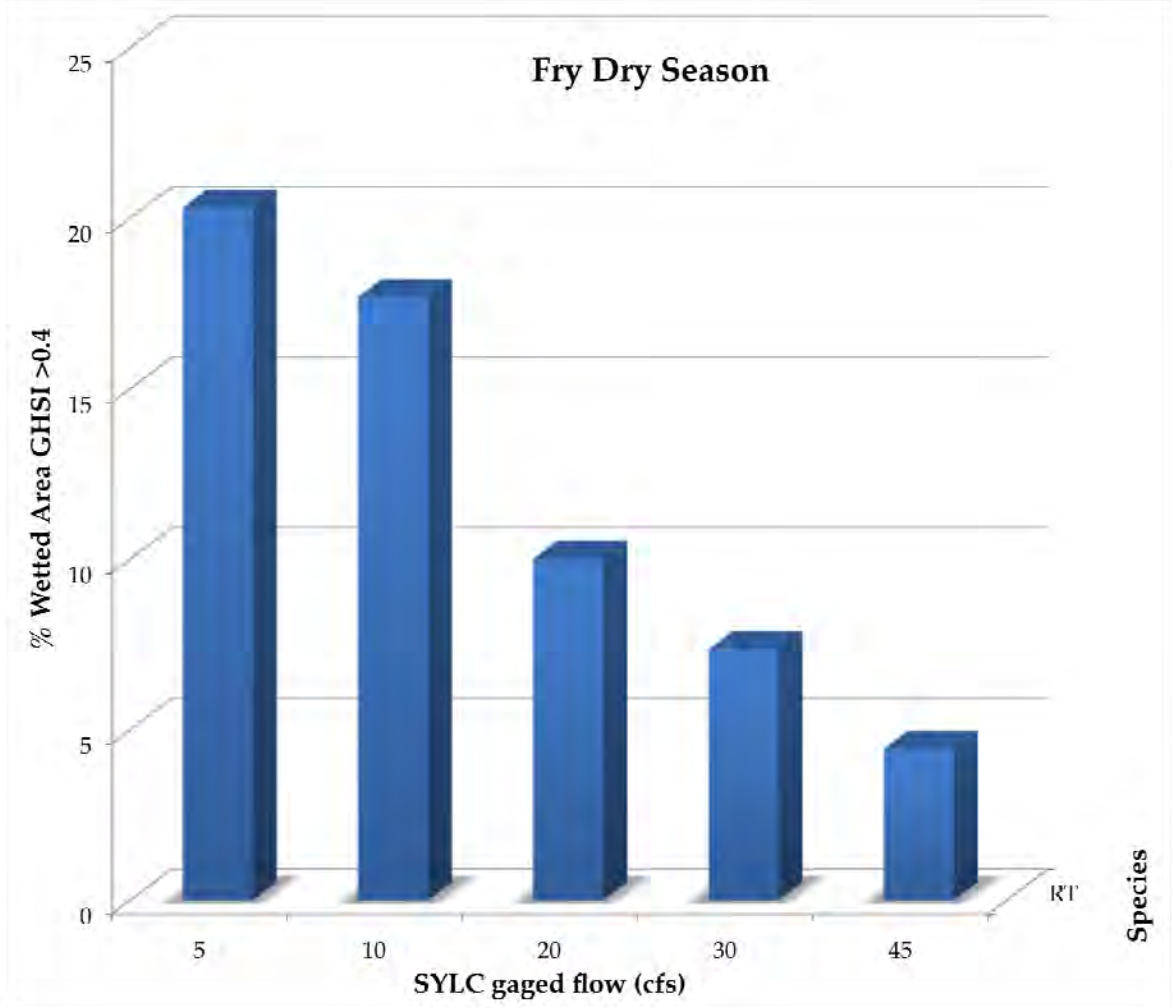

Figure 120. Dry season fry lifestage flow-dependent percent of the wetted study segment where the 2D model returned values of GHSI>0.4.

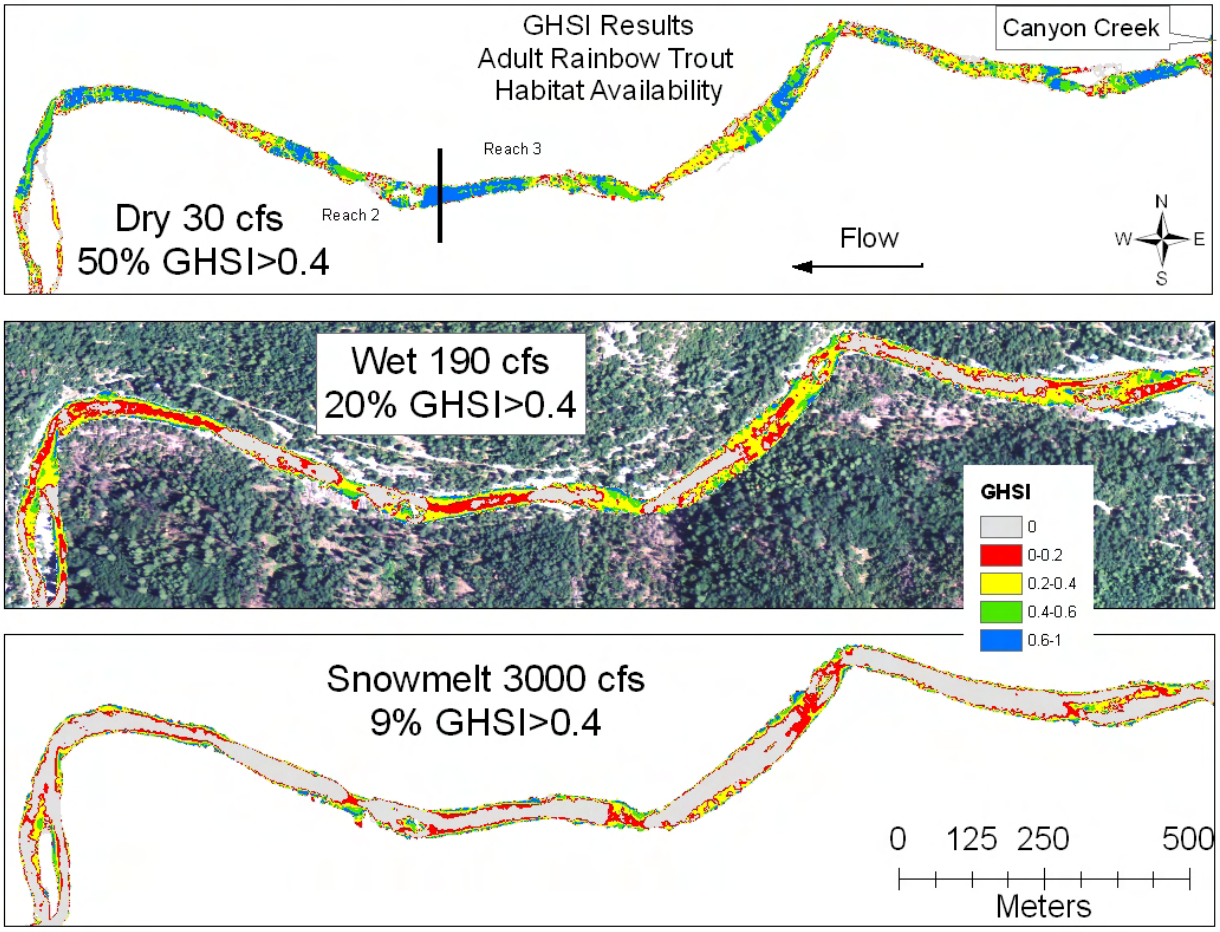

Figure 121. Example of season- and flow- rainbow trout adult preferred habitat in the upper part of Reach 2 and lower part of Reach 3, with Canyon Creek confluence just upstream of the image.

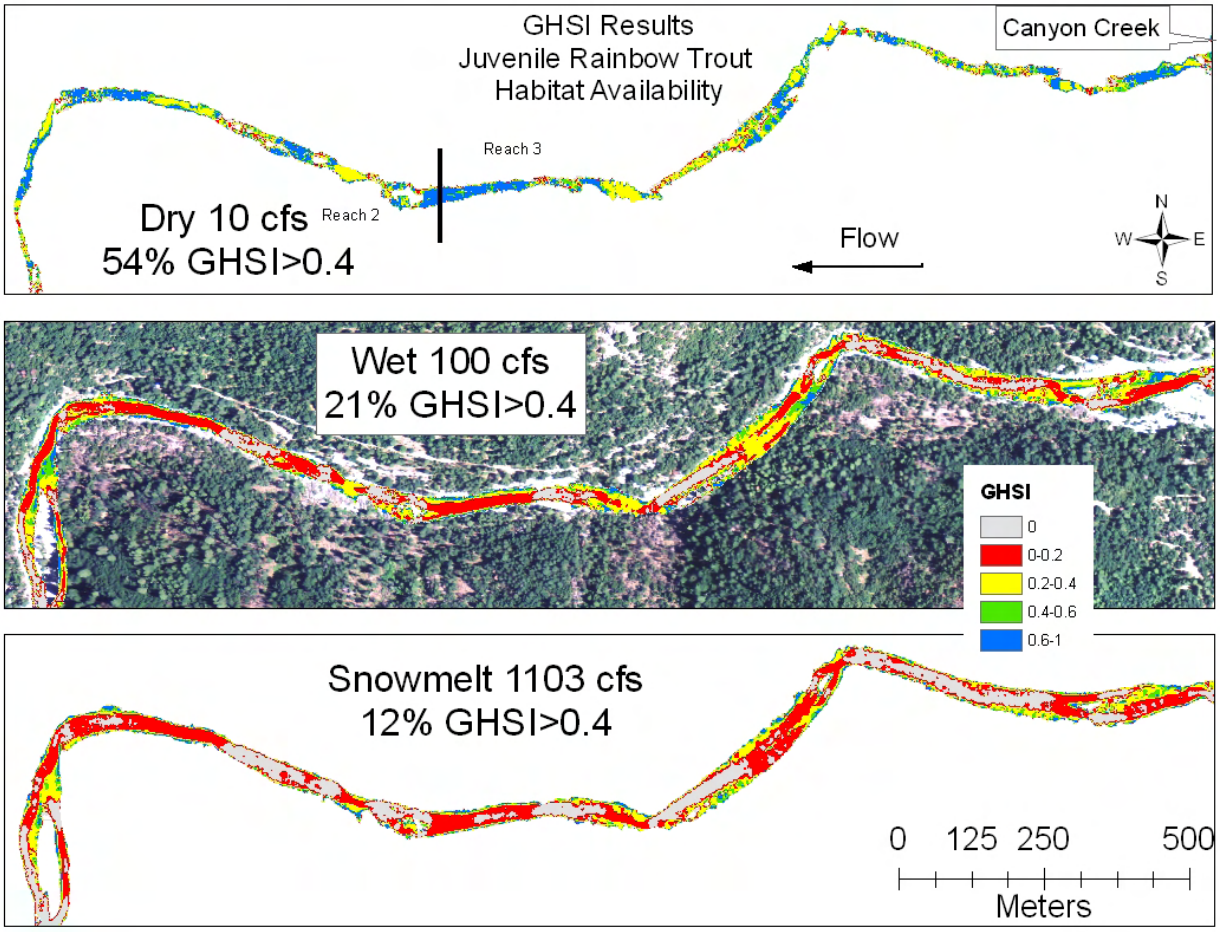

Figure 122. Example of season- and flow- rainbow trout juvenile preferred habitat in the upper part of Reach 2 and lower part of Reach 3, with Canyon Creek confluence just upstream of the image.

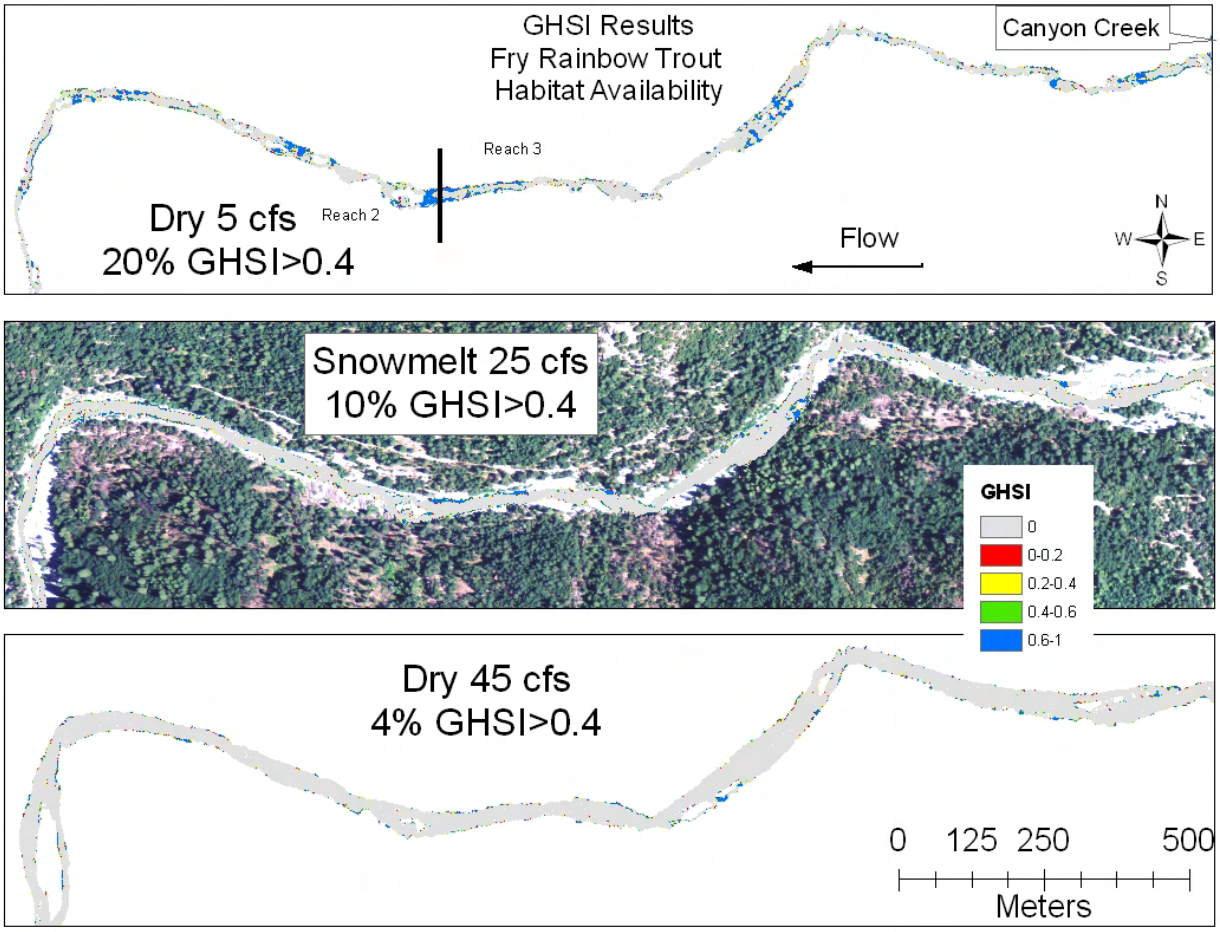

Figure 123. Example of season- and flow- rainbow trout fry preferred habitat in the upper part of Reach 2 and lower part of Reach 3, with Canyon Creek confluence just upstream of the image.

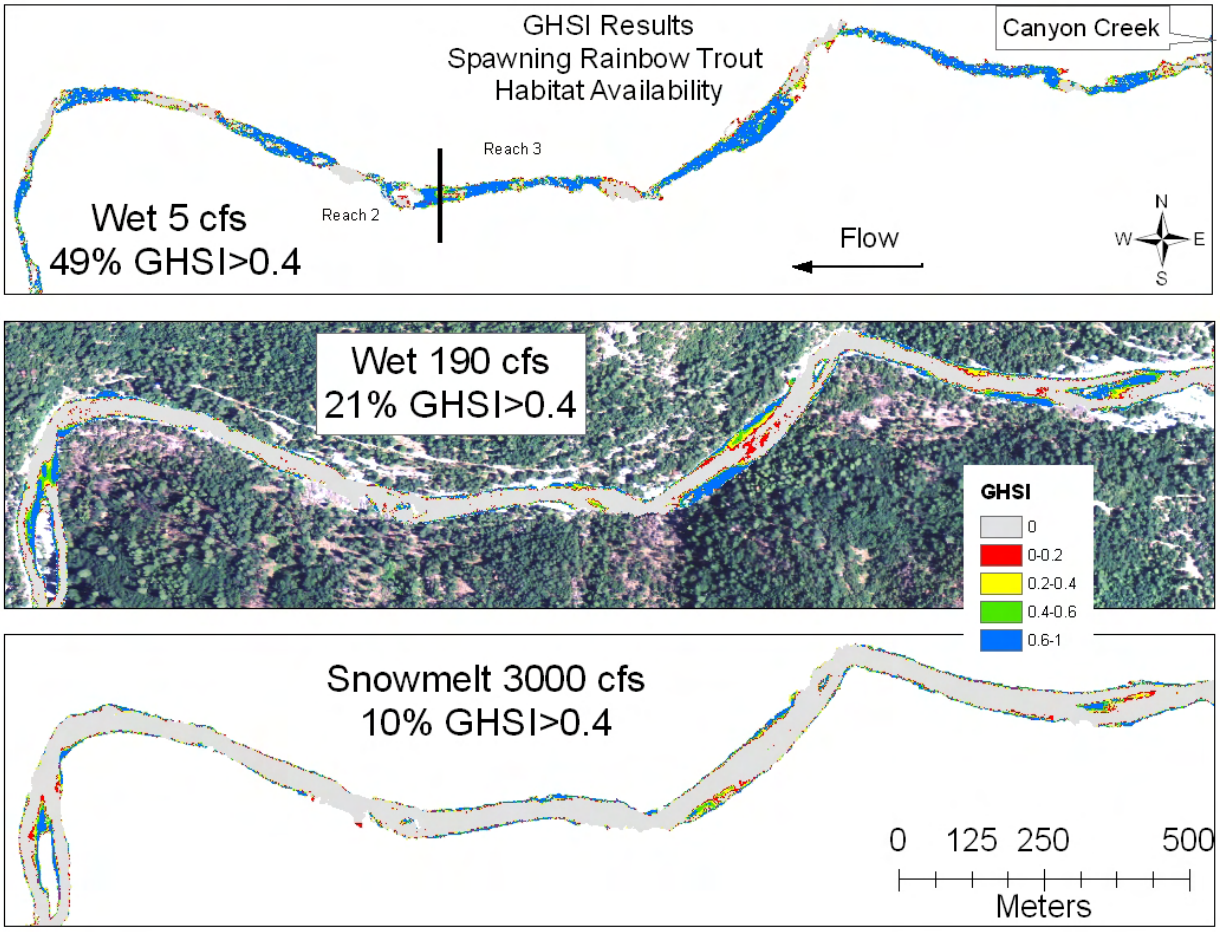

Figure 124. Example of season- and flow- rainbow trout spawner preferred habitat in the upper part of Reach 2 and lower part of Reach 3, with Canyon Creek confluence just upstream of the image.

11.4 Transect-based Microhabitat Analysis

11.4.1 Transect-based Physical Habitat Methods

In concert with a common approach to instream flow analysis, thirty transects were selected within the lower half of the study segment in easily accessible areas where there exist a diversity of morphological units (Chapter 6.0, section 8.6, 10.2). A key goal of obtaining these transects was to assess the effect of using a small number of samples to estimate accurate statistical characterization of microhabitat quality and area of preferred habitat. To achieve this controlled comparison, the analysis used the hydraulics from the 2D model to characterize the conditions at each point along each transect, thereby eliminating differences in hydraulic estimation/prediction from consideration. Consequently, this was not intended to be a test of the observation-based IFG4 tool within the PHABSIM program suite. What the analysis aimed to isolate was the single question of whether a small number of points can accurately represent the population of points in a long river segment. A test involving manual observations at cross-sections would not have accomplished this goal, as the test would then have used unequal data:

~1-m 2D model predictions versus empirical cross-section velocity and depth measures. Rather, the data for the 30 transects was explicitly extracted from the 2D model TINs representing depth and velocity. These data were assessed for their ability to represent morphological-unit populations and the population of the entire study segment. Transect-based sampling failed to accurately predict the hydraulics of morphological units, but it did yield a reasonable representation of the majority of the probability density functions for depth and velocity at the segment scale (section 10.2). As a result, it was worthwhile to propagate results to see what the effect would be on microhabitat assessment. As explained earlier, because this study matched 2D model hydraulics with transect-based sampling, the approach was termed the "2D transect" method.

The scheme used to determine the area of preferred habitat for each flow for each season with the 2D transect method involved five steps. First, GHSI values were computed at each 0.5-m spaced point across each transect. Second, points were stratified by morphological unit. Third morphological-unit-averaged GHSI values were computed. Fourth, each morphological unit type was binned by habitat quality category and simplified to preferred or avoided habitat. Fifth, unit types with preferred habitat were identified and their areas were summed to obtain the final result, the metric of total preferred habitat area for each species' lifestage. For the fifth step, two different ways of estimating area of each morphological unit with preferred habitat area were evaluated.

Based on this method, the 2D transect test for GHSI evaluated the combination of two effects. First, it tested the ability of transects to accurately estimate the morphological-unit average GHSI value as determined from the 2D model results (11.3.2). Second, it tested the ability of the transect method to estimate the area of preferred habitat based on the morphological units with preferred GHSI values >0.4. Testing the GHSI values themselves was straightforward, but accounting for areas was more challenging. One issue is that there is a mismatch in the concept of a flow-independent, laterally variable morphological unit versus a laterally uniform mesohabitat designation (section 8.4). The common approach to designating the mesohabitat type of transects involves assignment of a single mesohabitat type to a whole transect and all the points along it. No matter whether the flow is 10 or 1,000 cfs, a point out on the floodplain is the same mesohabitat type as a point in the center of a channel. As a result, the area of each mesohabitat simply scales with wetted area. Sometimes IFIM studies are only done for a small range of low flows, but often studies do include overbank flows, so this is a relevant concern.

In contrast, this study restricted morphological units to set areas on the basis of landform shape and size (section 8.4). The area of a single pool unit in this study did not change with flow, because the landform itself is fixed. For flows lower than baseflow, the wetted area has an unknown combination of morphological units for the transect method. For flows higher than baseflow, marginal areas outside the baseflow-wetted area were all designated as "floodplain". Since floodplain does not go across the channel, it is not represented by transects. The challenge was to determine what the area of transect-related morphologic units was, using this laterally variable scheme for characterizing them. In other words, using a more sophisticated approach to characterizing river features resulted in difficulties with using a simple transect approach. Consequently, a procedure was developed to account for areas below and above baseflow to facilitate the calculation of preferred area of habitat using transects.

For flows lower than baseflow, the solution involved calculating the area difference and the ratio of total wetted area between the flow of interest and baseflow (

Table 51). Then each morphological unit had its wetted area for that lower flow decreased by the same percent as was calculated for the total wetted area. This provided a simple area adjustment for lower flows that reflects the simplicity of the transect scheme (

Table 52). Although it would be possible to recalculate the actual wetted area of each morphological unit at lower flows in GIS, taking advantage of that additional information would not reflect what occurs with transect sampling, so that additional procedure was not done.

As flow increases above baseflow, all marginal areas outside the baseflow-wetted area were designated as floodplain. To account for this in the 2D transect method, the transect points on the floodplain at higher flows were assigned to the in-channel morphological-unit type that each transect was specified to represent (

Table 52). The morphological unit that dominated the thalweg of the channel at each transect became the designated morphologic-unit type for the complete transect. What this means is that the GHSI value of a specific transect designated as a pool might include plane bed, transition, and floodplain points; a steep inset channel might include inset channel, plane bed, as well as floodplain points (see Figure 55, Figure 56). The additional morphologic unit types were ignored and the entire baseflow-wetted channel was identified as the dominant morphologic unit type, while all areas above baseflow were defined as floodplain area. Transect points at 0.5-m intervals spanned the wetted channel at all flows, so each transect point-set was clipped in GIS to each wetted area flow shapefile. This resulted in some number of points at each end of each transect per flow, which were designated as floodplain points. Those points designated as floodplain at each flow were assigned the same morphological unit type as the original transect (Table 23, right-hand column). The total area of floodplain across the entire study segment was calculated for each flow and that area was distributed to each morphological unit type in proportion to the number of transect points for each unit type that had occurred on the floodplain (

Table 52).

Having determined the area of each morphological unit as a function of flow in terms of a transect-based method, the final step involved deciding how much of the total area of a unit type whose mean GHSI value was >0.4 should be considered preferred habitat. “Method A” involved an all-or-nothing strategy in which if the total area of a particular morphological unit type had a mean GHSI>0.4, then all area within the study segment designated as that unit type was considered preferred habitat, otherwise none of it was.

Table 53 shows Method A calculations performed for dry 5 cfs. The gray highlighted ratios are the mean GHSI values greater than 0.4 associated with a particular species' lifestage per morphological unit type. For example, pikeminnow/hardhead adult (PH Adult) mean GHSI values per morphologic unit are listed in the first row. Those units with an overall mean GHSI value >0.4 are highlighted in gray; the mean GHSI value for all transition area is 0.72, which is greater than 0.4, so all transition area (20,637 m^2) is designated as preferred habitat. Plane beds, on the other hand, have a mean GHSI value of 0.30, which is less than the necessary 0.4 value, so all plane bed area is considered avoided habitat, and thus a zero amount of area is assigned to plane bed for dry 5 cfs flows. Total possible area for each flow is found in

Table 52. “Method B” involved a proportional strategy in which the fraction of area of a particular morphological unit type with a mean GHSI>0.4 was equally assigned to the fraction of points identified as that unit type.

Table 59 shows Method B calculations for rainbow trout adults (RT Adult) for each flow during the dry season. In this method, rather than using an overall mean GHSI value, a calculation was performed to find what proportion of each morphological unit type had GHSI values >0.4. For instance, for dry 5 cfs, 33.5% of plane beds had values GHSI>0.4, whereas Method A found that overall, plane bed mean GHSI value was 0.30. Method A all or nothing designated plane beds as having no preferred habitat, whereas Method B proportionality assigned 33.5% of plane bed area as preferred habitat, for an area of 32,472 m^2 in dry 5 cfs (

Table 59; % GHSI>0.4 x total area = area assigned as preferred). Instream flow assessments might use either methodological approach when using transect-based analyses, so methods A and B were both evaluated. Tables and graphics depicting 2D transect results of percent distribution of GHSI categories, including those of low, very poor, and non-habitat, are available in Appendix D.

11.4.2 2D Transect Method A Results

The same styles of tables and metrics used to present and discuss 2D model results are used for all 2D transect results. Explanation of GHSI metrics can be found in section 11.3.1.

The area of preferred habitat (

Table 54) and percent area of preferred habitat (

Table 56) show RT adult dry 5 cfs available preferred habitat amounted to just 4784 m^2, or 1.8% of available area, while for dry 10 cfs, preferred habitat skyrocketed to 169119 m^2, or 64.7%. The reason for this dramatic difference is that morphologic unit values returned from dry 5 cfs results fell below the GHSI>0.4 threshold except for chutes, where GHSI = 0.57, versus the next highest GHSI value in transitions where GHSI = 0.38 (

Table 53). Thus, a very small total amount of area was considered preferred habitat for RT adults at dry season 5 cfs flow. The number of flows with habitat amounting to zero for a specific species' lifestage is significant using this method, 20% of dry season, 33% of wet season, and 44% of snowmelt season (

Table 54). Flows with zero habitat for every species and lifestage include wet season 350 cfs, snowmelt season 3000 cfs, and snowmelt 6921 cfs.

Weighted averages for preferred area (

Table 55) show wet season 15 cfs with the highest quantity of preferred habitat at 109,364 m^2, and rank order preference also returns wet 15 cfs. Snowmelt season 10 cfs returns preferred habitat of 141,368 m^2, but this time rank order returns a flow an order of magnitude higher, 210 cfs. Dry season 10 cfs returns highest area of preferred habitat at 109,364 m^2, while ranked order returns a higher flow preference of 30 cfs. The reason for the differences in flow preference may stem from the all or nothing approach of the method. Only if the overall average GHSI is >0.4 will the entire habitat within a specific morphologic unit be counted as habitat. This method resulted in many flows where zero preferred habitat was returned, which seems suspect even at the highest of the modeled flows, where some channel edge habitat should be available for fish species to hide in. Weighted averages, then, will suffer when zeroes are present, as this value is a legitimate result and thus must be considered in the weighted average calculation. Rank order, on the other hand, smoothed out the highs and lows of this method by ranking regardless of magnitude of differences or zeroes. Thus, available area in higher flows is at least partially reflected in the rank order analysis.

When analyzing preferred habitat per unit area (% area), absolute values no longer dominate. This can be seen in snowmelt season PH juvenile, where both 10 and 25 cfs return 92.6% of the wetted channel as preferred habitat, yet area-wise 25 cfs has over 30,000 m^2 more area. The same can be seen for all lifestages where more than one flow has the same % of preferred habitat (

Table 56). In this analysis, the equal weighting average and rank order return the same preferred flows (

Table 57); dry 10 cfs, wet 5 cfs, and snowmelt 10 cfs. These flows are markedly different than those of the area-only analysis of

Table 54 and

Table 55; dry 30 cfs, wet 15 cfs, and snowmelt 210 cfs.

A final metric, the weighted number of occurrences with highest individual area or % area, can be found in second and sixth columns of the analysis metrics table (

Table 58). Interestingly, once this metric was included in both the area and % area analyses, most preferred flow results dovetailed considerably. Refer to section 11.3.1 for complete descriptions of all metrics used in this analysis (same metrics as those used for the 2D model results).

2D transect Method A analysis metrics show that overall results are very similar when comparing metrics derived from total area of preferred habitat versus the % of preferred habitat per unit area (

Table 58). Specifically, the boxed flows in the right-hand column of

Table 58 indicate the overall best flow. Once the weighted # of occurrences was added to the equal weight result and the rank order result, the area metrics returned most preferred flows (highlighted in gray) of dry 10 cfs, wet 15 cfs, and snowmelt 10 cfs. Metrics for % area returned the same preferred flows (highlighted in blue) for dry and snowmelt season once all metrics were summed, with wet season returning 5 cfs as most preferred. And finally, the overall total of all metrics returned dry 10, wet 5, and snowmelt 10 cfs (boxed in right-hand column). This result shows that weighted # of occurrences could be considered a robust metric, as the addition of this metric closed the larger differences noted between area and % area metrics of

Table 55 and

Table 57. It is also notable that the results of the % area analysis were the same as the total of all metrics, suggesting that for this type of all-or-nothing analysis, % area may be a more robust metric than absolute area. Dry season 10 cfs, wet season 5 cfs, and snowmelt season 10 cfs received the highest overall totals and thus represent the flow that might best serve the most lifestages of the species present during the months of that specific season.

Taking a range of flows approach, dry season flows of 10 cfs appear to provide the most preferred habitat to the most species and lifestages during the months of August-November. Wet season flows of 5–15 cfs were most preferred for species' lifestages during the months of December-March. Snowmelt season flows of 10 cfs may be most advantageous for the species' lifestages present during the months April-July.

Table 51. Variance between observed baseflow area and model area per flow derived from raster-based area calculations.

Flow	Baseflow area (m^2)	Total modeled area (m^2)	Variance from baseflow area (m^2)	Ratio Total Area to baseflow
Dry (cfs)				
5	261,397	187,080	-74,318	0.72
10	261,397	198,471	-62,926	0.76
20	261,397	253,787	-7,610	0.97
30	261,397	295,294	33,897	1.13
45	261,397	344,483	83,086	1.32
Wet (cfs)				
5	261,397	226,555	-34,842	0.87
15	261,397	254,029	-7,368	0.97
30	261,397	285,995	24,597	1.09
55	261,397	325,174	63,777	1.24
100	261,397	369,243	107,846	1.41
190	261,397	425,183	163,786	1.63
350	261,397	499,551	238,153	1.91
Snowmelt (cfs)				
10	261,397	216,244	-45,154	0.83
25	261,397	253,122	-8,275	0.97
50	261,397	292,641	31,244	1.12
140	261,397	332,720	71,322	1.27
210	261,397	311,832	50,434	1.19
525	261,397	377,081	115,684	1.44
1103	261,397	433,858	172,461	1.66
3000	261,397	514,476	253,079	1.97
6921	261,397	610,780	349,383	2.34

Table 52. Allocation of area per flow to individual morphologic units.

Wetted Areas (m^2) Porportionally Allocated by Morphologic Unit for 2D Transect Method

Dry (cfs)	Transition	Plane Bed	Pool	Inset Channel	Chute	Steep Inset Channel	Step	TOTAL AREA
5	20637	96976	18468	33823	3424	13402	350	187080
10	21893	102881	19592	35882	3632	14218	371	198471
20	27995	131555	25053	45883	4645	18181	475	253787
30	31432	139267	26324	58039	5823	33921	489	295294
45	34345	145650	28414	75099	10149	50336	489	344483

Wet (cfs)	Transition	Plane Bed	Pool	Inset Channel	Chute	Steep Inset Channel	Step	TOTAL AREA
5	24991	117439	22365	40960	4146	16230	424	226555
15	28022	131681	25077	45927	4649	18198	475	254029
30	30071	138961	26299	54428	5649	30098	489	285995
55	32855	142432	27329	69165	8250	44653	489	325174
100	36707	148568	30527	82683	11711	58558	489	369243
190	41245	154932	36419	98044	19481	74573	489	425183
350	56020	160937	49651	117847	27200	87406	489	499551

Snowmelt (cfs)	Transition	Plane Bed	Pool	Inset Channel	Chute	Steep Inset Channel	Step	TOTAL AREA
10	23854	112094	21347	39096	3958	15491	404	216244
25	27922	131211	24987	45763	4633	18133	473	253122
50	30753	139337	26352	55892	5743	34074	489	292641
140	32976	144550	27491	71033	8465	47715	489	332720
210	31679	142515	26563	60531	6111	43943	489	311832
525	36292	150988	30585	86649	11285	60793	489	377081
1103	42189	158012	36488	98387	19665	78629	489	433858
3000	50910	167037	49654	120384	28042	97961	489	514476
6921	74295	178944	64115	138179	36496	118262	489	610780

Table 53. Example of area assigned to morphologic habitat units depending on GHSI greater than or less than 0.4. Blue highlights indicate GHSI>0.4, whereby all area for that morphologic unit is included in the GHSI>0.4 calculation.

Dry Season 5 (cfs) Flow Release at SYLC, Example of 2D Transect Method A Assignment of Areas When Average GHSI>0.4

	Transition	Plane Bed	Pool	Insct Channel	Chute	Steep Inset Channel	TOTAL AREA
PH Adult	0.72	0.30	0.83	0.11	0.64	0.10	
	20637	0	18468	0	3424	0	42529
PH Juvenile	0.87	0.63	0.64	0.32	0.81	0.23	
	20637	96976	18468	0	3424	0	139505
RT Adult	0.38	0.28	0.19	0.18	0.57	0.17	
	0	0	0	0	3424	0	3424
RT Fry	0.14	0.68	0.05	0.06	0.27	0.00	
	0	96976	0	0	0	0	96976
RT Juvenile	0.62	0.65	0.32	0.42	0.78	0.24	
	20637	96976	0	33823	3424	0	154860
SS Adult	0.65	0.04	0.26	0.00	0.40	0.00	
	20637	0	0	0	3424	0	24061
SS Juvenile	0.63	0.59	0.15	0.25	0.80	0.00	
	20637	96976	0	0	3424	0	121037

*Total possible area for dry 5 cfs flows equals 187,080 m^2, observed wetted area less step area of 350 m^2 where GHSI analyses were not conducted.

**GHSI value cells highlighted are those >0.4, preferred habitat for this species' lifestage.

Table 54. Area returned with GHSI>0.4 using 2D transect Method A.

Area (m^2) GHSI > 0.4 using 2D Transect Method A

		ADULT			JUVENILE			FRY	SPAWN
Dry (cfs)	Available Wetted Area (m^2)	SS	RT	PH	SS	RT	PH	RT	RT
5	187,080	24,061	3,424	42,529	121,037	154,860	139,505	96,976	na
10	198,471	25,526	128,407	45,118	128,407	164,289	183,882	102,881	na
20	253,787	27995	164,195	189,248	131,555	210,079	235,132	0	na
30	295,294	31,432	202,846	202,846	139,267	170,699	197,022	0	na
45	344,483	0	208,409	208,409	0	0	208,409	0	na

		ADULT			JUVENILE			FRY	SPAWN
Wet (cfs)	Available Wetted Area (m^2)	SS	RT	PH	SS	RT	PH	RT	RT
5	226,555	29,138	146,577	168,942	na	187,537	209,902	na	178,776
15	254,029	28,022	164,352	189,429	na	210,279	235,356	na	195,806
30	285,995	30,071	200,980	200,980	na	169,032	200,980	na	193,389
55	325,174	0	202,617	202,617	na	142,432	202,617	na	211,597
100	369,243	0	215,802	215,802	na	0	36,707	na	82,683
190	425,183	0	0	36,419	na	0	0	na	0
350	499,551	0	0	0	na	0	0	na	0

		ADULT			JUVENILE			FRY	SPAWN
Snowmelt (cfs)	Available Wetted Area (m^2)	SS	RT	PH	SS	RT	PH	RT	RT
10	216,244	27,811	139,905	161,252	139,905	179,001	200,348	112,094	170,638
25	253,122	32,555	163,765	188,753	131,211	209,528	234,515	0	195,107
50	292,641	30,753	202,186	286,409	**139,337**	170,090	202,186	0	195,229
140	332,720	32,976	205,017	205,017	0	144,550	205,017	0	215,583
210	311,832	31,679	206,868	206,868	0	174,194	206,868	0	203,047
525	377,081	0	217,865	217,865	0	0	217,865	0	147,442
1103	433,858	0	36,488	78,677	0	0	0	0	0
3000	514,476	0	0	0	0	0	0	0	0
6921	610,780	0	0	0	0	0	0	0	0

*Highlighted boxes indicate flows at which the highest estimated area of preferred habitat is available for a species' lifestage.

Table 55. 2D transect Method A results equal weighting average area (m^2) and rank order, where lowest rank equals highest amount of preferred habitat.

2D transect Method A results, Weighted Average Area (m^2) and Rank Order to test for most preferred flow scenario

Dry (cfs)	Equal Weighting Average	Rank Order**
5	86,260	29
10	109,364	22
20	103,357	15
30	**104,901**	14
45	69,470	22

Wet (cfs)	Equal Weighting Average	Rank Order
5	164,127	20
15	181,964	15
30	**174,135**	17
55	173,067	16
100	81,635	21
190	4,047	33
350	0	34

Snowmelt (cfs)	Equal Weighting Average	Rank Order
10	141,368	32
25	128,804	23
50	134,721	25
140	119,944	24
210	**119,635**	22
525	91,327	29
1103	9,597	46
3000	0	48
6921	0	48

* Highlighted boxes indicate flow each season with the highest estimated area using equal weighted average metric.

**Lowest rank order indicates highest ranked area of preferred habitat

Table 56. Percent area of GHSI>0.4 using 2D transect Method A.

% Area GHSI >0.4 using 2D Transect Method A

		ADULT			JUVENILE			FRY	SPAWN
Dry (cfs)	Available Wetted Area (m^2)	SS	RT	PH	SS	RT	PH	RT	RT
5	187,080	12.9	1.8	22.7	64.7	82.8	74.6	51.8	na
10	198,471	12.9	64.7	22.7	64.7	82.8	92.6	51.8	na
20	253,787	11.4	64.7	74.6	51.8	82.8	92.6	0.0	na
30	295,294	10.6	68.7	68.7	47.2	57.8	66.7	0.0	na
45	344,483	0.0	60.5	60.5	0.0	0.0	60.5	0.0	na

		ADULT			JUVENILE			FRY	SPAWN
Wet (cfs)	Available Wetted Area (m^2)	SS	RT	PH	SS	RT	PH	RT	RT
5	226,555	12.9	64.7	74.6	na	82.8	92.6	na	78.9
15	254,029	11.0	64.7	74.6	na	82.8	92.6	na	77.1
30	285,995	10.5	70.3	70.3	na	59.1	70.3	na	67.6
55	325,174	0.0	62.3	62.3	na	43.8	62.3	na	65.1
100	369,243	0.0	58.4	58.4	na	0.0	9.9	na	22.4
190	425,183	0.0	0.0	8.6	na	0.0	0.0	na	0.0
350	499,551	0.0	0.0	0.0	na	0.0	0.0	na	0.0

		ADULT			JUVENILE			FRY	SPAWN
Snowmelt (cfs)	Available Wetted Area (m^2)	SS	RT	PH	SS	RT	PH	RT	RT
10	216,244	12.9	64.7	74.6	64.7	82.8	92.6	51.8	78.9
25	253,122	12.9	64.7	74.6	51.8	82.8	92.6	0.0	77.1
50	292,641	10.5	69.1	97.9	47.6	58.1	69.1	0.0	66.7
140	332,720	9.9	61.6	61.6	0.0	43.4	61.6	0.0	64.8
210	311,832	10.2	66.3	66.3	0.0	55.9	66.3	0.0	65.1
525	377,081	0.0	57.8	57.8	0.0	0.0	57.8	0.0	39.1
1103	433,858	0.0	8.4	18.1	0.0	0.0	0.0	0.0	0.0
3000	514,476	0.0	0.0	0.0	0.0	0.0	0.0	0.0	0.0
6921	610,780	0.0	0.0	0.0	0.0	0.0	0.0	0.0	0.0

* Highlighted boxes indicate the flows at which the highest percent of preferred habitat per unit area is available.

Table 57. 2D transect Method A weighted average % area and rank order, where lowest value indicated highest amount of preferred habitat per unit area.

2D transect Method A results, Weighted Average Area (%) and Rank Order to test for most preferred flow scenario

Dry (cfs)	Equal Weighting Average	Rank Order**
5	46.1	18
10	55.1	11
20	42.0	14
30	35.5	21
45	20.2	29

Wet (cfs)	Equal Weighting Average	Rank Order
5	72.4	7
15	71.6	9
30	60.9	16
55	53.2	24
100	22.1	29
190	1.0	33
350	0.0	34

Snowmelt (cfs)	Equal Weighting Average	Rank Order
10	65.4	11
25	50.9	14
50	46.0	19
140	36.0	36
210	38.4	28
525	24.2	42
1103	2.2	46
3000	0.0	48
6921	0.0	48

* Highlighted boxes indicate the flow during each season with the highest estimated percent using equal weighting metric.

**Lowest rank order indicates highest ranked area of preferred habitat

Table 58. Analysis metrics of 2D transect Method A results. Boxed flow indicates overall preferred flow (right column). Boxed but not highlighted flows in right column indicate all analysis methods agree on boxed flow. Grey highlights indicate area analysis preferred flow; blue indicates % area preferred flow.

2D transect Method A	Area (m^2) Metrics				% Area Metrics				Most Preferred Flows, All Metrics	
Dry (cfs)	weighted # occurrences with highest individual area*	Equal Weight Average	Rank Order	Most Preferred flow using Area metrics only	weighted # occurrences with highest individual %*	Equal Weight Average	Rank Order	Most Preferred flow using % Area metrics only	TOTAL All Metrics	Dry (cfs)
5	0.00			0.00	2.00			2.00	2.00	5
10	1.00	1		2.00	2.00	1	1	4.00	6.00	10
20	0.66			0.66	1.00			1.00	1.66	20
30	0.66		1	1.66	0.33			0.33	1.99	30
45	0.66			0.66	0.00			0.00	0.66	45
Wet (cfs)	weighted # occurrences with highest individual area	Equal Weight Average	Rank Order	Most Preferred flow using Area metrics only	weighted # occurrences with highest individual %	Equal Weight Average	Rank Order	Most Preferred flow using % Area metrics only	TOTAL All Metrics	Wet (cfs)
5	0.00			0.00	2.3	1	1	4.33	4.33	5
15	1.00	1	1	3.00	1.0			1.00	4.00	15
30	0.33			0.33	0.3			0.33	0.66	30
55	1.00			1.00	0.0			0.00	1.00	55
100	0.66			0.66	0.0			0.00	0.66	100
190	0.00			0.00	0.0			0.00	0.00	190
350	0.00			0.00	0.0			0.00	0.00	350
Snowmelt (cfs)	weighted # occurrences with highest individual area	Equal Weight Average	Rank Order	Most Preferred flow using Area metrics only	weighted # occurrences with highest individual %	Equal Weight Average	Rank Order	Most Preferred flow using % Area metrics only	TOTAL All Metrics	Snowmelt (cfs)
10	1.33	1		2.33	3.33	1	1	5.33	7.66	**10**
25	0.66			0.66	1.00			1.00	1.66	25
50	0.33			0.33	0.66			0.66	0.99	50
140	1.33			1.33	0.00			0.00	1.33	140
210	0.00		1	1.00	0.00			0.00	1.00	210
525	0.33			0.33	0.00			0.00	0.33	525
1103	0.00			0.00	0.00			0.00	0.00	1103
3000	0.00			0.00	0.00			0.00	0.00	3000
6921	0.00			0.00	0.00			0.00	0.00	6921

*This metric uses the weighted # of occurrences with highest individual area or percent divided by total number of species in a lifestage, then summed within lifestage. For example each adult and each juvenile occurrence of highest area during dry season is assigned a weight of .33 because there is a one in three possibility of a particular species having the highest area. Conversely, dry season RT fry is assigned a weight of 1, as it is the only representative of the fry lifestage. Thus, dry 5 cfs total # occurrences with highest individual area only occur for RT fry, so the total for that flow equates to 1. Alternately, in dry 45 flows, two of three adult lifestages have the highest available preferred area during this flow, thus the metric total for dry 45 is 0.66 (0.33 + 0.33).

11.4.3 2D Transect Method B Results

The area of preferred habitat (

Table 60) and percent area of preferred habitat (

Table 62) of 2D transect method B show available habitat at every flow for every lifestage, a significant difference from 2D transect Method A results. Because percent area is calculated as a per unit area value, the highest preferred area can vary from the highest absolute area (m^2). This difference can be seen in adult SS, where in dry season the most area of preferred habitat occurs at 30 cfs with 64,071 m^2, while for % area the highest preference occurs in dry 20 cfs at 23.5% of available area.

Weighted averages (

Table 61) show wet season 30 cfs with the highest quantity of preferred habitat at 167,721 m^2, and rank order preference also returns wet 30 cfs. Snowmelt season 210 cfs returns preferred habitat of 132,892 m^2, and rank order returns the same flow, 210 cfs. Dry season 30 cfs returns highest area of preferred habitat at 110,031 m^2, while again ranked order returns a similar flow preference of 30 cfs, although a tie occurs here, with dry 20 cfs also a preferred flow.

The % area of preferred habitat (

Table 62) shows that more than one flow has the same %, which allows efficiency of habitat to gain significance rather than absolute value of area. RT juvenile in dry season is an example of three flows (5, 10, and 15 cfs) containing close to the same % area of preferred habitat (65.9%, 72.5%, and 70.0%, respectively), while area varied by over 50,000 m^2 (123,238 m^2, 143,838 m^2, and 177,561 m^2, respectively). Equal weighting averages of the % areas return preferred flows of dry 10 cfs, wet 15 cfs, and snowmelt 10 cfs (

Table 63). The rank order analysis returned preferred flows of dry 20 cfs, wet 15 and 30 cfs, and snowmelt 25 cfs.

The weighted number of occurrences with highest individual area (column two) or % area (column six) can be found in the analysis metrics table (

Table 64). Once this metric was included in both the area and % area analyses, preferred flow results dovetailed to some degree, though less than was the case in 2D transect Method A.

2D transect Method B metrics (

Table 64) show that results are similar when considering total area of preferred habitat versus the % of preferred habitat per unit area, with the exception of snowmelt flows. For the area metrics, the overall preferred flows were dry 30, wet 30, and 210 cfs. For % area metrics, overall preferred flow were dry 20, wet 15, and snowmelt 10 cfs. The boxed flows in the right-hand column of

Table 64 indicate the overall best flow, which takes into consideration all area and % area metrics. Dry season 20 cfs, wet season 30 cfs, and snowmelt season 210 cfs received the highest overall totals (boxed) and thus represent the flow that might best serve the most lifestages of the species present during the months of that specific season. Each boxed flow also represents either the flow most preferred by the area method or the % area method, but never both. The preferred flow for the area metric in wet and snowmelt seasons also were the most preferred flows totaling all metrics, while in the dry season the % area method was also the most preferred flow. Method B, which used a significantly different approach to amount of GHSI>0.4 area, produced better results using the area metrics (2 of 3 most preferred seasonal flows) rather than the % area metrics results that were more robust in Method A (3 of 3 most preferred seasonal flows). The results of Method B exhibit a large degree of variability in the preferred snowmelt flows (from 10 cfs to 210 cfs), while dry and wet seasons have less variability, falling within one 2D model simulation increment (i.e. dry season from 20 to 30 cfs).

Taking a range of flows approach, dry season flows of 20–30 cfs appear to provide the most preferred habitat to the most species and lifestages during the months of August-November. Wet season flows of 15–30 cfs were most preferred for species' lifestages during the months of December-March. Snowmelt season flows of 10 and 210 cfs may be most advantageous for the species' lifestages present during the months April-July.

Table 59. Application of 2D transect Method B to determine area of a morphologic unit assigned a GHSI>0.4 value.

Rainbow Trout Adult Dry Season Example

% of Morpho Units With GHSI>0.4, 2D Transect Method B

Flow (cfs)	Transition	Plane Bed	Pool	Inset Channel	Chute	Steep Inset Channel
5	49.1	33.5	3.4	23.8	72.9	14.5
10	69.4	52.9	10.4	35.7	76.9	7.9
20	81.3	74.7	32.9	52.0	84.9	25.6
30	83.5	83.9	75.2	47.1	56.4	19.3
45	63.5	75.1	78.2	41.2	25.6	23.1

Area (m^2)*	Possible Area (m^2) per Morphologic Unit at Dry 5 cfs					
	Transition	Plane Bed	Pool	Inset Channel	Chute	Steep Inset Channel
187080	20637	96976	18468	33823	3424	13402

Area (m^2) GHSI>0.4, Calculated as % Morpho Unit * Possible Area * 0.01

Flow (cfs)	Transition	Plane Bed	Pool	Inset Channel	Chute	Steep Inset Channel
5	10132	32472	634	8053	2495	1940
10	14329	51293	1916	12080	2634	1053
20	16772	72477	6074	17598	2906	3427
30	17234	81335	13890	15940	1932	2591
45	13095	72801	14444	13940	875	3095

*Less step area of 350 m^2, which was not analyzed for GHSI values

Table 60. Area (m2) where 2D transect Method B results returned a suitability index of medium or high quality habitat (i.e. GHSI > 0.4) per species, lifestage, and flow regime.

Area (m^2) GHSI > 0.4 using 2D Transect Method B

		ADULT			JUVENILE			FRY	SPAWN
Dry (cfs)	Available Wetted Area (m^2)	SS	RT	PH	SS	RT	PH	RT	RT
5	187,080	24,864	55,725	76,032	86,487	123,238	112,622	74,096	na
10	198,471	32,980	88,377	101,165	107,369	143,838	145,739	66,303	na
20	253,787	59,667	161,777	167,902	129,518	177,561	194,854	36,996	na
30	295,294	64,071	200,049	193,618	83,231	153,979	206,518	29,604	na
45	344,483	35,268	198,529	204,204	57,159	109,090	162,241	17,602	na

		ADULT			JUVENILE			FRY	SPAWN
Wet (cfs)	Available Wetted Area (m^2)	SS	RT	PH	SS	RT	PH	RT	RT
5	226,555	47,445	126,293	130,810	na	167,727	173,835	na	151,967
15	254,029	60,031	164,119	168,043	na	177,788	195,319	na	167,306
30	285,995	76,917	197,799	190,098	na	157,578	205,342	na	166,764
55	325,174	48,184	214,882	205,473	na	129,112	196,283	na	163,029
100	369,243	29,683	175,300	171,884	na	97,911	140,081	na	129,841
190	425,183	11,071	108,259	100,644	na	63,483	84,283	na	100,710
350	499,551	8,327	63,730	39,499	na	28,712	38,584	na	63,980

		ADULT			JUVENILE			FRY	SPAWN
Snowmelt (cfs)	Available Wetted Area (m^2)	SS	RT	PH	SS	RT	PH	RT	RT
10	216,244	37,518	99,784	113,117	116,677	158,444	160,576	67,051	141,435
25	253,122	57,568	160,459	167,119	131,651	179,830	195,752	38,445	168,732
50	292,641	77,877	199,927	194,419	89,628	160,030	206,728	32,845	171,221
140	332,720	46,950	214,991	205,953	69,109	130,681	210,390	22,919	167,922
210	311,832	86,497	208,457	201,625	86,495	163,738	213,336	27,933	183,585
525	377,081	29,558	209,059	213,377	50,786	109,808	162,750	12,768	144,979
1103	433,858	15,228	129,249	120,443	24,807	69,667	93,498	5,411	122,866
3000	514,476	9,325	58,173	44,670	13,912	33,377	42,709	5,165	55,940
6921	610,780	8,949	40,412	33,074	15,669	28,869	36,958	9,239	62,820

*Highlighted boxes indicate flows at which highest estimated area of preferred habitat is available for a species' lifestage.

Table 61. 2D transect Method B results equal weighting average area (m^2) and rank order, where lowest rank equals highest amount of preferred habitat.

2D transect Method B results, Weighted Average Area (m^2) and Rank Order to test for most preferred flow scenario

Dry (cfs)	Equal Weighting Average	Rank Order**
5	77,917	28
10	90,931	23
20	111,363	15
30	110,031	15
45	91,033	24

Wet (cfs)	Equal Weighting Average	Rank Order
5	141,421	24
15	161,530	15
30	167,721	11
55	160,635	14
100	124,820	26
190	82,639	36
350	44,938	42

Snowmelt (cfs)	Equal Weighting Average	Rank Order
10	109,298	38
25	126,159	24
50	128,401	24
140	120,883	28
210	132,892	19
525	104,048	37
1103	69,810	55
3000	32,123	67
6921	31,676	68

* Highlighted boxes indicate flow each season with the highest estimated area using equal weighted average metric.

**Lowest rank order indicates highest ranked area of preferred habitat

Table 62. Percent area where 2D transect Method B returned GHSI>0.4.

% Area GHSI >0.4 using 2D Transect Method B

		ADULT			JUVENILE			FRY	SPAWN
Dry (cfs)	Available Wetted Area (m^2)	SS	RT	PH	SS	RT	PH	RT	RT
5	187,080	13.3	29.8	40.6	46.2	65.9	60.2	39.6	na
10	198,471	16.6	44.5	51.0	54.1	72.5	73.4	33.4	na
20	253,787	23.5	63.7	66.2	51.0	70.0	76.8	14.6	na
30	295,294	21.7	67.7	65.6	28.2	52.1	69.9	10.0	na
45	344,483	10.2	57.6	59.3	16.6	31.7	47.1	5.1	na

		ADULT			JUVENILE				SPAWN
Wet (cfs)	Available Wetted Area (m^2)	SS	RT	PH	SS	RT	PH	RT	RT
5	226,555	20.9	55.7	57.7	na	74.0	76.7	na	67.1
15	254,029	23.6	64.6	66.2	na	70.0	76.9	na	65.9
30	285,995	26.9	69.2	66.5	na	55.1	71.8	na	58.3
55	325,174	14.8	66.1	63.2	na	39.7	60.4	na	50.1
100	369,243	8.0	47.5	46.6	na	26.5	37.9	na	35.2
190	425,183	2.6	25.5	23.7	na	14.9	19.8	na	23.7
350	499,551	1.7	12.8	7.9	na	5.7	7.7	na	12.8

		ADULT			JUVENILE				SPAWN
Snowmelt (cfs)	Available Wetted Area (m^2)	SS	RT	PH	SS	RT	PH	RT	RT
10	216,244	17.3	46.1	52.3	54.0	73.3	74.3	31.0	65.4
25	253,122	22.7	63.4	66.0	52.0	71.0	77.3	15.2	66.7
50	292,641	26.6	68.3	66.4	30.6	54.7	70.6	11.2	58.5
140	332,720	14.1	64.6	61.9	20.8	39.3	63.2	6.9	50.5
210	311,832	27.7	66.8	64.7	27.7	52.5	68.4	9.0	58.9
525	377,081	7.8	55.4	56.6	13.5	29.1	43.2	3.4	38.4
1103	433,858	3.5	29.8	27.8	5.7	16.1	21.6	1.2	28.3
3000	514,476	1.8	11.3	8.7	2.7	6.5	8.3	1.0	10.9
6921	610,780	1.5	6.6	5.4	2.6	4.7	6.1	1.5	10.3

* Highlighted boxes indicate the flows at which the highest percent of preferred habitat per unit area is available.

Table 63. 2D transect Method B results equal weighting average area (%) and rank order, where lowest rank equals highest amount of preferred habitat.

2D transect Method B results, Weighted Average Area (%) and Rank Order to test for most preferred flow scenario

Dry (cfs)	Equal Weighting Average	Rank Order**
5	**41.6**	25
10	45.8	17
20	43.9	12
30	37.3	20
45	26.4	31

Wet (cfs)	Equal Weighting Average	Rank Order
5	62.4	15
15	63.6	12
30	58.6	12
55	49.4	21
100	33.8	30
190	19.4	36
350	9.0	42

Snowmelt (cfs)	Equal Weighting Average	Rank Order
10	50.5	23
25	49.8	17
50	43.9	20
140	36.3	37
210	42.6	25
525	27.6	46
1103	16.1	57
3000	6.2	65
6921	5.2	70

* Highlighted boxes indicate the flow during each season with the highest estimated percent using equal weighting metric.

**Lowest rank order indicates highest ranked area of preferred habitat

Table 64. Analysis metrics of 2D transect Method B results. Boxed flow indicates overall preferred flow (right column). Grey highlights indicate area analysis preferred flow; blue indicates % area preferred flow.

2D transect Method B	Area (m2) Metrics				% Area Metrics				Most Preferred Flows, All Metrics	
Dry (cfs)	weighted # occurrences with highest individual area*	Equal Weight Average	Rank Order	Most Preferred flow using Area metrics only	weighted # occurrences with highest individual %*	Equal Weight Average	Rank Order	Most Preferred flow using % Area metrics only	TOTAL All Metrics	Dry (cfs)
5	1.00			1.00	1.00			1.00	2.00	5
10	0.00			0.00	0.66	1		1.66	1.66	10
20	0.66		0.5	1.16	1.00		1	2.00	3.16	20
30	1.00	1	0.5	2.50	0.33			0.33	2.83	30
45	0.33			0.33	0.00			0.00	0.33	45
Wet (cfs)	weighted # occurrences with highest individual area	Equal Weight Average	Rank Order	Most Preferred flow using Area metrics only	weighted # occurrences with highest individual %	Equal Weight Average	Rank Order	Most Preferred flow using % Area metrics only	TOTAL All Metrics	Wet (cfs)
5	0.00			0.00	1.33			1.33	1.33	5
15	1.50			1.50	0.33	1	0.5	1.83	3.33	15
30	0.83	1	1	2.83	1.00		0.5	1.50	4.33	30
55	0.66			0.66	0.00			0.00	0.66	55
100	0.00			0.00	0.00			0.00	0.00	100
190	0.00			0.00	0.00			0.00	0.00	190
350	0.00			0.00	0.00			0.00	0.00	350
Snowmelt (cfs)	weighted # occurrences with highest individual area	Equal Weight Average	Rank Order	Most Preferred flow using Area metrics only	weighted # occurrences with highest individual %	Equal Weight Average	Rank Order	Most Preferred flow using % Area metrics only	TOTAL All Metrics	Snowmelt (cfs)
10	1.00			1.00	1.66	1		2.66	3.66	10
25	0.66			0.66	1.33		1	2.33	2.99	25
50	0.00			0.00	0.66			0.66	0.66	50
140	0.33			0.33	0.00			0.00	0.33	140
210	1.66	1	1	3.66	0.33			0.33	3.99	210
525	0.33			0.33	0.00			0.00	0.33	525
1103	0.00			0.00	0.00			0.00	0.00	1103
3000	0.00			0.00	0.00			0.00	0.00	3000
6921	0.00			0.00	0.00			0.00	0.00	6921

*This metric uses the weighted # of occurrences with highest individual area or percent divided by total number of species in a lifestage, then summed within lifestage. For example each adult and each juvenile occurrence of highest area during dry season is assigned a weight of .33 because there is a one in three possibility of a particular species having the highest area. Conversely, dry season RT fry is assigned a weight of 1, as it is the only representative of the fry lifestage. Thus, dry 5 cfs total # occurrences with highest individual area only occur for RT fry, so the total for that flow equates to 1. Alternately, in dry 45 flows, two of three adult lifestages have the highest available preferred area during this flow, thus the metric total for dry 45 is 0.66 (0.33 + 0.33).

11.4.4 Comparison between 2D Model and 2D Transect Method A Results

To understand how 2D model and 2D transect Method A results compared, the 2D transect value was subtracted from the corresponding 2D model results value, the result divided by 2D model results value, and that result multiplied by 100 to produce a percent difference in preferred habitat with respect to 2D model results (

Table 65). A comparison by species lifestage (e.g. Sacramento sucker adult values averaged across all flows) reports average and standard deviation of all values except those of -999, absolute average and standard deviation of all values except those of -999, the number of positive and negative deviations from the 2D model results, and the number of cells where a zero quantity (shown as -999) precluded calculation (

Table 66). The overall preferred flow columns produced for each method (right-hand column,

Table 58) are used for comparison in

Table 67.

The 2D transect Method A over-predicted the percent area of GHSI>0.4 when compared to 2D model results 51.6% of the time and under-predicted them 13.4% of the time (

Table 65). A zero value occurred in Method A 35.0% of the time, which was designated as a value of -999 to indicate that 2D transect Method A returned no available habitat for those species' lifestages at the specified flow. No available habitat was taken to mean zero habitat, so these values are considered under-predictions when compared to the 2D model results method. Thus, 51.6% of 2D transect Method A values were under-predictions and 48.4% of values were over-prediction compared to 2D model results. The average absolute variance of 2D transect Method A results from 2D model results was 72.8 ± 18.9% (

Table 66).

The largest individual over-prediction occurred for RT fry during snowmelt season 10 cfs flows, at 227% (

Table 65). The biggest under-prediction was -92.3% for RT adults during dry season 5 cfs flows. The largest over-predictions for a species lifestage were rainbow trout fry at an absolute average of 191.7 ± 36.0%, and Sacramento sucker juveniles at 102.5 ± 31.0%. Under-predictions were consistently present across all flows for Sacramento sucker adult. An overall average of the averages in cases where 2D transect method A had a non-zero result, and using an equal weighted approach, yielded a 77.2 ± 39.2% over-prediction with respect to 2D model results.

This comparison shows a large amount of variation between individual results. The overall trend reveals that the 2D transect Method A either over-predicted the amount of available GHSI>0.4 habitat or reported a zero value which then moved the result into an under-prediction of available preferred habitat. Only 13.4% of 2D transect Method A values specifically under-predicted the amount of habitat with GHSI>0.4 (

Table 66). Method A over-predicted average habitat area for every species' lifestage except for SS adult, although the zero areas of habitat were not taken into account for these calculations.

A comparison between preferred flows as calculated using area and % area metrics (

Table 67) shows that 2D model results return a wider range of preferred flows than the 2D transect Method A analysis. The Method A approach suggests lower flows are more suitable in wet and snowmelt seasons, while in dry season the overall preferred flows are the same. 2D Model results show dry 10 cfs as most preferred, with 20 cfs also preferred, while Method A results all fall into the dry 10 cfs flow. Wet season 2D model results prefer 55 cfs, with 15 cfs also somewhat preferred, while Method A results show wet 5 cfs most preferred and wet 10 as also preferred. In snowmelt season, 2D model results prefer 25 cfs as well as 140 cfs, while Method A results show 10 cfs as most preferred.

Overall, over-predictions of habitat based on Method A moved preferred flows to lower SYLC discharge values compared to 2D model results, although there is overlap. 2D model results vary more in terms of the analysis methods used, such that dry season 'best' flows fall in the range of 10–20 cfs, wet season 'best' flows are 15 or 55 cfs, and snowmelt season 'best' flows are 25 and 140 cfs. The preferred flows and ranges for Method A fall into narrower and lower SYLC discharges, with dry season 'best' flows of 10 cfs, wet season flows a range of 5–15 cfs, and snowmelt 'best' flow of 10 cfs. Dry season preferred flows of 10 cfs were the only flow where the boxed most-preferred flows were in agreement between 2D model results and Method A.

Table 65. 2D transect Method A results compared to 2D model results.

% Difference in GHSI Area >0.4 Between 2D Transect Method A and 2D Model Results 100*(2D Transect-2D)/2D

		ADULT			JUVENILE			FRY	SPAWN
Dry (cfs)	Available Wetted Area (m^2)	SS	RT	PH	SS	RT	PH	RT	RT
5	261397	-28.8	-92.3	-45.9	81.5	70.3	32.3	155.1	na
10	261397	-35.3	81.9	-51.5	74.5	54.0	48.2	193.0	na
20	261397	-41.0	39.9	58.6	90.7	76.3	57.1	-999	na
30	280018	-31.3	37.7	46.3	140.2	51.6	24.5	-999	na
45	329883	-999	37.5	42.6	-999	-999	57.4	-999	na

		ADULT			JUVENILE			FRY	SPAWN
Wet (cfs)	Available Wetted Area (m^2)	SS	RT	PH	SS	RT	PH	RT	RT
5	261397	-33.2	66.5	64.4	na	66.3	56.6	na	61.8
15	261397	-42.3	39.7	58.7	na	77.6	57.4	na	53.2
30	271404	-36.3	40.8	48.9	na	47.7	27.3	na	40.5
55	310143	-999	28.4	37.5	na	41.5	35.9	na	49.1
100	355305	-999	55.8	56.8	na	-999	-67.3	na	-34.8
190	413455	-999	-999	-59	na	-999	-999	na	-999
350	488060	-999	-999	-999	na	-999	-999	na	-999

		ADULT			JUVENILE			FRY	SPAWN
Snowmelt (cfs)	Available Wetted Area (m^2)	SS	RT	PH	SS	RT	PH	RT	RT
10	261397	-31.6	87.7	69.1	89.8	65.3	58.3	227.0	68.5
25	261397	-33.5	42.9	59.7	86.9	74.5	57.2	-999	53.1
50	277074	-35.8	38.8	108.2	134.3	48.4	26.7	-999	40.1
140	317729	-16.3	26.8	37.1	-999	46.9	37.8	-999	50.6
210	296391	-32.1	32.8	44.0	-999	61.4	31.4	-999	42.0
525	363552	-999	49.7	52.6	-999	-999	82.7	-999	14.5
1103	421653	-999	-61.0	-18.3	-999	-999	-999	-999	-999
3000	504628	-999	-999	-999	-999	-999	-999	-999	-999
6921	601735	-999	-999	-999	-999	-999	-999	-999	-999

Note: -999 denotes no available habitat in 2D Transect Method A results

Table 66. Average, standard deviation, and number of positive and negative deviations of the 2D transect Method A results from the 2D model results.

% Difference Summary Metrics, 2D Transect Method A compared to 2D Model

	ADULT			JUVENILE			FRY	SPAWN
	SS	RT	PH	SS	RT	PH	RT	RT
Average %	-33.1	32.6	33.9	99.7	60.1	39.0	191.7	39.9
Standard Deviation	6.6	44.9	46.0	26.3	12.5	32.6	36.0	28.4
Average % using Absolute Values	33.1	50.6	53.3	99.7	60.1	47.4	191.7	46.2
Absolute Values Standard Deviation	6.6	20.5	18.2	26.3	12.5	16.9	36.0	14.5
# Positive deviations from 2D model	77							
# Negative deviations from 2D model	20							
# cells where a zero quantity from Method A precluded a calculation	52							

Table 67. Comparison of preferred flows for 2D model results and 2D transect Method A results.

Preferred Flows, 2D Model Results	Preferred Flows, 2D transect Method A
Dry (cfs)	Dry (cfs)
5	5
10*	10****
20**	20
30	30
45	45
Wet (cfs)	Wet (cfs)
5	5
15***	15
30	30
55	55
100	100
190	190
350	350
Snowmelt (cfs)	Snowmelt (cfs)
10	10
25	25
50	50
140	140
210	210
525	525
1103	1103
3000	3000
6921	6921

*Boxed indicates overall 'best' preferred flow

**Gray indicates preferred flow for greatest area

***Light blue indicates preferred flow for greatest habitat per unit area

****Pink indicates all metrics agree for that method (area, % area, and overall)

11.4.5 Comparison Between 2D Model and 2D Transect Method B Results, and between 2D Transect Method A and Method B results

Comparisons between 2D model results and 2D transect Method B results were conducted using the same approach as described in the first paragraph of section 11.4.4.

Transect Method B over-predicted the percent area of GHSI>0.4 when compared to 2D model results 91.3% of the time and under-predicted values the remaining 8.7% of the time (

Table 68). There were no zero values associated with 2D transect Method B. The largest over-predictions occurred for rainbow trout fry at lowest and highest flows in the snowmelt season, with values of 95.6% and 135.0%, respectively, as well as the highest average over-prediction at 47.7 ± 42.8% (

Table 69). Sacramento sucker adults had the next largest over-predicted average at 45.4 ± 24.7%. There were 13 under predictions (12.2% of total), the largest occurring for SS adults in wet season 190 cfs flows, with -37.6%. The average absolute variance of 2D transect Method B results from 2D model results was 32.9 ± 17.6%.

The 2D transect Method B consistently over-predicted individual amounts of available habitat with GHSI>0.4 compared to 2D model results, yet variation between individual results were smaller than the comparison between 2D model and 2D transect Method A results. This trend can be seen in the overall Method B over-prediction of 32.4 ± 23.7%, which was much closer to 2D model results than Method A over-prediction of 77.2 ± 39.2%. 2D transect Method B over-predicted over 88.8% of all values within a range of 1.6–134.1%.

A comparison between preferred flows as calculated using area and % area metrics (

Table 70) shows that overall preferred flows vary between methods. The Method B approach returned overall preferred flows of dry 20 cfs, wet 30 cfs, and snowmelt 210 cfs, while 2D model results return dry 10 cfs, wet 55 cfs, and snowmelt 25 cfs. 2D model preferred flows were lower in dry and snowmelt season and higher in wet season than Method B preferred flows. The most significant difference occurred within Method B where the % area analysis returned a preferred flow for snowmelt season of 10 cfs versus the area analysis and the overall total indicated a preferred 210 cfs flow. Overall, Method A under-predicted preferred flows with respect to 2D model results (

Table 67), while Method B results over-predicted preferred flows (

Table 70).

Table 68. 2D transect Method B results compared to 2D model results.

% Difference in GHSI Area >0.4 Between 2D Transect Method B and 2D Model Results 100*(2D Transect-2D)/2D

		ADULT			JUVENILE			FRY	SPAWN
Dry (cfs)	Available Wetted Area (m^2)	SS	RT	PH	SS	RT	PH	RT	RT
5	261397	-26.4	25.2	-3.3	29.7	35.6	6.8	94.9	na
10	261397	-16.5	25.2	8.7	45.9	34.9	17.4	88.8	na
20	261397	22.0	37.8	40.7	87.8	49.0	30.2	45.5	na
30	280018	40.0	35.8	39.7	43.5	36.8	30.5	36.2	na
45	329883	1.6	31.0	39.7	30.5	22.1	22.5	15.0	na

		ADULT			JUVENILE			FRY	SPAWN
Wet (cfs)	Available Wetted Area (m^2)	SS	RT	PH	SS	RT	PH	RT	RT
5	261397	8.8	43.5	27.3	na	48.8	29.7	na	37.6
15	261397	23.7	39.5	40.8	na	50.2	30.6	na	30.9
30	271404	62.8	38.5	40.9	na	37.7	30.1	na	21.1
55	310143	21.6	36.1	39.5	na	28.3	31.7	na	14.9
100	355305	3.6	26.6	24.9	na	29.0	24.6	na	2.4
190	413455	-37.6	24.6	14.0	na	23.3	16.6	na	10.7
350	488060	-34.8	11.9	-24.8	na	-15.4	-19.0	na	0.4

		ADULT			JUVENILE			FRY	SPAWN
Snowmelt (cfs)	Available Wetted Area (m^2)	SS	RT	PH	SS	RT	PH	RT	RT
10	261397	-7.7	33.9	18.7	58.3	46.3	26.8	95.6	39.7
25	261397	17.5	40.0	41.4	87.5	49.7	31.2	46.6	32.4
50	277074	62.6	37.2	41.4	50.7	39.6	29.6	49.4	22.9
140	317729	19.1	33.0	37.7	41.9	32.8	41.5	30.9	17.3
210	296391	85.4	33.8	40.3	58.5	51.7	35.5	37.3	28.4
525	363552	-1.0	43.6	49.5	35.7	40.9	36.5	3.4	12.6
1103	421653	-13.6	38.3	25.1	9.4	38.6	27.6	-21.5	31.4
3000	504628	-12.8	25.3	1.2	0.3	22.5	11.6	11.6	9.1
6921	601735	12.8	16.0	4.0	41.5	37.1	25.3	134.1	43.5

Table 69. Average, standard deviation, positive and negative deviations of 2D transect Method B results from 2D model results.

% Difference Summary Metrics, 2D Transect Method B compared to 2D Model

	ADULT			JUVENILE			FRY	SPAWN
	SS	RT	PH	SS	RT	PH	RT	RT
Average %	11.0	32.2	26.1	44.4	35.2	24.6	47.7	22.2
Standard Deviation	32.1	8.5	19.5	24.6	14.9	12.9	42.4	13.3
Average % using Absolute Values	25.3	32.2	28.7	44.4	36.7	26.4	47.4	22.2
Absolute Values Standard Deviation	22.1	8.5	15.1	24.6	10.5	8.4	38.3	13.3
# Positive deviations from 2D model	136							
# Negative deviations from 2D model	13							
# cells where a zero quantity from Method B precludes a calculation	0							

Table 70. Comparison of preferred flows for 2D model results and 2D transect Method B results.

Preferred Flows, 2D Model Results	Preferred Flows, 2D transect Method B
Dry (cfs)	Dry (cfs)
5	5
10*	10
20**	20
30	30
45	45
Wet (cfs)	Wet (cfs)
5	5
15***	15
30	30
55	55
100	100
190	190
350	350
Snowmelt (cfs)	Snowmelt (cfs)
10	10
25	25
50	50
140	140
210	210
525	525
1103	1103
3000	3000
6921	6921

*Boxed indicates overall 'best' preferred flow
**Gray indicates preferred flow for greatest area
***Light blue indicates preferred flow for greatest habitat per unit area

11.5 1D Model Microhabitat Analysis

International collaborator Hoang's 1D Model (Hoang et al. 2009) was run using 105 cross-sections across the entire study segment of thalweg length 13.52 km. The number of cross-sections included a significantly higher density than used on common professional practice and the spacing of the cross-sections was roughly uniform. Cross-sections included 12 chute, 14 pool, 16 plane bed, 17 transition, 19 inset channel, 27 steep inset channel, and 0 step units. All 30 of the transect-based method's cross-sections were included in the 1D numerical model, for a range of spacing 14–288 m between all cross-sections (Figure 44).

The goal of the physical habitat analysis using the 1D numerical model results was to enable a methodological comparison between 1D and 2D numerical models. It was shown in section 10.1 **Error! Reference source not found.**that the 1D numerical model performed poorly at representing the hydraulics of the study segment at the segment- and morphological-unit scales, because it is infeasible to obtain cross-sections located at all of the hydraulic controls that exist in a complex mountain river. The amount of effort needed to do that would render it more cost-effective to just map the whole river outright, in which case there is a significant benefit to running a 2D model over a 1D model, because the latter yields a higher resolution of spatially explicit results and velocity vectors can be oriented in any direction, not just downstream. Nevertheless, a thorough comparison requires an investigation into how 1D numerical model hydraulics propagate error into physical habitat metrics.

1D numerical model results were processed following the same methods detailed in section 11.4 for transect-based physical habitat analysis. Specifically, there was assignment of proportional floodplain area to morphologic units as model flows increased. Instead of considering the number of points in the floodplain as was done in the transect-based method to distribute floodplain area to morphological units, the analysis for the 1D numerical model's cross-sectionally averaged outputs involved distributing floodplain area on the basis of the proportional lengths of the cross-sections in the floodplain for each morphological unit.

A significant difference between 1D and 2D model results is that the 1D model natively returns one average depth and velocity magnitude value for each cross-section per modeled flow. As mentioned in section 7.3, it is possible to distribute depth across a cross-section making use of the water surface elevation and bed topography across the section. For velocity, a lateral extrapolation requires additional assumptions, empirical equations, and empirically estimated parameters (Ghanem et al. 1996). Even then, the lateral distribution of velocity magnitude is highly uncertain, and the velocity vector does not include a direction. In this study, the goal was to test the veracity of the 1D numerical model and its native output, not to determine whether additional layers of assumptions and empiricism can turn a native 1D numerical model into something else. A further test of such extrapolation would be interesting, but was beyond the scope of this study. The full range of % distribution of 1D Model GHSI categories, including those of low, very poor, and non-habitat, is available in Appendix E.

11.5.1 1D Model Method A Results

Method A as described and illustrated for 2D transect Method A (section 11.4.2) was applied to the 1D model results. The same styles of tables and metrics used to present and discuss 2D model results are used for all 1D model results. Explanation of metrics can be found in section 11.3.1.

The area of GHSI>0.4 (

Table 71) and percent area (

Table 73) illustrates that Method A returns habitat values of zero, regardless of whether a 2D or 1D model is used, although 1D Method A returned more zeros than 2D Method A. There is zero preferred habitat for rainbow trout fry, no matter the flow, in 1D Method A results. SS adult and juvenile lifestages are afforded a narrow range of flows at which some habitat is classified as suitable for lifestage maintenance using the 1D model Method A approach, which is also the case for RT juvenile lifestage. RT and PH adults appear to have resilience across the greatest range of flows. The number of flows with a zero value is significant in every season: 40.0% of dry season flows, 52.4% of wet season flows, and 66.7% of snowmelt season flows. Flows with zero-habitat for any species lifestage include wet season 190 and 350 cfs, and snowmelt season 1103, 3000, and 6921 cfs. Wet 100 cfs and snowmelt 525 cfs return ~12% of preferred habitat across the entire study segment for PH adults and zero for all others. These zeros amount to 43.9% of all modeled flows where little to no habitat is returned using a 1D numerical model methodology.

Equal weighted averages and ranked orders for areas (

Table 72) returned the same preferred flows for every season; wet season 15 cfs flows have the highest area of preferred habitat, at 192,780 m^2. The highest area for snowmelt season is at 25 cfs with 131,899 m^2; the highest dry season value is during 20 cfs flows with 104,727 m^2 of preferred habitat. The idea that rank order smooths variance between positive values and zeroes, discussed in section 11.4.2, does not seem to have played a part in this set of results. A possible explanation to may be that highest preferred areas were clustered within a narrower range - across flows during each season that were closest in available wetted area at ~250,000 m2. This result seems somewhat unlikely because of the variation in flow needs between species' lifestages, and may show how more smoothing results in a single preferred flow regardless of analysis metric used once the model results are computed.

When analyzing preferred habitat per unit area (% area), absolute values become less important (

Table 73). As an example, SS juvenile dry season 5 and 10 cfs preferred habitat return the same 62.9%, whereas areas vary by ~8,000 m^2. The same trend can be seen with other species and lifestages. The highest % area flows became even narrower for SS adults, with just two flows accounting for all dry (10 and 20 cfs), wet (5 and 15 cfs), and snowmelt (10 and 25 cfs) season preferred habitat. Rank order returned the same preferred flows as equal weighting averages (Table 74), although rank order had ties in wet season between 5 and 15 cfs, as well as in snowmelt season between 10 and 25 cfs, but varied in every season from the preferred flows using absolute area.

1D model Method A results metrics reveal a range of flows to be most preferred overall for the dry season, when rounding (3.99 versus 4.00) of the Total All Metrics value in 10 and 20 cfs flows occurs (

Table 75). In wet season, 15 cfs flows are most preferred overall, while snowmelt 25 cfs receives a similar distinction. Each boxed flow also represents the most preferred flow of the cumulative area metrics, while the % area metrics all come in at the next-lower flow. These results suggest a range of flows suitable to maintain a healthy proportion of preferred habitat for the greatest range of species and lifestages.

Taking a range of preferred flows approach, dry season flows of 10–20 cfs are most preferred, wet season flows of 5–15 cfs are most preferred, and snowmelt season flows of 10–25 cfs are most preferred.

Table 71. Area (m^2) where 1D transect Method A results returned a suitability index of medium or high quality habitat (i.e. GHSI > 0.4) per species, lifestage, and flow regime.

Area (m^2) GHSI >0.4, 1D Model Method A

		ADULT			JUVENILE			FRY	SPAWN
Dry (cfs)	Available Wetted Area (m^2)	SS	RT	PH	SS	RT	PH	RT	RT
5	187080	0	24,061	42,529	117,613	168,262	186,730	0	na
10	198471	21,893	178,507	147,999	124,775	178,507	198,100	0	na
20	253787	27,995	253,312	253,312	0	177,439	230,487	0	na
30	295294	0	288,982	197,022	0	0	170,699	0	na
45	344483	0	174,065	174,065	0	0	0	0	na

		ADULT			JUVENILE			FRY	SPAWN
Wet (cfs)	Available Wetted Area (m^2)	SS	RT	PH	SS	RT	PH	RT	RT
5	226555	24,991	201,140	168,942	na	199,620	226,132	na	203,767
15	254029	28,022	253,554	253,554	na	177,608	230,707	na	195,806
30	285995	0	279,856	255,408	na	138,961	195,331	na	223,487
55	325174	0	169,762	202,617	na	0	0	na	0
100	369243	0	0	30,527	na	0	0	na	0
190	425183	0	0	0	na	0	0	na	0
350	499551	0	0	0	na	0	0	na	0

		ADULT			JUVENILE			FRY	SPAWN
Snowmelt (cfs)	Available Wetted Area (m^2)	SS	RT	PH	SS	RT	PH	RT	RT
10	216244	23,854	194,492	161,252	135,948	161,150	215,839	0	194,492
25	253122	27,922	252,649	252,649	0	150,600	229,883	0	223,029
50	292641	0	286,409	258,078	0	95,517	196,443	0	195,229
140	332720	0	205,017	205,017	0	0	0	0	0
210	311832	0	261,288	206,868	0	16,227	0	0	0
525	377081	0	0	30,585	0	0	0	0	0
1103	433858	0	0	0	0	0	0	0	0
3000	514476	0	0	0	0	0	0	0	0
6921	610780	0	0	0	0	0	0	0	0

*Highlighted boxes indicate flows at which highest estimated area of preferred habitat is available for a species' lifestage.

Table 72. 1D model Method A results of equal weighting average area (m^2) and rank order, where lowest rank equals highest amount of preferred habitat.

1D Model Method A area (m^2) GHSI>0.4 results, Weighted Average and Rank Order to test for most preferred flow scenario

Dry (cfs)	Equal Weighting Average	Rank Order
5	59,910	22
10	94,420	14
20	104,727	11
30	72,967	18
45	38,681	23

Wet (cfs)	Equal Weighting Average	Rank Order
5	182,778	12
15	192,780	8
30	189,685	11
55	41,375	18
100	3,392	21
190	0	22
350	0	22

Snowmelt (cfs)	Equal Weighting Average	Rank Order
10	123,001	17
25	131,899	12
50	118,511	14
140	34,170	23
210	40,365	19
525	2,549	27
1103	0	28
3000	0	28
6921	0	28

* Highlighted boxes indicate the flow during each season with the highest estimated area using each metric.
**Lowest rank order indicates highest ranked area of preferred

Table 73. Percent area where 1D Method A returned GHSI>0.4.

% Area GHSI >0.4, 1D Model Method A

		ADULT			JUVENILE			FRY	SPAWN
Dry (cfs)	Available Wetted Area (m^2)	SS	RT	PH	SS	RT	PH	RT	RT
5	187080	0	12.9	22.7	62.9	89.9	99.8	0	na
10	198471	11.0	89.9	74.6	62.9	89.9	99.8	0	na
20	253787	11.0	99.8	99.8	0	69.9	90.8	0	na
30	295294	0	97.9	66.7	0	0	57.8	0	na
45	344483	0	50.5	50.5	0	0	0	0	na

		ADULT			JUVENILE			FRY	SPAWN
Wet (cfs)	Available Wetted Area (m^2)	SS	RT	PH	SS	RT	PH	RT	RT
5	226555	11.0	88.8	74.6	na	88.1	99.8	na	89.9
15	254029	11.0	99.8	99.8	na	69.9	90.8	na	77.1
30	285995	0	97.9	89.3	na	48.6	68.3	na	78.1
55	325174	0	52.2	62.3	na	0	0	na	0
100	369243	0	0	8.3	na	0	0	na	0
190	425183	0	0	0	na	0	0	na	0
350	499551	0	0	0	na	0	0	na	0

		ADULT			JUVENILE			FRY	SPAWN
Snowmelt (cfs)	Available Wetted Area (m^2)	SS	RT	PH	SS	RT	PH	RT	RT
10	216244	11.0	89.9	74.6	62.9	74.5	99.8	0	89.9
25	253122	11.0	99.8	99.8	0.0	59.5	90.8	0	88.1
50	292641	0	97.9	88.2	0	32.6	67.1	0	66.7
140	332720	0	61.6	61.6	0	0	0	0	0.0
210	311832	0	83.8	66.3	0	5.2	0	0	0.0
525	377081	0	0	8.1	0	0	0	0	0.0
1103	433858	0	0	0	0	0	0	0	0
3000	514476	0	0	0	0	0	0	0	0
6921	610780	0	0	0	0	0	0	0	0

* Highlighted boxes indicate the flows at which the highest percent of preferred habitat per unit area is available.

Table 74. 1D model Method A results of equal weighting average area (%) and rank order, where lowest rank equals highest amount of preferred habitat.

1D Model Method A area (%) GHSI>0.4 results, Weighted Average % and Rank Order to test for most preferred flow scenario

Dry (cfs)	Equal Weighting Average	Rank Order
5	32.0	17
10	47.6	10
20	41.3	13
30	**24.7**	20
45	11.2	24

Wet (cfs)	Equal Weighting Average	Rank Order
5	80.7	10
15	75.9	10
30	**66.3**	15
55	12.7	23
100	0.9	25
190	0.0	26
350	0.0	26

Snowmelt (cfs)	Equal Weighting Average	Rank Order
10	56.9	12
25	52.1	12
50	40.5	19
140	10.3	29
210	**12.9**	26
525	0.7	31
1103	0.0	32
3000	0.0	32
6921	0.0	32

* Highlighted boxes indicate the flow during each season with
**Lowest rank order indicates highest ranked area of preferred

Table 75. Analysis metrics of 1D Method A results. Boxed flow indicates overall preferred flow (right column). Grey highlights indicate area analysis preferred flow; blue indicates % area preferred flow.

1D Model, Method A	Area (m^2) Metrics				% Area Metrics				Most Preferred Flows, All Metrics	
Dry (cfs)	weighted # occurrences with highest individual area*	Equal Weight Average	Rank Order	Most Preferred flow using Area metrics only	weighted # occurrences with highest individual %*	Equal Weight Average	Rank Order	Most Preferred flow using % Area metrics only	TOTAL All Metrics	Dry (cfs)
5	0.00			0.00	1.00			1.00	1.00	5
10	0.66			0.66	1.33	1	1	3.33	3.99	10
20	1.00	1	1	3.00	1.00			1.00	4.00	20
30	0.30			0.30	0.00			0.00	0.30	30
45	0.00			0.00	0.00			0.00	0.00	45
Wet (cfs)	weighted # occurrences with highest individual area	Equal Weight Average	Rank Order	Most Preferred flow using Area metrics only	weighted # occurrences with highest individual %	Equal Weight Average	Rank Order	Most Preferred flow using % Area metrics only	TOTAL All Metrics	Wet (cfs)
5	0.50			0.50	2.0	1	0.5	3.50	4.00	5
15	0.83	1	1	2.83	1.0		0.5	1.50	4.33	15
30	1.66			1.66	0.0			0.00	1.66	30
55	0.00			0.00	0.0			0.00	0.00	55
100	0.00			0.00	0.0			0.00	0.00	100
190	0.00			0.00	0.0			0.00	0.00	190
350	0.00			0.00	0.0			0.00	0.00	350
Snowmelt (cfs)	weighted # occurrences with highest individual area	Equal Weight Average	Rank Order	Most Preferred flow using Area metrics only	weighted # occurrences with highest individual %	Equal Weight Average	Rank Order	Most Preferred flow using % Area metrics only	TOTAL All Metrics	Snowmelt (cfs)
10	0.66			0.66	2.33	1	0.5	3.83	4.49	10
25	1.66	1	1	3.66	1.00		0.5	1.50	5.16	25
50	0.66			0.66	0.00			0.00	0.66	50
140	0.00			0.00	0.00			0.00	0.00	140
210	0.00			0.00	0.00			0.00	0.00	210
525	0.00			0.00	0.00			0.00	0.00	525
1103	0.00			0.00	0.00			0.00	0.00	1103
3000	0.00			0.00	0.00			0.00	0.00	3000
6921	0.00			0.00	0.00			0.00	0.00	6921

*This metric uses the weighted # of occurrences with highest individual area or percent divided by total number of species in a lifestage, then summed within lifestage. For example each adult and each juvenile occurrence of highest area during dry season is assigned a weight of .33 because there is a one in three possibility of a particular species having the highest area. Conversely, dry season RT fry is assigned a weight of 1, as it is the only representative of the fry lifestage. Thus, dry 5 cfs total # occurrences with highest individual area only occur for RT fry, so the total for that flow equates to 1. Alternately, in dry 45 flows, two of three adult lifestages have the highest available preferred area during this flow, thus the metric total for dry 45 is 0.66 (0.33 + 0.33).

11.5.2 1D Model Method B Results

Method B as described and illustrated for 2D transect method B (section 11.4.3) was applied to the 1D model results. In this case it was not the proportion of points with individual GHSI values >0.4, but rather the proportion of cross-section length with individual cross-sectionally averaged GHSI values >0.4. The same styles of tables and metrics used to present and discuss 2D model results are used for all 2D transect results. Explanation of metrics can be found in section 11.3.1.

The area of GHSI>0.4 (

Table 76) and percent area (

Table 78) show that the 1D model Method B returns a significant number of zero values, an unexpected result considering that the 2D transect Method B returned positive values for every species lifestage at all flows. RT fry returned 6.6% preferred habitat at dry season 5 cfs and zero preferred habitat at every other flow. RT and PH adults and PH juveniles have the most available preferred habitat across flows and seasons. The number of flows with zero values for some lifestages per season was lower than for 1D model Method A, but still significant. In dry season, 17.1% of flows returned zero habitat; wet season 26.2%, and in snowmelt season 48.6% of the time, for an overall 32.7% of flows returning no preferred habitat. Flows where no habitat was returned for any species lifestage include wet season 350 cfs and snowmelt season 3000 cfs and 6921 cfs. Wet season 190 cfs and snowmelt season 1103 cfs returned a small amount of habitat for RT and PH adults, and for RT spawners only during wet season 190 cfs. This amounts to 34.9% of all modeled flows where avoided habitat is returned using the 1D model Method B, a significant amount of flows where no habitat area is available for one or more species' lifestages, yet also a lower value than the 43.9% of zero habitat returned in the 1D model Method A.

Weighted averages and ranked orders (

Table 77) analyses of area yielded the same preferred flows for each season. Wet season 15 cfs had the highest area of preferred habitat with 167,569 m^2. Snowmelt season 25 cfs had highest seasonal area at 115,563 m^2, and dry season returned 84,318 m^2. Highest amounts of preferred area fell within a range of three adjacent flows for wet and snowmelt season, while in dry season across four flows (gray highlighted areas in

Table 76).

Preferred habitat per unit area (% area) yielded somewhat different results. Highest preferred flows as represented by % area ranged across the four lowest flows in dry season, the three lowest flows in wet season, and the two lowest flows in snowmelt season (

Table 78). The highest weighted average % area for dry season was 10 cfs flows, for wet season was 5 cfs, and in snowmelt season at 10 cfs, compared to 20, 15, and 25 cfs, respectively, for 1D Method A. Ranked order varied from weighted average. In dry season, 10 and 20 cfs tied for most preferred flow, while in wet season 15 cfs was preferred and in snowmelt season it was 25 cfs.

1D model Method B results total, all metrics, suggest that overall, dry 20 cfs, wet 15 cfs, and snowmelt 25 cfs contain the most preferred habitat per season (

Table 80). Each boxed flow also represents the most preferred flow of the cumulative area metrics, while the % area metrics all prefer the next-lower flow.

The results of the 1D Method B analysis suggest that a small range of flows may be sufficient to maintain preferred habitat for the species and lifestages studied, in dry season 10–20 cfs, in wet season 5–15 cfs, and in snowmelt season 10–25 cfs. These ranges of flows are the same result as the 1D model Method A analysis (

Table 75). The similarity between 1D methods may point to the more pronounced inability of 1D transects, no matter the number, to legitimately represent hydraulic controls and instream habitat (see section 10.1.1 for details).

Table 76. Area (m^2) where 1D transect Method B results returned a suitability index of medium or high quality habitat (i.e. GHSI>0.4) per species, lifestage, and flow regime.

Area (m^2) GHSI >0.4, 1D Model Method B

		ADULT			JUVENILE			FRY	SPAWN
Dry (cfs)	Available Wetted Area (m^2)	SS	RT	PH	SS	RT	PH	RT	RT
5	187080	11,379	95,581	73,116	74,815	138,726	134,743	12,407	na
10	198471	14,648	138,942	113,856	83,616	151,150	164,606	0	na
20	253787	39,770	203,285	176,476	25,054	141,127	173,147	0	na
30	295294	32,591	218,379	200,415	0	86,622	163,404	0	na
45	344483	8,983	179,698	146,349	0	8,983	51,669	0	na

		ADULT			JUVENILE			FRY	SPAWN
Wet (cfs)	Available Wetted Area (m^2)	SS	RT	PH	SS	RT	PH	RT	RT
5	226555	24,279	173,365	140,103	na	173,886	179,967	na	191,412
15	254029	39,808	203,479	176,257	na	140,874	173,312	na	205,765
30	285995	34,006	222,875	201,139	na	121,800	166,218	na	169,849
55	325174	9,925	179,850	165,646	na	40,302	81,111	na	108,026
100	369243	0	111,003	114,798	na	0	29,981	na	20,549
190	425183	0	14,714	36,974	na	0	0	na	9,694
350	499551	0	0	0	na	0	0	na	0

		ADULT			JUVENILE			FRY	SPAWN
Snowmelt (cfs)	Available Wetted Area (m^2)	SS	RT	PH	SS	RT	PH	RT	RT
10	216244	16,742	155,540	121,994	92,014	161,150	177,369	0	185,628
25	253122	37,257	202,081	176,013	24,988	150,600	177,558	0	206,088
50	292641	34,440	225,711	192,233	0	95,517	157,570	0	168,848
140	332720	13,229	189,873	154,552	0	0	71,681	0	67,363
210	311832	28,225	206,506	176,202	0	16,227	120,993	0	102,033
525	377081	0	64,139	91,820	0	0	26,511	0	2,475
1103	433858	0	2,464	23,081	0	0	0	0	0
3000	514476	0	0	0	0	0	0	0	0
6921	610780	0	0	0	0	0	0	0	0

*Highlighted boxes indicate flows at which highest estimated area of preferred habitat is available for a species' lifestage.

Table 77. 1D model Method B results of equal weighting average area (m^2) and rank order, where lowest rank equals highest amount of preferred habitat.

1D Model Method B area (m^2) GHSI>0.4 results, Weighted Average and Rank Order to test for most preferred flow scenario

Dry (cfs)	Equal Weighting Average	Rank Order
5	62,842	24
10	74,091	17
20	84,318	13
30	77,935	17
45	43,965	27

Wet (cfs)	Equal Weighting Average	Rank Order
5	160,307	15
15	167,569	10
30	155,510	13
55	95,735	22
100	36,935	30
190	8,974	34
350	0	37

Snowmelt (cfs)	Equal Weighting Average	Rank Order
10	106,808	21
25	115,563	14
50	101,001	17
140	52,619	32
210	71,188	23
525	15,825	39
1103	2,129	43
3000	0	45
6921	0	45

* Highlighted boxes indicate the flow during each season with the highest estimated area using each metric.
**Lowest rank order indicates highest ranked area of preferred

Table 78. 1D model Method B results percent area where GHSI>0.4.

% Area GHSI >0.4, 1D Model Method B

		ADULT			JUVENILE			FRY	SPAWN
Dry (cfs)	Available Wetted Area (m^2)	SS	RT	PH	SS	RT	PH	RT	RT
5	187080	6.1	51.1	39.1	40.0	74.2	72.0	6.6	na
10	198471	7.4	70.0	57.4	42.1	76.2	82.9	0.0	na
20	253787	15.7	80.1	69.5	9.9	55.6	68.2	0.0	na
30	295294	11.0	74.0	67.9	0.0	29.3	55.3	0.0	na
45	344483	2.6	52.2	42.5	0.0	2.6	15.0	0.0	na

		ADULT			JUVENILE			FRY	SPAWN
Wet (cfs)	Available Wetted Area (m^2)	SS	RT	PH	SS	RT	PH	RT	RT
5	226555	10.7	76.5	61.8	na	76.8	79.4	na	84.5
15	254029	15.7	80.1	69.4	na	55.5	68.2	na	81.0
30	285995	11.9	77.9	70.3	na	42.6	58.1	na	59.4
55	325174	3.1	55.3	50.9	na	12.4	24.9	na	33.2
100	369243	0.0	30.1	31.1	na	0.0	8.1	na	5.6
190	425183	0.0	3.5	8.7	na	0.0	0.0	na	2.3
350	499551	0.0	0.0	0.0	na	0.0	0.0	na	0.0

		ADULT			JUVENILE			FRY	SPAWN
Snowmelt (cfs)	Available Wetted Area (m^2)	SS	RT	PH	SS	RT	PH	RT	RT
10	216244	7.7	71.9	56.4	42.6	74.5	82.0	0.0	85.8
25	253122	14.7	79.8	69.5	9.9	59.5	70.1	0.0	81.4
50	292641	11.8	77.1	65.7	0.0	32.6	53.8	0.0	57.7
140	332720	4.0	57.1	46.5	0.0	0.0	21.5	0.0	20.2
210	311832	9.1	66.2	56.5	0.0	5.2	38.8	0.0	32.7
525	377081	0.0	17.0	24.4	0.0	0.0	7.0	0.0	0.7
1103	433858	0.0	0.6	5.3	0.0	0.0	0.0	0.0	0.0
3000	514476	0.0	0.0	0.0	0.0	0.0	0.0	0.0	0.0
6921	610780	0.0	0.0	0.0	0.0	0.0	0.0	0.0	0.0

* Highlighted boxes indicate the flows at which the highest percent of preferred habitat per unit area is available.

Table 79. 1D model Method B results of equal weighting average area (%) and rank order, where lowest rank equals highest amount of preferred habitat.

1D Model Method B area (%) GHSI>0.4 results, Weighted Average % and Rank Order to test for most preferred flow scenario

Dry (cfs)	Equal Weighting Average	Rank Order
5	33.6	21
10	37.3	14
20	33.2	14
30	26.4	20
45	12.8	29

Wet (cfs)	Equal Weighting Average	Rank Order
5	70.8	12
15	66.0	10
30	54.4	14
55	29.4	24
100	10.0	30
190	2.1	34
350	0.0	37

Snowmelt (cfs)	Equal Weighting Average	Rank Order
10	49.4	16
25	45.7	12
50	34.5	19
140	15.8	34
210	22.8	26
525	4.2	39
1103	0.5	43
3000	0.0	45
6921	0.0	45

* Highlighted boxes indicate the flow during each season with
**Lowest rank order indicates highest ranked area of preferred

Table 80. Analysis metrics of 1D Method B results. Boxed flow indicates overall preferred flow (right column). Grey highlights indicate area analysis preferred flow; blue indicates % area preferred flow.

1D Model, Method B	Area (m^2) Metrics				% Area Metrics				Most Preferred Flows, All Metrics	
Dry (cfs)	weighted # occurrences with highest individual area*	Equal Weight Average	Rank Order	Most Preferred flow using Area metrics only	weighted # occurrences with highest individual %*	Equal Weight Average	Rank Order	Most Preferred flow using % Area metrics only	TOTAL All Metrics	Dry (cfs)
5	1.00			1.00	1.00			1.00	2.00	5
10	0.66			0.66	1.00	1	0.5	2.50	3.16	10
20	0.66	1	1	2.66	1.00		0.5	1.50	4.16	20
30	0.66			0.66	0.00			0.00	0.66	30
45	0.00			0.00	0.00			0.00	0.00	45
Wet (cfs)	weighted # occurrences with highest individual area	Equal Weight Average	Rank Order	Most Preferred flow using Area metrics only	weighted # occurrences with highest individual %	Equal Weight Average	Rank Order	Most Preferred flow using % Area metrics only	TOTAL All Metrics	Wet (cfs)
5	1.00			1.00	1.7	1		2.66	3.66	5
15	1.33	1	1	3.33	0.7		1.0	1.66	4.99	15
30	0.66			0.66	0.3			0.33	0.99	30
55	0.00			0.00	0.0			0.00	0.00	55
100	0.00			0.00	0.0			0.00	0.00	100
190	0.00			0.00	0.0			0.00	0.00	190
350	0.00			0.00	0.0			0.00	0.00	350
Snowmelt (cfs)	weighted # occurrences with highest individual area	Equal Weight Average	Rank Order	Most Preferred flow using Area metrics only	weighted # occurrences with highest individual %	Equal Weight Average	Rank Order	Most Preferred flow using % Area metrics only	TOTAL All Metrics	Snowmelt (cfs)
10	0.66			0.66	2.00	1		3.00	3.66	10
25	1.66	1	1	3.66	1.00		1	2.00	5.66	25
50	0.66			0.66	0.00			0.00	0.66	50
140	0.00			0.00	0.00			0.00	0.00	140
210	0.00			0.00	0.00			0.00	0.00	210
525	0.00			0.00	0.00			0.00	0.00	525
1103	0.00			0.00	0.00			0.00	0.00	1103
3000	0.00			0.00	0.00			0.00	0.00	3000
6921	0.00			0.00	0.00			0.00	0.00	6921

*This metric uses the weighted # of occurrences with highest individual area or percent divided by total number of species in a lifestage, then summed within lifestage. For example each adult and each juvenile occurrence of highest area during dry season is assigned a weight of .33 because there is a one in three possibility of a particular species having the highest area. Conversely, dry season RT fry is assigned a weight of 1, as it is the only representative of the fry lifestage. Thus, dry 5 cfs total # occurrences with highest individual area only occur for RT fry, so the total for that flow equates to 1. Alternately, in dry 45 flows, two of three adult lifestages have the highest available preferred area during this flow, thus the metric total for dry 45 is 0.66 (0.33 + 0.33).

11.5.3 Comparison Between 2D Model and 1D Model Method A Results

To understand how 2D model results and 1D model Method A compared between GHSI habitat area, the 1D model Method A percent value was subtracted from the corresponding 2D model results value, with the result divided by the 2D model results value and then multiplied by 100, to produce a percent difference in GHSI area greater than 0.4 with respect to 2D model results (

Table 81). A comparison by species lifestage (e.g. SS adult values averaged across all flows) reports average and standard deviation, absolute average and standard deviation, the number of positive and negative deviations from the 2D model results, and the number of cells where a zero quantity precluded calculation (

Table 82).

The 1D transect Method A over-predicted the percent area of GHSI>0.4 when compared to 2D model results 35.6% of the time and under-predicted them 8.0% of the time (

Table 82). A zero value occurred in Method A 52.8% of the time, which was designated as a value of -999 to indicate that the 1D Method A returned zero preferred habitat for those species' lifestages at the specified flow (

Table 81). No preferred habitat means zero habitat, so these values are considered under-predictions when compared to the 2D model results method. Thus, 35.6% of 1D transect method A values were over-predicted and 64.4% of values were under-predicted compared to 2D model results. The average absolute variance of 1D Method A results from 2D model results was 64.7 ± 17.9%.

The largest individual over-prediction of 1D Method A occurred for RT adults during snowmelt season 10 cfs flows, at 160.9%, and the biggest under-prediction occurred for PH adults during snowmelt season 525 cfs flows, at -78.2% (

Table 81). SS adult values were all under-predicted compared to 2D model results, making it the only negative average across flows at -42.8 ± 1.1%. Otherwise, all other species' lifestages over-predicted preferred habitat area when compared to 2D model results. The largest average over-prediction occurred for RT adults with 82.4 ± 60.4%. An overall average of the averages yielded a 49.4 ± 25.5% over-prediction with respect to 2D model results.

A comparison between preferred flows (

Table 83) shows that 2D model results vary from 1D Method A results. In dry season, 2D model results preferred 10 cfs with a lesser preference for 20 cfs flows, while 1D Method A results more habitat was preferred in 20 cfs with a lesser preference for 10 cfs flows. In wet season 55 cfs flows and with a lesser preference 15 cfs flows returned the most preferred habitat in 2D model results, while 1D Method A preferred flows were 15 cfs and to a lesser extent 5 cfs. In snowmelt season 2D model results, 25 cfs flows were preferred with a lesser preference for 140 cfs flow. Meanwhile, 1D model Method A preferred flows in dry season were 20 cfs, with a lesser preference for 10 cfs flows; wet season 15 cfs with a lesser preference for 5 cfs flows; and snowmelt season 25 cfs with a less preference for 10 cfs flows.

Preferred flows between the 2D method and the 1D Method A overlapped in the dry season, with both preferring a range of flows of 10–20 cfs. Wet season preferences diverged, with 2D model preferred flows at 15 and 55 cfs, while 1D Method A preferred flows were 5–15 cfs. Snowmelt season preferences also diverged, with 2D model preferred flow at 25 and 140 cfs, while 1D Method A preferred flows were 10–25 cfs.

Table 81. 1D transect Method A results compared to 2D model results.

% Difference in GHSI Area >0.4 Between 1D Method A and 2D Model Results (1D-2D)/2D*100

		ADULT			JUVENILE			FRY	SPAWN
Dry (cfs)	Available Wetted Area (m^2)	SS	RT	PH	SS	RT	PH	RT	RT
5	187080	-999	-45.9	-45.9	76.4	85.1	77.1	-999	na
10	198471	-44.5	152.9	59.0	69.6	67.4	59.6	-999	na
20	253787	-42.8	115.8	112.3	-999	48.9	54.0	-999	na
30	295294	-999	96.1	42.1	-999	-999	7.9	-999	na
45	344483	-999	14.8	19.1	-999	-999	-999	-999	na

		ADULT			JUVENILE			FRY	SPAWN
Wet (cfs)	Available Wetted Area (m^2)	SS	RT	PH	SS	RT	PH	RT	RT
5	226555	-42.7	128.5	64.4	na	77.1	68.7	na	84.5
15	254029	-42.3	115.5	112.4	na	50.0	54.2	na	53.2
30	285995	-999	96.0	89.3	na	21.4	23.8	na	62.3
55	325174	-999	7.5	37.5	na	-999	-999	na	-999
100	369243	-999	-999	-77.8	na	-999	-999	na	-999
190	425183	-999	-999	-999	na	-999	-999	na	-999
350	499551	-999	-999	-999	na	-999	-999	na	-999

		ADULT			JUVENILE			FRY	SPAWN
Snowmelt (cfs)	Available Wetted Area (m^2)	SS	RT	PH	SS	RT	PH	RT	RT
10	216244	-41.3	160.9	69.1	84.4	48.8	70.5	-999	92.1
25	253122	-43.0	120.4	113.8	-999	25.4	54.1	-999	75.0
50	292641	-999	96.6	87.6	-999	-17	23.1	-999	40.1
140	332720	-999	26.8	37.1	-999	-999	-999	-999	-999
210	311832	-999	67.7	44.0	-999	-85	-999	-999	-999
525	377081	-999	-999	-78.6	-999	-999	-999	-999	-999
1103	433858	-999	-999	-999	-999	-999	-999	-999	-999
3000	514476	-999	-999	-999	-999	-999	-999	-999	-999
6921	610780	-999	-999	-999	-999	-999	-999	-999	-999

Note: -999 denotes no available habitat in 1D results

Table 82. Average, standard deviation, and number of positive and negative deviations of the 1D transect Method A results from the 2D model results.

% Difference Summary Metrics, 1D Transect Method A compared to 2D Model

	ADULT			JUVENILE			FRY	SPAWN
	SS	RT	PH	SS	RT	PH	RT	RT
Average %	-42.8	82.4	42.8	76.8	32.2	49.3	*	67.9
Standard Deviation	1.1	60.4	62.2	7.4	50.8	23.2	*	19.6
Average % using Absolute Values	42.8	89.0	68.1	76.8	52.6	49.3	*	67.9
Absolute Values Standard Deviation	1.1	49.4	29.7	7.4	25.7	23.2	*	19.6
# Positive deviations from 2D model	53							
# Negative deviations from 2D model	12							
# cells where a zero quantity from Method A precluded a calculation	84							

*no preferred habitat at any flow

Table 83. 2D model preferred flows compared to 1D model Method A preferred flows.

Preferred Flows, 2D Model Results	Preferred Flows, 1D Model Method A
Dry (cfs)	Dry (cfs)
5	5
10*	10***
20**	20
30	30
45	45
Wet (cfs)	Wet (cfs)
5	5
15	15
30	30
55	55
100	100
190	190
350	350
Snowmelt (cfs)	Snowmelt (cfs)
10	10
25	25
50	50
140	140
210	210
525	525
1103	1103
3000	3000
6921	6921

*Boxed indicates overall 'best' preferred flow
**Gray indicates preferred flow for greatest area
***Light blue indicates preferred flow for greatest habitat per unit area

11.5.4 Comparison Between 2D Model and 1D Model Method B Results

To continue to understand differences between methods, comparisons between 2D model results and 1D transect Method B results were conducted using the same approach as described in section 11.4.4.

1D model Method B over-predicted the percent area of GHSI>0.4 when compared to 2D model results 36.2% of the time, under-predicted them 28.9% of the time, and returned a zero value 34.9% of the time (

Table 84,

Table 85). All zero values were designated -999 to indicate that the 1D transect Method B returned no available habitat for those species' lifestages at the specified flow. No available habitat means zero habitat, so these values are considered under-predictions. Thus, the 1D model Method B over-predicted GHSI>0.4 values 36.2% of the time and under-predicted them 63.8% of the time.

The largest individual over-prediction occurred for RT during dry season 5 cfs flows at 114.7% (

Table 84). The biggest under-prediction of preferred habitat area with respect to 2D model results was -97.3% during snowmelt season 1103 cfs flows. The largest average species lifestage over-prediction was for RT adults, at 35.3 ± 63.5%, and under-prediction was for SS adults at a negative 44.5 ± 21.5%. RT fry had a larger under-prediction at -67.4%, but only one value at dry season 5 cfs and all others a zero value, which resulted in no preferred habitat at any flows but dry season 5 cfs. An overall average of averages, using an equal weighted approach, yielded a 19.5 ± 51.1% under-prediction. The average absolute variance of 1D method B results from 2D model results was 52.4 ± 26.3%.

A comparison between preferred flows (

Table 86) shows that 2D model results vary from 1D model Method B results, which, incidentally, are exactly the same results as those returned using 1D model Method A results. In dry season, 2D model results preferred 10 cfs with a lesser preference for 20 cfs flows, in wet season 55 cfs flows and a lesser preference for 15 cfs flow, and in snowmelt season 25 cfs flows with a lesser preference for 140 cfs flow. Meanwhile, 1D model Method B preferred flows in dry season were 20 cfs, with a lesser preference for 10 cfs flows; wet season 15 cfs with a lesser preference for 5 cfs flows; and snowmelt season 25 cfs with a less preference for 10 cfs flows.

Table 84. 1D transect Method B results compared to 2D model results.

% Difference in GHSI Area >0.4 Between 1D Method B and 2D Model Results (1D-2D)/2D*100

		ADULT			JUVENILE			FRY	SPAWN
Dry (cfs)	Available Wetted Area (m^2)	SS	RT	PH	SS	RT	PH	RT	RT
5	187080	-66.3	114.7	-7.0	12.2	52.6	27.8	-67.4	na
10	198471	-62.9	96.9	22.3	13.6	41.7	32.6	-999	na
20	253787	-18.7	73.2	47.9	-63.7	18.4	15.7	-999	na
30	295294	-26.7	49.4	46.3	-999	-21.5	4.9	-999	na
45	344483	-73.3	20.4	1.4	-999	-89.6	-60.1	-999	na

		ADULT			JUVENILE			FRY	SPAWN
Wet (cfs)	Available Wetted Area (m^2)	SS	RT	PH	SS	RT	PH	RT	RT
5	226555	-44.3	96.9	36.4	na	54.2	34.3	na	73.3
15	254029	-18.0	72.9	47.6	na	19.0	15.9	na	61.0
30	285995	-26.0	56.9	50.7	na	8.7	6.9	na	24.5
55	325174	-74.4	15.9	13.9	na	-58.8	-44.3	na	-22.8
100	369243	-999	-18.8	-15.3	na	-999	-72.6	na	-83.5
190	425183	-999	-82.8	-57.7	na	-999	-999	na	-89.1
350	499551	-999	-999	-999	na	-999	-999	na	-999

		ADULT			JUVENILE			FRY	SPAWN
Snowmelt (cfs)	Available Wetted Area (m^2)	SS	RT	PH	SS	RT	PH	RT	RT
10	216244	-58.8	108.7	28.0	24.8	48.8	40.1	-999	83.3
25	253122	-23.9	76.3	49.0	-64.4	25.4	19.0	-999	61.7
50	292641	-26.1	55.7	41.3	-999	-14.5	0.2	-999	22.6
140	332720	-65.6	18.7	4.5	-999	-999	-50.7	-999	-52.8
210	311832	-38.3	33.1	23.8	-999	-84.7	-21.9	-999	-28.3
525	377081	-999	-55.3	-35.2	-999	-999	-77.4	-999	-98.1
1103	433858	-999	-97.3	-75.8	-999	-999	-999	-999	-999
3000	514476	-999	-999	-999	-999	-999	-999	-999	-999
6921	610780	-999	-999	-999	-999	-999	-999	-999	-999

Note: -999 denotes no available habitat in 1D results

Table 85. Average, standard deviation, and number of positive and negative deviations of the 1D transect Method B results from the 2D model results.

% Difference Summary Metrics, 1D Transect Method B compared to 2D Model

	ADULT			JUVENILE			FRY	SPAWN
	SS	RT	PH	SS	RT	PH	RT	RT
Average %	-45.2	34.7	11.6	-15.5	-0.6	-8.7	-67.4	-4.4
Standard Deviation	21.3	63.6	38.0	44.6	50.8	40.6	na	67.0
Average % using Absolute Values	45.2	63.2	33.1	35.8	41.6	33.0	67.4	58.4
Absolute Values Standard Deviation	21.3	33.1	20.6	26.3	26.5	23.9	na	28.2
# Positive deviations from 2D model	54							
# Negative deviations from 2D model	43							
# cells where a zero quantity from Method B precluded a calculation	52							

Table 86. 2D model preferred flows compared to 1D model Method B preferred flows.

Preferred Flows, 2D Model Results	Preferred Flows, 1D Model Method B
Dry (cfs)	Dry (cfs)
5	5
10*	10***
20**	20
30	30
45	45
Wet (cfs)	Wet (cfs)
5	5
15	15
30	30
55	55
100	100
190	190
350	350
Snowmelt (cfs)	Snowmelt (cfs)
10	10
25	25
50	50
140	140
210	210
525	525
1103	1103
3000	3000
6921	6921

*Boxed indicates overall 'best' preferred flow
**Gray indicates preferred flow for greatest area
***Light blue indicates preferred flow for greatest habitat per unit area

11.6 Microhabitat Analysis Summary

The extensive microhabitat analyses and methodological comparisons conducted for this study using standard methods to arrive at GHSI values has, firstly, analyzed 2D model results, where depth and velocity values were representative of every 0.5x0.5 m raster cell throughout the full 13.52 km model domain (section 11.3). To test differences between the 2D model results analysis and analyses using more common transect methodologies, 30 transects were selected and velocity and depth measures extracted along each transect at 0.5 m increments to represent the study segment (section 11.4). A separate 1D numerical model was run with 105 cross-sections, where one averaged depth and one averaged velocity value were returned for each cross-

section per model run, as it is professionally used for river science and management for long river segments (section 11.5).

The *first notable conclusion* is that there was a large degree of variation across all methods in individual species' lifestage results that returned preferred area as indicated by GHSI>0.4. Both the transect-based and 1D numerical model methods were compared against the 2D model results to understand the differences between these methods (Table 87). No other method matched the 2D model results; taking into account variance, Methods A & B results deviated by a minimum of 56.1% and a maximum of 118.6%. Since the 2D transect-based method used the hydraulics from the 2D model, then it is necessarily true that any difference between the 2D model results and the 2D transect method reveals a flaw in the transect-based sampling approach. Such flaws can stem from the limited sampling, the upscaling framework, or a combination of those.

- 2D transect Method A results were the highest averaged over-predicted results and the second-highest standard deviation of all methods, at 78.8 ± 39.7%. The standard deviation is an indication of the variability across a species' lifestage when the seasons were averaged together.
- 1D Method A results were second highest in over-prediction with 53.4 ± 20.3%.
    - 1D Method A results returned the highest over-predictions, with 2D model results the most variable.
- 2D transect Method B results were over-predicted on average 32.4 ± 23.7% in relation to 2D model results. The improved performance of this method hinged on avoiding statistical averaging when upscaling point-scale habitat indices to segment-scale habitat areas. However, in common instream flow assessment practice, statistical averaging is used to compute mesohabitat averaged combined suitability indices, before a weighted usable area is calculated.
- 1D Method B results were the only overall under-predicted results, and were on average within 19.5 ± 51.1% of 2D model results. The standard deviation for this result was highest among methods. While the overall average amount of preferred habitat was closest to 2D model results, the variability in results was also greatest.
    - 1D Method B returned results closest to those of the 2D model results.

The *second notable conclusion* is that there was a great deal of variance within methods, as indicated in the high standard deviations (Table 87) and over- and under-predictions of values with respect to 2D model results (Table 88).

- 2D transect Method A results were almost evenly split between over- and under-predictions.
- 1D Method A results were almost 2/3 under-predicted versus 1/3 over-predicted, yet the analysis over-predicted results overall by 53.4%. The apparent disconnect between these results is explained by the number of zero predictions of preferred habitat which were using in Table 88 calculations but not in Table 87 calculations.

- 2D transect Method B results were the only results that were heavily weighted toward over-prediction, with over 90% of results over-predicted. This was also the only other method besides the 2D model results themselves that returned habitat values for all species lifestages at every flow. Again, this was due to the avoidance of statistical averaging.
- 1D Method B results were split very similarly to 1D method A results, with almost 2/3 under-predicted and 1/3 over-predicted, yet there was a greater than 70 percentage-point difference between the 1D Method A and B results.

Metrics were developed to determine which flows returned the most area of habitat indicated as most preferred by GHSI>0.4 values by the most species and/or lifestages, described throughout the ecological analysis section.

Table 89 summarized the top two preferred flows per season for each analysis method.

- Preferred flows for the dry season fall within the range of 10–20 cfs for all methods except 2D transect Method B, which has a range of 20–30 cfs.
- Preferred flows for the wet season vary widely, with 2D model results preferring 55 cfs with a secondary preference of 15 cfs. 2D transect Method B comes closest to the 2D model results with preferred flows of 30 and 15 cfs. All other methods range between 5 and 15 cfs, though preferences are inverted among them.
- Preferred flows for the snowmelt season vary widely, with 2D model results preferring 25 cfs with a secondary preference of 140 cfs. 2D Method B results come closest to the 2D model results with preferred flow of 210 and 10 cfs, so although the range is most similar, the preference is inverted. All other methods range between 10–25 cfs.
    - Overall, 2D model results return the largest range of preferred flows, suggesting that more species' lifestage needs are revealed using near-census data than for other methods.
    - 2D transect Method B results returned ranges more similar to those of the 2D model method than any other method, and thus could be considered the second-best overall results. This method returned no zero habitat in any flow, and as such was also most similar to 2D model results.
    - 2D transect Method A, 1D Method A, and 1D Method B results were most similar to one another. These methods all returned numerous zero habitats especially across higher flows. The similarity between 2D transect Method A and 1D Method A suggests that this method is the least useful method, especially considering the 'all-or-nothing' approach taken to determining habitat area.
    - 1D Method A and B results returned the exact same preferred and secondary flows, suggesting that Method A and Method B performed equally using the 1D hydrodynamic modeling method. The similarity between 1D methods may point to the more pronounced inability of 1D transects, no matter the number, to legitimately represent hydraulic controls and instream habitat.

The *final conclusions* of the microhabitat analysis are that the 2D model results are considered the best result *since all approaches used were either models or subsamples of models*, with 2D transect Method B results next best, since it avoided statistical averaging. This study did not compare models against observation-based methods, though it did test some of the key steps used in processing observational data sets to arrive at habitat-flow relationships. The range of flows returned by these two methods may indicate the ability of these analyses to differentiate between and/or identify the needs of various species' lifestages (

Table 89). All other methods returned similar, narrowly defined, preferred flows, indicating that those methods were less able to uncover nuances between species or lifestage needs. The Method A all-or-nothing approach suggested that higher flows (e.g. no suitable flows in dry season for RT fry,

Table 81) provide no habitat, which seems suspect. For the 1D transect approach, no matter how many cross-sections a 1D numerical model might utilize, the ability to adequately represent hydraulic controls is questionable (Figure 103, Figure 104). Further analyses that focused on individual species and/or individual lifestages would be appropriate to better understand the methods.

This study illustrates the opportunities and constraints in using a 2D model as the centerpiece of instream flow assessment for complex mountain rivers:

- The numbers of depth and velocity data points are 10^2-10^3 greater than any other method available for this study segment (see Chapter 0). Achieving a near-census of hydraulic sampling will perform best at representing the maximum ranges and standard deviations of hydraulics variables.
- Even though modeling has inaccuracies and uncertainties at the point-scale (see sections 4.3-4.5and 6.2), this study found that the variation of depth and velocity throughout a 13.52-km river segment (which is still small compared to the totality of instream flow assessment needs in the watershed) can only be represented with modeling. Science is a long way off from developing technologies for remote sensing of the spatial distribution of velocity. Direct observation at transects will miss deep areas and fast areas.
- Transect-based assessments have no predictive capability and are not recommended for a dynamic channel subjected to diverse societal uses and cumulative impacts. Because they are not mechanistic or predictive, they have little to no utility for river rehabilitation design and evaluation as part of actions required after an instream flow assessment finds problems in a study area. River management involves both flow allocation and channel maintenance. When a 2D model is used for instream flow assessment, it is immediately available for further use in a diversity of river management needs, including rehabilitation designs.
- At present, the dominant philosophy among practitioners is that the habitat-flow relationship is and will remain the centerpiece of instream flow assessment. Even though 2D modeling can be used to construct a habitat-flow relationship, such an outcome is not the primary goal of a shift in methodology. Instead, the opportunity lies in the fact that 2D modeling enables explicit spatial analysis of habitat, which is essential for instream flow assessment, because many important ecological functions are linked to specific locations or migratory pathways.
- As technologies become available that span ever-larger spatial domains with finer detailed data at lower cost, the perceived barriers preventing adoption of 2D modeling in professional practice will fall down. Companies that adopt this method will eventually outcompete those that do not, because the opportunities for spatial analysis will provide added value in bids compared to just having a statistical flow-habitat relationship.

Beyond accuracy of predicting GHSI and area of preferred physical habitat, at some point instream flow analysis must consider the spatial pattern of habitat as well as non-habitat related

metrics of ecological functions in rivers. 2D model results have the capability to grow in these vital future directions, whereas transect-based sampling methods do not. That limits the future potential for transect-based methods, despite the fact that some encouraging results were found in using them in this study.

Table 87. The over- or under-prediction average and standard deviation of averages of all methods compared against 2D model results.

Prediction Variance per Method when compared to 2D Model Census Results*

	Method A		Method B	
	2D v. 2D Transect A	2D v. 1D Method A	2D v. 2D Transect B	2D v. 1D Method B
Overprediction	78.5 ± 39.7%	53.4 ± 20.3%	32.4 ± 23.7%	
Underprediction				-19.5 ± 51.1%

* Of values where a zero quantity did not preclude a comparative calculation

Table 88. Percent of positive and negative values returned from the equation ((Method X value – 2D model value)/2D model value) * 100.

% of GHSI>0.4 values Over- and Underpredicted in Relation to 2D Model Census Results*

	Method A		Method B	
	2D Transect A	1D Method A	2D Transect B	1D Method B
Overpredicted	51.6	35.6	91.3	36.2
Underpredicted	48.4	64.4	8.7	63.8

* Including -999 values as underpredictions in all methods except 2D Transect Method B, where no zero values were returned

Table 89. Flow per season with highest average % preferred habitat using equal weighting per species lifestage.

Seasonal preferred flows, using cumulative metrics

Dry Season (cfs)	2D Model Results	2D Transect Method A	1D Model Method A	2D Transect Method B	1D Model Method B
Preferred flow	10	10	20	20	20
Secondary preference	20	10	10	30	10
Wet Season (cfs)					
Preferred flow	55	5	15	30	15
Secondary preference	15	15	5	15	5
Snowmelt Season (cfs)					
Preferred flow	25	10	25	210	25
Secondary preference	140	10	10	10	10

CHAPTER 12:
Conclusions and Recommendations

The primary goal of this project involved developing a spatially explicit, high-resolution instream flow analysis procedure by blending new and existing technologies. A combination of innovative ground-based and remotely-sensed data collection technologies, data-processing methods, mechanistic models, and GIS-based spatial and 3D analyses were tested for proof-of-concept to determine which would be the most useful in producing relevant information that could be incorporated into future instream flow assessments. Readers are invited to evaluate each section of the report and draw their own conclusions as to whether the various techniques and methodologies might prove useful in future assessments. Based on the experience of producing this study, the single most important tool that can be developed to support in-depth analyses to inform instream flow assessment in the 21st century is as detailed and accurate of a topographic map as possible. Secondarily, having a mechanistic 2D hydrodynamic model capable of integrating flow inputs and detailed topography is the next most important tool for instream flow assessment. The authors believe that at this time and for the next 5–10 years, 2D modeling of water mass and momentum conservation provides the best mechanistic tool commensurate with the topographic detail available and level of knowledge available in river science. Remote-sensing tools are developing so rapidly that it is both difficult and exciting to conjecture just how easily development and adoption of new methods will be that might reveal specific metrics useful for instream flow assessments; special sessions on this topic are now a regular feature of river science conferences.

Regardless of scientific advancement, all methods for instream flow assessment have uncertainty and always will. There is no way around that, because all observation methods and numerical models are developed using assumptions. Every model is simplified compared to any river segment, reach, morphological unit, or hydraulic unit. Simple approaches, such as some types of transect-based or 1D numerical modeling efforts, have easily understood assumptions that should render them unsuitable for instream flow. For example, a transect-based approach in which Manning's equation is used to estimate discharge is never appropriate, but is still commonly used in diverse river science and management applications (Brown and Pasternack, 2009). Also, this study found that transect-based methods that use averaging to arrive at mesohabitat-average combined suitability indices perform poorly. Other transect-based (e.g. PHABSIM) and 1D numerical modeling schemes are sufficiently sophisticated that they are reasonable for some river settings, though mountain rivers present the most complex channel forms in which simple hydraulic estimation and extrapolation from a small set of point observations is most questionable at representing the range of hydraulics naturally present (Chapter 0 and sections 11.4-11.5). Meanwhile, 2D modeling also has a lot of uncertainty in the potential for significant errors in topographic characterization (sections 4.3-4.5), roughness parameterization, and turbulence closure.

What is most important to acknowledge when using hydrodynamic models or hydraulic-sampling observation schemes is that whatever approach is used, analysis of uncertainty should be integrated into study design and reported in any results. In this study, uncertainty was accounted for in every phase of the project by cross-checking different data types and different analysis methods as part of the forward-looking 2D model analysis: 1) LIDAR data was compared against ground-based data and a correction factor introduced to bring the two data

sets into closer agreement (Chapter 4.0), 2) 2D model predictions were compared against field observations (section 6.2) and were found to be on par with other 2D model studies, 3) hydraulic results were analyzed at multiple spatial scales using both statistical and spatial analyses, 4) model results were used to evaluate hydraulic and geomorphic patterns and processes to evaluate dynamism and resilience in the system relative to geomorphic theory, 5) physical habitat modeling used binary binning of GHSI values prior to calculating habitat area for the habitat-flow relationships to significantly reduce error, relative to the common practice of using the weighted usable area metric with no uncertainty assessment.

A complete study of its own could be conducted to understand the uncertainties between the various topographic data collection methods, all of the 2D model predictions based on various input parameters, and how the ecological analyses might change if a field-based effort were undertaken to determine if the habitat suitability curves reflect conditions. What this study sought to accomplish was to be scientifically transparent by acknowledging uncertainties where they exist, performing tests to understand what those uncertainties might be, and reducing uncertainty by simplifying results into more-certain metrics. There are always more and better uncertainty analyses possible, but at this time the main conclusion is that an instream flow assessment that does not include any uncertainty checks is inadequate.

12.1 Methodological Conclusions and Recommendations

The total financial allocation for this project was $218,640, and that included not only the cost of a 2D modeling instream flow assessment, but a hydrological analysis, a geomorphic analysis, and a thorough habitat-flow relationship methodological comparison. It effectively began with flood stage observations on May 4, 2009 and ended with completing this final report on March 31, 2011—a period of 23 months. The intensive field campaign during summer 2009 was a four-month effort by four people working 40 hours a week. It involved integrating several diverse, state-of-the-art technologies, which required patience and diligence. Once the data was in hand, it took substantially more effort than expected to check the quality of all data sources iteratively and repeatedly bring all of the topographic data into agreement (Chapter 4.0). Methods for checking data quality and for processing data were developed as part of the underlying science in this study and were implemented with the aid of ArcGIS and Microsoft Excel software. Even though 2D hydrodynamic modeling is a well-established tool, this project required a few months of testing different 2D mesh generation methods to determine what would work best for the setting and available data. It was not a sure thing that 2D modeling would be feasible for the waterfalls and other complex river features in the study segment, although in the end the SRH-2D model performed well (section 6.2). After ~6 months of 2D modeling, ~6 months were spent on GIS-based hydraulic, geomorphic, and microhabitat analyses using 2D model results. Meanwhile, remote-sensing image processing and analysis was done concurrently over a year of effort. Methods to analyze the data were developed as opportunities and challenges arose. In the final stage of the study, quality checks required some analyses to be re-done and still more new analyses to be conducted. Overall, the project turned out to be ambitious and rewarding, yielding this report as well as a robust dataset that has the potential for further analyses.

One of the important methodological questions asked in this study was whether a 2D hydraulic model could be used as the focal lens through which instream flow assessment could be conducted. The researchers conclude yes, the 2D hydraulic model used for this study proved extremely versatile in what it could lend insight into. The geomorphic analysis section in this

study is almost completely based on 2D model results and includes several new discoveries about scale-dependent geomorphic patterns and processes that would not have been possible without the use of a 2D model. Microhabitat analysis with 2D modeling yielded a detailed dataset of paired depth and velocity points with higher resolution than other instream flow assessment methods. Even with the evident ~20-30% inaccuracy in velocity predictions, the ability to span the widest statistical diversity in hydraulics means that 2D modeling is not missing anything that other commonly used methods might reveal. Most importantly, 2D modeling at ~1-m resolution provides a near-census of spatially distributed hydraulic and habitat conditions, which in the future will enable assessment of the patterns of flow conditions and physical habitats. Someday, when there is the technology and data to enable it, current 2D models that cannot reveal sub-meter hydraulics will have to be discarded and replaced with models that accurately cope with pebble-scale roughness and turbulence that influence the sub-meter flow field. In this study patterns of flow were explored in terms of morphological units and in terms of stage-dependent flow convergence, but there was insufficient time to explore the attributes of the spatial patterns in microhabitats. Nevertheless, the habitat maps in Appendix C illustrate that the potential for making more discoveries by way of spatial analysis is available when high-resolution 2D modeling is used.

Another forward-looking question involved ascertaining the value of various high-resolution remote-sensing methods in the data collection phase of an instream flow assessment. Red-light LIDAR data collection provides remarkable point density, in this study at a density of ~0.7 points per m^2. However, vendors provide few and inadequate data quality checks, necessitating a significant amount of effort to check data quality by the end-user. In the last 18 months, the PI of this project has worked with three different LIDAR vendors and all three have produced significant errors in delivered data; had the PI not caught those manually, then the faulty data would have been used with a false high degree of confidence. This illustrated that the uncertainty tests used by vendors are not reliable. The challenge is that large datasets are difficult and time consuming to check. If problems are not found quickly (i.e. before payment is made), vendors show little interest in solving problems and there is little professional or financial accountability. A dataset with >10 million points is too big to independently check completely, but a substantial effort is mandatory for good results and for characterizing remaining uncertainty.

Beyond LIDAR, this study also investigated the use of ultra-high-resolution kite-blimp imagery. The goal was to achieve sub-centimeter resolution, as had been done in the past. Because kite-blimp flight altitudes were fixed to span the active channel width, the final resolution achieved after georeferencing turned out to be ~4 cm. Images collected at this resolution were mostly stunning and adequate to perform an array of analyses, though there was inadequate time in this study to achieve the full potential. Admittedly, the project team was not trained enough to be able to do all possible types of image correction available and known to photography experts. In the proposal the plan called for rubber-sheeting the blimp images onto 1-m resolution NAIP imagery, but the resolution mismatch between 1 m and 4 cm turned out to make this method impossible. Unpaid (volunteer) undergraduate students from University of California at Davis spent countless hours October 2009 through August 2010 manually georeferencing the images. This approach would be untenable in the private sector. However, aerial image vendors now regularly collect 10-cm resolution imagery using fixed wing aircraft, so less time-consuming methods of achieving a similar output are foreseeable. Utah State University now has the AggieAir Flying Circus (http://aggieair.usu.edu) aerial imagery system

that uses an unmanned aerial drone and GPS tracking to obtain ultra-high-resolution imagery that is adequately georeferenced. The potential for remote sensing of rivers remains very high, but is presently labor intensive and not getting to useful hydrogeomorphic and ecologic products fast enough at low enough cost.

In contrast to 2D modeling, this study found that 1D hydrodynamic modeling is not viable for accurately predicting hydraulics in mountain rivers. In this setting, there are so many hydraulic controls (stage-dependent width constrictions, bed oscillations, and multiple scales of channel roughness) that no reasonable number of cross-sections can capture them. Evenly spaced cross-sections are commonly used, but they make no sense whatsoever for 1D hydraulic prediction. Absent a digital elevation model of the wetted channel in advance, the process of establishing cross-sections at the necessary hydraulic controls is highly uncertain. Even if all hydraulic controls were included, there is enough rapid variation in channel form that cross-sections would not be representative on conditions between them. Also, many locations in the complex channel had 2D flow paths that a 1D model cannot represent. This study found that 1D modeling performed poorly at predicting even XS-averaged depth and velocity, and then those performed poorly at predicting hydraulic habitat quality. Averaging to morphological units did not help.

There is no formally standardized framework for conducting transect-based instream flow analysis, and each relicensing process involves stakeholder-negotiated study designs. As a result, this study could only investigate aspects of the method amenable to direct comparison against a near-census approach using a 2D modeling to characterize hydraulics at the 1-m spatial scale. The key finding was that for a complex mountain river (not a "small" or "large" river, but one with a high ratio of bed-roughness scale to water-depth scale), transect points had mixed performance with respect to their utility for a statistics-based hydraulics and physical habitat assessment. In the absence of 2D modeling, there would be no geomorphic analysis chapter and a greatly curtailed hydraulics component to the study, with no spatial hydraulics component at all. That is a large drawback to relying on a transect-based framework for instream flow analysis. With regard to their statistical capability, the transect sampling did represent the majority of the depth and velocity distributions well, but it did not span the range of hydraulics encountered and performed worse as discharge increased. Mountain rivers have more local hydraulic detail than 30 transects capture. Also, transects performed poorly at yielding statistical metrics at the morphological-unit scale, which is an important step in habitat analysis. In addition, when coupled with a commensurate area estimation method to upscale point observations to morphological units and then on to larger reach and segment scales, transect points performed poorly at estimating the total area of preferred hydraulic habitat across multiple species' lifestages, except when statistical averaging was avoided using the Method B approach.

One reason why transects may have a mixed performance is that only a few are used to represent each mesohabitat type and they are often placed in the same relative location within individual units for each type. Hydraulics at the entrance, middle, exit, centerline, thalweg, and periphery of an individual unit can vary over a wide range and transects fail to capture that diversity. Given limited time and resources, it would be preferable to thoroughly map the 2D flow pattern in a few individual pools completely rather than having many transects in a similar relative location of many different pools, for example.

The results of this study show that hydraulic conditions are more diverse within morphological units than presently recognized in current transect-based sampling schemes. A key factor is that the commonly used method of characterizing laterally uniform mesohabitats based on aerial videography is invalid as a method for distinguishing either ”homogeneous” or “representative” units in mountain rivers. The morphological units uncovered by an objective classification of low-flow channel hydraulics at 1-m resolution turned out to be spatially variable, with discrete smaller units (e.g. steps, pools, chutes, and steep inset channels) surrounded by much larger but more amorphous units (e.g. transition and plane bed). All these in-channel units are bounded by a normally dry active river corridor termed the “floodplain” in this study, though admittedly it was composed of bedrock and alluvial substrates as well as erosive and depositional surfaces. Assigning overbank points to in-channel habitat conceptions in terms of mesohabitats is highly questionable. Further, the aerial videography method is subjective and cannot yield accurate delineations of in-channel and overbank morphological units, so that is a serious limitation impacting transect-based methods.

Finally, transect-based and 1D-model based instream flow assessments provide virtually no process-based hydrogeomorphic insights. A common critique of 2D modeling for instream flow assessment is that the expenditure is unnecessary to obtain statistical habitat-flow relationships. The philosophy that instream flow assessment boils down to flow-habitat relationships (with or without a habitat “time-series analysis”) is flawed. Instream flow assessment ought to involve a lot more than just a statistical microhabitat assessment of weighted usable area as a function of flow and time. Often instream flow assessments give a terse geomorphic assessment (if at all) in which it is simply and conveniently concluded that the river is “stable” no matter the real dynamics present, so standard transect-based methods are deemed appropriate. This study illustrated a wide range of “spatial structure” analyses along the lines of new developments by YARMT (2009). Figuring out the key physical processes responsible for forming and maintaining physical habitat conditions ought to be a larger part of instream flow assessment, and that cannot be achieved with a transect-based study design and aerial videography.

Furthermore, river ecology involves far more than habitat occurrence. Migration, competition, predation, reproduction, habitat renewal, disturbance regimes, and other topics are all components of a comprehensive assessment of the status and dynamics of a river’s ecological functionality. It is unlikely that habitat assessment alone can serve as an indicator for overall ecosystem status.

Ultimately, conducting a 2D-model based instream flow assessment of a 13.52 km river segment is viewed by some as wholly inadequate relative to the need for mountain-wide assessment of the entire Sierra Nevada range. On a practical level, it is claimed that transect-based sampling is the only timely and affordable way to do relicensing. This claim is rapidly unraveling in light of the demonstrated efforts to map and model the ~37.5 km of the lower Yuba River and the ~88 km of the lower Stanislaus River, both substantially longer and wider than the river segment of this study. Over the last 10 years, the ability to map and model river channels at high resolution using a desktop personal computer has matured from ~0.1 km to ~100 km of river length. At this point, it is just a matter of time before it is possible to do 10,000 km of river length and beyond. . In just the last year alone, the computational time to solve a speed-benchmark 2D model decreased in half, with the transition from the Intel Xeon Nehalen 5504 processor at 2.0 GHz to the Intel i7 X980 extreme edition processor at 3.33 GHz. There is no fundamental limitation at play. Methods for mapping river channels continue to advance with shocking

speed. The efficiency of 2D modeling codes also improves, and with the pending onset of parallel-processing codes capable of using multiple computer cores simultaneously, the size and detail of desktop 2D model simulations will grow on par with mapping advances.

12.2 Scientific Conclusions

This project was funded to conduct applied research with direct methodological value for hydropower dam relicensing in the near future. Nevertheless, the use of forward-looking methods resulted in many basic discoveries of varying broad interest. The simplest example of a new discovery was the development of a new technology for characterizing the spatial pattern of emergent boulders in mountain river channels. To actually represent every boulder >0.3 m above the water surface is a novel scientific development. It turned out that the longitudinal distribution of emergent boulders was relatively uniform, but it did vary by morphological unit and could be used to evaluate the scope of "pocket water" in the river. The pattern of extracted boulders proved most useful for georeferencing kite-blimp imagery and evaluating the ability of 2D models to capture emergent boulders and boulder clusters with different types of computational meshes.

The hydrology of the northern Sierra Nevada is poorly documented in the peer-reviewed scientific literature. Government agencies and hydro-facility licensees primarily track water supplies as present in the form of snow and streamflow. Relatively rudimentary hydrological models are being used to predict and track water supplies for mountain water management compared to the state-of-the-art in hydrologic science. Very few basic studies report on the mechanisms of water flux and the interactions between hydrology, ecology, and geomorphology. There has been a rush to evaluate the impacts of climate change for the Sierras using inadequate data, models, and methodologies, yielding highly questionable results with no accountability.

Within this uncertain hydrological context, the novelty and significance of the results of the data-driven hydrologic analysis conducted in this study are unclear. Hydrologic analysis was undertaken out of necessity in support of 2D modeling, but turned out to be sufficiently involved to stand on its own. There is no standardized approach for performing flow-accretion analysis, so in this study methods were developed to evaluate flow accretion, generate synthetic equations to predict it, and then test those equations with direct field observations. The most basic finding was that flow accretion provides several times more flow than is released by hydro-facilities in the dry and wet seasons. Further, although the Jones Bar gage indicates that 2003-2009 had significantly less flow accretion than 1965-172, interannual variability in flow accretion dwarfs the trend. Analysis of historical climate change indicators found no long-term trend in streamflow in the unregulated North Yuba at Goodyear's Bar. Therefore, it is most likely that the changes observed in the Jones Bar record are due to water-management changes and land use/land cover changes. Even with those changes, a comparison of predictions against direct field observations found that the equations for 1965-1972 did not systematically over predict flow accretion.

During the mid to late 1990s two systems for describing and classifying "channel units" in mountain rivers were published in the peer reviewed literature (Grant et al., 1990; Montgomery and Buffington, 1997). Both systems involve a visual identification of channel units and then a statistical analysis of their geomorphic attributes. In recent years, some studies have been shifting away from subjective visual classification of channel units toward objective hydraulic

classification schemes. In these schemes there are still subjective decisions to be made using expert judgment in terms of the number of classes to recognize and the exact numerical thresholds between them. Because water flow and its numerical variables are continuous in space and time, mechanistic thresholds between hydraulic metrics of channel-unit types do not appear to exist. That means that there will have to be some subjectivity in determining the numerical thresholds delineating unit types. However, once the depth-velocity thresholds are set, then the actual spatial pattern of units in the river is determined objectively. That is a significant scientific advance, because it yields precise boundaries between units that are perfectly repeatable.

This study was the first to perform hydraulics-based channel classification at 1-m resolution in a steep mountain river. Discovery of laterally explicit morphological units and the geomorphic and hydraulic characterization of their specific spatial organization is a major scientific advance. The exact names used for some of the morphological units is somewhat different from other studies, but is not particularly important. What is scientifically novel is that new methods were developed to characterize the spatial structure of the units, and that revealed that the fluvial landforms in the study segment are spatially organized, not randomly located. Some units are preferentially located further upstream or downstream within the segment. Each unit has a statistically significant higher likelihood (i.e. "preference") of occurrence adjacent to a subset of other unit types. This spatial organization has a strong influence on physical meso- and micro-habitat conditions. It requires further inquiry into its origin and mechanisms of maintenance.

A major scientific question in fluvial geomorphology involves determining the relative roles of near-uniform channel and valley-wide abstractions of fluvial landforms versus their complex, non-uniform true nature. As summarized by White et al., (2010), there is a consensus for gravel-bed rivers that there exist multiple spatial scales of landform nonuniformity and that the processes governing channel form are primarily due to the flow-dependent expression of this nonuniformity. Processes such as stage-dependent flow convergence, helical flow and sediment routing through meander bends, turbulence-induced local scour at flow obstructions, and particle queuing all hinge on channel non-uniformity. Presently the science of fluvial geomorphology is just beginning to have the tools necessary to reveal the processes as they occur in nature, and 2D modeling is one of the tools that is proving useful (Sawyer et al., 2010).

In this study, the process of stage-dependent flow convergence was thoroughly investigated in the study segment over the range of flows observed in 2009-2010. Indicators of stage-dependent flow convergence were sought after in 2D-model-predicted velocity as well as the derivative variables of maximum critical bed material size and Shields stress for a gravel/cobble mixture. The results found that flows >3000 cfs (SYLC gage) cause channel-altering changes to gravel/cobble substrates, but the framework of boulders that dominates the river corridor requires flows beyond what was studied to cause channel change. It was a disappointment to not be able to model sufficiently large/rare floods, but there was no way to know in advance just how large a flood would be sufficient to alter the channel. The rain-on-snow flood that occurred in January 1997 had ~30,000 cfs in the study reach. Toward the end of this study local residents revealed the locations of some high-water marks that were then surveyed. It might be possible to simulate that even in the near future as part of a subsequent study.

Scientifically, the significance of what was discovered using the 2D model of the 6921 cfs flood is that it confirms the notion that mountain rivers with a framework of boulders requires very large and rare floods to cause channel-altering conditions. Whether stage-dependent flow

convergence plays a role in that is unclear at this time. It is self-evident that if the observed lack of scour conditions in pools were to hold over the full range of flows, then the pools would fill in with material scoured out of the steep inset channel and inset channel areas. Therefore, there has to be some higher flow during which time the pools are preferentially scoured more than other units, causing them to be deeper. The relative roles of stage-dependent flow convergence versus turbulence-induced local scour is unknown, but could be answered if sufficient data existed to simulate a sufficiently large flood.

Although the scope of microhabitat analyses performed with the 2D model did not span the range of what was possible with the available data due to lack of time and resources, this study provides some useful scientific advances. In the process of performing velocity measurements for hydraulic validation, observers had to wade into the river with a sensor and position themselves securely to collect the data. The range of "velocity observation habitat" was 0-2.5 m/s surface velocity for depths of 0-1.5 m, consistent with pre-existing studies of safe wading practices. What turned out to be interesting during data collection was the spatial availability of velocity observation habitat as experienced by the field crew. At low flow (~5-25 cfs) this habitat occurred widely within the wetted channel, with the exception of pools, transitions, and the center of chutes. When flow was > ~100 cfs, the area of velocity observation habitat shifted to the plane bed units at the periphery of the channel, some limited inset channel units, and onto the floodplain. This observation illustrates the importance of the link between microhabitat conditions, morphological units, and flow.

Since the majority of the habitat suitability curves used in this study (except rainbow trout adult and juvenile as well as pikeminnow/hardhead juvenile lifestages) involved lower depths and velocities than suitable for velocity observation, there is no question from both direct observation and from model predictions that habitat availability shifts as discharge increases. The microhabitat analyses show the shifts and they show that some hydraulic habitats therefore increase at higher discharges, while others decrease. The fact that the active river corridor is filled with hydraulic mining sediment means that there is terrestrial alluvial on a floodplain-like surface that is available for fish to migrate to at higher flow. When flow is between 5-50 cfs, there is not as consistent of a stage-dependent habitat dynamic across species' lifestages. Some species' lifestages experience increased area of preferred habitat as water floods out on to the floodplain and others experience decreased area. Once flows are >100 cfs in any season, the maps shown in Appendix C illustrate that there is not a 1-to-1 trade-off in preferred habitat availability relative to the baseflow regime. Instead, at these higher flows there is significantly less area of preferred habitat as discharge increases over a unique range for each species' lifestage.

Remaining pockets of habitat at flows >100 cfs are essentially refugia. As habitat shifts to the channel periphery and onto the floodplain, it comes into contact with more riparian cover and streamwood cover, which may yield an additional benefit beyond what is accounted for in the reported results. The channel itself was found to have a significant amount of roughness at multiple scales, so it does not appear that the amount of cover is different, just the type of cover. Although refugia habitat was not thoroughly investigated in this study, the 2D model produced sufficient results that such an analysis is within grasp if desired.

12.3 Management Conclusions and Recommendations

Multiple concurrent societal impacts on the upper South Yuba River, including accelerated hillslope wasting, presence of historic mining sediment, instream gold mining, roads, land use, and flow regulation interact in complex ways- it is inappropriate to attribute all "blame" to flow regulation. In fact, the dominant aspect of societal impacts on the study segment is the vast amount of sedimentary infill of the river corridor as a direct consequence of historic hydraulic gold mining and regular in-channel dredger gold mining that only ended in late summer 2009. Flow regulation is a factor, but occurs on top of the pre-existing historical reality of extensive direct intervention into natural channel conditions. It would be incorrect to say that in the absence of flow regulation, the channel would experience a natural hydrogeomorphic regime. As Brown and Pasternack (2008) explain, anthropogenic boundary controls have a strong impact on instream habitat than flow regulation. Several case studies around the world have concluded that re-regulating flows as a river restoration strategy in lieu of actively rehabilitating the impacts of anthropogenic boundary controls yields very limited benefits (Pasternack et al. 2008a).

From a habitat perspective, there are three different consequences of the history of mining effects. First and foremost, the extent to which the hydraulic mining debris in the river at this time is "stable" is highly uncertain. Traditionally it is has been thought that rivers possess the capability of adjusting their attributes to accommodate flow and sediment transport regimes so that sediment in- and out-fluxes are balanced and landform conditions are "stable". However, in reality geomorphic drivers and boundary conditions are much more independently dynamic and fast changing than classically envisioned, such that landforms may always be in a state of adjustment in response to external drivers and internal free oscillations that is normal and appropriate. Rather than thinking of landforms as "stable", it is more appropriate to think of them and the ecosystem functions they are associated with as resilient in the face of change. Knowledge of historic, pre-human baseline conditions or regional reference conditions is limited and may not be as useful in understanding natural geomorphic and ecosystem services as once envisioned. In light of this natural complexity, a geomorphic assessment of conditions after a large dam or other facility is built and operated may not be as simple as documenting geomorphic instability and attributing that to human impacts relative to the presumed stable baseline conditions. What this study provides is an extremely rich geomorphic baseline assessment of conditions in 2009-2010 that can be used in future studies to assess channel change and ecohydraulic resilience.

Second, the presence of a large amount of mining sediment in the river means that as stage rises, fish habitat can and does shift from channel-center to overbank margins, enabling preferred habitat to exist over a wide range of flows. The type and amount of habitat may shift to refugia at high flows, but it is still there and it is coincident with availability of diverse cover types.

Third, the channel has an abundance of gravel/cobble substrates suitable for fish spawning. These sizes are ubiquitous throughout the river, but primary occur within a structured framework of boulders. More than 36,000 emergent boulder features were mapped in the study segment. These emergent boulder features create a "pocket water" effect that traps smaller substrates in their lee. In addition, hydraulic sorting occurs in which larger and deeper patches

of sand or gravel accumulate. Kite-blimp imagery captured these features, but it was not feasible to map them in GIS with the available time and budget.

Beyond the effect of hydraulic mining sediment, another non-regulated aspect of the system was found to be essential to channel processes and hydraulic habitat- flow accretion. Flow accretion may not occur within the topmost channel length below Spaulding Dam (or any dam), but it is essential to have sufficient gaging stations in a system to characterize it. Presently, every hydro-facility affecting the study segment is gaged, while none of the accretionary segments of the mainstem river or major tributaries are gaged. Also, the extent to which non-point discharge of groundwater is occurring along the length of the river is unknown.

Flow accretion represents a large source of uncertainty in both instream flow assessment and in subsequent flow regime specifications. This study found a significant amount of interannual variation in flow accretion, such that only two out of seven independent tests of predicted versus observed flow accretion were within 10% of each other. It is recommended that dam licenses for mountain rivers require establishing a network of gages to monitor accretionary flows. This would build datasets that would enable future generations to more thoroughly and accurately assess flow accretion. Further, to the extent that instream flow requirements are shifting away from the concept of minimum flow requirements to a more balanced flow regime that serves more geomorphic processes and ecological functions at the right times, credit ought to be given to the role of accretionary flows in leveraging beneficial environmental outcomes. Determining the exact length of channel below a dam for which flow accretion has no relevance, would be useful.

REFERENCES

Ackers, P., White, W., Perkins, J., Harrison, A. 1978. Weirs and flumes for flow measurement. John Wiley & Sons, New York.

Arthington, A.H., Bunn, S.E., Poff, N.L., and Naiman, R.J. 2006. The challenge of providing environmental flow rules to sustain river ecosystems. Ecological Applications 16(4): 1311-1318.

Barbour, M.G., Keeler-Wolf, T., and Schoenherr, A.A. 2007. 3rd Ed. Terrestrial vegetation of California. University of California Press, Berkeley, CA.

Bates, P.D., Anderson, M.G., Baird, L., Walling, D.E., Simm, D. 1992. Modeling floodplain flow with a two dimensional finite element scheme. Earth Surface Processes and Landforms 17, 575-588.

Bates, P.D., Anderson, M.G., Hervouet, J.M., Hawkes, J.C. 1997. Investigating the behaviour of two-dimensional finite element models of compound channel flow. Earth Surface Processes and Landforms 22 (1), 3-17.

Bates, P.D., Horritt, M.S., Hervouet J.M. 1998. Investigating two-dimensional, finite element predictions of floodplain inundation using fractal generated topography. Hydrological Processes 12 (8), 1257-1277.

Barker, J.R., Pasternack, G.B., Bratovich, P., Massa, D., Reedy, G., Johnson, T. 2010. Method to Rapidly Collect Thousands of Velocity Observations to Validate Million-Element 2D Hydrodynamic Models. Abstract EP51C-0571 presented at 2010 Fall Meeting, AGU, San Francisco, Calif., 13-17 Dec.

Beechie, T.J., Collins, B.D., and Pess, G.R. 2001. Holocene and recent geomorphic processes, land-use and fish habitat in two Puget Sound watersheds. In: Dorava, J.M., Montgomery, D.R., Palcsak, B., Fitzpatrick, F. (Eds.), Geomorphic Processes and River Habitat. American Geophysical Union, Washington D.C., pp. 37–54.

Beechie, T.J., Pess, G., Beamer, E., and Lucchetti, G. 2003. Role of watershed assessments in recovery planning for salmon. In: Montgomery, D.R., Bolton, S., Booth, D.B., Wall, L. (Eds.), Restoration of Puget Sound Rivers. University of Washington Press, Seattle, WA, pp. 194–225.

Beechie, T.J., Liermann, M., Pollock, M.M., Baker, S., and Davies, J. 2006. Channel pattern and river-floodplain dynamics in forested mountain river systems. Geomorphology 78: 124-141.

Benda, L., Hasson, M.A., Church, M., and May, C.L. 2005. Geomorphology of steepland headwaters: the transition from hillslopes to channels. Journal of the American Water Resources Association 04071: 835-851.

Booker, D.J., Acreman, M.C. 2007. Generalisation of physical habitat-discharge relationships. Hydrology and Earth System Sciences 11: 141-157.

Booker, D.J., Sear, D.A., Payne, A.J. 2001. Modeling three-dimensional flow structures and patterns of boundary shear stress in a natural pool–riffle sequence. Earth Surface Processes and Landforms 26 (5): 553–576.

Bovee, K.D. 1982. A guide to stream habitat analysis using the instream flow incremental methodology. Instream Flow Information Paper 12. U.S.D.I. Fish Wildl. Serv., Office of Biol. Serv. FWS/OBS-82/26: 248 pp.

Bovee, K.D. 1986. Development and evaluation of habitat suitability criteria for use in the instream flow incremental methodology. Instream Flow Information Paper 21, U. S. Fish and Wildlife Service Biological Report 86(7), U. S. Fish and Wildlife Service.

Brandt, S.A. 2000. Classification of geomorphological effects downstream of dams. Catena 40(4): 375-401.

Brierly, G. J., Fryirs, K. 2000. River styles, a geomorphic approach to catchment characterization: implications for river rehabilitation in Bega catchment, New South Wales, Australia. Environmental Management 25, 661-679.

Brasington, J., Rumsby, B.T. and McVey, R.A. 2000. Monitoring and modelling morphological change in a braided gravel-bed river using high resolution GPS-based survey. Earth Surface Processes and Landforms 25(9): 973-990.

Brown, R.A., and Pasternack, G.B. 2008. Engineered channel controls limiting spawning habitat rehabilitation success on regulated gravel-bed rivers. Geomorphology 97: 631-654.

Brown, R.A., and Pasternack, G.B. 2009. Comparison of Methods for Analyzing Salmon Habitat Rehabilitation Designs For Regulated Rivers. River Research and Applications 25: 745-772.

Brunner GW. 1998. HEC-RAS: River Analysis System. Unpublished Users Manual, Version 2.2. U.S. Army Corps of Engineers: CA.

Buffington, J.M., Lisle, T.E., Woodsmith, R.D., Hilton, S. 2005. Controls on the size and occurrence of pools in coarse-grained forest rivers. River Research and Applications 18: 507–531.

Bunte, K., Abt, S.R. 2001. Sampling surface and subsurface particle-size distributions in wadable gravel-and cobble-bed streams for analyses in sediment transport, hydraulics, and streambed monitoring. Gen. Tech. Rep. RMRS-GTR-74. Fort Collins, CO: U.S. Department of Agriculture, Forest Service, Rocky Mountain Research Station. 428 p.

Buscombe, D., Rubin, D.M., Warrick, J.A. 2010. A universal approximation of grain size from images of no cohesive sediment: Journal of Geophysical Research, v.115, F02015, doi:10.1029/2009JF001477.

California Data Exchange Center (CDEC). 2010. Accessed October 23, 2010. http://cdec.water.ca.gov/

Carling, P.A. 1991. An appraisal of the velocity-reversal hypothesis for stable pool riffle sequences in the River Severn, England. Earth Surface Processes and Landforms 16 (1): 19-31.

Cao, Z.X., Carling, P., Oaky, R. 2003. Flow reversal over a natural pool–riffle sequence: a computational study. Earth Surface Processes and Landforms 28 (7): 689-705.

Castleberry, D.T., Czech, J.J., Erma, D.C., Hankins, D., Healey, M., Kondolf, G.M., Mangle, M., Mohr, M., Moyle, P.B., Nielsen, J., Speed, T.P., and Williams, J.G. 1996. Uncertainty and instream flow standards. Fisheries 21(8): 20-21.

Cavallo, B., Kurt, R., Kidnap, J., Seesholtz, A., Perrone, M. 2003. Distribution and habitat use of steelhead and other fishes in the lower feather river, 1999-2001. Interim Report. SPF10, Task 3a, California Department of Water Resources, Division of Environmental Services.

Clifford, N.J. 1993. Differential bed sedimentology and the maintenance of a riffle-pool sequence. Catena 20, 447-468.

Clifford, N.J. and French, J.R. 1998. Restoration of channel physical environment in smaller, moderate gradient rivers: geomorphological bases for design criteria. In: R.G. Bailey, P.V. Jose and B.R. Sherwood (Editors), United Kingdom Floodplains. Westbury Academic & Scientific Publishing, Westbury, pp. 72-76.

Clifford, N.J., Richards, K.S. 1992. The reversal hypothesis and the maintenance of riffle–pool sequences: a review and field appraisal. In: Lowland Floodplain Rivers: Geomorphological Perspectives. Edited by Carling, P.A., Petts, G.E. John Wiley & Sons, Chichester, 43-70 pp.

Clifford, N.J., Soar, P.J., Harmar, O.P., Gurnell, A.M., Petts, G.E., Emery, J.C. 2005. Assessment of hydrodynamic simulation results for eco-hydrological and eco-hydraulic applications: a spatial semivariance approach. Hydrological Processes 19: 3631–3648.

Cox, C. 2007. Research needs assessment for hydropower relicensing processes in California: developing tools for more efficient and effective resource management. California Energy Commission, PIER Program.

Crowder D.W., Diplas P. 2000. Using two-dimensional hydrodynamic models at scales of ecological importance. Journal of Hydrology 230: 172-191.

Curtis, J.A., Flint L.E, Alpers, C.N. and Yarnell, S.M. 2005. Conceptual model of sediment processes in the upper Yuba River watershed, Sierra Nevada, CA. Geomorphology 68:149-166.

Darby S.E., Van de Wiel M.J. 2003. Models in fluvial geomorphology. *In* Tools in fluvial geomorphology, Kondolf, GM. Piégay, H (Eds). Wiley: Chichester.

Dendy, F.E., Bolton, G.C. 1976. Sediment yield-runoff drainage area relationships in the United States. Journal of Soil and Water Conservation 31, 264-266.

Department of Water Resources (DWR). 2004. SP F-16 Phase 2 report, evaluation of project effects on instream flows and fish habitat. Oroville Facilities Relicensing, FERC Project No. 2100.

Dreamflows. Flow information for California rivers. http://www.dreamflows.com/

Elkins, E.E., Pasternack, G.B., Merz, J.E. 2007. The Use of Slope Creation for Rehabilitating Incised, Regulated, Gravel-Bed Rivers. Water Resources Research 43(W05432): doi:10.1029/2006WR005159.

Elliott, C.R.N., Johnson, I.W., Sekulin, A.E., Dunbar, M.J., Acreman, M.C. 1996. Guide to the use of the Physical Habitat Simulation system. R&D Technical Report W20. Environment Agency: Bristol, UK.

Escobar, M.I. and Pasternack, G.B. 2009. A Hydrogeomorphic Dynamics Approach to Assess In-Stream Ecological Functionality Using the Functional Flows Model, Part 1 - Model Characteristics . River Research and Applications, doi: 10.1002/rra.1316.

Gallagher, S.P., Gard, M.F. 1999. Relationship between chinook salmon (Oncorhynchus tshawytscha) redd densities and PHABSIM-predicted habitat in the Merced and American Rivers, California. Canadian Journal of Fisheries and Aquatic Sciences 56: 570-577.

Gard, M. 2003. Flow-habitat relationships for spring-run Chinook salmon spawning in Butte Creek, U.S. Fish and Wildlife Service, Energy Planning and Instream Flow Branch, Butte Creek 2-D Modeling Final Report.

Geist, D.R., Dauble, D.D. 1998. Redd site selection and spawning habitat use by fall chinook salmon: the importance of geomorphic features in large rivers. Environmental Management 22, 655-669.

Ghanem, A., Steffler, P., Hicks, F. 1996. Two-dimensional hydraulic simulation of physical habitat conditions in flowing streams. Regulated Rivers: Research & Management 12:185-200.

Gibson, S., Nygaard, C., Sclafani, P. 2010. Mobile bed modeling of the Cowlitz River using HEC-RAS: Assessing flooding risk and impact due to system sediment. United States Army Corps of Engineers, 2nd Joint Federal Interagency Conference, Las Vegas, NV, June 27 - July 1, 2010.

Gilbert, G.K. 1917. Hydraulic-Mining Debris in the Sierra Nevada: U.S. Geological Survey Professional Paper 105, 154 p. Geological Society of America Bulletin 102: 340-352.

Good, T.P., Beechie, T.J., McElhany, P., McClure, M.M., Ruckelshaus, M.H. 2007. Recovery planning for Endangered Species Act-listed Pacific salmon: Using science to inform goals and strategies. Fisheries, 32:426-440.

Gore, J.A., Nestler, J.M. 1988. Instream flow studies in perspective. Regulated Rivers: Research and Management 93-101.

Grant, G.E., Swanson, F.J., Wolman M.G. 1990. Pattern and origin of stepped-bed morphology in high-gradient streams, Western Cascades, Oregon.

Grant, G.E., Schmidt, J.C., Lewis, S.L. 2003. A Geological Framework for Interpreting Downstream Effects of Dams on Rivers. In A Peculiar River. Edited by J.E. O'Connor and G.E. Grant. American Geophysical Union, Water Science And Applications Series, Vol. 7, Washington, D.C. pp. 209-223.

Guay, J.C., Boisclair, D., Rioux, D., Leclerc, M., Lapointe, M., Legendre, P. 2000. Development and validation of numerical habitat models for juveniles of Atlantic salmon (salmo salar). Canadian Journal of Fisheries and Aquatic Sciences 57: 2065-2075.

Gurnell, A.M., Piegay, H., Swanson, F.J., Gregory, S.V. 2002. Large wood and fluvial processes. Freshwater Biology 47: 601-619.

Hanrahan, T.P., 2007. Bedform morphology of salmon spawning areas in a large gravel-bed river. Geomorphology 86, 529–536.

Hardy, R.J., Bates, P.D., Anderson, M.G. 1999. The importance of spatial resolution in hydraulic models for floodplain environments. Journal of Hydrology 216 (1-2), 124-136.

Harrison, L.R., Keller, E.A. 2007. Modeling forced pool–riffle hydraulics in a boulder-bed stream, southern California. Geomorphology 83, 232-248.

Hatfield T, Bruce J. 2000. Predicting salmonid habitat-flow relationships for streams from western North America. North American Journal of Fisheries Management 20: 1005–1015.

Heritage, G.L., Milan, D.J., Large, A.R.G., Fuller, I. 2009. Influence of survey strategy and interpolation model upon DEM quality. Geomorphology, doi:10.1016/j.geomorph.2009.06.024.

Hoang, Q.H., Kubo N., Hoang, N.G., Tanji H. 2009. Operation of the Ba Lai irrigation system in the Mekong Delta, Vietnam. Paddy Water Environ., doi:10.1007/s10333-009-0155-0.

Horritt, M.S., Bates, P.D., Mattinson, M.J. 2006. Effects of mesh resolution and topographic representation in 2D finite volume models of shallow water fluvial flow. Journal of Hydrology 329 (1-2), 306-314.

Jacobson, R.B., Galat, D.L. 2006. Flow and form in rehabilitation of large-river ecosystems – an example from the lower Missouri River. Geomorphology 77, 249-269.

Jackson, D.A., Peres-Neto, P.R., Olden, J.D. 2001. What controls who is where in freshwater fish communities- the roles of biotic, abiotic, and spatial factors. Canadian Journal of Fisheries and Aquatic Sciences 58: 157-170.

James, L.A. 1995. Diversion of the upper Bear River: Glacial diffluence and Quaternary erosion, Sierra Nevada, California. Geomorphology 14: 131-148.

James, L.A., Harbor, J., Fabel, D., Dahms, D., Elmore, D. 2002. Late Peistocene glaciations in the northwestern Sierra Nevada, California. Quarternary Research 57: 409-419.

James, L.A. 2005. Sediment from hydraulic mining detained by Englebright and small dams in the Yuba basin. Geomorphology 71: 202-226.

Johannesen H., Parker G. 1989. Linear theory of river meanders. *In* Ikeda, S. and Parker, G., eds. River meandering American Geophysical Union Water Research Monograph 12 379-415.

Johnson, A.D. 1997. The Nevada "Rome" Powerhouse and the Birth of PG&E. Accessed October 23, 2010. http://www.ncgold.com/Museums_Parks/syrp/hydrohis.html.

Kattelmann, K. 1997. Rapid changes in snow cover at low elevations in the Sierra Nevada, California, U.S.A., Annals of Glacialogy 25: 367-370.

Keller, E.A. 1971. Areal sorting of bed-load material: the hypothesis of velocity reversal. Geological Society of America Bulletin 82: 753–756.

Keller, E.A. Florsheim, J.L. 1993. Velocity-Reversal Hypothesis - a Model Approach. Earth Surface Processes and Landforms, 18(8): 733-740.

Kendall, B.E., Fox, G.A. 2002. Variation Among Individuals and Reduced Demographic Stochasticity. Conservation Biology 16:109-116.

Kieffer, S.W. 1985. The 1983 hydraulic jump in Crystal Rapid: implications for river running and geomorphic evolution in the Grand Canyon. Journal of Geology 93, 385-406.

Kieffer, S.W. 1989. Geologic nozzles. Reviews of Geophysics 27, 3-38.

Knighton, A.D. 1998. Fluvial Forms and Processes: A New Perspective. Arnold, London. 383 p. ISBN 0 340 66313 8.

Kondolf, G.M., Larsen, E.W., Williams, J.G. 2000. Measuring and modeling the hydraulic environment for assessing instream flows. . North American Journal of Fisheries and Management 1016-1028.

Lamb, B.L., Sabaton, C. Souchon, Y. 2004. Use of the instream flow incremental methodology: introduction to the special issue. Hydroécologie Appliquée 14(1): 1-7.

Lane, S.N., Bradbrook, K.F., Richards, K.S., Biron, P.A., Roy, A.G. 1999. The application of computational fluid dynamics to natural river channels: three-dimensional versus two-dimensional approaches. Geomorphology 29(1-2): 1-20.

Lane, S.N., Richards, K.S. 1998. High resolution, two-dimensional spatial modelling of flow processes in a multi-thread channel. Hydrological Processes 12 (8), 1279-1298.

Lawless, M. Robert, A. 2001. Scales of boundary resistance in coarse-grained channels: turbulent velocity profiles and implications. Geomorphology 39(3-4): 221-238.

Lax P.D., Wendroff B. 1960. *Systems of conservation laws*, Communication on Pure and Applied Mathematics, Vol. 13, pp. 217–237.

Leclerc, M., Boudreault, A., Bechara, J.A., Corfa, G. 1995. 2-dimensional hydrodynamic modeling - a neglected tool in the instream flow incremental methodology. Transactions of the American Fisheries Society 124: 645-662.

Leopold, L.B., Wolman, M.G., Miller, J.P. 1964. Fluvial Processes in Geomorphology. San Francisco: Freeman.

Lisle, T.E. 1979. A sorting mechanism for a riffle-pool sequence: Geological Society of America Bulletin 90: 1142-1157.

Lisle, T.E. 1986. Stabilization of a gravel channel by large streamside obstructions and bedrock bends, Jacoby Creek, Northwestern California. Geological Society of America Bulletin 97, 999–1011.

Lisle, T.E., Nelson, J.M., Pitlick, J., Madej, M.A., Barkett, B.L. 2000. Variability of bed mobility in natural, gravel-bed channels and adjustments to sediment load at local and reach scales. Water Resources Research 36 (12): 3743-3755.

MacWilliams, M.L., Wheaton, J.M., Pasternack, G.B., Kitinidis, P.K., Street, R.L. 2006. The Flow Convergence-Routing Hypothesis for Pool-Riffle Maintenance in Alluvial Rivers. Water Resources Research 42(W10427): doi:10.1029/2005WR004391.

May, C.L., Pryor, B., Lisle, T.E., Lang, M.M. 2007. Assessing the risk of redd scour on the Trinity River. Report prepared for the Bureau of Reclamation, Trinity River Restoration Program, Weaverville, CA. 63p.

McCabe, G.J., Clark, M.P. 2005. Trends and Variability in Snowmelt Runoff in the Western United States. Journal of Hydrometeorology, 6(4): 476-482.

McElhany, P., Ruckelshaus, M.H., Ford, M.J., Wainwright, T.C., Bjorkstedt, E.P. 2000. Viable salmonid populations and the recovery of evolutionarily significant units. U.S. Dept. Commer. NOAA Tech. Memo. NMFS-NWFSC-42, 156 pp.

McKelvey, K.S. Johnson, J.G. 1992. Historical perspectives on forests of the Sierra Nevada and the Transverse Ranges of Southern California: forest conditions at the turn of the century. USDA Forest Service Gen. Tech. Rep. PSW-GTR-133. Chapter 11, 225-246.

Milan, D.J., Heritage, G.L., Large, A.R.G., Charlton, M.E. 2001. Stage-dependent variability in tractive force distribution through a riffle–pool sequence. Catena 44(2): 85-109.

Milhous, R.T., Updike, M.A., Schneider, D.M. 1989. Physical Habitat Simulation Reference Manual—Version II. Instream Flow Information Paper No. 26, Biological Report 89(16). US Fish and Wildlife Service: Fort Collins, Colorado.

Miller, A.J. 1994. Debris-fan constrictions and flood hydraulics in river canyons: some implications from two-dimensional flow modeling. Earth Surface Processes and Landforms 19, 681–697.

Miller, A.J., Cluer, B.L. 1998. Modeling considerations for simulation of flow in bedrock channels. *In*: Wohl, E.E., Tinkler, K.J. (Eds.), Rivers Over Rock: Fluvial Processes in Bedrock Channels. Geophysical Monograph Series, Vol. 107., American Geophysical Union, Washington, DC, pp. 61-104.

Moir, H.J., Pasternack, G.B. 2008. Relationships between mesoscale morphological units, stream hydraulics and Chinook salmon (Oncorhynchus tshawytscha) spawning habitat on the Lower Yuba River, California. Geomorphology 100: 527-548.

Moir, H.J., Pasternack, G.B. 2010. Substrate requirements of spawning Chinook salmon (*Oncorhynchus tshawytscha*) are dependent on local channel hydraulics. River Research and Applications 26:456-468.

Moir H.J., Gibbins, C.N., Soulsby, C., Webb J. 2004. Linking channel geomorphic characteristics to spatial patterns of spawning activity and discharge use by Atlantic salmon (*salmo salar l.*). Geomorphology 60: 21-35.

Moir, H.J., Gibbins, C.N., Soulsby, C., Youngson, A.F. 2005. PHABSIM modelling of Atlantic salmon spawning habitat in an upland stream: Testing the influence of habitat suitability indices on model output. River Research and Applications 21: 1021-1034.

Montgomery, D.R., Buffington, J.M. 1997. Channel-reach morphology in mountain drainage basins. GSA Bulletin 109(5): 596-611.

Montgomery, D.R., Buffington, J.M., Smith, R.D., Schmidt, K.M., Pess, G. 1995. Pool spacing in forest channels. Water Resources Research 31, 1097–1105.

Moyle, P.B. 1994. The decline of anadromous fishes in California. Conservation Biology 8(3): 869-870.

Moyle, P.B., Check, J.J. 2004. Fishes: An introduction to ichthyology, Pearson Prentice Hall, Upper 23 Saddle River, NJ.

Moyle, P.B., Randall, P.J. 1998. Evaluating the biotic integrity of watersheds in the Sierra Nevada, California. Conservation Biology 12: 1318-1326.

Naden, P.S., Brayshaw, A.C. 1987. Small and medium-scale bedforms in gravel-bed rivers. River channels environment and process. *In*: Richards (Ed.), I.B.G. Special Publication, 17. Blackwell, Oxford, pp. 249–271.

National Agricultural Imagery Program (NAIP). http://www.fsa.usda.gov/FSA/apfoapp?area=home&subject=prog&topic=nai

National Oceanic and Atmospheric Administration (NOAA). 2010. California Nevada River Forecast Center. Accessed October 23, 2010. http://www.cnrfc.noaa.gov/rainfall_data.php.

Nelson, J.M., Bennett, J.P., Wiele, S.M. 2003. Flow and sediment-transport modeling. In Tools in fluvial geomorphology, Kondolf GM, Piégay, H (Eds). Wiley, Chichester, 539-576.

Newson, M.D., Newson, C.L. 2000. Geomorphology, ecology and river channel habitat: mesoscale approaches to basin-scale challenges. Progress in Physical Geography 24, 195-217.

Nevada Irrigation District (NID). 2005. Project History, Nevada Irrigation District & Yuba-Bear Hydroelectric Project (FERC Project No. 2266), Draft relicensing process plan and schedule.

Nevada Irrigation District (NID) Facilities and Features schematic. 2007. Yuba-Bear Hydroelectric Project (FERC No. 2266). Yuba-Bear and Drum-Spaulding Projects Schematic (Modeling Version).

Nevada Irrigation District (NID) and Pacific Gas and Electric Company (PG&E). 2008. Study Proposal, Instream Flow, dated May 6, 2008.

Nicholas, A.P., Mitchell, C.A. 2003. Numerical simulation of overbank processes in topographically complex floodplain environments. Hydrological Processes 17, 727-746.

Pacific Gas & Electric Company (PG&E). 2010. Accessed October 23, 2010. http://www.pgecorp.com/aboutus/history/.

Pacific Gas and Electric Company (PG&E) Facilities and Features Schematic. 2007. Drum-Spaulding Project (FERC No. 2310). Pacific Gas and Electric Company.

Padmore, C. L., Newson, M. D., Charlton, M. E. 1998. Instream habitat in gravel bed rivers: identification and characterisation of biotopes. In: Klingeman, P. C., Beschta, R. L., Komar, P. D., Bradley, J. B. (Eds.), Gravel bed rivers in the environment. Water Resources Publications, Highlands Ranch, Colorado, pp. 345-364.

Parasiewicz, P. 2007. The Mesohabsim Model Revisited. River Research and Applications 23: 893-903.

Park, J. K., 1992. Suspended Sediment Transport in a Mountainous Catchment. Science Reports of the Institute of Geoscience, Univ. of Tsukuba, 13(A): 137-197.

Parker, G., Toro-Escobar, C.M., Ramey, M., Beck, S. 2003. The effect of floodwater extraction on the morphology of mountain streams. Journal of Hydraulic Engineering 129(11): 885-895.

Pasternack, G. B. 2008a. Spawning habitat rehabilitation: advances in analysis tools. *In* (D.A. Sear, P. DeVries, S. Greig, Eds) Salmonid spawning habitat in rivers: physical controls, biological responses, and approaches to remediation. Symposium 65, American Fisheries Society, Bethesda, MD, p. 321-348.

Pasternack, G. B. 2008b. SHIRA-Based River analysis and field-based manipulative sediment transport experiments to balance habitat and geomorphic goals on the lower Yuba River. Cooperative Ecosystems Studies Unit (CESU) 81332 6 J002 Final Report, University of California at Davis, Davis, CA, 569pp.

Pasternack, G.B., Bounrisavong, M.K., Parikh, K.K. 2008. Backwater control on riffle-pool hydraulics, fish habitat quality, and sediment transport regime in gravel-bed rivers. Journal of Hydrology 357(1-2): 125-139.

Pasternack, G.B., Gilbert, A.T., Wheaton, J.M., Buckland, E.M. 2006a. Error Propagation for Velocity and Shear Stress Prediction Using 2D Models For Environmental Management. Journal of Hydrology 328: 227-241.

Pasternack, G.B., Ellis, C. Leier, K.A., Valle, B.L., Marr, J.D. 2006b. Convergent hydraulics at horseshoe steps in bedrock rivers. Geomorphology 82:126-145.

Pasternack, G.B., Wang, C.L., Merz, J.E. 2004. Application of a 2D hydrodynamic model to design of reach-scale spawning gravel replenishment on the Mokelumne River, California. River Research and Applications 20(2): 205-225.

Pasternack, G.B., Maneta, M.P., Pan, L.L., Chen, S.H., Fogg, G.E., Grismer, M.E., Harter, T., Hopmans, J.W., Puente, C.E., Ustin, S.L., Wallender, W.W. Submitted. Resiliency of a high-precipitation water supply region in California to future climatic change. Water Resources Research.

Partridge, J., Baker V.R. 1987. Palaeoflood hydrology of the Salt River, Arizona. Earth Surface Processes and Landforms 12: 109-125.

Payne, T.R., Bremm, D.J. 2003. The influence of multiple velocity calibration sets on the PHABSIM habitat index. Paper presented to International IFIM User's Workshop, June 1-5, 2003, Ft. Collins, CO.

Payne, T.R., Eggers, S.D., Parkinson, D.B. 2004. The number of transects required to compute a robust PHABSIM habitat index. Hydroécologie Appliquée 14(1): 27-53.

Payne, T.R. 2004. A Roadmap for PIER Research on Instream Flow Determinations for Hydropower Applications in California. California Energy Commission, PIER Program.

Perry, C.A. 2000. Significant floods in the United States during the 20th Century- USGS measures a century of floods. United States Geological Survey, Fact Sheet 024-00, 4pp.

Poff, N.L., Allan, J.D., Bain, M.B., Karr, J.R., Prestegaard, K.L., Richter, B.D., Sparks, R.E., Stromberg, J.C. 1997. The natural flow regime. Bioscience 47: 769-784.

Power, M.E., Dietrich, W.E., Finlay, J.C. 1996. Dams and Downstream Aquatic Biodiversity: Potential Food Web Consequences of Hydrologic and Geomorphic Change. Environmental Management 20(6): 887-895.

Pyearce, R.S., Ashmore, P.E. 2005. Bedload path length and point bar development in gravel-bed river models. Sedimentology 52(4): 839–857.

Reeves, G.H., Everest, F.H., Nickelsen, T.E. 1989. Identification of physical habitats limiting the production of coho salmon in western Oregon and Washington. U.S. Forest Service General Technical Report PNW-GTR-245, Boise, ID.

Rathburn, S., Wohl, E. 2003. Predicting fine sediment dynamics along a pool-riffle mountain channel. Geomorphology 55: 111-124.

Reid, L.M. 2001. Cumulative watershed effects: then and now. WMC Networker Summer 2001, p. 24-33.

Repetto, R., Tubino, M., Paola, C. 2002. Planimetric instability of channels with variable width. Journal of Fluid Mechanics 457: 79–109.

Richter, B.D., Baumgartner, J.V., Powell, J., Braun, D.P. 1996. A method for assessing hydrologic alteration within ecosystems. Conservation Biology 10(4): 1163-1174.

Rosgen, D.L. 1996. Applied River Morphology. Wildland Hydrology, Pagosa Springs, Colorado.

Sandoval-Solis, S., McKinney, D.C., Loucks, D.P. 2010. Sustainability index for water resources planning and management. Journal of Water Resources Planning and Management, doi:10.1061/(ASCE)WR.1943-5452.0000134.

Sawyer, A.M., Pasternack, G.B., Moir, H.J., Fulton, A.A. 2010. Riffle-Pool Maintenance and Flow Convergence Routing Confirmed on a Large Gravel Bed River. Geomorphology 114:143-160.

Slyter, R.J., Slyter, G.J. 1976. Historical notes of the early Washington, Nevada County, California Mining District.

Stewart, G.B., 2000. Two-dimensional hydraulic modeling for making instream-flow recommendations. Masters Thesis, Colorado State University, Fort Collins, CO, 80 pp.

Stewart, I.T., Cayan, D.R., Dettinger, M.D. 2005. Changes toward Earlier Streamflow Timing across Western North America. Journal of Climate, 18(8): 1136-1155.

Stewardson, M.J., McMahon, T.A. 2002. A stochastic model of hydraulic variations within stream channels. Water Resources Research 38 (1). doi:10.1029/2000WR000014.

Stockdale, R.J., McLelland, S.J., Middleton, R., Coulthard, T.J. 2007. Measuring river velocities using GPS River Flow Tracers (GRiFTers). Wiley InterScience, Earth Surf. Process. Landforms (2007), DOI: 10.1002/esp. 1614.

Storer, T.I., Usinger, R.L., Lukas, D. 2004. Revised Ed. Sierra Nevada Natural History. University of California Press, Berkeley.

Tharme, R.E. 2002. A global perspective on environmental flow assessment: emerging trends in the development and application of environmental flow methodologies for rivers. *In*: Proceedings of the International Conference on Environmental Flows for River Systems, incorporating the 4th International Ecohydraulics Symposium. Cape Town, South Africa. March 2002.

Tharme, R.E. 2003. A global perspective on environmental flow assessment: emerging trends in the development and application of environmental flow methodologies for rivers. River Research and Applications 19: 397-441.

Thomas, J.A., Bovee, K.D. 1993. Application and testing of a procedure to evaluate transferability of habitat suitability criteria. Regulated Rivers: Research and Management: 285-294.

Thomson, J.R., Taylor, M.P., Fryirs, K.A., Brierley, G.J. 2001. A geomorphological framework for river characterization and habitat assessment. Aquatic Conservation-Marine and Freshwater Ecosystems 11(5): 373-389.

Thompson, D.M. 2001. Random controls on semi-rhythmic spacing of pools and riffles in constriction-dominated rivers. Earth Surface Processes and Landforms 26, 1195–1212.

Tiffan, K.F., Garland, R.D., Rondorf, D.W. 2002. Quantifying flow-dependent changes in subyearling fall chinook salmon rearing habitat using two-dimensional spatially explicit modeling. North American Journal of Fisheries Management 22(3): 713-726.

Tinkler, K.J., Wohl, E.E. 1998. Rivers over rock- fluvial processes in bedrock channels. American Geophysical Union, Geophysical Monograph Series, Vol. 107, Washington, D.C.

United States Geological Survey (USGS). 1992. Policy Statement on Stage Accuracy. Office of Surface Water, Technical Memorandum Number 93.07, Washington, D.C.

United States Geological Survey (USGS). 2010. National Water Information System (NWISWeb). Accessed October 24, 2010. http://waterdata.usgs.gov/nwis/inventory?agency_code=USGS&site_no=11417000.

United States Geological Survey (USGS). Surface water field techniques. http://wwwrcamnl.wr.usgs.gov/sws/fieldmethods/Indirects/nvalues/index.htm

Upper Yuba River Studies Program Team (UYRSPT). 2007. Upper Yuba River watershed Chinook salmon and steelhead habitat assessment. Prepared for California Department of Water Resources.

URS Corporation. 2004. Hydraulic Model of the Merced River Dredger Tailings Reach. Prepared for Stillwater Sciences, Berkeley, CA.

Valle, B.L., Pasternack, G.B. 2006. Field mapping and digital elevation modelling of submerged and unsubmerged hydraulic jump regions in a bedrock step-pool channel. Earth Surface Processes and Landforms 31(6): 646-664.

Van Asselt, M.B.A., Rotmans, J. 2002. Uncertainty in integrated assessment modelling. Climatic Change 54: 75-105.

Waddle, T.J. 2001. PHABSIM for Windows User's Manual and Exercises. United States Geologica Survey, Fort Collins, CO.

Waddle, T.J., Steffler, P., Ghanem, A., Katopodis, C., Locke, A. 2000. Comparison of one and two-dimensional open channel flow models for a small habitat stream. Rivers 7(3): 205-220.

Warrick J.A., Rubin, D.M. Ruggiero, P., Harney, J., Draut, A.E., Buscombe, D. 2009. Cobble Cam: Grain-size measurements of sand to boulder from digital photographs and autocorrelation analyses. Earth Surface Processes and Landforms 34 (13): 1811-1821.

Western Regional Climate Center (WRCC). 2010. Western U.S. Historical Summaries by State, Annual Precipitation Averages and Extremes. Accessed October 23, 2010. http://www.wrcc.dri.edu/htmlfiles/ca/ca.ppt.ext.html.

Wheaton, J.M., Pasternack, G.B., Merz, J.E. 2004a. Spawning habitat rehabilitation-I. conceptual approach and models. International Journal of River Basin Management 2(1): 3-20.

Wheaton, J.M., Pasternack, G.B., Merz, J.E. 2004b. Spawning habitat rehabilitation-II. Using hypothesis development and testing in design, Mokelumne River, California, U.S.A. International Journal of River Basin Management 2(1): 21-37.

Wheaton, J.M., Brasington, J., Darby, S., Merz, J.E., Pasternack, G.B., Sear, D.A., Vericat, D. 2010. Linking geomorphic changes to salmonid habitat at a scale relevant to fish. River Research and Applications 26:469-486.

White, J.Q., Pasternack, G.B., Moir, H.J. 2010. Valley width variation influences riffle-pool location and persistence on a rapidly incising gravel-bed river. Geomorphology 121:206-221.

Wilcock, P.R., Barta, A.F., Shea, C.C., Kondolf, G.M., Matthews, W.V.G., Pitlick, J.C. 1996. Observations of flow and sediment entrainment on a large gravel-bed river. Water Resources Research 32: 2897-2909.

Wilcock, P.R., Barta, A.F., Shea, C.C., Kondolf, G.M., Matthews, W.V.G., Pitlick, J.C. 1996. Observations of flow and sediment entrainment on a large gravel-bed river. Water Resources Research 32, 2897-2909.

Wilcock, P.R., Kondolf, G.M., Barta, A.F., Matthews, W.V.G., Shea, C.C. 1995. Spawning gravel flushing during trial reservoir releases on the Trinity River: field observations and recommendations for sediment maintenance flushing flows. Report submitted to the U.S. Fish and Wildlife Service. 220pp.

Wilkinson, S.N., Rutherfurd, I.D., Keller, R.J., 2008. An experimental test of whether bar instability contributes to the formation, periodicity and maintenance of pool–riffle sequences. Earth Surface Processes and Landforms 33 (11), 1742–1756.

Williams, J.G. 2010. Sampling for Environmental Flow Assessments. Fisheries 35 (9): 434-443.

Williams, T.H., Reeves, G.H. 2003. Ecosystem Diversity and the Extinction Risk of West Coast Salmonid Populations. In: MacCall, A.D., Wainwright, T.C. (editors), Assessing Extinction

Risk for West Coast Salmon: Proceedings of the Workshop. NOAA Tech. Memo. NMFS-NWFSC-56. pp. 107-115. Seattle, Washington: U.S. Department of Commerce.

Williams, G.P., Wolman, M.G. 1984. Downstream effects of dams on alluvial rivers. Professional Paper 1286, U.S. Geological Survey, Washington, D.C.

Willson, M.F., Halupka, K.C. 1995. Anadromous Fish as Keystone Species in Vertebrate Communities. Conservation Biology, 9(3): 489-497.

Wu, R-S, Mao, C-T. 2007. The assessment of river ecology and habitat using a two-dimensional hydrodynamic and habitat model. Journal of Marine Science and Technology 15(4): 322-330.

Wyrick, J.R., Pasternack, G.B. 2008. Modeling energy dissipation and hydraulic jump regime responses to channel nonuniformity at river steps. Journal of Geophysical Research 113: F03003.

Yuba Accord River Management Team (YARMT). 2009. Lower Yuba River Accord Monitoring and Evaluation Plan. Review Draft. February 2009.

GLOSSARY

Accretionary flow	Additional ungaged water input to the river segment
ADCP	Acoustic doppler current profiler
a priori	Known or decided ahead of time
ATV	All terrain vehicle
Bioverification	Independent testing of the validity of HSC in the study area
CCB	Canyon Creek below Bowman
Competence	The upper limit of grain size capable of being moved by a discharge
Cross-section	Lateral span of channel where detailed environmental observations are made (also see transect)
DEM	Digital elevation model
DHSI	Depth habitat suitability index
Ecological functions	How organisms interact with each other and their environment
ESU	Evolutionarily Significant Unit (related to fish populations and survival viability)

FERC	Federal Energy Regulatory Commission
Flow convergence	Stage-dependent oscillatory focusing of high velocity jets through riffle and pools driven by multiple scales of landform variability
First returns	LIDAR signals that bounce off of canopy without hitting the ground and thus have a slightly faster return than any other returns
GHSI	Global habitat suitability index, represents the joint distribution of DHSI and VHSI
GIS	Geographic information system
Habitat units in rivers	Also known as physical habitat, are defined as zones with characteristic physical attributes where organisms perform ecological functions,
HSC	Habitat suitability curve for aquatic species' lifestages
Hysteresis	A difference in stage-discharge curves on the rising limb versus the falling limb of a hydrograph
IFIM	Instream Flow Incremental Methodology
IHA	Instream habitat assessment
Last returns	LIDAR signals classified by signal-strength identification and return time as ground points
LIDAR	Light detection and ranging, a remote sensing technology that uses a laser beam to acquire topographic data

Mesohabitat	Interdependent set of the same physical variables over a morphological unit at a given discharge
MMB	Marsh-McBirney velocity sensor
Microhabitat	Localized depth, velocity, temperature, and substrate at a point in a river without regard to the surrounding conditions
Morphologic unit	Discernible landform in the river valley that is typically visible at the spatial scale of 1-10 channel widths; defined this this study by a joint distribution of depth and velocity predictions at low flow
NAIP	National Agricultural Imagery Program, which acquires periodic 1-m resolution imagery of areas within the USA
PH	Pikeminnow/hardhead fish species, Ptychocheilus grandis/Mylopharodon conocephalus
PHABSIM	Physical Habitat Simulation System
Phase-space plot	Joint distribution plots of depth and velocity
QA/QC	Quality assurance/quality control; a process of checking the accuracy of data
RMS	Root mean squared statistical measure
RT	Rainbow trout, Oncorhynchus mykiss
RTK-GPS	Real-time kinematic geographic positioning system

Scale factors	Used to constrain distortion across a projected coordinate system
Secular	An underlying unidirectional shift in magnitude ignoring short-term fluctuations
SMS	Surface water modeling system
SRH-2D	Sedimentation and River Hydraulics—Two-Dimensional model
SS	Sacramento sucker, Catostomus occidantalis
Stage-discharge relation, 'rating curve'	Empirical relationship between WSE and total discharge
SYJB	USGS stream gage at South Yuba at Jones Bar
SYLC	USGS stream gage, South Yuba River at Langs Crossing
synthetic	Empirically derived from observation data
SYWA	USGS gage, South Yuba at Washington, California
Tailwater	Back-flood, which can occur naturally and in modeling
TIN	Triangular irregular network

Total station	A surveying technology which provides precise measures from known locations
Transect	Lateral span of channel where detailed environmental observations are made (also see cross-section)
USGS gage	United States Geological Survey station where total stream discharge is measured
Velocity area method	Taking depth and velocity measures along a transect to calculate total discharge
VHSI	Velocity habitat suitability index
VSP	Viable salmonid population
YARMT	Yuba Accord River Management Team
WSE	Water surface elevation